Universidad de Valladolid

Escuela de Doctorado Universidad de Valladolid

PROGRAMA DE DOCTORADO EN FÍSICA

TESIS DOCTORAL:

"Synthesis, Foaming Kinetics and Physical Properties of Cellular Nanocomposites Based on Rigid Polyurethane"

Presentada por Mercedes Santiago Calvo para optar al grado de
Doctora por la Universidad de Valladolid

Dirigida por:
Dr. Miguel Ángel Rodríguez Pérez
Dr. Fernando Villafañe González

0- Resumen de la tesis en castellano

1- Introduction

2- Background and state of the art

CHACTER 0:

RESUMEN DE LA TESIS EN CASTELLANO

Mercedes Santiago Calvo

0.1- Introducción

Desde sus comienzos, durante y después de la Segunda Guerra Mundial, la producción de plástico ha resultado en un crecimiento rápido y continuo (**Figura 0.1.A**). Las necesidades de desarrollar polímeros sintéticos y los avances científicos relevantes han permitido la expansión de un conjunto completo de polímeros que ahora generalmente se reconocen como "plásticos". Estos polímeros se comercializaron fácilmente debido al objetivo de aligerar el peso de los productos y ofrecer alternativas económicas a los materiales naturales y metálicos. En 2017, la producción mundial de plástico alcanzó más de 350 millones de toneladas, de las cuales 64,4 se fabricaron en Europa [1]. Uno de los polímeros más versátiles es el poliuretano (PU), ya que sus propiedades únicas han permitido su uso en una amplia gama de diferentes sectores industriales, como automoción, construcción, muebles, envases, equipos médicos, deportivos, etc. [2]. La **Figura 0.1.B** muestra que el polímero de PU representó el 7,7% del consumo europeo de plástico en 2017 [1]. El área de negocios de PU involucra billones de dólares estadounidenses en todo el mundo y está en constante crecimiento, estimándose en $ 60.5 billones en 2017, y se prevé que llegará a más de $ 79 billones en 2021 [3].

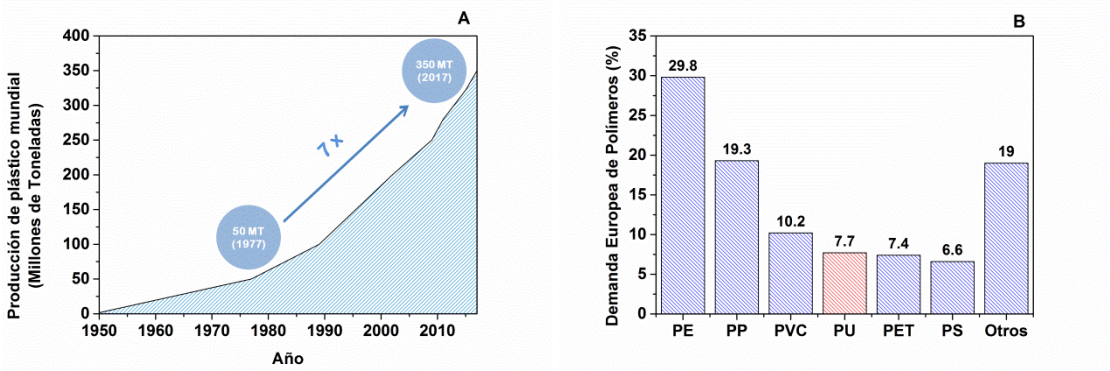

Figura 0.1. A) Producción global de plástico después de la Segunda Guerra Mundial hasta el presente (Adaptado de [1]). B) Demanda europea de plástico por tipos de polímeros en 2017: polietileno (PE), polipropileno (PP), cloruro de polivinilo (PVC), poliuretano (PU), tereftalato de polietileno (PET), poliestireno (PS), otros (Adaptado de [1]).

Debido a la diversidad de formas en que se pueden sintetizar los PUs, hay muchos tipos diferentes de materiales de PU disponibles: espumas flexibles y rígidas, elastómeros, adhesivos y selladores, recubrimientos, entre otros [2]. La **Figura 0.2** claramente muestra que las espumas de PU (referidas a las espumas termoestables de PU) cubren la mayor parte del mercado de PU, ocupando el 67% como espumas flexibles, rígidas y moldeadas, mientras que el 33% restante incluye el resto de los tipos de PU, como adhesivos, elastómeros, recubrimientos y otros [4, 5]. El uso máximo (31% del mercado de PU) se asigna a las espumas flexibles, que se utilizan principalmente en colchones, cojines y otros. Les siguen las espumas rígidas (25% del mercado de PU), que se utilizan ampliamente en el aislamiento térmico de

edificios, refrigeradores, aislamiento de tuberías y transporte refrigerado. Las espumas moldeadas (11% del mercado de PU) se utilizan principalmente en las industrias del automóvil y de muebles. Por otro lado, es importante tener en cuenta que los elastómeros (6% del mercado de PU) incluyen materiales de poliuretano termoplástico (TPU), que también incluyen las espumas de TPU.

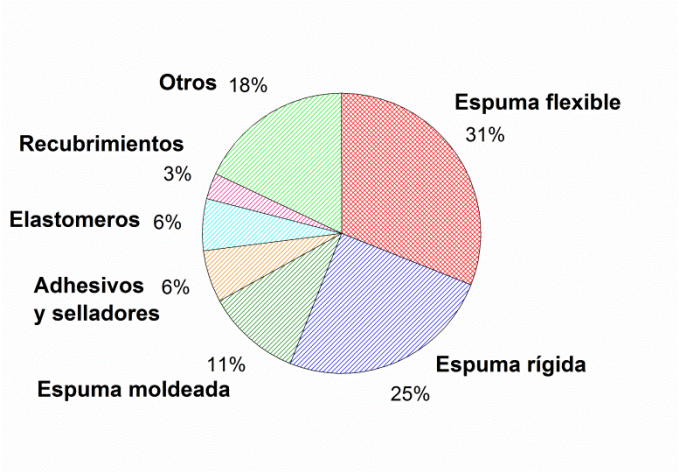

Figure 0.2. Consumo mundial de poliuretano por tipos in 2016 (Adaptado de [4, 5]).

Los datos anteriores muestran que la mayoría de los PU obtenidos industrialmente son espumas de PU. El mercado de las espumas poliméricas se divide en PU, poliestireno (PS), cloruro de polivinilo (PVC), fenólicas, poliolefinas, melamina y otras espumas. Las espumas de PU son uno de los segmentos más grandes del mercado de espumas poliméricas, puesto que representan más del 50% del volumen global de espumas poliméricas [6]. La causa de este alto valor se debe principalmente a la alta aplicabilidad de las espumas de PU, que se basa principalmente en la posibilidad de adaptar las propiedades finales del material cambiando adecuadamente los tipos o cantidades de los componentes iniciales: isocianato, poliol, surfactantes, catalizadores y agentes espumantes. Además, la simplicidad de la tecnología de espumación ha hecho que estos materiales sean muy competitivos desde una perspectiva económica. Por lo tanto, la investigación de estos materiales ha atraído mucho interés desde su descubrimiento en 1941.

0.2- Marco de esta tesis

Esta tesis, titulada **"Synthesis, foaming kinetics and physical properties of cellular nanocomposites based on rigid polyurethane"**, se ha realizado en el Laboratorio de Materiales Celulares (CellMat) del Departamento de Física de la Materia Condensada de la Universidad de Valladolid (UVa) durante los últimos cinco años. El objetivo principal del trabajo

es obtener nuevos conocimientos científicos en el campo de las espumas rígidas de poliuretano (RPU). Esta tesis ha sido supervisada por los profesores Dr. Miguel Ángel Rodríguez-Pérez y Dr. Fernando Villafañe.

CellMat fue establecido en 1999 en la Universidad de Valladolid por los profesores Dr. Jóse Antonio de Saja y Dr. Miguel Ángel Rodríguez-Pérez, después de la defensa de la tesis doctoral de Miguel Ángel Rodríguez Pérez sobre las propiedades de las espumas de base poliolefinas, con el propósito de estudiar materiales celulares [7]. Como resultado, al principio, la actividad de investigación se centró en la caracterización de la microestructura y las propiedades físicas de los polímeros celulares comerciales basados en poliolefinas, para evaluar sus relaciones estructura-propiedades [8-32]. En los años siguientes, los temas de investigación se han ampliado al desarrollo de nuevas espumas poliméricas y sus rutas de producción. A lo largo de los años, comenzó una nueva línea de investigación centrada en la producción y caracterización de espumas metálicas [33-37]. El trabajo de nuestro grupo ha permitido aumentar el conocimiento científico sobre los mecanismos de formación de espuma involucrados en los procesos de fabricación, así como sobre las relaciones de producción-estructura-propiedades de los materiales estudiados [38, 39]. Las aplicaciones finales de los materiales desarrollados en CellMat también se han considerado siempre, porque uno de los principios fundamentales de nuestro laboratorio es la transferencia de conocimiento y tecnología entre la Universidad y la industria.

En la actualidad, se están desarrollando cinco temas principales de investigación en CellMat, todos supervisados por el Prof. Dr. Miguel Ángel Rodríguez-Pérez: polímeros nanocelulares [40-45], materiales celulares multifuncionales [46-48], nanocompuestos celulares [49-52], materiales celulares bioplásticos [53-57] y espumas de PU [58-61]. Además, el grupo de investigación ha participado en muchos proyectos de investigación financiados por instituciones públicas y privadas, y mantiene colaboraciones con un número significativo de grupos de investigación en todo el mundo. Como resultado de este trabajo, se han publicado hasta el momento 30 tesis de doctorado y más de 200 artículos científicos sobre materiales celulares, lo que convierte a CellMat en un laboratorio de referencia internacional en este campo.

La presente tesis es parte del trabajo desarrollado en el laboratorio CellMat en el campo de las espumas de PU. Esta línea de investigación se inició en 2014 con la tesis defendida posteriormente por Sergio Estravis, que trata sobre espumas termoestables de PU [59]. Una de las razones clave que llevaron a CellMat a establecer este nuevo tema fue la gran demanda de estos materiales en el mercado mundial de espumas, debido a sus diversas aplicaciones y peso económico. CellMat ya tenía conocimiento sobre la incorporación de nanopartículas en diferentes espumas, lo cual es un enfoque interesante para la industria de los materiales y, en particular, para el campo de las espumas de PU. Estos rellenos pueden reforzar la matriz de PU, aumentando las propiedades mecánicas, y también pueden actuar como agentes nucleantes y/o bloqueadores de infrarrojo, mejorando así sus propiedades de aislamiento térmico entre otros efectos. El Dr. Estravis realizó un estudio detallado sobre los efectos de la adición de nanoclays a la microestructura, propiedades mecánicas y térmicas de las espumas RPU comerciales, cuyas aplicaciones principales fueron la gestión térmica en edificios, sistemas

de refrigeración y transporte. En particular, la principal conclusión de este trabajo fue que la conductividad térmica de las espumas RPU puede mejorar significativamente con la presencia de cantidades muy bajas de nanoclays (1% en peso o incluso menos). Al mismo tiempo, la presencia de nanoclays en los sistemas de PU mejoró ligeramente el módulo elástico y disminuyó la resistencia a la compresión. La presencia de nanoclays no empeoró la estructura celular, de hecho se obtuvieron tamaños celulares más pequeños y, por lo tanto, la disminución observada de las propiedades mecánicas podría atribuirse a la alteración de la cinética de reacción involucrada en la formación de espuma de PU que causa una morfología del polímero diferente. Esto indicó que la adición de partículas afectaba a la modificación química de la matriz de PU. Sin embargo, el efecto de las partículas en las principales reacciones químicas de las espumas de PU (espumado y polimerización) no se pudo estudiar en este trabajo, pero se señaló como la clave principal para futuros trabajos. Esta tesis fue el primer contacto del laboratorio CellMat con espumas de PU y permitió establecer la metodología necesaria para la fabricación y caracterización de espumas de PU en futuros proyectos y tesis. Los principales temas tratados por CellMat pueden resumirse como un tetraedro (**Figura 0.3**), y la tesis del Dr. Estravis es una contribución definitiva a los cuatro tres vértices de su base.

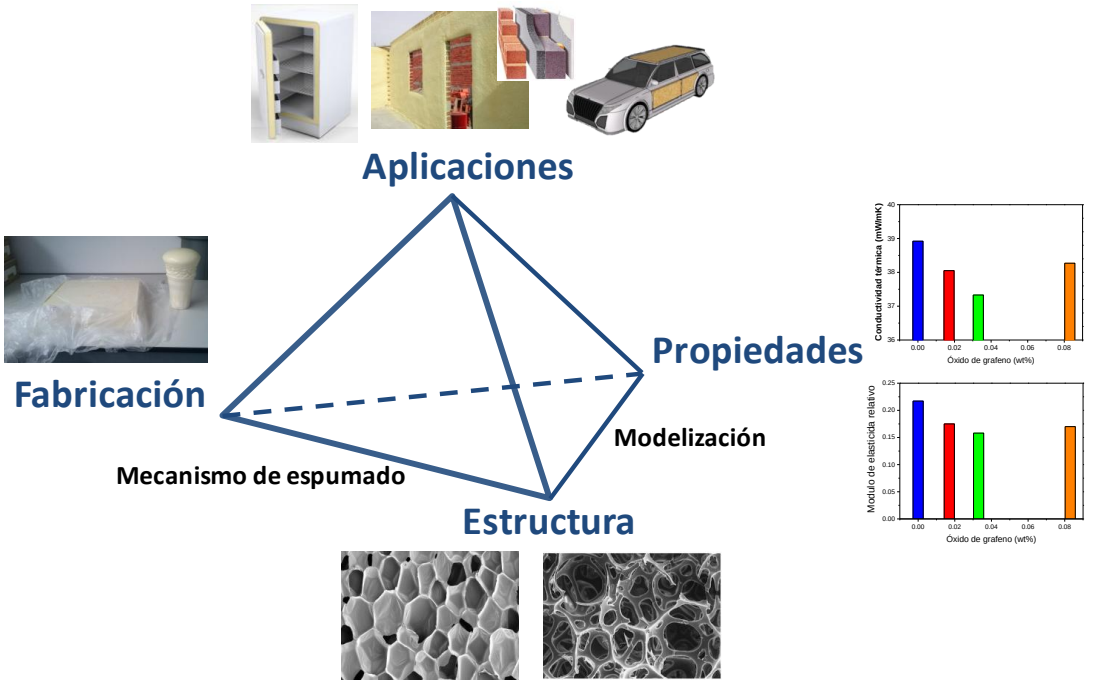

Figure 0.3. Tetraedro de los materiales referido a espumas de PU.

El trabajo de investigación descrito en la presente tesis anima a continuar la investigación basada en espumas de PU, pero esta vez se centra principalmente en los aspectos químicos. Las espumas de PU termoestables se producen mediante espumación reactiva, y el equilibrio

entre las reacciones implicadas en la formación de espuma de PU es crucial para obtener las propiedades deseadas. Como ya lo observó el Dr. Estravis, la inclusión de nanopartículas en las espumas de RPU también puede modificar la cinética de las reacciones. Esto daría lugar a consecuencias inesperadas en las propiedades de la matriz de PU final, ya que algunas propiedades de la espuma pueden mejorarse, pero otras pueden empeorar. Por lo tanto, comprender estos efectos se vuelve esencial para hacer un mejor uso de las nanopartículas y, finalmente, para obtener una mejor estructura celular y propiedades de espuma. Uno de los objetivos principales de la presente tesis fue el desarrollo de una metodología que permita seguir las reacciones químicas que ocurren durante la formación de PU. El objetivo final era controlar la formulación de PU para obtener el mejor rendimiento del composite de espuma de PU termoestable.

Por lo tanto, con el inicio de la presente tesis (finales de 2014) CellMat comenzó el estudio de las espumas de PU desde un punto de vista químico. El primer paso fue desarrollar la metodología para monitorear la espuma de PU termoestable, que es clave para entender las propiedades de la espuma final y también para optimizarlas. Esta metodología se basa en el uso de las siguientes técnicas complementarias: espectroscopia de FTIR, expandometría infrarroja, medidas de temperatura interna y radioscopia de rayos X. Además, por primera vez, pudimos desarrollar nuestras propias formulaciones de PU, en lugar de las formulaciones comerciales utilizadas anteriormente en nuestro laboratorio. El diseño de una formulación propia ha sido una forma adicional de controlar las propiedades finales de las espumas. Por lo tanto, en esta tesis hemos podido mejorar significativamente la calidad de nuestra investigación sobre espumas de PU, controlando mejor todos los aspectos clave del proceso, incluida la materia prima utilizada.

Además de las espumas de PU termoestables, es posible fabricar materiales celulares basados en TPU. Para adquirir conocimientos en este campo, se realizó una estancia de tres meses de junio a agosto de 2017 en el Grupo de Investigación de Polymers & Peptides en la Escuela de Materiales de la Universidad de Manchester (Reino Unido), bajo la supervisión del Profesor Alberto Saiani. Este grupo de investigación fue establecido en 2004 por los Profs. Aline F. Miller y Alberto Saiani y se centra en la caracterización de materiales polímericos, biopoliméricos y peptídicos en diferentes escalas de longitud, destacando el estudio de los materiales de TPU. Su investigación se dirige principalmente a la comprensión de las correlaciones de propiedades de químicas, termodinámicas, estructurales y físicas en sistemas complejos para controlar procesos y productos. Durante la estancia de investigación en Manchester, el trabajo se centró en la síntesis y caracterización de TPUs, que posteriormente se espumaron en CellMat mediante espumación por disolución de gas. Esta es la primera vez que CellMat logra espumar TPU sintetizado. Esta estancía de investigación permite cumplir con los requisitos para obtener un doctorado con la Mención Internacional.

En resumen, el trabajo realizado en esta tesis ha generado conocimiento en los dos métodos que pueden usar para producir materiales espumados basados en PU, es decir, mediante espumación reactiva (espumas de PU termoestables) y espumación por disolución de gas (espumas de TPU) (**Figura 0.4**). El primero de ellos es la parte principal de la tesis, ya que el estudio de las espumas de PU termoestables se llevó a cabo durante los primeros tres años. El

estudio de las espumas de TPU es complementario a este y se realizó principalmente durante los tres meses de estancia y además se desarrolló durante el último año de esta tesis.

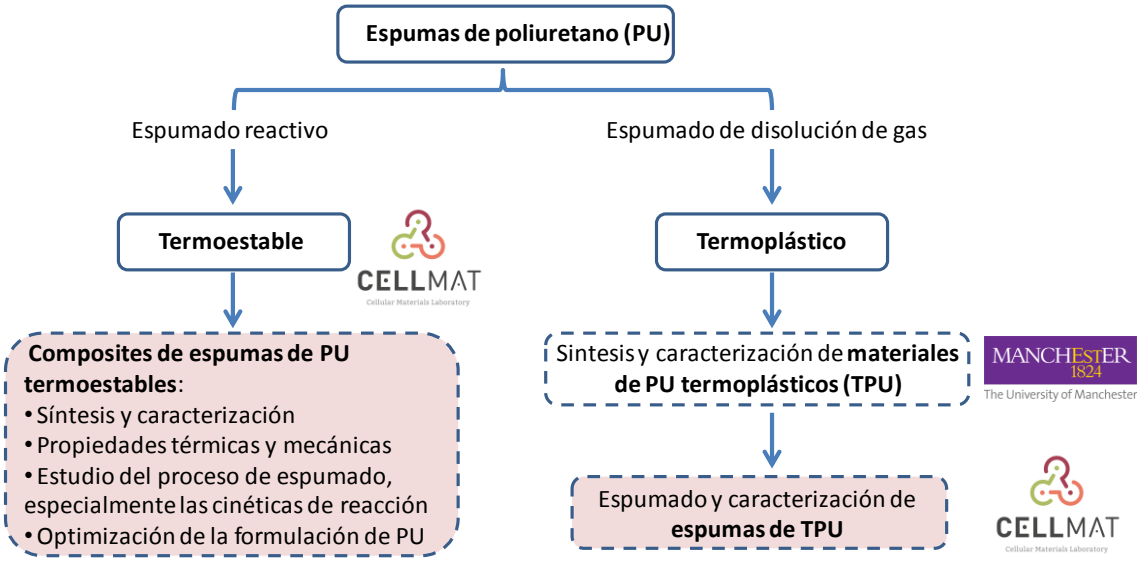

Figure 0.4. Esquema simplificado de las investigaciones desarrolladas en esta tesis.

0.3- Objetivos

El **objetivo de la presente tesis** es adquirir nuevos conocimientos sobre las espumas de PU termoestables (particularmente las espumas de RPU), centrándose en el estudio del proceso de espumado, especialmente en la cinética de reacción de la generación de gas (reacción de espumado) y polimerización (reacción de polimerización) cuando las micro- y/o nanopartículas se incorporan a la matriz de PU para mejorar las propiedades térmicas y mecánicas.

El **segundo aspecto importante** a estudiar es el efecto que la modificación de la reacción podría tener en la estructura y propiedades de los materiales finales.

El **tercer aspecto importante** es optimizar las formulaciones de los sistemas RPU que contienen partículas utilizando la información obtenida en el estudio cinético.

Para alcanzar estos objetivos generales, se han considerado los siguientes objetivos específicos:

• Modelización de la conductividad térmica de espumas de RPU modificadas con micropartículas y/o nanopartículas para estudiar el efecto de las partículas (Capítulo 5).

- Desarrollar nuestras formulaciones propias de PU para poder controlar las características finales de los sistemas RPU.
- Desarrollar y validar la metodología que permitirá estudiar la cinética de las principales reacciones químicas (espumado y polimerización) y la morfología de la matriz polimérica durante el proceso de espumación de las espumas RPU (**Capítulo 4**).
- Desarrollar y validar la metodología que permitirá estudiar las cinéticas de expansión que se producen en la producción de espumas RPU (**Capítulo 4**).
- Aplicar otras metodologías existentes que permitan estudiar la estructura microcelular interna durante el proceso de espumación de las espumas RPU (**Capítulo 4**).
- Aplicar las metodologías de monitorización del proceso de espumado a los sistemas RPU modificados con micropartículas y/o nanopartículas para evaluar el efecto de las partículas en el proceso de espumado, especialmente en la cinética de reacción y la morfología final de la matriz polimérica (**Capítulo 6**).
- Establecimiento de correlaciones entre la cinética de reacción, la morfología final de la matriz polimérica, la estructura celular y las propiedades físicas de los sistemas de RPU modificados con micropartículas y/o nanopartículas (**Capítulo 6**).
- Optimización de la formulación de RPU modificada con micropartículas y/o nanopartículas a partir de la información cinética obtenida (**Capítulo 6**).
- Para sistemas RPU modificados con micropartículas y / o nanopartículas, establecer correlaciones entre la temperatura de espumación y la evolución de su conductividad térmica con el tiempo (**Capítulo 5**).
- Modelización de la conductividad térmica de espumas de RPU modificadas con micropartículas y/o nanopartículas para estudiar el efecto de las partículas (**Capítulo 5**).

Otro objetivo de la presente tesis es estudiar el comportamiento de espumado de los materiales de TPU utilizando la espumación por disolución de gas, para generar conocimiento sobre las espumas de TPU (**Capítulo 7**).

0.4- Principales resultados y conclusiones

1. La principal novedad de la tesis.

Hasta ahora, la literatura científica actual [59, 62-75], que describe espumas de PU reforzadas con micro y/o nanopartículas, sigue el enfoque descrito en la **Figura 0.5**, que se centra principalmente en la producción y caracterización de las espumas, sin poner especial atención al efecto de estos aditivos en las reacciones de polimerización y espumación.

Figura 0.5. Esquema seguido por la literatura científica actual sobre espumas de PU reforzadas con micro- y/o nanopartículas.

Sin embargo, una comprensión clara del efecto de las partículas en la cinética de reacción es esencial, ya que afecta al proceso de formación de la espuma, pero también a la morfología final de la matriz de PU, y por lo tanto a las propiedades finales de la espuma resultante. Por esta razón, nuestra investigación se basa en un enfoque novedoso representado en la **Figura 0.6**, basado en el estudio simultáneo de la modificación de la cinética de la reacción y de la microestructura y propiedades físicas de los sistemas de RPU que contienen micro y/o nanopartículas.

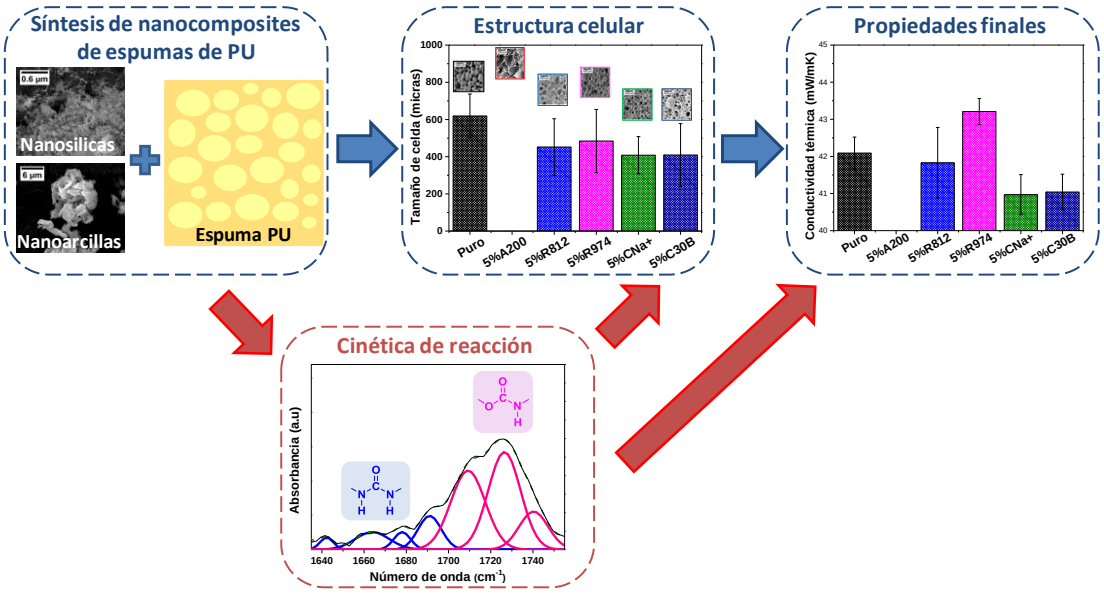

Figura 0.6. Novedoso esquema seguido en esta tesis para el estudio de espumas RPU reforzadas con nanopartículas.

2. Novedades sobre el estudio del proceso de espumado para espumas de RPU (Capítulo 4).

Como punto de partida, se requirió el diseño de una metodología basada en la espectroscopia *in situ* FTIR que consiste en la monitorización y la posterior deconvolución de la región carbonílica (que contiene los productos de reacción). Esto permitiría saber cómo las principales reacciones se ven afectadas por la incorporación de partículas en la matriz de PU. Esta metodología se ha probado en espumas de RPU reforzadas con diferentes tipos de nanosilicas o nanoclays (5% en peso), demostrando cómo los diferentes tipos y superficies (hidrofóbicas

y/o hidrofílicas) de las nanopartículas afectan a la cinética de la reacción de diferentes maneras. Además, se discute el efecto de la modificación de la cinética de reacción sobre la densidad, la estructura celular, la conductividad térmica y las propiedades mecánicas de las espumas de RPU.

Además, en esta tesis se ha desarrollado una metodología novedosa llamada "Expandometría infrarroja", para caracterizar simultáneamente la cinética de expansión (altura frente al tiempo y volumen frente al tiempo) y la evolución de la temperatura de la superficie de las espumas de PU. Esto se logra mediante el uso de la radiación infrarroja emitida por la reacción exotérmica de la espuma de PU. Para probar esta metodología, se ha elegido una formulación de RPU donde el agente espumante (agua) y/o el catalizador de espumado se cambian sistemáticamente.

Finalmente, el proceso de espumado también se ha estudiado mediante radioscopia de rayos X, que mide la densidad relativa, el tamaño de celda y la densidad de nucleación celular en función del tiempo. Esta técnica se ha utilizado para comparar el comportamiento de espumado de dos series de espumas: las preparadas a partir de polioles funcionalizados con óxido de grafeno (GO) y las que contienen GO dispersado en el poliol mediante mezclado a alta cizalla (0.017 y 0.083% en peso). Los resultados obtenidos con esta técnica permiten demostrar que el uso de poliol funcionalizado con GO mejora mucho la estructura celular y también hace que los resultados sean más reproducibles.

3. Novedades sobre las propiedades físicas de las espumas RPU reforzadas con partículas (Capítulo 5).

El efecto de las nanofibras de carbono (CNF) en el mecanismo de conducción de calor de un sistema de PUR espumado con agua se ha estudiado en profundidad, midiendo el coeficiente de extinción y modelizando la conductividad térmica. Se logra una mejora térmica del 2% con solo el 0,1% en peso de CNFs, ya que los CNFs como absorbentes de radiación infrarroja aumentando el coeficiente de extinción de la espuma y, como consecuencia, hay una clara reducción de la contribución radiativa. Este es un resultado notable teniendo en cuenta que las espumas en estudio tienen densidades relativamente altas (56 kg/m^3) y, por lo tanto, la contribución radiativa tiene un peso bajo.

Además, se ha estudiado el efecto de diferentes partículas sobre la conductividad térmica de una espuma de RPU con ciclopentano y agua a lo largo de aproximadamente tres años. En los primeros días después de la producción de espuma, las espumas que contienen partículas mejoran en gran medida la conductividad térmica en comparación con el material de referencia, principalmente debido a la disminución significativa en el tamaño de la celda promovida por las partículas que reducen la contribución radiativa. Sin embargo, después de un tiempo, esta primera mejora se pierde en muchos sistemas, porque la composición del gas dentro de las celdas evoluciona de manera diferente. Por primera vez, la diferente evolución de la conductividad térmica en las primeras medidas se ha relacionado con la temperatura de espumación alcanzada por cada sistema. Las partículas que alcanzan una temperatura de espumación más alta presentan una mayor evolución de la conductividad térmica, ya que esto

causa un mayor gradiente de presión entre las celdas y la atmósfera, lo que genera una mayor velocidad de difusión del gas.

4. Novedades sobre la optimización de las propiedades físicas de las espumas de RPU reforzadas con partículas a partir de los resultados cinéticos (Chapter 6).

Se ha investigado el efecto de los polioles funcionalizados con GO en el proceso de espumado, la morfología de la matriz de PU, la estructura celular, la conductividad térmica y las propiedades mecánicas de compresión de las espumas de RPU. En este estudio, el uso de partículas de GO unidas químicamente a las cadenas de poliol impide la aglomeración de nanofillers, evitando los problemas habituales de dispersión de partículas en nanocompuestos poliméricos. Solo con un 0,033% en peso de GO, la conductividad térmica se incrementa en alrededor del 4% sin modificaciones decisivas de otros aspectos importantes de la estructura celular, mientras que las propiedades mecánicas empeoran, lo que podría deberse a una modificación negativa de la morfología del polímero. Por este motivo, se lleva a cabo un estudio en profundidad del efecto de las partículas GO en el proceso de espumado y la morfología del PU utilizando la expandometría infrarroja, la espectroscopia de in situ FTIR y las medidas de la temperatura de espumado. En conclusión, la presencia de GO disminuye la conversión de isocianato y favorece la reacción de polimerización (generación de uretanos), dando lugar a una reticulatión inferior dentro de la espuma de RPU. Basándose en los resultados del estudio cinético, las propiedades mecánicas de la espuma con 0.033% en peso de GO podrían mejorarse finalmente cambiando la formulación de PU, mientras que al mismo tiempo la conductividad térmica se mantiene o mejora.

5. La novedad de la estancia de investigación en la Universidad de Manchester (Capítulo 7).

El comportamiento de espumado de una nueva serie de TPUs sintetizados con diferentes contenidos de segmentos duros (HS) se ha analizado exhaustivamente en diferentes condiciones de saturación y espumación mediante un proceso de espumado por disolución de gas en un solo paso. El estudio también incluye la densidad y la estructura celular de las espumas resultantes. La mayoría de los trabajos anteriores publicados en la literatura han estudiado la espumación en TPU comerciales en los que la composición no suele conocerse, pero esta investigación permite relacionar la composición del TPU con el comportamiento de espumación.

0.5- Estructura y metodología de la tesis

Esta tesis se escribe como un compendio de 8 artículos científicos, y se divide en 7 capítulos, en los que se incluyen los artículos (ver **Tabla 0.1**). Además, esta tesis cumple con los requisitos para ser acreditada con la Mención Internacional.

Cada capítulo incluye la siguiente información:

-Capítulo 1: Introducción. Se presenta la introducción, el marco de la investigación, los objetivos, las principales novedades, la estructura de la tesis y la lista de las publicaciones resultantes, comunicaciones en conferencias y proyectos de investigación.

-Capítulo 2: Antecedentes y estado del arte. Revisa los conceptos básicos relacionados con las espumas de PU, como su química básica, morfología polimérica, estructura celular, materias primas comunes, proceso de espumación, propiedades y aplicaciones. Además, se describe el estado del arte del seguimiento del proceso de espumado de los materiales compuestos de espuma de PU.

-Capítulo 3: Materiales. Describe los componentes de las formulaciones de PU utilizadas en este trabajo, como los polioles, isocianatos, catalizadores, surfactantes y agentes espumantes, así como los diferentes rellenos agregados a las formulaciones de PU.

-Capítulo 4: Desarrollo de una metodología para seguir el proceso de espumado de espumas rígidas de poliuretano. Explica la metodología desarrollada durante esta tesis para estudiar el proceso de espumado de las espumas RPU que permite controlar la morfología química y, en consecuencia, las propiedades de la espuma. Esta metodología se basa en el uso de espectroscopia FTIR, expandometría infrarroja y radioscopia de rayos X, cuyos resultados son complementarios. Este capítulo contiene tres artículos que tratan cada uno de una técnica diferente para monitorear el proceso de formación de espuma.

-Capítulo 5: Efecto de las partículas sobre la estructura celular y las propiedades físicas de las espumas rígidas de poliuretano. Este capítulo contiene dos artículos. El primero describe el efecto de las CNFs en las propiedades morfológicas, térmicas y mecánicas de las espumas de PUR espumadas con agua. El segundo artículo describe el efecto de diferentes tipos de partículas (talco, tierra de diatomeas y sílice no porosa) sobre el envejecimiento de la conductividad térmica durante tres años para las espumas de RPU que contienen ciclopentano y agua como agentes espumantes.

-Capítulo 6: La optimización de la formulación de poliuretano a partir de los resultados cinéticos para obtener espumas de poliuretano rígidas reforzadas con óxido de grafeno con mejores propiedades térmicas y mecánicas. Contiene dos artículos. El primero investiga el efecto de un poliol funcionalizado con GO en la estructura celular y las propiedades termo-mecánicas de las espumas de RPU obtenidas. Además, se lleva a cabo un estudio cinético detallado utilizando la metodología desarrollada en esta tesis, que permite identificar el efecto del GO en la cinética de reacción y, por consiguiente, en la morfología del polímero final. El segundo artículo se basa en la información recopilada del estudio cinético anterior y describe cómo se puede ajustar la formulación de PU que contiene GO para mejorar las propiedades térmicas y mecánicas al mismo tiempo.

-Capítulo 7: Estancia internacional de investigación: Espumas de poliuretano termoplástico. Incluye el trabajo realizado durante la estadía de investigación internacional y se ocupa de las espumas de TPU producidas por el proceso de espumado por disolución de gas.

-Capítulo 8: Conclusiones y trabajo futuro. Resume las conclusiones finales obtenidas durante toda la tesis y también el trabajo futuro.

0.6- Publicaciones, conferencias y actividades complementarias

Un total de 8 artículos científicos, enumerados en la **Tabla 0.1**, se han redactado durante el desarrollo de esta tesis. Varios de ellos han sido publicados y otros han sido enviados (pendientes de publicación), todos en revistas internacionales. El capítulo en el que se incorporan estos artículos también se especifica en la **Tabla 0.1**.

Tabla 0.1. Artículos científicos de esta tesis.

	ARTÍCULOS CIENTÍFICOS	Capítulo
1	M. Santiago-Calvo, J. Tirado-Mediavilla, J.L. Ruiz-Herrero, M.A. Rodríguez-Pérez, F. Villafañe. **The effects of functional nanofillers on the reaction kinetics, microstructure, thermal and mechanical properties of water blown rigid polyurethane foams.** Polymer 150 (**2018**) 138-149.https://doi.org/10.1016/j.polymer.2018.07.029	4
2	M. Santiago-Calvo, S. Pérez-Tamarit, J. Tirado-Mediavilla, F. Villafañe , M.A. Rodríguez-Pérez. **Infrared expandometry: a novel methodology to monitor the expansion kinetics of cellular materials produced with exothermic foaming mechanisms.** Polymer Testing 66 (**2018**) 383-393. https://doi.org/10.1016/j.polymertesting.2018.02.004	4
3	M. Santiago-Calvo, S. Pérez-Tamarit, P. Cimavilla-Román, V. Blasco, C. Ruiz, R. París, F. Villafañe , M.A. Rodríguez-Pérez. **X-ray radioscopy validation of a polyol functionalized with graphene oxide for producing rigid polyurethane foams with improved cellular structures.** European polymer journal 118 (**2019**) 404-411. https://doi.org/10.1016/j.eurpolymj.2019.06.012	4
4	M. Santiago-Calvo, J. Tirado-Mediavilla, J.C. Rauhe, L.R. Jensen, J.L. Ruiz-Herrero, F. Villafañe, M.A. Rodríguez-Pérez. **Evaluation of the thermal conductivity and mechanical properties of water blown polyurethane rigid foams reinforced with carbon nanofibers.** European polymer journal 108 (**2018**) 98-106. https://doi.org/10.1016/j.eurpolymj.2018.08.051	5
5	M. Santiago-Calvo, J. Tirado-Mediavilla, J.L. Ruiz-Herrero, M.A. Rodríguez-Pérez, F. Villafañe. **Long-thermal conductivity aging of cyclopentane-water blown rigid polyurethane foams reinforced with different types of fillers.** Polymer International (**2019**).https://doi.org/10.1002/pi.5893	5
6	M. Santiago-Calvo, V. Blasco, C. Ruiz, R. París, F. Villafañe, M.A. Rodríguez-Pérez. **Synthesis, characterization and physical properties of rigid polyurethane foams prepared with poly(propylene oxide) polyols containing graphene oxide.** European Polymer Journal 97 (**2017**) 230–240.https://doi.org/10.1016/j.eurpolymj.2017.10.013	6
7	M. Santiago-Calvo, V. Blasco, C. Ruiz, R. París, F. Villafañe, M.A. Rodríguez-Pérez. **Improvement of thermal and mechanical properties by control of formulations in rigid polyurethane foams from polyols functionalized with graphene oxide.** Journal of Applied Polymer Science, 136 (**2019**) 47474. DOI: 10.1002/app.47474	6

	ARTÍCULOS CIENTÍFICOS	Capítulo
8	M. Santiago-Calvo, H. Naji, V. Bernardo, J. Martín-de León, A. Saiani, F. Villafañe, M.A. Rodríguez-Pérez. **Synthesis, characterization, and foaming of thermoplastic polyurethane with different hard segment contents.** Pending publication	7

Además, el trabajo desarrollado en esta tesis ha sido presentado en conferencias nacionales e internacionales, como se recoge en la **Tabla 0.2**.

Table 0.2. Comunicaciones en conferencias relacionadas con el trabajo de esta tesis.

	CONTRIBUCIONES EN CONGRESOS
1	M. Santiago-Calvo, J. Tirado-Mediavilla, J.L. Ruiz-Herrero, M.A. Rodríguez-Pérez, F. Villafañe. FTIR studies to characterize the kinetics of nanocomposite polyurethane foams. **XII Simposio de Investigadores Jóvenes RSEQ-Sigma Aldrich.** November 2015, Barcelona, Spain. (Poster)
2	M. Santiago-Calvo, J. Tirado-Mediavilla, J.L. Ruiz-Herrero, M.A. Rodríguez-Pérez, F. Villafañe. An approach to follow the kinetics of nanocomposite polyurethane foam formation by FTIR spectroscopy. **VIII Jornadas de Jóvenes Investigadores en Física Atómica y Molecular (J2IFAM).** February 2016, Valladolid, Spain. (Talk)
3	M. Santiago-Calvo, J. Tirado-Mediavilla, J.L. Ruiz-Herrero, M.A. Rodríguez-Pérez, F. Villafañe. FTIR studies to characterize the kinetics of nanocomposite polyurethane foams. **XIV Reunión del Grupo Especializado de Polímero (GEP).** September 2016, Burgos, Spain. (Poster)
4	M. Santiago-Calvo1, V. Blasco, C. Ruiz, R. París, F. Villafañe, M.A. Rodríguez-Pérez. Synthesis, properties and kinetic study of rigid polyurethane foams obtained from poly(propylene oxide) polyols functionalized with graphene oxide. **15th International Conference on Advances in Foam Materials & Technology (FOAMS).** October 2017, Bayreuth, Germany. (Poster)
5	M. Santiago-Calvo, H. Naji, V. Bernardo, J. Martín-de León, A. Saiani, F. Villafañe, M.A. Rodríguez-Pérez. Synthesis, characterization and foaming of thermoplastic polyurethane synthesized with different soft/hard segment ratio and graphene nanoplatelet contents. **1st International congress PDFA, Polymers: Design, Function and Application.** March 2018, Barcelona, Spain. (Poster)
6	M. Santiago-Calvo1, V. Blasco, C. Ruiz, R. París, F. Villafañe, M.A. Rodríguez-Pérez. Synthesis, properties and kinetic study of rigid polyurethane foams obtained from poly(propylene oxide) polyols functionalized with graphene oxide. **5th International Conference on Cellular Materials (CellMAT).** October 2018, Bad Staffelstein, Germany. (Talk)
7	M. Santiago-Calvo, H. Naji, V. Bernardo, J. Martín-de León, A. Saiani, F. Villafañe, M.A. Rodríguez-Pérez. Synthesis, characterization and foaming of thermoplastic polyurethane synthesized with different soft/hard segment ratio and graphene nanoplatelet contents. **5th International Conference on Cellular Materials (CellMAT).** October 2018, Bad Staffelstein, Germany. (Poster)

Ya que se presenta esta tesis para obtener un doctorado con Mención Internacional, se ha llevado a cabo una estancia en una institución extranjera. Todos los detalles están incluidos en la **Tabla 0.3**.

Tabla 0.3. Estancias en otro centro de investigación durante la investigación.

ESTANCIA DE INVESTIGACIÓN INTERNACIONAL
Polymers & Peptides Research Group, The University of Manchester (UK). **From June to August 2017 (3 months).** Under the supervision of Prof. Alberto Saiani. Research work: Synthesis and characterization of thermoplastic polyurethane (TPU) in order to produce TPU foams by gas dissolution foaming process.

Uno de los trabajos de investigación desarrollados durante la tesis ganó el Premio al Mejor Póster 2017 en la 15th International Conference on Advances in Foam Materials & Technology (FOAMS 2017), celebrada en Bayreuth (Alemania). Esto se enumera en la **Tabla 0.4**.

Table 0.4. Trabajos de investigación premiados.

PREMIOS
M. Santiago-Calvo1, V. Blasco, C. Ruiz, R. París, F. Villafañe, M.A. Rodríguez-Pérez. **Synthesis, properties and kinetic study of rigid polyurethane foams obtained from poly(propylene oxide) polyols functionalized with graphene oxide.** 5th International Conference on Cellular Materials (CellMAT). October 2017, Bayreuth, Germany. Best Poster selected by the Society of Plastics Engineers: Thermoplastic Materials & Foams Division.

El conocimiento generado en el presente trabajo se ha desarrollado y aplicado en diferentes proyectos de investigación en colaboración con empresas privadas, recogidos en la **Tabla 0.5**. Este es un indicador decisivo de la importancia principal de esta investigación para importantes sectores industriales como la refrigeración, la automoción, la construcción, etc. Además, la investigación aquí desarrollada también se ha financiado con fondos públicos (también recogidos en la **Tabla 0.5**).

Tabla 0.5. Proyectos privados y públicos que han financiado la investigación realizada en el presente trabajo.

	PROYECTOS DE INVESTIGACIÓN
1	Título del proyecto: **"Improvement of short and long term thermal conductivity for rigid polyurethane foams through the use of specific additives and the control of kinetic reactions".** Fecha inicial: **Dicienbre 2013** Fecha final: **Noviembre 2016** Entidad financiadora: **BOSH AND SIEMENS HOME APPLIANCES (Navarra).** Investigador principal: **Miguel Ángel Rodríguez Pérez**
2	Título del proyecto: **"Innovative additives for foams with better thermal insulation performance and fire behavior (NEOADFOAM)".** Fecha inicial: **Septiembre 2015** Fecha final: **Diciembre 2018** Entidad financiadora: **MINECO, PROYECTO RETOS EN COLABORACIÓN CON TOLSA SA E IMDEA (Madrid).** Investigador principal: **Miguel Ángel Rodríguez Pérez**
3	Título del proyecto: **"Development of advanced cellular materials".** Fecha inicial: **Abril 2016** Fecha final: **Diciembre 2016** Entidad financiadora: **Parque Científico. Universidad de Valladolid (Valladolid).** Investigador principal: **Miguel Ángel Rodríguez Pérez**
4	Título del proyecto: **"Analysis of a rigid polyurethane system: manufacturing, study of the reaction kinetics and characterization of the structure and properties".** Fecha inicial: **Mayo 2016** Fecha final: **Diciembre 2016** Entidad financiadora: **REPSOL S.A (Madrid).** Investigador principal: **Miguel Ángel Rodríguez Pérez**
5	Título del proyecto: **"Comparative analysis of the cellular structure and reaction kinetics for three systems based on polyurethane".** Fecha inicial: **Abril 2016** Fecha final: **Diciembre 2018** Entidad financiadora: **GRUPO ANTOLÍN INGENIERÍA (Burgos).** Investigador principal: **Miguel Ángel Rodríguez Pérez**
6	Título del proyecto: **"Study of polyurethane formulations by X-ray radioscopy".** Fecha inicial: **Enero 2017** Fecha final: **Junio 2017** Entidad financiadora: **SOPREMA (France).** Investigador principal: **Miguel Ángel Rodríguez Pérez**
7	Título del proyecto: **"Research on applications of advanced carbon nanomaterials to improved performance of polyurethane matrices with interest in the automotive sector".** Fecha inicial: **Abril 2017** Fecha final: **2019** Entidad financiadora: **GRUPO ANTOLÍN INGENIERÍA (Burgos).** Investigador principal: **Miguel Ángel Rodríguez Pérez**
8	Título del proyecto: **"Study of polyisocyanurate foam formulations".** Fecha inicial: **Enero 2019** Fecha final: **2019** Entidad financiadora: **DUPONT (USA).** Investigador principal: **Miguel Ángel Rodríguez Pérez**

Finalmente, la **Tabla 0.6** muestra las actividades adicionales desarrolladas durante esta tesis relacionadas con el campo de las espumas de PU.

Tabla 0.6. Actividades adicionales llevadas durante esta tesis.

ARTÍCULOS CIENTÍFICOS
S. Estravís, J. Tirado-Mediavilla, M. Santiago-Calvo, J.L. Ruiz-Herrero, M.A. Rodríguez-Pérez, F. Villafañe. **Rigid polyurethane foams with infused nanoclays: Relationship between cellular structure and thermal conductivity.** European Polymer Journal 80 **(2016**) 1–15. https://doi.org/10.1016/j.eurpolymj.2016.04.026
P. Acuña, M. Santiago-Calvo, F. Villafañe, M.A. Rodríguez-Perez, J. Rosas, De-Yi Wanga. **Impact of Expandable Graphite on Flame Retardancy and Mechanical Properties of Rigid Polyurethane Foam.** Polymer composites (**2018**). https://doi.org/10.1002/pc.25127
P. Acuña, Z. Li, M. Santiago-Calvo, F. Villafañe, M.A. Rodríguez-Perez, De-Yi Wanga. **Influence of the characteristics of expandable graphite on the morphology, thermal properties, fire behaviour and compression performance of a rigid polyurethane foam.** Polymers 11 (**2019**) 168. https://doi.org/10.3390/polym11010168
A. Galakhova, M. Santiago-Calvo, J. Tirado-Mediavilla, F. Villafañe, M.A. Rodríguez-Pérez and G. Riess. **Identification and Quantification of Cell Gas Evolution in Rigid Polyurethane Foams by Novel GCMS Methodology.** Polymers 11 (**2019**) 1192. https://doi.org/10.3390/polym11071192

CONTRIBUCIONES A CONGRESOS
P. Cimavilla-Román, S. Pérez-Tamarit, M. Santiago-Calvo, M.A. Rodríguez-Pérez. In situ analysis, by X-ray radioscopy, of the foaming process of aerogel-polyurethane cellular composites. **10th European School on Molecular Nanoscience (ESMolNa2017).** May 2017, El Escorial, Madrid, Spain. (Talk)
P. Cimavilla-Román, S. Pérez-Tamarit, M. Santiago-Calvo, M.A. Rodríguez-Pérez. In-situ physicochemical analysis of the foaming process of aerogel-rigid polyurethane composite foams. **12th European Conference on Foams, Emulsions and Applications (EUFOAM).** July 2018, Liege (Belgium). (Talk)

ACTIVIDADES ACADÉMICAS
Proyecto final de master: Characterization and in-situ analysis of the cellular structure and foaming process of aerogel-polyurethane composites by means of X-ray radioscopy and tomography. Autora: P. Cimavilla-Román. Tutores: M.A. Rodríguez-Pérez, S. Pérez-Tamarit y M. Santiago-Calvo. Fecha de publicación: 2017. Titulación universitaria: Máster en Nanociencia y Nanotecnología Molecular. http://uvadoc.uva.es/handle/10324/26203

CHARLAS DE DIVULGACIÓN CIENTÍFICA
Ciclo de conferencias: Woman Researchers of the University of Valladolid in the Adventure of Science and Technology. -En **2016**: Study of formation reactions of polyurethane foam nanocomposites by FTIR spectroscopy. (Talk) -En **2017**: Polyurethane foams from polyols functionalized with graphene oxide. (Talk) -En **2018**: Synthesis and characterization of thermoplastic polyurethanes (TPUs) with different contents of hard segments in order to prepare TPU foams. (Talk)

PROYECTOS DE INVESTIGACIÓN
Título del proyecto: **"Evolution: The Electric Vehicle revolution enhabled by advanced materials highly into ligh".** Fecha inicial: **Octubre 2013** Duración: **1 año** Entidad financiadora: **EUROPEAN UNION (FPVII).** Investigador principal: **Miguel Ángel Rodríguez Pérez**
Título del proyecto: **"ACTIBIOPACK: Envasado activo y biodegradable de champiñón en fresco y carne fresca".** Fecha inicial: **October 2014** Duración: **3 months** Entidad financiadora: **MINECO.** Investigador principal: **Miguel Ángel Rodríguez Pérez**

0.7- Referencias

[1] Plastics Europe (the Association of Plastics Manufacturers in Europe). https://www.plasticseurope.org/en/resources/market-data.

[2] M. Szycher, Szycher's Handbook of Polyurethanes, Second ed., CRC Press Boca Raton, Florida, USA, 2012.

[3] Polyurethane Global Market Size Forecast 2021. Available online: https://www.statista.com/statistics/720449/global-polyurethane-market-size-forecast/ (accessed on 22 February 2019).

[4] Plastics Insight: https://www.plasticsinsight.com/resin-intelligence/resin-prices/polyurethane/.

[5] Statista: https://www.statista.com/statistics/615265/distribution-of-polyurethane-consumption-worldwide-by-end-use/.

[6] Polymer Foams Market Expected to Consume 25.3 Million Tonnes by 2019. http://www.smithersrapra.com/news/2014/may/polymer-foam-market-to-consume-25-3-million-tonnes, 2014 (accessed 16 July 2019).

[7] M.Á. Rodríguez-Pérez, PhD Thesis: Thermal and mechanical properties of polyolefin foams University of Valladolid, 1999.

[8] M.A.Rodríguez-Pérez, O.Alonso, J. Souto, J.A.d. Saja, Thermal Conductivity of Crosslinked Closed Cell Polyolefin Foams, Polymer Testing, 16 (1997) 287-298.

[9] M.A. Rodríguez-Pérez, S. Rodríguez-Llorente, J.A.d. Saja, Dynamic Mechanical Properties of Polyolefin Foams Studied by DMA Techniques, Polym. Eng. Sci., 37 (1997) 959-966.

[10] M.A.Rodríguez-Pérez, A.Duijsens, J.A.d. Saja, Effect of Addition of EVA on the Technical Properties of Extruded Foam Profiles of Low-Density Polyethylene/EVA Blends, J.Applied Polymer Science (1998) 1237-1244

[11] M.A.Rodriguez, S.Diez, J.A.d. Saja, The recovery behaviour of crosslinked closed cell polyolefin foams, Polymer Eng. & Sci, (1998) 831-838.

[12] M.A.Rodríguez-Pérez, O.Alonso, A.Duijsens, J.A.d. Saja, Thermal Expansion of Crosslinked Closed-Cell Polyethylene Foams, J.Polymer Sci. , 36 (1998) 2587-2596.

[13] M.A. Rodríguez-Pérez, J.A.D. Saja, The effect of blending on the physical properties of crosslinked closed cell polyrthylene foams, Cellular Polymers 18 (1999) 1-20.

[14] M.A. Rodríguez-Pérez, O. Almanza, J.A.D. Saja, Anomalous thickness increase in crosslinked closed cell polyolefin foams during heat treatments. , Journal of Applied Polymer Science, 73 (1999) 2825–2835.

[15] J.I. Velasco, A.B. Martinez, D. Arencon, M.A. Rodriguez-Perez, J.A.D. Saja, Application of instrumented falling dart impact to the mechanical characterization of thermoplastic foams, Journal of Materials Science, 34 (1999) 431–438.
[16] O.A. Almanza, M.A. Rodríguez-Pérez, J.A.D. Saja, Prediction of the radiation term in the thermal conductivity of crosslinked closed cell polyolefin foams, Journal of Polymer Science Part B: Polymer Physics, 38 (2000) 993–1004.
[17] M.A. Rodriguez-Perez, J.I. Velasco, D. Arencon, O. Almanza, J.A.D. Saja, Mechanical Characterization of Closed-CellPolyolefin Foams, Journal of Applied Polymer Science, 75 (2000) 156 –166.
[18] M.A. Rodríguez-Pérez, J.A.d. Saja, Dynamic mechanical analysis applied to the characterisation of closed cell polyolefin foams, Polymer Testing, 19 (2000) 831–848.
[19] J.I. Velasco, A.B. Martinez, D. Arencon, M.A. Rodriguez-Perez, J.A.d. Saja, Rigidity characterisation of flexible foams by falling dart robound tests, Cellular Polymers, 19 (2000) 115–133.
[20] O. Almanza, M.A. Rodriguez-Perez, J.A.D. Saja, The microestructure of polyethylene foams produced by a nitrogen solution process, Polymer, 42 (2001) 7117–7126.
[21] O. Almanza, L.O.A.y. Rabago, M.A.Rodriguez-Perez, A. Gonzalez, J.A.d. Saja, Strucutre-property relationships in polyolefin foams, Journal of Macromolecular Science, Part B 40 (2001) 603–613.
[22] J.A. Martinez-Diez, M.A. Rodriguez-Perez, J.A.d. Saja, L.O.A.y. Rabago, O.A. Almanza, The thermal conductivity of a polyethylene foam block produced by a compression molding process, Journal of Cellular Plastics, 37 (2001) 21–42.
[23] N.J. Mills, M.A. Rodriguez-Perez, Modelling the Gas-loss Creep Mechanism in EVA Foam from Running Shoes, Cellular Polymers, 20 (2001) 79–100.
[24] M.A. Rodriguez-Perez, O. Almanza, J.L.D. Valle, A. Gonzalez, J.A.D. Saja, Improvement of the measurement process used for the dynamic mechanical characterization of polyolefin foams in compression, Polymer Testing, 20 (2001) 253–267.
[25] M.A. Rodriguez-Perez, The effect of chemical composition, density and cellular structure on the dynamic mechanical response of polyolefin foams, Cellular Polymers, 21 (2002) 117–136.
[26] M.A. Rodriguez-Perez, J.I. Gonzalez-Peña, N. Witten, J.A.D. Saja, Morphology of semicrystalline foams based on polyethylene, Journal of Macromolecular Science: Part B – Physics 41 (2002) 761–775.
[27] M.A. Rodriguez-Perez, J.I. Gonzalez-Peña, N. Witten, J.A.D. Saja, The Effect of Cell Size on the Physical Properties of Crosslinked Closed Cell Polyethylene Foams Produced by a High Pressure Nitrogen Solution Process, Cellular Polymers, 21 (2002) 165–194.
[28] O. Almanza, M.A. Rodríguez-Pérez, J.A. de Saja, Applicability of the Transient Plane Source Method To Measure the Thermal Conductivity of Low-Density Polyethylene Foams, Journal of Polymer Science: Part B: Polymer Physics, 42 (2004) 1226–1234.
[29] O. Almanza, Y. Masso-Moreu, N.J. Mills, M. A.Rodriguez-Perez, Thermal expansion coefficient and bulk modulus of polyethylene closed-cell foams, Journal of Polymer Science, Part B: Polymer Physics, 42 (2004) 3741–3749.
[30] O. Almanza, M.A. Rodriguez-Perez, J.A.d. Saja, Measurement of the thermal diffusivity andspecific heat capacity of polyethylene foamsusing the transient plane source technique, Polymer International 2004, 53, , 53 (2004) 2038–2044.
[31] R.A. Campo-Arnáiz, M.A. Rodríguez-Pérez, B. Calvo, J.A. de Saja, Extinction coefficient of polyolefin foams, Journal of Polymer Science Part B: Polymer Physics, 43 (2005) 1608-1617.
[32] O. Almanza, M.A. Rodríguez-Pérez, B. Chernev, J.A.d. Saja, P. Zipper, Comparative study on the lamellar structure of polyethylene foams, European Polymer Journal, 41 (2005) 599–609.
[33] J.A. Reglero-Ruiz, PhD Thesis: Manufacture and characterization of aluminium foams: Applications in the aeronautical sector, University of Valladolid, 2007.

[34] E. Solórzano, PhD Thesis: Aluminium foams: Foaming process, cellular structure and properties, University of Valladolid, 2008.
[35] J.A. Reglero, M.A. Rodriguez-Perez, D. Lehmhus, M. Windmann, J.A.d. Saja, A. Fernandez, An experimental study on the inhomogeneities of aluminum foams measuring the thermal conductivity by using the transient plane source method, Materials Science Forum 480-481 (2005) 133–138.
[36] E. Solórzano, M.A. Rodríguez-Pérez, J.A. Reglero, J.A.d. Saja, Density gradients in aluminium foams: characterisation by computed tomography and measurements of the effective thermal conductivity, Journal of Materials Science, 42 (2007) 2557–2564.
[37] E. Solórzano, J.A. Reglero, M.A. Rodríguez-Pérez, J.A.d. Saja, M.L. Rodríguez-Méndez, Improvement of the foaming process for 4045 and 6061 aluminium foams by using the Taguchi methodology, Journal Material Science, 42 (2007) 7227–7238.
[38] C. Saiz-Arroyo, PhD thesis: Fabricación de Materiales Celulares Mejorados Basados en Poliolefinas. Relación procesado-composición-estructura-propiedades, University of Valladolid, 2012.
[39] S. Pardo, PhD Thesis: X-Ray Imaging Applied to the Characterization of Polymer Foams' Cellular Structure and its Evolution, University of Valladolid, 2014.
[40] J. Pinto, PhD Thesis: Fabrication and characterization of nanocellular polymeric materials from nanostructured polymers., University of Valladolid, 2014.
[41] B. Notario-Collado, PhD Thesis: Fabrication and characterization of the physical properties of nanocellular polymers: The transition from the micro to the nanoscale., University of Valladolid, 2016.
[42] J.A.R. Ruiz, M. Dumon, J. Pinto, M.A. Rodriguez-Perez, Low-Density Nanocellular Foams Produced by High-Pressure Carbon Dioxide, Macromol. Mater. Eng., 296 (2011) 752-759.
[43] J. Pinto, M. Dumon, M. Pedros, J. Reglero, M.A. Rodriguez-Perez, Nanocellular CO2 foaming of PMMA assisted by block copolymer nanostructuration, Chem. Eng. J., 243 (2014) 428-435.
[44] B. Notario, J. Pinto, E. Solorzano, J.A. de Saja, M. Dumon, M.A. Rodriguez-Perez, Experimental validation of the Knudsen effect in nanocellular polymeric foams, Polymer, 56 (2015) 57-67.
[45] J. Martin-de Leon, V. Bernardo, M.A. Rodriguez-Perez, Key Production Parameters to Obtain Transparent Nanocellular PMMA, Macromol. Mater. Eng., 302 (2017) 5.
[46] B. Notario, A. Ballesteros, J. Pinto, M.A. Rodriguez-Perez, Nanoporous PMMA: A novel system with different acoustic properties, Mater. Lett., 168 (2016) 76-79.
[47] J.A. Reglero-Ruiz, C. Saiz-Arroyo, M. Dumon, M.A. Rodríguez-Perez, L. Gonzalez, Production, cellular structure and thermal conductivity ofmicrocellular (methyl methacrylate)–(butyl acrylate)–(methyl methacrylate) triblock copolymers, Polymer International, 60 (2011) 146-152.
[48] M. Dumon, J.A.R. Ruiz, J.P. Sanz, M.A.R. Perez, J.-M. Tallon, M. Pedros, E. Cloutet, P. Viot, Block Copolymer-Assisted Microcellular Supercritical CO2 Foaming of Polymers and Blends, Cellular Polymers, 31 (2012) 207-222.
[49] J.I. Velasco, M. Antunes, O. Ayyad, J.M. López-Cuesta, P. Gaudon, C. Saiz-Arroyo, M.A. Rodríguez-Pérez, J.A. de Saja, Foaming behaviour and cellular structure of LDPE/hectorite nanocomposites, Polymer, 48 (2007) 2098-2108.
[50] C. Saiz-Arroyo, M.A. Rodriguez-Perez, J.I. Velasco, J.A. de Saja, Influence of foaming process on the structure-properties relationship of foamed LDPE/silica nanocomposites, Compos. Pt. B-Eng., 48 (2013) 40-50.
[51] E. Laguna-Gutierrez, J. Escudero, V. Kumar, M.A. Rodriguez-Perez, Microcellular foaming by using subcritical CO2 of crosslinked and non-crosslinked LDPE/clay nanocomposites, Journal of Cellular Plastics, 54 (2018) 257-282.

[52] M. Ardanuy, J.I. Velasco, M. Antunes, M.A. Rodriguez-Perez, J.A. de Saja, Structure and Properties of Polypropylene/Hydrotalcite Nanocomposites, Polymer Composites, 31 (2010) 870-878.
[53] M.A. Rodriguez-Perez, R.D. Simoes, C.J.L. Constantino, J.A.D. Saja, Structure and Physical Properties of EVA/Starch Precursor Materials for Foaming Applications, Journal of Applied Polymer Science, 121 (2011) 2324-2330.
[54] M.A. Rodriguez-Perez, R.D. Simoes, S. Roman-Lorza, M. Alvarez-Lainez, C. Montoya-Mesa, C.J.L. Constantino, J.A.d. Saja, Foaming of EVA/Starch Blends: Characterization of the Structure, Physical Properties and Biodegradability, Polymer Enginnering and Science, 52 (2012) 62-70.
[55] A. Lopez-Gil, F. Silva-Bellucci, D. Velasco, M. Ardanuy, M.A. Rodriguez-Perez, Cellular structure and mechanical properties of starch-based foamed blocks reinforced with natural fibers and produced by microwave heating, Industrial Crops and Products, 66 (2015) 194-205.
[56] A. López-Gil, PhD Thesis: Development of environmentally friendly cellular polymers for packaging and structural applications. Study of the relationship cellular structure-mechanical properties, University of Valladolid, 2016.
[57] H. Ventura-Casellas, PhD Thesis: Development of new lightweight green composites reinforced with nonwoven structures of flax fibers, University of Valladolid, 2017.
[58] S. Pardo-Alonso, E. Solórzano, S. Estravís, M.A. Rodríguez-Perez, J.A. de Saja, In situ evidence of the nanoparticle nucleating effect in polyurethane–nanoclay foamed systems, Soft Matter, 8 (2012) 11262.
[59] S. Estravis, PhD Thesis: Cellular nonocomposites based on rigid polyurethane and nanoclays: fabrication, caharacterization and modelling of the mechanical and thermal properties, University of Valladolid, 2014.
[60] S. Pardo-Alonso, E. Solórzano, M.A. Rodriguez-Perez, Time-resolved X-ray imaging of nanofiller-polyurethane reactive foam systems, Colloids and Surfaces A: Physicochemical and Engineering Aspects, 438 (2013) 119-125.
[61] S. Pardo-Alonso, E. Solórzano, L. Brabant, P. Vanderniepen, M. Dierick, L. Van Hoorebeke, M.A. Rodríguez-Pérez, 3D Analysis of the progressive modification of the cellular architecture in polyurethane nanocomposite foams via X-ray microtomography, European Polymer Journal, 49 (2013) 999–1006.
[62] L. Madaleno, R. Pyrz, A. Crosky, L.R. Jensen, J.C.M. Rauhe, V. Dolomanova, A.M.M.V. de Barros Timmons, J.J. Cruz Pinto, J. Norman, Processing and characterization of polyurethane nanocomposite foam reinforced with montmorillonite–carbon nanotube hybrids, Composites Part A: Applied Science and Manufacturing, 44 (2013) 1–7.
[63] X. Cao, L. James Lee, T. Widya, C. Macosko, Polyurethane/clay nanocomposites foams: processing, structure and properties, Polymer, 46 (2005) 775–783.
[64] G. Harikrishnan, T.U. Patro, D.V. Khakhar, Polyurethane Foam-Clay Nanocomposites: Nanoclays as Cell Openers, Industrial and Engineering Chemistry Research, 45 (2006) 7126–7134.
[65] M.M.A. Nikje, Z.M. Tehrani, Thermal and mechanical properties of polyurethane rigid foam/modified nanosilica composite, Polymer Engineering & Science, 50 (2010) 468–473.
[66] M.M.A. Nikje, Z.M. Tehrani, Polyurethane Rigid Foams Reinforced by Doubly Modified Nanosilica, Journal of Cellular Plastics, 46 (2010) 159–172.
[67] T. Widya, C. Macosko, Nanoclay-Modified Rigid Polyurethane Foam, Journal of Macromolecular Science, Part B: Physics, 44 (2005) 897-908.
[68] M.C. Saha, M.E. Kabir, S. Jeelani, Enhancement in thermal and mechanical properties of polyurethane foam infused with nanoparticles, Materials Science and Engineering: A, 479 (2008) 213-222.
[69] M.M.A. Nikje, Z.M. Tehrani, The Effects of Functionality of the Organifier on the Physical Properties of Polyurethane Rigid Foam/Organified Nanosilica, Designed Monomers and Polymers, 14 (2012) 263-272.

[70] M.M.A. Nikje, Z.M. Tehrani, Novel Modified Nanosilica-Based on Synthesized Dipodal Silane and Its Effects on the Physical Properties of Rigid Polyurethane Foams, Designed Monomers and Polymers, 13 (2012) 249-260.
[71] M.E. Kabir, M.C. Saha, S. Jeelani, Effect of ultrasound sonication in carbon nanofibers/polyurethane foam composite, Materials Science and Engineering: A, 459 (2007) 111-116.
[72] C. Caglayan, I. Gurkan, S. Gungor, H. Cebeci, The Effect of CNT-Reinforced Polyurethane Foam Cores to Flexural Properties of Sandwich Composites, Composites: Part A, (2018).
[73] S.-X. Wang, H.-B. Zhao, W.-H. Rao, S.-C. Huang, T. Wang, W. Liao, Y.-Z. Wang, Inherently flame-retardant rigid polyurethane foams with excellent thermal insulation and mechanical properties, Polymer, 153 (2018) 616-625.
[74] S. Sathiyamoorthy, G. Girijakumrai, P. Kannan, K. Venugopal, S.T. Shanmugam, P. Veluswamy, K.D. Wael, H. Ikeda, Tailoring the functional properties of polyurethane foam with dispersions of carbon nanofiber for power generator applications, Applied Surface Science, (2018).
[75] N. Nazeran, J. Moghaddas, Synthesis and characterization of silica aerogel reinforced rigid polyurethane foam for thermal insulation application, Journal of Non-Crystalline Solids, 461 (2017) 1-11.

CHAPTER 1:

INTRODUCTION

Mercedes Santiago Calvo

1.1- Introduction

From its early beginnings during and after World War II, plastic production has resulted in a rapid and continuous growth (**Figure 1.1.A**). The needs to develop synthetic polymers and relevant scientific advances have allowed the expansion of a complete set of polymers which are now usually recognized as "plastics". These polymers were easily commercialized due to the aim to lighten the weight of products and to offer economic alternatives to natural and metallic materials. In 2017, the world plastic production reached over 350 million tonnes of which 64.4 were manufactured in Europe [1]. One of the most versatile polymers is polyurethane (PU), since their unique properties have allowed its usage in a wide range of different industrial sectors, such as automotive, construction, furniture, packaging, medical, sports equipment, etc [2]. **Figure 1.1.B** shows that PU polymer represented 7.7% of the European plastic consumption in 2017 [1]. The business area of PU involves billions of U.S. dollars throughout the World and it is constantly growing, being estimated at $60.5 billion in 2017, and it is forecasted that it will reach over $79 billion in 2021 [3].

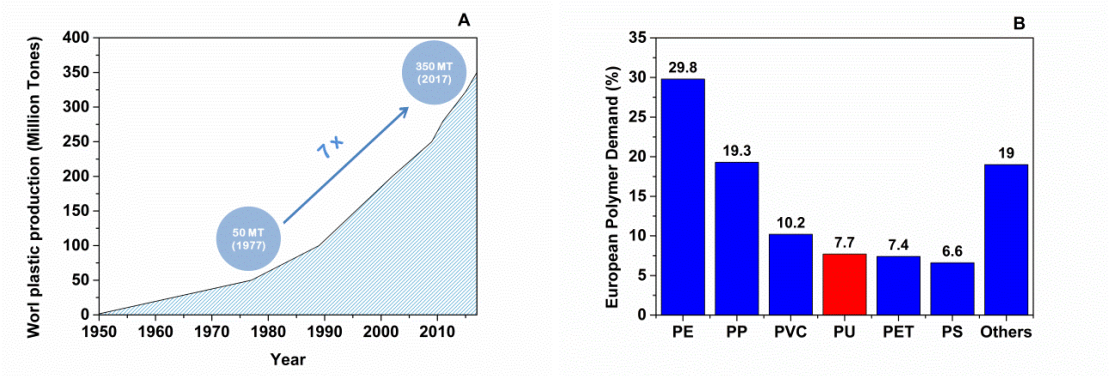

Figure 1.1. A) Global plastic production after World War II to the present (Adapted from [1]). **B)** European plastic demand by polymer types in 2017: Polyethylene (PE), Polypropylene (PP), Polyvinyl chloride (PVC), Polyurethane (PU), Polyethylene terephthalate (PET), Polystyrene (PS), others (Adapted from [1]).

Because of the diversity of ways in which PUs can be synthesized, many different types of PU materials are available: flexible and rigid foams, elastomers, adhesives and sealants, coatings, among others [2]. **Figure 1.2** clearly shows that the PU foams referred to thermoset PU foams cover the majority of the PU market, occupying 67% as flexible, rigid and molded foams, whereas the remaining 33% includes the rest of PU types, such as adhesives, elastomers, coating and other [4, 5]. The maximum usage (31% of PU market) is allocated to flexible foams, which are used principally in mattresses, cushions and others. They are followed by rigid foams (25% of PU market), which are widely used in thermal insulation of buildings, refrigerators, pipe insulation and refrigerated transport. Molded foams (11% of PU market) are mainly used in automotive and furniture industries. On the other hand, it is important to note that

elastomers (6% of PU market) include thermoplastic polyurethane (TPU) materials, which also enclose the TPU foams.

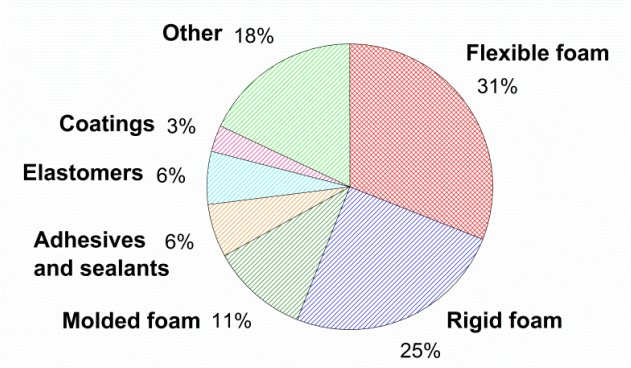

Figure 1.2. World consumption of polyurethane by types in 2016 (Adapted from [4, 5]).

The preceding data clearly show that most of the PUs industrially obtained are PU foams. The polymer foam market is divided into PU, polystyrene (PS), polyvinylchloride (PVC), phenolic, polyolefin, melamine, and other foams. PU foams are one of the largest segments of polymeric foam markets, representing more than 50% of the global volume of polymeric foams [6]. The cause of this high value is mainly due to the high applicability of PU foams, what is mainly based on the possibility of tailoring the final properties of the material by adequately changing the types or quantities of the initial components: isocyanate, polyol, surfactants, catalysts and blowing agents. In addition, the simplicity of the foaming technology has made these materials very competitive from an economic perspective. Thus, the investigation of these materials has attracted a lot of interest from their discovery in 1941.

1.2- Framework of this thesis

This thesis, entitled **"Synthesis, foaming kinetics and physical properties of cellular nanocomposites based on rigid polyurethane"**, has been carried out in the Cellular Materials Laboratory (CellMat) of the Department of Física de la Materia Condensada of the Universidad of Valladolid (UVa) during the last five years. The main target of the work is gaining new scientific knowledge in the field of rigid polyurethane (RPU) foams. This thesis has been supervised by professors Dr. Miguel Ángel Rodríguez-Pérez and Dr. Fernando Villafañe.

CellMat was established in 1999 at the University of Valladolid by professors Dr. Jóse Antonio de Saja and Dr. Miguel Ángel Rodríguez-Pérez, after the defense of PhD thesis of Miguel Ángel Rodríguez Pérez dealing with the properties of polyolefins based foams, with the purpose of studying cellular materials [7]. As a result, at the beginning, the research activity was focused on the characterization of the microstructure and physical properties of commercial cellular

polymers based on polyolefins, in order to evaluate their structure-properties relationships [8-32]. In the following years, the research topics have been extended to the development of novel polymeric foams and their production routes. Over the years, a new research line started focused on the production and characterization of metal foams [33-37]. The work of our group has allowed to increase the scientific knowledge about the foaming mechanisms involved in the manufacturing processes, as well as about the production-structure-properties relationships of the materials studied [38, 39]. The final applications of the materials developed in CellMat have also been always considered, because one of the main principles of our laboratory is transferring knowledge and technology between the University and the industry.

At present, five main research topics are being developed in CellMat laboratory, all supervised by Prof. Dr. Miguel Ángel Rodríguez-Pérez: nanocellular polymers [40-45], multifunctional cellular materials [46-48], cellular nanocomposites [49-52], bioplastic cellular materials [53-57], and PU foams [58-61]. Furthermore, the research group has participated in many research projects funded both by public and private institutions, and it maintains collaborations with a significant number of research groups all around the world. As a result of this work, a total of 30 PhD theses and more than 200 scientific papers have been published so far on cellular materials, what makes CellMat laboratory an international reference in this field.

The present thesis is part of the work developed in CellMat laboratory in the field of PU foams. This research line was started in 2014 with the thesis later defended by Sergio Estravis, dealing with thermoset PU foams [59]. One of the key reasons what led CellMat to establish this new topic was the very high demand of these materials in the global foams market, due to their diverse applications and economical weight. CellMat had already knowledge on the incorporation of nanoparticles to different foams, what is an interesting approach for the material industry, and in particular for the field of PU foams. These fillers can reinforce the PU matrix, increasing the mechanical properties, and also can act as nucleating agents and/or infrared blockers, thus improving their thermal insulating properties among other effects. Dr. Estravis carried out a detailed study on the effects of the addition of nanoclays to the microstructure, mechanical and thermal properties of commercial RPU foams, whose main applications were the thermal management in buildings, refrigeration systems and transport. Notably, the main conclusion of this work was that the thermal conductivity of the RPU foams may improve significantly with the presence of very low amounts of nanoclays (1 wt% or even less). At the same time, the presence of nanoclays in the PU systems slightly improved the elastic modulus and decreased the compression strength. The presence of nanoclays did not worsen the cellular structure, in fact smaller cell size were obtained, and therefore the observed decrease of the mechanical properties could be attributed to the alteration of the reaction kinetics involved in the PU foam formation causing a different polymer morphology. This indicated that the addition of particles affected the chemical modification of the PU matrix. However, the effect of particles on the main chemical reactions of PU foams (blowing and gelling) could not be studied in this work, but it was underlined as a main key for future works. This thesis was the first contact of CellMat laboratory with PU foams and it allowed establishing the methodology needed for manufacturing and characterizing PU foams in future

projects and theses. The main issues addressed by CellMat may be summarized as a tetrahedron (**Figure 1.3**), and Dr. Estravis thesis is a definite contribution to the four three vertexes of its base.

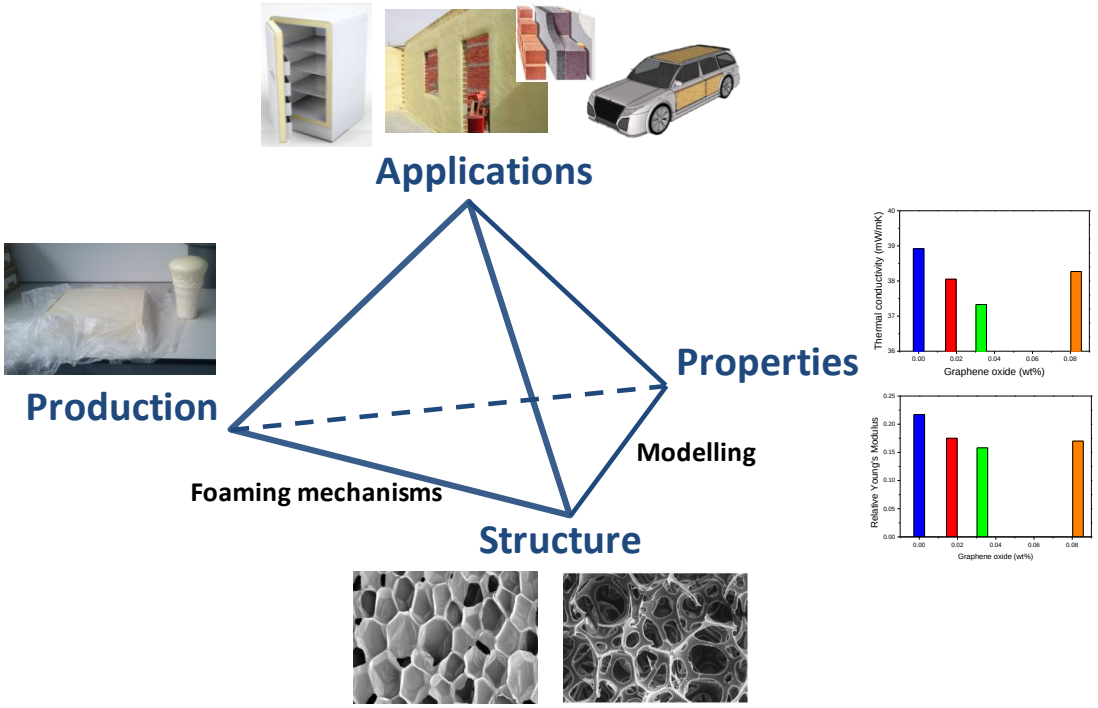

Figure 1.3. Tetrahedron of materials referring to PU foams.

The research work described in the present thesis aims to continue the research based on PU foams, but this time mainly focusing the research on the chemical aspects. The thermoset PU foams are produced by reactive foaming, and the balance between the reactions implicated in the PU foam formation is crucial in order to obtain the desired properties. As it was already observed by Dr. Estravis, the inclusion of nanoparticles into the RPU foams may also modify the kinetics of the reactions. This would give rise to unexpected consequences on the properties of the final PU matrix, since some foam properties may be improved, but others may be worsened. Therefore, understanding these effects becomes essential to make a better use of nanoparticles, and finally to get better cellular structure and foam properties. One of the main targets of the present thesis was the development of a methodology which allows to follow the chemical reactions occurring during the PU formation. The final purpose was controlling the PU formulation in order to obtain the best performance of the thermoset PU foam composite.

Hence, with the beginning of the present thesis (end of 2014) CellMat started the study of PU foams from a chemical point of view. The first step was developing the methodology to monitor the thermoset PU foaming, which are key to understand the properties of final foam

and also to optimize them. This methodology is based on the use of the following complementary techniques: FTIR spectroscopy, infrared expandometry, temperature measurements, and X-ray radioscopy. Moreover, for the first time we could develop our own PU formulations, instead of the commercial formulations previously used in our laboratory. The design of an own formulation has been an additional way to control the final properties of the foams. Therefore, in this thesis we have been able to improve significantly the quality of our research on PU foams, having a better control on all the key aspects of the process, including the raw material used.

In addition to thermoset PU foams, it is possible to manufacture cellular materials based on TPU. In order to gain knowledge in this field, a three-months stay was carried out from June to August 2017 in the Polymers & Peptides Research Group at the School of Materials of the University of Manchester (UK), under the supervision of Professor Alberto Saiani. This research group was established in 2004 by Profs. Aline F. Miller and Alberto Saiani and is focused on the characterization of polymer, biopolymer and peptide materials across different length scales, highlighting the study of TPU materials. Their research is mainly intended to the understanding of the chemical architecture-thermodynamic-structure-physical properties correlations in complex systems in order to control processes and products. During the research stay in Manchester, the work was focused on the synthesis and characterization of TPUs, which were later on foamed in CellMat by gas dissolution foaming. This is the first time that CellMat has achieved foaming of synthesized TPU. This research stay allows fulfilling the requirements to obtain a PhD with the International Mention.

In summary, the work carried out in this thesis has generated knowledge in the two methods that can be used to produce foamed materials based on PU, that is, by reactive foaming (thermoset PU foams) and by gas dissolution foaming (TPU foams) (**Figure 1.4**). The first of them is the main part of the Thesis, since the study of thermoset PU foams was carried out during the first three years. The study of TPU foams is complementary to this and was mainly conducted during the three-months stay and further developed during the last year of this thesis.

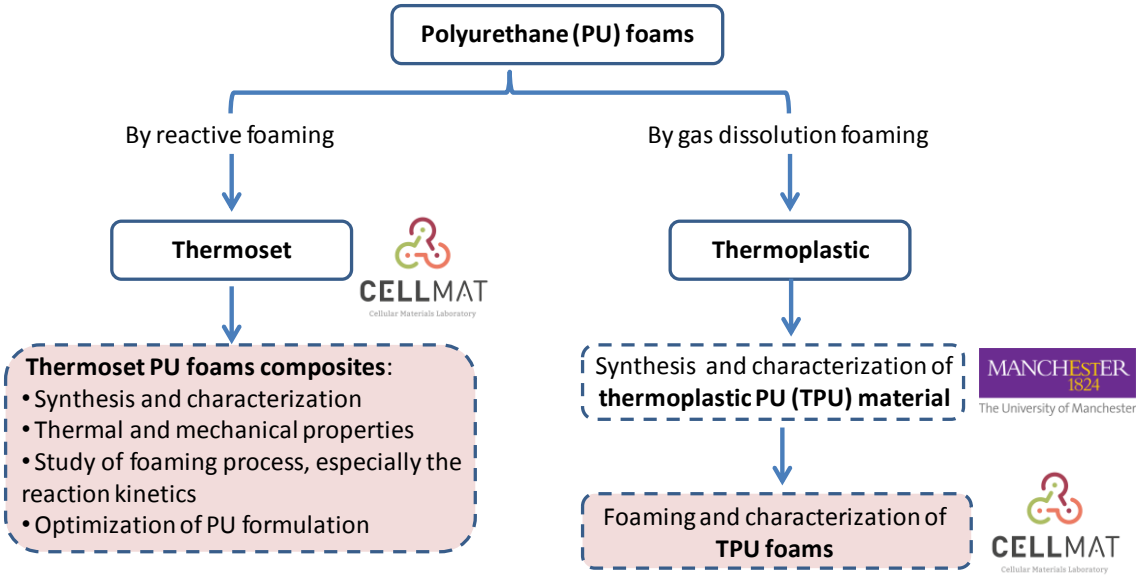

Figure 1.4. Simplified scheme of the investigations developed in this thesis.

1.3- Objectives

The **aim of the present thesis** is to acquire new knowledge about the **thermoset PU foams** (particularly RPU foams), focusing on the study of the foaming process, especially the reaction kinetics of the gas generation (blowing reaction) and polymerization (gelling reaction) when micro- and/or nanoparticles are incorporated into the PU matrix to improve the thermal and mechanical properties.

The **second important aspect** to study is the effect that modifying the reaction could have on the structure and properties of the final materials.

The **third important aspect** is to optimize the formulations of RPU systems containing particles using the kinetic information obtained.

In order to achieve these general objectives, the following specific targets have been considered:

- Developing our own PU formulations in order to can control the final characteristics of the RPU systems.

- Developing and validating the methodology which will allow to study the kinetics of the main chemical reactions (blowing and gelling) and the morphology of the polymeric matrix during the foaming process of RPU foams (**Chapter 4**).
- Developing and validating the methodology which will allow to study the expansion kinetics occurring in the production of RPU foams (**Chapter 4**).
- Applying other existing methodologies which will allow to study the internal microcellular structure during foaming process of RPU foams (**Chapter 4**).
- Applying the methodologies of monitoring the foaming process to RPU systems modified with microparticles and/or nanoparticles in order to evaluate the particles effect on the foaming process, especially on the reaction kinetics and final morphology of the polymer matrix (**Chapter 6**).
- Establishing correlations between the reaction kinetics, the final morphology of the polymer matrix, the cellular structure and the physical properties of the RPU systems modified with microparticles and/or nanoparticles (**Chapter 6**).
- Optimizing the RPU formulation modified with microparticles and/or nanoparticles from kinetic information obtained (**Chapter 6**).
- For RPU systems modified with microparticles and/or nanoparticles, establishing correlations between the foaming temperature and the evolution of their thermal conductivity with time (**Chapter 5**).
- Modeling of the thermal conductivity of RPU foams modified with microparticles and/or nanoparticles to study the particles effect (**Chapter 5**).

Other objective of the present thesis is to study the foaming behavior of **TPU materials** using gas dissolution foaming in order to generate knowledge about TPU foams (**Chapter 7**).

1.4- Main novelties

1. The main novelty of the thesis.

So far, the current scientific literature [59, 62-75], describing PU foams reinforced with micro- and/or nanoparticles, follows the approach depicted in **Figure 1.5**, which is mainly focused on the production and characterization of the foams, without paying particular attention to the effect of these additives on the gelling and blowing reactions.

Figure 1.5. Scheme followed by the current scientific literature on PU foams reinforced with micro- and/or nanoparticles.

Nevertheless, a clear understanding of the effect of particles on the reaction kinetics is essential, because it affects to the foaming process, but also to the final morphology of the PU matrix, and therefore to the final properties of the resulting foam. For this reason, our research is based on a novel approach depicted in **Figure 1.6**, based on the simultaneous study of the modification of the reaction kinetics, and of the microstructure and physical properties of RPU systems containing micro- and/or nanofillers.

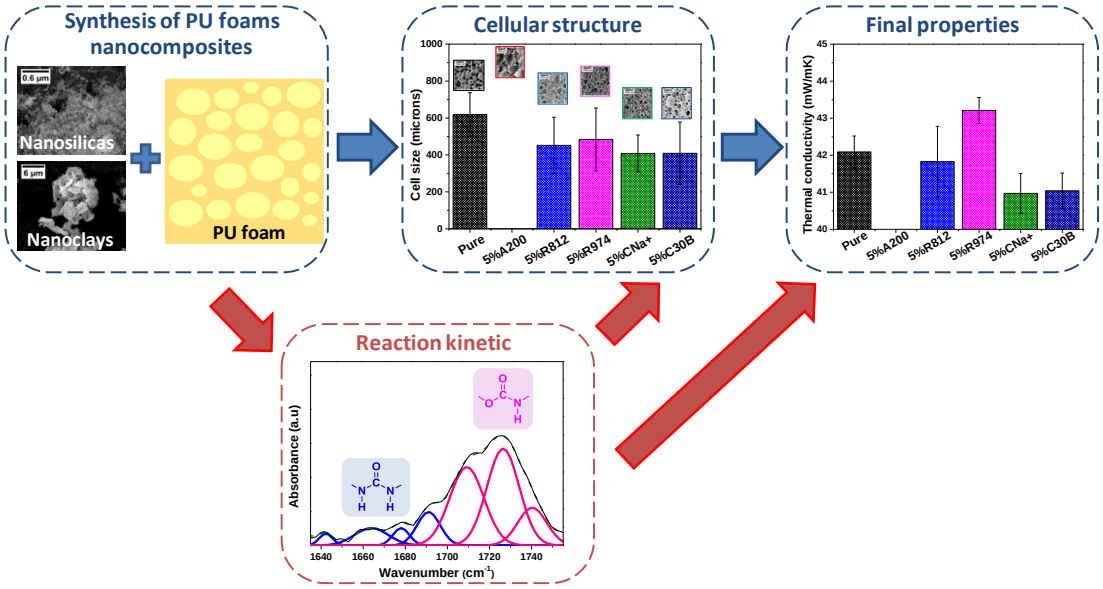

Figure 1.6. Novel scheme followed in this thesis for the study of RPU foams reinforced with nanoparticles.

2. Novelties about the study of foaming process for RPU foams (Chapter 4).

As a starting point, designing a methodology based on *in-situ* FTIR spectroscopy consisting on monitoring and further deconvolution of the carbonyl region (which contains the reaction products) was required. This would allow to know how the main reactions are affected by the incorporation of particles into the PU matrix. This methodology has been tested in RPU foams reinforced with different types of nanosilicas or nanoclays (5 wt%), demonstrating how the different types and surfaces (hydrophobic and/or hydrophilic) of nanoparticles affect the reaction kinetics on different ways. Moreover, the effect of the modification of the reaction kinetics on the density, cellular structure, thermal conductivity and mechanical properties of RPU foams are discussed.

In addition, a novel methodology called "Infrared Expandometry" has been developed in this thesis, in order to characterize simultaneously both the expansion kinetics (height vs. time and volume vs. time) and the surface temperature evolution of the PU foams. This is achieved by using the infrared radiation emitted by the exothermic PU foaming reaction. In order to test this methodology, a RPU formulation has been chosen where the blowing agent (water) and/or the blowing catalyst are systematically changed.

Finally, the foaming process has been also studied by X-ray radioscopy, measuring the relative density, cell size, and cell nucleation density versus time. This technique has been used in order to compare the foaming behavior of two series of foams: those prepared from polyols functionalized with graphene oxide (GO) and those containing GO dispersed in the polyol by high shear mixing (loading of 0.017 and 0.083 wt%). The results obtained with this technique allow to demonstrate that the use of polyol functionalized with GO highly improves the cellular structure and also makes the results more reproducible.

3. Novelties about the physical properties of RPU foams reinforced with particles (Chapter 5).

The effect of carbon nanofibers (CNFs) on the heat conduction mechanism of a water-blown PUR system is herein described by measuring the extinction coefficient and by modelling the thermal conductivity. A thermal enhancement of 2% is achieved with only 0.1 wt.% of CNFs, since the CNFs as infrared radiation absorbents increases the extinction coefficient of the foam, and as consequence there is a clear reduction of the radiative contribution. This is a remarkable result taking into account that the foams under study have relatively high densities (56 kg/m^3) and thus the radiative contribution has a low weight.

In addition, the effect of different particles on the long-thermal conductivity of cyclopentane-water blown RPU foams is also studied along around three years. In the early days after foam production, the foams containing particles highly enhances the thermal conductivity in comparison with reference material, principally due to the significant decrease in cell size promoted by the particles which reduce the radiative contribution. However, after some time, this first improvement is lost in many systems, because the gas composition inside the cell evolves differently. For first time, the different thermal conductivity evolution at the first measurements has been related to the foaming temperature reached by each system. Those particles reaching higher foaming temperature present higher thermal conductivity evolution, because this causes a higher pressure gradient between the cells and the atmosphere, causing higher gas diffusion rates.

4. Novelties about the optimization of the physical properties of RPU foams reinforced with particles from the kinetic results (Chapter 6).

The effect of the polyols functionalized with GO on the foaming process, morphology of PU matrix, cellular structure, thermal conductivity, and compressive mechanical properties of the RPU foams is investigated. In this study, the use of GO particles chemically linked to polyol chains precludes the agglomeration of nanofillers, avoiding the usual problems of particles

dispersion in polymer nanocomposites. Only with a 0.033 wt% of GO, the thermal conductivity is enhanced by around 4% without decisive modifications of other important aspects of the cellular structure, whereas the mechanical properties are worsen, what could be due to a negative modification of the polymer morphology. For this reason, an in-depth study of the effect of GO particles on the foaming process and PU morphology is carried out using infrared expandometry, *in-situ* FTIR spectroscopy and temperature measurements. In conclusion, the presence of GO decreases the isocyanate conversion and favours the polymerization reaction (urethane generation), giving rise to a lower crosslinking network inside the RPU foam. Based on these foaming results, the mechanical properties of the foam with 0.033 wt% GO could be finally improved by changing the PU formulation, while at the same time the thermal conductivity is maintained or improved.

5. The novelty of the research stay at the University of Manchester (Chapter 7).

The foaming behavior of a new series of TPUs synthesized with different hard segments (HS) contents is extensively analyzed at different saturation and foaming conditions by one-step gas dissolution foaming process. The study also includes the density and cellular structure of the resulting foams. Most of the previous works reported in the literature have studied the foaming of commercial TPUs in which the composition is not usually known, but this research allows to relate the TPU composition to the foaming behaviour.

1.5- Structure of the thesis

This thesis is written as a compendium of 8 scientific papers, and is divided into 7 chapters, in which the articles are included (see **Table 1.1**). In addition, this thesis meets the requirements to be accredited with the International Mention.

Each chapter includes the following information:

-Chapter 1: Introduction. It presents the introduction, the framework of the research, the objectives, the main novelties, the structure of the thesis, and the list of the resulting publications, communications in conferences and related research projects.

-Chapter 2: Background and state of the art. It revises the basic concepts related to PU foams such as their basic chemistry, polymeric morphology, cellular structure, common raw materials, foaming process, properties and applications. Moreover, the state of the art of the monitoring of foaming process of the PU foam composites is described.

-Chapter 3: Materials. It describes the components of the PU formulations used in this work such as polyols, isocyanates, catalysts, surfactants and blowing agents, as well as the different fillers added to the PU formulations.

-Chapter 4: Development of a methodology to follow the foaming process of rigid polyurethane foams. It explains the methodology developed during this thesis in order to

study the foaming process of the RPU foams which allows to control the chemistry morphology and, as a consequence, the foam properties. This methodology is based on the use of FTIR spectroscopy, infrared expandometry and X-ray radioscopy, whose results are complementary. This chapter contains three articles dealing each with a different technique to monitor the foaming process.

-Chapter 5: Effect of fillers on the cellular structure and physical properties of rigid polyurethane foams. It contains two articles. The first one describes the effect of CNFs on the morphological, thermal and mechanical properties of water-blown PUR foams. The second article reports the effect of different types of particles (talc, diatomaceous earth, and non-porous silica) on the thermal conductivity aging during three years of RPU foams containing cyclopentane and water as blowing agents.

-Chapter 6: Optimization of the polyurethane formulation from the kinetics results in order to obtain rigid polyurethane foams reinforced with graphene oxide with better thermal and mechanical properties. It contains two articles. The first one investigates the effect of a polyol functionalized with GO on the cellular structure and thermal-mechanical properties of the RPU foams obtained from it. Moreover, a detailed kinetic study using the methodology developed in this thesis is carried out, allowing to identify the effect of GO on the reaction kinetics, and consequently on the final polymer morphology. The second article is based on the information collected from this previous kinetic study, and describes how the PU formulation containing GO can be tuned in order to improve both the thermal and mechanical properties at the same time.

-Chapter 7: International research stay: Thermoplastic polyurethane foams. It includes the work carried out during the international research stay, and deals with TPU foams produced by gas dissolution foaming process.

-Chapter 8: Conclusion and future work. It summarizes the final conclusions obtained during the whole thesis and also the future work.

1.6- Publications, conferences and complementary activities

A total of 8 scientific articles, listed in **Table 1.1**, have been drafted during the development of this thesis. Several of them have been published and others have been submitted (pending publication), all in international journals. The chapter in which these articles are incorporated is also specified in **Table 1.1**.

Table 1.1. Scientific articles of this thesis.

	RESEARCH ARTICLES	Chapter
1	M. Santiago-Calvo, J. Tirado-Mediavilla, J.L. Ruiz-Herrero, M.A. Rodríguez-Pérez, F. Villafañe. **The effects of functional nanofillers on the reaction kinetics, microstructure, thermal and mechanical properties of water blown rigid polyurethane foams.** Polymer 150 (**2018**) 138-149. https://doi.org/10.1016/j.polymer.2018.07.029	4
2	M. Santiago-Calvo, S. Pérez-Tamarit, J. Tirado-Mediavilla, F. Villafañe , M.A. Rodríguez-Pérez. **Infrared expandometry: a novel methodology to monitor the expansion kinetics of cellular materials produced with exothermic foaming mechanisms.** Polymer Testing 66 (**2018**) 383-393. https://doi.org/10.1016/j.polymertesting.2018.02.004	4
3	M. Santiago-Calvo, S. Pérez-Tamarit, P. Cimavilla-Román, V. Blasco, C. Ruiz, R. París, F. Villafañe , M.A. Rodríguez-Pérez. **X-ray radioscopy validation of a polyol functionalized with graphene oxide for producing rigid polyurethane foams with improved cellular structures.** European polymer journal 118 (**2019**) 404-411. https://doi.org/10.1016/j.eurpolymj.2019.06.012	4
4	M. Santiago-Calvo, J. Tirado-Mediavilla, J.C. Rauhe, L.R. Jensen, J.L. Ruiz-Herrero, F. Villafañe, M.A. Rodríguez-Pérez. **Evaluation of the thermal conductivity and mechanical properties of water blown polyurethane rigid foams reinforced with carbon nanofibers.** European polymer journal 108 (**2018**) 98-106. https://doi.org/10.1016/j.eurpolymj.2018.08.051	5
5	M. Santiago-Calvo, J. Tirado-Mediavilla, J.L. Ruiz-Herrero, M.A. Rodríguez-Pérez, F. Villafañe. **Long-thermal conductivity aging of cyclopentane-water blown rigid polyurethane foams reinforced with different types of fillers.** Polymer International (**2019**). https://doi.org/10.1002/pi.5893	5
6	M. Santiago-Calvo, V. Blasco, C. Ruiz, R. París, F. Villafañe, M.A. Rodríguez-Pérez. **Synthesis, characterization and physical properties of rigid polyurethane foams prepared with poly(propylene oxide) polyols containing graphene oxide.** European Polymer Journal 97 (**2017**) 230–240.https://doi.org/10.1016/j.eurpolymj.2017.10.013	6
7	M. Santiago-Calvo, V. Blasco, C. Ruiz, R. París, F. Villafañe, M.A. Rodríguez-Pérez. **Improvement of thermal and mechanical properties by control of formulations in rigid polyurethane foams from polyols functionalized with graphene oxide.** Journal of Applied Polymer Science, 136 (**2019**) 47474. https://doi.org/10.1002/app.47474	6
8	M. Santiago-Calvo, H. Naji, V. Bernardo, J. Martín-de León, A. Saiani, F. Villafañe, M.A. Rodríguez-Pérez. **Synthesis, characterization, and foaming of thermoplastic polyurethane with different hard segment contents.** Pending publication	7

In addition, the work developed in this thesis has been presented in national and international conferences, as collected in **Table 1.2**.

Table 1.2. Communications in conferences related to the thesis work.

CONTRIBUTIONS TO CONGRESS	
1	M. Santiago-Calvo, J. Tirado-Mediavilla, J.L. Ruiz-Herrero, M.A. Rodríguez-Pérez, F. Villafañe. FTIR studies to characterize the kinetics of nanocomposite polyurethane foams. **XII Simposio de Investigadores Jóvenes RSEQ-Sigma Aldrich.** November 2015, Barcelona, Spain. (Poster)
2	M. Santiago-Calvo, J. Tirado-Mediavilla, J.L. Ruiz-Herrero, M.A. Rodríguez-Pérez, F. Villafañe. An approach to follow the kinetics of nanocomposite polyurethane foam formation by FTIR spectroscopy. **VIII Jornadas de Jóvenes Investigadores en Física Atómica y Molecular (J2IFAM).** February 2016, Valladolid, Spain. (Talk)
3	M. Santiago-Calvo, J. Tirado-Mediavilla, J.L. Ruiz-Herrero, M.A. Rodríguez-Pérez, F. Villafañe. FTIR studies to characterize the kinetics of nanocomposite polyurethane foams. **XIV Reunión del Grupo Especializado de Polímero (GEP).** September 2016, Burgos, Spain. (Poster)
4	M. Santiago-Calvo1, V. Blasco, C. Ruiz, R. París, F. Villafañe, M.A. Rodríguez-Pérez. Synthesis, properties and kinetic study of rigid polyurethane foams obtained from poly(propylene oxide) polyols functionalized with graphene oxide. **15th International Conference on Advances in Foam Materials & Technology (FOAMS).** October 2017, Bayreuth, Germany. (Poster)
5	M. Santiago-Calvo, H. Naji, V. Bernardo, J. Martín-de León, A. Saiani, F. Villafañe, M.A. Rodríguez-Pérez. Synthesis, characterization and foaming of thermoplastic polyurethane synthesized with different soft/hard segment ratio and graphene nanoplatelet contents. **1st International congress PDFA, Polymers: Design, Function and Application.** March 2018, Barcelona, Spain. (Poster)
6	M. Santiago-Calvo1, V. Blasco, C. Ruiz, R. París, F. Villafañe, M.A. Rodríguez-Pérez. Synthesis, properties and kinetic study of rigid polyurethane foams obtained from poly(propylene oxide) polyols functionalized with graphene oxide. **5th International Conference on Cellular Materials (CellMAT).** October 2018, Bad Staffelstein, Germany. (Talk)
7	M. Santiago-Calvo, H. Naji, V. Bernardo, J. Martín-de León, A. Saiani, F. Villafañe, M.A. Rodríguez-Pérez. Synthesis, characterization and foaming of thermoplastic polyurethane synthesized with different soft/hard segment ratio and graphene nanoplatelet contents. **5th International Conference on Cellular Materials (CellMAT).** October 2018, Bad Staffelstein, Germany. (Poster)

As this thesis is presented to obtain a PhD with International Mention, a stay in a foreign institution has been carried out. All the details are included in **Table 1.3**.

Table 1.3. Stays in another research centre during the investigation.

INTERNATIONAL RESEARCH STAY
Polymers & Peptides Research Group, The University of Manchester (UK). **From June to August 2017 (3 months).** Under the supervision of Prof. Alberto Saiani. Research work: Synthesis and characterization of thermoplastic polyurethane (TPU) in order to produce TPU foams by gas dissolution foaming process.

One of the research works developed during the thesis won the 2017 Best Poster Award at the 15th International Conference on Advances in Foam Materials & Technology (FOAMS 2017), celebrated in Bayreuth (Germany). This is listed in **Table 1.4**.

Table 1.4. Research works awarded.

AWARDS
M. Santiago-Calvo1, V. Blasco, C. Ruiz, R. París, F. Villafañe, M.A. Rodríguez-Pérez. **Synthesis, properties and kinetic study of rigid polyurethane foams obtained from poly(propylene oxide) polyols functionalized with graphene oxide.** 5th International Conference on Cellular Materials (CellMAT). October 2017, Bayreuth, Germany. Best Poster selected by the Society of Plastics Engineers: Thermoplastic Materials & Foams Division.

The knowledge generated in the present work has developed and applied in different research projects in collaboration with private companies, collected in **Table 1.5**. This is a decisive indicator of the main importance of this research for important industrial sectors such as refrigeration, automotive, construction, etc. Moreover, the research herein developed has also been financed by public funding (also collected in **Table 1.5**).

Table 1.5. Private and public projects which have financed the investigation performed in the present work.

	RESEARCH PROJECTS
1	Project Title: **"Improvement of short and long term thermal conductivity for rigid polyurethane foams through the use of specific additives and the control of kinetic reactions".** Initial date: **December 2013** Final date: **November 2016** Financial entity: **BOSH AND SIEMENS HOME APPLIANCES (Navarra).** Principal researcher: **Miguel Ángel Rodríguez Pérez**
2	Project Title: **"Innovative additives for foams with better thermal insulation performance and fire behavior (NEOADFOAM)".** Initial date: **September 2015** Final date: **December 2018** Financial entity: **MINECO, PROYECTO RETOS EN COLABORACIÓN CON TOLSA SA E IMDEA (Madrid).** Principal researcher: **Miguel Ángel Rodríguez Pérez**
3	Project Title: **"Development of advanced cellular materials".** Initial date: **April 2016** Final date: **December 2016** Financial entity: **Parque Científico. Universidad de Valladolid (Valladolid).** Principal researcher: **Miguel Ángel Rodríguez Pérez**
4	Project Title: **"Analysis of a rigid polyurethane system: manufacturing, study of the reaction kinetics and characterization of the structure and properties".** Initial date: **May 2016** Final date: **December 2016** Financial entity: **REPSOL S.A (Madrid).** Principal researcher: **Miguel Ángel Rodríguez Pérez**

RESEARCH PROJECTS	
5	Project Title: **"Comparative analysis of the cellular structure and reaction kinetics for three systems based on polyurethane".** Initial date: **April 2016** Final date: **December 2018** Financial entity: **GRUPO ANTOLÍN INGENIERÍA (Burgos).** Principal researcher: **Miguel Ángel Rodríguez Pérez**
6	Project Title: **"Study of polyurethane formulations by X-ray radioscopy".** Initial date: **January 2017** Final date: **June 2017** Financial identity: **SOPREMA (France).** Principal researcher: **Miguel Ángel Rodríguez Pérez**
7	Project Title: **"Research on applications of advanced carbon nanomaterials to improved performance of polyurethane matrices with interest in the automotive sector".** Initial date: **April 2017** Final date: **2019** Financial entity: **GRUPO ANTOLÍN INGENIERÍA (Burgos).** Principal researcher: **Miguel Ángel Rodríguez Pérez**
8	Project Title: **"Study of polyisocyanurate foam formulations".** Initial date: **January 2019** Final date: **2019** Financial entity: **DUPONT (USA).** Principal researcher: **Miguel Ángel Rodríguez Pérez**

Finally, **Table 1.6** shows additional activities developed during this thesis related to the field of PU foams.

Table 1.6. Additional activities carried out during this thesis.

RESEARCH ARTICLES
S. Estravís, J. Tirado-Mediavilla, M. Santiago-Calvo, J.L. Ruiz-Herrero, M.A. Rodríguez-Pérez, F. Villafañe. **Rigid polyurethane foams with infused nanoclays: Relationship between cellular structure and thermal conductivity.** European Polymer Journal 80 (**2016**) 1–15. https://doi.org/10.1016/j.eurpolymj.2016.04.026
P. Acuña, M. Santiago-Calvo, F. Villafañe, M.A. Rodríguez-Perez, J. Rosas, De-Yi Wanga. **Impact of Expandable Graphite on Flame Retardancy and Mechanical Properties of Rigid Polyurethane Foam.** Polymer composites (**2018**). https://doi.org/10.1002/pc.25127
P. Acuña, Z. Li, M. Santiago-Calvo, F. Villafañe, M.A. Rodríguez-Perez, De-Yi Wanga. **Influence of the characteristics of expandable graphite on the morphology, thermal properties, fire behaviour and compression performance of a rigid polyurethane foam.** Polymers 11 (**2019**) 168. https://doi.org/10.3390/polym11010168
A. Galakhova, M. Santiago-Calvo, J. Tirado-Mediavilla, F. Villafañe, M.A. Rodríguez-Pérez and G. Riess. **Identification and Quantification of Cell Gas Evolution in Rigid Polyurethane Foams by Novel GCMS Methodology.** Polymers 11 (**2019**) 1192. https://doi.org/10.3390/polym11071192

CONTRIBUTIONS TO CONGRESS
P. Cimavilla-Román, S. Pérez-Tamarit, M. Santiago-Calvo, M.A. Rodríguez-Pérez. In situ analysis, by X-ray radioscopy, of the foaming process of aerogel-polyurethane cellular composites. **10th European School on Molecular Nanoscience (ESMolNa2017).** May 2017, El Escorial, Madrid, Spain. (Talk)
P. Cimavilla-Román, S. Pérez-Tamarit, M. Santiago-Calvo, M.A. Rodríguez-Pérez. In-situ physicochemical analysis of the foaming process of aerogel-rigid polyurethane composite foams. **12th European Conference on Foams, Emulsions and Applications (EUFOAM).** July 2018, Liege (Belgium). (Talk)
ACADEMIC ACTIVITIES
Final Master Project: Characterization and in-situ analysis of the cellular structure and foaming process of aerogel-polyurethane composites by means of X-ray radioscopy and tomography. Author: P. Cimavilla-Román. Tutors: M.A. Rodríguez-Pérez, S. Pérez-Tamarit, M. Santiago-Calvo. Document published: 2017. University qualification: Máster en Nanociencia y Nanotecnología Molecular. http://uvadoc.uva.es/handle/10324/26203
DIVULGATION TALKS
Cycle of conferences: Woman Researchers of the University of Valladolid in the Adventure of Science and Technology. -In **2016**: Study of formation reactions of polyurethane foam nanocomposites by FTIR spectroscopy. (Talk) -In **2017**: Polyurethane foams from polyols functionalized with graphene oxide. (Talk) -In **2018**: Synthesis and characterization of thermoplastic polyurethanes (TPUs) with different contents of hard segments in order to prepare TPU foams. (Talk)
RESEARCH PROJECTS
Project Title: "Evolution: The Electric Vehicle revolution enhabled by advanced materials highly into ligh". **Initial date: October 2013 Duration: 1 year** **Financial entity: EUROPEAN UNION (FPVII).** **Principal researcher: Miguel Ángel Rodríguez Pérez**
Project Title: "ACTIBIOPACK: Envasado activo y biodegradable de champiñón en fresco y carne fresca". **Initial date: October 2014 Duration: 3 months** **Financial entity: MINECO.** **Principal researcher: Miguel Ángel Rodríguez Pérez**

1.7- References

[1] Plastics Europe (the Association of Plastics Manufacturers in Europe). https://www.plasticseurope.org/en/resources/market-data.
[2] M. Szycher, Szycher's Handbook of Polyurethanes, Second ed., CRC Press Boca Raton, Florida, USA, 2012.
[3] Polyurethane Global Market Size Forecast 2021. Available online: https://www.statista.com/statistics/720449/global-polyurethane-market-size-forecast/ (accessed on 22 February 2019).
[4] Plastics Insight: https://www.plasticsinsight.com/resin-intelligence/resin-prices/polyurethane/.
[5] Statista: https://www.statista.com/statistics/615265/distribution-of-polyurethane-consumption-worldwide-by-end-use/.

[6] Polymer Foams Market Expected to Consume 25.3 Million Tonnes by 2019. http://www.smithersrapra.com/news/2014/may/polymer-foam-market-to-consume-25-3-million-tonnes, 2014 (accessed 16 July 2019).
[7] M.Á. Rodríguez-Pérez, PhD Thesis: Thermal and mechanical properties of polyolefin foams University of Valladolid, 1999.
[8] M.A.Rodríguez-Pérez, O.Alonso, J. Souto, J.A.d. Saja, Thermal Conductivity of Crosslinked Closed Cell Polyolefin Foams, Polymer Testing, 16 (1997) 287-298.
[9] M.A. Rodríguez-Pérez, S. Rodríguez-Llorente, J.A.d. Saja, Dynamic Mechanical Properties of Polyolefin Foams Studied by DMA Techniques, Polym. Eng. Sci., 37 (1997) 959-966.
[10] M.A.Rodríguez-Pérez, A.Duijsens, J.A.d. Saja, Effect of Addition of EVA on the Technical Properties of Extruded Foam Profiles of Low-Density Polyethylene/EVA Blends, J.Applied Polymer Science (1998) 1237-1244
[11] M.A.Rodriguez, S.Diez, J.A.d. Saja, The recovery behaviour of crosslinked closed cell polyolefin foams, Polymer Eng. & Sci, (1998) 831-838.
[12] M.A.Rodríguez-Pérez, O.Alonso, A.Duijsens, J.A.d. Saja, Thermal Expansion of Crosslinked Closed-Cell Polyethylene Foams, J.Polymer Sci. , 36 (1998) 2587-2596.
[13] M.A. Rodríguez-Pérez, J.A.D. Saja, The effect of blending on the physical properties of crosslinked closed cell polyrthylene foams, Cellular Polymers 18 (1999) 1-20.
[14] M.A. Rodríguez-Pérez, O. Almanza, J.A.D. Saja, Anomalous thickness increase in crosslinked closed cell polyolefin foams during heat treatments. , Journal of Applied Polymer Science, 73 (1999) 2825–2835.
[15] J.I. Velasco, A.B. Martinez, D. Arencon, M.A. Rodriguez-Perez, J.A.D. Saja, Application of instrumented falling dart impact to the mechanical characterization of thermoplastic foams, Journal of Materials Science, 34 (1999) 431–438.
[16] O.A. Almanza, M.A. Rodríguez-Pérez, J.A.D. Saja, Prediction of the radiation term in the thermal conductivity of crosslinked closed cell polyolefin foams, Journal of Polymer Science Part B: Polymer Physics, 38 (2000) 993–1004.
[17] M.A. Rodriguez-Perez, J.I. Velasco, D. Arencon, O. Almanza, J.A.D. Saja, Mechanical Characterization of Closed-CellPolyolefin Foams, Journal of Applied Polymer Science, 75 (2000) 156 –166.
[18] M.A. Rodríguez-Pérez, J.A.d. Saja, Dynamic mechanical analysis applied to the characterisation of closed cell polyolefin foams, Polymer Testing, 19 (2000) 831–848.
[19] J.I. Velasco, A.B. Martinez, D. Arencon, M.A. Rodriguez-Perez, J.A.d. Saja, Rigidity characterisation of flexible foams by falling dart robound tests, Cellular Polymers, 19 (2000) 115–133.
[20] O. Almanza, M.A. Rodriguez-Perez, J.A.D. Saja, The microestructure of polyethylene foams produced by a nitrogen solution process, Polymer, 42 (2001) 7117–7126.
[21] O. Almanza, L.O.A.y. Rabago, M.A.Rodriguez-Perez, A. Gonzalez, J.A.d. Saja, Strucutre-property relationships in polyolefin foams, Journal of Macromolecular Science, Part B 40 (2001) 603–613.
[22] J.A. Martinez-Diez, M.A. Rodriguez-Perez, J.A.d. Saja, L.O.A.y. Rabago, O.A. Almanza, The thermal conductivity of a polyethylene foam block produced by a compression molding process, Journal of Cellular Plastics, 37 (2001) 21–42.
[23] N.J. Mills, M.A. Rodriguez-Perez, Modelling the Gas-loss Creep Mechanism in EVA Foam from Running Shoes, Cellular Polymers, 20 (2001) 79–100.
[24] M.A. Rodriguez-Perez, O. Almanza, J.L.D. Valle, A. Gonzalez, J.A.D. Saja, Improvement of the measurement process used for the dynamic mechanical characterization of polyolefin foams in compression, Polymer Testing, 20 (2001) 253–267.
[25] M.A. Rodriguez-Perez, The effect of chemical composition, density and cellular structure on the dynamic mechanical response of polyolefin foams, Cellular Polymers, 21 (2002) 117–136.

[26] M.A. Rodriguez-Perez, J.I. Gonzalez-Peña, N. Witten, J.A.D. Saja, Morphology of semicrystalline foams based on polyethylene, Journal of Macromolecular Science: Part B – Physics 41 (2002) 761–775.
[27] M.A. Rodriguez-Perez, J.I. Gonzalez-Peña, N. Witten, J.A.D. Saja, The Effect of Cell Size on the Physical Properties of Crosslinked Closed Cell Polyethylene Foams Produced by a High Pressure Nitrogen Solution Process, Cellular Polymers, 21 (2002) 165–194.
[28] O. Almanza, M.A. Rodríguez-Pérez, J.A. de Saja, Applicability of the Transient Plane Source Method To Measure the Thermal Conductivity of Low-Density Polyethylene Foams, Journal of Polymer Science: Part B: Polymer Physics, 42 (2004) 1226–1234.
[29] O. Almanza, Y. Masso-Moreu, N.J. Mills, M. A.Rodriguez-Perez, Thermal expansion coefficient and bulk modulus of polyethylene closed-cell foams, Journal of Polymer Science, Part B: Polymer Physics, 42 (2004) 3741–3749.
[30] O. Almanza, M.A. Rodriguez-Perez, J.A.d. Saja, Measurement of the thermal diffusivity andspecific heat capacity of polyethylene foamsusing the transient plane source technique, Polymer International 2004, 53, , 53 (2004) 2038–2044.
[31] R.A. Campo-Arnáiz, M.A. Rodríguez-Pérez, B. Calvo, J.A. de Saja, Extinction coefficient of polyolefin foams, Journal of Polymer Science Part B: Polymer Physics, 43 (2005) 1608-1617.
[32] O. Almanza, M.A. Rodríguez-Pérez, B. Chernev, J.A.d. Saja, P. Zipper, Comparative study on the lamellar structure of polyethylene foams, European Polymer Journal, 41 (2005) 599–609.
[33] J.A. Reglero-Ruiz, PhD Thesis: Manufacture and characterization of aluminium foams: Applications in the aeronautical sector, University of Valladolid, 2007.
[34] E. Solórzano, PhD Thesis: Aluminium foams: Foaming process, cellular structure and properties, University of Valladolid, 2008.
[35] J.A. Reglero, M.A. Rodriguez-Perez, D. Lehmhus, M. Windmann, J.A.d. Saja, A. Fernandez, An experimental study on the inhomogeneities of aluminum foams measuring the thermal conductivity by using the transient plane source method, Materials Science Forum 480-481 (2005) 133–138.
[36] E. Solórzano, M.A. Rodríguez-Pérez, J.A. Reglero, J.A.d. Saja, Density gradients in aluminium foams: characterisation by computed tomography and measurements of the effective thermal conductivity, Journal of Materials Science, 42 (2007) 2557–2564.
[37] E. Solórzano, J.A. Reglero, M.A. Rodríguez-Pérez, J.A.d. Saja, M.L. Rodríguez-Méndez, Improvement of the foaming process for 4045 and 6061 aluminium foams by using the Taguchi methodology, Journal Material Science, 42 (2007) 7227–7238.
[38] C. Saiz-Arroyo, PhD thesis: Fabricación de Materiales Celulares Mejorados Basados en Poliolefinas. Relación procesado-composición-estructura-propiedades, University of Valladolid, 2012.
[39] S. Pardo, PhD Thesis: X-Ray Imaging Applied to the Characterization of Polymer Foams' Cellular Structure and its Evolution, University of Valladolid, 2014.
[40] J. Pinto, PhD Thesis: Fabrication and characterization of nanocellular polymeric materials from nanostructured polymers., University of Valladolid, 2014.
[41] B. Notario-Collado, PhD Thesis: Fabrication and characterization of the physical properties of nanocellular polymers: The transition from the micro to the nanoscale., University of Valladolid, 2016.
[42] J.A.R. Ruiz, M. Dumon, J. Pinto, M.A. Rodriguez-Perez, Low-Density Nanocellular Foams Produced by High-Pressure Carbon Dioxide, Macromol. Mater. Eng., 296 (2011) 752-759.
[43] J. Pinto, M. Dumon, M. Pedros, J. Reglero, M.A. Rodriguez-Perez, Nanocellular CO2 foaming of PMMA assisted by block copolymer nanostructuration, Chem. Eng. J., 243 (2014) 428-435.
[44] B. Notario, J. Pinto, E. Solorzano, J.A. de Saja, M. Dumon, M.A. Rodriguez-Perez, Experimental validation of the Knudsen effect in nanocellular polymeric foams, Polymer, 56 (2015) 57-67.

[45] J. Martin-de Leon, V. Bernardo, M.A. Rodriguez-Perez, Key Production Parameters to Obtain Transparent Nanocellular PMMA, Macromol. Mater. Eng., 302 (2017) 5.
[46] B. Notario, A. Ballesteros, J. Pinto, M.A. Rodriguez-Perez, Nanoporous PMMA: A novel system with different acoustic properties, Mater. Lett., 168 (2016) 76-79.
[47] J.A. Reglero-Ruiz, C. Saiz-Arroyo, M. Dumon, M.A. Rodríguez-Perez, L. Gonzalez, Production, cellular structure and thermal conductivity ofmicrocellular (methyl methacrylate)–(butyl acrylate)–(methyl methacrylate) triblock copolymers, Polymer International, 60 (2011) 146-152.
[48] M. Dumon, J.A.R. Ruiz, J.P. Sanz, M.A.R. Perez, J.-M. Tallon, M. Pedros, E. Cloutet, P. Viot, Block Copolymer-Assisted Microcellular Supercritical CO2 Foaming of Polymers and Blends, Cellular Polymers, 31 (2012) 207-222.
[49] J.I. Velasco, M. Antunes, O. Ayyad, J.M. López-Cuesta, P. Gaudon, C. Saiz-Arroyo, M.A. Rodríguez-Pérez, J.A. de Saja, Foaming behaviour and cellular structure of LDPE/hectorite nanocomposites, Polymer, 48 (2007) 2098-2108.
[50] C. Saiz-Arroyo, M.A. Rodriguez-Perez, J.I. Velasco, J.A. de Saja, Influence of foaming process on the structure-properties relationship of foamed LDPE/silica nanocomposites, Compos. Pt. B-Eng., 48 (2013) 40-50.
[51] E. Laguna-Gutierrez, J. Escudero, V. Kumar, M.A. Rodriguez-Perez, Microcellular foaming by using subcritical CO2 of crosslinked and non-crosslinked LDPE/clay nanocomposites, Journal of Cellular Plastics, 54 (2018) 257-282.
[52] M. Ardanuy, J.I. Velasco, M. Antunes, M.A. Rodriguez-Perez, J.A. de Saja, Structure and Properties of Polypropylene/Hydrotalcite Nanocomposites, Polymer Composites, 31 (2010) 870-878.
[53] M.A. Rodriguez-Perez, R.D. Simoes, C.J.L. Constantino, J.A.D. Saja, Structure and Physical Properties of EVA/Starch Precursor Materials for Foaming Applications, Journal of Applied Polymer Science, 121 (2011) 2324-2330.
[54] M.A. Rodriguez-Perez, R.D. Simoes, S. Roman-Lorza, M. Alvarez-Lainez, C. Montoya-Mesa, C.J.L. Constantino, J.A.d. Saja, Foaming of EVA/Starch Blends: Characterization of the Structure, Physical Properties and Biodegradability, Polymer Enginnering and Science, 52 (2012) 62-70.
[55] A. Lopez-Gil, F. Silva-Bellucci, D. Velasco, M. Ardanuy, M.A. Rodriguez-Perez, Cellular structure and mechanical properties of starch-based foamed blocks reinforced with natural fibers and produced by microwave heating, Industrial Crops and Products, 66 (2015) 194-205.
[56] A. López-Gil, PhD Thesis: Development of environmentally friendly cellular polymers for packaging and structural applications. Study of the relationship cellular structure-mechanical properties, University of Valladolid, 2016.
[57] H. Ventura-Casellas, PhD Thesis: Development of new lightweight green composites reinforced with nonwoven structures of flax fibers, University of Valladolid, 2017.
[58] S. Pardo-Alonso, E. Solórzano, S. Estravís, M.A. Rodríguez-Perez, J.A. de Saja, In situ evidence of the nanoparticle nucleating effect in polyurethane–nanoclay foamed systems, Soft Matter, 8 (2012) 11262.
[59] S. Estravis, PhD Thesis: Cellular nonocomposites based on rigid polyurethane and nanoclays: fabrication, caharacterization and modelling of the mechanical and thermal properties, University of Valladolid, 2014.
[60] S. Pardo-Alonso, E. Solórzano, M.A. Rodriguez-Perez, Time-resolved X-ray imaging of nanofiller-polyurethane reactive foam systems, Colloids and Surfaces A: Physicochemical and Engineering Aspects, 438 (2013) 119-125.
[61] S. Pardo-Alonso, E. Solórzano, L. Brabant, P. Vanderniepen, M. Dierick, L. Van Hoorebeke, M.A. Rodríguez-Pérez, 3D Analysis of the progressive modification of the cellular architecture in polyurethane nanocomposite foams via X-ray microtomography, European Polymer Journal, 49 (2013) 999–1006.

[62] L. Madaleno, R. Pyrz, A. Crosky, L.R. Jensen, J.C.M. Rauhe, V. Dolomanova, A.M.M.V. de Barros Timmons, J.J. Cruz Pinto, J. Norman, Processing and characterization of polyurethane nanocomposite foam reinforced with montmorillonite–carbon nanotube hybrids, Composites Part A: Applied Science and Manufacturing, 44 (2013) 1–7.
[63] X. Cao, L. James Lee, T. Widya, C. Macosko, Polyurethane/clay nanocomposites foams: processing, structure and properties, Polymer, 46 (2005) 775–783.
[64] G. Harikrishnan, T.U. Patro, D.V. Khakhar, Polyurethane Foam-Clay Nanocomposites: Nanoclays as Cell Openers, Industrial and Engineering Chemistry Research, 45 (2006) 7126–7134.
[65] M.M.A. Nikje, Z.M. Tehrani, Thermal and mechanical properties of polyurethane rigid foam/modified nanosilica composite, Polymer Engineering & Science, 50 (2010) 468–473.
[66] M.M.A. Nikje, Z.M. Tehrani, Polyurethane Rigid Foams Reinforced by Doubly Modified Nanosilica, Journal of Cellular Plastics, 46 (2010) 159–172.
[67] T. Widya, C. Macosko, Nanoclay-Modified Rigid Polyurethane Foam, Journal of Macromolecular Science, Part B: Physics, 44 (2005) 897-908.
[68] M.C. Saha, M.E. Kabir, S. Jeelani, Enhancement in thermal and mechanical properties of polyurethane foam infused with nanoparticles, Materials Science and Engineering: A, 479 (2008) 213-222.
[69] M.M.A. Nikje, Z.M. Tehrani, The Effects of Functionality of the Organifier on the Physical Properties of Polyurethane Rigid Foam/Organified Nanosilica, Designed Monomers and Polymers, 14 (2012) 263-272.
[70] M.M.A. Nikje, Z.M. Tehrani, Novel Modified Nanosilica-Based on Synthesized Dipodal Silane and Its Effects on the Physical Properties of Rigid Polyurethane Foams, Designed Monomers and Polymers, 13 (2012) 249-260.
[71] M.E. Kabir, M.C. Saha, S. Jeelani, Effect of ultrasound sonication in carbon nanofibers/polyurethane foam composite, Materials Science and Engineering: A, 459 (2007) 111-116.
[72] C. Caglayan, I. Gurkan, S. Gungor, H. Cebeci, The Effect of CNT-Reinforced Polyurethane Foam Cores to Flexural Properties of Sandwich Composites, Composites: Part A, (2018).
[73] S.-X. Wang, H.-B. Zhao, W.-H. Rao, S.-C. Huang, T. Wang, W. Liao, Y.-Z. Wang, Inherently flame-retardant rigid polyurethane foams with excellent thermal insulation and mechanical properties, Polymer, 153 (2018) 616-625.
[74] S. Sathiyamoorthy, G. Girijakumrai, P. Kannan, K. Venugopal, S.T. Shanmugam, P. Veluswamy, K.D. Wael, H. Ikeda, Tailoring the functional properties of polyurethane foam with dispersions of carbon nanofiber for power generator applications, Applied Surface Science, (2018).
[75] N. Nazeran, J. Moghaddas, Synthesis and characterization of silica aerogel reinforced rigid polyurethane foam for thermal insulation application, Journal of Non-Crystalline Solids, 461 (2017) 1-11.

CHAPTER 2:

BACKGROUND AND STATE OF THE ART

Mercedes Santiago Calvo

2.1- Introduction

Polyurethane (PU) foams (referred to thermoset PU foams) are discussed in more detail in most sections of this chapter, since the largest part of this thesis is centered in them. The following sections summarize these aspects about PU foams:

- Their discovery (**section 2.2**).
- Their basic chemistry (main reactions), polymer morphology and cellular structure (**section 2.3**).
- The common raw materials used to produce them (**section 2.4**).
- The steps of foaming process and cell degeneration mechanisms (**section 2.5**).
- Their properties and applications (**section 2.6**).
- PU foam composites (**section 2.7**).
- The monitoring of foaming process of PU foams (**section 2.8**).

The last section (**2.9**) is focused on thermoplastic polyurethane (TPU) foams, whose study was carried during the international stay. It is also important to mention that a detailed state of the art of the different topics considered during the thesis is discussed in each paper included in **chapters 4** to **7**.

2.2- Discover of polyurethane: Polyurethane foams

In 1849, Charles Adolphe Wurtz discovered the reaction of urethane formation (-NH-CO-O-) by reacting aliphatic monofunctional isocyanates with alcohols [1]. However, it was not until the 1930s that Professor Dr. Otto Bayer and his co-workers at the laboratories of I.G. Farben in Leverkusen, Germany rediscovered and patented the novel polymerization reaction called polyaddition reaction for the synthesis of PUs by reacting diisocyanates and compounds containing at least two hydroxyl and/or amine groups [2]. Initially, their work was focused on the production of fibers to be used for textile applications, but unfortunately these fibers based on PU were not long enough for their initial purpose. This is why they decided to study PU moldable masses, what gave instead products containing undesired bubbles, as a result of the use of an impure polyester component which contained carboxyl groups, which react with isocyanates forming amides and CO_2 [3]. Therefore, it was by chance that Professor Dr. Otto Bayer and his team obtained thermoset PU foams in 1941. Subsequently, they used a small amount of water to obtain PU foams with the desired amount of CO_2 [3]. **Figure 2.1** shows a photograph of Bayer showing his discovery of PU foam.

The first patent of a flexible polyurethane (FPU) foam preparation was assigned to Zaunbrecher and Barth in 1942 [4]. But the commercial production of FPU foam had to wait until the early fifties, and it was based on the reaction between toluene diisocyanate (TDI) and polyester polyols. These reactants were also used to produce other types of PUs, such as rigid foams, gum rubber, or elastomers. In 1956 DuPont launched poly(tetramethylene glycol) (PTMG), the first commercial polyether polyol. Polyether polyols became more popular than

polyester polyols due to their advantages, such as lower cost, easier handling, and higher resistance to water [5]. Moreover, new and better catalysts, such as triethylenediamine or organotin compounds, were developed. All these contributions allowed the emergence of the so-called one-shot process in 1958, eliminating the earlier need of an intermediate prepolymer step [6]. In 1960, a new polymeric isocyanate, polymeric diphenylmethane diisocyanate (pMDI), was introduced by the Carwin (later Upjohn and Dow) Company. Thus, the availability of polyether polyols, polymeric isocyanates such as pMDI and new catalysts and blowing agents increased the use of rigid foams as high-performance insulation materials. By 1967, the availability of pMDI allowed the development of polyisocyanurate (PIR) foams with high thermal and flammability resistance[5]. In the subsequent decades, many further developments in the field of PU foams have been achieved, such as the use of physical blowing agents with low ozone depleting potential, the gradual replacement of TDI by less volatile pMDI or MDI, the utilization of vegetable oil-based polyols, the use of PU foam composites, the PU foams free of isocyanate, or the use of carbon dioxide-based polyols, among others [7].

Figure 2.1. Prof. Otto Bayer, recognized as “the father of polyurethane chemistry”, in 1952, demonstrating his creation, the polyurethane foam.

2.3- Basic chemistry, polymeric morphology and cellular structure of polyurethane foams

2.3.1- Basic chemistry

Considering the thermoset PU foams, their synthesis is a complicated process because many components and multiple simultaneous reactions are involved. Rigid, flexible or semirigid foams can be obtained just by changing the starting materials. The chemistry involved in the synthesis of the different PU foams is mainly centred on the isocyanate reactions, since isocyanates groups (-N=C=O) are highly reactive towards hydrogen active compounds, such as those contain -OH or –NH functional groups [1]. This high reactivity between isocyanate groups

and hydrogen active compounds is due to the elevated electrophilic character of the central carbon atom in the isocyanate group, which is thus easily attacked by the highly electronegative oxygen or nitrogen atoms. **Table 2.1** collects the relative reaction rates of isocyanates with different hydrogen active compounds, resulting from their reactivities.

Table 2.1. Relative reaction rates of isocyanates with varying reaction partners (Adapted from [8]).

Hydrogen active compound	Structure	Relative uncatalyzed reaction rate at 25°C
Primary amine	R-N**H**$_2$	100.000
Secondary aliphatic amine	R_2N-**H**	20.000-50.000
Primary aromatic amine	Ar-N**H**$_2$	200-300
Primary hydroxyl	R-CH_2-O**H**	100
Water	**H**$_2$O	100
Carboxylic acid	R-COO**H**	40
Secondary hydroxyl	R_2CHO**H**	30
Urea	R-N**H**-CO-N**H**-R	15
Tertiary alcohol	R_3CO**H**	0.5
Urethane	R-N**H**-COOR	0.3
Amide	R-CO-N**H**$_2$	0.1

The main reaction involved in the synthesis of PU products (foams, elastomers, coating, etc), occurs between the isocyanate and a polyol, which produces urethanes, as shown in **scheme 2.1**. This reaction is known as polymerization or gelling reaction in the PU field. When polyfunctional reagents (polyisocyanates and polyols) are used, it is a polyaddition process which forms a highly crosslinked covalent polymeric structure. The reaction is exothermic, with a heat of reaction of -93.9 KJ/mol [9], and it occurs at a relatively slow rate at room temperature when no catalysts are added.

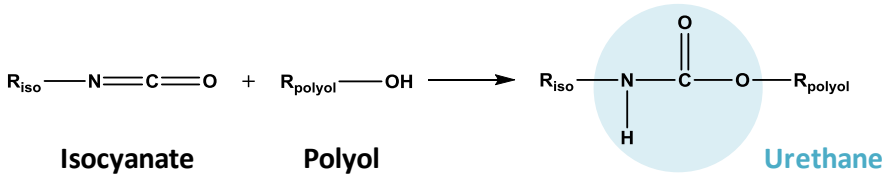

Scheme 2.1. Polymerization or gelling reaction: the reaction between isocyanate and polyol to generate urethane groups. R_{iso} and R_{polyol} are the structures of the isocyanate and the polyol, respectively.

The second main process during PU foams formation is called blowing or foaming reaction, and occurs due to the generation of gas from a chemical blowing agent, a physical blowing agent, or a mixture of both [10]. It occurs at the same time that the polymerization or gelling reaction. The physical blowing agents are low boiling blowing agents, such as cyclopentane, n-pentane, isopentane, etc, which are volatilized during the exothermic foaming process. The chemical blowing agents, such as water, produce gas by a chemical reaction. In many applications of PU foams, water is the most common blowing agent used nowadays. In these water-blown PU foams, an isocyanate with a strong affinity to water (**Table 2.1**) reacts with it to give an unstable carbamic acid, which spontaneously decomposes into CO_2 and the corresponding amine. The generated gas provides the foam expansion, helping to create the porous structure of foams (first reaction in **Scheme 2.2**). The amine produced in the first reaction continues reacting with a second isocyanate generating urea groups (second reaction in **Scheme 2.2**). Both reactions are exothermic with a heat of reaction of -125.5 kJ/mol [9].

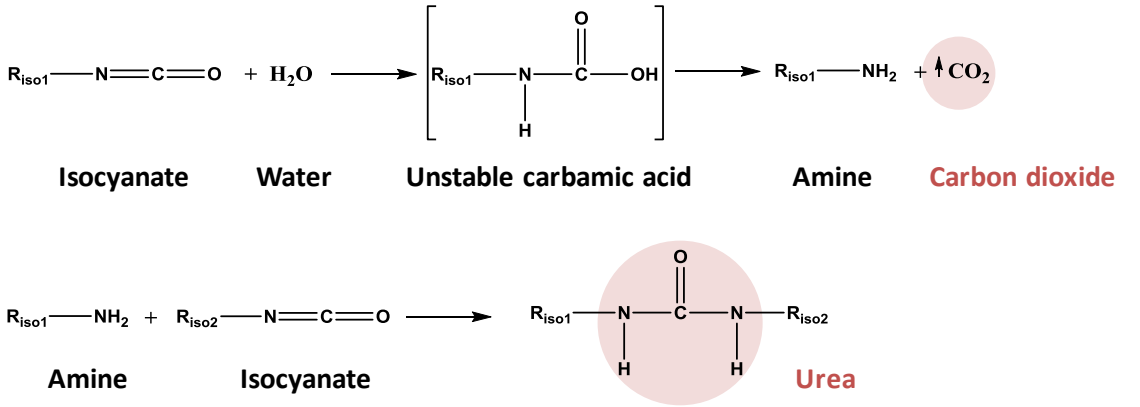

Scheme 2.2. Foaming or blowing reaction: the reaction between isocyanate and water to generate carbon dioxide and urea. R_{iso} and R_{polyol} are the structures of the isocyanate and the polyol, respectively.

In addition to the two main reactions based on the starting components (polyol, isocyanate and water), other reactions are produced in water-blown PU foams: They may occur due to the high reactivity of the isocyanate group, to the adiabatic heat buildup in the reacting mass, or to local inhomogeneities in the component concentration [11]. Therefore, the isocyanate continues to react in the foaming process forming additional chemical functional groups, such as allophanate, biuret, isocyanurate, carbodiimide, uretidinedione, among others, which contribute to the overall structure and rigidity of the material [8, 12-16] . While the gelling and blowing reactions generate urethane and urea products at room temperature (and up to 50°C), the reactions producing allophanate, biuret, or isocyanate linkages occur at higher temperatures (lower than 150°C) [12].

The reactions of isocyanate with the products corresponding to the main reactions, urea and urethane, lead to allophanate (**scheme 2.3**) and biuret compounds (**scheme 2.4**), respectively.

These reactions occur under the presence of an excess of isocyanate and, as indicated above, more readily at elevated temperatures. In addition, allophanate and biuret linkages are thermo-reversible to give the starting components, free isocyanates and urethane or urea compounds [8]. The dissociation temperatures of allophanate and biuret are ca. 100–120°C and ca. 115–125°C, respectively [12].

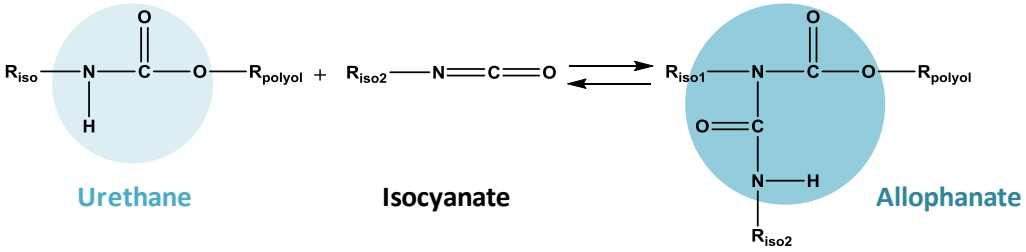

Scheme 2.3. The reaction between urethane and isocyanate to give allophanate. R_{iso} and R_{polyol} are the structures of the isocyanate and the polyol, respectively.

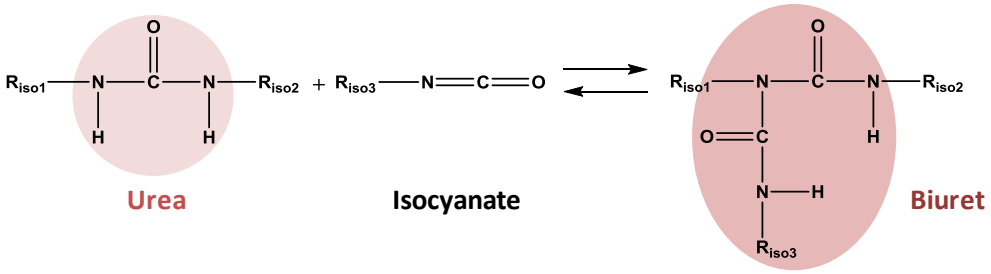

Scheme 2.4. The reaction between urea and isocyanate to form biuret. R_{iso} and R_{polyol} are the structures of the isocyanate and the polyol, respectively.

Isocyanate groups may react with themselves to form oligomers (mainly dimers or trimers) whit excess of isocyanate and the appropriate conditions. The trimerization reaction forms cyclic trimers called isocyanurates (**scheme 2.5**). These isocyanurate rings act as extremely stable crosslinks in the PU network, increasing the thermal stability and flame retardance of the PU foams. This cyclotrimerization reaction is exothermic, and their heat of reaction is -91.2 kJ/mol [5]. This reaction may be also used to produce polyisocyanurate (PIR) foams, when isocyanates are the predominant species (isocyanate index = 200-600) [1].

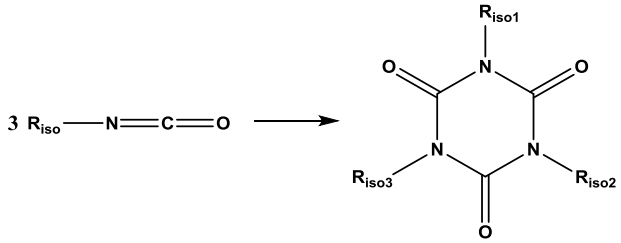

Isocyanate **Isocyanurate**

Scheme 2.5. Trimerization of isocyanate to form isocyanurate. R_{iso} is the structure of the isocyanate.

Isocyanates may undergo two types of dimerization reactions: formation of uretidione rings (**scheme 2.6**) or carbodiimides (**scheme2. 7**). The heat of formation of uretidione is nearly zero and its dissociation occurs at relatively low temperatures (80-100°C) [11]. While the formation of uretidione is a reversible process, carbodiimide is instead generated by a catalyzed irreversible dimerization reaction of isocyanate groups (**scheme 2.7**). The carbodiimide continues reacting with the excess of isocyanate to generate an uretonimine structure (**scheme 2.7**). This reaction is reversible and the opposite process occurs at a rapid rate when the temperatures are above 130°C.

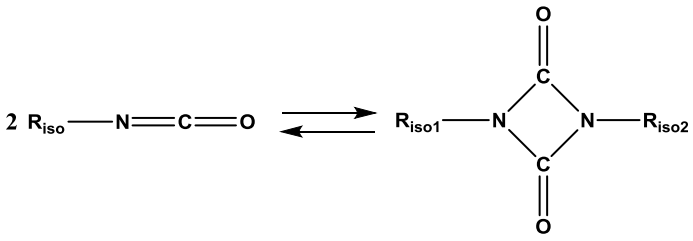

Isocyanate **Uretidione (dimer)**

Scheme 2.6. Dimerization of isocyanate to form uretidione. R_{iso} is the structure of the isocyanate.

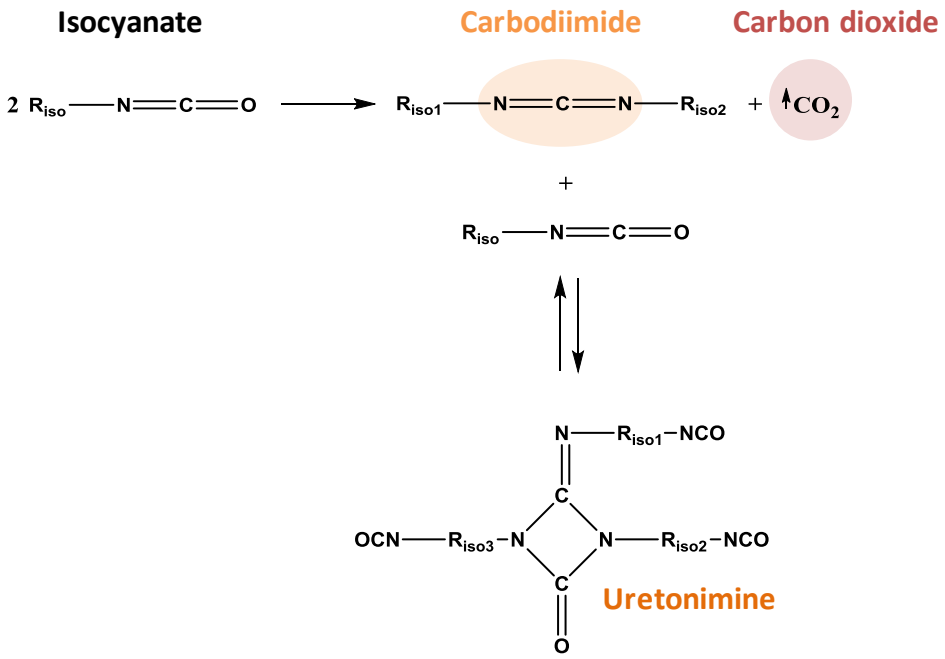

Scheme 2.7. Dimerization of isocyanate to form carbodiimide and carbon dioxide, followed by the reaction of carbodiimide and isocyanate to form uretonimine. R_{iso} is the structures of the isocyanate.

Additionally, the isocyanate groups can react with other functional groups also present in the starting components or fillers of PU foams. For example, isocyanate reacts with carboxylic acids to form an intermediate anhydride, which undergoes a further break down generating an amide group and carbon dioxide (**scheme 2.8**).

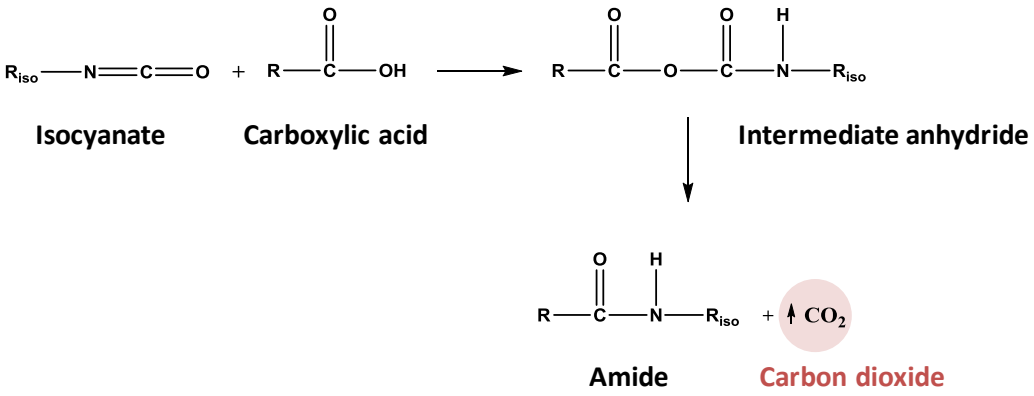

Scheme 2.8. The reaction of isocyanate and carboxylic acid to form the intermediate anhydride and the final amide. R_{iso} is the structures of the isocyanate.

As a conclusion, a number of side reactions may take place, depending predominantly on the reaction conditions, such as temperature, the ratio between polyol and isocyanate, and the presence of catalysts. Moreover, these side products may suppose a supplementary source of crosslinking to the PU network. Since the PU formulations used in the present thesis are for rigid foams in which the excess of isocyanate is not high, the amount of products corresponding to the side reactions is very small in comparison with that of the main reactions (gelling and blowing) and thus the side reactions can be despised.

2.3.2- Polymer morphology

PU foams present a complex polymer morphology composed of alternating hard and soft segments. Soft segments (SS) are composed of polyol chains such as polyether or polyester polyols, which offer flexibility and elastomeric properties at room temperature. Hard segments (HS) are derived from the main simultaneous reactions of isocyanate with polyol and water, which provide rigidity [17]. The polymerization reaction creates progressively a chemical crosslinking network based on urethane structures, while the blowing reaction generates CO_2 and polyurea-based HS which are chemical incompatibility with polyol SS and tends to form microphase separation where polyureas are aggregated via hydrogen bonding [17, 18]. The urea groups in foams have stronger specific hydrogen-bonding interaction and high stiffness compared to those of the urethane groups, making them more appropriate for microphase separation as compared to the urethane groups [17]. For this reason the hydrogen-bonded urea, in particular ordered urea (bidentate urea), is frequently used for estimating the degree of microphase separation [19, 20]. The formation of the microphase separation into urea HS and polyol SS depends on the kinetics and thermodynamic effects in foam formation, and it is favoured in flexible foams [21, 22].

On the one hand, flexible foams have a wide meshed cross-linked structure formed by the reactions of low functionalized long-chain polyols with water and diisocyanate [23]. Moreover, the flexible foams are characterized by the phase separation into urea HS and polyol SS (**Figure 2.2.A**). Consequently, the polymer morphology of the flexible foams consists of an elastic network of strong covalent cross-links in the soft domains and weaker physical cross-links in the hard domains. On the other hand, rigid foams have a close meshed cross-linked structure generated by the reaction between highly functionalized low-chain polyols with polyfunctional isocyanates [23]. Moreover, the excess of isocyanate used in RPU or PIR foams generates additional cross-linking points such as allophanate, biuret or isocyanurate groups (**Figure 2.2.B**) [23].

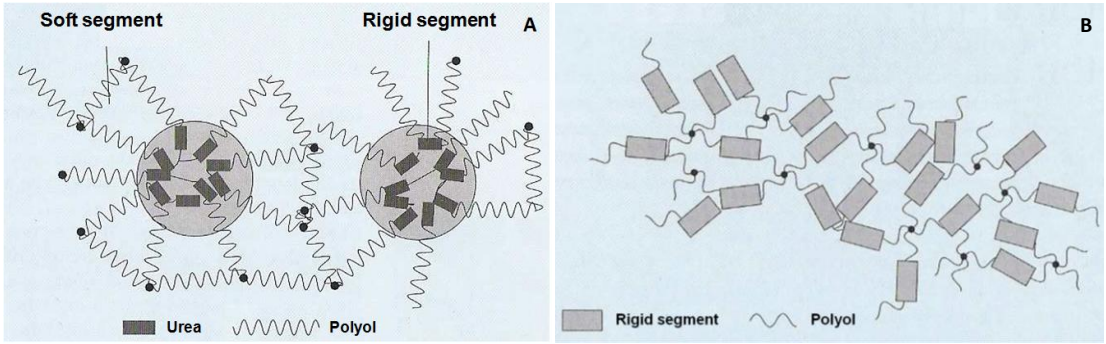

Figure 2.2. A) Polymer morphology of flexible polyurethane foam and B) rigid polyurethane foam [24].

2.3.3. Cellular structure and density

RPU and FPU foams differ not only on the polymer morphology but also on the type of cellular structure. Two types of cellular structures are present in PU foams: closed cell structure and open cell structure. The cellular structure is predominantly closed for rigid foams (**Figure 2.3.A**), which means that the cells present cell walls and contain the dispersed gas completely enclosed. However, in FPU, the cellular structure is predominantly open (**Figure 2.3.B**), which means that the cell walls are interconnected and are filled with air. These types of cellular structures depend on the starting components and their amounts, as it will be explained in **section 2.4**. In addition to the open or closed cellular structure, the cell size is very relevant since many applications require either large or small cells. The cell shape (isotropy or anisotropy) and the uniformity of cellular structure are other important factors. It is very common to have PU foams with anisotropic cellular structures, with cells elongated (with a large cell site) in the growing direction (**Figure 2.3.C**). As a consequence of the type of structure, rigid foams have lower thermal conductivities and high mechanical properties, whereas flexible foams have excellent shock absorption, acoustic absorption, absorptive capacity for water and moisture and higher permeability to gas and vapor [5, 25].

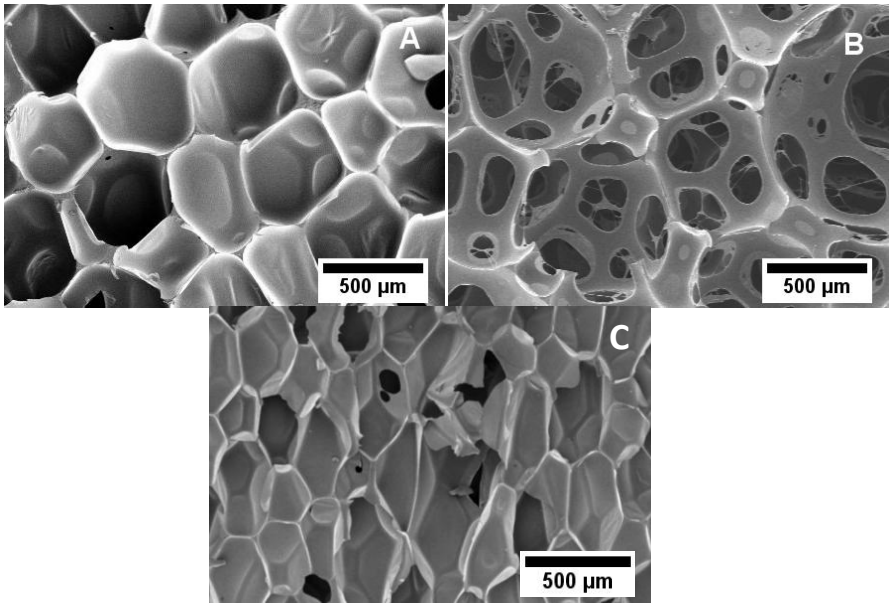

Figure 2.3. SEM micrographs of polyurethane foams: A) rigid and B) flexible and C) rigid with anisotropic cells in the growing direction.

The density of the PU foams is another very important parameter, because it determines the performance and cost of a foam, by measuring how much of a foam is air and how much is solid polymer [26]. The final density of PU foams, which determines a wide range of applications, can be easily modified by changing the amount of blowing agents. RPU foams may have densities between 20 and 800 kg/m^3 [5]. RPU foams with lower densities (lower than 50 kg/m^3) are used as insulating materials, while RPU foams with higher densities are most used as structural materials. FPU foams are produced with densities ranging from 20 to 45 kg/m^3 [27].

2.4- Common raw materials of polyurethane foams

Polyols and isocyanates are the most important raw materials to build the complex structure of a PU polymer. Isocyanates are highly reactive groups, as already indicated in **section 2.2**, but their reaction with polyols is relatively slow at room temperature due to the phase incompatibility between the relatively non-polar and denser isocyanate phase, and the more polar and less-dense polyol phase [8]. A similar situation occurs when isocyanate reacts with water. Moreover, the successful production of PU foams requires an adequate balance of the kinetics of the reaction. It is therefore necessary to use surfactants to improve the phase compatibilization, and also catalysts to enhance or regulate the rate of blowing and gelling reactions. Hence, the PU foam formulations usually include many different components, such as polyols, isocyanates, catalysts, surfactants, blowing agents, and additives (cell openers, flame retardants, antioxidants, and light stabilizers, among others) in order to obtain a final

product with the desired properties. The essential components of the PU foam formulation are discussed next.

2.4.1- Polyol

Polyols contain multiple hydroxyl functional groups intended to react with isocyanate groups, to give urethane linkages (**scheme 2.1**). There are two main types of polyols available: polyether polyols and polyester polyols.

Polyether polyols contain ether and hydroxyl groups in their backbone, and are normally produced by the reaction of an alkylene oxide (epoxide) with an initiator in the presence of an acid or a base acting as a catalyst. The initiator is an active hydrogen compound containing functionality from 2 to 8 (**scheme 2.9**). Some examples of initiators are ethylene glycol (EG), propylene glycol, glycerin, pentaerythritol, trimethylolpropane, sucrose, or sorbitol, while ethylene oxide (EO), propylene oxide (PO), mixtures of EO and PO, or tetrahydrofuran (THF) are examples of alkylene oxides commonly used. Polyether polyols are widely used for producing foams and other PU products because they present several advantages over polyester polyols: their functionalities and equivalent weight can be widely changed, lower cost production, lower viscosities, and resulting foams which are resistant to hydrolysis [28]. However, a disadvantage of polyether polyols is their resistance to oxidation, which is lower compared to that of polyester polyols based foams.

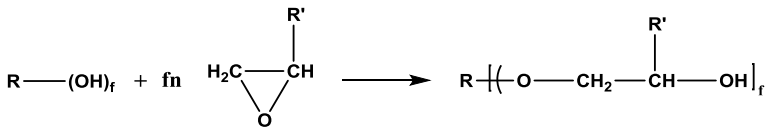

Scheme 2.9. Example of anionic polymerization of alkylene oxides, such as ethylene or propylene oxide, to obtain polyether polyols. "fn" is the functionality of the initiator, "R-(OH)f" is the initiator, n is the number of moles of alkylene oxide molecules, and R' is H or CH_3 (Adapted from [28]).

Polyester polyols contain ester and hydroxyl groups in the backbone, and are generally produced by the polycondensation reaction of multifunctional carboxylic acids and polyols (**scheme 2.10**), or by the ring opening polymerization of a lactone with a polyol (**scheme 2.11**). Some examples of compounds used to produce polyester polyols are glycerine, trimethylolpropane (TMP), EG or diethyleneglycol (DEG) as polyols, and adipic acid or azelaic acid as a carboxylic acid. A large number of ester groups, which are highly polar, may give rise to polyester-based PUs with strong cohesive strength and adhesion, and thus to high strength and wear resistance.

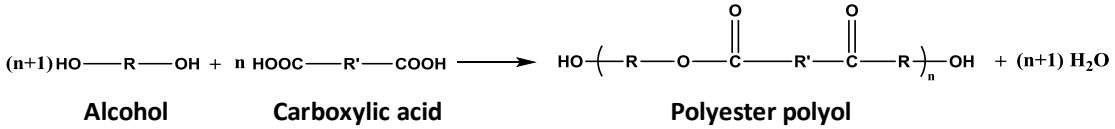

Scheme 2.10. Example of polycondensation reaction to obtain polyester polyols. n is the number of moles of carboxylic acid molecules.

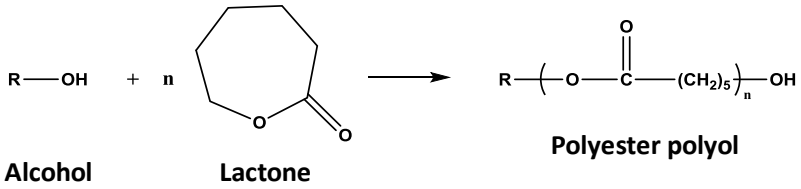

Scheme 2.11. Example of the ring-opening polymerization of lactones to obtain polyester polyols. n is the number of moles of lactone molecules.

Polyols may be designed to have different structures and characteristics by varying the types of starting materials. Some important features for polyols are: hydroxyl number, functionality, molecular weight, acid value, moisture, viscosity, density, and color. The main important feature is the hydroxyl number or hydroxyl index, which is the quantitative value defined by the amount of hydroxyl groups available for the reaction with isocyanates. It is expressed as milligrams of potassium hydroxide by gram of sample (mg KOH/g). Lower hydroxyl numbers indicate longer polyol chain lengths and higher molecular weights and vice versa. Functionality is the second important characteristic of polyols, and is defined as the number of hydroxyl groups by each molecule of polyol. The functionality is based on the initiator or on the mixture of initiators used for producing the polyols. Hydroxyl number, functionality and molecular weight are the main polyol features which determine the rigid or flexible behavior of the final foam (**Table 2.2**), but the rest of characteristics must also be considered for the foam formulation. In general, all the foams are crosslinked, being the rigid foams those highly crosslinked. Hence, rigid foams are produced from polyols with high hydroxyl number, high functionality and low molecular weight. Instead, flexible foams are obtained from polyols with low hydroxyl number, low functionality and high molecular weight.

Table 2.2. Characteristics of polyols used for both rigid and flexible PU foams (Adapted from [12, 28]).

Polyol	Rigid foam	Flexible foam
Hydroxyl number (mg KOH/g)	350-560	5.6-70
Functionality	3.0-8.0	2.0-3.1
Molecular weight range (Da)	150-1000	1000-6500

2.4.2-Isocyanate

The isocyanate component reacts with functional groups from the polyol (**scheme 2.1**), with water (**scheme 2.2)**, with themselves (**schemes 2.5-7**), and with other components on the formulation (**schemes 2.3, 2.4 and 2.8**). The isocyanates used in the production of PU foams contain at least two NCO groups per molecule, and are usually aromatic isocyanates, such as toluene diisocyanate (TDI) or diphenyl methane diisocyanate (MDI). They present higher reactivity and thermal stability compared to aliphatic isocyanates, such as isophorone diisocyanate (IPDI) or hexamethylene iscocyanate (HDI) [29]. The phosgenation of amines, reported by Hentschel in 1884, is the most important commercial method for isocyanate production (**Scheme 2.12**). Isocyanate is obtained by the reaction of gaseous phosgene with amines or amine salt precursors. The main trouble about this commercial process of isocyanate production is the use of phosgene, which is a colorless, very reactive, and a highly toxic gas. Exposure to this toxic gas can cause severe respiratory effects, ocular irritation and burns to the eye and to the skin, and eventually to death [30]. Moreover, the isocyanates monomers thus obtained (MDI and TDI) also are harmful [30, 31]. As a consequence, the Occupational Safety and Health Administration of the United States and the European Agency for Safety and Health at Work have released regulations about the hazards and exposure limits to isocyanates.

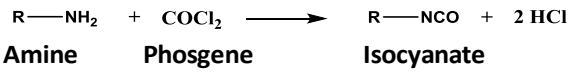

Scheme 2.12. Example of isocyanate production by the reaction of gaseous phosgene with amines.

Compared to polyols, there are fewer types of commonly used isocyanates, being TDI and MDI in their oligomeric forms those most employed. Commercial TDI is a liquid of low viscosity at room temperature, and contains a mixture of 2,4- and 2,6-isomers (**scheme 2.13**) in an either 80/20 or 65/35 w/w ratio, being the latter mixture less reactive. TDI is the most common isocyanate used for flexible foams. Modified TDI or undistilled TDI can be used for preparing rigid foams and semirigid foams. However, TDI is not suitable for PIR foams.

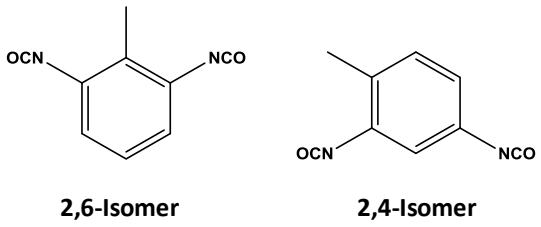

Scheme 2.13. Chemical Structure of TDI.

Pure MDI (or monomeric MDI) is difunctional, is a solid at room temperature, and is used for elastomers and coatings. Polymeric and oligomeric MDI are commercialized as liquids, what enhaces processing and/or properties. The 4,4'-isomer, which usually contains a small amount of 2,2'-isomer and up to 10% of the 2,4-isomer (**Scheme 2.14**) is the mixture more commonly used. Its average functionality is in the range 2.3-3.0. Its functionality and its liquid nature make pMDI to be widely used to obtain rigid and semirigid foams, as well as PIR foams. Currently new products based on pMDI are being developed in order to substitute the TDI of the flexible foams, due to the higher toxicity levels of TDI compared to pMDI.

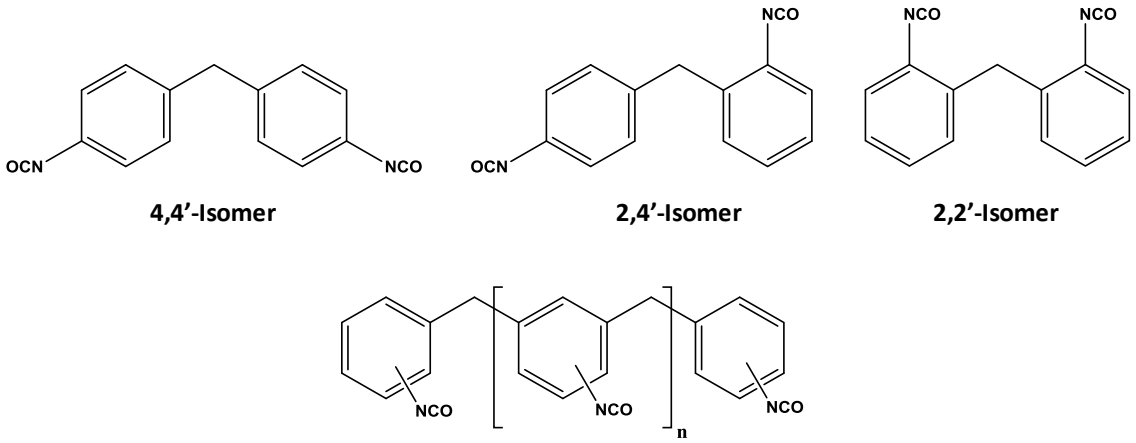

Scheme 2.14. Chemical structures of MDI isomers and pMDI.

The isocyanates are characterized by their NCO content, functionality, viscosity and acidity (HCl percent). NCO content, normally given in % by weight of NCO, represents the weight percent of an isocyanate comprised of NCO groups. Functionality is defined as the number of NCO groups by molecule of isocyanate. Acidity is a measure of the acid content derived from the synthesis of isocyanate (**Scheme 2.12**), which can influence its reactivity.

It is very important to employ the correct stoichiometry in order to carry out the polymerization reaction. Normally, the total number of isocyanate groups must be higher than, or equal to, the sum of the active hydrogen-containing groups in the reacting system (hydroxyl groups of polyols plus water in water-blown PU foams). This concept is expressed by the isocyanate index or the isocyanate/hydroxyl equivalent ratio (**equation 2.1**) [32]. Depending on the foam system to be manufactured (for example, rigid or flexible), the isocyanate index is fixed, and thus the amount of isocyanate required to react with the polyol and with any other reactant in the formulation must be calculated in terms of theoretically stoichiometric equivalents. Therefore, the actual amount of isocyanate used in the foam is obtained from these two terms. The isocyanate index of flexible foams usually goes from 90 to 110 [26], whereas the range for rigid foams is usually 105–120 [12]. Isocyanate indexes above 100 imply

the use of an excess of isocyanate groups relative to the active hydrogen-containing groups in the reacting mixture, which may generate isocyanate reactions with itself (**schemes 2.5-7**). Obviously, PIR foams present higher isocyanate indexes, up to 300 even more in order to form the isocyanurate group [33].

$$Isocyanate\ Index = \frac{Actual\ amount\ of\ isocyanate\ used}{Theoretical\ amount\ of\ isocyanate\ required} x\ 100 \quad (Equation\ 2.1)$$

2.4.3-Surfactant

Surfactants or foam stabilizers are frequently used to improve the properties of PU foams. Surfactants consist of block copolymers of either polydimethylsiloxane-polyoxyalkylene, nonylphenol ethoxylates, silicone oils or some other organic compounds [29]. The most used surfactants for PU foams are polydimethylsiloxane-polyoxyalkylene copolymers. These surfactants are copolymers of poly(dimethylsiloxane) or PDMS $[\text{-Si}(CH_3)_2\text{-O-}]_n$ and oxyalkylene chains, such as polyethylene oxide chain $(EO)_x$ and polypropylene oxide chains $(PO)_y$ (**Scheme 2.15**). These copolymers can be linear or branched (pendant). Structural parameters of the silicone surfactants, such as the balance/content of hydrophobic PDMS and hydrophilic oxyalkylene chains, significantly affect their functions [28].

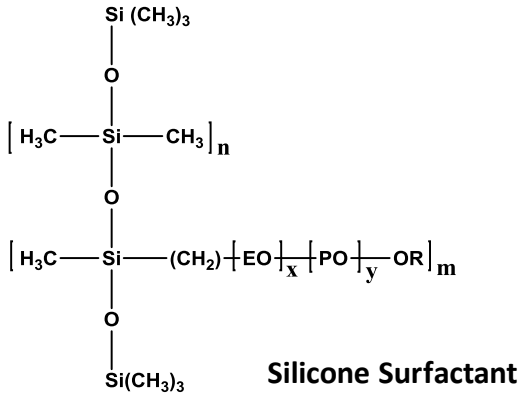

Scheme 2.15. Chemical structure of polydimethylsiloxane-polyoxyalkylene copolymers (Adapted from [28]).

In PU foams, surfactants act mainly in three ways: (1) lowering the surface tension of the PU-air interface, thus promoting the generation of bubbles which evolve into the foam cells; (2) offering emulsification for the whole components, what affects to the speed of the reactions, because the concentration of reagents available is then increased; and (3) controlling the stability of the foam structure, thus preventing the collapse and regulating the voids at the

sub-surface [11, 12, 29]. The surfactants requirements for rigid and flexible foams are different, since the compatibility of the starting materials and the cellular structure of the final rigid and flexible foams are different, but the general surfactant behavior is similar. In rigid foams the starting components are incompatible and cells are completely closed, whereas in flexible foams the starting components are homogeneously miscible and the cells are open. The process of cell opening consists of draining the walls towards the struts, and the emulsion of components depends mainly on the surfactant structure. Flexible foams require surfactants which promote improved cell-wall drainage in order to open the cell walls during the foaming reaction, whereas rigid foams require the opposite. However, it should be emphasized that rigid foams present more stable growth than flexible foams, because the drainage effect is reduced due to the high increase in viscosity during the PU formation. In this case there is no danger of collapsing by separation of a solid phase of polyurea, as it happens in the formation of flexible foam [12].

2.4.4-Catalyst

Catalysts are required in PU foam formulations to accelerate the reactions involved in the foaming process at room temperature. At the same time, catalysts are able to maintain an adequate balance between the gelling and blowing reactions, as well as the side reactions. PU catalysts can be classified into two categories: amine compounds and organometallic compounds. Common amine catalysts are tertiary amines, such as dimethylcyclohexylamine (DMCHA), dimethylethanolamine (DMEA) and triethylenediamine [29]. Organometallic compounds usually contain metals such as bismuth, lead, zinc, tin or mercury. The basic mechanism of any of these two types of catalysts consists on increasing polarization of either the isocyanate or the hydroxyl compounds by polar interactions (**Scheme 2.16**) [11]. According to this, the catalyst enhances de polarity of the bonds and therefore its reactivity.

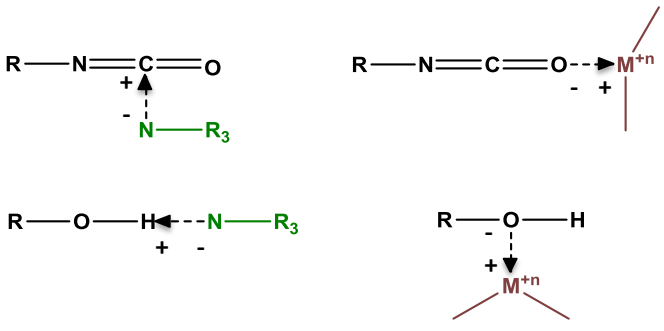

Scheme 2.16. Examples of bond polarization mechanisms by tertiary amines (NR3) or organometallic compounds as catalysts (Adapted from [11]).

The catalytic activity of tertiary amines is controlled by their structure and their basicity, increasing with the increasing basicity and decreasing with the steric hindrance of the substituents of the nitrogen atom [7]. Amine catalysts are able to promote both gelling and blowing reactions (urethane and urea products) at the same time, as well as different side reactions, depending on isocyanate excess, catalyst concentration, temperature, etc [11]. However, specific amine catalysts can be designed to preferably catalyze either the gelling or the blowing reactions, thus their appropriate combinations may help to achieve the desired properties of the final foam.

On the other hand, organometallic catalysts favor almost exclusively the gelling reaction. Some examples of organometallic catalysts are stannous octoate, dibutyltindilaurate, and tin mercaptides. The advantages of these catalysts respect to tertiary amines are based on their lower volatility, what facilitates their maintenance in the foam without causing odors which is an important issue in automotive applications, for example. The odor problem of amine catalysts can be also solved by using amines containing functional groups able to react with isocyanate, such as OH- or NH_2, which react during the foaming process and are eventually bonded to the foams [12]. Organometallic catalysts can be used either alone or in combination with amine catalysts in order to achieve the expected balance of reaction rates in the PU foam formation.

2.4.5-Blowing agent

PU foam expansion occurs due to the presence of either a chemical blowing agent, a physical blowing agent, or a mixture of both. Physical blowing agents (such as solvents with low boiling point: pentane, hexane, acetone, hydrochlorofluorocarbons (HCFCs) or hydrofluoroolefins (HFOs)) provide gas for PU expansion by vaporization during the foaming process, what is an endothermic process [34]. Chemical blowing agents are compounds which release gas during the foam formation, due to either a thermal decomposition or to a chemical reaction. This is the role of water, which is the most common chemical blowing agent in PU formation [26]. Until recently, chlorofluorocarbons (CFCs) and HCFCs were commonly used as physical blowing agents, but they have been recently prohibited because they play a decisive role in the destruction of the ozone layer. For this reason, more environmentally friendly blowing agents, such as cyclopentane (CP), HFOs or water, are currently being used in most of the industrial applications. The CP evaporated during the foaming process as a result of the heat produced during the polymerization reaction may be occluded as a physical blowing agent inside the cells. As indicated before (**Schemes 2.2, 2.7, and 2.8**) water acts as a chemical blowing agent expanding PU due to the carbon dioxide generated during different exothermic reactions, during water-blown RPU foams production.

The blowing agents play an important role in both the production and performance of the PU foams. Thus, the amount of blowing agent greatly determines the foam density of the final foam, and influences the cellular microstructure and the polymer morphology of the PU foams: these are essential parameters in order to describe their final behavior [26]. Thermal

conductivity is the most important property for PUR or PIR foams used for thermal insulating applications. These foams must contain closed cells and the blowing agent must be retained inside the cellular structure, until it eventually diffuses out of the cell. Thus, key strategies for improving the thermal properties of foams are the use of blowing agents with low thermal conductivities, or which are able to enhance the overall long-term performance of the foam [26]. For example, CP or HCFCs are retained in the cells for longer periods of time compared to CO_2, since the latter leaves the foam in a time period shorter than one month [35]. In flexible foams, the blowing agents have no influence on the performance of the foam, although they do determine their resulting cellular structure and polymer morphology.

2.5- Foaming process of polyurethane foams

PU foams are normally prepared by one-shot free-foaming method at room temperature in which the reactive components (isocyanate and polyol blend) are mixed using plastic cups or molds. The reaction mixture is constantly expanded by the blowing gases released from chemical or physical blowing agents, and the polymerization reactions help to encapsulate the gas phase, creating a cellular structure when the polymeric matrix solidifies. Depending on the cellular structure and morphology formed, the resulting PU foams will have some properties or others. Therefore, it is fundamental to analyze the foaming process in order to understand the final cellular structure and morphology obtained. For water-blown rigid polyurethane foams, the following stages are characteristic of the reactions and foaming process of water-blown PU foams [36-38] (**Figure 2.4**):

1. Cream stage. Bubble nucleation occurs when the CO_2 generated in the reaction between water and isocyanate reaches the solubility limit, giving a creamy appearance to the reactive mixture, which is defined as cream time. For foams blown with a physical blowing agent, the nucleation starts when the physical blowing agent is evaporated as the temperature rises, due to the exothermic polymerization reaction [39]. Increasing the amount of gas molecules (CO_2 or physical blowing agent) into the polymer will enhance the probability of aggregation between molecules to produce a nucleus/bubble, and consequently, the nucleation density.

2. Rise stage. The reactive mixture begins to expand when CO_2 from the liquid phase (zones with higher pressure) diffuses to previously created nuclei (zones with lower pressure). The liquid foam presents a metastable state that evolves dynamically due to several processes: simultaneous reactions (principally blowing and gelling), cell growth and corresponding macroscopic expansion, and cell degeneration mechanisms (drainage, coarsening and cells coalescence).

3. Packing stage. The bubbles grow until the foam rises to a maximum. Urethane and urea formation continues, increasing the viscosity of the liquid phase until the equilibrium with expansion forces is reached. At maximum rise, the cells are filled with hot gas due to the exothermic foaming process, but as the foam cools, the pressure inside the cells drops. Rigid foams are strong enough to maintain a partial vacuum in each cell and hence a closed-packed

structure without shrinkage is formed [26]. In the case of flexible foams, both the pressure inside each bubble and the precipitation of urea microdomains provokes rupture of cell walls, that divide cells, creating open channels [26]. If the flexible foam contains too many closed cells, the foam will shrink when it cools due to the partial vacuum inside the closed cells and the low stiffness of the polymer.

4. Gelation stage. The foam reaches its final structure. The rigidity of the fluid is high enough so that the final size of the bubbles is reached, and expansion or degeneration mechanisms are no longer produced.h

5. Solidification stage. The solidification stage is reached when the PU mass has gelled, obtaining the final structure and almost the final mechanical properties. Crosslinking finishes and foam starts to cool down a curing period where the polymer cells become fully solidified.

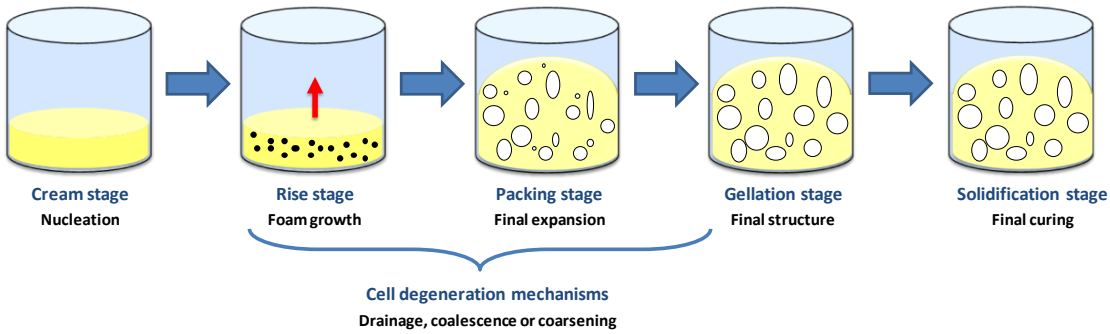

Figure 2.4. Diagram showing the distinct stages of the foaming process for PU foams.

As mentioned above, cell degeneration mechanisms can take place during the foaming process (at the rise and packing stages), and can change the final cellular structure. A brief description of cell degeneration mechanisms is included below (see **Figure 2.5**) [40]:

Drainage is caused by capillary forces action that produces transport of the liquid material from the cell walls towards the struts. This mechanism is most frequently found in the case of low viscosity systems, such as flexible foams.
Coalescence is the rupture of a cell wall separating adjacent cells due to the excessive cell wall thinning, caused by microscopic drainage or other mechanisms. This phenomenon is responsible for cellular structure degeneration because it reduces the number of cells and increases cell size.
Coarsening consists of gas motion promoted by diffusion from the smaller cells (with higher internal pressure) to the larger adjacent cells (with lower internal pressure). Therefore, the small cells disappear and increase the average size of those remaining, or the cellular structure present larger and small cells being very heterogeneous.

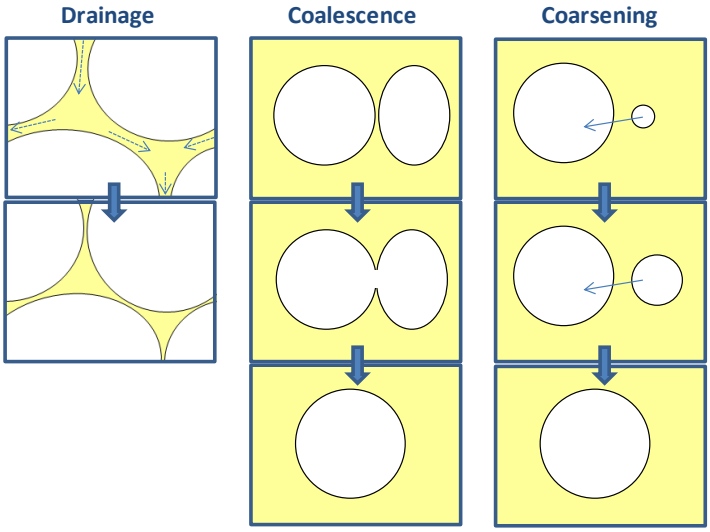

Figure 2.5. Diagram of the cell degeneration mechanisms produced during the foaming process.

2.6- Properties and applications of polyurethane foams

Nowadays PU foams are a fundamental part of our lives since they are employed in a wide range of applications. The final properties of PU foams are the result of a combination of polymer phase morphology, cellular structure and density.

On the one hand, FPU foams with lower cross-linking network and open cell structure have the following properties:

- Lightweight, with good elasticity.
- High load-bearing capacity
- Tearing resistance.
- Breathability.
- Ability to control noise and vibrations.
- Chemically and biologically resistant.
- Long-lasting.
- Easily cut or molded for almost any shape.

FPU foams are cushioning materials used in almost all furniture and bedding, and also they are used as packaging material to protect delicate instruments.

Regarding RPU foams present the following properties, due to their highly cross-linking network and closed cell structure [26, 28]:

- High thermal insulation properties with low thickness.
- Lightweight, with high stiffness and high mechanical strength.
- Chemically and biologically resistant.

- Long-lasting.
- Satisfies fire regulations for particular applications (once they are properly formulated including flame retardants).
- Quickly and easily foaming on site such as spray foaming in place, pour-in-place foaming and one-component foaming by moisture in the air.

Due to their low thermal conductivity and to their high mechanical properties at low weights, the main fields of application for RPU foams include construction, refrigeration, and piping/tubing industries [25]. In the construction industry, RPU foams generally are used to make insulating panels, and to spray *in situ* in order to insulate. RPU foams are one of the most popular foam insulators in the construction industry because they achieve a high insulating capability with thinner material, which supposes lower space requirements. Moreover, their application in construction keeps growing because the regulations for saving energy in buildings are becoming more stringent around the world, as a result of climate change and rising energy cost. In the refrigeration industry, RPU foams are the insulating material most used because they allow the highest energy efficiency. They are also used for this application because they have good mechanical properties, good adhesion of PU foam to the outer shells used in refrigeration appliances, and they allow an easily filling of the complex cavities of refrigerators. RPU foams are used as well for insulating pipes since they reduce very efficiently the heat exchange between the conveyed medium and the environment. In addition to the applications mentioned, they have other applications in windows frames, core of sandwich panels, or in hot-water tanks and boilers, among others.

2.7- Polyurethane foam composites

PU foams display excellent properties, but the incorporation of fillers in PU formulations is a promising strategy to improve their properties even more. This is achieved by the use of micro or nanofillers, which allow to perform and exceed the increasingly demanding requirements of some applications, such as construction, refrigeration and automotive. Moreover, the fillers could lead to save weight, energy and cost.

Since the main applications of RPU foams are on the field of thermal insulation, reducing the thermal conductivity as well as the mechanical properties is an essential issue. Three heat transfer mechanisms account for thermal conductivity: conduction through the gas phase and solid phase, radiation, and convention, which can be considered negligible for cell sizes below 2 mm [41]. Fillers could act as nucleating agent, decreasing the cell size, but could act also as infrared radiation blockers, by reducing the radiation contribution to the thermal conductivity. For example, carbon-based nanofillers such as carbon nanofibers (CNFs), carbon nanotubes (CNTs), graphene derivates or carbon black are good infrared absorbers [42], since they increase the extinction coefficient of PU foams, reducing the thermal conductivity. On the other hand, mechanical properties depend on the properties of the solid material, on the relative density and on the cellular structure of the foam (cell size, cell anisotropy, cell size distribution and fraction of mass in the struts (f_s)). Thus, fillers can enhance the mechanical properties of PU foams by solid PU matrix improvement and by microstructure optimization.

For example, nanoparticles such as CNTs, graphite, graphene, graphene oxide (GO), nanoclays or carbon black have high mechanical and physical properties, and thus their incorporation into PU foams could enhance their mechanical performance of the solid phase [43]. Moreover, fillers may also improve the cellular structure (reducing cell size, improving cellular structure homogeneity, reducing f_s, or increasing anisotropy) what also contributes to improve the mechanical properties.

In particular, fillers of nanoscale sizes (length scale ranging from 0.1 nm to 100 nm) are attracting a great deal of attention nowadays in order to obtain PU foams with enhanced properties based on the modification of the cellular structure and on the reinforcement of the polymeric matrix. The nanofillers present several advantages over microfillers, such as their dimensions below the size of cell walls and struts, as well as their high specific surface area compared to that of microparticles, which allows a higher interaction with the polymer matrix. Due to this, a low amount of nanofillers may induce important modifications on the properties of the PU foam. This is very convenient in the case of RPU foams, because the use of higher amounts of fillers would preclude the production of foams with the low densities required for thermal insulation and structural applications. These reasons have encouraged the research on the incorporation of different types of nanofillers into PU foams, such as nanoclays [44-47], nanosilicas [48, 49], CNTs [50-54], CNFs [55-58] or graphene derivates [51] [59, 60]. As a result of the nanoparticles inclusion, some properties of the PU foams can be improved, such as mechanical and thermal insulation, or new properties can emerge, such as electrical conductivity. Nevertheless, only the addition of nanofillers does not guarantee optimal results, but a good distribution and dispersion are also required. Strong interactions between the nanofillers and the polymeric matrix, which depend on the surface chemistry, size and shape of the nanoparticles, are other requirements [43]. For this reason, many research efforts have been dedicated to the surface modification of the nanoparticles in order to achieve a better compatibility with the polymer chains, and also a better dispersion. This means that testing and development of dispersion techniques, such as the use of ultrasonication, high shear mixing, surfactants, and functionalization of the nanoparticles, are also decisive factors.

An important aspect which is often not considered in most of the research articles published to date is how the incorporation of micro or nanofillers into PU matrix may affect to the reactions involved in PU formation [61]. On the one hand, the functional groups of the fillers surface could interact or react with the functional groups of the PU components (hydroxyl or isocyanate) and/or with the chemical blowing agent (water), thus modifying the urethane/urea products ratio and the isocyanate conversion. On the other hand, the fillers could affect to the rate of polymerization and in particular the rate of the blowing and/or the gelling reaction, which would give rise to changes in the rheological behavior of the reaction mixture and/or the interaction of the nanofiller surface groups with the PU components. Moreover, the fillers could also affect the microphase separation of urethane and urea in PU foams by interfering with the hydrogen bonds formed between ureas or urethanes [62].

Therefore, the presence of fillers may modify the foaming process by increasing or decreasing reaction ratios, leading to a modification of urethane and/or urea linkages, of isocyanate consumption and of microphase separation of urethane and ureas. Thus, the cross-linking

density and the final morphology of the PU matrix, and consequently the properties of the final foam may be also influenced [63]. The fillers have also greater or lesser effects on PU foams depending on several factors, such as the filler content, filler size, filler chemical surface, and PU components, among others. In many cases the fillers improve some properties of PU foams, but they may be worsened sometimes. Hence, understanding how the reactions change when fillers are incorporated in PU foams could help to correct the reaction imbalance by changing the PU formulation. As a consequence, this would allow developing PU formulations reinforced with fillers with positive effects on all the properties. Given the importance of this issue, the metrologies used to follow the changes in the PU reactions are addressed in the following section.

Despite the importance of studying the effect of fillers on the foaming process, most studies to date do not always take it into account, as can be seen in **Table 2.3.** This table collects recent studies focused on improving the thermal and mechanical properties of RPU foams by incorporation of fillers. As we can see, very few of these studies carry out an in-depth evaluation of the effect of fillers on the foaming process and the morphology of the PU matrix. Even many of these studies do not analyze the cellular structure parameters (cell size, anisotropy, open cell content, etc) which also are essential to understand the resulting properties of the foams. Moreover, the table collects the foam properties which are improved or not depending on the type of filler or its content. As a conclusion of these investigations, understanding the effect of the fillers on the foaming kinetics would be essential to make a better use of fillers, and finally to get better cellular structure and foam properties.

Table 2.3. Review of recent research into RPU foam composites: system studied, study of the foaming process, study of the cellular structure parameters, and foam properties (MAINLY thermal conductivity and mechanical properties).

Ref.	System studied (filler used)	Study of the foaming process	Study of the cellular structure parameters	Thermal conductivity and mechanical properties
[64]	Water-blown RPU foam with silica aerogel.	No.	No. Only SEM images were commented without calculating cellular structure parameters.	Compressive mechanical properties and thermal conductivity were enhanced.
[65]	Water-blown RPU biofoam with hydroxyl-functionalized multi-walled carbon nanotubes (MWCNTs) (0.5, 1, 1.5 and 2 wt%).	Yes. FTIR spectroscopy was employed to analyze the reaction or interaction between the PU matrix and the filler.	No. Only SEM images were commented without calculating cellular structure parameter.	Compressive and flexural mechanical properties were enhanced.
[66]	Water-blown RPU foam with ground granulated blast furnace slag and fly ash 5, 8, 10, 20, 40, and 60 wt% of each filler in polyol).	No.	Yes. Cell diameter, cell number density and mean strut thickness were calculated from SEM images.	For both fillers, an increase in tensile strength was observed up to the electrical percolation threshold. Thermal conductivity was not improved.

Ref.	System studied (filler used)	Study of the foaming process	Study of the cellular structure parameters	Thermal conductivity and mechanical properties
[67]	Water-blown RPU foam with nanosilica (Aerosil 380) and nanosilica suspension of nanosilica and ionic liquid (0.5, 1, and 2 wt% of nanosilica).	Yes. The characteristic foaming times (cream, gel and tack-free times) and the maximum foaming temperature were measured.	Yes. Cell diameter, wall thickness and cell size distribution were calculated from SEM images.	0.5 and 1 wt% of nanosilica and nanosilica suspension improved the physic-mechanical properties (compressive strength, three-point bending test, apparent density) and thermal conductivity. However, 2 wt% of content was not improved these properties.
[68]	Water-blown RPU foam with two types of polyhedral oligomeric silsesquioxanes (POSSs) (0.5, 1.5 and 5 wt%).	Yes. The characteristic foaming times (cream, gel and tack-free times) and the maximum foaming temperature were measured.	Yes. Cell diameter, wall thickness and cell size distribution were calculated from SEM images.	The addition of both fillers in an amount of 5 wt% led to samples with reduced compression modulus, compressive strength, thermal transitions, and storage modulus with respect to the foams containing 0.5 and 1.5 wt% of the fillers, mainly due to damaging changes induced by the fillers.
[69]	Water-blown RPU foam reinforced with nanoclay and Silica aerogel (2 and 4 wt% in polyol).	No.	No. Only SEM images were commented without calculating cellular structure parameters.	Thermal conductivity was highly enhanced only for nanoclay addition. In general, the compressive and tensile properties improved with the fillers.
[70]	Water-blown RPU foam with raw and functional MWCNTs (up to 0.2 wt%).	No.	Yes. Cell size, cell wall thickness, cell edge length and cell density were calculated from SEM images.	Fillers showed an enhancement of 13% in compressive strength compared to neat PU foam.
[71]	Water-blown RPU foam filled with MWCNTs and poly (ethylene oxide) grafted MWCNTs (up to 3 wt%).	Yes. The characteristic foaming times (cream, gel and tack-free times).	Yes. Cell size, cross section of cells and anisotropy were calculated from SEM images.	The specific compressive properties (property/density) were improved with the fillers, improving more with poly (ethylene oxide) grafted MWCNTs.
[72]	Water-blown semi-rigid PU foam with aluminum microfibers (0.5, 1, 1.5 and 2 wt%).	No.	No.	This increase in properties (61.81%-compressive strength and 71.29%-energy absorption) was obtained by adding up to 1.5%.
[73]	Water-blown RPU foam filled with silanized MWCNTs (1.5 and 3 wt%)	No.	Yes. SEM images are shown and cell density was calculated.	Tensile mechanical properties were improved with 1.5 wt% of fillers, whereas foams with 3 wt% showed poor results.
[62]	Water-blown RPU foam reinforced with fullerene soot, modified fullerene soot, AL_2O_3 and CrO_3 (up to 0.6 wt%).	Yes. The degree of micro-phase separation in polyurethane-polyurea matrix was determined by deconvolution of carbonyl band in FTIR spectra of the final foams.	Yes. Optical images analysis allowed determining cell size and cell size distribution.	The introduction of nanofillers leads to increase of mechanical strength of the foam with the exception of CrO_3. The predicted thermal conductivity increased with the nanofillers addition.
[74]	Water-blown RPU foam with various contents of graphene oxide (GO) (up to 0.7 wt%) and graphite (up to 5 wt%).	No.	No. Only SEM images were commented without calculating cellular structure parameters.	The compressive strength improved by 5% and by 10% for 1 wt% of graphite and 0.05 wt% of GO, respectively. Thermal conductivity was not reduced with GO, but it was slightly reduced by 0.1% with 1 wt% of graphite.
[75]	Cyclopentane- water blown RPU foam reinforced with TiO_2 nanoparticles and halloysite clay nanotubes (uo to 10 wt%).	No.	Yes. Cell size and cell density were calculated by SEM analysi.	The compressive mechanical properties were enhanced only with high contents of fillers (6, 8 and 10 wt%). Thermal conductivity was reduced with fillers addition after 3 days of foam production, but this worsen in all the foams after 10 days.

Ref.	System studied (filler used)	Study of the foaming process	Study of the cellular structure parameters	Thermal conductivity and mechanical properties
[76]	A series of RPU foams with different types of blowing agents (CFC-11, cyclopentane, pentane or hexane) and with silica aerogel (1–5 wt%).	No. FTIR spectroscopy was used in order to observe if there is reaction between silica aerogel and isocyanate or polyol matrix.	No. Only SEM images were commented without calculating cellular structure parameters.	The thermal conductivity of nanocomposite foams for all blowing agents was less than the pure foams. Also, the mechanical properties improved for nanocomposite foams, particularly for lower silica aerogel contents (1 wt.% and 3 wt%).
[77]	Three different types of water-blown RPU foams with granular silica aerogel and powdered silica aerogel (up to 4 wt%).	No.	No. Only SEM images were commented without calculating cellular structure parameters.	Thermal conductivity of foams did not enhance by adding silica aerogel.
[78]	Water-blown RPU foam reinforced with nanoporous graphene (0.5–5 wt%).	No.	No. Only SEM images were commented without calculating cellular structure parameters.	Only 0.25 wt % of fillers improved compressive strength and modulus respectively by 10.7% and 66.5%.
[79]	Cyclopentane-water blown RPU foam reinforced with glass fibre (5, 10 and 20 wt%).	No.	No. Only SEM images were commented without calculating cellular structure parameters.	Fibre reinforcements increased the mechanical properties of the foam in a significant manner (up to 121% increase in stiffness and 101% increase in strength), proportionally with the increase in fibre mass content.
[80]	Water-blown RPU foam with titanium dioxide, zinc oxide, and magnetite nanofillers (1 or 10 wt% in polyol)	Yes. Reaction kinetics were followed by FTIR spectroscopy (isocyanate conversion was studied).	Yes. Some parameters of cellular structure were measured or commented from SEM images.	Thermal and mechanical properties did not study.
[81]	RPU foam blown HCFC-141 b and filled with MWCNTs (0.1, 1 and 2 wt%)	No.	Yes. Optical and SEM images were commented and cell size and cellular density were calculated.	The thermal conductivity showed a modest increase with increased MWCNTs content.

2.8- Monitoring of foaming process of polyurethane foams

As indicated previously (**section 2.3.1**), the reaction kinetics of PU foams are very complex because they involve simultaneous reactions which are responsible for the final morphology of the PU matrix and microstructural characteristics, and therefore affect to final properties of the resulting foams. The balance of the PU reactions can be modified by the addition of the fillers, by changes in PU components, or by foaming conditions, among others, and for this reason understanding how these reactions take place is a decisive factor. Historically, Fourier transform infrared (FTIR) spectroscopy has proven to be a very useful tool to investigate both the reaction kinetics and the morphology development during the foaming process [82-85]. In PU foams, analysis of the FTIR spectra must be carried out by studying specific bands. The most studied bands are the isocyanate band at 2270 cm^{-1}, corresponding to asymmetric stretching vibrations of the isocyanate group, and the amide I or carbonyl region (1800-1600 cm^{-1}) corresponding to stretching vibrations of the carbonyl groups present in reaction products. However, the carbonyl region may contain many hidden bands corresponding mainly to the gelling reaction (urethane compounds such as free urethane and hydrogen-bonded urethanes), and blowing reaction (urea compounds such as free urea and hydrogen-bonded

ureas, which include both monodentate, or disordered, and bidentate, ordered) (see **Table 2.4**). The frequencies of the hidden bands in the carbonyl region can be established from the second-derivative spectra, and then each absorption can be identified, separated, and quantified by deconvolution [82, 83, 86-89]. Given the difficulty of the deconvolution analysis of the carbonyl region, most of the investigations studied only the intensity changes of the total bands (amide I).

Table 2.4. Carbonyl stretching assignments in PU foams.

Functional group	Frequency (cm^{-1})	Band assignment	Structure
ν (C=O) Urethane (Gelling reaction)	1740-1730	**Free urethane** (Urethane groups free from hydrogen bonds). [19, 85, 90-94]	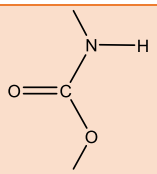
	1730-1725	**Hydrogen-bonded urethane hard segment/soft interaction** (Ether polyol hydrogen-bonded urethane). [90-94]	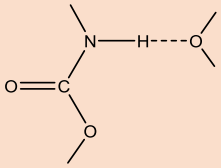
	1715-1700	**Hydrogen-bonded urethane hard segment/ hard segment interaction** [90-94]	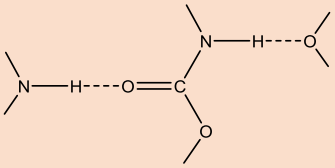
ν (C=O) Urea (Blowing reaction)	1700-1690	**Free Urea** (Urea groups free from hydrogen-bonds). [84, 85, 90, 95]	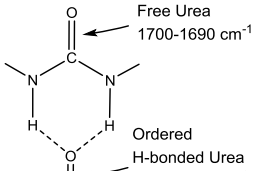
	1690-1650	**Monodentate or disordered hydrogen-bonded urea** [19, 90]	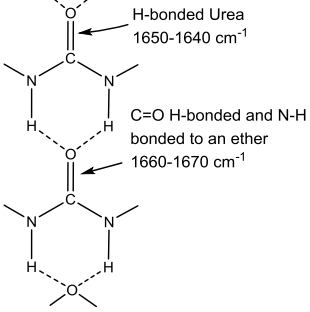
	1670-1660	**C=O Hydrogen-bonded and N-H bonded to an ether group** [95]	
	1650-1640	**Bidentate or ordered hydrogen-bonded urea** [19, 84, 85, 90, 95-97]	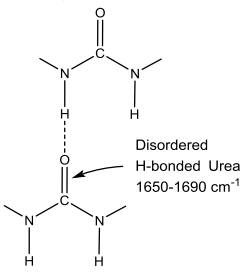

Since the inclusion of fillers in the PU matrix is an attractive strategy to enhance the properties of PU foams, most of the published articles have been focused on the production and characterization of the foams. Some of these studies are focused on the effect of fillers on the reaction kinetics and on the development of the PU morphology during the foaming process [62, 80, 96, 98, 99]. The following paragraphs collect a brief summary of those studies focused on the effect of fillers on the reaction kinetics and/or the morphology of PU foams monitoring the isocyanate and/or carbonyl bands by ATR-FTIR spectroscopy.

Wilkinson *et al.*(2007) [98] prepared water-blown FPU foams infused with unmodified Na^+ montmorillonite (MMT) at a concentration of 5 or 10 wt% in the final foam. FTIR data showed a significant increase in the rate of isocyanate decay as MMT content was increased, in agreement with the adiabatic temperature rise profiles that were also measured. The absorbance changes in soluble and hydrogen-bonded urea group contents in the HS phases were used to determine the microphase-separation times. These times decreased for nanocomposites foams, but the formation of hydrogen-bonded urea of HS phase was higher for reference foam (without MMT) at longer times.

Bernal *et al.*(2011) [96] investigated the influence of chemically inert multi-walled CNTs (MWCNTs) and functionalized MWCNTs (f-MWCNTs) bearing oxygen-containing groups over the surface on the foaming process of water-blown FPU foams. They studied foams containing 0.1 or 0.5 phpp (parts by hundred parts of polyol), which correspond to 0.06 or 0.33 wt% of the final foam. A decrease of isocyanate conversion rates at the early stages was observed when the MWCNTs amount increases, what was explained considering that the high initial viscosity of the systems with MWCNTs induced a lower mobility of the molecules during the reaction. Moreover, the onset of the microphase separation (the formation of ordered hydrogen-bonded urea) was influenced by the presence of functional groups on the MWCNT surface. The same group (2012) [99] later reported a kinetic study of water-blown FPU foams with two contents of HS (25% or 32.5%) filled with MWCNTs, f-MWCNTs or functionalized graphene sheets (FGS) (0.5 phpp which correspond to 0.33 wt% of the final foam). **Figure 2.6** shows the deceleration of the rate of polymerization due to the increase of the HS content and to the inclusion of the nanoparticles. In the case of HS systems, the decrease in the rate and isocyanate conversion was attributed to an increase in the viscosity of the system and thus to a restriction of the chain mobility due to the larger HS content. In the case of the nanofillers system, the chain mobility was also affected by both the viscosity effect and by the hindrance to the formation of hydrogen bonds between the HS.

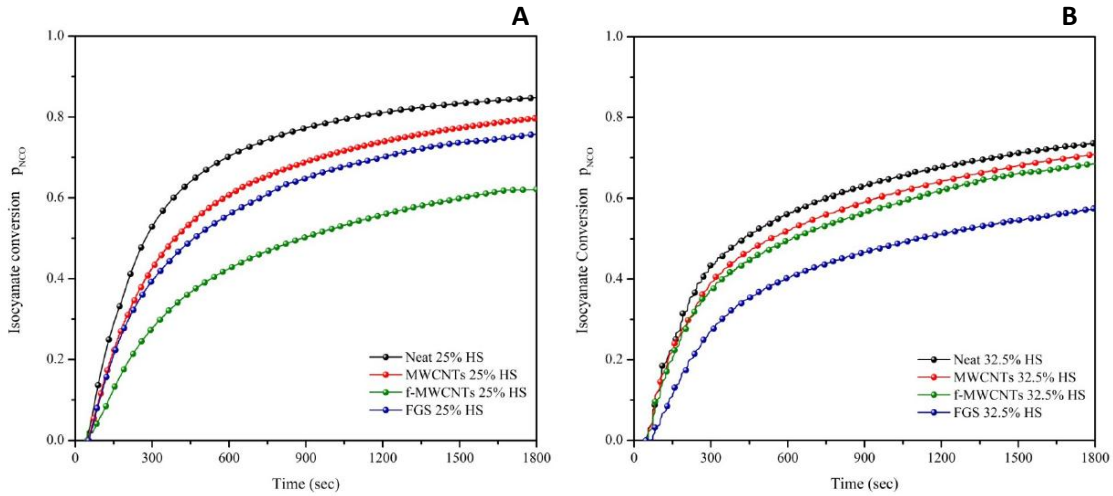

Figure 2.6. Isocyanate conversion, pNCO, for FPU nanocomposite foams with 25%HS (A) and for FPU nanocomposite foams with 32.5%HS (B). [100]

Akkoyun *et al.*(2016) [80] studied the effects of different different types, shapes and concentrations of titanium dioxide, zinc oxide, and magnetite nanofillers (1 or 10 wt% in polyol) on the RPU foam formation reaction. The results of the isocyanate conversion showed that, regardless of the nanofiller type, the reaction rate increased as the surface area increased beyond a critical surface area of nanofillers (30 m^2 in this study). Moreover, the nanofillers reduced the final cell size below the critical surface area, whereas above this critical value the cell size distribution was wider. Thus, the increase of the reaction rate facilitated uncontrolled cell nucleation, growth, and hence coalescence, which resulted in an uncontrolled foam structure.

Pikhurov *et al.*(2018) [62] prepared water-blown RPU foams reinforced with nanofillers of different nature (fullerene soot containing fullerenes with hydrophobic surface, modified fullerene soot with neutral hydrophilic surfaces, Al_2O_3 nanoparticles with acidic or basic hydrophilic surfaces, or Cr_2O_3 nanoparticles with acidic hydrophilic surfaces) at concentrations 0.075–0.6 wt%. The effects of these fillers on the foam morphology were investigated by using ATR-FTIR spectroscopy. The different hidden peaks of the free and hydrogen-bonded groups were obtained by deconvolution of the carbonyl region in order to calculate the degree of phase separation (DPS) for urethane bonds and for urea bonds (**equation 2.2**), thus obtaining a measurement of the micro-phase separation (**Table 2.5** collects the DPS values).

$$DPS = \frac{A_b}{A_f + A_b} \qquad (Equation\ 2.2)$$

A_b and A_f are the deconvoluted area of hydrogen-bonded and free molecular groups, respectively. The FTIR results indicate that the foams with hydrophilic nanofillers (modified fullerene soot, Al_2O_3 and Cr_2O_3), able to form hydrogen bonds with urethane and urea groups, increased DPS for urethane bonds in all concentrations, compared to the reference foam. However, DPS for the urea bonds were practically the same as that in the reference and did

not depend on concentration or type of filler. However, no correlations could be found between mechanical performance and DPS.

Table 2.5. DPS values obtained from FTIR analysis (Adapted from [62]).

Loading (wt%)	DPS for urethane bonds	DPS for urea bonds
Reference	0.915	0.557
Fullerene soot		
0.075	0.799	0.214
0.15	0.733	0.23
0.3	0.747	0.225
0.6	0.858	0.437
Modified fullerene soot		
0.075	0.988	0.589
0.15	0.990	0.625
0.3	0.989	0.621
0.6	0.993	0.63
Al_2O_3		
0.075	0.959	0.547
0.15	0.956	0.545
0.3	0.959	0.534
0.6	0.959	0.525
CrO_3		
0.075	0.966	0.535
0.15	0.981	0.544
0.3	0.953	0.547
0.6	0.960	0.573

In addition to FTIR spectroscopy, other methods can be used to obtain additional kinetic information, such as measuring the adiabatic temperature raise. It is directly measured during the foaming process by thermocouples inside the foam, since the gelling and blowing reactions are exothermic. Once the cellular structure of the PU foam has been formed, the center of foam is isolated from its surroundings, so it may be considered as an adiabatic system. Thus, the adiabatic temperature monitoring of the PU foam may be related to the kinetics of the reaction, and hence to the consumption of isocyanate in both gelling and blowing reactions [101]. The foaming temperature as a function of time has been measured in several articles to determine the effect caused on the reaction kinetics of PU foams by: different blowing agents [102, 103], different contents of bio-polyols [9, 104] or nanofillers [59, 98, 105].

Some studies of nanocomposite foams described an increase of the foaming temperature when nanofillers are incorporated in water-blown RPU foams [59, 98, 105]. Bernal *et all.* (2014) [59] studied RPU foams filled with MWCNTs, f-MWCNTs or FGS (0.4 or 0.8 phpp, which corresponded to 0.17 or 0.35 wt% of the final foam) to obtain electromagnetic interference (EMI) shielding materials. The extent of conversion of RPU nanocomposite foams was followed by adiabatic temperature raise (**Figure 2.7**). The final degree of conversion was similar for all

samples, but those with nanofillers showed faster conversion rates during the initial stages of the reaction than the reference foam. The acceleration of the reaction was favoured by the high thermal conductivity in the system with MWCNTs, and by the low viscosities and surface functionalities in the system with f-MWCNTs and FGS. Similar results were obtained by Wilkinson *et al.*(2007) [98] using the adiabatic temperature rise method for RPU foams with MMT (0, 5 or 10 wt% in foam). In the initial stage, a significant increase in the rate of reaction when increasing MMT content was detected, due possibly to a surface catalytic effect related to the high-surface area of the MMT. Ahn *et al.* (2015) [105] also observed a faster and higher temperature raise with time for RPU foams containing MWCNTs (0.005-0.1 phpp). This could be understood as a result of the creation of cells with smaller sizes and of a more uniform cell size distribution due to the nucleating effect of MWCNT.

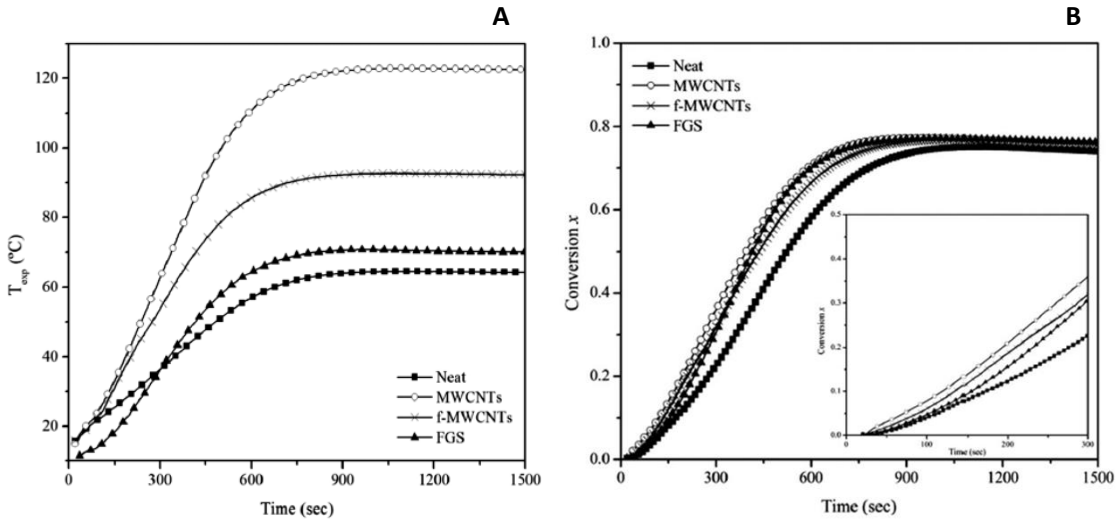

Figure 2.7. (A) Variation of the experimental temperature (T_{exp}) with time for RPU nanocomposite foams. (B) Variation of the conversion x with time for RPU nanocomposite foams [59].

Finally, X-ray radioscopy allows to collect a great deal of information of the PU foaming process. The use of this technique in combination with image analysis allows determining the evolution of relative density and cell size, as well as to calculate cell nucleation density during the whole foaming process (**Figure 2.8**). This technique was applied for the first time by our group (Pardo-Alonso *et al*, 2012) [106] in order to evaluate the effect of nanoclays content (0.5, 1, 3 or 5 wt% of Cloisite®30B) on the foaming process of water-blown RPU foams. No significant changes of the relative density were found (**Figure 2.8.A**). However, a noticeable cell size reduction was observed as the amount of nanoclays increased, being reduced to a half for the foam with 5 wt% nanoclays (**Figure 2.8.B**). The cell nucleation density also increased with the content of nanoclays, and it remained constant with time, thus confirming the absence of cell coalescence (**Figure 2.8.C**). Our group (2013) [107] also analyzed by X-ray

radioscopy the effect of different nanofillers (1 or 5 wt% contents of nanoclays (Cloisite®30B) or nanosilicas (Aerosil®A200 and Aerosil®R812)) on the cellular structure of water-blown RPU foams. Both nanoclays and nanosilicas showed a significant cell size reduction, being nanoclays those promoting higher cell nucleation density. Moreover, none of the nanoparticles induced coalescence in the RPU system. Another X-ray radioscopy study was carried out by Bernal *et al.* (2014) [108]. The cellular structure and density evolution were monitored for water-blown FPU foams with MWCNTs, f-MWCNTs or FGS (0.5 phpp, which corresponded to 0.33 wt% of the final foam). At early stage, a significant cell nucleation enhancement was detected for MWCNT (hydrophobic surface) and FGS (hydrophobic/hydrophilic surface), but these particles induced higher coalescence and thus the cell size reduction was lost at the final stage. Instead, f-MWCNT (hydrophilic surface) promoted a similar number of cells than neat FPU foam without coalescence. Thus, the surface nature of the carbon nanoparticles affected the physical events occurring on the PU nanocomposite foams, what is correlated with the chemical modifications observed for these systems by in situ FTIR [99].

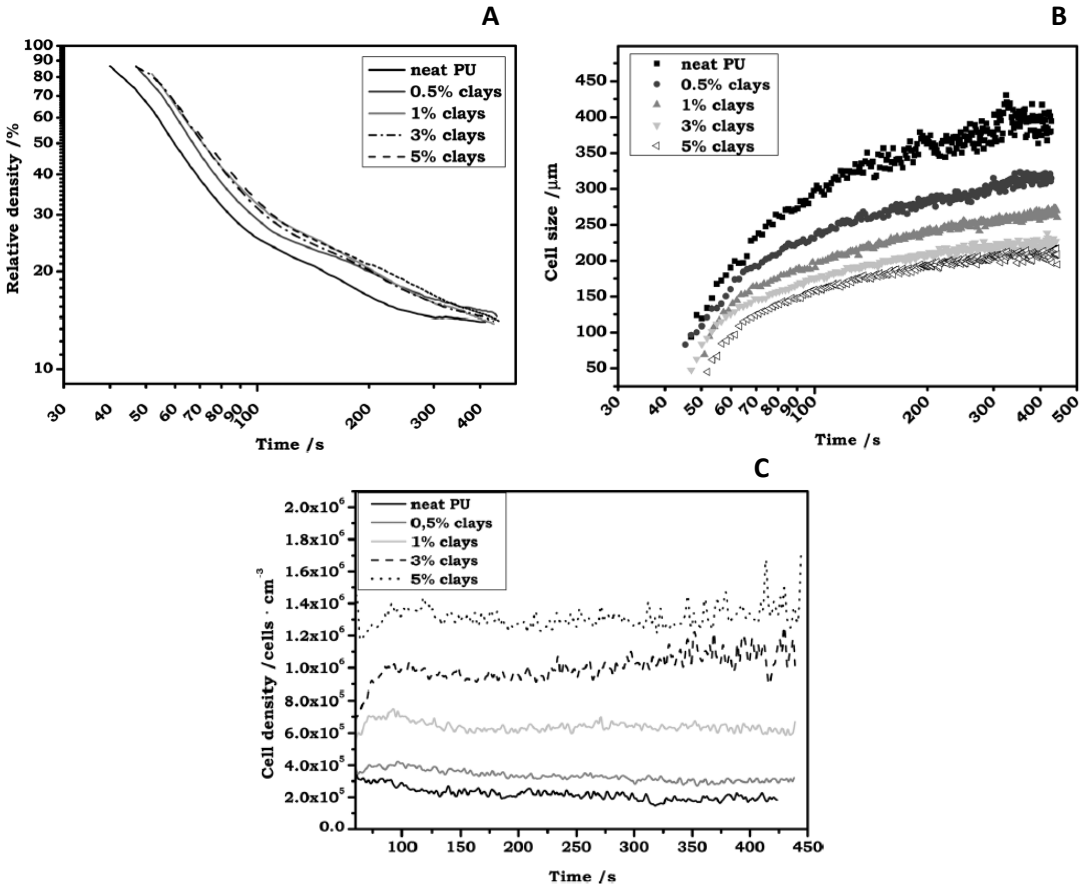

Figure 2.8. (A) Relative density evolution; **(B)** cell size evolution and **(B)** cell density evolution during the PU foaming process for neat PU foam and foams containing 0.5, 1, 3 or 5 wt% of nanoclays [106].

The review of the different techniques used to study the foaming process allows concluding that they provide complementary information. FTIR spectroscopy allows to follow the reaction kinetics and the composition of PU matrix during the foam formation. The measurements of foaming temperature also provide information on the reactivity of the system. Finally, the X-ray radioscopy allows analysing the foaming mechanisms produced (cell nucleation and growth and degeneration mechanisms such as nucleation, cell growth, pore coalescence and coarsening) at all intermediate stages during the foaming process. Thus, the combination of the information provided by each technique can help us to understand the final properties of the PU foams, and thus to improve the PU formulation. As it was explained in **Chapter 1**, this is one of the main objectives of this research.

2.9- Thermoplastic polyurethane foams

2.9.1- Thermoplastic polyurethanes

One of the most important types of PU material is TPU, which is a thermoplastic elastomer discovered in 1958 [109]. TPU combines advantages of both thermoplastics (melt-processability) and elastomers (elasticity). Hence, TPUs are very versatile materials, which can exhibit properties ranging from very soft thermoplastic elastomers to strong, rigid thermoplastics, depending on their chemical composition, backbone structures and resultant microphase separation [88]. Given the possible combinations of TPU properties, these materials have many applications in automotive components, textile fibers, adhesives, wire and cable sheathings, footwear, and biomaterials [27, 29].

TPUs are usually produced by the polyaddition reaction of a diisocyanate with two other reactants: a macrodiol and a low chain diol or diamine, that acts as chain extender (**scheme 2.1**). TPUs consist of linear segmented block copolymers composed of alternating SS and HS which are flexible (SS) and rigid (HS) polymeric chains which resemble the behavior of an elastomer, but they lack permanent cross-links. The thermodynamic incompatibility between SS and HS gives rise to a two-phase microstructure, in which the HS from the diisocyanate and the chain extender segregate into semicrystalline domains through physical cross-links, whereas the SS from the macrodiol chains form amorphous domains in which the HS are dispersed (**Figure 2.9**) [110]. Therefore, HS offers rigidity, and SS provides flexibility to the TPU material, and their ratio and distribution are determined by different chemical and structural factors, including the polymerization procedure used for their synthesis and the processing conditions [111]. Moreover, the final properties of TPUs are generally attributed to their morphological structure, and they can be adequately tuned by changing the components, the ratio of SS and HS and the reaction steps.

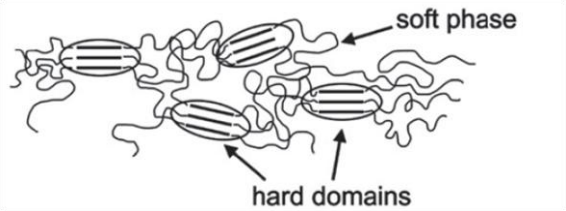

Figure 2.9. Schematic illustration of TPU morphology [112].

TPUs with different properties can be manufactured due to the commercial availability of a large number of starting compounds. These are the following: diisocyanate, macrodiol and chain extender.

-Isocyanates: are difunctional and monomeric with a low molecular weight of around 150-250 [113]. Isocyanates in TPUs have a double function: (1) reacting with the macrodiol to produce the urethane-sparse TPU SS, and (2) reacting with the chain extender to generate HS in the TPU backbone [113]. The isocyanates most used are TDI and MDI (see **section 2.4.2**).

-Macrodiols: are polyester or polyether diols with long chains with molecular weights of around 500-4000 [113]. Macrodiols comprise the SS, so as for example longer macrodiols give more flexible TPUs. Some examples of macrodiol are polyethylene oxide glycol, oxytetramethylene glycol and poly (tetramethylene adipate) glycol.

-Chain extenders: are typically diols or diamines with low chains of molecular weight around 100-350 [113]. For example, shorter chain extenders favor more crystalline TPUs, that are tougher and with a higher strength [114]. Some examples of chain extenders are 1-ethanediol, 1,3-propanediol, 1,5-pentanediol or ethylene diamine.

TPUs can be synthesized by two basic polymerization methods: one-step process and two-step process (the latter also called pre-polymer process) [113].

- One-step process: All of TPU components (diisocyanate, macrodiol and chain extender) are mixed together at the same time (**Scheme 2.17**).

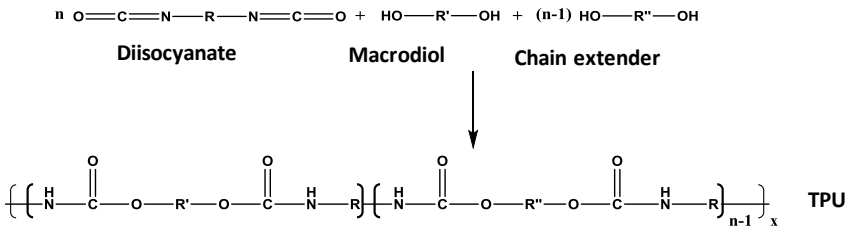

Scheme 2.17. Synthesis of TPU by one-step process [113].

-Two-steps process: In a first step, the macrodiol reacts with an excess of the diisocyanate to form an isocyanate-terminated prepolymer. Then, the isocyanate-terminated prepolymer

reacts with the chain extender in the presence of other additives such as solvent and catalyst, resulting in the formation of the high molecular weight TPU (**Scheme 2.18**). This two-steps is the one used in our research.

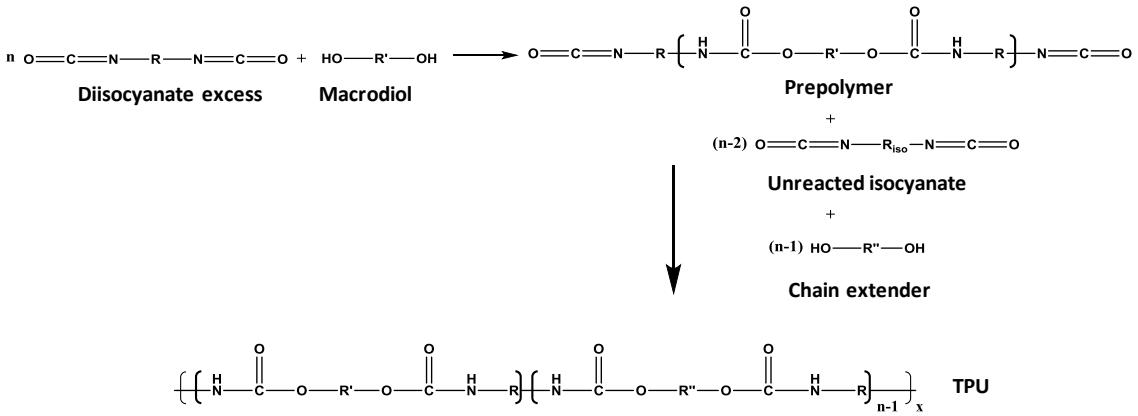

Scheme 2.18. Synthesis of TPU by two-step or pre-polymer process [113].

Synthesized TPUs are marketed as a fully reacted product which can be processed by conventional thermoplastic processing methods such as injection molding, compression molding, and extrusion, in order to obtain their final form, or by solvent processing to form coatings, adhesives, and films.

2.9.2- Foaming of thermoplastic polyurethanes

The use of TPU products has some limitations, such as their high cost and the middle up to high hardness. These limitations can be reduced by TPU foaming, which allows decreasing the weight of the material for a given part and thus its cost. Moreover, foamed TPU reduce the material hardness without additional plasticizers, being able to produce soft grades. Thus, TPU foams have interesting properties, such as light-weight, highly flexible, a great cushioning effect, and fast energy restoration in compression [115]. Furthermore, the use of TPU foams shows enormous advantages compared to thermoset PU foams, given that TPU foams are elastic thermoplastically processable materials, and also they can be reprocessed or recycled due to their non-chemical crosslinked structure. For all this, TPU foamed products are nowadays very interesting materials for several industries, such as furniture, automotive, sportswear, and packaging [115].

Several foaming processes have been used to produce TPU foams, such as extrusion foaming [116], injection foaming [117, 118] reaction foaming [119], and gas dissolution foaming in an autoclave [120, 121]. The two most popular processes are extrusion and injection foaming, due to their higher production efficiencies. On the other hand, the gas dissolution foaming in an autoclave gives rise to high quality foams, and for this reason it has been recently used to

produce foamed TPU at the lab scale [120-127]. Due to its interest, we chose this process in order to study the foaming of a series of TPU materials synthesized with different HS contents (**chapter 7**). The gas dissolution process is a discontinuous (batch) foaming process, in which the polymer is saturated with a gas (usually CO_2) at constant temperature and pressure inside a high-pressure vessel (autoclave). Then the system is supersaturated by reducing pressure, leading to the phase separation of the dissolved gas and thus promoting the nucleation and growth of cells. It is remarkable that in TPU foaming, the solubility of CO_2 is significantly higher in the polyol (SS) than in the HS [123], thus the TPU morphology directly affects to its foaming behavior and final foam structure. Changing the starting components, the HS/SS ratio, or the production process allows creating microcellular or even nanocellular foams which would have a high interest as superinsulating materials.

This paragraph collects a review of those investigations focused on studying the foaming behavior of TPU by gas dissolution foaming in an autoclave. Dai et al. [122] foamed TPU films synthesized from 4,4-diphenylmethanediisocyanate (MDI), poly-tetramethyleneglycol (PTMG) and 1,3-propylenediamine components by a one-step foaming method. Processing conditions, such as pressure, temperature, and foaming time, and their effect on the foam morphology were investigated. The resulting TPU foams showed an improvement in their damping performance. TPU foamed at 35 °C, 18 MPa and 160 min reached the lowest cell size of *ca*. 4μm, a cell density of *ca*. 10^{11} cells/cm^3 and a foam density of *ca*. 0.4 g/cm^3. Ito et al. [123] studied the effect of the chain length of the SS and the HS contents on the cellular structure of TPU foams obtained by a two-step foaming. They concluded that the solubility of CO_2 in the SS is considerably higher than that in the HS. Rizvi et al. [124] obtained TPU nanocomposites foams produced by one-step foaming from a commercial TPU reinforced with different concentration (from 0 to 10 wt%) of multiwall carbon nanotubes (MWCNTs). TPU foam with 4 wt% of MWNT has the smallest cell size of 2.7 μm, the greatest cell density of 6.7 x 10^{10} cells/cm^3 and a relative density of *ca.* 0.46. The thermal, electrical and piezoresistive properties of these nanocomposites foams were investigated and correlated with the MWNT concentration, and with the microstructure of the materials. Prasad et al. [125] used commercial TPUs with different hardness to obtain porous chemical mechanical polishing (CMP) pads, changing the processing conditions. They concluded that the cellular structure of the TPU foams synthesized by a two-step foaming is related to the hardness of the polymer matrix. Yeh et al. [120] foamed a commercial TPU with Cloisite® 30B nanoclay (1,3 and 5 wt%) in order to promote cell nucleation and to increase the cell density. The cell size of the final nanocomposite foams decreased to 1 μm, and the cell density increased to 3 x 10^{11} cells/cm^3 even after using a short foaming time of 5 s either at 150°C in a two-step foaming, either at a lower foaming temperature (70°C) in a one-step foaming. In a later study, this group [126] obtained a nanocellular TPU foam by adding Cloisite® 30B nanoclay, at 60°C in a one-step foaming. The lowest cell size reached was *ca*. 0.45 μm when the saturation and foaming conditions were 13.79 MPa and 50°C. This foaming process gave a cell density of 10^{11} cells/cm^3, and a relative density of 0.9–0.95. The same group [121] later reported the synthesis of a TPU based on MDI, 1,4-butanediol (BD) and polypropylene glycol (PPG). One-step foaming afforded a cell size reduction up to 2 μm when the foaming temperature decreased up to 20°C. The decrease of cell size was stabilized at 20°C, but the foam presented a non-uniform cell structure below 20°C. Moreover, the authors also reported that pre-mixing TPU before

foaming produced a higher cell size reduction, and a more homogeneous cellular structure. In a posterior study, these researchers [127] used three different approaches in order to obtain TPU nanocellular foams by a one-step foaming from previously synthesized TPU: increasing the HS content, replacing the SS type, and adding a graphene nucleation agent. All three approaches were able to produce cell sizes of less than 1 µm. Although increasing the HS content generated a minimum average cell size of 0.5 µm, the cell size distribution was heterogeneous and the relative density was as high as 0.91, for saturation and foaming conditions of 50°C and 13.6 MPa. The best results were obtained for TPU foams with 0.1 wt% of graphene, because their cell structure was homogeneous with an average cell size of 0.7 µm, the cell density improved to 4.94×10^{11} cells/cm^3, and a low relative density of 0.77 was reached, for saturation and foaming conditions of 20°C and 13.6 MPa.

As we have seen, most of the previous works reported in the literature have studied the foaming of commercial TPUs in which their chemical composition is not usually known and thus it is harder to understand their foaming behaviour. For this reason, our research,included in **chapter 7**, has focused on obtaining a new series of synthesized TPUs with known chemical composition in order to relate this to the foaming behavior.

2.10- References

[1] M. Ionescu, Chemistry and Technology of Polyols for Polyurethanes, Rapra Technology Limited: Shawbury, UK, 2005.
[2] O. Bayer, W. Siefken, H. Rinke, L. Orthner, H. Schild, German Patent DRP 728981: Verfahren zur Herstellung von Polyurethanen bzw. Polyharnstoffen. "A process for the production of polyurethanes and polyureas". in: I.G.Farbenindustrie (Ed.)Germany, 1942.
[3] R.B. Seymour, Pioneers in Polymer Science, Dordrecht/Boston/London: Kluwer Academic Publishers, 1989.
[4] K. Zaunbrecher, h. Barth, Japanese Patent Publication Nº. Sho-33-8094,1958, in: F. A.G. (Ed.), 1942.
[5] A.S. Dutta, Polyurethane Foam Chemistry, (2018) 17-27.
[6] J.W. Gooch, Urethane Polymers, in: J.W. Gooch (Ed.) Encyclopedic Dictionary of Polymers, Springer New York, New York, NY, 2011, pp. 785-785.
[7] E. Sharmin, F. Zafar, Polyurethane: An Introduction, (2012).
[8] P. Cognard, Handbook of Adhesives and Sealants: Basic Concepts and High Tech Bonding, 2005.
[9] S. Tan, T. Abraham, D. Ference, C.W. Macosko, Rigid polyurethane foams from a soybean oil-based Polyol, Polymer, 52 (2011) 2840-2846.
[10] G. Oertel, Polyurethane Handbook 2nd ed., Hanser Publishers, Munich, 1993.
[11] M.F. Sonnenschein, Polyurethanes: Science, Technology, Markets, and Trends, 2015.
[12] M. Szycher, Szycher's Handbook of Polyurethanes, Second ed., CRC Press Boca Raton, Florida, USA, 2012.
[13] A. Lapprand, F. Boisson, F. Delolme, F. Méchin, J.P. Pascault, Reactivity of isocyanates with urethanes: Conditions for allophanate formation, Polymer Degradation and Stability, 90 (2005) 363-373.
[14] D.K. Chattopadhyay, K.V.S.N. Raju, Structural engineering of polyurethane coatings for high performance applications, Progress in Polymer Science, 32 (2007) 352-418.

[15] K. Dusek, M. Spirkova, I. Havlicek, Network Formation of Polyurethanes Due to Side Reactions, Macromolecules, 23 (1990) 1774-1781.
[16] M. Špirková, M. Kubín, K. Dušek, Side Reactions in the Formation of Polyurethanes: Model Reactions Between Phenylisocyanate and 1-Butanol, Journal of Macromolecular Science: Part A - Chemistry, 24 (1987) 1151-1166.
[17] J. Zou, Y. Chen, M. Liang, H. Zou, Effect of hard segments on the thermal and mechanical properties of water blown semi-rigid polyurethane foams, Journal of Polymer Research, 22 (2015).
[18] N. Mahmood, J. Kressler, K. Busse, Structure analysis in polyurethane foams at interfaces, Journal of Applied Polymer Science, 98 (2005) 1280-1289.
[19] W. Li, A.J. Ryan, Effect of Chain Extenders on the Morphology Development in Flexible Polyurethane Foam, Macromolecules, 35 (2002) 6306–6312.
[20] A.M. Heintz, D.J. Duffy, C.M. Nelson, Y. Hua, S.L. Hsu, W. Suen, C.W. Paul, A Spectroscopic Analysis of the Phase Evolution in Polyurethane Foams, Macromolecules, 38 (2005) 9192-9199.
[21] D.V. Dounis, G.L. Wilkes, Structure-property relationships of flexible polyurethane foams, Polymer 38 (1997) 2819-2828.
[22] D. Klempner, V. Sendijarevic, Handbook of Polymeric Foams and Foam Technology, Hanser 1991.
[23] K. Efstathiou, PhD Thesis: Synthesis and characterization of a Polyurethane Prepolymer for the development of a novel Acrylate-based polymer foam, Budapest University of Technology and Economics (BME), 2011.
[24] R. Leppkes, Polyurethanes, material with many faces, Verlag Moderne Industrie AG; 4th edition, (2004).
[25] H.W. Engels, H.G. Pirkl, R. Albers, R.W. Albach, J. Krause, A. Hoffmann, H. Casselmann, J. Dormish, Polyurethanes: versatile materials and sustainable problem solvers for today's challenges, Angewandte Chemie, 52 (2013) 9422-9441.
[26] Handbook of Polymer Foams, Rapra Technology Limited, Shawbury, Shrewsbury, Shropshire, SY4 4NR, UK, 2004.
[27] Herman F. Mark: Encyclopedia of Polymer Science and Technology, concise, 3rd Edition, 2008.
[28] K. Ashida, Polyurethane and related foams: Chemistry and Technology, CRC Press2007.
[29] J.O. Akindoyo, M.D.H. Beg, S. Ghazali, M.R. Islam, N. Jeyaratnam, A.R. Yuvaraj, Polyurethane types, synthesis and applications – a review, RSC Advances, 6 (2016) 114453-114482.
[30] G. Rokicki, P.G. Parzuchowski, M. Mazurek, Non-isocyanate polyurethanes: synthesis, properties, and applications, Polymers for Advanced Technologies, 26 (2015) 707-761.
[31] D.C. Allport, D.S. Gilbert, S.M. Outterside, MDI and TDI: A Safety, Health and the Environment: A Source Book and Practical Guide., John Wiley & Sons Ltd., Chichester, 2003.
[32] S.T. Lee, N.S. Ramesh, Polymeric foams: mechanisms and materials, Boca Raton, Florida, USA, 2004.
[33] H. Ulrich, Kirk-Othmer Encyclopedia of Chemical Technology, 1937 (2006).
[34] K.H. Choe, D.S. Lee, W.J. Seo, W.N. Kim, Properties of Rigid Polyurethane Foams with Blowing Agents and Catalysts, Polymer Journal, 36 (2004) 368-373.
[35] S. Estravís, J. Tirado-Mediavilla, M. Santiago-Calvo, J.L. Ruiz-Herrero, F. Villafañe, M.A. Rodríguez-Pérez, Rigid polyurethane foams with infused nanoclays: Relationship between cellular structure and thermal conductivity, European Polymer Journal, 80 (2016) 1–15.
[36] C. Torres-Sánchez, J. Corney, Identification of formation stages in a polymeric foam customised by sonication via electrical resistivity measurements, Journal of Polymer Research, 16 (2008) 461-470.
[37] A.J. ROJAS, J.H. MARCIANO, R.J. WILLIAMS, Rigid Polyurethane Foams: A Model of the Foaming Process, POLYMER ENGlNEERlNG AND SCIENCE, 22 (1982) 840-844.

[38] R.A. Neff, C.W. Macosko, Simultaneous measurement of viscoelastic changes and cell opening during processing of flexible polyurethane foam, Rheologica Acta, 35 (1996).
[39] D. Niyogi, R. Kumar, K.S. Gandhi, Water Blown Free Rise Polyurethane Foams, Polymer engineering and science, 39 (1999) 199-209.
[40] I. Cantat, S. Cohen-Addad, F. Elias, F. Graner, R. Höhler, O. Pitois, F. Rouyer, A. Saint-Jalmes, S. Cox, Foams: Structure and Dynamics, Oxford University Press2013.
[41] L. Glicksman, Low Density Cellular Plastics: Physical Basis of Behaviour, Springer Netherlands, London, 1994.
[42] J. Shen, X. Han, L.J. Lee, Nanoscaled Reinforcement of Polystyrene Foams using Carbon Nanofibers, Journal of Cellular Plastics, 42 (2016) 105-126.
[43] A. Kausar, Polyurethane Composite Foams in High-Performance Applications: A Review, Polymer-Plastics Technology and Engineering, 57 (2017) 346-369.
[44] X. Cao, L. James Lee, T. Widya, C. Macosko, Polyurethane/clay nanocomposites foams: processing, structure and properties, Polymer, 46 (2005) 775–783.
[45] S.H. Kim, M.C. Lee, H.D. Kim, H.C. Park, H.M. Jeong, K.S. Yoon, B.K. Kim, Nanoclay reinforced rigid polyurethane foams, Journal of Applied Polymer Science, 117 (2010) 1992-1997.
[46] Z. Xu, X. Tang, A. Gu, Z. Fang, Novel preparation and mechanical properties of rigid polyurethane foam/organoclay nanocomposites, Journal of Applied Polymer Science, 106 (2007) 439-447.
[47] G. Harikrishnan, T.U. Patro, D.V. Khakhar, Polyurethane Foam-Clay Nanocomposites: Nanoclays as Cell Openers, Industrial and Engineering Chemistry Research, 45 (2006) 7126–7134.
[48] M.M.A. Nikje, Z.M. Tehrani, Polyurethane Rigid Foams Reinforced by Doubly Modified Nanosilica, Journal of Cellular Plastics, 46 (2010) 159–172.
[49] M.M.A. Nikje, Z.M. Tehrani, Thermal and mechanical properties of polyurethane rigid foam/modified nanosilica composite, Polymer Engineering & Science, 50 (2010) 468–473.
[50] L. Zhang, E.D. Yilmaz, J. Schjødt-Thomsen, J.C. Rauhe, R. Pyrz, MWNT reinforced polyurethane foam: Processing, characterization and modelling of mechanical properties, Composites Science and Technology, 71 (2011) 877-884.
[51] D. Yan, L. Xu, C. Chen, J. Tang, X. Ji, Z. Li, Enhanced mechanical and thermal properties of rigid polyurethane foam composites containing graphene nanosheets and carbon nanotubes, Polymer International, 61 (2012) 1107-1114.
[52] D.-X. Yan, K. Dai, Z.-D. Xiang, Z.-M. Li, X. Ji, W.-Q. Zhang, Electrical conductivity and major mechanical and thermal properties of carbon nanotube-filled polyurethane foams, Journal of Applied Polymer Science, 120 (2011) 3014-3019.
[53] N. Athanasopoulos, A. Baltopoulos, M. Matzakou, A. Vavouliotis, V. Kostopoulos, Electrical conductivity of polyurethane/MWCNT nanocomposite foams, Polymer Composites, 33 (2012) 1302-1312.
[54] L. Madaleno, R. Pyrz, A. Crosky, L.R. Jensen, J.C.M. Rauhe, V. Dolomanova, A.M.M.V. de Barros Timmons, J.J. Cruz Pinto, J. Norman, Processing and characterization of polyurethane nanocomposite foam reinforced with montmorillonite–carbon nanotube hybrids, Composites Part A: Applied Science and Manufacturing, 44 (2013) 1–7.
[55] M.C. Saha, M.E. Kabir, S. Jeelani, Enhancement in thermal and mechanical properties of polyurethane foam infused with nanoparticles, Materials Science and Engineering: A, 479 (2008) 213-222.
[56] G. Harikrishnan, S.N. Singh, E. Kiesel, C.W. Macosko, Nanodispersions of carbon nanofiber for polyurethane foaming, Polymer, 51 (2010) 3349-3353.
[57] M.C. Saha, B. Barua, S. Mohan, Study on the Cure Kinetic Behavior of Thermosetting Polyurethane Solids and Foams: Effect of Temperature, Density, and Carbon Nanofiber, Journal of Engineering Materials and Technology, 133 (2011) 011015.

[58] M.E. Kabir, M.C. Saha, S. Jeelani, Effect of ultrasound sonication in carbon nanofibers/polyurethane foam composite, Materials Science and Engineering: A, 459 (2007) 111-116.
[59] M.M. Bernal, M. Martin-Gallego, I. Molenberg, I. Huynen, M.A. López Manchado, R. Verdejo, Influence of carbon nanoparticles on the polymerization and EMI shielding properties of PU nanocomposite foams, RSC Advances, 4 (2014) 7911.
[60] A. Lorenzetti, M. Roso, A. Bruschetta, C. Boaretti, M. Modesti, Polyurethane-graphene nanocomposite foams with enhanced thermal insulating properties, Polymers for Advanced Technologies, 27 (2016) 303-307.
[61] N.V. Gama, A. Ferreira, A. Barros-Timmons, Polyurethane Foams: Past, Present, and Future, Materials, 11 (2018).
[62] D.V. Pikhurov, A.S. Sakhatskii, V.V. Zuev, Rigid polyurethane foams with infused hydrophilic/hydrophobic nanoparticles: Relationship between cellular structure and physical properties, European Polymer Journal, 99 (2018) 403-414.
[63] N. Gama, L.C. Costa, V. Amaral, A. Ferreira, A. Barros-Timmons, Insights into the physical properties of biobased polyurethane/expanded graphite composite foams, Composites Science and Technology, 138 (2017) 24-31.
[64] M.E. Li, S.X. Wang, L.X. Han, W.J. Yuan, J.B. Cheng, A.N. Zhang, H.B. Zhao, Y.Z. Wang, Hierarchically porous SiO2/polyurethane foam composites towards excellent thermal insulating, flame-retardant and smoke-suppressant performances, Journal of hazardous materials, 375 (2019) 61-69.
[65] X. Luo, Y. Cai, L. Liu, F. Zhang, Q. Wu, J. Zeng, Soy Oil-Based Rigid Polyurethane Biofoams Obtained by a Facile One-Pot Process and Reinforced with Hydroxyl-Functionalized Multiwalled Carbon Nanotube, Journal of the American Oil Chemists' Society, 96 (2019) 319-328.
[66] M. Akkoyun, S. Akkoyun, Blast furnace slag or fly ash filled rigid polyurethane composite foams: A comprehensive investigation, Journal of Applied Polymer Science, 136 (2019) 47433.
[67] S. Członka, A. Strąkowska, K. Strzelec, A. Kairytė, S. Vaitkus, Composites of rigid polyurethane foams and silica powder filler enhanced with ionic liquid, Polymer Testing, 75 (2019) 12-25.
[68] S. Czlonka, A. Strakowska, K. Strzelec, A. Adamus-Wlodarczyk, A. Kairyte, S. Vaitkus, Composites of Rigid Polyurethane Foams Reinforced with POSS, Polymers (Basel), 11 (2019).
[69] F. Stazi, C. Urlietti, C. Di Perna, G. Chiappini, M. Rossi, F. Tittarelli, Thermal and mechanical optimization of nano-foams for sprayed insulation, Construction and Building Materials, 201 (2019) 828-841.
[70] C. Caglayan, I. Gurkan, S. Gungor, H. Cebeci, The Effect of CNT-Reinforced Polyurethane Foam Cores to Flexural Properties of Sandwich Composites, Composites: Part A, (2018).
[71] K. Chen, F. Cao, S. Liang, J. Wang, C. Tian, Preparation of poly(ethylene oxide) brush-grafted multiwall carbon nanotubes and their effect on morphology and mechanical properties of rigid polyurethane foam, Polymer International, 67 (2018) 1545-1554.
[72] E. Linul, C. Valean, P.A. Linul, Compressive Behavior of Aluminum Microfibers Reinforced Semi-Rigid Polyurethane Foams, Polymers (Basel), 10 (2018).
[73] A. Yaghoubi, M.M. Alavi Nikje, Silanization of multi-walled carbon nanotubes and the study of its effects on the properties of polyurethane rigid foam nanocomposites, Composites Part A: Applied Science and Manufacturing, 109 (2018) 338-344.
[74] J.-M. Kim, J.-H. Kim, J.-H. Ahn, J.-D. Kim, S. Park, K.H. Park, J.-M. Lee, Synthesis of nanoparticle-enhanced polyurethane foams and evaluation of mechanical characteristics, Composites Part B: Engineering, 136 (2018) 28-38.
[75] C. Lorusso, V. Vergaro, F. Conciauro, G. Ciccarella, P.M. Congedo, Thermal and mechanical performance of rigid polyurethane foam added with commercial nanoparticles, Nanomaterials and Nanotechnology, 7 (2017) 184798041668411.

[76] N. Nazeran, J. Moghaddas, Synthesis and characterization of silica aerogel reinforced rigid polyurethane foam for thermal insulation application, Journal of Non-Crystalline Solids, 461 (2017) 1-11.
[77] A. Dourbash, C. Buratti, E. Belloni, S. Motahari, Preparation and characterization of polyurethane/silica aerogel nanocomposite materials, Journal of applied Polymer Science, 134 (2017) 44521.
[78] M. Hoseinabadi, M. Naderi, M. Najafi, S. Motahari, M. Shokri, A study of rigid polyurethane foams: The effect of synthesized polyols and nanoporous graphene, Journal of Applied Polymer Science, 134 (2017) 45001.
[79] D.-A. Şerban, O. Weissenborn, S. Geller, L. Marşavina, M. Gude, Evaluation of the mechanical and morphological properties of long fibre reinforced polyurethane rigid foams, Polymer Testing, 49 (2016) 121-127.
[80] M. Akkoyun, E. Suvaci, Effects of TiO2, ZnO, and Fe3O4 nanofillers on rheological behavior,microstructure, and reaction kinetics of rigid polyurethane foams, Journal of Applied Polymer Science, 133 (2016).
[81] J.J. Espadas-Escalante, F. Avilés, P.I. Gonzalez-Chi, A.I. Oliva, Thermal conductivity and flammability of multiwall carbon nanotube/polyurethane foam composites, Journal of Cellular Plastics, 53 (2016) 215-230.
[82] M.M. Coleman, K.H. Lee, D.J. Skrovanek, P.C. Painter, Hydrogen bonding in polymers. 4. Infrared temperature studies of a simple polyurethane, Macromolecules, 19 (1986) 2149–2157.
[83] R.D. Priester, J.V. McClusky, R.E. O'Neill, R.B. Turner, M.A. Harthcock, B.L. Davis, FT-IR-A Probe into the Reaction Kinetics and Morphology Development of Urethane Foams, Journal of Cellular Plastics, 26 (1990) 346-367.
[84] M.J. Elwell, A.J. Ryan, H.J.M. Grünbauer, H.C.V. Lieshout, In-Situ Studies of Structure Development during the Reactive Processing of Model Flexible Polyurethane Foam Systems Using FT-IR Spectroscopy, Synchrotron SAXS, and Rheology, Macromolecules, 29 (1996).
[85] M.J. Elwell, A.J. Ryan, An FT i.r. study of reaction kinetics and structure development in model flexible polyurethane foam systems, Polymer, 37 (1996) 1353–1361.
[86] Y. Shi, X. Zhan, Z. Luo, Q. Zhang, F. Chen, Quantitative IR characterization of urea groups in waterborne polyurethanes, Journal of Polymer Science Part A: Polymer Chemistry, 46 (2008) 2433-2444.
[87] D.P. Queiroz, M.N. de Pinho, C. Dias, ATR-FTIR Studies of Poly(propylene oxide)/Polybutadiene Bi-Soft Segment Urethane/Urea Membranes, Macromolecules, 36 (2003) 4195–4200.
[88] I. Yilgor, E. Yilgor, I.G. Guler, T.C. Ward, G.L. Wilkes, FTIR investigation of the influence of diisocyanate symmetry on the morphology development in model segmented polyurethanes, Polymer, 47 (2006) 4105-4114.
[89] L.-S. Teo, C.-Y. Chen, J.-F. Kuo, Fourier Transform Infrared Spectroscopy Study on Effects of Temperature on Hydrogen Bonding in Amine-Containing Polyurethanes and Poly(urethane-urea)s, Macromolecules, 30 (1997) 1793-1799.
[90] A.L. Daniel-da-Silva, J.C.M. Bordado, J.M. Martín-Martínez, Moisture curing kinetics of isocyanate ended urethane quasi-prepolymers monitored by IR spectroscopy and DSC, Journal of Applied Polymer Science, 107 (2008) 700–709.
[91] Michael M. Coleman, Maria Sobkowiak, George J. Pehlert, P.C. Painter, Infrared temperature studies of a simple polyurea, Macromolecular Chemistry Physis, 198 (1997) 117–134.
[92] L. Ning, W. De-Ning, Y. Sheng-Kang, Hydrogen-Bonding Properties of Segmented Polyether Poly(urethane urea) Copolymer, Macromolecules, 30 (1997) 4405–4409.

[93] V. Zharkov, A. Strikovsky, T. Verteletskaya, Amide I absorption band: description of the urethane group association scheme in polyether urethane elastomers, Polymer, 34 (1993) 935–941.
[94] A. Strikovsky, V. Zharkov, Infra-red spectroscopy study of equilibrium association of urethane groups in poly(ether urethane)s, Polymer, 34 (1993) 3397.
[95] A. Marcos-Fernández, A.E. Lozano, L. González, A. Rodríguez, Hydrogen Bonding in Copoly(ether-urea)s and Its Relationship with the Physical Properties, Macromolecules, 30 (1997) 3584–3592.
[96] M.M. Bernal, M.A. Lopez-Manchado, R. Verdejo, In situ Foaming Evolution of Flexible Polyurethane Foam Nanocomposites, Macromolecular Chemistry and Physics, 212 (2011) 971–979.
[97] R. Versteegen, R. Sijbesma, E. Meijer, Synthesis and Characterization of Segmented Copoly(ether urea)s with Uniform Hard Segments, Macromolecules, 38 (2005) 3176–3184.
[98] A.N. Wilkinson, N.H. Fithriyah, J.L. Stanford, D. Suckley, Structure Development in Flexible Polyurethane Foam-Layered Silicate Nanocomposites, Macromolecular Symposia, 256 (2007) 65-72.
[99] M.M. Bernal, M. Martin-Gallego, L.J. Romasanta, A.-C. Mortamet, M.A. López-Manchado, A.J. Ryan, R. Verdejo, Effect of hard segment content and carbon-based nanostructures on the kinetics of flexible polyurethane nanocomposite foams, Polymer, 53 (2012) 4025-4032.
[100] M.M. Bernal, PhD Thesis: Estudio de nanocompuestos de espumas de poliuretano reforzadas con nanocargas en base carbono, Polytechnic University of Valencia, 2012.
[101] L.D. Artavia, C.W. Macosko, Foams kinetics, Journal of Cellular Plastics, 26 (1990) 490-511.
[102] M. Modesti, V. Adriani, F. Simioni, Chemical and Physical Blowing Agents in Structural Polyurethane Foams: Simulation and Characterization, Polymer Engineering & Science, 40 (2000).
[103] M. Kuranska, A. Prociak, S. Michalowski, K. Zawadzinska, The influence of blowing agents type on foaming process and properties of rigid polyurethane foams, Polimery, 63 (2018) 672-678.
[104] M. Kurańska, A. Prociak, The influence of rapeseed oil-based polyols on the foaming process of rigid polyurethane foams, Industrial Crops and Products, 89 (2016) 182-187.
[105] W. Ahn, J.-M. Lee, Effect of CNT as a Nucleating Agent on Cell Morphology and Thermal Insulation Property of the Rigid Polyurethane Foams, Journal of Nanoscience and Nanotechnology, 15 (2015) 9125-9130.
[106] S. Pardo-Alonso, E. Solórzano, S. Estravís, M.A. Rodríguez-Perez, J.A. de Saja, In situ evidence of the nanoparticle nucleating effect in polyurethane–nanoclay foamed systems, Soft Matter, 8 (2012) 11262.
[107] S. Pardo-Alonso, E. Solorzano, M.A. Rodriguez-Perez, Time-resolved X-ray imaging of nanofiller-polyurethane reactive foam systems, Colloid Surf. A-Physicochem. Eng. Asp., 438 (2013) 119-125.
[108] M. Mar Bernal, S. Pardo-Alonso, E. Solórzano, M.Á. Lopez-Manchado, R. Verdejo, M.Á. Rodriguez-Perez, Effect of carbon nanofillers on flexible polyurethane foaming from a chemical and physical perspective, RSC Advances, 4 (2014) 20761.
[109] C.S. Schollenberger, H. Scott, G.R. Moore, Rubber Worls, 137 (1958) 549.
[110] C. Prisacariu, Polyurethane elastomers, Wien New York: Springer, 2011.
[111] Y. He, D. Xie, X. Zhang, The structure, microphase-separated morphology, and property of polyurethanes and polyureas, Journal of Materials Science, 49 (2014) 7339-7352.
[112] I. Javni, O. Bilić, N. Bilić, Z.S. Petrović, E.A. Eastwood, F. Zhang, J. Ilavský, Thermoplastic polyurethanes with controlled morphology based on methylenediphenyldiisocyanate/isosorbide/butanediol hard segments, Polymer International, 64 (2015) 1607-1616.

[113] Handbook of Elastomers, in: A.K. Bhowmick, H. Stephens (Eds.), CRC Press2000.
[114] K.E. Kear, Developments in Thermoplastic Elastomers, in: R.R. Reports (Ed.), 2003.
[115] X. Sun, H. Kharbas, L.-S. Turng, Fabrication of highly expanded thermoplastic polyurethane foams using microcellular injection molding and gas-laden pellets, Polymer Engineering & Science, 55 (2015) 2643-2652.
[116] C. Dai, C. Zhang, W. Huang, K.-C. Chang, L.J. Lee, Thermoplastic polyurethane microcellular fibers via supercritical carbon dioxide based extrusion foaming, Polymer Engineering & Science, 53 (2013) 2360-2369.
[117] X.-C. Wang, X. Jing, Y.-Y. Peng, Z.-K. Ma, C.-T. Liu, L.-S. Turng, C.-Y. Shen, The effect of nanoclay on the crystallization behavior, microcellular structure, and mechanical properties of thermoplastic polyurethane nanocomposite foams, Polymer Engineering & Science, 56 (2016) 319-327.
[118] H.-Y. Mi, X. Jing, M.R. Salick, X.-F. Peng, L.-S. Turng, A novel thermoplastic polyurethane scaffold fabrication method based on injection foaming with water and supercritical carbon dioxide as coblowing agents, Polymer Engineering & Science, 54 (2014) 2947-2957.
[119] Baralu Jagannatha Rashmi, D. Rusu, K. Prashantha, M.F. Lacrampe, P. Krawczak, Development of Water-Blown Bio-Based Thermoplastic Polyurethane Foams Using Bio-Derived Chain Extender, Journal of Applied Polymer Science, 128 (2013) 292–303.
[120] S.-K. Yeh, Y.-C. Liu, W.-Z. Wu, K.-C. Chang, W.-J. Guo, S.-F. Wang, Thermoplastic polyurethane/clay nanocomposite foam made by batch foaming, Journal of Cellular Plastics, 49 (2013) 119-130.
[121] C.-C. Chu, S.-K. Yeh, S.-P. Peng, T.-W. Kang, W.-J. Guo, J. Yang, Preparation of microporous thermoplastic polyurethane by low-temperature supercritical CO2 foaming, Journal of Cellular Plastics, 53 (2017) 135-150.
[122] X. Dai, Z. Liu, Y. Wang, G. Yang, J. Xu, B. Han, High damping property of microcellular polymer prepared by friendly environmental approach, The Journal of Supercritical Fluids, 33 (2005) 259-267.
[123] S. Ito, K. Matsunaga, M. Tajima, Y. Yoshida, Generation of microcellular polyurethane with supercritical carbon dioxide, Journal of Applied Polymer Science, 106 (2007) 3581-3586.
[124] R. Rizvi, H. Naguib, Porosity and composition dependence on electrical and piezoresistive properties of thermoplastic polyurethane nanocomposites, Journal of Materials Research, 28 (2013) 2415-2425.
[125] A. Prasad, G. Fotou, S. Li, The effect of polymer hardness, pore size, and porosity on the performance of thermoplastic polyurethane-based chemical mechanical polishing pads, Journal of Materials Research, 28 (2013) 2380-2393.
[126] S.-K. Yeh, Y.-C. Liu, C.-C. Chu, K.-C. Chang, S.-F. Wang, Mechanical Properties of Microcellular and Nanocellular Thermoplastic Polyurethane Nanocomposite Foams Created Using Supercritical Carbon Dioxide, Industrial & Engineering Chemistry Research, 56 (2017) 8499-8507.
[127] S.-K. Yeh, Y.-R. Chen, T.-W. Kang, T.-J. Tseng, S.-P. Peng, C.-C. Chu, S.-P. Rwei, W.-J. Guo, Different approaches for creating nanocellular TPU foams by supercritical CO2 foaming, Journal of Polymer Research, 25 (2017) 30.

CHAPTER 3:

MATERIALS, FOAM PRODUCTION AND EXPERIMENTAL TECHNIQUES

Mercedes Santiago Calvo

3.1- Introduction

This chapter describes in detail the polyurethane (PU) formulations, the fillers and the procedures for foams production employed in this research work. A summary of the information included in this chapter is collected in **Table 3.1**. The experimental techniques, enumerated together with the standards used in each case, will be collected later (**Tables 3.12-15**).

Table 3.1. Summary of PU commercial and own formulations, fillers and foaming process employed in the different chapters of this research.

	RESEARCH ARTICLES	Chapter	Formulations	Fillers	Foaming process
1	The effects of functional nanofillers on the reaction kinetics, microstructure, thermal and mechanical properties of water blown rigid polyurethane foams.	4	Commercial formulation of water-blown RPU foam	Nanosilicas and nanoclays	Reactive foaming: Free expansion in a plastic cup
2	Infrared expandometry: a novel methodology to monitor the expansion kinetics of cellular materials produced with exothermic foaming mechanisms.	4	Own formulations of water-blown RPU foams		Reactive foaming: Free expansion in a plastic cup
3	X-ray radioscopy validation of a polyol functionalized with graphene oxide for producing rigid polyurethane foams with improved cellular structures.	4	Own formulations of water-blown RPU foams from polyols functionalized with GO and polyols with GO dispersed	GO	Reactive foaming: Free expansion in a plastic cup
4	Evaluation of the thermal conductivity and mechanical properties of water blown polyurethane rigid foams reinforced with carbon nanofibers.	5	Commercial formulation of water-blown RPU foam	CNFs	Reactive foaming: Free expansion using a mould
5	Long-thermal conductivity of cyclopentane-water blown rigid polyurethane foams reinforced with different types of fillers.	5	Commercial formulation of cyclopentane-water blown RPU foam	Talc (T), Non-porous silicas (NPS), Diatomeous earth (DE)	Reactive foaming: Restricted expansion using a mould
6	Synthesis, characterization and physical properties of rigid polyurethane foams prepared with poly(propylene oxide) polyols containing graphene oxide.	6	Own formulations of water-blown RPU foams from polyols functionalized with GO	GO	Reactive foaming: Free expansion in a plastic cup
7	Improvement of thermal and mechanical properties by control of formulations in rigid polyurethane foams from polyols functionalized with graphene oxide.	6	Own formulations of water-blown RPU foams from a polyol functionalized with 1000 ppm of GO	GO	Reactive foaming: Free expansion in a plastic ckkup
8	Synthesis, characterization, and foaming of thermoplastic polyurethane with different hard segment contents.	7	Own formulation of TPU foam		Gas dissolution foaming by 1-step in a autoclave

3.2- Polyurethane formulations

Both commercial and own formulations of rigid polyurethane (RPU) foams were used in this thesis (**Table 3.1**). In addition, the study of TPU foams was carried out with our own

formulations of thermoplastic polyurethane (TPU) materials (**Table 3.1**). In the case of commercial formulations, we do not have a complete information about the characteristics and the amounts of the components included in each formulation. We only have the information provided by the company producing these formulations.

3.2.1- Commercial formulation of water-blown rigid polyurethane foam

The commercial formulation of water-blown RPU foam, supplied by "BASF Poliuretanos Iberia S.A.", is formed by the polyol component (Elastopor H 1501/2) and by the isocyanate component (IsoPMDI 92140) [1, 2]. This formulation was chosen for two of the studies of this thesis because this is a typical PU formulation commonly used for the core material of sandwich insulating panels. Firstly, this commercial formulation was employed in order to evaluate the modification of the reaction kinetics by FTIR spectroscopy when different functional nanofillers (nanosilicas and nanoclays) were incorporated into water-blown RPU formulation (**article 1** included in **chapter 4**, **Table 3.1**). Secondly, this commercial formulation was used to study both the thermal and mechanical properties of RPU foams reinforced with different contents of carbon nanofibers (CNFs) (**article 4** included in **chapter 5**, **Table 3.1**). The main characteristics of this PU formulation, provided by BASF, are summarized in **Table 3.2**.

Table 3.2. Features of commercial formulation of water-blown RPU foam from BASF Poliuretanos Iberia S.A (**article 1** included in **chapter 4** and **article 4** included in **chapter 5**).

Product	Features	
Elastopor H 1501/2 (Polyol component)	Chemical composition	Polyether polyols, catalysts, flame retardant agents, stabilizers and blowing agent (water)
	OH index (mg KOH/g)	651
	Viscosity (20°C)(mPa·s)	650
	Density (20°C) (g/cm^3)	1.07
IsoPMDI 92140 (Isocyanate component)	Chemical composition	Polymeric diphenylmethane diisocyanate (pMDI)
	Isocyanate content Weight (%)	31.5
	Viscosity (20°C)(mPa·s)	170-250
	Density (20°C) (g/cm)	1.23
Foam	Polyol/isocyanate ratio (by weight)	100/160
	Density (Kg/m^3, free foaming)	52±5
	Cream time (s)	45±7
	Gel time (s)	145±18
	Rise time (s)	232±21

3.2.2- Commercial formulation of cyclopentane-water blown rigid polyurethane foam

The same formulation included in **Table 3.2** has been the starting point to develop a cyclopentane-water blown RPU foam. The proportions of the three components used were set at 100/160/13 by weight for the polyol (Elastopor H 1501/2), isocyanate (IsoPMDI 92140) and cyclopentane (99.9% purity from Sigma Aldrich) in order to have a free foaming density of 30 kg/m^3. This RPU system has a low thermal conductivity due to its low density, and also to the

use of CP as physical blowing agent. Due to its excellent insulating properties, this formulation was chosen to produce RPU foams with different types of fillers, such as talc (T), Diatomaceous earth (DE) or non-porous silica (NPS), and to study the thermal conductivity aging during these years (**article 5** included in **chapter 5**, **Table 3.1**).

3.2.3- CellMat formulations of water-blown rigid polyurethane foams

RPU formulations were developed in our laboratory in order to have a better control on the foam properties and to have the possibility of understanding the relation between formulation, reaction kinetics, cellular structure and properties. The chemical and physical characteristics of several formulation components (isocyanate, surfactant, catalysts and blowing agent) used to produce the RPU foams are collected in **Table 3.3**. On the other hand, **Table 3.4** shows the characteristics of Alcupol® R4520, a commercial polyol supplied by Repsol S.A., and collects four non-commercial polyols synthesized by Repsol in order to carry out several works of this thesis: a polyol without GO (to obtain the reference material), and three polyols chemically functionalized with low amounts of GO (GO-f) (500, 1000, and 2500 rpm).

Table 3.3. General features of formulation components used to produce own RPU foams.

Components	Commercial product	Features of PU components	
Isocyanate	**IsoPMDI 92140**	Supplier	BASF Poliuretanos Iberia S.A
		Chemical composition	Polymeric diphenylmethane diisocyanate (pMDI)
		Isocyanate content Weight (%)	31.5
		Viscosity (20°C)(mPa·s)	170-250
		Density (20°C) (g/cm^3)	1.23
Surfactant	**TEGOSTAB® B 8522**	Supplier	Evonik
		Chemical composition	Non - hydrolysable poly-ether - polydimethyl-siloxane
		Specific gravity (25 °C) (g/cm^3)	1.035 - 1.055
		Viscosity (25°C)(mPa·s)	600 - 1 000
		pH value (4 % hydrous solution)	6.0 - 8.0
Catalyst	**TEGOAMIN® DMCHA**	Supplier	Evonik
		Chemical composition	N,N-dimethylcyclohexylamine (DMCHA)
		Content (%)	≥ 98.0
		Water content (%)	≤ 0.25
	TEGOAMIN® PMDETA	Supplier	Evonik
		Chemical composition	N,N,N',N'',N''-Pentamethyldiethylenetriamine (PMDETA)
Blowing agent	**Distilled water**		

Table 3.4. General features of a commercial polyol from Repsol and non-commercial polyols from Repsol used to produce RPU foams with own formulations.

Commercial product	Features of polyols	
Alcupol® R4520	Supplier	Repsol S.A.
	Chemical composition	Polyether polyol
	Starter	Sucrose/ Glycerol
	Functionality	4.5
	OH index (mg KOH/g)	455
	Viscosity (25°C)(mPa·s)	5250
	Molecular weight (g/mol)	555
	Density (25°C) (g/cm^3)	1.08
	Water content (%)	0.1
	Alkaline content (ppm)	≤ 130
Non-commercial product	**Features of polyols**	
Polyol: 0 ppm GO-f (pure poliol)	Supplier	Repsol S.A.
	Chemical composition	Polyether polyol
	Starter	Glycerol
	Functionality	3
	OH index (mg KOH/g)	426.4
	Viscosity (25°C)(mPa·s)	476.85
	Molecular weight (g/mol)	488
Polyol: 500 ppm GO-f	Supplier	Repsol S.A.
	Chemical composition	Polyether polyol
	Starter	Glycerol
	Functionality	3
	OH index (mg KOH/g)	399.3
	Viscosity (25°C)(mPa·s)	553.30
	Molecular weight (g/mol)	494
Polyol: 1000 ppm GO-f	Supplier	Repsol S.A.
	Chemical composition	Polyether polyol
	Starter	Glycerol
	Functionality	3
	OH index (mg KOH/g)	358.6
	Viscosity (25°C)(mPa·s)	547.59
	Molecular weight (g/mol)	570
Polyol: 2500 ppm GO-f	Supplier	Repsol S.A.
	Chemical composition	Polyether polyol
	Starter	Glycerol
	Functionality	3
	OH index (mg KOH/g)	377.5
	Viscosity (25°C)(mPa·s)	4463.23
	Molecular weight (g/mol)	675

Table 3.5 summarizes four formulations developed during the research work. From the formulation collected in **Table 3.5**, four different RPU foams were obtained, which differ in the amount of water (2 or 5 ppw) and in the blowing catalyst used (TEGOAMIN® PMDETA) (0 or 2 ppw). These materials were selected in order to describe a new methodology called "Infrared Expandometry", appropriate to characterize simultaneously the expansion kinetics (height vs. time, and volume vs. time) and the surface temperature evolution of cellular materials **(article 2** included in **chapter 4**, **Table 3.1**).

Table 3.6 shows two series of RPU foams formulations: one contains polyols functionalized with GO (GO-f), and the second one GO dispersed (GO-d) into the pure polyol. A pure polyol without GO was used to obtain a pure material as a reference for both series. These formulations were used in order to study the effect of both GO-f and GO-d, on the foaming mechanisms by using X-ray radioscopy (**article 3** included in **chapter 4**, **Table 3.1**).

This previous work allowed concluding that incorporating GO chemically linked to the polyol chains clearly improves the characteristics of RPU foams nanocomposites. Therefore, we decided to produce water-blown RPU foams from polyols functionalized with low amounts of GO-f (0.017, 0.033 and 0.088 wt. % in the foam) following the formulations collected in **Table 3.7**. The influence of the amount of GO-f on density, cellular structure, thermal conductivity and mechanical properties were investigated (**article 6** included in **chapter 6**, **Table 3.1**). Furthermore, a detailed study of foaming process was carried out by FTIR spectroscopy, infrared expandometry and temperature evolution, in order to evaluate the effect of GO-f on the reaction kinetics and foam formation process. The main conclusion of this work was that the better performance was displayed by the foam containing 0.033 wt% GO-f, because it reduced the thermal conductivity. However the mechanical properties were not improved in comparison to the reference foam.

Finally, this optimum system with 0.033 wt% GO-f was further studied in the last work herein collected, in order to improve their mechanical properties without loss of their thermal properties (**article 7** included **chapter 6** shown in **Table 3.1**). For this purpose, the data obtained from the previous modifications of the reaction kinetics induced by the presence of GO in the polyol, led us to obtain a series of RPU foams by varying the isocyanate index, the amounts of catalyst, the amounts of surfactant, or a combination of these components. The formulations used for this purpose are included in **Table 3.8**.

Table 3.5. Own formulations of water-blown RPU foams (**article 2** included in **chapter 4**).

	Isocyanate component	Polyol component (ppw)				
	Isocyanate index	Polyol	Surfactant	Catalyst		Blowing agent
Samples	IsoPMDI 92140	Alcupol® R4520	TEGOSTAB® B 8522	TEGOAMIN® DMCHA	TEGOAMIN® PMDETA	Water
PUR1	110	100	1	1	0	2
PUR2	110	100	1	1	2	2
PUR3	110	100	1	1	0	5
PUR4	110	100	1	1	2	5

Table 3.6. Own formulations of water-blown RPU foams from polyols functionalized with GO and polyols with GO dispersed (**article 3** included in **chapter 4**).

	Isocyanate component	Polyol component (ppw)					
	Isocyanate index	Polyol			Surfactant	Catalyst	Blowing agent
Samples	IsoPMDI 92140	0 ppp GO-f	500 ppm GO-f	2500 ppm GO-f	TEGOSTAB® B 8522	TEGOAMIN® DMCHA	Water
Pure (Reference)	120	100			1	**0.3**	5
0.017%GO-f	120		100		1	**0.3**	5
0.083%GO-f	120			100	1	**0.3**	5
0.017%GO-f	120	100			1	**0.3**	5
0.083%GO-d	120	100			1	**0.3**	5

Table 3.7. Own formulations of RPU foams from polyols functionalized with GO (**article 6** included in **chapter 6**).

	Isocyanate component	Polyol component (ppw)						
	Isocyanate index	Polyol				Surfactant	Catalyst	Blowing agent
Samples	IsoPMDI 92140	0 ppp GO-f	500 ppm GO-f	1000 ppm GO-f	2500 ppm GO-f	TEGOSTAB® B 8522	TEGOAMIN® DMCHA	Water
Pure (Reference)	120	100				1	**1**	5
0.017%GO-f	120		100			1	**1**	5
0.033%GO-f	120			100		1	**1**	5
0.083%GO-f	120				100	1	**1**	5

Table 3.8. Own formulations of RPU foams from a polyol functionalized with 1000 ppm of GO-f (0.033 wt% GO-f in the foam) (**article 7** included **chapter 6**).

	Isocyanate component	Polyol component (ppw)			
	Isocyanate index	Polyol	Surfactant	Catalyst	Blowing agent
Samples	IsoPMDI 92140	1000 ppm GO-f	TEGOSTAB® B 8522	TEGOAMIN® DMCHA	Water
PU-115ISO	**115**	100	1	1	5
PU-120ISO (Reference)	**120**	100	1	1	5
PU-125ISO	**125**	100	1	1	5
PU-130ISO	**130**	100	1	1	5
PU-0.5CAT	120	100	1	**0.5**	5
PU-1CAT (Reference)	120	100	1	**1**	5
PU-1.5CAT	120	100	1	**1.5**	5
PU-2CAT	120	100	1	**2**	5
PU-1SURF (Reference)	120	100	**1**	1	5
PU-2SURF	120	100	**2**	1	5
PU-120ISO-1CAT-1SURF (Reference)	120	100	1	1	5
PU-130ISO-2CAT-1SURF	**130**	100	1	**2**	5
PU-130ISO-2CAT-2SURF	**130**	100	**2**	**2**	5

3.2.4- CellMat formulations of thermoplastic polyurethane foams

Table 3.9 shows the characteristics of the TPU foam components: isocyanate, macrodiol, chain extender, catalyst, solvent and blowing agent. Firstly, three TPU materials with different weight fraction of hard segments (HS) (40%HS, 50%HS and 60%HS) were synthesized, as collected in **Table 3.10**. A total of 100 g of TPU material was produced in each synthesis. These TPUs were synthesized using a two-steps process in order to study their foaming behavior by a one-step gas dissolution foaming process (**article 8** included in **chapter 7**, **Table 3.1**).

Table 3.9. Properties of TPU foam components.

Components	Commercial product	Features of TPU foam components	
Isocyanate	**4,4'-MDI**	Supplier	Sigma Aldrich
		Chemical composition	Methylene diphenyl diisocyanate (MDI)
		Functionality	2
		Molecular weight (g/mol)	250.25
		Melting point (°C)	42- 45
		Boiling point (5 mm Hg) (°C)	200
		Purity (%)	98
		Density (25°C) (g/ml)	1.18
Macrodiol	**Poly(propylene glycol)-block-poly(ethylene glycol)-block-poly(propylene glycol) average Mn ~2,000**	Supplier	Sigma Aldrich
		Chemical composition	Poly(ethylene glycol)-block-poly(propyleneglycol-block-poly(ethylen-glycol) structure (PEG-PPG-PEG)
		Functionality	2
		OH index (mg KOH/g)	56-59
		Molecular weight (g/mol)	Mn ~2000
Chain extender (diol)	**1,5-pentanediol**	Supplier	Sigma Aldrich
		Chemical composition	1,5-pentanediol (1,5-PDO)
		Functionality	2
		Molecular weight (g/mol)	104.15
		Purity (%)	≥97.0
		Density (25°C) (g/ml)	0.994
Calatyst	**1,4-Diazabicyclo[2.2.2]octane (DABCO)**	Supplier	Sigma Aldrich
		Chemical composition	1,4-Diazabicyclo[2.2.2]octane (DABCO)
		Density (25°C) (g/ml)	**1.02**
		Melting point (°C)	**156-159**
Solvent	**N,N dimethylene-acetamide**	Supplier	Sigma Aldrich
		Chemical composition	N,N dimethylene-acetamide (DMAC)
		Molecular weight (g/mol)	87.12
		Melting point (°C)	-20
		Boiling point (760 mm Hg) (°C)	164-166
Blowing agent	**Carbon dioxide**	Supplier	Air Liquide
		Chemical composition	Carbon dioxide
		Purity (%)	99.9

Table 3.10. The amount of each component used for first and second step of TPU synthesis.

	First step			Second step	
	Isocyanate	Polyol	PREPOLYMER	Isocyanate	Chain extender
Samples	MDI	PEG-PPG-PEG	PREPOLYMER	MDI	1,5-PDO
40%HS	43.8 g, 0.175 mol	85.8 g, 0.043 mol	90.6 g	0	9.4 g, 0.090 mol
50%HS	64.2 g, 0.257 mol	85.8 g, 0.043 mol	87.4 g	0	12.6 g, 0.121 mol
60%HS	64.2 g, 0.257 mol	85.8 g, 0.043 mol	69.9 g	13.4 g, 0.054 mol	16.7 g, 0.160 mol

3.3- Fillers

Different fillers were used for the production of composite foams (**Table 3.1**). Their main characteristics are collected in **Table 3.11**.

The properties of composites resulting from the incorporation of nanoscale size fillers such as nanoclays or nanosilicas have been widely studied [3-12]. However the effect of these additives on the PU reactions has been so far very scarcely explored. For this reason, these types of nanoparticles were selected in a part of this thesis. Nanoclays and nanosilicas with different superficial treatments (**Table 3.11**): hydrophilic (Aerosil®A200 and Cloisite®Na+), hydrophobic (Aerosil®R812), or partially hydrophilic (or containing both hydrophilic and hydrophobic groups, such as Aerosil®R974 or Cloisite®30B) were used to determine their effect on the reaction kinetics of water-blown RPU foams (**article 1** included in **chapter 4**, **Table 3.1**).

On the one hand, CNFs (**Table 3.11**) were added to water-blown RPU foams in order to study their effect on the heat conduction mechanisms by measuring the extinction coefficient and by modelling the thermal conductivity (**article 4** included in **chapter 5**, **Table 3.1**). CNFs were selected in this work since their nanometric size as well as their high superficial area makes possible their use as infrared blocker, even for very small contents. As a consequence, the radiative contribution to the thermal conductivity is then reduced.

Different types of particles, such as talc (T), diatomeous earth (DE), or non-porous silicas (NPS) (**Tables 3.11 to 3.8**), were added to RPU foams containing CP and water as blowing agents, in order to investigate their effect on the thermal conductivity along three years of aging (**article 5** included in **chapter 5**, **Table 3.1**). T and DE were selected mainly due to their low cost, and also they are easy to be dispersed because they are micrometric particles. In the case of DE, these particles have a porous silica structure at the nanoscale [18], what favor increasing their superficial area and therefore favor the nucleation too. On the other hand, NPS were selected because being nanometric particles, their nucleation potential is very high even for low contents. Due to the low contents used and their nanometric size, a smaller impact on the properties of cell walls and therefore on the diffusion of the gases should be expected.

A series of polyols functionalized with GO (**Table 3.11**) were used in order to obtain blown RPU foams. The effect of the polyol functionalized with GO on the foaming kinetics, cellular structure, thermal conductivity, and compressive mechanical properties of the RPU foams was investigated in several works of this thesis (**article 4** included in **chapter 4** and **articles 6** and **7** included in **chapter 6**, **Table 3.1**). GO is a two-dimensional graphene layer which has multiple oxygen functional groups, such as hydroxyl, epoxy, and carboxylic acid, on its basal planes and edges. Thus, GO particles were selected because these functional groups can facilitate the reactivity of GO with the starting components of polyols to produce polyols functionalized with GO. Moreover, GO acts as an infrared blocker and a nucleating agent, what could favor a decrease of the radiative contribution of thermal conductivity in RPU foams. The main advantages of the use of GO particles chemically incorporated into the polyol chains are that agglomeration of fillers is precluded. Therefore even very low amounts of GO can generate RPU foams with promising characteristics.

Table 3.11. Main characteristics of the fillers used in this thesis.

Fillers	Commercial product	Features of fillers	
Nanosilicas	**Aerosil®A200 (A200)** [13]	Supplier	Evonik Industries AG (Evonik Degussa)
		Chemical composition	Silica nanoparticles without any further treatment [13-15]
		Diameter (nm)	12
		Specific surface area (m^2/g)	175-225
	Aerosil®R974 (R974) [13]	Supplier	Evonik Industries AG (Evonik Degussa)
		Chemical composition	Silica nanoparticles post-treated with dimethyldichlorosilane (50%) [3, 6, 7]
		Particle size (nm)	12
		Specific surface area (m^2/g)	150-190
	Aerosil®R812 (R812) [13]	Supplier	Evonik Industries AG (Evonik Degussa)
		Chemical composition	Silica nanoparticles post-treated with hexamethyldisilazane (90%) [13, 16]
		Particle size (nm)	7
		Specific surface area (m^2/g)	230-290
Nanoclays	**Cloisite®Na+ (CNa+)** [17]	Supplier	Southern Clay Products Inc
		Chemical composition	Natural Montmorillonite [17-19]
		Specific surface area (m^2/g)	700-786
		Lateral size (microns)	2-13
	Cloisite®30B (C30B) [17]	Supplier	Southern Clay Products Inc
		Chemical composition	Organically modified montmorillonite with methyl tallow bis-2-hydroxyethyl quaternary ammonium chloride (30%) [17-19]
		Specific surface area (m^2/g)	760
		Lateral size (microns)	2-13
Carbon nanofibers (CNFs)	**Pyrograf® III PR-24-XT-PS**	Supplier	Applied Sciences Inc
		Chemical composition	Graphitic tubular carbon nanofibers with a minimal chemically vapor deposited (CVD) layer of carbon on their surface
		Diameter (nm)	100
		Length (microns)	50-200
		Surface area (m^2/gm)	45
		Iron (ppm)	<100
Talc (T)	**Luzenac HAR® T84**	Supplier	Imerys
		Chemical composition	Talc
		Particle size (microns)	2
Diatomaceous earth (DE)	**Kieselguhr Diasol nº 2 Mo**	Supplier	Cekesa
		Chemical composition	CO_3Ca (34.5%), SiO_2 (62%), Al_2O_3 (1.4%), Fe_2O_3 (0.72%), traces (1.4%)
		Particle size (microns)	0.58-28
Non-porous silica (NPS)	**PNPP0.15NA C18-10**	Supplier	Glantreo
		Chemical composition	Non-porous nanosilica with a superficial treated with C18 groups
		Particle size (microns)	0.15
		Surface area (m^2/g)	<20
Graphene oxide (GO)	**Graphenea Graphene oxide (GO)**	Supplier	Graphenea S.A.
		Chemical composition	Dispersion of GO sheets in water (4 mg/ml concentration)
		Monolayer content (measured in 0.5 mg/ml)	>95%

3.4- Foams production

3.4.1- Rigid polyurethane foams

RPU foams studied in this thesis were obtained by reactive foaming process which occurs when two reactive components (isocyanate and polyol blend) are mixed. This chemical reaction generates gaseous products and the polymerization process helps to encapsulate the gas phase. In order to produce the RPU foams, the procedures included the next steps (**Figure 3.1**):

- Pre-mixture of polyol component.

In the case of the commercial formulations, pre-mixing the polyol component, which contains a variety of additives, is necessary in order to maintain the homogeneity of the mixture before being used. Thus, the polyol component was mixed at 250 rpm for 2-5 minutes. In the case of our own formulations (**Table 3.5-8**), the calculated amounts of polyol, catalysts, surfactants and blowing agents were first prepared and then mixed at 250 rpm for 2 minutes in order to obtain a homogenous polyol blend. An overhead stirrer (EUROSTAR Power control-visc P1, IKA) with a 50 mm diameter Lenart disc stirrer was used to premix the polyol component in both commercial and CellMat formulations.

- Dispersion of fillers.

For the production of RPU foams infused with fillers (nanoclays, nanosilicas, CNFs, T, NPS, DE or GO), an extra step is required previously to carry out the mixture isocyanate-polyol: particles must be dispersed into one of the two components. In each case, the component chosen to disperse the particles was selected taking into account both tests and previous studies. The technique employed to disperse all the particles was mechanical shear mixing. Particles were dried under vacuum at 50°C overnight before being dispersed into the isocyanate or polyol component, in order to avoid any moisture which could react with the isocyanate.

Nanoclays and nanosilicas were dispersed into the isocyanate component during 5 minutes (at 1200 rpm during the first minute and the remaining time at 250 rpm), whereas T, NPS, DE and GO were dispersed into the polyol component for 5 minutes at 250 rpm. All the particles were dispersed using the same stirrer than that used for the pre-mixture of the polyol blend. CNFs particles were previously dispersed into the polyol by using a Silverson L5M high shear mixer running at 4000 rpm for 30 minutes.

- Addition of CP to the polyol component.

In the case of the commercial formulation of the CP-blown RPU foam, CP was previously mixed with the polyol blend both for pure foam or for the polyol blend containing particles. For foams with T, NPS or DE at 250 rpm, the mixtures were stirred for 3 minutes using an overhead stirrer (EUROSTAR Power control-visc P1, IKA) with a 50 mm diameter Lenart disc stirrer.

- Mixture of polyol and isocyanate components.

For most of systems, the polyol and isocyanate components were mixed at 1200 rpm for 10 seconds by using an overhead stirrer (EUROSTAR Power control-visc P1, IKA) with a 50 mm diameter Lenart disc stirrer. Different mixing conditions were used for the RPU foams containing CNFs, in this case the isocyanate and the polyol components were stirred using a Pendraulik TD100 mechanical mixer running at 2500 rpm for 30s.

For most of the studies in this thesis (**Table 3.1**), the foams were produced by one-pot free expansion in a plastic cup whose dimensions were 10 cm of diameter and 15 cm of height.

However, for two of the studies herein reported (**Table 3.1**), the isocyanate and polyol mixture was poured over a mould and thus the foams were produced by one-pot free or restricted expansion. For materials with CNFs, the mold used was 25 x 25 x 25 cm^3, whereas for materials with CP, the mold dimensions were 30 x 35 x 5 cm^3.

- Curing process of foams.

After the foaming, the materials were cured during at least 48 hours at room temperature and then they were cut for complete characterization.

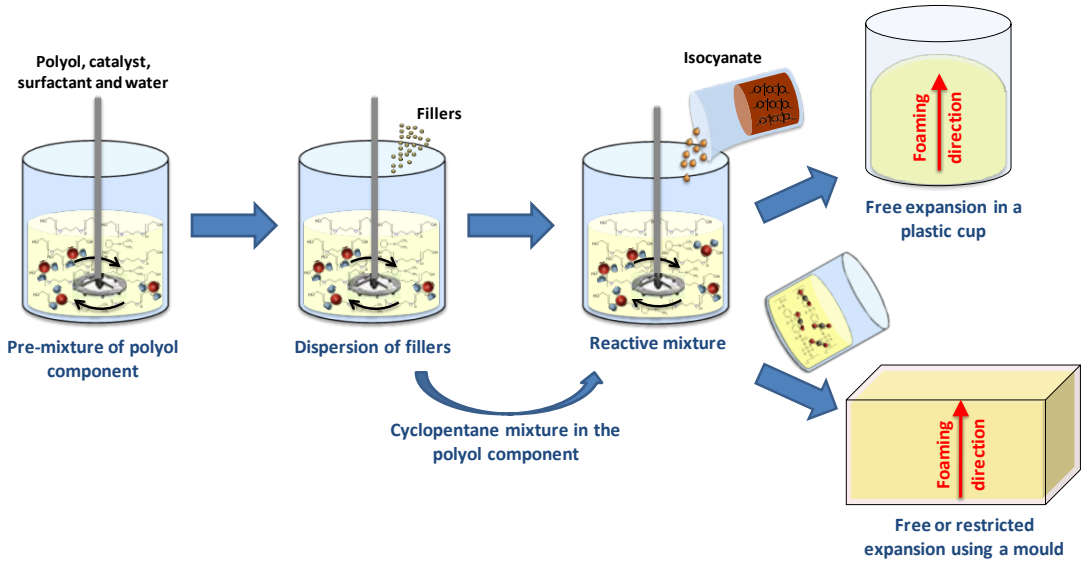

Figure 3.1. ble Scheme of RPU foams production by reactive foaming.

3.4.2- Thermoplastic polyurethane foams

TPUs were synthesized with different weight fraction of HS (40%HS, 50%HS and 60%HS) **(Ta 3.10)** and then were foamed by gas dissolution foaming using CO_2 as physical blowing agent (**article 8** included in **chapter 7**, **Table 3.1**). All the steps are detailed next (**Figure 3.2** and **Figure 3.3**):

- Synthesis of solid TPUs.

The synthesis of TPUs was carried out in a closed reaction flask by a two-step, pre-polymer method under dry nitrogen atmosphere (TPU formulations are collected in **Table 3.10**). The molar ratio of NCO/OH was adjusted to 1.02. First, PEG-PPG-PEG was added dropwise from a addition funnel to MDI and this mixture was heated into an oil bath at 80°C for 2 h with stirring at 400 rpm. In this first step of synthesis, the molar ratio of MDI and PEG-PPG-PEG polyol was 6:1 for TPU 50%HS and TPU 60%HS, and 4:1 for TPU 40%HS. In the second step, the mixture of

the additional amount of MDI and the prepolymer previously obtained in DMAc (240 mL), was added dropwise from the addition funnel to a preheated mixture of 1,5-PDO and DABCO (0.3 g, 0.003 mmol, 0.3%) in DMAc (60 mL). This reaction mixture was stirred at 400 rpm for 2h into an oil bath at 80°C. Finally, the solution containing the TPU was poured into silicone moulds without exclusion of air and maintained in an oven at 80°C for 3 days in order to obtain TPU casts.

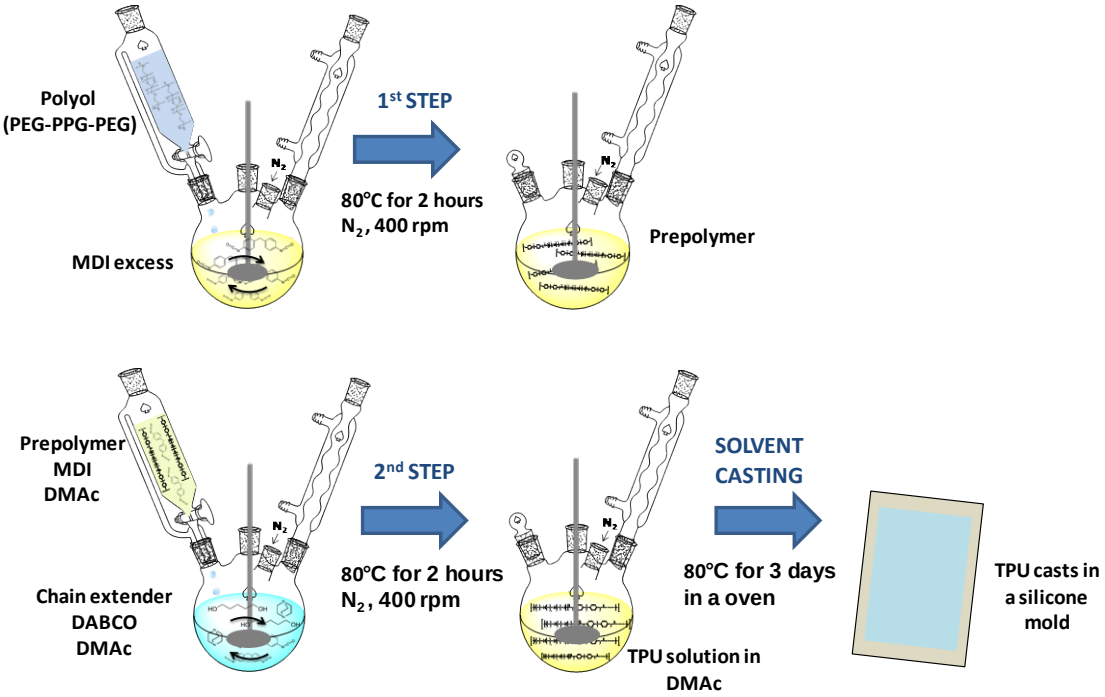

Figure 3.2. Scheme of TPU synthesis by pre-polymer method.

- Samples preparation.

Extruded samples with 1.5 ± 0.5 mm of diameter were prepared by TWELVindex extrusion plastometer from ATS Faar using a temperature above melting temperature (between 165-180 °C) in order to carry out the foaming tests.

Compression molded samples were prepared by using a hot plate press in order to characterize their using different techniques: shore hardness, WAXD, DMTA and rheology (**Table 3.15**). The material was first heated at a temperature above melting temperature (between 165-180 °C) for 3 min, raising the pressure to 10 MPa at 0.05 MPa/s. Then the samples were pressed under a constant pressure of 10 MPa for 7 min, lowering the temperature to 60°C at 25°C/min.

- Foamed of solid TPUs.

The extruded samples were foamed by a one-step gas dissolution foaming process using CO_2 as physical blowing agent (**Figure 3.3**). A high pressure vessel provided by Parr Instrument Company (model PARR 4681), with a capacity of 1 L, and capable of operating at a maximum temperature of 350° C and a maximum pressure of 41 MPa was used to obtain the TPU foams. The pressure was automatically controlled by an accurate pressure pump controller (model SFT-10) provided by Supercritical Fluid Technologies Inc. The vessel is equipped with a clamp heater of 1200 W, and the temperature is controlled by a CAL 3300 temperature controller. This set up has been used to carry out a set of experiments by using a one-step foaming process. Samples were first introduced in the pressure vessel under certain pressure and temperature conditions for the saturation stage. After saturation, pressure was rapidly released and the samples expanded in the pressure vessel after depressurization.

Two sets of experiments were performed. First, the effect of the foaming temperature was analyzed by fixing the saturation pressure to 20 MPa and the saturation time to 1 h, whereas varying the foaming temperature at 140, 150, 160, 170 and 180 °C. Second, the influence of the saturation pressure was evaluated by choosing four different saturation pressures: 10, 15, 20 and 25 MPa at fixed temperature and time: 170 °C for 1 h. Extruded TPU samples were foamed and then the remaining CO_2 was allowed to desorb before measuring their density and characterizing their cellular structure.

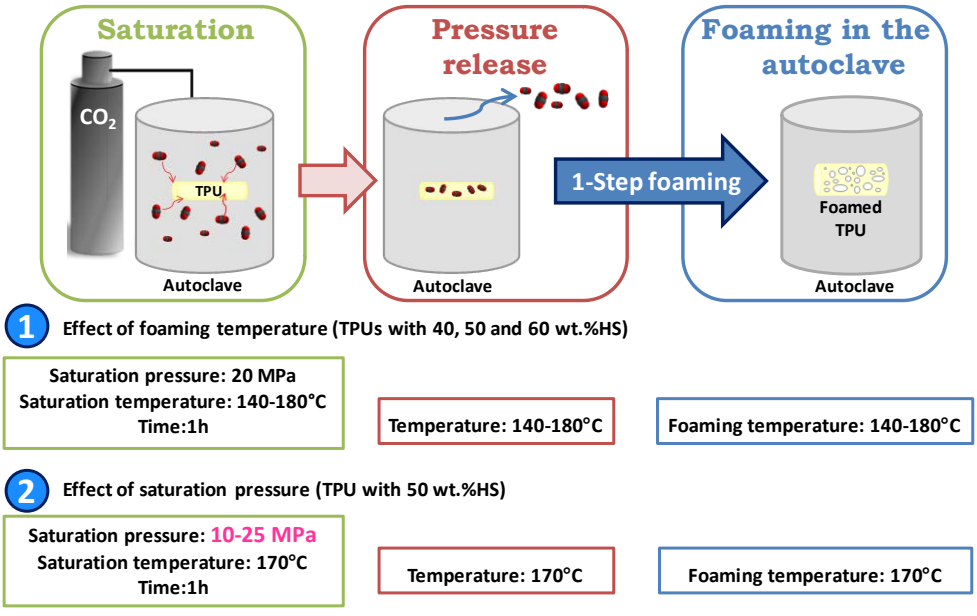

Figure 3.3. Scheme of TPU foam production by 1-step gas dissolution foaming process in an autoclave.

3.5- Experimental techniques

3.5.1- Summary of experimental techniques

Several standard and well-known experimental techniques were employed in order to characterize the materials studied in this research work. A full description of these experimental techniques has been already provided in the scientific articles included in this thesis, therefore only a brief description of them is collected in **Tables 3.12 to 3.15**. Instead, detailed descriptions of those experimental techniques used to monitor the reaction kinetics of the RPU foams (FTIR spectroscopy, X-ray radioscopy, infrared expandometry and adiabatic temperature rise, **Table 3.12.**) are herein detailed, since these techniques are the most important ones in this research.

Table 3.12. Summary of the experimental techniques used for the characterization and the monitoring of foaming process of RPU foams.

CHARACTERIZATION OF RPU FOAMS		
EXPERIMENTAL TECHNIQUE	Purpose	Chapter
Density determination (Geometric method) ASTM D1622/D1622M-14 [20]	Obtain the foam density	4, 5 and 6
Open cell content determination (Gas picnometry) ASTM D6226-10 [21] Gas pycnometer Accupyc II 1340 from Micromeritics	Calculate the open cell content	4, 5 and 6
Scanning Electron Microscopy (SEM) JEOL JSM-820 microscope.	Determine the average cell size (Φ_{3D}), anisotropy ratio (AR), the standard deviation (SD) of the cell size distribution and the normalized standard deviation (NSD)	4, 5 and 6
Optical Microscopy (OM) Leica DM2500M microscope	Locate the position of CNFs in the foam structure	5
Thermal conductivity by transient method ISO 22007‑2:2008 [22] Hot-disk transient plane source (TPS) thermal constant analyzer	Measure the thermal conductivity	5
Thermal conductivity by stationary method UNE12667 [47] Rapid K heat flowmeter from Holometrix	Measure the thermal conductivity	5
Mechanical tests in compression ASTM D1621-10 [44] Instron Machine (model 5.500R6025)	Measure Young´s modulus and collapse stress.	4, 5 and 6
Fourier transform infrared (FTIR) spectroscopy by transmission Bruker Tensor 27 spectrometer	Calculate the spectral extinction coefficient	5
Fourier transform infrared (FTIR) spectroscopy by transmission and attenuated total reflectance (ATR) Bruker Tensor 27 spectrometer	Characterize the premix of the nanoparticles with the isocyanate component	4
Dynamical mechanical analysis (DMA). PerkinElmer DMA7 dynamic mechanical analzer	Analyze the viscoelastic behavior of foamed samples. Measure the sample thickness to calculate the spectral extinction coefficient	4 and 5
FOLLOW THE FOAMING PROCESS OF RPU FOAMS		
EXPERIMENTAL TECHNIQUE	Purpose	Chapter
FTIR spectroscopy by ATR Bruker ALPHA spectrometer	Follow the isocyanate conversion and the generation of products during the foaming process	4 and 6
Infrared expandometry Infrared camera (model Hotfind L) from SDS	Follow the foam expansion to determine the surface temperature, height and volume evolution	4
X-ray radioscopy Home-designed equipment	Follow the cellular structure evolution, measuring the relative density, cell size and cell nucleation density evolution	4 and 6
Adiabatic temperature rise	Follow the temperature evolution to extract complementary information about the reactions	4 and 6

Table 3.13. Summary of the experimental techniques used for the characterization of polyol functionalized with GO.

CHARACTERIZATION OF POLYOL FUNCTIONALIZED WITH GO		
EXPERIMENTAL TECHNIQUE	**Purpose**	**Chapter**
Hydroxyl number determination ASTM D-4274 [23]	Determine hydroxyl numbers	6
Viscosity determination Brookfield DV-III ULTRA Rheometer.	Determine viscosity	6
Differential scanning calorimeter (DSC) DSC TA Instruments Q2000.	Measure the glass transition temperature (Tg).	6
Gel-permeation chromatography (GPC) Bruker 3800 equipped with a deflection RI detector.	Measure the weigh-averaged molecular weights (M_w) and polydispersity index (PDI).	6

Table 3.14. Summary of the experimental techniques used for fillers characterization.

CHARACTERIZATION OF FILLERS		
EXPERIMENTAL TECHNIQUE	**Purpose**	**Chapter**
Fourier transform infrared (FTIR) spectroscopy by attenuated total reflectance (ATR) method Bruker Tensor 27 spectrometer	Identify the surface groups of nanoclays and nanosilicas	4
Thermogravimetric analysis (TGA) Mettler Toledo TGA/SDTA 851	Analyze the thermal decomposition of nanoclays and nanosilicas	4
Environmental scanning electron microscope (ESEM) Quanta 200 FEG	Examine the morphologies of nanoclays and nanosilicas	4
Scanning Electron Microscopy (SEM) Zeiss EVO LS15	Characterize the dimensions of CNFs	5

Table 3.15. Summary of the experimental techniques used for solid TPU and TPU foams.

CHARACTERIZATION OF SOLID TPU AND TPU FOAMS		
EXPERIMENTAL TECHNIQUE	**Purpose**	**Chapter**
Density determination (Gas picnometry) Gas pycnometer Accupyc II 1340 from Micromeritics	Density of the solid TPUs	7
Shore hardness A and D ISO 868:2003 [24] Bareiss U72 durometer	Analyze the difference in the shore hardness of the solid TPUs	7
Gel-permeation chromatography (GPC)	Analyze the difference in the molecular weight of the solid TPUs	7
Differential scanning calorimetry (DSC) DSC30 Mettler Toledo Instrument.	Detect variations in the glass transition temperature of the solid TPUs	7
Wide angle X-ray diffraction (WAXD) PANalytical X'Pert Pro (XRD 5) Instrument.	Analyze the difference in the crystallinity of the solid TPUs	7
Dynamic mechanical thermal analysis (DTMA) Q800 DMA instrument (TA)	Analyze the viscoelastic properties of the solid TPUs	7
Shear rheology ARES-G2, TA Instruments	Characterize the rheological properties of the solid TPUs	7
Density determination (Archimedes method) (Precision Balance AT 261 from Mettler)	Obtain the density of TPU foams	7
Scanning Electron Microscopy (SEM) JEOL JSM-820 microscope.	Determine the average cell size (Φ_{3D}), anisotropy ratio (AR), the standard deviation (SD) of the cell size distribution, the normalized standard deviation (NSD) and cell nucleation density (N_0) of TPU foams.	7

3.5.2- Experimental techniques for the monitoring of foaming process

3.5.2.1- FTIR spectroscopy

Aiming at investigating the reaction kinetics of RPU foams, a methodology based on *in-situ* FTIR spectroscopy by ATR was established in the **article 1** included in **chapter 4** of this thesis and was also applied in **article 6**, included in **chapter 6** of this thesis. The RPU foam formation may be monitored by *in-situ* FTIR by following the isocyanate consumption from the isocyanate asymmetric stretching vibration at 2270 cm^{-1}. The generation of urethane and urea products associated with the gelling and blowing reactions can be also deduced from the carbonyl stretching vibrations of the Amide I or carbonyl region (in the range of 1610-1760 cm^{-1}). Therefore, only the main reactions, that are the most critical ones in most of the cases, have been considered for the analysis of products.

A Bruker ALPHA spectrometer working in ATR method was employed in order to collect the *in-situ* FTIR spectra of the samples. The measurements were carried out following the next steps (**Figure 3.4**):

1. Sample preparation: A low amount of reacting foam (ca. 1 mL of the reactants mixture) extracted from a mixture made with the usual amounts to produce the foams with higher dimensions in a plastic cup (as explained in the **section 3.3.1** of this chapter), was poured on the ATR surface. The addition of the isocyanate was taken as time t = 0.

2. Measurement parameters of FTIR spectra: FTIR spectra were measured during 30 min each 20 or 30 sec. (16 scans, 4 cm^{-1} of resolution in the range 4000-400 cm^{-1}). The sample was maintained during all the experiment at 70°C in order to reproduce the high temperatures characteristic of the exothermic foaming process of RPU foam with higher dimensions.

3. Processing of FTIR spectra: First, a background spectrum was deduced from each spectrum. Second, baseline correction was conducted in order to correct the intensity shifts at lower frequencies. The asymmetric CH stretching band at 2972 cm^{-1} (whose concentration remains constant during the reaction) was used as internal reference band to correct the concentration or density changes during the foaming process [25-28].

4. Isocyanate analysis: The isocyanate conversion during the foaming process was quantified by the area decay of the isocyanate absorption band. The limits chosen to carry out these measurements are 2500 and 2000 cm^{-1} (explained in the **article 1** included in **chapter 4**).

5. Amide I or carbonyl region analysis: The carbonyl absorptions of the urethane and urea groups obtained from the blowing and gelling reactions were identified by their second derivative technique, and they were separated and quantified by deconvolution using PeakFit program (**Figure 3.5**). The deconvoluted region (1601-1760 cm^{-1}) was chosen in order to avoid the absorption effects of other side bands from the aromatic C=C ring stretching and/or from amide II bands. Gaussian bands were used to be deconvoluted [29, 30], which finished once a correlation coefficient with at least three nines was obtained in the curve fittings. The parameter used to quantify the different bands contained in the carbonyl region and the

global urea and urethane content are detailed in the **article 1** included in **chapter 4**. Quantitative analysis was performed in this study assuming that the urethane and urea compounds in carbonyl region present similar extinction coefficients.

Figure 3.4. Scheme of the procedure followed to carry out the FTIR measurements with time.

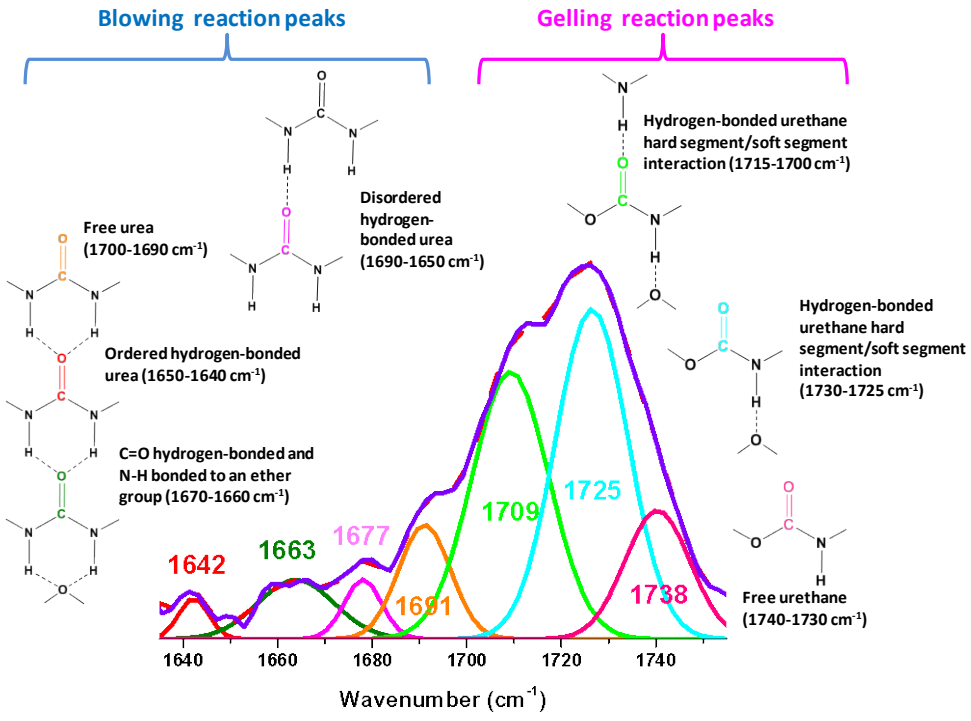

Figure 3.5. Example of deconvolution of Amide I region. Hidden bands in the carbonyl region associated with blowing and gelling reactions and their corresponding structure.

3.5.2.2- Infrared expandometry

A novel experimental technique named "Infrared Expandometry" was defined and introduced in the **article 2** included in **chapter 4** of this thesis. It allows monitoring simultaneously the expansion kinetics (height vs. time and volume vs. time), and the evolution of surface temperature of the RPU foams. A infrared camera detects the infrared radiation emitted by the foam during the exothermic foaming process, and transforms the infrared radiation into luminous images visible by the human eye. The acquired images are then analyzed in order to obtain quantifiable information. This technique was also applied in the **article 6** included in **chapter 6** of this thesis in order to study the differences of the expansion kinetics of RPU foams with different types of GO.

In order to record the foam expansion, an infrared camera (model HotFind L) from SDS Infrared was employed. Other experimental details of this technique for the expansion characterization of RPU foams are detailed next (**Figure 3.6**):

1. Sample preparation: The foams are produced in a plastic cup, as explained in the **section 3.3.1** of this chapter, and situated at 1,00 m of the infrared camera in order to record the foam expansion. The addition of the isocyanate to the polyol component was taken as time t = 0. From this moment, 25 frames per second (fps) were recorded during 7 minutes for every sample.

2. Temperature calibration: The infrared camera detects the surface temperature, which depends on the atmosphere transmittance. The latter is conditioned by the environmental conditions (mainly temperature and relative humidity of the surrounding atmosphere) and by the emissivity of the samples. Therefore, the environmental conditions were measured for each experiment, and the emissivity of the PU foams under study was fixed at 0.82 during the whole process.

3. Image analysis: Once the infrared images sequence of each sample has been acquired (see an example in **Figure 3.7**), an image analysis methodology based on ImageJ/Fiji software tool [31, 32] was implemented in order to extract the quantitative information of the foaming process. The main steps of the image analysis methodology are the following: (1) the 25 frames corresponding to one second were condensed into an average for these 25 images, (2) a binarization process after a filter application, and (3) binarized images were used to determine the quantitative parameters of the foaming process. Therefore, this technique allows evaluating the evolution of height, volume, expansion rate, expansion acceleration, and superficial temperatures (minimum, maximum and average), as well as the inhomogeneities in the sample surface. More details of the image analysis protocol and the parameters determined are detailed in the **article 2** included in **chapter 4** of this thesis.

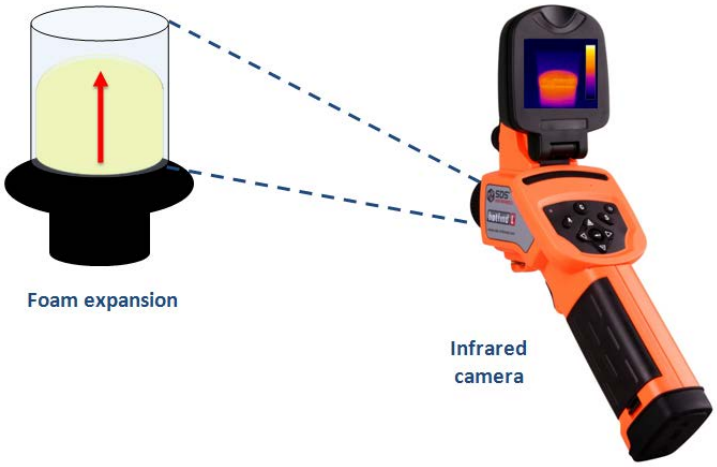

Figure 3.6. Scheme of the infrared radiation detection system in order to record the expansion of PU foam in a plastic cup.

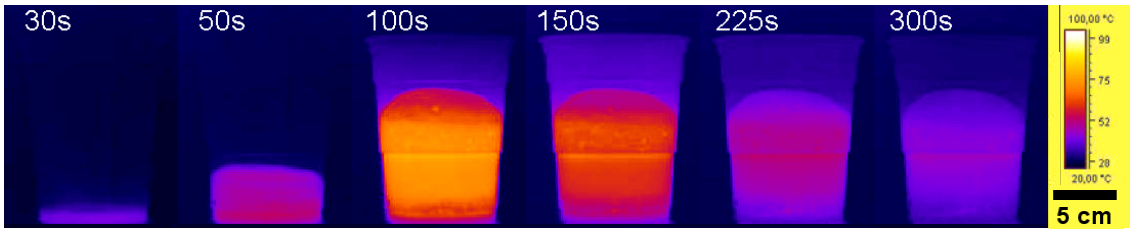

Figure 3.7. Example of infrared images at different times of the foaming process.

3.5.2.3- X-ray radioscopy

X-ray radioscopy, in which sequences of radiographies are acquired during foaming, has been demonstrated to be a useful tool for the *in-situ* inspection of the foaming process of PU materials. Several articles have been previously published in our laboratory on this methodology [33-35], which was applied in the **article 4** included in **chapter 4** of this thesis.

A home-designed equipment of X-ray was employed in order to follow the foaming process of RPU foams by X-ray radioscopy. The main experimental aspects of this technique are detailed next (**Figure 3.8**):

1. Sample preparation: The usual amount of isocyanate and polyol components were mixed in a plastic cup, as explained in the **section 3.3.1** of this chapter. Then 0.020 ± 0.009 mL of the reaction mixture were deposited on a specific foaming mould designed to perform the X-ray radioscopy experiments. This specific foaming mould is made of stainless steel, and consists on a central cylindrical hole (Ø = 6mm, thickness = 0.6 mm) where the reaction mixture was

poured. The hole is enclosed between two polypropylene plastic covers (25 µm thick) and the sample thickness is invariable during the process due to two lateral evacuation conduits. Two materials of known relative density (air, relative density = 0, and a TPU disc of the same thickness, relative density = 1) are situated into two smaller holes at each side of the main one, and scanned with the evolving sample to calibrate *in-situ* the X-ray acquired signal. Typically, lower amount of catalyst (0.3 ppw) is used in these studies because the cream time must be increased, in order to properly observe the foaming behaviour with the X-ray setup.

2. Measurement parameters of X-ray radioscopy: The X-ray tube was adjusted at 40 kV and 120 µA in order to obtain the optimum contrast of the acquired radiographies. Moreover, an exposure time of 800 ms was selected in order to record motionless and sharp images. A total of 700 radiographies were acquired, corresponding to *ca.* 9 min of the foaming process. A initial period of 50s is needed in order to place the foaming frame inside the X-ray cabinet.

3. Image Analysis: Once the radiographies of each sample were acquired (see an example in **Figure 3.9**), an image analysis protocol based on ImageJ/Fiji software tool [37,38] was applied to quantify the relative density, the cell size, and the nucleation cell density. All the details of the image analysis protocol and the parameters determined are detailed in the **article 3** included in **chapter 4** of this thesis.

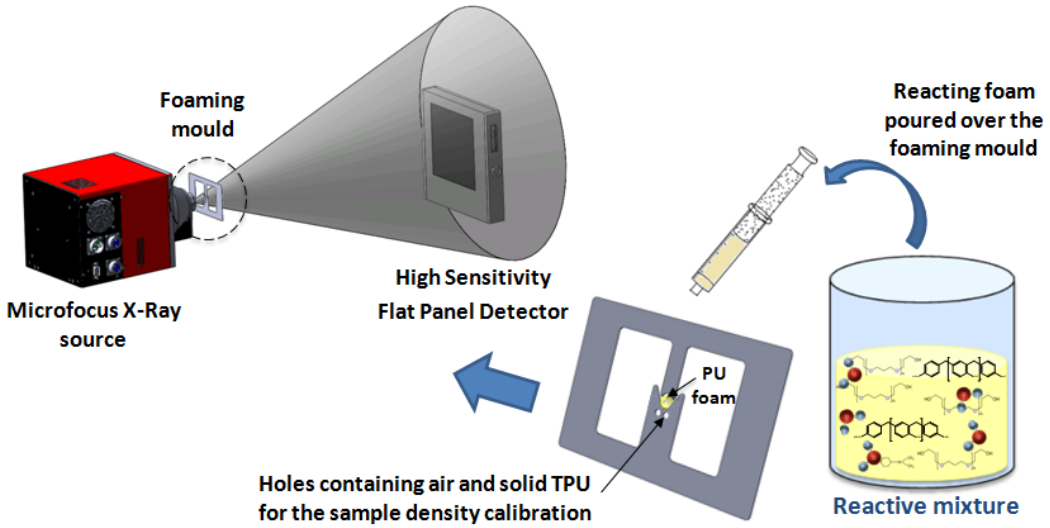

Figure 3.8. Scheme of the system employed to perform the X-ray radioscopy experiments.

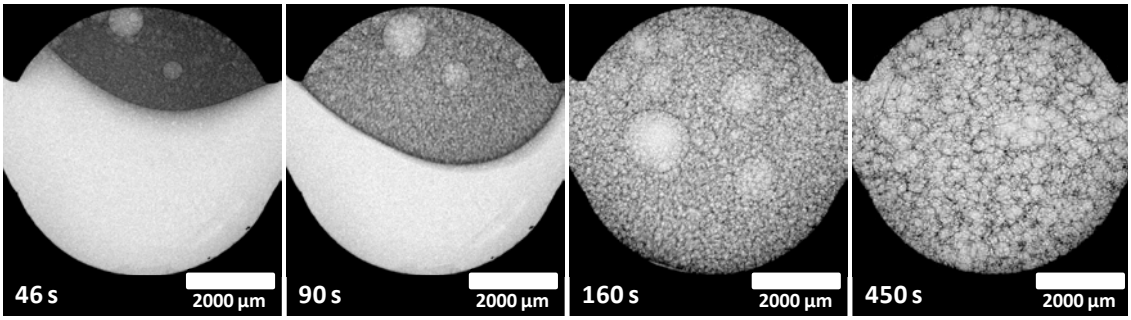

Figure 3.9. Example of X-ray radiographies obtained for two RPU foams at 75 and 420 seconds of the foaming process.

3.5.2.4- Adiabatic temperature rise

Adiabatic temperature rise is a technique used to follow the foaming temperature evolution with time. It is directly measured during the foaming process by thermocouples inside the foam, since the gelling and blowing reactions are exothermic. Because this is a fast and easy technique, several articles have been used to obtain information about the foaming process [36-40]. This technique was applied in the **article 2** (**chapter 4**), in the **article 5** (**chapter 5**) and in the **article 6** (**chapter 6**).

In order to measure the foaming temperature evolution, several thermocouples type K were introduced in the plastic cup which contains the reactive mixture (produced as explained in **section 3.3.1** of this chapter). The thermocouples are placed vertically in the center of plastic cup at the different heights from the base (**Figure 3.8**). The data collected by the thermocouples were registered in a computer.

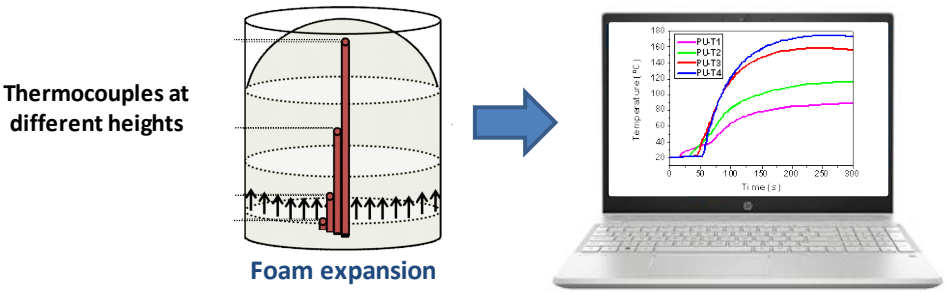

Figure 3.8. Scheme of the system employed to follow the foaming temperature reached with time. The position and number of thermocouples were fixed for each formulation of this thesis.

3.6- References

[1] IsoPMDI 92140 Technical Data Sheet. BASF Poliuretanos Iberia S.A.
[2] Elastopor H 1501/2 Technical Data Sheet. BASF Poliuretanos Iberia S.A.

[3] L. Madaleno, R. Pyrz, A. Crosky, L.R. Jensen, J.C.M. Rauhe, V. Dolomanova, A.M.M.V. de Barros Timmons, J.J. Cruz Pinto, J. Norman, Processing and characterization of polyurethane nanocomposite foam reinforced with montmorillonite–carbon nanotube hybrids, Composites Part A: Applied Science and Manufacturing, 44 (2013) 1–7.
[4] X. Cao, L. James Lee, T. Widya, C. Macosko, Polyurethane/clay nanocomposites foams: processing, structure and properties, Polymer, 46 (2005) 775–783.
[5] G. Harikrishnan, T.U. Patro, D.V. Khakhar, Polyurethane Foam-Clay Nanocomposites: Nanoclays as Cell Openers, Industrial and Engineering Chemistry Research, 45 (2006) 7126–7134.
[6] S. Estravis, PhD Thesis: Cellular nonocomposites based on rigid polyurethane and nanoclays: fabrication, caharacterization and modelling of the mechanical and thermal properties, University of Valladolid, 2014.
[7] M.M.A. Nikje, Z.M. Tehrani, Thermal and mechanical properties of polyurethane rigid foam/modified nanosilica composite, Polymer Engineering & Science, 50 (2010) 468–473.
[8] M.M.A. Nikje, Z.M. Tehrani, Polyurethane Rigid Foams Reinforced by Doubly Modified Nanosilica, Journal of Cellular Plastics, 46 (2010) 159–172.
[9] T. Widya, C. Macosko, Nanoclay-Modified Rigid Polyurethane Foam, Journal of Macromolecular Science, Part B: Physics, 44 (2005) 897-908.
[10] M.C. Saha, M.E. Kabir, S. Jeelani, Enhancement in thermal and mechanical properties of polyurethane foam infused with nanoparticles, Materials Science and Engineering: A, 479 (2008) 213-222.
[11] M.M.A. Nikje, Z.M. Tehrani, The Effects of Functionality of the Organifier on the Physical Properties of Polyurethane Rigid Foam/Organified Nanosilica, Designed Monomers and Polymers, 14 (2012) 263-272.
[12] M.M.A. Nikje, Z.M. Tehrani, Novel Modified Nanosilica-Based on Synthesized Dipodal Silane and Its Effects on the Physical Properties of Rigid Polyurethane Foams, Designed Monomers and Polymers, 13 (2012) 249-260.
[13] Technical data sheet: Products AEROSIL® fumed silica from Evonik Industries AG (Evonik Degussa). www.aerosil.com/product/aerosil/en/products.
[14] H.J. Walls, J. Zhou, J.A. Yerian, P.S. Fedkiw, S.A. Khan, M.K. Stowe, G.L. Baker, Fumed silica-based composite polymer electrolytes: synthesis, rheology, and electrochemistry, Journal of Power Sources, 89 (2000) 156–162.
[15] S.R. Raghavan, J. Hou, G.L. Baker, S.A. Khan, Colloidal Interactions between Particles with Tethered Nonpolar Chains Dispersed in Polar Media: Direct Correlation between Dynamic Rheology and Interaction Parameters, Langmuir 16 (2000) 1066–1077.
[16] A. Chuiko, Y. Gorlov, Chemistry of a Silica Surface, Kiev, 1992.
[17] Technical data sheet: Cloisite nanoclays from Southern Clay Products.
[18] J.M. Cervantes-Uc, J.V. Cauich-Rodríguez, H. Vázquez-Torres, L.F. Garfias-Mesías, D.R. Paul, Thermal degradation of commercially available organoclays studied by TGA–FTIR, Thermochimica Acta, 457 (2007) 92–102.
[19] A.B. Inceoglu, U. Yilmazer, Synthesis and mechanical properties of unsaturated polyester based nanocomposites, Polymer Engineering & Science 43 (2003) 661–669.
[20] ASTM D1622-08: Standard Test Method for Apparent Density of Rigid Cellular Plastics.
[21] ASTM D6226-10: Standard Test Method for Open Cell Content of Rigid Cellular Plastics.
[22] ISO 22007-2:2008. Plastics-Determination of Thermal Conductivity and Thermal Diffusivity—Part 2: Transient Plane Heat Source (Hot Disc) Method.
[23] ASTM D4274 - 16: Standard Test Methods for Testing Polyurethane Raw Materials: Determination of Hydroxyl Numbers of Polyols.
[24] ISO 868:2003: Plastics and ebonite. Determination of indentation hardness by means of a duromer (Shore hardness).

[25] M.J. Elwell, A.J. Ryan, H.J.M. Grünbauer, H.C.V. Lieshout, In-Situ Studies of Structure Development during the Reactive Processing of Model Flexible Polyurethane Foam Systems Using FT-IR Spectroscopy, Synchrotron SAXS, and Rheology, Macromolecules, 29 (1996).
[26] M.J. Elwell, A.J. Ryan, An FT i.r. study of reaction kinetics and structure development in model flexible polyurethane foam systems, Polymer, 37 (1996) 1353–1361.
[27] L. Ning, W. De-Ning, Y. Sheng-Kang, Crystallinity and hydrogen bonding of hard segments in segmented poly(urethane urea) copolymers, Polymer, 37 (1996) 3577-3583.
[28] M.M. Bernal, M.A. Lopez-Manchado, R. Verdejo, In situ Foaming Evolution of Flexible Polyurethane Foam Nanocomposites, Macromolecular Chemistry and Physics, 212 (2011) 971–979.
[29] D.P. Queiroz, M.N. de Pinho, C. Dias, ATR-FTIR Studies of Poly(propylene oxide)/Polybutadiene Bi-Soft Segment Urethane/Urea Membranes, Macromolecules, 36 (2003) 4195–4200.
[30] A. Marcos-Fernández, A.E. Lozano, L. González, A. Rodríguez, Hydrogen Bonding in Copoly(ether-urea)s and Its Relationship with the Physical Properties, Macromolecules, 30 (1997) 3584–3592.
[31] C.A. Schneider, W.S. Rasband, K.W. Eliceiri, NIH Image to ImageJ: 25 years of image analysis, Nature Methods, 9 (2012) 671-675.
[32] M.D. Abràmoff, P.J. Magalhães, S.J. Ram, Image Processing with ImageJ, Biophotonics International, 11 (2004) 36-42.
[33] S. Pardo-Alonso, E. Solórzano, S. Estravís, M.A. Rodríguez-Perez, J.A. de Saja, In situ evidence of the nanoparticle nucleating effect in polyurethane–nanoclay foamed systems, Soft Matter, 8 (2012) 11262.
[34] S. Pardo-Alonso, E. Solórzano, M.A. Rodriguez-Perez, Time-resolved X-ray imaging of nanofiller-polyurethane reactive foam systems, Colloids and Surfaces A: Physicochemical and Engineering Aspects, 438 (2013) 119-125.
[35] M. Mar Bernal, S. Pardo-Alonso, E. Solórzano, M.Á. Lopez-Manchado, R. Verdejo, M.Á. Rodriguez-Perez, Effect of carbon nanofillers on flexible polyurethane foaming from a chemical and physical perspective, RSC Advances, 4 (2014) 20761.
[36] S. Tan, T. Abraham, D. Ference, C.W. Macosko, Rigid polyurethane foams from a soybean oil-based Polyol, Polymer, 52 (2011) 2840-2846.
[37] M. Kurańska, A. Prociak, The influence of rapeseed oil-based polyols on the foaming process of rigid polyurethane foams, Industrial Crops and Products, 89 (2016) 182-187.
[38] A.N. Wilkinson, N.H. Fithriyah, J.L. Stanford, D. Suckley, Structure Development in Flexible Polyurethane Foam-Layered Silicate Nanocomposites, Macromolecular Symposia, 256 (2007) 65-72.
[39] M.M. Bernal, M. Martin-Gallego, I. Molenberg, I. Huynen, M.A. López Manchado, R. Verdejo, Influence of carbon nanoparticles on the polymerization and EMI shielding properties of PU nanocomposite foams, RSC Advances, 4 (2014) 7911.
[40] W. Ahn, J.-M. Lee, Effect of CNT as a Nucleating Agent on Cell Morphology and Thermal Insulation Property of the Rigid Polyurethane Foams, Journal of Nanoscience and Nanotechnology, 15 (2015) 9125-9130.

CHAPTER 4:

DEVELOPMENT OF A METHODOLOGY TO FOLLOW THE FOAMING PROCESS OF RIGID POLYURETHANE FOAMS

Mercedes Santiago Calvo

4.1- Introduction

The enhancement of the insulating properties of Rigid Polyurethane (RPU) is necessary for some applications, where requirements are getting more exigent. The addition of fillers to RPU foams offers an efficient way to increase their thermal and mechanical properties, enlarging the range of their applications. Although many investigations have been focused on the production and characterization of PU foams reinforced with micro and/or nanofillers, the effect of these fillers on the foaming process and reaction kinetics has barely been explored, in part due to the complexity of PU systems in which several chemical reactions are involved. In fact, a static observation of the different stages of the foaming process is often hindered.

When fillers are incorporated into the PU matrix, some foam properties may be improved, whereas others can be worsened. It is therefore important to understand how the fillers modify the PU reactions in order to explain the resulting morphology and properties of the foams. In addition, their possible negative effects should be compensated.

This chapter includes three scientific articles which have a common purpose: **developing/applying a methodology to monitor the foaming process of PU foams and thus understand their final structure and properties**. The articles are:

-Article 1: The effects of functional nanofillers on the reaction kinetics, microstructure, thermal and mechanical properties of water blown rigid polyurethane foams. Polymer 150 (**2018**) 138-149.

-Article 2: Infrared expandometry: a novel methodology to monitor the expansion kinetics of cellular materials produced with exothermic foaming mechanisms. Polymer Testing 66 (**2018**) 383-393.

-Article 3: X-ray radioscopy validation of a polyol functionalized with graphene oxide for producing rigid polyurethane foams with improved cellular structures. European Polymer Journal 118 (**2019**) 404-411.

Different techniques, which are complementary to each other, are set-up in order to monitor the foaming behavior of water-blown RPU foams: ***in-situ* FTIR spectroscopy**, **infrared expandometry** and ***in-situ* X-ray radioscopy** (see **Figure 4.1**). In addition to these techniques, the **rise** of the **adiabatic temperature** can be also used to obtain information about the foaming process by using thermocouples inside the foam. This method is used in the second article, which is focused on the introduction of infrared expandometry. A brief summary of the three articles are presented in the next paragraphs.

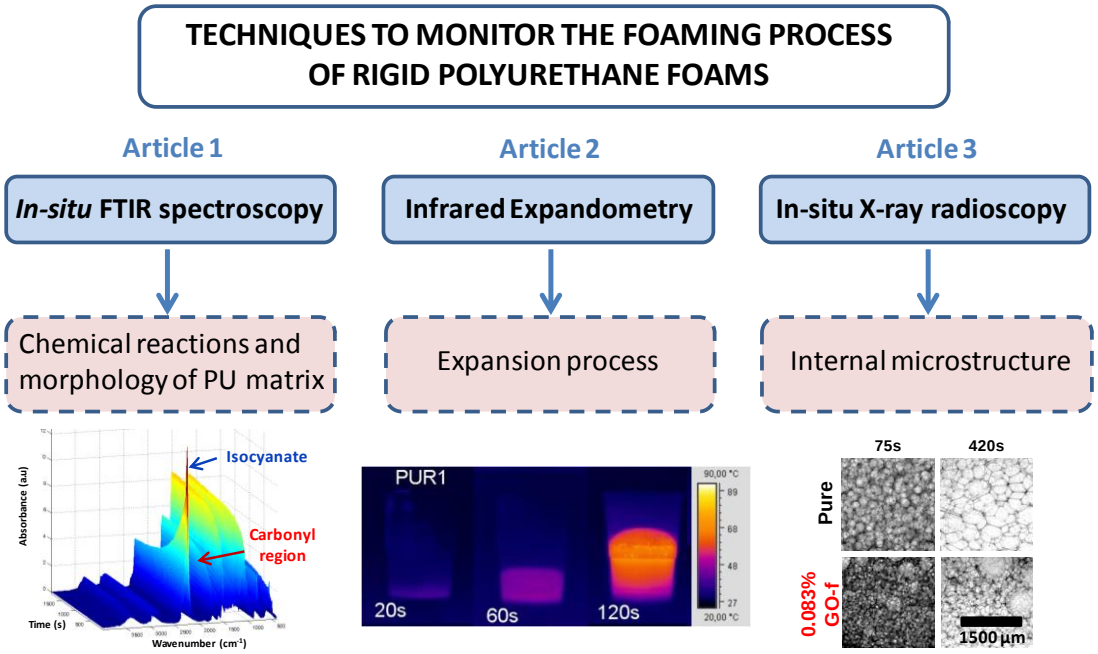

Figure 4.1. Scheme of the techniques used to follow the foaming process of RPU foams.

In the first article, the first experimental method to follow the foaming process is discussed. ***In-situ* FTIR spectroscopy** is used to monitor **the evolution of both the reactions and the morphology of the PU matrix** for RPU foams reinforced with different types of nanosilicas or nanoclays (5 wt%). For this purpose, a low amount of reacting foam (around 1 mL) extracted from a higher amount of reactive mixture, is poured on the ATR surface. The contribution of both blowing and gelling reactions (urea and urethane compounds) are studied by deconvolution of the carbonyl region. The FTIR results demonstrate how the different types and surfaces (hydrophobic and/or hydrophilic) of nanoparticles affect the reaction kinetics on different ways. The foams with nanosilicas show higher isocyanate conversion than those with nanoclays, being the conversion higher when hydrophobic groups are present on their surface. Moreover, hydrophobic nanoparticles promote the gelling reaction generating higher urethane groups, whereas hydrophilic nanoparticles enhance the blowing reactions increasing the urea groups. On the other hand, the effect of the modification of the reaction kinetics on the density, cellular structure, thermal conductivity and mechanical properties of RPU foams are also discussed.

Infrared expandometry, a novel experimental technique, developed in the second article, for monitoring **the expansion process** of a RPU foam, by taking advantage of their exothermic foaming process. In order to test this methodology, a RPU formulation has been chosen where the blowing agent (water) and/or the blowing catalyst are systematically changed. Thus, the expansion evolution of the foam can be followed from the initial to final times without any restrictions in the sample size. For example, the foaming process is monitored in this article in a plastic cup (15 cm of height by 10 cm of diameter). Important parameters of the foaming process are determined using the approach developed in this paper, such as the evolution of

height, volume, expansion rate, acceleration rate and surface temperature, among others. Moreover, the measurement of surface temperature can be quantified at certain areas of the surface or calculated for the whole sample surface, in both cases without interfering with the expansion process, what is a remarkable advantage compared to the traditional measurement of internal temperature using thermocouples. Thus, this article demonstrates the potential of this technique in order to follow the expansion kinetics of PU foams.

In-situ X-ray radioscopy is used in the third article to visualize the evolution of the **internal microstructure** of the foams during their production, obtaining relative density, cell size and cell nucleation density vs. time. These data are obtained by using a very low amount of the reacting components (around 0.02 mL), which is poured on the foaming mold after being extracted from a higher amount of reactive mixture. In the article, this technique has been used in order to compare the foaming behavior of two series of foams: those prepared from polyols functionalized with GO (GO-f) and those containing GO dispersed in the polyol (GO-d) by high shear mixing (loading of 0.017 and 0.083 wt%). The results obtained allow us evaluating which is the preponderant mechanism (nucleation or degeneration) in these systems. The foams containing GO-f present a cell size reduction as the amount of GO-f increases, whereas in the foams containing GO-d there is a decrease of cell size at low contents, because it is most difficult to achieve a proper dispersion of the fillers when the amount increases. Although the systems with GO-f present a high coalescence, the enhanced nucleation experienced by these foams prevails at final stages over the cell degeneration processes. The results obtained demonstrate that the use of polyol functionalized with GO-f highly improves the cellular structure and also makes the results more reproducible.

Taking into account the objectives of this thesis (**chapter 1**, **section 1.2**), the results obtained from these three works have allowed establishing and validating a methodology for monitoring the reaction and expansion kinetics, the morphology of the polymeric matrix, and the internal structure during foaming process of PU foams. Moreover, this methodology has allowed us understanding the effect produced by the fillers on the foaming process. This knowledge is fundamental in order to analyze and to understand the cellular structure and properties of the foamed materials.

Polymer 150 (**2018**) 138-149
https://doi.org/10.1016/j.polymer.2018.07.029

The effects of functional nanofillers on the reaction kinetics, microstructure, thermal and mechanical properties of water blown rigid polyurethane foams

Mercedes Santiago-Calvo[1,*], Josías Tirado-Mediavilla[1], José Luis Ruiz-Herrero[1], Miguel Ángel Rodríguez-Pérez[1], Fernando Villafañe[2]

[1] Cellular Materials Laboratory (CellMat), Condensed Matter Physics Department, Faculty of Science, University of Valladolid, Campus Miguel Delibes, Paseo de Belén 7, 47011 Valladolid, Spain

[2] GIR MIOMeT-IU Cinquima-Química Inorgánica. Faculty of Science, University of Valladolid, Campus Miguel Delibes, Paseo de Belén 7, 47011 Valladolid, Spain

* Corresponding author: mercesc@fmc.uva.es

Abstract

The use of functional nanofillers to improve the properties of rigid polyurethane (PU) foams has caused the need for a better understanding of how these nanofillers modify the reaction kinetic of the PU system. In this study, different nanoclays and nanosilicas are used as functional nanofillers. Analysis of the kinetic data obtained by *in-situ* FTIR spectroscopy monitoring allows to correlate the isocyanate consumption with the type of nanoparticles. The quantification of urethane and urea, obtained by deconvolution of the carbonyl region absorptions, enables to follow the blowing and gelling reactions during the foaming process. These reactions are correlated to the nature of the chemical groups present on the surface of the nanoparticles added. In addition, the effect of the modification of the reaction kinetics on the density, cellular structure, thermal conductivity and mechanical properties is herein discussed.

Keywords: Polyurethane foam; nanoclay; nanosilica; reaction kinetics; thermal properties; mechanical properties

Development of a methodology to follow the reaction kinetics of rigid polyurethane foams

1. Introduction

Polyurethanes (PUs) are multipurpose polymers, since they are present in a wide range of industrial sectors, like automotive, medical, construction, furniture, appliances, etc [1]. PUs can be found commercially as solid thermoplastics (known as TPU), coatings, adhesives, sealants, binders, elastomers, and foams [2].

PUs foams are usually classified according to their mechanical behavior as flexible foams (such as those used for furniture, mattresses or automotive seats), or rigid foams (which can be applied for insulation and structural materials) [3]. PU foams represent almost a 50% of the global market of foams, and their use is still substantially growing over the years [4]. Thermal management in buildings and transportation insulation or refrigeration systems are the core applications of rigid PU foams with closed cells [**Figure 1(a)**]. These applications have been extensively studied both theoretically [5-7] and experimentally [8-11].

Incorporating additives to the PU formulation is an excellent method to improve the mechanical, thermo-mechanical, or thermal properties of the foam. Nanoscale size fillers are becoming a promising option in order to obtain improved properties [12, 13]. For a PU foam with closed cells, with a density of 50 kg/m^3, the cell wall thickness is usually in the range of 1 to 2.5 microns [**Figure 1(c)**], and therefore the typical sizes of cells and struts are slightly higher [**Figures 1(a) and 1(b)**] [14, 15]. These features should be taken into account in order to select an appropriate filler for modifying its physical properties, and a logical approach is adding fillers with at least one of the dimensions clearly below the thickness of the cell walls (i.e. smaller than 1 micron).

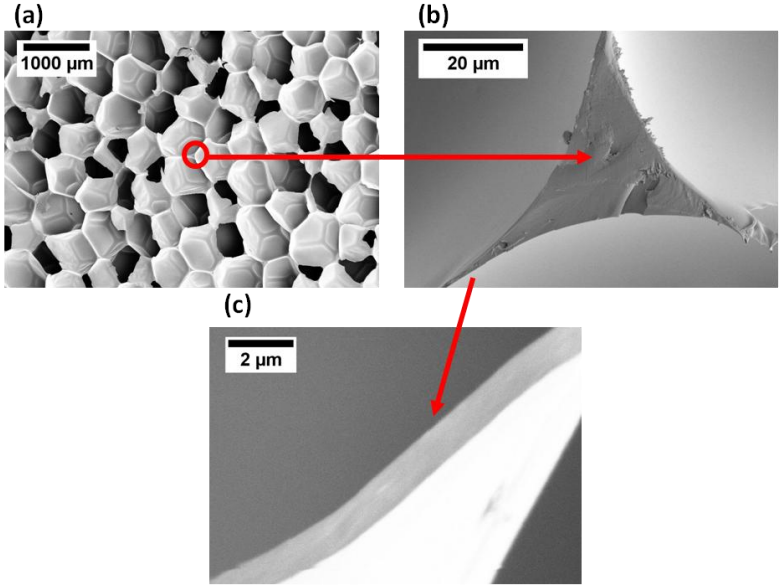

Figure 1. SEM micrographs of the microstructure of a closed cell rigid PU foam: (a) Microstructure formed by closed cells. The components of closed cells are (b) struts, and (c) cell walls with thickness in the range of 1 to 2.5 microns.

These reasons have encouraged the research on the incorporation of nanofillers into a variety of materials and foams [16, 17]. These works have allowed concluding that the properties on the final composite depend, among other aspects, on the nanofiller chemical composition and on the size and shape of the nanoparticles [18, 19].

So far, the reinforcing inorganic materials probably more extensively used are layered nanoclays, especially those based on montmorillonite, $[(Na,Ca)_{0.33}(Al,Mg)_2(Si_4O_{10})(OH)_2 \bullet nH_2O]$. This is due to their cation exchange capacity, high surface and reactivity, and adsorptive properties. The structure of montmorillonite is based on a central octahedral sheet of alumina, sandwiched between two external silica tetrahedral sheets. The interlayer galleries (of about 1 nm in thickness and 100 nm in width and length) are occupied by cations (usually Na^+ and Ca^{2+}). The presence of these cations in the interlayer spaces makes montmorillonite hydrophilic, which is the main reason for its poor compatibility with organic polymers. Thus, metallic cations must be substituted by hydrophobic organic cations (alkylammonium or -phosphonium quaternary salts) in order to both enhance a better layer separation, and to improve compatibility with the polymer matrix. Introducing nanoclays based on montmorillonite into PUs allows overcoming some of the weaker aspects of these foams, such as their relatively poor thermal stability, or their low gas-barrier properties. Thus, these type of PU-montmorillonite composites have been studied,[14, 20-22] and many investigations have been focused on their methods of preparation, structure, hydrogen bonding, degree of clay dispersion or exfoliation, microphase morphology, rheology, mechanical properties, thermal stability, flame retardancy, water sorption, or barrier properties [23].

On the other hand, the number of papers describing polymers reinforced with dispersed silica nanoparticles is also high [24, 25]. Nanosilica surface is hydrophilic due to the presence of hydroxyl groups, which generate hydrogen bonding and therefore significant interactions between particles. For this reason, nanoparticles tend to agglomerate, what should be precluded in order to favor the dispersion of nanoparticles into the polymer matrix. The degree of nanoparticles dispersion and the interfacial adhesion are important drawbacks to obtain appropriate materials, [26] and surface modification is the best way to reduce the preference for agglomeration of nanosilica particles [27]. Thus, the replacement of silanol groups by non-polar silyl groups removes the active hydrogen bonds on the surface, and changes the hydrophilicity of the filler surface into hydrophobic. The studies carried out on PU/nanosilica composites reveal that the addition of surface modified nanosilicas can improve the thermal, rheological, mechanical, and adhesion properties of PUs [17].

The properties of composites resulting from the addition of either nanoclays or nanosilicas to PU foams have been studied to some extent, [21, 24] but most of the reports are mainly focused on the production and characterization of the foams, paying particular attention to the nanoparticles dispersion. However, the effect of these additives on the chemical reactions occurring during foaming has been very scarcely explored. PUs are obtained when isocyanate

react with active hydrogen containing compounds, such as the hydroxyl groups of long polyether or polyester chains (polymerization or gelling reaction), or water (blowing reaction) to give urethane or urea linkages respectively. These two simultaneous processes should be adequately controlled in order to obtain a polymer foam with the desired cellular structure and physical properties [3, 28, 29]. The presence of additives such as nanofillers may modify the kinetics of these chemical reactions, by increasing or decreasing reaction ratios leading to a modification of urethane and/or urea linkages, thus affecting the foaming process and the final morphology of the PU matrix, and consequently the properties of the final foam. The modification of the reaction kinetics, microstructure and physical properties of PU systems containing nanofillers is a topic which depends on many interconnected factors, and therefore requires a high degree of systematization.

The aim of this work is to study systematically the effect of different nanoparticles on the reaction kinetics of rigid PU foams formation, and to analyze how these modifications affect the cellular structure and physical properties of the foams.

2. Experimental

2.1. Reactants

A commercial, bi-component formulation of rigid PU foam from "BASF Poliuretanos Iberia S.A." was used in this investigation. The polyol component, Elastopor H 1501/2 (OH index 651 mg KOH/g, density 1.07 g cm^{-3}, viscosity 650 mPa·s) is a mixture of components containing polyether polyol, catalysts and stabilizers [30]. The formulation uses water as blowing agent. The isocyanate component, IsoPMDI 92140 (31.5% NCO, density 1.23 g cm^{-3}, viscosity 170-250 mPa·s), is a polymeric diphenylmethane diisocyanate (pMDI) [30, 31]. According to supplier technical data sheet, the proportions of the two component formulation were set at 100/160 by weight for the polyol and isocyanate. Other features provided for BASF formulation are: free foaming density of 52±5 kg/m^3, cream time (45±7), gel time (145±18) and rise time (232±21).

2.2. Nanofillers Reactants

Table 1 collects the nanofillers used: two nanoclays (Cloisite®Na^+ and Cloisite®30B) and three nanosilicas (Aerosil®A200, Aerosil®R812 and Aerosil®R974). The hydrophobic or hydrophilic character of these particles has been previously established in several studies referenced in **Table 1**, and has been confirmed in this research through the characterization of nanoparticles by FTIR spectroscopy and Thermogravimetric analysis (TGA).

AEROSIL® fumed silica supplied by Evonik Industries AG (Evonik Degussa) are: (a) Aerosil®A200 (without modifier) with a specific surface area of 175-225 m^2/g; (b) Aerosil® R812 (post-treated

with hexamethyldisilazane) with a specific surface area of 230-290 m^2/g; and (c) Aerosil® R974 (post-treated with dimethyldichlorosilane) with a specific surface area of 150-190 m^2/g [32]. Nanoclays supplied by Southern Clay Products Inc are: Cloisite®Na^+ with a specific surface area of 700-786 m^2/g (CNa+, natural montmorillonite), and Cloisite®30B (organically modified montmorillonite with methyl tallow bis-2-hydroxyethyl quaternary ammonium chloride) with a specific surface area of 760 m^2/g. Cloisite®30B contains both hydrophilic (hydrogen bonded water molecules in the silicate layer surfaces) and hydrophobic groups (hydrocarbon chains of either 18, 16 or 14 carbon atoms in the methyl-bis-2-hydroxyethyl-tallow quaternary ammonium cation) [33, 34].

Table 1. Additives used in this study describing the surface groups and their hydrophilic/hydrophobic nature.

Additive	Surface groups	Type of surface
Aerosil®A200 (A200)	Silica nanoparticles without any further treatment [32, 35, 36]	Hydrophilic
Aerosil®R812 (R812)	Silica nanoparticles post-treated with hexamethyldisilazane (90%) [32, 37]	Hydrophobic
Aerosil®R974 (R974)	Silica nanoparticles post-treated with dimethyldichlorosilane (50%) [32, 35, 36]	Partially hydrophilic/partially hydrophobic
Cloisite®Na^+ (CNa+)	Natural Montmorillonite [33, 38, 39]	Hydrophilic
Cloisite®30B (C30B)	Organically modified montmorillonite with methyl tallow bis-2-hydroxyethyl quaternary ammonium chloride (30%) [33, 38, 39]	Partially hydrophilic/partially hydrophobic

2.3. Synthesis of the PU Foams

Six different PU foam systems were studied: the pure material, and those containing either 5 wt% A200, 5 wt% R812, 5 wt% R974, 5 wt% CNa+ or 5 wt% C30B.

"Pure" corresponds to the PU foam without additives that will be considered as the reference material. The nanoparticles (5% in weight) were previously dried under vacuum at 50°C overnight before being dispersed into the isocyanate component. An overhead stirrer (EUROSTAR Power control-visc P1, IKA) with a 50 mm diameter Lenart disc stirrer was used to premix the nanoparticles with the isocyanate component during 300 seconds for an optimal dispersion (at 1200 rpm during the first minute and the remaining time at 250 rpm). The polyol and isocyanate were mixed in a plastic cup with a ratio of 100:160 by weight at 1200 rpm for 10 seconds to promote the chemical reactions and the foaming process. Foams with cylindrical sizes of 100 mm x 200 mm (diameter x height) were produced. After the foaming and curing at room temperature for 2 days, samples were characterized.

2.4. Nanofillers characterization

Three methods were used for the characterization of the nanoparticles. Surface groups were identified by Fourier transform infrared (FTIR) spectroscopy, using a Bruker Tensor 27 spectrometer in the attenuated total reflectance (ATR) method. Thermogravimetric analysis (TGA) was performed with a Mettler Toledo TGA/SDTA 851 from 50 to 1000 °C at a heating rate of 20 °C/min, under inert atmosphere (N_2). Morphological characterization was carried out using a Quanta 200 FEG environmental scanning electron microscope (ESEM).

2.5. Foam characterization

2.5.1. Density

Foam density was measured as described by ASTM D1622/D1622M-14 [40]. Three different cylindrical samples of 30 mm x 25 mm (diameter x height) for each material were measured.

2.5.2. Open cell content

The open cell content (OC) was measured by using a gas pycnometer Accupyc II 1340 from Micromeritics, according to ASTM D6226-10 [41]. The OC was measured in three cylindrical samples of each material after measuring their densities.

2.5.3. Scanning electron microscopy (SEM)

The cellular structure of the foam and SEM micrographs were acquired by Scanning electron microscopy (SEM) with a JEOL JSM-820 microscope. The cured foams were cut in order to ensure a smooth surface, which was examined by SEM after vacuum coating with a gold monolayer. SEM micrographs were obtained for the growth plane (z plane) of the foam.

An image analysis technique [42] was used to determine the main characteristics of the cellular structure: average cell size (Φ3D), anisotropy ratio (AR)) and the homogeneity of the cell size distribution measured using the parameter normalized standard deviation (NSD), which is the ratio of the standard deviation (SD) of the cell size distribution and the Φ3D.

2.5.4. Thermal Conductivity measurements

The thermal conductivity was determined at 20°C using a hot-disk transient plane source (TPS) thermal constant analyzer according to ISO 22007-2:2008 method [43]. Transient methods are based on the analysis of the thermal response of a sample submitted to a controlled transient heat flow. The measurements were performed using two cylindrical samples of 30 mm x 25 mm (diameter x height) for each material. A disk shaped TPS sensor with a radius of 3.189 mm was used in all measurements, after being located in contact with the xy plane (perpendicular to growth plane) of the two samples.

2.5.5. Dynamical mechanical analysis (DMA)

Dynamical mechanical analysis (DMA) was carried out using a PerkinElmer DMA7 dynamic mechanical analyzer using a heating rate of 3°C/min from 25 to 200°C. A parallel-plate system with a top plate of 12 mm in diameter was used on a cylindrical sample of 12 mm x 7 mm (diameter x height). The storage modulus (E'), loss modulus (E''), and loss factor (tan δ) curves were obtained from DMA measurements. The glass transition temperature (Tg) of the polymer was calculated from the curve of tanδ vs. temperature.

2.5.6. Mechanical Tests

Mechanical tests in compression were performed according to ASTM D1621-10 [44]. An Instron Machine (model 5.500R6025) was used for this purpose. Stress (σ)–strain (ε) curves in compression were obtained at room temperature at a strain rate of 10 mm/min. The maximum static strain was 75% for all the experiments, and the compression tests were always performed in a direction parallel to the growing direction. The samples were prepared with rigorously parallel contact surfaces. Young´s modulus (E) and collapse stress (σ) were measured in three cylindrical samples of 30 mm x 25 mm (diameter x height) for each material.

2.6. Foaming kinetics: FTIR measurements

In-situ FTIR spectra of the samples were collected using a Bruker ALPHA spectrometer working in ATR method. 1 mL of the reacting foam was poured on the surface of the ATR cell to obtain the variation of FTIR spectra vs time. In order to ensure the uniformity of the reacting foam, a higher amount of polyol (30 g) and isocyanate (48 g) (similar amounts to those used to produce the foams with the dimensions mentioned in section 2.2) were mixed at 1200 rpm for 10 seconds, and then 1 mL of this reacting foam was poured on the ATR surface. This method was designed in order to make uniform the low amount of reaction mixture used in FTIR experiments. The addition of the isocyanate was taken as time t = 0. The maximum elapsed time between the addition of isocyanate and the acquisition of the first scan was

approximately 1 minute. Each FTIR spectrum was obtained after 16 scans, with a resolution of 4 cm^{-1} in the range 4000-400 cm^{-1}. In order to reproduce the high temperatures characteristics of the exothermic foaming process of PU, FTIR experiments were carried out at 70°C, using the plate available in the FTIR equipment. A background spectrum was deduced from each reaction spectra, and a total of 90 spectra were run for each experiment, which lasted 30 minutes. Baseline correction was conducted in order to correct the intensity shifts at lower frequencies. According to the literature [45, 46], the asymmetric CH stretching band at 2972 cm^{-1} (which remains constant during the reaction) was used as internal reference band to correct the concentration or density changes during the foaming process. The results herein reported are the average of three experiments. The maximum error reached for the isocyanate conversion was a 3% and a 5% for urea and urethane quantification.

The overlapped absorptions in the amide I region (carbonyl region) were deconvoluted using Gaussian bands. Curve fittings were adjusted using methods previously reported.[47, 48] Hidden bands were identified following the second derivative technique, and correlation coefficient with at least three nines was obtained in the fittings. The deconvolution range was chosen to give appropriate adjustment within the range 1790-1570 cm^{-1}. These limits were chosen in order to avoid the absorption effects of side bands from the aromatic C=C ring stretching and from amide II bands.

In addition, the premix of the nanoparticles with the isocyanate component was characterized by FTIR spectra (blank experiments), using a Bruker Tensor 27 spectrometer in ATR method.

3. Results and discussion

3.1. Nanoparticles characterization

Table 1 summarizes the nanoparticles used in this study, as well as the hydrophilic and/or hydrophobic nature of the surface groups present in them. These groups are critical on several aspects of the foams production, such as the dispersion of the fillers, their interaction with the PU matrix, and the possible nucleating effect during foaming. In addition, these surface groups can interact both with the functional groups of the reactants, and with the polymer molecules formed during the reaction. All these aspects may affect the reaction kinetics, so we decide to carry out a complete characterization of the selected additives in order to understand the phenomena occurring during the reactions.

3.1.1. FTIR spectroscopy

FTIR spectra of nanosilicas are shown in **Figure S1** (**supporting information**). The spectrum of A200 (unmodified nanosilica) shows an absorption peak *ca.* 3334 cm^{-1} (O-H stretching vibrations), which may be assigned to the silanol groups on the nanosilica surface. The spectra

of R812 and R974 (modified nanosilicas with methyl groups on their surface collected in **Table 1**) also show absorptions of O-H stretching vibrations at 3334 cm^{-1}, which have lower intensity than those of the unmodified nanosilica A200. Moreover, in the spectra of R812 and R974, the presence of methyl groups of surface modifier was confirmed by absorption peaks of the C-H stretching vibrations at 2964 cm^{-1} for R812 or 2971 cm^{-1} for R974. The absorptions at 1052 cm^{-1} and at 807 cm^{-1} detected in all nanosilicas are attributed to the asymmetric and symmetric Si-O-Si stretching vibrations. The FTIR spectra confirm the presence of hydrophobic groups in the surface of R812 and R974.

FTIR spectra of nanoclays are shown in **Figure S2** (**supporting information**). The spectra of both CNa+ (natural nanoclay) and C30B (organically modified nanoclay) show bands in the 3100-3700 cm^{-1} region (assigned to O-H stretching of silicate and water hydroxyl groups), at 1634 cm^{-1} (O-H bending), at *ca.* 990 cm^{-1} (Si-O-Si stretching of silicates), and at 917 cm^{-1} (Al-O-Al deformation of aluminates) [38]. Some absorptions displayed by the organically modified nanoclay (C30B) spectrum, which are not exhibited by natural nanoclay (CNa+), belong to the organic fragment of the modifier collected in **Table 1**, and are located at 2926 cm^{-1} (CH_2 stretching), 2852 cm^{-1} (CH_3 stretching), 1469 cm^{-1} (CH_2 bending), and 1374 cm^{-1} (CH_3 bending).[38] These FTIR results support the partially hydrophobic character of C30B in comparison with CNa+, which is entirely hydrophilic since its surface has not been modified.

3.1.2. Thermogravimetric analysis (TGA)

Thermograms of nanosilicas are shown in **Figure S3** (**supporting information**). Nanoparticles thermograms present mass loss from 50 to 1000 °C of *ca.* 0.81% for A200, *ca.* 2.70% for R812, and *ca.* 0.83% for R974. The weight loss for A200 (unmodified nanosilica) is attributed to the removal of adsorbed water on the nanosilicas surface. Considering R812 and R974 (modified nanosilicas with methyl groups on their surface), the mass loss is attributed to adsorbed water, as well to the content of the organic moieties. Therefore, R812 (with a 90% of hydrophobic groups in the surface) has a higher mass loss than R974 (with only a 50% of them).

Thermograms of nanoclays are shown in **Figure S4** (**supporting information**). The main differences between the thermograms of CNa+ (natural nanoclay) and C30B (organically modified nanoclay) are due to the decomposition of the organo-modifier present in the latter. The residual mass of CNa+ (92.02%) is composed of inorganic material and is higher than that of C30B (69.98%), due to the loss of the organic modifier. The mass loss below 150°C, attributed to weakly chemical bonded water volatilization, is higher for natural nanoclay (1.57%) than for the organically modified nanoclay (0.57%). This means that C30B contains less water, what should be expected taking into account its partially hydrophobic nature.

3.1.3. Scanning electron microscopy (SEM)

The particle morphologies were examined by SEM (**Figure 2**), supporting the particles size provided by the supplier. The micrographs show the spherical size (with a particle size of around 7 nm for R812 and 12 nm for A200 and R974) of nanosilicas, whereas CNa+ and C30B present platelet shapes with lateral sizes in micrometric dimensions (*ca.* 2-13 µm) and thickness of individual platelets in the nanoscale.

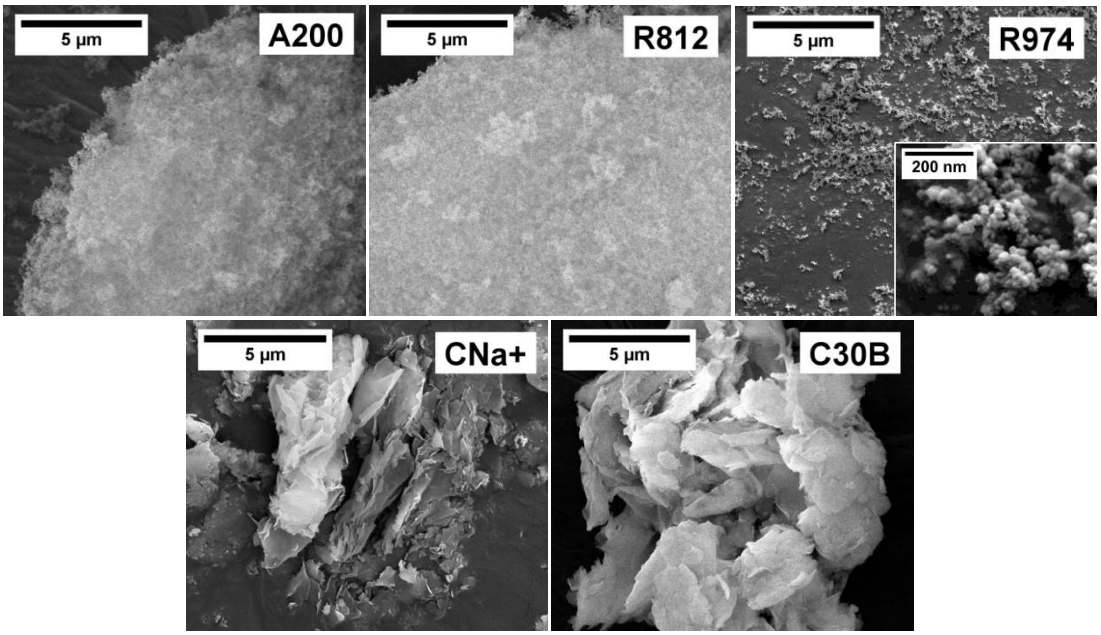

Figure 2. SEM micrographs of the nanoparticles used for this study.

3.2. Kinetics studies: FTIR measurements

In-situ FTIR spectroscopy is a useful technique to monitor the reaction kinetics of PU foams. The isocyanate consumption can be followed by the isocyanate asymmetric stretching vibration at 2270 cm^{-1}. In addition, carbonyl stretching vibrations of the Amide I Region (in the range of 1610-1760 cm^{-1}) allow following the generation of urethane and urea products connected with the gelling and blowing reactions respectively. An example of the reaction monitoring of the pure PU foam by *in-situ* FTIR spectra is depicted in **Figure 3**, where the isocyanate consumption and products generation are highlighted.

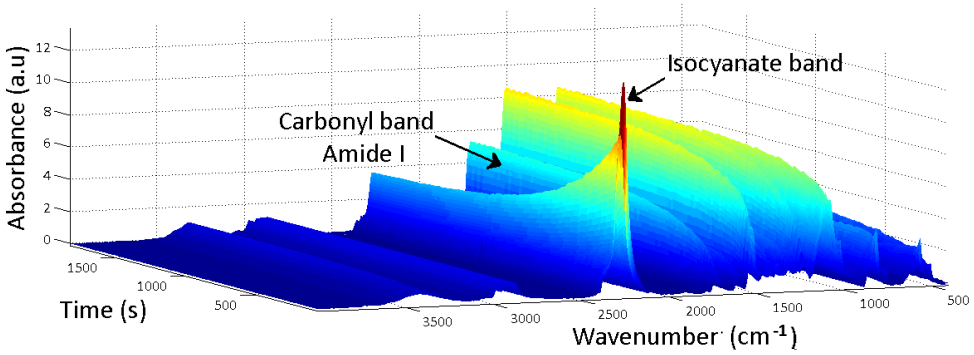

Figure 3. FTIR spectra for pure PU foam for 30 minutes.

3.2.1. Isocyanate analysis

The decay of the isocyanate absorption band (located between 2500 and 2000 cm^{-1}) was used to quantify the isocyanate group conversion during polymerization. The isocyanate conversion (*p*NCO) is defined by **Equation 1** [46]:

$$pNCO = \frac{A_0 - A_{max}}{A_0} \quad \textbf{(1)}$$

where A_0 is the extrapolated absorbance (measured as the area under the isocyanate band) of the isocyanate band at t = 0, and A_{max} is the integrated absorbance of the isocyanate band at time = t. **Figure 4** shows the isocyanate conversion obtained from this equation for all the systems under study. These data indicate that for all the materials the isocyanate conversion increases with time and reaches an almost constant value at 15 minutes. However, the isocyanate is not entirely consumed even after the 30 minutes of reaction which have been monitored; and therefore its complete conversion into PU requires longer times and/or higher temperatures. The conversion curves show a higher isocyanate conversion for foams containing surface treated nanosilicas than for foams containing nanoclays, whereas the pure foam conversion is similar to those containing nanosilicas. In the case of the foam with nanosilica A200, the isocyanate conversion is slightly higher than that of the pure foam in the early part of the foaming reaction (until 400 seconds), but slightly lower after that point.

Different factors such as the amount, type, shape, specific surface area and functionality of nanofillers determine the isocyanate conversion in nanocomposite foams. Several authors [49] have concluded that the reaction kinetics depends mainly on the viscosity of the mixture when the nanocomposite foam contains low concentrations of nanofillers. As the concentration of nanoparticles increases, the type and shape have a definitive effect on the reaction kinetics [50]. In our case, all the systems studied contain the same amount of nanoparticles (5 wt.%), but those with nanosilicas give rise to higher isocyanate conversions. Thus, isocyanate reaction can be related to the type of particles (nanoclays or nanosilicas). In addition, the foams containing nanosilicas R812 (hydrophobic) and R974 (partially hydrophilic and partially

hydrophobic) show higher isocyanate consumption than the foam with nanosilica A200 (hydrophilic), whereas the foam with C30B (partially hydrophilic and partially hydrophobic) presents a higher isocyanate conversion than that containing nanoclay CNa+ (hydrophilic). Therefore, the isocyanate reaction rate depends also on the nature of the superficial groups present in each type of particle, being this conversion higher when hydrophobic groups are present.

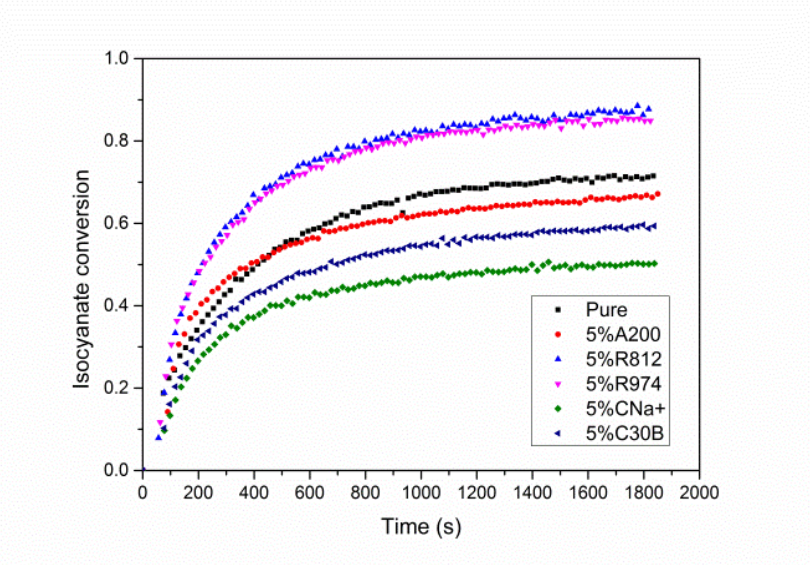

Figure 4. Isocyanate conversion as a function of time for the systems under studied.

3.2.2. Amide I region analysis

Figure 5(a) shows the time evolution of the amide I band. The vibrations associated with urea and urethane groups present in this region were detected and separated after deconvolution [47]. **Figure 5(b)** shows an example of the second derivative spectrum calculated in order to perform the deconvolution. **Figure 5(c)** shows an example of the deconvolution of the amide I zone of the spectrum and **Table 2** summarizes all the bands used to carry out this deconvolution, as well as their assignment.

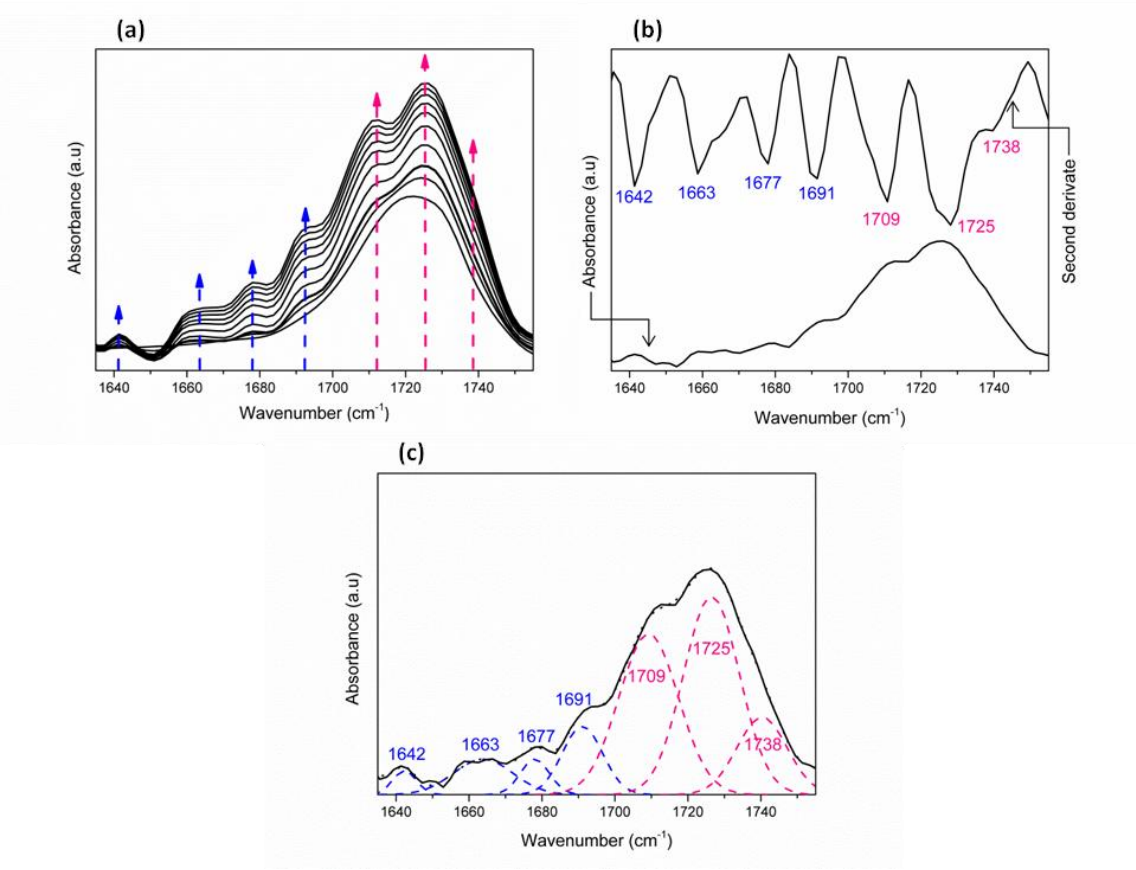

Figure 5. Example of the deconvolution of amide I region for the PU foam containing 5% C30B: **(a)** Evolution of the amide I region. **(b)** Spectrum of the amide I region at the bottom and the corresponding second derivative at the top. **(c)** Curve-fitting in the amide I region.

TABLE 2 Carbonyl stretching assignments in PU foams.

Functional group	Frequency (cm^{-1})	Band assignment
v(C=O) Urethane	1740-1730	Free urethane [46, 51-56](Urethane groups free from hydrogen-bonds)
	1730-1725	Hydrogen-bonded urethane hard segment/soft segment interaction [51-55](Ether polyol hydrogen-bonded urethane)
	1715-1700	H-bonded urethane HS/HS interaction [51-55]
v(C=O) Urea	1700-1690	Free Urea [45, 46, 48, 51] (Urea groups free from hydrogen-bonds)
	1650-1690	Disordered hydrogen-bonded urea [51, 56]
	1660-1670	C=O hydrogen-bonded and N-H bonded to an ether group [48]
	1650-1640	Ordered hydrogen-bonded Urea [45, 46, 48, 49, 51, 56, 57]

The deconvolution of the amide I absorptions allows obtaining quantitative measurements of the amounts of the different carbonyl groups present in the reaction mixture (seven peaks collected in **Table 2**). The relative area percentage for each peak was obtained by dividing the corresponding peak area by the total amide I area (sum of areas of seven peaks present in this region ($\sum A_{c=oUrea} + \sum A_{c=oUrethane} = A_{amide\ I}$)) at each time. Moreover, this analysis provides the total relative area percentages of the total ureas (sum of areas correspond to all urea peaks ($\sum A_{c=o\ Urea}$) divided by the total amide I area ($A_{amide\ I}$)), and the total urethanes (sum of areas correspond to all urethane peaks ($\sum A_{c=o\ Urethane}$) divided by the total amide I area ($A_{amide\ I}$)). Thus, **Equations (2)** and **(3)** give results for the two main reactions: the blowing reaction associated to the urea groups and the gelling reaction associated to the urethane groups. **Table 3** summarizes the urethane/urea ratios obtained for different times, calculated from the relative area percentages of urethanes divided by the relative area percentages of ureas as given in **Equation (4)**. **Figure 6** shows the relative area percentage associated to urea and urethane detected in the amide I region at a time of 30 minutes.

$$\text{Relative Area \% of total Urea} = \frac{\sum A_{c=oUrea}}{\sum A_{c=oUrea} + \sum A_{c=oUrethane}} = \frac{\sum A_{c=o\ Urea}}{\text{amide I}} \quad (\mathbf{2})$$

$$\text{Relative Area \% of total Urethane} = \frac{\sum A_{c=oUrethane}}{\sum A_{c=oUrea} + \sum A_{c=oUrethane}} = \frac{\sum A_{c=o\ Urethane}}{\text{amide I}} \quad (\mathbf{3})$$

$$\text{Urethane/Urea ratio} = \frac{\text{Relative Area \% of total Urethane}}{\text{Relative Area \% of total Urea}} = \frac{\sum A_{c=o\ Urethane}}{\sum A_{c=o\ Urea}} \quad (\mathbf{4})$$

Table 3. The urethane/urea ratio of PU foam as a function of the time.

Time (*ca.* min.)	Urethane/Urea ratio					
	Pure	**5%A200**	**5%R812**	**5%R974**	**5%CNa+**	**5%C30B**
1	2.35	2.50	2.54	2.54	3.13	3.01
3	2.12	1.79	1.94	2.32	2.75	2.83
5	1.82	1.52	1.94	1.73	1.76	1.95
15	1.89	1.65	2.05	1.73	2.07	2.88
20	1.95	1.50	2.15	1.66	2.09	2.86
30	2.01	1.60	2.39	1.65	1.92	2.72

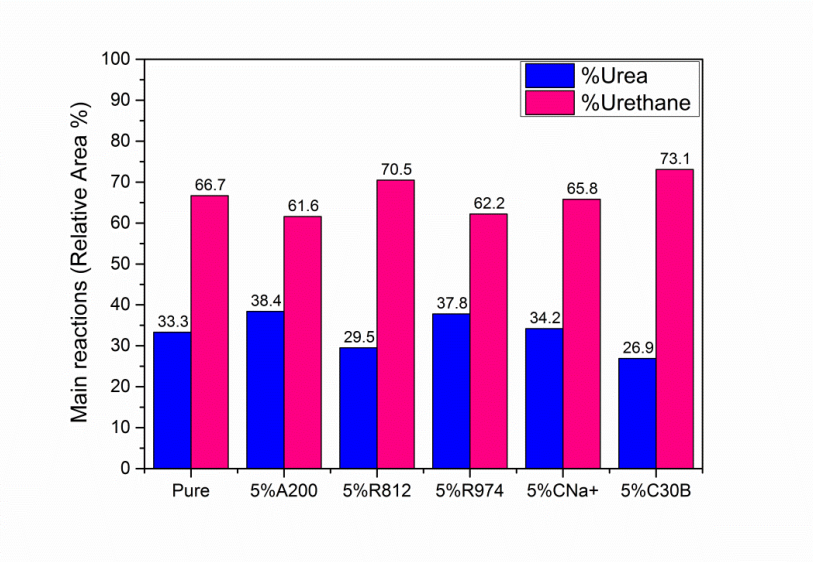

Figure 6. Relative area percentage of the total absorbance associated to urea and urethane detected in the amide I region after a time of 30 minutes.

Table 3 and **Figure 6** clearly reflect how the presence of nanoparticles severely affects the overall reaction kinetics. A clear trend in the first five minutes is observed in **Table 3**, since the urethane/urea ratio decreases for all the systems, showing that more blowing reaction is occurring (more urea products) because the foam is expanding. Hence, the final urethane/urea ratio depends on the type of nanoparticle incorporated into the PU foam.

As indicated in **Table 3** the urethane/urea ratio of the system containing the A200 nanosilica is the lowest from 3 to 30 minutes. These data indicate that the blowing reaction, (responsible of both urea linkages formation and gas formation) is highly enhanced when A200 is added. The high imbalance between blowing and gelling reactions (38.4% of ureas and 61.6% urethanes, as shown in **Figure 6**) precludes the production of a foam with a low density and a homogeneous cellular structure. This will be discussed in the next section.

The data show that A200 (the more hydrophilic nanosilica), and R974 (which contains both hydrophilic and hydrophobic groups on their surface), behave similarly: low values of the urethane/urea ratio and high proportion of ureas at 30 minutes, although proper foam is obtained in this case. For R974 the urethane/urea ratio is the second lower considering all the formulations used (see **Table 3**), thus the blowing reaction is again enhanced. There are previous reports on the somehow anomalous behavior of the nanosilica R974, what has been attributed to its dual behavior, which sometimes evinces a "split personality", due to the presence of both hydrophilic and hydrophobic groups in its surface [48]. In our experiments, R974 hydrophilic behavior seems to prevail.

Instead, R812, which is the nanosilica containing only hydrophobic groups on the surface (90% methyl groups), gives rise to a slight increase of the urethane/urea ratio with respect to the

pure material (see **Table 3**). This occurs during the whole reaction process, and the final urethane/urea ratio for the PU containing R812 is the highest among those containing nanosilicas.

Table 3 and **Figure 6** also show the effects of adding nanoclays. The natural nanoclay CNa+, which contains hydrophilic groups, shows urethane/urea ratios similar to those of the pure foam (all the values between 3 and 30 minutes are similar, some of them higher, some lower, see **Table 3**). Moreover, the final content of urea groups for this foam is slightly higher than that of the reference system.

However, the modified nanoclay C30B, which contains both hydrophilic and hydrophobic groups on their surface, induces higher values of the urethane/urea ratio during all the experiment (**Table 3**) and the highest increase of the urethane/urea ratio values after 30 minutes (**Figure 6**). The gelling reaction is greatly enhanced when this additive is present. As it is shown in **Figure 6**, this is the system more affected by the inclusion of nanoparticles.

In summary, nanoparticles containing hydrophilic groups on their surface (A200 and CNa+) lead to a slight increase of the urea groups (and therefore of the blowing reaction) with respect to the pure foam. Moreover, R974 also exhibits a blowing reaction increase, due to its dual behavior with hydrophilic and hydrophobic groups on its surface. One of the possible reasons for the increase of blowing reaction could be the water present on these particles, which could be released during the foaming process. This water could be the adsorbed water (higher ratios on A200 and R974 nanosilicas surface), and the chemically bonded water (higher amount in the CNa+ nanoclays), as was observed in TGA analysis.

However, establishing further relationships between the nature or surface of the nanoparticles added and their effect on the reaction is rather difficult. These data neither clarify whether a chemical interaction (weak, through hydrogen bonds, or strong, through covalent bonds) between the nanoparticles and the reactants (isocyanate, polyol, catalysts, surfactants and water) and/or the final product (PU), occurs or not. This is a very controversial point according to literature precedents, as some reports support a chemical reaction between the starting isocyanate and the OH groups present in nanoclays, [58-61] whereas other reports conclude that hydrogen bonds are the only type of interactions present,[62, 63] or that interactions do not occur at all [64-67]. In order to clarify this question, blank experiments were carried out by mixing the nanoparticles with isocyanate carrying out FTIR experiments. **Figures 7** and **S5-S8** (**supporting information**) show the isocyanate band and the Amide I region in the FTIR spectra of the isocyanate and of the starting premixture of isocyanate with nanoparticles. The spectra clearly indicate that the intensity of isocyanate absorption does not decrease, what indicates that there is no consumption of isocyanate reactant when the nanoparticles are dispersed into it. However, the intensity of the isocyanate band slightly increases, what might be due to weak hydrogen bonds interactions between the isocyanate groups and the hydroxyl groups present in the nanoparticles. The absence of reaction between the nanoparticles and the isocyanate is also shown by the lack of urethane absorptions observed in the Amide I region. Therefore, we can conclude that the hydroxyl groups present in nanoparticles do not react with the

isocyanate groups of the isocyanate component in the conditions used in this experiment. This also means that the water included in the nanoparticles neither reacts with the isocyanate groups, very possibly because a higher temperatures would be needed in order to release the water from the nanoparticles surface.

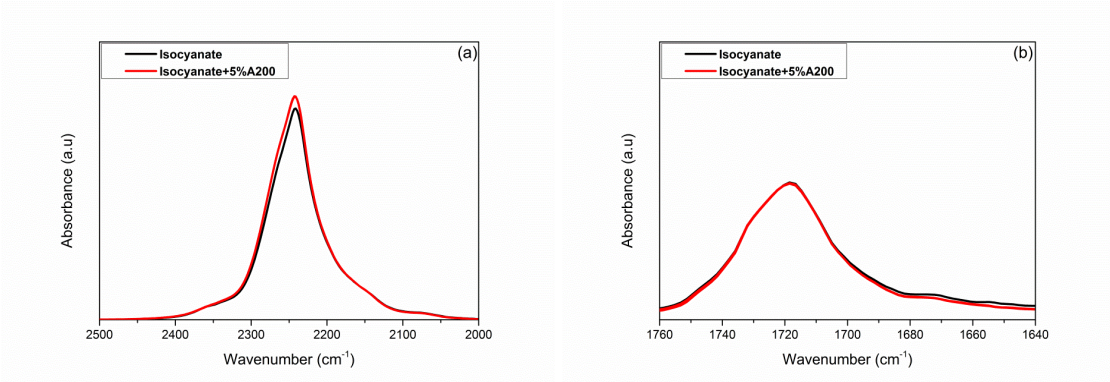

Figure 7. Spectra of isocyanate component and of the dispersion of 5% A200 in isocyanate: **(a)** isocyanate band and **(b)** Amide I region.

Clearly, the modifications induced in the kinetics of the reactions by the nanoparticles will play a role on the final structure and properties of the foams. This is the main focus of the next sections.

3.3. Cellular structure and properties of final foams

The density and the main characteristics of the cellular structure of the foams are collected in **Table 4**. The density may be related to the amount of gas generated during the foaming process and with the stability of the foam. The higher density value is reached for system containing A200. This foam, as indicated above, collapsed due to the strong imbalance between the two main reactions (i.e. part of the gas was released too soon, when the viscosity of the reactive mixture was not enough to hold the gas phase inside). The other two materials based on partially hydrophilic particles, R974 and CNa+, show a lower density than that of the pure foam. This interesting effect can be explained taking into account that the blowing reaction is favored for these systems. This means that more gas is available when the viscosity is not too high in order to promote a higher expansion ratio. Finally, the foams containing R812 and C30B nanoparticles, where the urethane/urea ratio is higher (more gelling reaction) than that of the pure foam (see **Table 4**), have a higher density than that of the pure system. This result can be understood taking into account that in this case the gelling reaction was quicker,

and the viscosity of the system was also higher during foaming, giving as a consequence a lower expansion ratio.

On the other hand, there is an evident increase of the open cell content (OC) (which range from *ca.* 8 to 23%) with the addition of nanoparticles, as compared to that found in the pure foam (which is only *ca.* 5%). Clearly, nanosilicas give rise to higher OC compared to those of nanoclays, as shown in **Table 4**. Moreover, nanosilicas containing more OH groups on their surface give higher values of OC, and the same trend is observed for nanoclays. This significant increase of the open cell content should be connected to additional phenomena taking place during foaming, because it occurs in a higher or lower extent for all the nanoparticles considered. One possible reason is the high amount of particles used (5 wt%), which leads to possible agglomerations, what could promote opening of the cell walls, as previously proved for polypropylene foams containing clays [68]. This effect would be more important in those systems based on hydrophilic particles, in which a worse dispersion is expected.

The analysis of the SEM micrographs (**Figure 8**) in the growth plane allows measuring cell size (Φ3D), anisotropy ratio (AR), and the homogeneity of the cell size distribution (NSD) (**Table 4**). Cell size is highly reduced up to 34% by nanoclays, and up to 22% by nanosilicas, compared to the value of the pure foam. As previously reported, the cell size reduction for similar systems to the those herein studied is due to a nucleation effect of the nanofillers [69]. Thus, this cell size reduction is due to a physical phenomenon not directly connected to the different reaction kinetics caused by the presence of the different particles. From this perspective, nanoclays seem to be more effective than nanosilicas, possibly because the specific surface area of nanoclays is higher than those of nanosilicas. All the foams (pure and those containing nanoclays) can be considered isotropic, as their anisotropy is close to one in all the cases. However, there are several differences between samples, due to the inaccuracy of the measurements. Moreover, all the samples display a high homogeneity, as their NSD values (related to the width of the cell size distributions) are small. All the particles increase the value of NSD, what is a typical result for systems in which the particles act as nucleating sites. This effect is associated to the presence of a combination of cells (typically smaller), nucleated in the particles and cells nucleated in a similar way to those nucleated in the reference material [69].

Table 4. Density, OC, Φ3D, AR and NSD and AC for the foams under study. Sample A200 was not characterized due to its very deteriorated cellular structure.

Material	Density (Kg/m^3)	OC (%)	Φ3D (μm)	AR	NSD
Pure	57.15±0.31	5.00±0.53	619±118	1.10±0.23	0.19
5%A200	67.52±3.15	-	-	-	-
5%R812	57.43±0.65	15.22±0.78	452±152	1.34±0.37	0.34
5%R974	55.92±0.65	22.67±1.32	484±170	1.23±0.38	0.35
5%CNa+	51.00±0.15	11.56±0.18	408±100	1.10±0.18	0.25
5%C30B	59.03±1.55	8.13±0.83	409±169	1.06±0.21	0.41

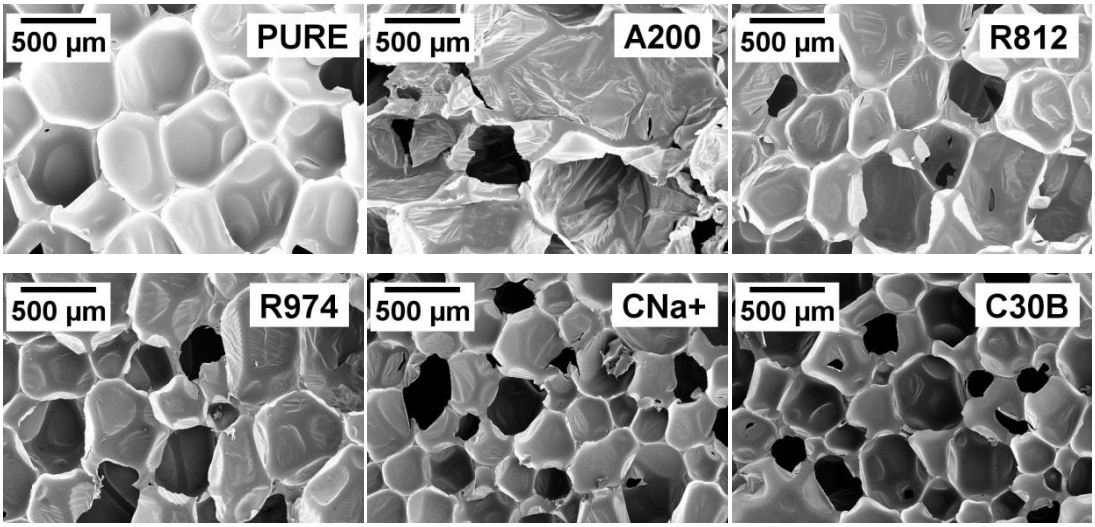

Figure 8. SEM micrographs of PU foam: (a) Pure material, (b) with 5% wt.A200, (c) with 5% wt.R812, (d) with 5% wt.R974, (e) with 5% wt. CNa+ and (f) with 5% C30B.

3.4. Thermal conductivity

Figure 9 shows the thermal conductivity of the pure foam and of those containing nanofillers (except for the A200 material; as its poor quality precluded to characterize the physical properties of this material). The values have been measured when the cells contain only atmospheric air, that is, once the carbon dioxide produced in the blowing reaction has completely diffused outside the cells (this occurs *ca.* 2 weeks after production), being substituted by atmospheric air [11].

The conductivity of the two systems containing nanoclays is lower than that of the reference system. This result is due to a combination of facts. As previously reported [11], a cell size reduction in these systems promotes the reduction of the heat transfer by radiation. In addition to this, the open cell content of these two systems does not increase significantly in comparison with that of the pure foam, so the expected increase of thermal conductivity due to the higher open cell content does not compensate the effect of the reduced cell size. Finally,

for the system containing the CNa+ clay, the density reduction due to the different kinetics of this material (see previous section) also contributes to the reduction of the thermal conductivity.

The two systems containing nanosilica particles present similar (R812) or higher (R974) thermal conductivity than of the reference material. This is probably due to the high open cell content of these two materials, which induces a significant increase of the heat transfer by radiation in spite of their reduced cell size. Considering these two foams the one with a smaller thermal conductivity (R812) is showing a lower open cell content.

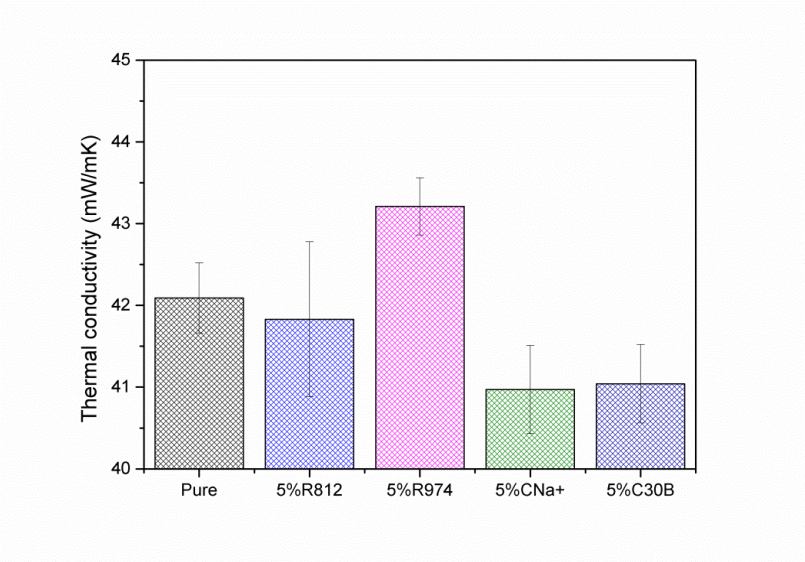

Figure 9. Thermal conductivity values for PU nanocomposite foams.

3.5. Dynamic mechanical analysis (DMA)

Table 5 summarizes the viscoelastic properties of the PU foams measured by DMA. The first column in **Table 5** collects the glass transition temperatures (Tg), which are associated with the α relaxation of soft domains in the foams. Both Tg and the maximum of tan δ account for the polymer chain mobility. The foam with the nanosilica R812 (hydrophobic) displays the highest Tg, whereas the hydrophilic nanoclay CNa+ affords the lowest Tg value. These values are in accordance with the isocyanate conversion (**Figure 4**), and show how the formation of more products (higher isocyanate conversion) gives rise to higher Tg values, and therefore to restrict the chain mobility. Obviously, lower products formation (low isocyanate conversion) leads to lower Tg, and to a higher chain mobility. Therefore, these results show that the reaction kinetics is directly connected to the chain mobility and to the viscoelastic behavior of the foams.

Table 5. The DMA data for pure foam and the foams containing nanoparticles.

Material	Tg (°C)	Maximun Tan δ
Pure	149.9±1.7	0.549±0.031
5%R812	157.5±2.6	0.292±0.023
5%R974	161.2±2.6	0.333±0.007
5%CNa+	118.6±2.7	0.491±0.031
5%C30B	149.1±2.2	0.495±0.022

3.6. Mechanical properties

The effect of the functional nanofillers on the mechanical properties of the PU foams obtained was also studied. The mechanical properties of the PU foams mainly depend on the foam density, the cellular morphology (cell size, OC, cell wall thickness, etc), the polymeric matrix morphology (reaction products generated, etc), and the compatibility of nanoparticles with the matrix.

As the foams studied have slightly different densities. The Gibson and Ashby relationship between mechanical properties and density [70] is used to exclude these differences in densities. **Figure 10** shows the compressive modulus and collapse stress divided by the relative density of the foam. These values allow to compare the mechanical properties of the PU foams containing different nanofillers, and therefore with different densities.

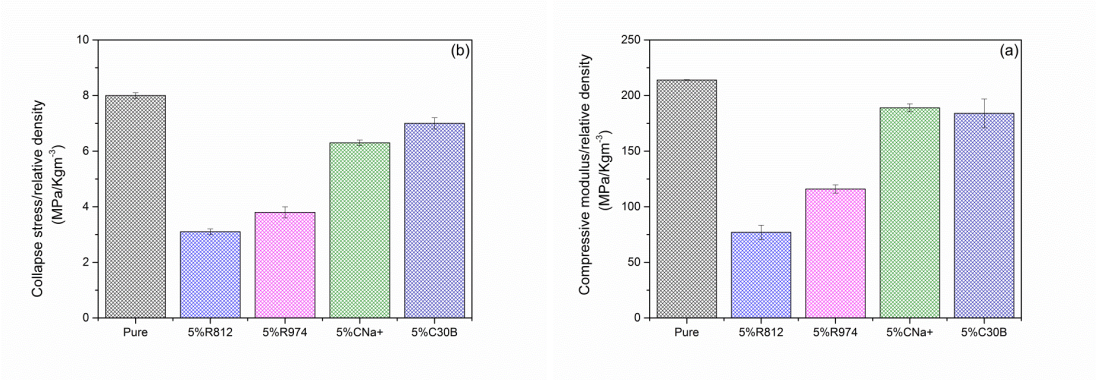

Figure 10. Relative compressive modulus **(a)** and relative collapse stress **(b)** for pure foam and foams with particles correspond to compression test.

As shown in **Figure 10**, the foams containing nanosilicas show a significant decrease of the compression properties, whereas this decrease for the foams containing nanoclays is smaller. Compared to the pure PU foam, those containing nanoclays present a decrease of 12% (for CNa+) and of 14% (for C30B) in compressive modulus, and a decrease of 21% and 13% (respectively) in their collapse stress. The higher decrease for foams containing nanosilicas

reaches a 64% for R812 and a 46% for R974 in their compressive modulus, whereas the reduction of their collapse stress is 61% and 53% (respectively).

The reduction of the final mechanical properties for the four systems compared to the reference foam is mainly due to the increase of the open cell content, due to the presence of the particles. In fact, the materials containing nanosilica with a higher open cell content present reduced compressive properties. In addition to this, the better properties of the nanosilica systems are displayed by R794, which contains higher amounts of urea in the final foam (see **Figure 6**). The increase of the mechanical properties due to the increase of urea content has been already described [71].

4. Conclusions

The effects of nanofillers (nanosilicas and nanoclays) on the reaction kinetics, microstructure, thermal conductivity, viscoelastic properties and compressive mechanical properties of rigid PU foams are herein systematically studied. The reaction kinetics are studied by *in-situ* FTIR spectroscopy. The isocyanate conversion depends on the type of particles used in PU formulation, and on their superficial groups. Therefore, the foams containing nanosilicas show higher isocyanate conversions than those containing nanoclays, whereas those nanoparticles containing hydrophilic groups afford lower isocyanate conversions. The quantification of urea and urethane groups by deconvolution of the carbonyl region can be also correlated to the chemical groups present on the surface of the nanoparticles added, what allows to conclude that hydrophilic nanoparticles enhance the blowing reaction, giving higher ratios of urea groups.

The modifications of the reaction kinetics induced by the nanoparticles have consequences on the density, cellular structure and physical properties of the final foams. Density is reduced for systems in which the blowing reaction is enhanced (foams with R974 and CNa+). However, when the blowing reaction is accelerated in a significant extent the strong decoupling between blowing and gelling promotes a deterioration of the cellular structure, as observed for the A200 system. The conversion degree clearly affects the viscoelastic properties of the foams, since a higher conversion degree promotes both a higher glass transition temperature and a lower degree of mobility of the polymer chains. In addition, the presence of a higher urea ratio in the final foams allows improving the compressive properties.

In addition to these effects, the particles also modify the foaming mechanisms. In this particular case, all the analyzed nanoparticles act as nucleating agents during the process, reducing the average cell size and decreasing the homogeneity of the cell size distribution. Moreover, the high content of particles used induces an increase of the open cell content. These modifications of the cellular structure lead to a reduction of the thermal conductivity for the systems containing clays, and to a decrease of the compressive properties for all the analyzed foams.

Acknowleggements

Financial assistance from MINECO, FEDER, UE (MAT2015-69234-R) and the Junta de Castile and Leon (VA011U16) are gratefully acknowledged.

References

[1] U. Meier-Westhues, Polyurethanes: Coatings, Adhesives and Sealants., Vincentz Network, Hannover, 2007.
[2] M. Szycher, Szycher's Handbook of Polyurethanes, Second ed., CRC Press Boca Raton, Florida, USA, 2012.
[3] D. Klempner, V. Sendijarevic, Handbook of Polymeric Foams and Foam Technology, Hanser 1991.
[4] Polymer Foams Market Expected to Consume 25.3 Million Tonnes by 2019.
[5] L. Glicksman, Low Density Cellular Plastics: Physical Basis of Behaviour, Springer Netherlands, London, 1994.
[6] R.J.J. Williams, C. Aldao, Thermal Conductivity of Plastic Foams, Polymer Engineering and Science, 23 (1983) 293–298.
[7] O.A. Almanza, M.A. Rodríguez-Pérez, J.A.D. Saja, Prediction of the radiation term in the thermal conductivity of crosslinked closed cell polyolefin foams, Journal of Polymer Science Part B: Polymer Physics, 38 (2000) 993–1004.
[8] J.W. Wu, W.F. Sung, H.S. Chu, Thermal conductivity of polyurethane foams, International Journal of Heat and Mass Transfer, 31 (1999) 1100–1106.
[9] M.S. Han, S.J. Choi, J.M. Kim, Y.H. Kim, W.N. Kim, H.S. Lee, J.Y. Sung, Effects of Silicone Surfactant on the Cell Size and Thermal Conductivity of Rigid, Macromolecular Research, 17 (2009) 44–50.
[10] C.-j. Tseng, M. Vamaguch, T. Ohmori, Thermal conductivity of polyurethane foams from room temperature to 20 K, Cryogenics, 37 (1997) 305–312.
[11] S. Estravís, J. Tirado-Mediavilla, M. Santiago-Calvo, J.L. Ruiz-Herrero, F. Villafañe, M.A. Rodríguez-Pérez, Rigid polyurethane foams with infused nanoclays: Relationship between cellular structure and thermal conductivity, European Polymer Journal, 80 (2016) 1–15.
[12] E.P. Giannelis, Polymer Layered Silicate Nanocomposites, Advanced Materials, 8 (1996) 29–35.
[13] Y. Chen, S. Zhou, H. Yang, L. Wu, Structure and properties of polyurethane/nanosilica composites, Journal of Applied Polymer Science, 95 (2005) 1032–1039.
[14] S. Estravis, PhD Thesis: Cellular nonocomposites based on rigid polyurethane and nanoclays: fabrication, caharacterization and modelling of the mechanical and thermal properties, University of Valladolid, 2014.
[15] S. Pardo-Alonso, E. Solórzano, L. Brabant, P. Vanderniepen, M. Dierick, L. Van Hoorebeke, M.A. Rodríguez-Pérez, 3D Analysis of the progressive modification of the cellular architecture in polyurethane nanocomposite foams via X-ray microtomography, European Polymer Journal, 49 (2013) 999–1006.
[16] A.J. Crosby, J.Y. Lee, Polymer Nanocomposites: The “Nano” Effect on Mechanical Properties, Polymer Reviews, 47 (2007) 217–229.
[17] M.A. Samir, F. Alloin, A. Dufresne, Review of Recent Research into Cellulosic Whiskers, Their Properties and Their Application in Nanocomposite Field, Biomacromolecules, 6 (2005) 612–626.

[18] Y. Rao, J.M. Pochan, Mechanics of Polymer-Clay Nanocomposites, Macromolecules 40 (2007) 290–296.
[19] R. Van Hooghten, S. Gyssels, S. Estravis, M.A. Rodriguez-Perez, P. Moldenaers, Understanding the effect of particle surface free energy on the structural and mechanical properties of clay-laden rigid polyurethane foams, European Polymer Journal, 60 (2014) 135–144.
[20] L. Madaleno, R. Pyrz, A. Crosky, L.R. Jensen, J.C.M. Rauhe, V. Dolomanova, A.M.M.V. de Barros Timmons, J.J. Cruz Pinto, J. Norman, Processing and characterization of polyurethane nanocomposite foam reinforced with montmorillonite–carbon nanotube hybrids, Composites Part A: Applied Science and Manufacturing, 44 (2013) 1–7.
[21] X. Cao, L. James Lee, T. Widya, C. Macosko, Polyurethane/clay nanocomposites foams: processing, structure and properties, Polymer, 46 (2005) 775–783.
[22] G. Harikrishnan, T.U. Patro, D.V. Khakhar, Polyurethane Foam-Clay Nanocomposites: Nanoclays as Cell Openers, Industrial and Engineering Chemistry Research, 45 (2006) 7126–7134.
[23] I.V. Khudyakov, D.R. Zopf, N.J. Turro, Polyurethane Nanocomposites, Designed Monomers & Polymers, 12 (2009) 279–290.
[24] M.M.A. Nikje, Z.M. Tehrani, Thermal and mechanical properties of polyurethane rigid foam/modified nanosilica composite, Polymer Engineering & Science, 50 (2010) 468–473.
[25] M.M.A. Nikje, Z.M. Tehrani, Polyurethane Rigid Foams Reinforced by Doubly Modified Nanosilica, Journal of Cellular Plastics, 46 (2010) 159–172.
[26] D. Qi, Y. Bao, Z. Weng, Z. Huang, Preparation of acrylate polymer/silica nanocomposite particles with high silica encapsulation efficiency via miniemulsion polymerization, Polymer, 47 (2006) 4622–4629.
[27] O. Aso, J.I. Eguiazábal, J. Nazábal, The influence of surface modification on the structure and properties of a nanosilica filled thermoplastic elastomer, Composites Science and Technology, 67 (2007) 2854–2863.
[28] S.T. Lee, N.S. Ramesh, Polymeric foams: mechanisms and materials, Boca Raton, Florida, USA, 2004.
[29] G. Woods, Flexible Polyurethane Foams: Chemistry and Technology, London, 1982.
[30] Elastopor H 1501/2 Technical Data Sheet. BASF Poliuretanos Iberia S.A.
[31] IsoPMDI 92140 Technical Data Sheet. BASF Poliuretanos Iberia S.A.
[32] Technical data sheet: Products AEROSIL® fumed silica from Evonik Industries AG (Evonik Degussa). www.aerosil.com/product/aerosil/en/products.
[33] Technical data sheet: Cloisite nanoclays from Southern Clay Products.
[34] N.K. Borse, M.R. Kamal, Melt processing effects on the structure and mechanical properties of PA-6/clay nanocomposites, Polymer Engineering & Science, 46 (2006) 1094–1103.
[35] H.J. Walls, J. Zhou, J.A. Yerian, P.S. Fedkiw, S.A. Khan, M.K. Stowe, G.L. Baker, Fumed silica-based composite polymer electrolytes: synthesis, rheology, and electrochemistry, Journal of Power Sources, 89 (2000) 156–162.
[36] S.R. Raghavan, J. Hou, G.L. Baker, S.A. Khan, Colloidal Interactions between Particles with Tethered Nonpolar Chains Dispersed in Polar Media: Direct Correlation between Dynamic Rheology and Interaction Parameters, Langmuir 16 (2000) 1066–1077.
[37] A. Chuiko, Y. Gorlov, Chemistry of a Silica Surface, Kiev, 1992.
[38] J.M. Cervantes-Uc, J.V. Cauich-Rodríguez, H. Vázquez-Torres, L.F. Garfias-Mesías, D.R. Paul, Thermal degradation of commercially available organoclays studied by TGA–FTIR, Thermochimica Acta, 457 (2007) 92–102.

[39] A.B. Inceoglu, U. Yilmazer, Synthesis and mechanical properties of unsaturated polyester based nanocomposites, Polymer Engineering & Science 43 (2003) 661–669.
[40] ASTM D1622-08: Standard Test Method for Apparent Density of Rigid Cellular Plastics.
[41] ASTM D6226-10: Standard Test Method for Open Cell Content of Rigid Cellular Plastics.
[42] J. Pinto, E. Solorzano, M.A. Rodriguez-Perez, J.A. de Saja, Characterization of the cellular structure based on user-interactive image analysis procedures, Journal of Cellular Plastics, 49 (2013) 555–575.
[43] ISO 22007-2:2008. Plastics-Determination of Thermal Conductivity and Thermal Diffusivity—Part 2: Transient Plane Heat Source (Hot Disc) Method.
[44] ASTM D1621: Standard Test Method for Compressive Properties Of Rigid Cellular Plastics.
[45] M.J. Elwell, A.J. Ryan, H.J.M. Grünbauer, H.C.V. Lieshout, In-Situ Studies of Structure Development during the Reactive Processing of Model Flexible Polyurethane Foam Systems Using FT-IR Spectroscopy, Synchrotron SAXS, and Rheology, Macromolecules, 29 (1996).
[46] M.J. Elwell, A.J. Ryan, An FT i.r. study of reaction kinetics and structure development in model flexible polyurethane foam systems, Polymer, 37 (1996) 1353–1361.
[47] D.P. Queiroz, M.N. de Pinho, C. Dias, ATR-FTIR Studies of Poly(propylene oxide)/Polybutadiene Bi-Soft Segment Urethane/Urea Membranes, Macromolecules, 36 (2003) 4195–4200.
[48] A. Marcos-Fernández, A.E. Lozano, L. González, A. Rodríguez, Hydrogen Bonding in Copoly(ether-urea)s and Its Relationship with the Physical Properties, Macromolecules, 30 (1997) 3584–3592.
[49] M.M. Bernal, M.A. Lopez-Manchado, R. Verdejo, In situ Foaming Evolution of Flexible Polyurethane Foam Nanocomposites, Macromolecular Chemistry and Physics, 212 (2011) 971–979.
[50] M. Akkoyun, E. Suvaci, Effects of TiO2, ZnO, and Fe3O4 nanofillers on rheological behavior,microstructure, and reaction kinetics of rigid polyurethane foams, Journal of Applied Polymer Science, 133 (2016).
[51] A.L. Daniel-da-Silva, J.C.M. Bordado, J.M. Martín-Martínez, Moisture curing kinetics of isocyanate ended urethane quasi-prepolymers monitored by IR spectroscopy and DSC, Journal of Applied Polymer Science, 107 (2008) 700–709.
[52] Michael M. Coleman, Maria Sobkowiak, George J. Pehlert, P.C. Painter, Infrared temperature studies of a simple polyurea, Macromolecular Chemistry Physis, 198 (1997) 117–134.
[53] L. Ning, W. De-Ning, Y. Sheng-Kang, Hydrogen-Bonding Properties of Segmented Polyether Poly(urethane urea) Copolymer, Macromolecules, 30 (1997) 4405–4409.
[54] V. Zharkov, A. Strikovsky, T. Verteletskaya, Amide I absorption band: description of the urethane group association scheme in polyether urethane elastomers, Polymer, 34 (1993) 935–941.
[55] A. Strikovsky, V. Zharkov, Infra-red spectroscopy study of equilibrium association of urethane groups in poly(ether urethane)s, Polymer, 34 (1993) 3397.
[56] W. Li, A.J. Ryan, Effect of Chain Extenders on the Morphology Development in Flexible Polyurethane Foam, Macromolecules, 35 (2002) 6306–6312.
[57] R. Versteegen, R. Sijbesma, E. Meijer, Synthesis and Characterization of Segmented Copoly(ether urea)s with Uniform Hard Segments, Macromolecules, 38 (2005) 3176–3184.
[58] Y.I. Tien, K.H. Wei, High-Tensile-Property Layered Silicates/Polyurethane Nanocomposites by Using Reactive Silicates as Pseudo Chain Extenders, Macromolecules, 34 (2001) 9045–9052.
[59] A. Pattanayak, S.C. Jana, Synthesis of thermoplastic polyurethane nanocomposites of reactive nanoclay by bulk polymerization methods, Polymer, 46 (2005) 3275–3288.
[60] A. Pattanayak, S.C. Jana, Thermoplastic polyurethane nanocomposites of reactive silicate clays: effects of soft segments on properties, Polymer, 46 (2005) 5183–5193.

[61] Y.I. Tien, K.H. Wei, The effect of nano-sized silicate layers from montmorillonite on glass transition, dynamic mechanical, and thermal degradation properties of segmented polyurethane, Journal of Applied Polymer Science, 86 (2002) 1741–1748.
[62] Y.I. Tien, K.H. Wei, Hydrogen bonding and mechanical properties in segmented montmorillonite/polyurethane nanocomposites of different hard segment ratios, Polymer 42 (2001) 3213–3221.
[63] J. Vega-Baudrit, V. Navarro-Bañón, P. Vázquez, J.M. Martín-Martínez, Addition of nanosilicas with different silanol content to thermoplastic polyurethane adhesives, International Journal of Adhesion and Adhesives, 26 (2006) 378–387.
[64] T.-K. Chen, Y.-I. Tien, K.-H. Wei, Synthesis and characterization of novel segmented polyurethane/clay nanocomposites, Polymer 41 (2000) 1345–1353.
[65] M.A. Osman, V. Mittal, M. Morbidelli, U.W. Suter, Polyurethane Adhesive Nanocomposites as Gas Permeation Barrier, Macromolecules 36 (2003) 9851–9858.
[66] Y. Zhu, D.-x. Sun, Preparation of Silicon Dioxide/Polyurethane Nanocomposites by a Sol–Gel Process, Journal of Applied Polymer Science, 92 (2004) 2013–2016.
[67] S.M. Lai, C.K. Wang, H.F. Shen, Properties and preparation of thermoplastic polyurethane/silica hybrid using sol-gel process, Journal of Applied Polymer Science, 97 (2005) 1316–1325.
[68] E. Laguna-Gutierrez, R.V. Hooghten, P. Moldenaers, M.A. Rodriguez-Perez, Effects of extrusion process, type and content of clays, and foaming process on the clay exfoliation in HMS PP composites, Journal of Applied Polymer Science, 132 (2015).
[69] S. Pardo-Alonso, E. Solórzano, S. Estravís, M.A. Rodríguez-Perez, J.A. de Saja, In situ evidence of the nanoparticle nucleating effect in polyurethane–nanoclay foamed systems, Soft Matter, 8 (2012) 11262.
[70] L. Gibson, M. Ashby, Cellular solids: structure and properties, Pergamon Press, Oxford, 1988.
[71] W.J. Seo, H.C. Jung, J.C. Hyun, W.N. Kim, Y.B. Lee, K.H. Choe, S.B. Kim, Mechanical, morphological, and thermal properties of rigid polyurethane foams blown by distilled water, Journal of Applied Polymer Science, 90 (2003) 12–21.

Supplementary material

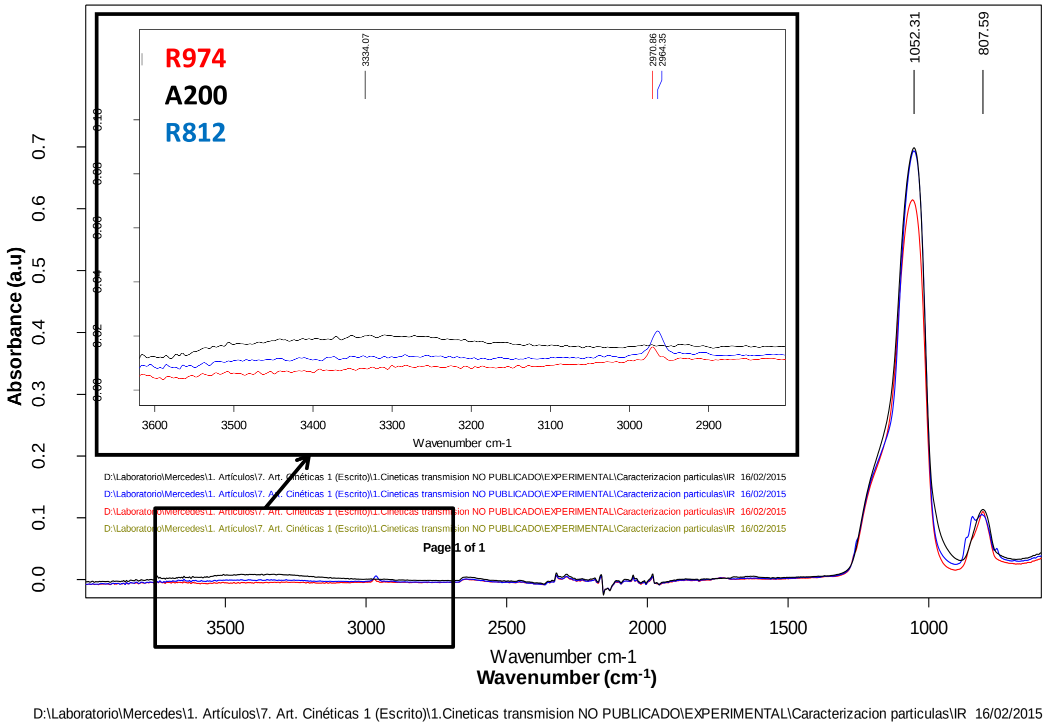

Figure S1. FTIR spectra of nanosilicas: **A200, R812** and **R974.**

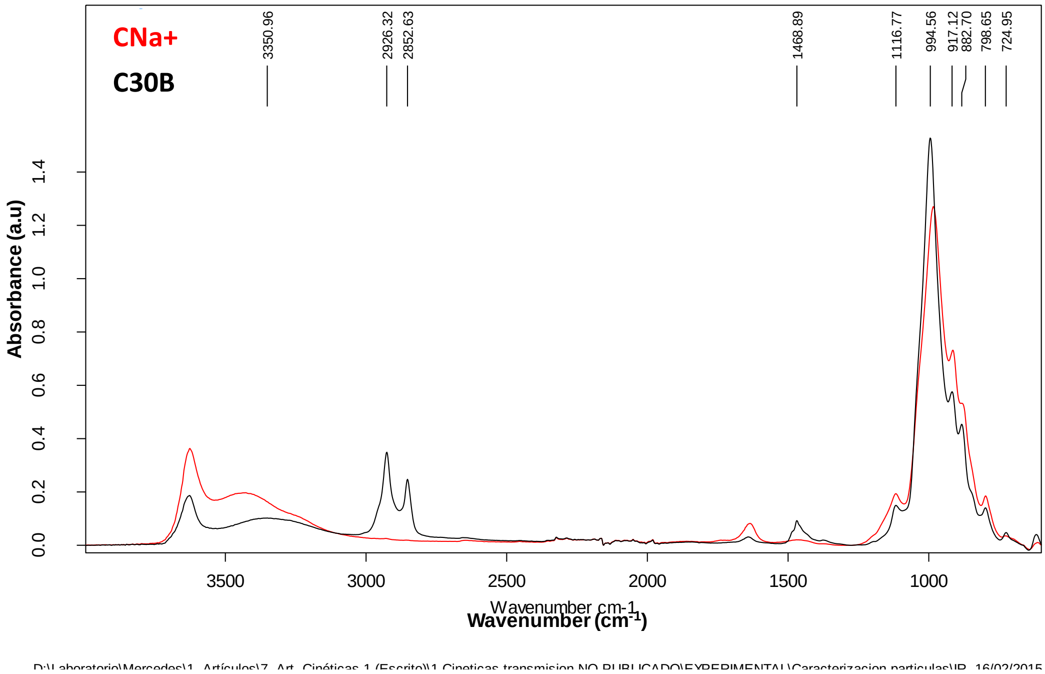

Figure S2. FTIR spectra of nanoclays: **CNa+** and **C30B.**

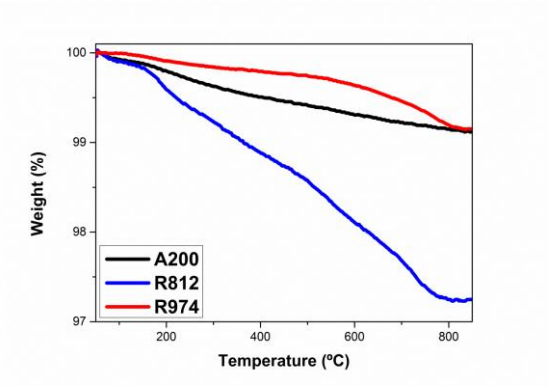

Figure S3. TGA thermograms of the nanosilicas: **A200**, **R812** and **R974**.

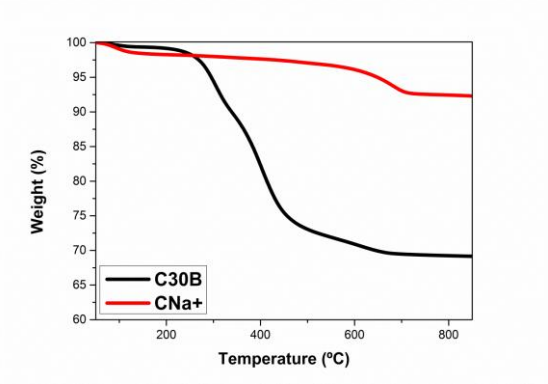

Figure S4. TGA thermograms of the nanoclays: **CNa+** and **C30B.**

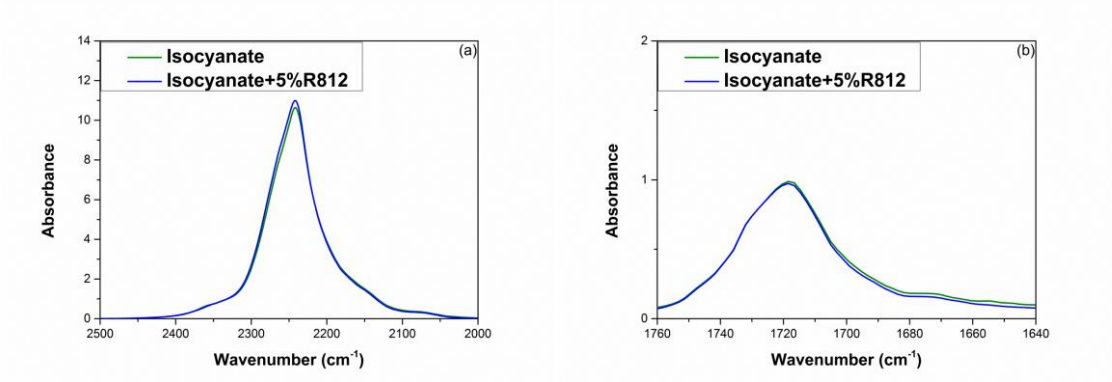

Figure S5. FTIR spectra of the isocyanate component and the dispersion of 5%**R812** in isocyanate: **(a)** isocyanate band and **(b)** Amide I region.

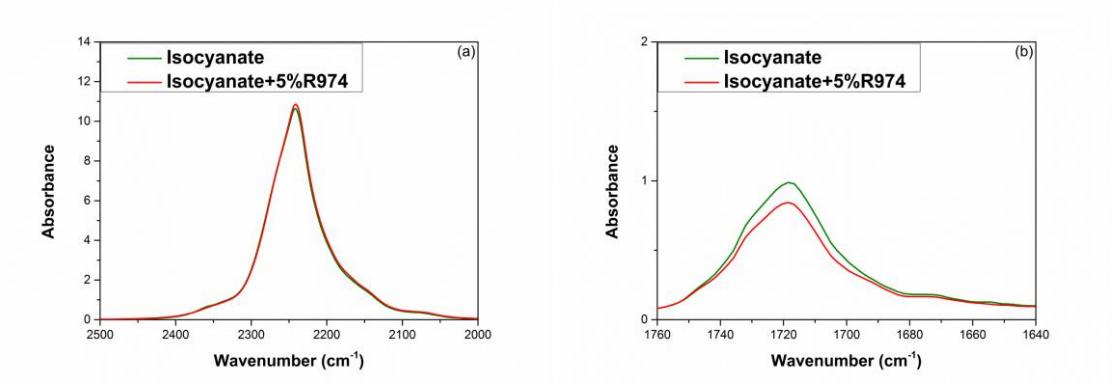

Figure S6. FTIR spectra of the isocyanate component and the dispersion of 5%**R974** in isocyanate: **(a)** isocyanate band and **(b)** Amide I region.

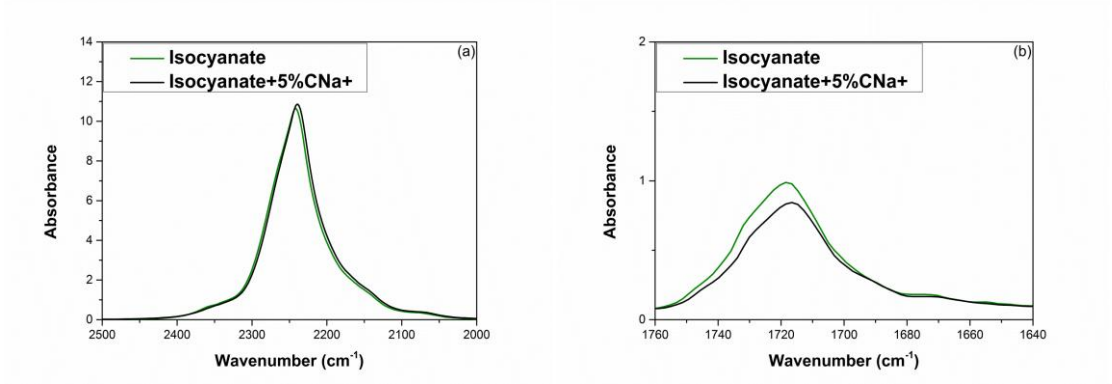

Figure S7. FTIR spectra of the isocyanate component and the dispersion of 5%**CNa+** in isocyanate: **(a)** isocyanate band and **(b)** Amide I region.

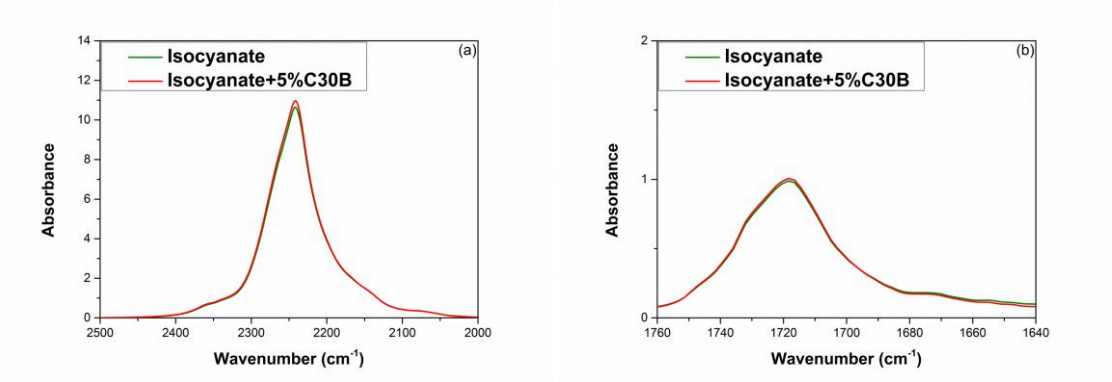

Figure S8. FTIR spectra of the isocyanate component and the dispersion of 5%**C30B** in isocyanate: **(a)** isocyanate band and **(b**) Amide I region.

Development of a methodology to follow the reaction kinetics of rigid polyurethane foams

Polymer testing 66 (**2018**) 383-393
https://doi.org/10.1016/j.polymertesting.2018.02.004

Infrared expandometry: a novel methodology to monitor the expansion kinetics of cellular materials produced with exothermic foaming mechanisms

Mercedes Santiago-Calvo [1,*], Saúl Pérez-Tamarit [1], Josías Tirado-Mediavilla [1], Fernando Villafañe [2], Miguel Ángel Rodríguez-Pérez [2]

[1] Cellular Materials Laboratory (CellMat), Condensed Matter Physics Department, Faculty of Science , Campus Miguel Delibes, University of Valladolid, Paseo de Belén 7, 47011 Valladolid, Spain.

[2] GIR MIOMeT-IU Cinquima-Química Inorgánica, Faculty of Science, University of Valladolid, Campus Miguel Delibes, Paseo de Belén, 7, 47011 Valladolid, Spain.

* Corresponding author: mercesc@fmc.uva.es

Abstract

This paper presents a new methodology called "Infrared Expandometry" appropriate to characterize simultaneously the expansion kinetics (height *vs.* time and volume *vs.* time) and the temperature evolution of cellular materials by using the infrared radiation emitted when a body reaches a certain temperature. Therefore, a mandatory feature of the foamed samples to be studied by this methodology is the internal generation of heat during the growing step, i.e. the foaming process must be exothermic. The evolution of the surface temperature *vs*. time is determined by calibrating the intensity of the acquired images. From this information and by using image analysis, the kinetics of foaming is characterized. The presented technique provides very valuable information during the foaming process, such as height, volume, temperature evolution and temperature homogeneity, being a fast, clean and simple characterization technique. In order to demonstrate the use of this new technique to monitor the foaming kinetics of cellular materials, the formation of a polyurethane foam system is herein described.

Keywords: infrared imaging; polyurethane foams; kinetics; foamability

1. Introduction

Polymeric cellular materials have a wide range of applications in different industrial sectors, such as construction, cushioning, packaging, automotive, and many others. In the last decades, the use of polymeric cellular materials has increased due to their low density, which results from the inclusion of the gas phase in the structure. This has allowed manufacturing materials with an extensive range of specific properties by using a reduced amount of raw materials, thus also reducing the production costs. In addition, the study and production of new polymeric cellular materials with improved properties is an exciting research topic. However, to develop new and improved materials it is needed a deep understanding of the foaming process and novel techniques able to provide this understanding are essential. In this investigation, we present a new method that we have named "Infrared Expandometry" to monitor the foaming process of different polymer cellular materials which are obtained by exothermic blowing processes.

A large number of thermoset polymer cellular materials, such as polyurethanes (PUs), polyisocyanurates (PIRs), phenolics, epoxies or silicones, among others, are obtained by exothermic foaming processes [1]. Therefore they are appropriate candidates to be studied by "Infrared Expandometry". A gaseous component (chemical foaming agent) is generated in these exothermic foaming processes, and polymerization contributes to enclose the gas phase. Alternatively, a physical blowing agent, such as some organic volatiles evaporated during the polymerization reaction, may also be used. Hence, the exothermic foaming process involves both foaming and polymerization reactions, and both gas and heat are generated. The thermoset cellular polymers more widely used, which are obtained by exothermic foaming processes, are briefly reviewed in the following paragraphs.

PU foams are the most extensively used and well-known cellular polymers, representing more than half of the global market of foams, with a sustained growth over the years [2]. PU foams are obtained by two simultaneous reactions: (a) isocyanate and polyol (polymerization or gelling reaction, **Figure 1.a**) give urethane groups which form the polymeric structure; and (b) a second reaction where a gas is generated (foaming or blowing reaction) due to the addition of physical or chemical blowing agents [3]. Water is the most common chemical blowing agent, since it reacts with isocyanate giving CO_2 and urea groups, what produces the foam expansion (**Figure 1.b**). Moreover, physical blowing agents, such as cyclopentane, are commonly used in PU foams manufacture, since their vaporization contributes to the foam expansion. Both gelling and blowing reactions are exothermic, their heat of reaction being –125.5 kJ/mol for the blowing reaction (when water is the only blowing agent) and–93.9 kJ/mol for gelling reaction [4].

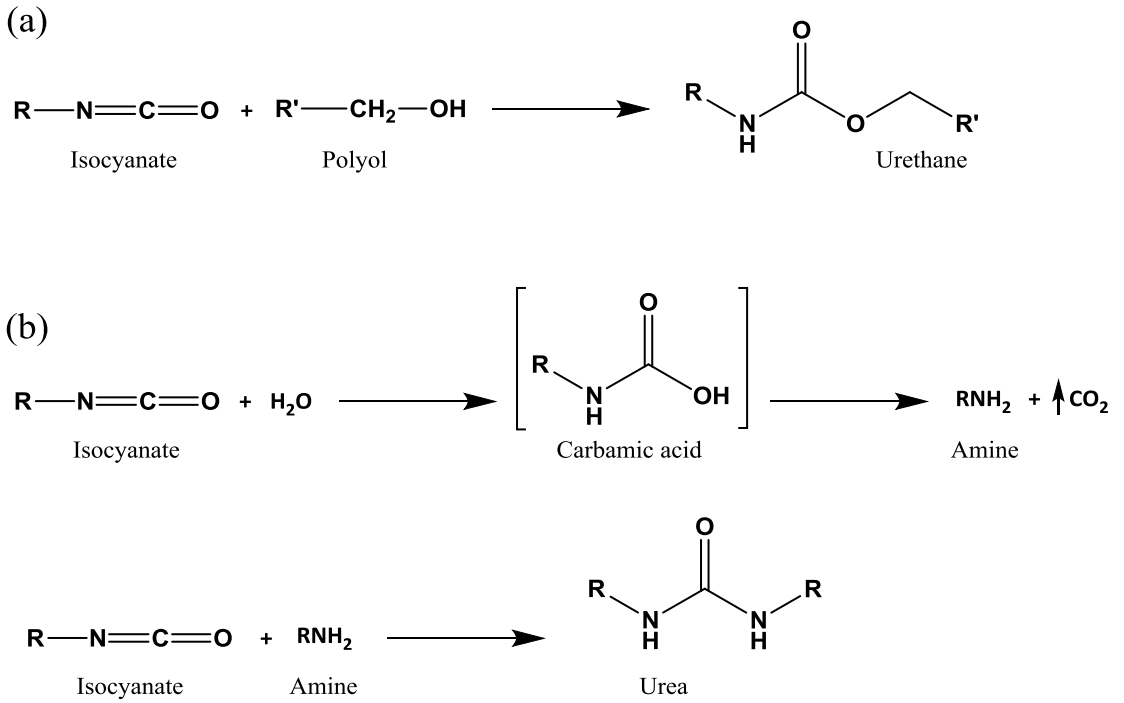

Figure 1. Main reaction of PU foams: (a) gelling and (b) blowing reactions.

PIR foams are obtained from the polycyclotrimerization reaction of a blowing (chemical or physical) agent with either diisocyanates or isocyanate-terminated prepolymers (**Figure 2**). As a result, PIR foams consist of highly crosslinked six-member isocyanurate rings, what make them extremely fragile. For this reason, PIR foams are usually modified with the addition of polyols, which are connected to isocyanurate rings via urethane groups, giving rigid polyurethane-polyisocyanurate (PUR–PIR) foams. Therefore, this type of foams is obtained by the same main reactions of PU foams, but including also a cyclotrimerization reaction. All of these processes are exothermic reactions, and the heat of reaction of the cyclotrimerization reaction is –91.2 kJ/mol [5].

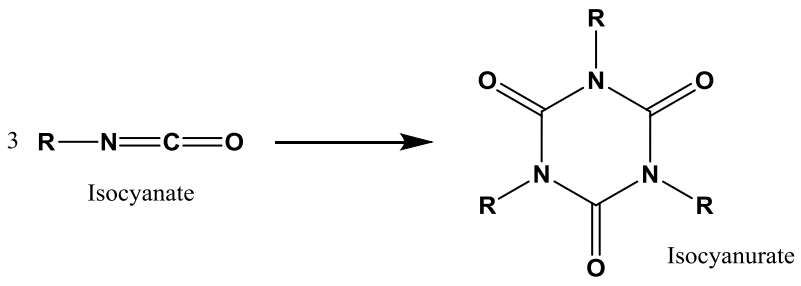

Figure 2. Polycyclotrimerization reaction of isocyanates.

Finally, epoxy resin foams are obtained by an exothermic crosslinking reaction called curing reaction, which occurs between an epoxy resin and a curing agent (usually a primary amine, polyphenol or anhydride). The heat released during this reaction helps to evaporate a physical blowing agent, such as hexane or cyclohexane, generating the foam expansion. An alternative is the use of a chemical blowing agent, such as polysiloxane, which reacts with the curing agent releasing the foaming gas. **Figure 3** shows these two parallel reactions that occur during the foaming process of the epoxy-amine system, with siloxane as blowing agent. The reaction between the epoxy resin and the amine is also exothermic, being its heat of reaction ⍰105 kJ/mol [1].

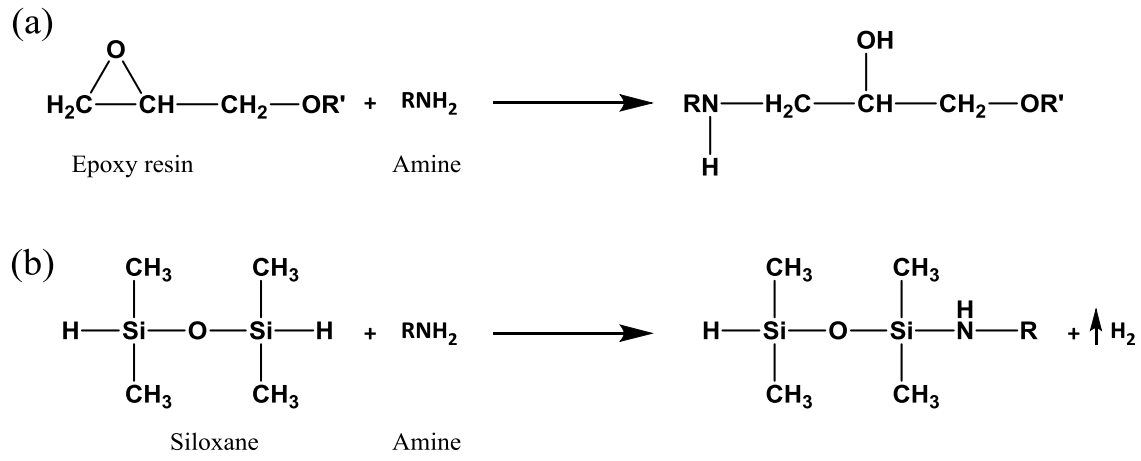

Figure 3. Reactions of the epoxy resin foams: **(a)** curing reaction with amine as curing agent, and **(b)** blowing reaction with siloxane as blowing agent.

The expansion process is an important step in the production of the aforementioned foams, and therefore it has been studied by a wide number of techniques. Typically, *ex-situ* techniques are those more frequently considered for the study of foaming processes. This type of characterization techniques usually only accounts for the initial and final states of the foamed specimen. [1, 6] Foaming is a complex phenomenon where many physical and chemical mechanisms occur simultaneously [7, 8], cell generation (nucleation and growth), and degeneration (coalescence, drainage, coarsening…) playing all of them a key role during foaming. Due to this, ex-situ techniques are not enough to obtain a proper understanding of foaming.

Several advances regarding the *in-situ* analysis of the foaming behaviour have been presented in recent years. The first and simpler expansion kinetic characterization experiments were based on thermo-mechanical analysis equipments [9, 10]. In this type of tests, a precursor containing the thermally decomposing blowing agent is located between two parallel plates. This allows measuring the linear thermal expansion of samples by using Linear Variable Differential Transformer (LVDT) components. All the system follows a specific temperature

profile, providing the temporal evolution of the sample height. Mechanical expandometers, based on similar principles, were also initially used and supplied similar results [11, 12]. These devices were then sequentially replaced by optical contactless systems, such as the so-called laser beam expandometer [13, 14]. However, all these techniques detected the growing in only one single direction, whereas the other two dimensions were excluded, even though they could be crucial in order to understand the real expansion kinetics in a free foaming process, as shown in **Figure 4**. This has been recently solved by measuring the bidimensional expansion of samples, which can be easily extrapolated to a volumetric expansion. For this purpose, both optical methods [15] and X-rays imaging systems have been used. The latter techniques also evaluate the evolution of the internal structure of the foams [16-19].

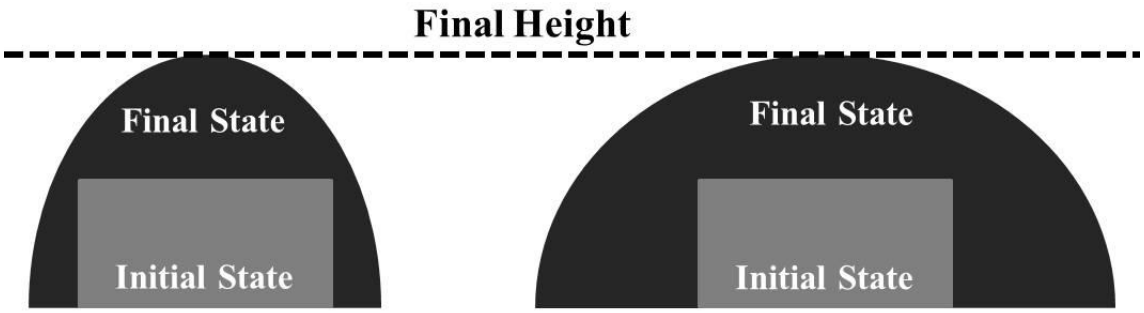

Figure 4. Schematic representation of two foamed samples reaching the same final lineal expansion, but different volume expansions.

We have focused this research on polymer foams based on thermoset polymers. These are interesting materials for the experimental technique herein presented, since they involve exothermic blowing processes and are usually foamed at room temperature and at atmospheric pressure. This is why the foaming set-up to follow the expansion kinetics is the simplest, since no furnace is required in order to promote the blowing mechanism. In addition, the impact of thermoset foams in polymer industry and market is large [20].

Several reports have been already published dealing with the *in-situ* study of the foaming behaviour of thermoset cellular polymers. Considering PU foams, several characterization methods have been described during the last decades. These include the use of floats located in the surface of the sample [21], or measuring the foam height with rulers [22], or optical devices [23, 24]. More sophisticated methods to characterize the expansion process have been developed in recent years [25], such as the use of ultrasonic fan sensors. Nevertheless, thermocouples are required for all the cited characterization techniques in order to record (either simultaneously or not) the temperature evolution during foaming. The use of these thermocouples results in very local temperature measurements that can affect the foaming process.

The new method presented in this paper has some interesting features. This technique allows following *in-situ* the evolution of the material from the start to the final of the expansion process, without any restrictions about the sample size. This is rather important because with other methods, such as X-rays imaging systems, there are limitations on the samples size. A second benefit of Infrared Expandometry is that provides accurate information about the volume expansion of the system. This method also allows measuring the surface temperature without interfering with the expansion process, and the temperatures may be quantified either at certain points of the surface or for the whole sample surface. These are remarkable advantages compared to the information provided by traditional thermocouple measurements. Moreover, the measurement of the surface temperature simplifies monitoring heterogeneities such as hot spots produced by an inadequate dispersion of the components in the reactive mixture. Finally, this technique allows a quick and simple processing of the images by image analysis due to the important temperature differences between the sample and the background that gives a high image contrast. In conclusion, Infrared Expandometry supplies full information about the expansion process in a quick and easy way.

In order to show the use of Infrared Expandometry to monitor blowing kinetics of cellular materials, the results obtained for a PU foam system are herein described.

2. Experimental

2.1. Materials

IsoPMDI 92140 (31.5% NCO, density 1.23 g cm^{-3}, viscosity 170-250 mPa·s), a polymeric diphenylmethane diisocyanate (pMDI) from "BASF Poliuretanos Iberia S.A", was used to produce the PUR foams. The polyol employed was Alcupol R4520 (OH index 455 mg KOH/g, viscosity 5250 mPa·s), from Repsol. Tegoamin® DMCHA (N,N-dimethylcyclohexylamine) and Tegoamin® PMDETA (N,N,N',N'',N''-Pentamethyldiethylenetriamine) from Evonik, were used as gelling and blowing catalysts respectively. Tegostab® B 8522 (a non- hydrolysable poly-ether-polydimethyl-siloxane–stabilizer) from Evonik, was used as a surfactant. Distilled water was used as blowing agent.

Four different PUR foams were studied, labelled as PUR1, PUR2, PUR3 and PUR4, according to the formulations shown in **Table 1**, which differ in the amount of water (2 and 5 ppw) and blowing catalysts used (0 and 2 ppw). An overhead stirrer (EUROSTAR Power control-visc P1, IKA) with a 50 mm diameter Lenart disc stirrer was used to premix the polyol with the catalysts, the surfactant, and the blowing agent during 2 minutes at 250 rpm, thus giving different homogenous polyol blends (Polyol component), collected in **Table 1**. Each polyol blend was mixed with isocyanate (isocyanate index = 110), in a polypropylene plastic container (thickness of walls of 0.3 millimetres) during 10 seconds at 1200 rpm, for PUR1 and PUR3 formulations, and during 3 seconds at 1200 rpm, for PUR2 and PUR4 formulations. The latter grow faster due to the presence of blowing catalyst in the polyol blend.

Table 1. PUR formulation.

	Isocyanate component	Polyol component				
Samples	Isocyanate index	Polyol (ppw)	Surfactant (ppw)	Gelling catalyst (ppw)	Blowing catalyst (ppw)	Blowing agent (H_2O) (ppw)
PUR1	110	100	1	1	0	2
PUR2	110	100	1	1	2	2
PUR3	110	100	1	1	0	5
PUR4	110	100	1	1	2	5

2.2. Experimental setup

2.2.1. Infrared imaging system

An infrared camera (model HotFind L) from SDS Infrared was employed for this study. This camera provides a 320x240 pixels^2 infrared detector (type microbolometer UFPA) covering 8-14 microns of spectral range, and detects temperatures from -20ºC up to 1000ºC, with a temperature accuracy of ±2ºC until *ca.* 100 ºC or ±2% of measured temperature for temperatures above 100 ºC.

Each pixel of the camera comprises basically a micro-resistor which changes its resistance as heats up due to IR radiation absorption. The camera electronics convert the changes in resistance to a thermal signal. A lens must to be placed between the monitored object and the detector in order to obtain a focused thermal image.

The object to be monitored (the expanding foam) radiates in a wide range of wavelengths. The maximum of radiance corresponds to its own temperature, as predicted by Wien's displacement law. As the emitting object is not a black-body, the theoretical emitted spectral energy distribution must be multiplied by the surface emissivity of the object (ε). When the temperature increases the total energy emitted also increases and it is emitted at lower average wavelengths, in accordance with both Stefan-Boltzmann's and Wien's laws.

The energy reaching the sensor, W_T, is not only a contribution of the object, since both the surroundings and the atmosphere also emit energy that should be taken into account. The energy W_{sur} radiated by the surroundings is reflected by the object, according to its reflectivity $R = 1-\varepsilon$. Consequently, the object irradiates according to its temperature and emissivity, and it also reflects radiation from the surroundings. Furthermore, the atmosphere between the object and the infrared camera modifies the two radiative contributions from the object, which are given by its transmittance τ, and it also radiates energy itself (W_{atm}), thus contributing by a certain amount of energy.

The energy emitted by the object (W_{obj}) can then be expressed in terms of the total energy reaching the camera, and the contributions by both atmosphere and environment (**Equation 1**) [26]:

$$obj = \frac{1}{\varepsilon\tau} \quad T - \frac{1-\tau}{\tau} \quad sur - \frac{1-\tau}{\varepsilon\tau} \quad atm \qquad (1)$$

The internal calibration of the camera allows transforming into temperature the energy received in the operating IR range. The temperature read by the camera depends mainly on two parameters: object emissivity and atmosphere transmittance. The first one is related to the characteristics of the analysed sample, whereas the second one depends on the environmental conditions (mainly surroundings temperature and relative humidity). For this reason, the environmental conditions at the beginning of the stirring process have to be taken into account in order to adequately calibrate the surface temperature detected by the infrared camera. The emissivity of the samples was fixed at 0.82 during the whole process. This assumption is correct taking into account that the material is expanding inside a container that does not change its nature during the process. The camera is located at a distance of *ca*. one meter from the sample, resulting in an effective field of view (FOV) of 40x30 cm^2. For every sample 25 frames per second (fps) were recorded during 7 minutes and starting from the moment of mixing the polyol blend and the isocyanate. A scheme of the infrared detection experimental set-up is shown in **Figure 5**.

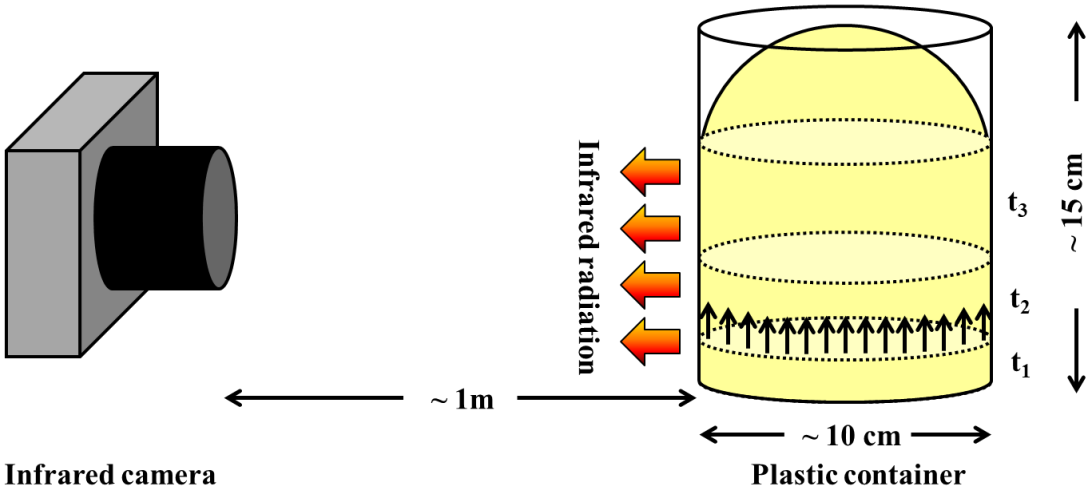

Figure 5. Schematic view of the infrared radiation detection system. The sample grows in a plastic container emitting radiation that is recorded by the camera.

2.2.2. Image analysis

After the image acquisition, an image analysis procedure based on ImageJ/Fiji software tool [27, 28] was implemented to extract quantitative information about the infrared image sequence of every tested sample. First of all, a sequential image averaging was applied in order

to condensate the 25 frames for every second into an average temperature for these 25 images. As a consequence, the individual image contrast was also enhanced by eliminating random noise in the images. After that, the temperature and distances in the images were suitably calibrated. To this purpose, a known distance in the images is selected (for example the upper part of the foam container) for spatial calibration, thus allowing obtaining the real pixel size of the images. On the other hand, temperature is calibrated by using the two temperature limits (maximum and minimum) of the temperature scale supplied by the infrared camera post-processing software. Once the corresponding grey level limits are known, any temperature between them is calculated assuming a linear relationship between temperature and grey level.

Next, an edge-preserving filter (median filter of variable radius depending on the image height) was applied in order to homogenize the grey level on the images, and to facilitate the subsequent automatic binarization process. The latter allows obtaining the mask images needed for calculating all the relevant parameters of the foaming process, such as sample height, sample volume, expansion rate, expansion acceleration or superficial temperatures (minimum, maximum and average).

The sample area is calculated measuring the area of the mask during the process. The sample height is directly obtained by considering the vertical dimension of the binarized mask. Finally, sample volume and expansion rate/acceleration are indirectly determined by using the following expressions, which are obtained considering the symmetry of the system:

$$V = \frac{\pi}{4}\frac{A^2}{h} \quad (\mathbf{2})$$

$$v = \frac{dV}{dt} \quad (\mathbf{3})$$

$$a = \frac{dv}{dt} \quad (\mathbf{4})$$

Where *V* is the sample volume, *A* is the area of the binarized mask, *h* is the height, *v is* the expansion rate, *t* is the time and finally *a* is the expansion acceleration.

Furthermore, as explained above, the surface temperature is calculated considering the grey level intensity of the region of interest (ROI), marked by the binarized mask. The maximum, minimum and average grey intensity of the pixels inside the contour of the ROI are calculated in order to determine the corresponding surface temperatures considering the temperature calibration explained before. **Figure 6** shows the main steps of the image analysis protocol.

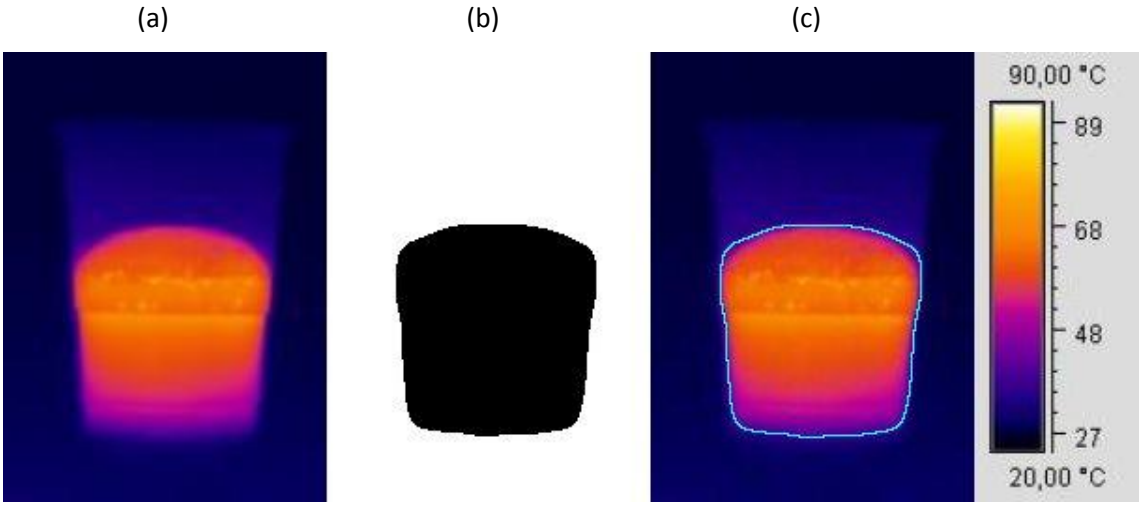

Figure 6. Main steps of the image analysis methodology. **(a)** Acquired image after the condensation of the 25 frames corresponding to one second. **(b)** Binarized mask image after the filter application. **(c)** Original image with overlaid ROI that allows determining superficial temperatures.

One interesting advantage of this technique is the possibility to evaluate temperature inhomogeneities in the sample surface. We define three different strategies for this purpose. Two of them provide quantitative information about this feature, whereas the last one adds a visual component.

The first property, denominated normalized standard deviation (*NSD*), consists on the determination of the standard deviation of the grey level of the pixels inside the contour of the ROI divided by the average value described above for every instant of time.

The second one, designated normalized temperature variation (*NΔT*), is simply the difference between the maximum and minimum temperatures in the images, divided by the corresponding average temperature.

Finally, the last feature permits obtaining 2D temperature maps showing the evolution with time of a determined vertical profile as shown in **Figure 7**. To accomplish this, a rectangular region is selected in the images (green rectangle in the coloured version of **Figure 7**). Every value of the vertical profile is then the result of averaging all the temperature values corresponding to the same row of the rectangle. Thus, obtaining the vertical profile of the same region for all the images allows condensing all the information on a 2D temperature map (**Figure 7**, bottom). In these maps, the x-axis is the time, the y-axis is the height on the vertical profile and the colour map displays the measured temperature. These representations allow discerning the temperature variation (and also its inhomogeneity) along the whole video in one single image.

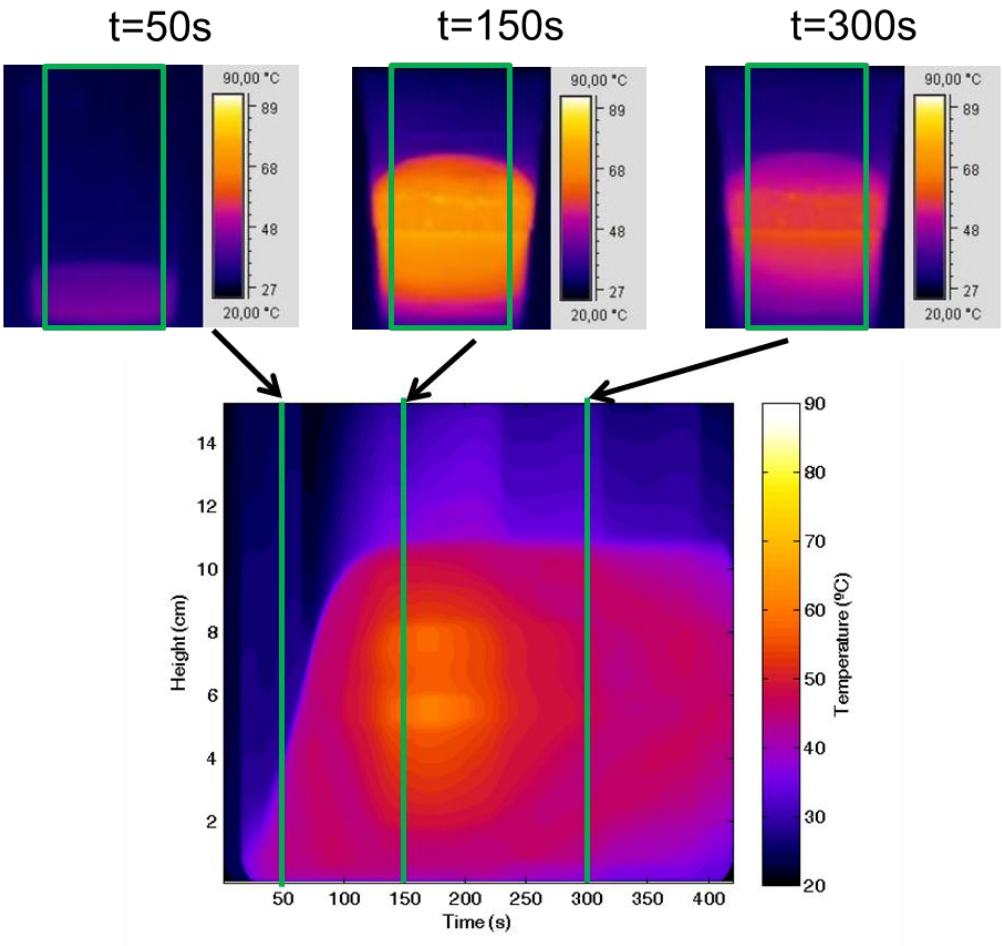

Figure 7. The evolution of the vertical profile of temperature for the PUR1.

Furthermore, the spatial capabilities of the presented technique allow identifying the presence of "hot spots" in the sample surface, due for example to a non proper mixing of the components. In order to show this aspect, we manufactured two samples with the same formulation as PUR3, but a small amount of blowing catalyst was added to one of them once the mixing process of the polyol blend and isocyanate had been completed. The results of this specific experiment are shown in the Results and Discussion section.

2.2.3. Validation of the temperatures measured by the IR camera

Temperature profiles during foaming process were measured and collected. For some specific experiments a thermocouple was introduced in the plastic container in order to measure the internal temperature during the time of the experiment (**Figure 8**). The thermocouple was located as close as possible to the container wall at half height of the plastic container. The thermocouple position has been chosen in order to get information about the temperatures at

the surface to validate the temperatures obtained by the IR camera. All the data provided by the thermocouple were registered in a computer.

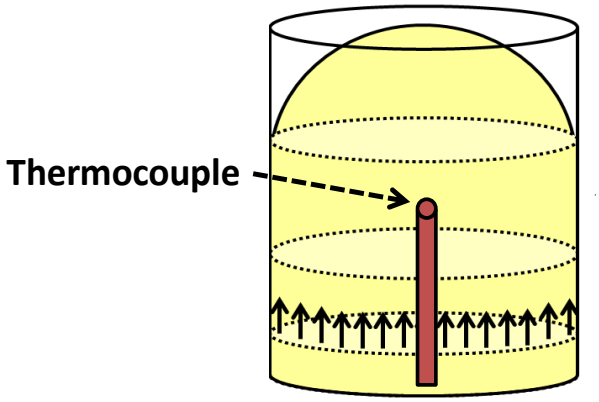

Figure 8. Schematic view of the plastic cup used to produce the foams when a thermocouple was located in internal surface of the cup to evaluate the accuracy of the temperature measurements of the IR camera.

3. Results and Discussion

As mentioned before, after the 25 frames condensation the infrared camera allowed obtaining a video with 420 images for every analysed sample. In order to show the main highlights of the recorded foaming process, four different moments have been selected (20s, 60s, 120s and 240s). The images are shown in **Figure 9** for the four samples under study.

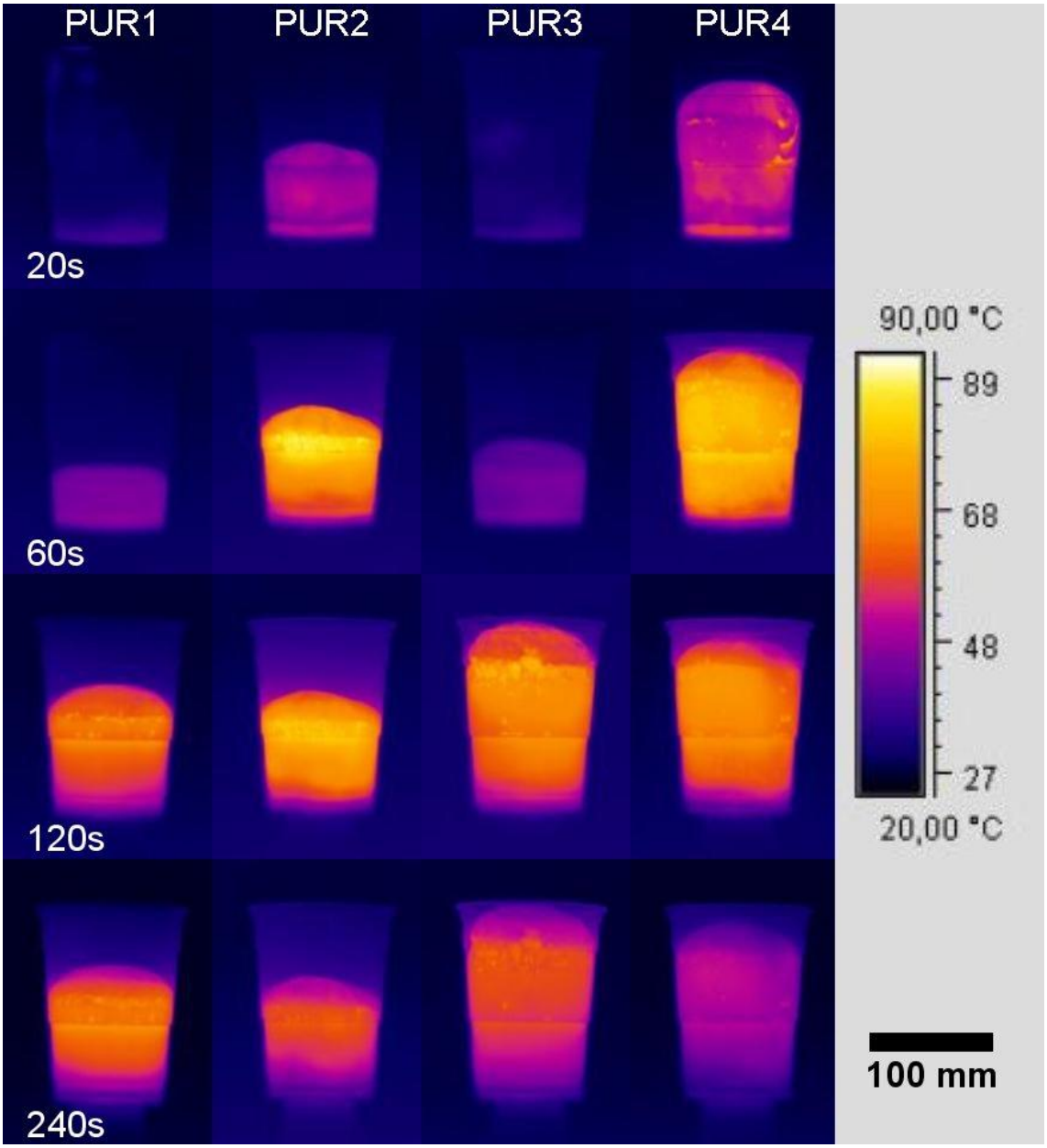

Figure 9. Acquires images for all the analysed (PUR1, PUR2, PUR3 and PUR4) samples at selected times.

From the images of figure 9 the expansion height and expansion volume were measured (Figure 10). Considering the final reached expansion, the samples may be separated into two groups. On one hand, PUR1 and PUR2 reach approximately 9 cm in height (**Figure 10a**), and consequently *ca*. 600 cm^3 in volume (**Figure 10b**) due to the container symmetry. On the other hand, PUR3 and PUR4 show a higher final expansion, reaching 15 cm in height (**Figure 10a**), and reaching a total volume close to 1000 cm^3 (**Figure 10b**).

This different behaviour is in accordance with the PUR formulation of each sample (**Table 1**), since the final expansion of a cellular material (obviating cell degeneration processes [29]) is mainly determined by the amount of blowing agent [30]. In our case, PUR1 and PUR2 have been obtained by using the same amount of water in the PU formulation (2 ppw), which is lower than that used in foams PUR3 and PUR4 (5 ppw). Since water acts a blowing agent, the final expansion of the two latter foams is higher. In addition, a slight shrinkage (reduction of height and volume) is observed in the volume expansion curves for PUR2 and PUR4 for high times. For these two materials a blowing catalyst was added to the reactants.

(a) (b)

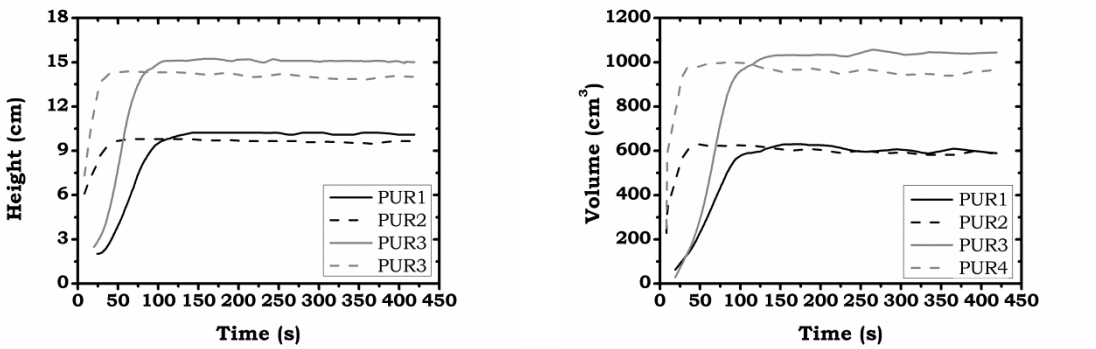

Figure 10. (a) Sample height, and **(b)** sample volume results.

The expansion rate and the expansion acceleration obtained (**Figure 11**) from these experiments are crucial parameters to understand the expansion kinetics. Once again, the studied samples may be divided into two separated groups depending in this case on the presence of the blowing catalyst in the PU formulation. PUR1 and PUR3 do not contain blowing reaction catalyst, and they expand relatively slowly, with a maximum peak in the expansion rate curves located at *ca*. 70s (**Figure 11a**). Therefore an inflexion point is detected in their acceleration behaviour at the same point (**Figure 11b**). Since the formulation of PUR2 and PUR4 contain 2 parts of the blowing reaction catalyst, the expansion of these two samples is very fast. Thus, in this case the observation of the mentioned two (maximum/inflexion) points in the expansion rate and acceleration curves occurs before the first data are obtained and therefore they are not observed (**Figure 11**). On the other hand, when foams with the same amount of catalyst are compared (PUR1 *vs*. PUR3, and PUR2 *vs*. PUR4) foams containing higher amounts of water in the PU formulation (PUR3 and PUR4) reach higher maximum expansion rates.

(a) (b)

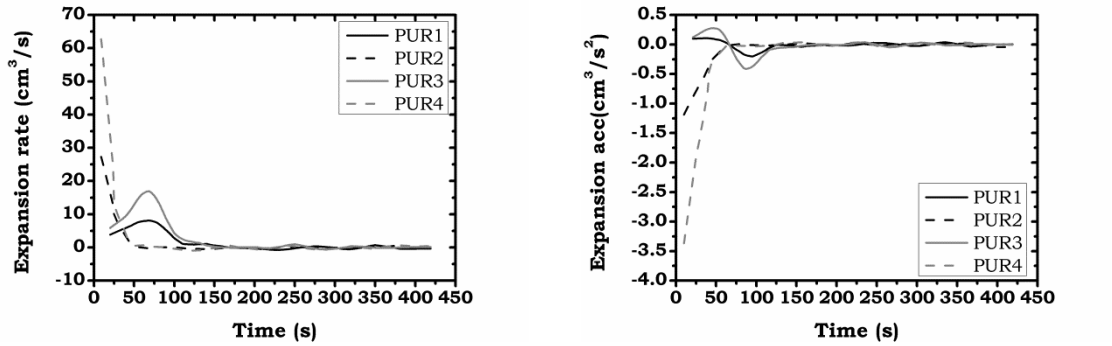

Figure 11. (a) Expansion rate, and **(b)** expansion acceleration for all the samples tested by infrared expandometry.

In addition, the analysis of infrared sequences allows quantifying the surface temperatures considering the whole sample. As indicated above, this is a clear advantage compared to thermocouples, which measure the temperature only in a specific region of the sample.

The PU blowing reaction is extremely exothermic [4] and samples containing blowing catalyst should reach higher temperatures. Besides, the presence of blowing catalyst in the PU formulation should also lead to a faster heating of the samples in comparison with the samples without blowing catalyst. This expected trends can be clearly detected in the samples studied, as shown in **Figure 12** PUR2 and PUR4, which contain the blowing catalyst, reach higher temperatures (both average and maximum temperatures), and these temperatures are reached in a shorter time compared with PUR1 and PUR3, which do not contain blowing catalyst.

When formulations containing the same amount of catalyst are compared, the presence of water in the reaction also accelerates the sample heating. Thus, PUR3 and PUR4 reach the highest temperature before PUR1 and PUR2, even though they reach lower maximum temperatures (**Figure 12b**).

(a) (b)

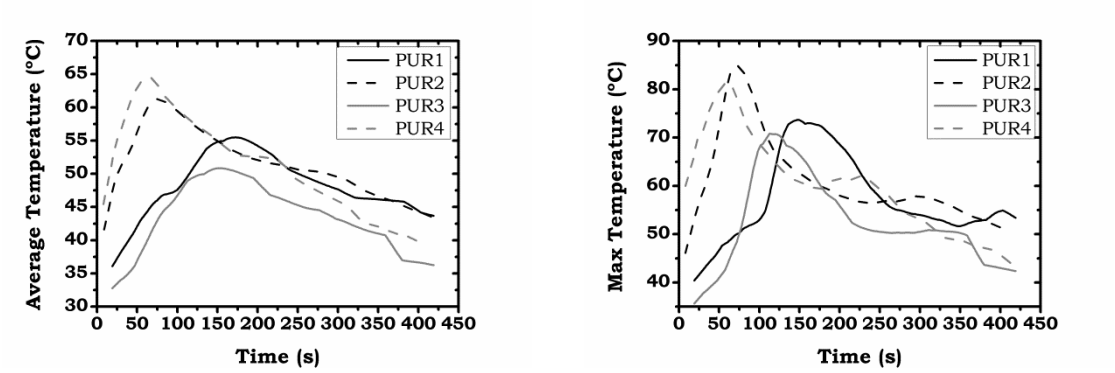

Figure 12. (a) Average and **(b)** maximum surface temperatures detected by the infrared camera for all the analysed samples.

In addition to the surface temperature measured during foaming with the infrared camera, we have also measured the temperature evolution with a thermocouple placed in the surface of the plastic container (see section 2.2.3). The surface temperatures measured by thermocouples for all samples are shown in **Figure 13**. The comparison between the temperatures registered by both methods (surface thermocouple in **Figure 13** and infrared camera in **Figure 12**) evidences that both temperatures display the same trends. Therefore, these results support the observations described above and show that the approach followed allows an accurate comparison of the behaviour of different materials.

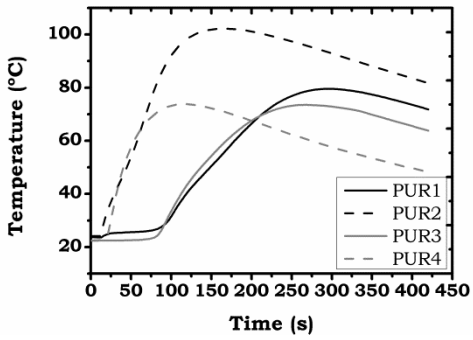

Figure 13. Surface temperature measured by a thermocouple for all the systems under study.

Figure 14 shows the evolution of the temperature parameters *versus* time. These parameters allow evaluating the inhomogeneity of the temperature in the samples. The analysis of *NSD* (**Figure 14a**) allows establishing two intervals. The inflexion point between these two parts

(indicated by vertical lines in **Figure 14a**) depends on the sample but, as expected, it occurs before in those samples containing blowing catalyst (PUR2 and PUR4) which heat up faster. Focusing on the first interval, the maximum values of *NSD* correspond roughly to the moment when the highest temperature is reached (**Figure 12b**). Furthermore, the samples with lower amount of blowing agent (PUR1 and PUR2) are less homogeneous in this step of the process. The study of the second interval shows that samples with higher amounts of blowing agent (PUR3 and PUR4) evolve more inhomogeneously than samples with lower amounts of blowing agent (PUR1 and PUR2).

The values of *NΔT* (**Figure 14b**) show similar trends to those shown by the measurements of maximum temperature (**Figure 12b**). Samples with higher amounts of blowing catalyst (PUR2 and PUR4) reach the higher temperature before, and consequently the maximum point of *NΔT* is also reached earlier. However, a quantitative evaluation of the inhomogeneity results does not show any direct relation between formulations and the values obtained from this parameter.

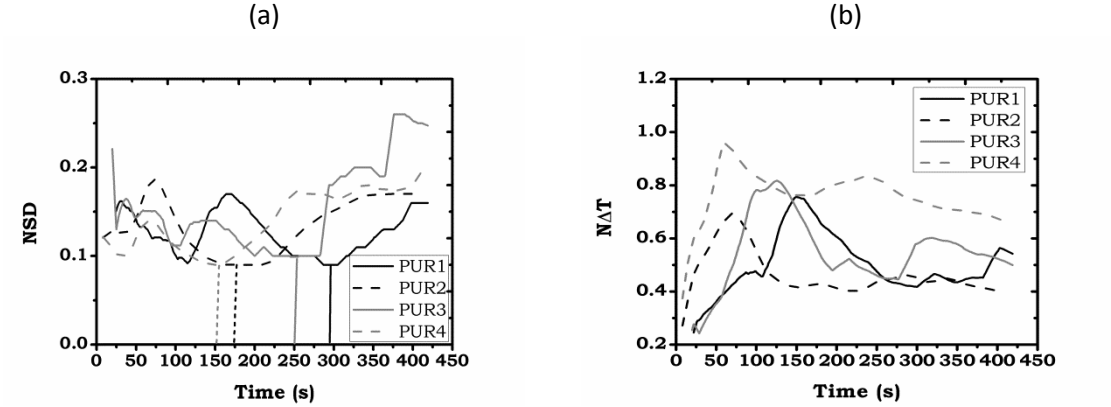

Figure 14. (a) Normalised standard deviation (*NSD*) of the temperature and **(b)** normalised temperature variation (*NΔT*) for the samples under study.

The evolutions of the vertical profiles of surface temperature are shown in **Figure 15**. This parameter accounts for the inhomogeneities of temperature in the surface of the samples. **Figure 15** shows that all the foams reach the maximum temperature approximately in the centre of the sample. The vertical profiles of surface temperature for the foams containing blowing catalyst (PUR2 and PUR4) are less homogeneous than those for foams without blowing catalyst (PUR1 and PUR3). The samples with blowing catalyst reach higher temperatures and these temperatures are reached faster.

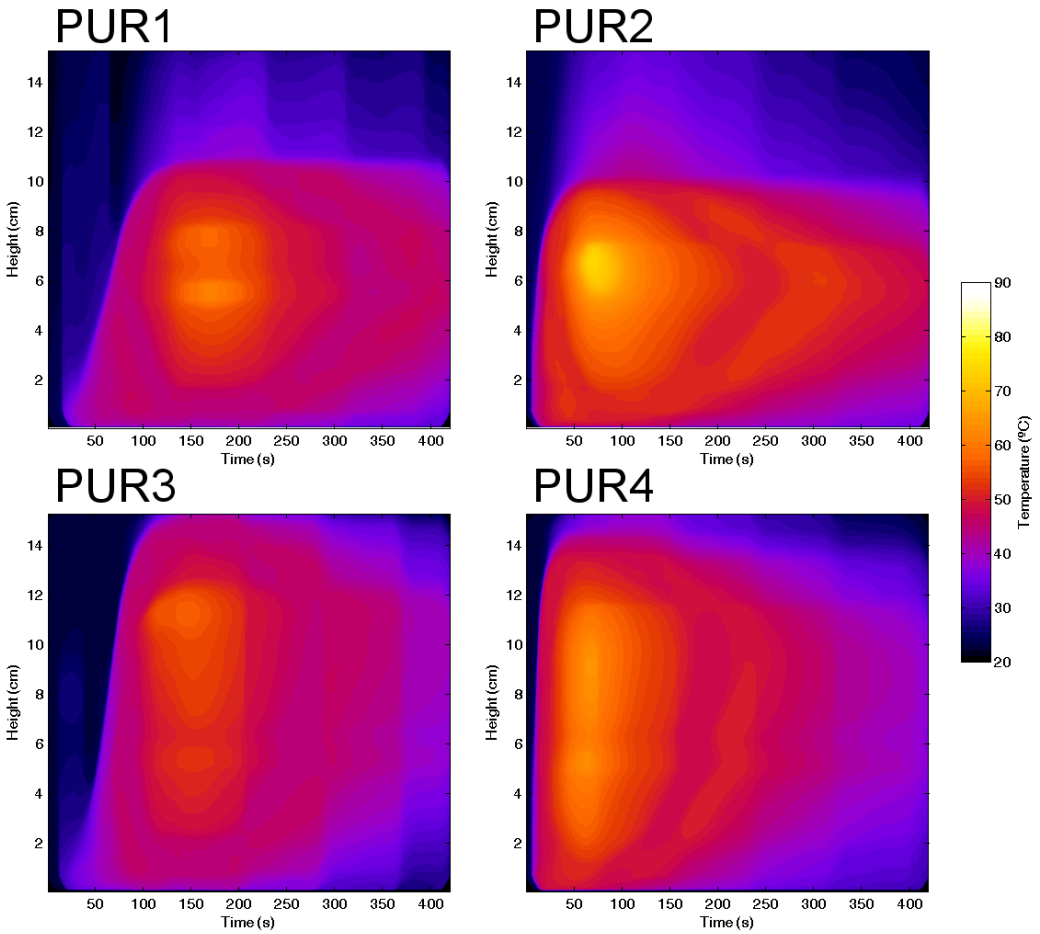

Figure 15. The evolution of the vertical profile of temperature for all the systems under study.

Figure 16 exhibits an example of a possible application of Infrared Expandometry. **Figure 16a** and **Figure 16b** show images of the foaming process for PUR3 without blowing catalyst and with an additional amount of blowing catalyst, respectively. **Figure 16b**, shows a hot spot during foam expansion. The temperature differences between both processes can be clearly observed. Therefore, Infrared Expandometry also allows detecting heterogeneities in the formulations, such as this hot spot, which in our case is due to an inadequate dispersion of the components into the mixture reaction.

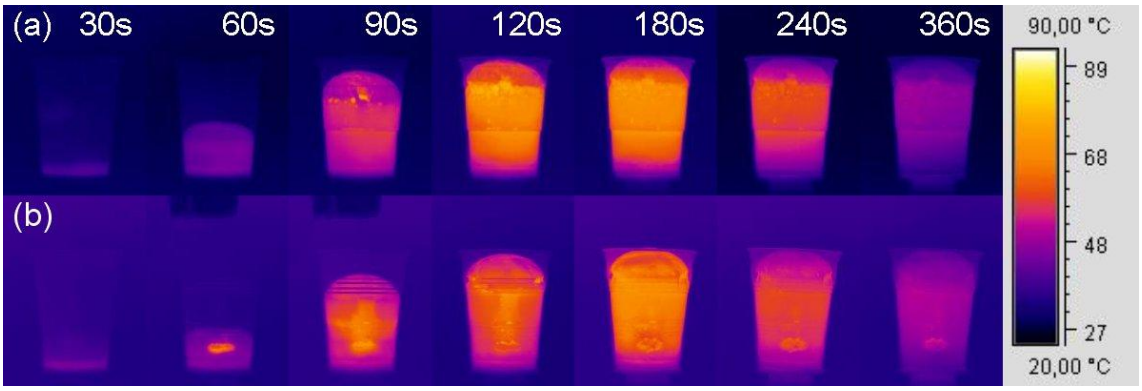

Figure 16. Several moments of the recorded expansion process exhibiting the possibility of detection of hot spots: **(a)** PUR3 **(b)** PUR3 with additional blowing catalyst none properly dispersed that promotes this hot spot.

7. Conclusions

Herein we have introduced Infrared Expandometry, a novel experimental technique adequate to monitor the expansion kinetics of thermoset cellular materials obtained by exothermic foaming processes. It is based on the infrared radiation emitted by a body at a given temperature, and it has been successfully tested in PU foams.

The analysis of the images acquired by the infrared camera allows determining the evolution *vs.* time of important parameters of the foaming process, such as height, volume, expansion rate, acceleration rate, and surface temperature. Moreover, the homogeneity of the surface temperature can be evaluated by several parameters such as the normalized standard deviation of the surface temperature and the normalized temperature variation. In addition, the evolution of the vertical profile of the surface temperature can also be obtained by this technique.

Infrared Expandometry has some interesting features. Since it allows following *in-situ* the evolution of the material from the initial time, it is possible to study samples without size restrictions and compared with traditional thermocouple measurements. Infrared Expandometry does not interfere with the foam expansion, and temperatures may be quantified either at any point of the surface or for the whole sample.

Acknowledgements

Financial assistance from MINECO and FEDER program (MAT2015-69234-R) and the Junta de Castile and Leon (VA011U16) are gratefully acknowledged. Predoctoral contract of S. Perez-

Tamarit by University of Valladolid (E-47-2015-0094701) and co-financed by Banco Santander is also acknowledged.

References

[1] D. Klempner, V. Sendijarevic, Handbook of Polymeric Foams and Foam Technology, Hanser 1991.
[2] Polymer Foams Market Expected to Consume 25.3 Million Tonnes by 2019. http://www.smithersrapra.com/news/2014/may/polymer-foam-market-to-consume-25-3-million-tonnes, 2014 (accessed 16 July 2019).
[3] G. Oertel, Polyurethane Handbook 2nd ed., Hanser Publishers, Munich, 1993.
[4] S. Tan, T. Abraham, D. Ference, C.W. Macosko, Rigid polyurethane foams from a soybean oil-based Polyol, Polymer, 52 (2011) 2840-2846.
[5] A.K. Bonetskaya, M.A. Kravchenko, T.M. Frenkel', V.A. Pankratov, S.V. Vinogradova, V.V. Korshak, The kinetics and the heat of cyclotrimerization of aryl- and alkylisocyanates, Polymer Science U.S.S.R., 27 (1985) 1422-1427.
[6] M.A. Rodríguez-Pérez, J.A.D. Saja, The effect of blending on the physical properties of crosslinked closed cell polyrthylene foams, Cellular Polymers 18 (1999) 1-20.
[7] L. Gibson, M. Ashby, Cellular solids: structure and properties, Pergamon Press, Oxford, 1988.
[8] D. Weaire, S. Hutzler, The Physics of Foams, Oxford University Press2001.
[9] J.I. Velasco, M. Antunes, O. Ayyad, C. Saiz-Arroyo, M.A. Rodríguez-Pérez, F. Hidalgo, J.A. de Saja, Foams based on low density polyethylene/hectorite nanocomposites: Thermal stability and thermo-mechanical properties, Journal of Applied Polymer Science, 105 (2007) 1658-1667.
[10] J.I. Velasco, M. Antunes, O. Ayyad, J.M. López-Cuesta, P. Gaudon, C. Saiz-Arroyo, M.A. Rodríguez-Pérez, J.A. de Saja, Foaming behaviour and cellular structure of LDPE/hectorite nanocomposites, Polymer, 48 (2007) 2098-2108.
[11] S. Asavavisithchai, A.R. Kennedy, Effect of powder oxide content on the expansion and stability of PM-route Al foams, Journal of colloid and interface science, 297 (2006) 715-723.
[12] A.R. Kennedy, S. Asavavisitchai, Effects of TiB2 particle addition on the expansion, structure and mechanical properties of PM Al foams, Scripta Materialia, 50 (2004) 115-119.
[13] I. Duarte, J. Banhart, A study of aluminium foam formation–kinetics and microstructure, 48 (2000) 2349-2362.
[14] H. Stanzick, J. Banhart, L. Helfen, T. Baumbach, In-situ monitoring of metal foam evolution and decay, Eurofoam 2000: Foams, emulsions and applications, 2000, pp. 290-296.
[15] E. Solórzano, M. Antunes, C. Saiz-Arroyo, M.A. Rodríguez-Pérez, J.I. Velasco, J.A. de Saja, Optical expandometry: A technique to analyze the expansion kinetics of chemically blown thermoplastic foams, Journal of Applied Polymer Science, 125 (2012) 1059-1067.
[16] E. Solórzano, J. Pinto, S. Pardo, F. Garcia-Moreno, M.A. Rodriguez-Perez, Application of a microfocus X-ray imaging apparatus to the study of cellular polymers, Polymer Testing, 32 (2013) 321-329.
[17] S. Pardo-Alonso, E. Solórzano, S. Estravís, M.A. Rodríguez-Perez, J.A. de Saja, In situ evidence of the nanoparticle nucleating effect in polyurethane–nanoclay foamed systems, Soft Matter, 8 (2012) 11262.
[18] F. Garcia-Moreno, M. Mukherjee, C. Jiménez, A. Rack, J. Banhart, Metal Foaming Investigated by X-ray Radioscopy, Metals, 2 (2011) 10-21.
[19] F. García Moreno, M. Fromme, J. Banhart, Real-time X-ray Radioscopy on Metallic Foams Using a Compact Micro-Focus Source, Advanced Engineering Materials, 6 (2004) 416–420.

[20] http://www.prnewswire.com/news-releases/thermoset-plastics-market---forecasts-from-2016-to-2021---by-material-type-thermoset-moulding-process-type-industry--geography---research-and-markets-300407804.html.
[21] R. Jennings, Instrumental Analysis of the performance Characteristics of figid urethane foaming systems, Journal of Cellular Plastics, 5 (1969) 159-172.
[22] R.L. Rowton, A simple method for developing gel rise profiles of urethane foams, Journal of Cellular Plastics, 16 (1980) 287-292.
[23] A.V. Thuyne, B. Zeegers, Kinetic study on flexible polyurethane foams formation, Journal of Cellular Plastics, 14 (1978.) 150-160.
[24] Y. Jianqiu, Z. Jianyuan, W. Dening, H. Chunpu, Y. Shengkang, C. Yiou, C. Yufu, C.X. Ziqian, S. Jin, W. Yin, A modified method for developing gel rise profile of urethane foams, Journal of Cellular Plastics, 26 (1990) 39-47.
[25]http://www.tracomme.ch/fileadmin/user_upload/Datenblaetter/E-PI_Polyurethane_Testing_Equipment_2009.pdf.
[26] X.P. Maldague, Theory and Practice of Infrared Technology for Nondestructive Testing, New York 2001.
[27] C.A. Schneider, W.S. Rasband, K.W. Eliceiri, NIH Image to ImageJ: 25 years of image analysis, Nature Methods, 9 (2012) 671-675.
[28] M.D. Abràmoff, P.J. Magalhães, S.J. Ram, Image Processing with ImageJ, Biophotonics International, 11 (2004) 36-42.
[29] I. Cantat, S. Cohen-Addad, F. Elias, F. Graner, R. Höhler, O. Pitois, F. Rouyer, A. Saint-Jalmes, S. Cox, Foams: Structure and Dynamics, Oxford University Press2013.
[30] G. Harikrishnan, D.V. Khakhar, Modeling the dynamics of reactive foaming and film thinning in polyurethane foams, AIChE Journal, 56 (2010) 522-530.

European polymer journal 118 (**2019**) 404-411
https://doi.org/10.1016/j.eurpolymj.2019.06.012

X-ray radioscopy validation of a polyol functionalized with graphene oxide for producing rigid polyurethane foams with improved cellular structures

Mercedes Santiago-Calvo [1,*], Saúl Pérez-Tamarit[1], Paula Cimavilla-Román[1], Victoria Blasco[2], Carolina Ruiz[2], Rodrigo París[2], Fernando Villafañe[3], Miguel Ángel Rodríguez-Pérez[1]

[1] Cellular Materials Laboratory (CellMat), Condensed Matter Physics Department, Faculty of Science, University of Valladolid, Campus Miguel Delibes, Paseo de Belén 7, 47011 Valladolid, Spain

[2] D.C. Technology and Corporate Venturing, Repsol S.A. C/ Agustín de Betancourt s/n, 28935 Móstoles, Spain

[3] GIR MIOMeT-IU Cinquima-Química Inorgánica, Faculty of Science, University of Valladolid, Campus Miguel Delibes, Paseo de Belén 7, 47011 Valladolid, Spain

* Corresponding author: mercesc@fmc.uva.es

Abstract

Fillers can be dispersed in polyurethane (PU) components to produce PU foams with improved properties by different methods. Herein, graphene oxide (GO) is chemically linked to polyol chains in order to suppress fillers agglomeration. Then the foaming behaviour of rigid polyurethane (RPU) foams from polyols functionalized with GO (GO-f) is compared with the one of RPU foams containing GO dispersed in the polyol (GO-d) by high shear mixing. Relative density, cell size, and cell nucleation density of the RPU foam nanocomposites are monitored during the foaming process by using X-ray radioscopy. The results obtained demonstrate that the use of polyol functionalized with GO-f offers a high improvement of the cellular structure and also makes the results more reproducible.

Keywords: Polyurethane foam; Graphene oxide; filler agglomeration; X-ray radioscopy

Development of a methodology to follow the reaction kinetics of rigid polyurethane foams

1. Introduction

The exceptional characteristics of rigid polyurethane (RPU) foams, such as their low thermal conductivity, low density, high strength-to-weight ratio, and low moisture permeability, make them very useful materials for thermal insulation in different sectors such as transportation, refrigeration systems, automotive industry, and building construction, among others [1-3]. Moreover, properties such as mechanical, acoustic, flammability or thermal may be considerably improved by introducing nanoparticles in the formulation of polyurethane (PU) foams [4, 5]. The effect of nanoparticles on the properties of the foams depends on their concentration, their particle size and shape, their functionality, their compatibility with the polymer matrix, as well as on their degree of dispersion. The latter factor is crucial because the effect of nanoparticles on the properties of foams is mainly correlated with an optimal dispersion into the PU matrix [3-5]. However, reaching a suitable dispersion of nanoparticles is often a complicated task. Fillers are commonly dispersed into either the isocyanate or the polyol components by using high shear mixing and/or ultrasounds [6-12], although there are also a scarce number of studies describing PU components functionalized with fillers [13-16].

In a previous study we reported the synthesis of water-blown RPU foams from polyols chemically functionalized with low amounts of graphene oxide (GO) nanoparticles (0.017, 0.033 and 0.083 wt%) [14], that resulted in lower cell sizes and thermal conductivities in comparison with the material without nanoparticles. Moreover, the main advantage of using GO particles chemically linked to polyol chains was avoiding nanoparticles agglomeration, and thus the usual problems of nanoparticles dispersion were precluded. In order to support the idea that the use of polyols functionalized with GO improves the characteristics of RPU foams nanocomposites, we herein evaluate the influence on some of the characteristics of the foams by using X-ray radioscopy of either the GO chemically linked to polyol chains or the GO dispersed into the polyol.

X-ray radioscopy is a *in situ* technique that allows collecting real-time information about the internal microstructure and about the density of foaming materials such as metals [17] or polymers [18, 19] with a temporal resolution in the range of seconds. Thus, this technique allows evaluating the intermediate stages of the dynamic foaming process, which cannot be estimated by conventional ex situ techniques, such as SEM, X-ray tomography or density determination. This technique was applied for the first time on RPU foams by our group in order to evaluate the effect of nanoclays content on the foaming process [18]. In addition, other two works have described the use of this technique in order to study the effect of nanoparticles on PU foaming [20, 21]. Therefore, this approach has been very helpful in order to observe the nucleation and degeneration mechanisms (coalescence and coarsening) which can be promoted by the incorporation of nanoparticles during the PU foaming process.

In the present article, we describe the evolution of relative density, cell size, and cell nucleation density of the RPU foam nanocomposites by using X-ray radioscopy. The effect of GO (either GO chemically linked to polyol chains or GO dispersed into polyol) on the microstructure and on the foaming mechanisms (cell nucleation, growth and degeneration

mechanisms such as pore coalescence) at all the intermediate stages during the foaming process have been evaluated.

2. Experimental

2.1. Materials

Three poly(propylene oxide) polyols synthesized by Repsol S.A. (Spain) were used in this study: the pure polyol without GO (functionality 3, OH index 426.4 mg KOH/g, viscosity 476.9 mPa·s, 488 Dalton), and two functionalized with GO: 500 ppm of GO (functionality 3, OH index 399.3 mg KOH/g, viscosity 553.3 mPa·s, 494 Dalton) and 2500 ppm of GO (functionality 3, OH index 377.5 mg KOH/g, viscosity 4463.2 mPa·s, 675 Dalton) [14].

Two series of RPU foams were studied (Table 1): (1) foams synthesized with the polyols functionalized with GO (GO chemically linked to polyol chains were labelled as GO-f): a RPU foam containing 0.017 wt% GO-f (obtained from a polyol with 500 ppm of GO) and a RPU foam containing 0.083 wt% GO-f (obtained from a polyol with 2500 ppm of GO); and (2) foams synthesized with GO dispersed (GO dispersed into pure polyol were labelled as GO-d) into the pure polyol: a RPU foam containing 0.017 wt% GO-d and a RPU foam containing 0.083 wt% GO-d. A pure material (obtained with pure polyol without GO) was used as a reference for both series. In order to prepare both series of RPU foams the same GO is used: liquid highly concentrated GO (with a concentration of 2.5 mg/mL of GO sheets dispersed in water with a GO particle size distribution: D90 29.05-32.9 μm; D50 13.3-16.6 μm; D10 5.9-6.63 μm) from Graphenea S.A. (Spain) [22]. In the case of the series of foams in which the GO is added as a water dispersion, the amount of water from the GO particles is taken into account for adjusting the required amount of water in the formulation.

The series of RPU foams with GO-f were synthesized following the next steps and the formulation collected in Table 1. An overhead stirrer (EUROSTAR Power control-visc P1, IKA) with a 50 mm diameter Lenart disc stirrer was used to premix a mixture of polyol [14] (100 parts by weight (ppw)), TEGOAMIN® DMCHA catalyst from Evonik Nutrition & Care GmbH (Germany), (0.3 ppw), TEGOSTAB® B 8522 surfactant from Evonik Nutrition & Care GmbH (Germany), (1 ppw), and distilled water as blowing agent (5 ppw). A lower amount of catalyst (0.3 ppw) is used in this study because the cream time must be increased in order to observe properly the foaming behaviour with the X-ray setup. The mixture of the components was stirred during 2 minutes at 250 rpm in order to obtain homogenous polyol blends (Part B). IsoPMDI 92140 (2.7 functionality, 31.5% NCO, density 1.23 g cm^{-3}, viscosity 170-250 mPa·s), a polymeric diphenylmethane diisocyanate (pMDI) from "BASF Poliuretanos Iberia S.A" (Spain), was used. Part B and Part A were then mixed in a plastic cup at 1200 rpm for 10 seconds. The isocyanate index was fixed in 120 [1] [23].

The series of RPU foams with GO-d into the pure polyol were synthesized following the same steps and the same formulation as for RPU foams with GO-f (**Table 1**). However, a new step is necessary in the latter case: the production of the premix of GO with the polyol blend. In this

case, the GO water dispersion and the polyol blend were previously stirred during 5 minutes at 250 rpm for an optimal dispersion.

A total amount of 30 g (Part A and Part B) were mixed in a plastic cup, and then 0.020±0.009 mL of this reaction mixture was poured on a specific foaming mould in order to carry out the X-ray radioscopy experiments (section 2.3). In addition, the material not used in the radioscopy test was allowed to grow in the plastic cup and the resulting foam with a cylindrical size of 100 mm x 100 mm (diameter x height) was characterized (section 2.2).

Table 1. Formulations of RPU foams from polyols functionalized with GO (GO-f) and polyols with GO dispersed (GO-d).

	Part A (ppw)	**Part B (ppw)**					
	Isocyanate[a]	**Polyol with different GO content**			**Surfactant**	**Catalyst**	**Blowing agent**
RPU foams with different GO wt%	**IsoPMDI 92140**	**0 ppp GO (pure)**	**500 ppm GO**	**2500 ppm GO**	**TEGOSTAB ® B 8522**	**TEGOAMIN ® DMCHA**	**Water**
Pure (Reference)	211	100			1	0.3	5
0.017%GO-f	203		100		1	0.3	5
0.083%GO-f	197			100	1	0.3	5
0.017%GO-d	211	100[b]			1	0.3	5
0.083%GO-d	211	100[b]			1	0.3	5

[a] The ppw of isocyanate are calculated from the isocyanate index (fixed in 120) and the hydroxyl equivalents as it is explained in the references [1] [23].

[b] The GO is added as a water dispersion into the polyol in order to produce foams with the corresponding content of GO, 0.017 wt% and 0.083 wt% respectively. The amount of water from the GO particles is taken into account for adjusting the required amount of water in the formulation.

2.2. Characterization of final foam

Density, open cell content and mean cell size of the resulting foams obtained in a plastic cup (as mentioned in section 2.1) were measured in order to validate the X-ray radioscopy results. The values obtained were compared with those corresponding to the last monitored instant in radioscopy. Density was measured as described by ASTM D1622/D1622M-14 [24]. Relative density was obtained as the ratio between the foam density and the solid material density (1160 kg/m^3). Open cell content (OC) was measured by using a gas pycnometer Accupyc II 1340 from Micromeritics, according to ASTM D6226-10 [25]. Moreover, the microstructure of the foams was examined by Scanning Electron Microscopy (SEM) with a JEOL JSM-820 microscope. Then, an image analysis protocol [26] was applied on SEM micrographs to

determine the mean 3D cell size (Φ_{3D}). The width of the all cell size distribution (WCD) is calculated as the relation between the standard deviation of the cell size distribution and the mean 3D cell size (Φ_{3D}).

2.3. X-ray Radioscopy

2.3.1. Set-up

X-ray radioscopy, in which sequences of radiographies are acquired over time, has been demonstrated to be a useful tool for the *in-situ* inspection of the foaming process of polymeric materials [18, 20, 21]. The basic elements of the radioscopy set-up used in this research are: a low energy micro-focus X-ray source which produces X-rays (L10101, Hamamatsu. Voltage: 20-100 kV, Current: 0-200 µA), and a high sensitivity flat panel detector which forms the X-ray images (C7940DK-02, Hamamatsu. 2240x2344 pixels, 50 µm pixel size). Both elements are positioned at a distance (source to detector distance, SDD) of 580 mm (**Figure 1a**). Furthermore, the magnification factor (*M*) is determined by the position of the monitored object between source and detector (SOD, source to object distance), considering the cone-beam provided by the X-ray source (Equation 1).

$$= \frac{SDD}{SOD} \quad \textbf{(1)}$$

In this study, SOD = 46.4 mm, what leads to *M*=12.5, that resulted in an effective pixel size of 8 µm, by using pixel binning 2x2.

2.3.2. Monitoring

A specific foaming mould (**Figure 1b**) was designed and fabricated using stainless steel in order to perform the X-ray radioscopy experiments. It consists on a central cylindrical hole (Ø = 6mm, thickness = 0.6 mm) with two lateral evacuation cavities. The amount of the isocyanate-polyol mixture introduced in the central area of the mould was 0.020±0.009 mL (PU droplet in **Figure 1b**). This blend was deposited in this area immediately after the stirring process, as mentioned in section 2.1. Foaming occurred between two polypropylene plastic covers (25 µm thick) which, helped by the evacuation cavities, permitted to maintain invariable the sample thickness during the process. Two smaller holes are located just below the centred one which enables an *in-situ* calibration of the X-ray acquired signal (**Figure 1b**). Two materials with known relative density (air, relative density = 0 and a thermoplastic polyurethane (TPU) disc of the same thickness, relative density = 1) are located in these holes and scanned with the evolving sample. The image analysis calculations in which this calibration is used are explained in the following section.

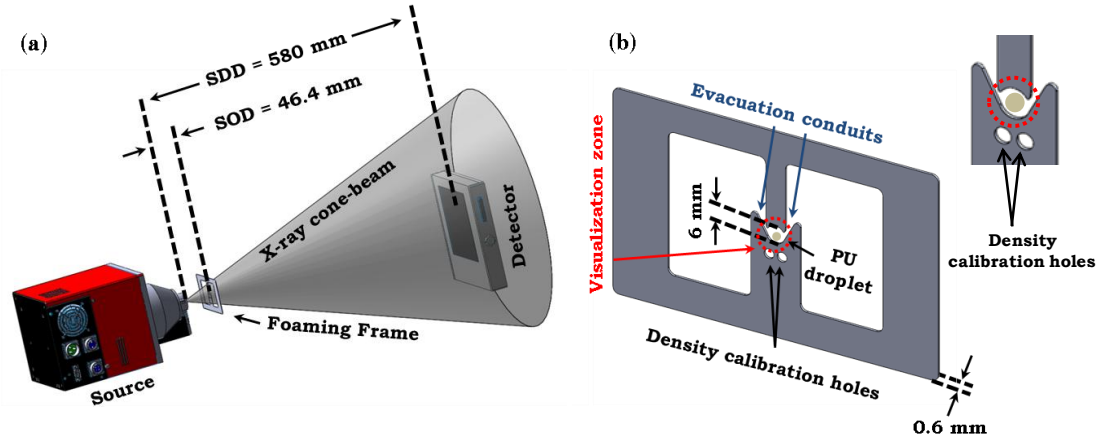

Figure 1. 3D sketch of the system employed to perform the X-ray radioscopy experiments. (**a**) X-ray system and relative position of the foaming mould with respect to the X-ray source and detector and (**b**) designed mould for PU foaming (foaming frame).

The X-ray tube was adjusted at 40 kV and 120 µA in order to obtain the optimum contrast on the acquired radiographies. The low amount of catalyst allowed us to slow down the foaming kinetics. For this reason, an exposure time of 800 ms was selected in order to record motion-less and sharp images. A total of 700 radiographies were acquired, corresponding to *ca.* 9 min of the foaming process. The first 50s are needed in order to place the foaming frame inside the X-ray cabinet. Three foaming tests were carried out for every material in order to obtain a representative behaviour of each formulation.

2.4. Image Analysis

Dedicated image analysis protocols have been programmed using ImageJ/Fiji as image analysis tool [27, 28]. These protocols were applied to all the acquired radiographs in order to quantify both the relative density and the cell size to finally calculate the cell nucleation density.

Density (ρ) evolution can be extracted by using the Beer-Lambert attenuation law [19], which allows calculating the density of the materials from the transmitted intensity collected in the detector (I), as expressed by **Equation 2**:

$$I = I_0 exp(-\mu \rho t) \quad \textbf{(2)}$$

where both the X-ray attenuation coefficient (μ) and the thickness of the sample (t) exponentially reduce the original intensity from the source (I_0). Relative density (density of the sample divided by density of the solid precursor) (ρ_r) evolution was obtained by calibrating the acquired average intensity on the sample (I) by using the intensity of both materials with known relative density. The zone used to determine the intensity on the sample has been adjusted over time to the surface occupied by the sample in the visualization zone from a little

drop at the start of the process to the full 6 mm hole of the foaming frame at the end. The intensity used to determine the relative density is the average intensity in these zones over time/images. In our case, air (I_{air}) and solid TPU of 0.6 mm of thickness (I_{ref}) were located in the smaller holes of the foaming frame (**Figure 1b**). Zones of the same area in each of the mentioned holes have been used to calculate the average intensities of air and solid TPU respectively during the whole process. After a logarithmic conversion of the acquired intensity, relative density was calculated as the ratio between these two extreme calibration points (**Equation 3** for general calibration equation and **Equation 4** for our particular case with relative densities 0 and 1 as limits) [19].

$$r = {}_r{}^{air} + \frac{log\left(\frac{I}{I_{air}}\right)}{log\left(\frac{I_{ref}}{I_{air}}\right)}\left(\rho_r{}^{ref} - {}_r{}^{air}\right) \quad \textbf{(3)}$$

$$r = \frac{log\left(\frac{I}{I_{air}}\right)}{log\left(\frac{I_{ref}}{I_{air}}\right)} \quad \textbf{(4)}$$

Several sequential steps were involved in the *in-situ* determination of the cell size. Firstly, the real pixel size was scaled considering a known distance to the images. Then, an edge preserving filter allowed to homogenize the intensity of the images, thus facilitating subsequent binarization. As sample intensity is exponentially decreasing (as well as relative density), the threshold limits were varied automatically being adapted to the intensity of the images, thus enabling a proper binarization of the whole sequence. After that, a watershed algorithm [29] was applied in order to separate every single pore. In order to minimise cell size quantification errors, maximum and minimum cell size at the start and at the end of the process are evaluated by the user on the images. After that, the image analysis software allowed interpolating both values for the whole sequence assuming a $t^{1/2}$ law for the cell growth, typically considered in the literature [30, 31]. As a result, maximum and minimum cell sizes are obtained during the full expansion process. In addition, only objects with circularity higher than 0.8 were included in order to refine the cell size characterization. Using both restrictions (size and circularity) we were able to avoid pore overlapping problems in addition to binarization and watershed mistakes during the image analysis process. Once the cell size is characterized on the radiographs (2D), it is transformed to 3D values using the typical scale factor of 1.27 [26].

Once cell size (ϕ) and relative density (ρ_r) were adequately monitored, the evolution of the cell nucleation density (N_o) or number of cells per unit volume of the unfoamed material was determined using **Equation 5**.

$$N_o = \frac{6}{\pi\phi^3}\left(\frac{1}{\rho_r} - 1\right) \quad \textbf{(5)}$$

Finally, we have defined the average normalized standard deviation (Average NSD) of the three experiments performed for each sample (**Equation 6)**. It is calculated for each parameter studied during the foaming process: relative density, cell size and cell density. Average NSD is obtained by averaging the NSD for each time of the foaming process, NSD being the ratio of the standard deviation (SD) of the parameter studied (relative density, cell size or cell density)

divided by its average value for each time, once considered the three radioscopy experiments performed for the same sample.

$$Average\ NSD = \frac{1}{i}\sum_i NSD \quad ; \quad i = \#time \qquad \textbf{(6)}$$

Since Average NSD is calculated from three experiments performed for each sample, this parameter accounts for the reproducibility of the experiments carried out for each material.

3. Results and discussion

3.1. Foaming behaviour

X-ray radioscopy allows following in-situ the foaming process of RPU foams. **Figure 2** shows a comparative of the acquired radiographies at two different times (after 75 and 420 s) for two samples of each system studied. In order to compare the foams containing GO-f and those containing GO-d, three parameters have been evaluated during the foaming process: relative density, cell size, and cell nucleation density.

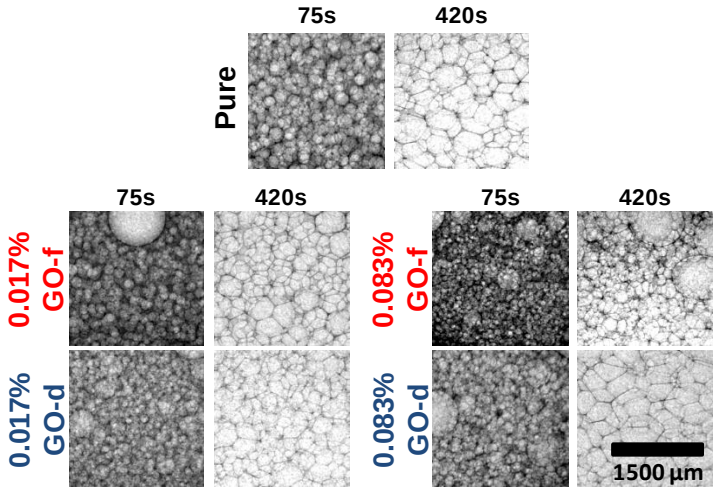

Figure 2. X-ray radiographies of the materials under study at 75 and 420 seconds of the foaming process.

Figure 3 shows the evolution of the relative density during the foaming process. In general, the two series of RPU nanocomposite foams present slower expansion than the pure material at the early stages of the foaming process (60-200 s). This behaviour could be attributed to the higher viscosity of both the polyols with GO-f and the polyols with GO-d as well as to the

possible chemical interaction (weak, through hydrogen bonds, or strong, through covalent bonds) between functional groups present on GO surface and the PU components.

At the end of the foaming process (*ca.* 560 s), the foams with GO-f reach relative densities slightly higher than that of the reference material, as the amount of GO-f increases. However, the opposite result is found for the foam with higher GO-d content (0.083 wt. %), since a slightly decrease in relative density with respect to pure material is observed. The reason for this behaviour could be related to the presence of the oxygenated functional groups (epoxy, carboxyl and hydroxyl) in the GO-d surface, that can form hydrogen bonds with water, and this adsorbed water would be released at the final stages of the foaming process, by producing CO_2 after reacting with the isocyanate component. However, the sample with 0.017 wt. % of GO-d has higher relative density than that of the reference foam, what could indicate that, for lower GO-d contents, the higher viscosity of polyol with GO-d predominates over the effect of the adsorbed water, present due to the oxygen functional groups in the surface. In the samples with GO-f, the effect of the adsorbed water is not observed maybe because part of the functional groups on their surface have reacted during the synthesis of polyol functionalized with GO, and thus GO-f has less functional groups available on their surface than GO-d, which is dispersed in the polyol. On the other hand, the sample with low content of GO-d (0.017 wt. %) presents higher relative density than the foam with same amount but of GO-f: this may be explained considering that GO-d particles have more amount of functional groups on their surface, what could interact with the PU components, decreasing their mobility and thus increasing the viscosity of the reactive mixture.

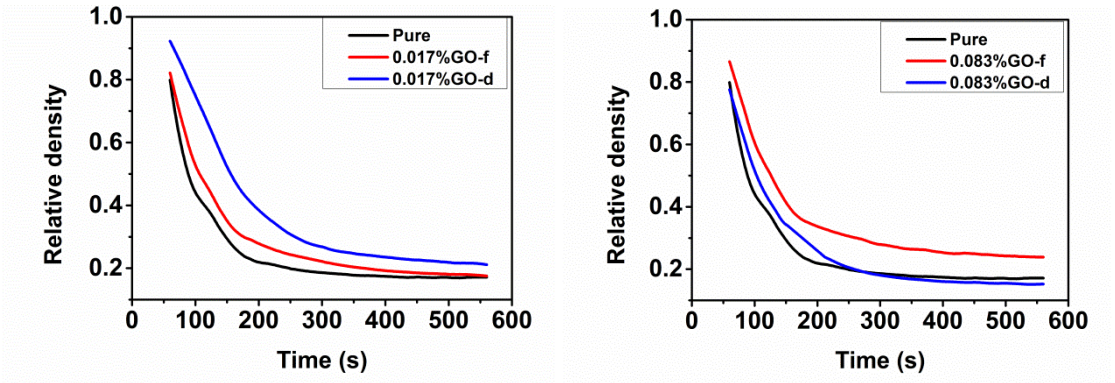

Figure 3. Evolution of relative density, measured by X-ray radioscopy, during the foaming process for the materials under study.

Figure 4 shows the values of cell size evolution, which point to a cell size reduction for both type of foams (with GO-f and with GO-d) at the beginning of PU formation. This cell size reduction is the same for low content (0.017 wt. %) of GO-f and of GO-d, whereas at high content of GO-f (0.083 wt. %) the cell size is also decreased. However, the GO-d material with a higher content of particles presents a similar cell size to that of the reference system. This result could be explained considering that a low content of GO may be easily dispersed,

whereas a high content could form aggregates. In conclusion, the cell size decreases as the GO-f content increases in comparison to the reference system, the reduction reached for 0.017 wt. % and 0.083 wt. % of GO-f being 16 % and 30%, respectively. Conversely, the cell size is reduced by *ca.* 20% for the foam with 0.017 wt. % GO-d, whereas the cell size is not reduced for the foam with 0.083 wt. % GO-d in comparison to the values of the reference material. These cell size reductions for the foams with GO can be appreciated in the radiographies at 420 s, shown in **Figure 1**.

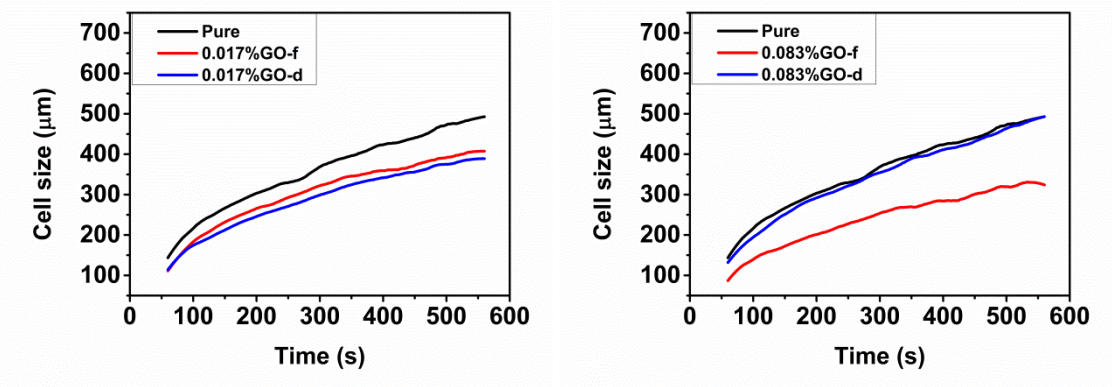

Figure 4. Evolution of the cell size, measured by X-Ray radioscopy, during the foaming process for the materials under study.

Figure 5 shows the cell nucleation density evolution during the PU formation calculated by equation 3. In all the samples there is an increase of the cell nucleation density in the first instants, reaching a maximum. Then, a drop of the cell nucleation density is observed because the mechanisms of degeneration start to appear. At the early stages, the results show that the number of nucleation sites increases for the samples with GO-f compared to the reference material. Thus, for those foams with GO-d, the cell nucleation density for the highest GO-f content is superior. The evolution of the cell nucleation density shows that there is coalescence in all the systems under study, because the cell nucleation density decreases with time, this coalescence being more pronounced in systems with GO-f. Despite this, the enhanced nucleation experienced by foams with GO-f prevails at the final stages over the cell degeneration processes, what is in accordance with the cell size reduction described above.

All the above can be explained by the hydrophilic or hydrophobic character of GO particles. As mentioned earlier, the GO-d contains more oxygen functional groups than GO-f, and as a consequence, GO-d presents more hydrophilic character, whereas GO-f is more hydrophobic. In this way, the hydrophobic surface of GO-f favours the nucleation mechanisms due to its non-wetting surface, and also causes destabilizing effects in the cell walls [20]. The opposite effect occurs in the case of foams with GO-d particles which have a more hydrophilic surface, and thus less destabilization occurs during the foaming process [20]. In addition to this, the results of cell nucleation density could also be related to the improved dispersion of the particles in the system GO-f.

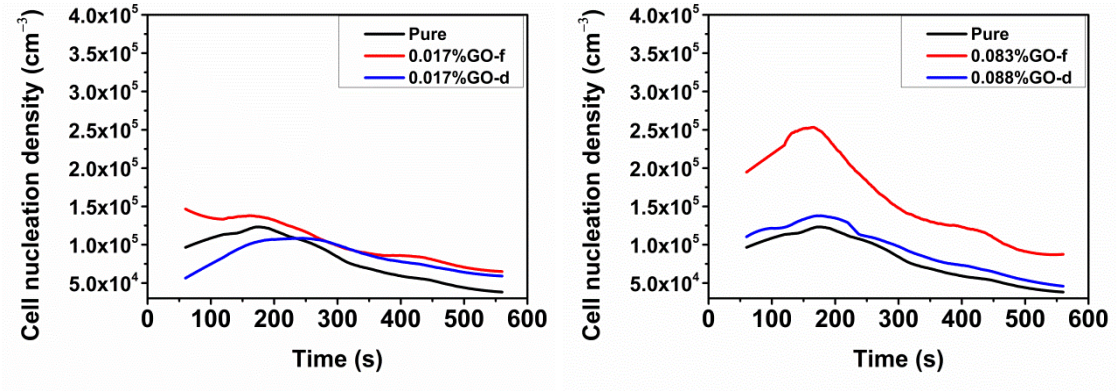

Figure 5. Evolution of the cell nucleation density, measured by X-ray radioscopy, during the foaming process for the materials.

Average NSD values have been calculated for each parameter studied during the foaming process: relative density, cell size and cell density (**Figure 6**). In general, the average NSD of the systems with GO-d is larger for several of the parameters measured, followed by those with GO-f. This is clearly observed by the values of NSD for relative densities and cell nucleation densities. Hence, the reproducibility of the RPU foams with GO-d is worse than that of the foams with GO-f probably because the degree of GO dispersion is poorer in the GO-d system. Instead, the disadvantage of the filler dispersion is removed by using polyols functionalized with GO (GO-f).

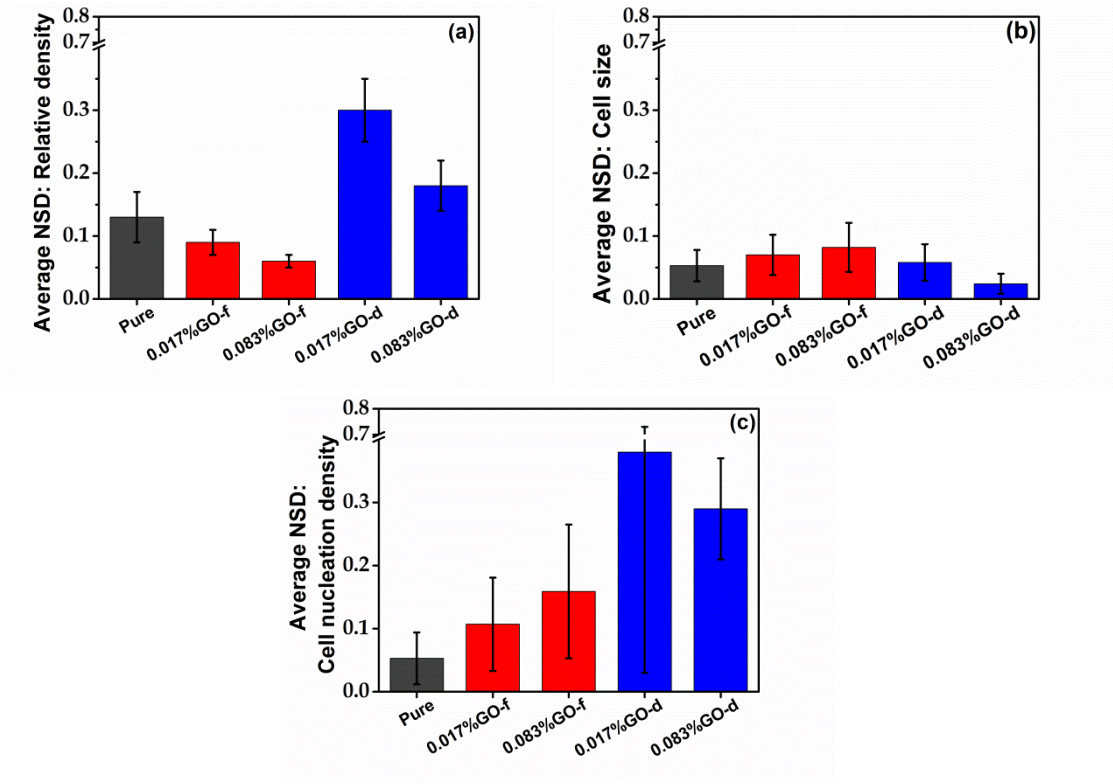

Figure 6. Average NSD for the three main parameters considered in this investigation: (a) Relative density (b) cell size and (c) cell density.

3.2. Comparison of results obtained from the radioscopy experiments and from the final foam

Table 2 collects the relative densities and cell sizes for foams obtained with a small drop of PU mixture (0.020±0.009 ml) at 560 s of X-ray radioscopy experiment, and those for final foams with a larger size (100 mm of diameter x 100 mm of height). The foams produced during the X-ray radioscopy experiment present higher values of relative density (0.155±0.031 more) and smaller values of cell size (118±22 less) than those of the final foams. This is because these parameters are measured for smaller samples after 560 s, when the foaming process has not been yet completed, and the reduced size of the samples scanned by radioscopy limits the temperature generation reducing the foam expansion. However, the trends observed in the radioscopy samples correspond to those of the larger samples, what allows validating the X-ray radioscopy results. The foams containing GO-f have higher relative densities than that of the reference material, whereas the foams with GO-d present a decrease in relative density with respect to the reference material. On the other hand, the average cell size decreases when the amount of GO-f increases. The decrease of the cell size for the sample containing 0.017 wt. % GO-d is similar to that of the sample with the same content of GO-f, whereas the cell size of the foam with 0.083 wt. % GO-d is hardly reduced. Moreover, the reduction of cell size observed by the radioscopy experiments is very similar to those obtained for the final

materials. The different factors (relative density, cell size and cell size reduction) for radioscopy foams and for final foams are represented in **Figure 7**, in order to show their correlations. In the cases of cell size (**Figure 7. b**) and cell size reduction (**Figure 7.c**), there is a good linear correlation with a coefficient of determination (R^2) near to 1. However, the correlation between relative density for radioscopy foams and for final foams is not so evident.

On the other hand, the widths of cell size distribution (WCD) for radioscopy foams and final foams follow the same trend (**Table 2**). The WCD of the foam with a low GO-f content (0.017 wt. %) is similar to that of the reference foam, whereas it is wider for the foam with high GO-f content (0.083 wt.%). In the case of the foams with GO-d, a wider WCD is obtained compared to that of the reference foam. Moreover, the highest WCD value corresponds to the foam with high GO-f content which is the one that presents more coalescence (**Figure 5**).

In addition, the open cell content data of the final samples indicate that the addition of GO promotes the interconnection between cells (**Table 2**). This is more intense when GO-d particles are added. In fact, the GO-d material with a GO content of 0.083 wt. % has a high open cell content of 70%.

Table 2. Relative density, cell size, width of cell size distribution (WCD) and cell size reduction for radioscopy foams. Moreover, relative density, cell size, WCD, cell size reduction and open cell content (OC) for final foams.

Material	**Radioscopy foam at 560 seconds of foaming process (smaller size)**				**Final foam (higher size)**				
	Relative density	**Cell size (µm)**	**WCD**	**Cell size reduction (%)**	**Relative density**	**Cell size (µm)**	**WCD**	**Cell size reduction (%)**	**OC (%)**
Pure	0.170	489	0.12		0.0340	616	0.22		7.47±0.61
0.017%GO-f	0.178	413	0.13	16	0.0381	524	0.23	15	5.98±0.02
0.083%GO-f	0.239	341	0.30	30	0.0404	476	0.29	23	14.40±1.05
0.017%GO-d	0.210	390	0.17	20	0.0339	523	0.29	15	12.03±0.13
0.083%GO-d	0.151	502	0.21	0	0.0249	585	0.27	5	70.51±1.87

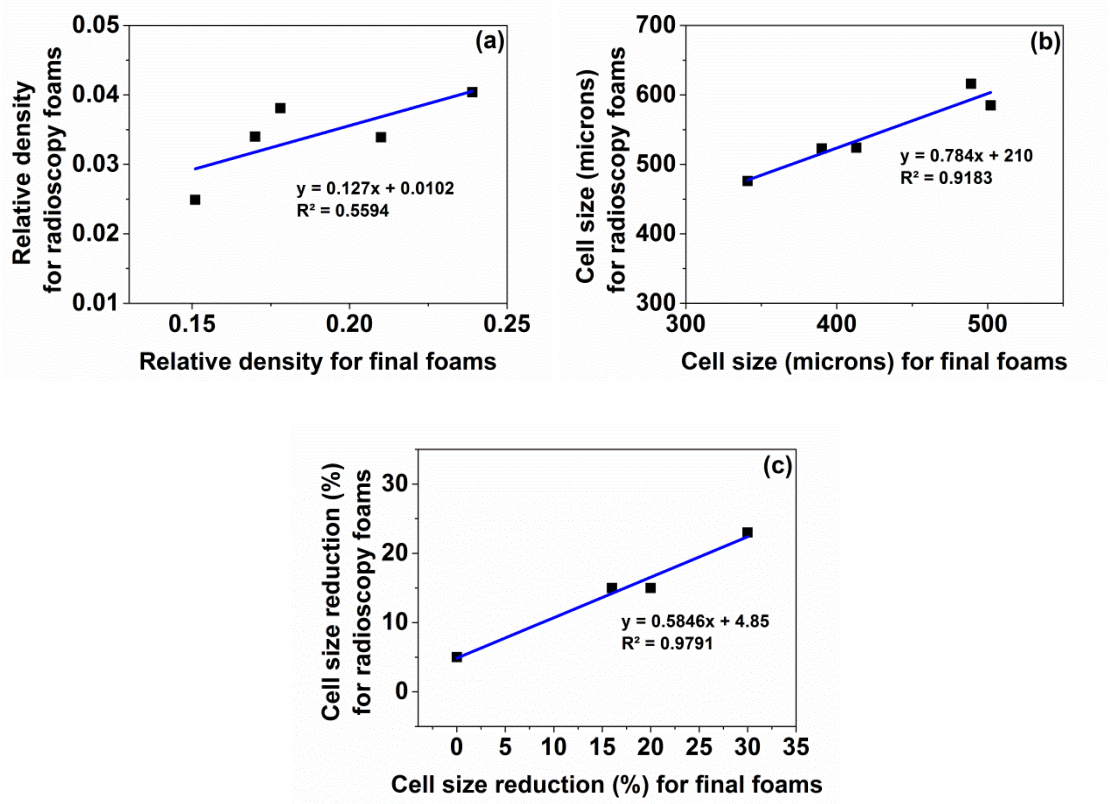

Figure 7. **(a)** Relative density for radioscopy foams versus relative density for final foams. **(b)** Cell size for radioscopy foams versus cell size for final foams. **(c)** Cell size reduction for radioscopy foams versus cell size reduction for final foams.

4. Conclusions

X-ray radioscopy allows obtaining the relative density, cell size and cell nucleation density during the foaming process of RPU foams containing GO nanoparticles. These particles have been introduced by two different methods: by using polyols functionalized with GO or by dispersing the particles into the polyol using high shear mixing.

The radioscopy results show that the addition of the particles improves the nucleation process, reducing the cell sizes in the early stages of the foaming process. This improvement is progressive for the systems containing GO-f particles, i.e. a higher amount of particles results in better improvements, resulting in larger cell nucleation density and a cell size decrease of 30% for the highest GO-f content of 0.083 wt%. However, for systems containing GO-d particles, the improvement almost disappears when a larger amount of particles is added (0.083 wt% GO-d) possibly due to the difficulty of achieving a proper dispersion of the fillers when the amount increases. Furthermore, the systems with GO-d present higher average NSD values of the relative density and cell nucleation density than those of the systems with GO-f.

Therefore, the reproducibility of the experiments is better for the foams obtained with GO-f mainly because the intrinsic dispersion is better in these materials.

Acknowledgements

Financial assistance from MINECO, FEDER, UE (MAT2015-69234-R) and the Junta de Castilla and Leon (VA275P18) are gratefully acknowledged. Authors thank Graphenea S.A. for supplying us with Graphene Oxide and for the technical discussion. Predoctoral contract of S. Perez-Tamarit by University of Valladolid (E-47-2015-0094701) and co-financed by Banco Santander is also acknowledged. Financial support from Junta de Castilla y León predoctoral grant of P. Cimavilla-Román, co-financed by the European Social Fund is also acknowledged.

References

[1] M. Szycher, Szycher's Handbook of Polyurethanes, Second ed., CRC Press Boca Raton, Florida, USA, 2012.
[2] C. Hopmann, R. Wagner, K. Fischer, A. Böttcher, One Step Production of Highperformance Sandwich Components, Cellular Polymers, 36 (2017).
[3] J.O. Akindoyo, M.D.H. Beg, S. Ghazali, M.R. Islam, N. Jeyaratnam, A.R. Yuvaraj, Polyurethane types, synthesis and applications – a review, RSC Advances, 6 (2016) 114453-114482.
[4] N.V. Gama, A. Ferreira, A. Barros-Timmons, Polyurethane Foams: Past, Present, and Future, Materials, 11 (2018).
[5] A. Kausar, Polyurethane Composite Foams in High-Performance Applications: A Review, Polymer-Plastics Technology and Engineering, 57 (2017) 346-369.
[6] M.C. Saha, M.E. Kabir, S. Jeelani, Enhancement in thermal and mechanical properties of polyurethane foam infused with nanoparticles, Materials Science and Engineering: A, 479 (2008) 213-222.
[7] S. Estravís, J. Tirado-Mediavilla, M. Santiago-Calvo, J.L. Ruiz-Herrero, F. Villafañe, M.A. Rodríguez-Pérez, Rigid polyurethane foams with infused nanoclays: Relationship between cellular structure and thermal conductivity, European Polymer Journal, 80 (2016) 1–15.
[8] M. Santiago-Calvo, J. Tirado-Mediavilla, J.L. Ruiz-Herrero, M.Á. Rodríguez-Pérez, F. Villafañe, The effects of functional nanofillers on the reaction kinetics, microstructure, thermal and mechanical properties of water blown rigid polyurethane foams, Polymer, 150 (2018) 138-149.
[9] E. Malewska, A. Prociak, The effect of nanosilica filler on the foaming process and properties of flexible polyurethane foams obtained with rapeseed oil-based polyol, Polimery, 60 (2015) 472-479.
[10] A. Hasani Baferani, A.A. Katbab, A.R. Ohadi, The role of sonication time upon acoustic wave absorption efficiency, microstructure, and viscoelastic behavior of flexible polyurethane/CNT nanocomposite foam, European Polymer Journal, 90 (2017) 383-391.
[11] S. Sathiyamoorthy, G. Girijakumrai, P. Kannan, K. Venugopal, S.T. Shanmugam, P. Veluswamy, K.D. Wael, H. Ikeda, Tailoring the functional properties of polyurethane foam with dispersions of carbon nanofiber for power generator applications, Applied Surface Science, (2018).

[12] C. Caglayan, I. Gurkan, S. Gungor, H. Cebeci, The Effect of CNT-Reinforced Polyurethane Foam Cores to Flexural Properties of Sandwich Composites, Composites: Part A, (2018).
[13] M.C. Lopes, H. Ribeiro, M.C.G.a. Santos, L.M. Seara, F.L.Q. Ferreira, R.L. Lavall, G.G. Silva, High performance polyurethane composites with isocyanate-functionalized carbon nanotubes: Improvements in tear strength and scratch hardness, Journal of applied polymer science, 134 (2017) 1-13.
[14] M. Santiago-Calvo, V. Blasco, C. Ruiz, R. París, F. Villafañe, M.Á. Rodríguez-Pérez, Synthesis, characterization and physical properties of rigid polyurethane foams prepared with poly(propylene oxide) polyols containing graphene oxide, European Polymer Journal, 97 (2017) 230-240.
[15] A.-K. Appel, R. Thomann, R. Mülhaupt, Hydroxyalkylation and Polyether Polyol Grafting of Graphene Tailored for Graphene/Polyurethane Nanocomposites, Macromolecular Rapid Communications, 34 (2013) 1249-1255.
[16] M.W. Kim, S.H. Kwon, H. Park, B.K. Kim, Glass fiber and silica reinforced rigid polyurethane foams, Express Polymer Letters, 11 (2017) 374-382.
[17] F. García Moreno, M. Fromme, J. Banhart, Real-time X-ray Radioscopy on Metallic Foams Using a Compact Micro-Focus Source, Advanced Engineering Materials, 6 (2004) 416–420.
[18] S. Pardo-Alonso, E. Solórzano, S. Estravís, M.A. Rodríguez-Perez, J.A. de Saja, In situ evidence of the nanoparticle nucleating effect in polyurethane–nanoclay foamed systems, Soft Matter, 8 (2012) 11262.
[19] E. Solórzano, J. Pinto, S. Pardo, F. Garcia-Moreno, M.A. Rodriguez-Perez, Application of a microfocus X-ray imaging apparatus to the study of cellular polymers, Polymer Testing, 32 (2013) 321-329.
[20] M. Mar Bernal, S. Pardo-Alonso, E. Solórzano, M.Á. Lopez-Manchado, R. Verdejo, M.Á. Rodriguez-Perez, Effect of carbon nanofillers on flexible polyurethane foaming from a chemical and physical perspective, RSC Advances, 4 (2014) 20761.
[21] S. Pardo-Alonso, E. Solórzano, M.A. Rodriguez-Perez, Time-resolved X-ray imaging of nanofiller-polyurethane reactive foam systems, Colloids and Surfaces A: Physicochemical and Engineering Aspects, 438 (2013) 119-125.
[22] Product Date sheet: Graphenea Graphene Oxide (GO) (2.5 wt% concentration). https://www.graphenea.com/collections/graphene-oxide/products/highly-concentrated-graphene-oxide-2-5-wt-concentration.
[23] S.T. Lee, N.S. Ramesh, Polymeric foams: mechanisms and materials, Boca Raton, Florida, USA, 2004.
[24] ASTM D1622-08: Standard Test Method for Apparent Density of Rigid Cellular Plastics.
[25] ASTM D6226-10: Standard Test Method for Open Cell Content of Rigid Cellular Plastics.
[26] J. Pinto, E. Solorzano, M.A. Rodriguez-Perez, J.A. de Saja, Characterization of the cellular structure based on user-interactive image analysis procedures, Journal of Cellular Plastics, 49 (2013) 555–575.
[27] M.D. Abràmoff, P.J. Magalhães, S.J. Ram, Image Processing with ImageJ, Biophotonics International, 11 (2004) 36-42.
[28] C.A. Schneider, W.S. Rasband, K.W. Eliceiri, NIH Image to ImageJ: 25 years of image analysis, Nature Methods, 9 (2012) 671-675.
[29] L. Vincent, P. Soille, Watersheeds in digital spaces: an efficient algorithm based on immersion simulations, IEEE Transactions on Pattern Analysis and Machine Intelligence, 13 (1991) 583 - 598.
[30] M. Amon, C.D. Denson, A study of the dynamics of foam growth: Analysis of the growth of closely spaced spherical bubbles, Polymer Engineering & Science, 24 (1984) 1026-1034.
[31] R. D.Patel, Bubble growth in a viscous Newtonian liquid, Chemical Engineering Science, 35 (1980) 2352-2356.

CHAPTER 5:

EFFECT OF FILLERS ON CELLULAR STRUCTURE AND PHYSICAL PROPERTIES OF RIGID POLYURETHANE FOAMS

Mercedes Santiago Calvo

5.1- Introduction

The most important objective of employing fillers in rigid polyurethane (RPU) foams is the improvement of their thermal and mechanical properties, since their main applications are focused on the thermal insulation of buildings, refrigerators, pipes, among others. Mechanical properties of RPU foams depend mainly on both the properties of the PU matrix and the characteristics of the cellular structure, therefore the fillers can help to improve them by reinforcing the solid PU matrix and/or by optimizing the microstructure (reducing the average cell size and/or giving more homogeneous structure because the fillers are nucleating agents). Considering thermal conductivity, it can be described by four heat transfer contributions: conduction through the gas phase and solid phase, convention and radiation. The latter can be enhanced by the addition of fillers, which reduces the radiation contribution to the total thermal conductivity, because they can act as nucleating agents decreasing the cell size and/or as infrared radiation blockers. On the other hand, the gas phase contribution supposes the highest contribution to the total thermal conductivity (sometimes higher than 60%), since the gas phase of RPU foams represents more than 95% of their volume. However, the gas phase contribution changes with time because insulation gases diffuse out of the foam and atmospheric air diffuses into the foam, consequently the total thermal conductivity value increases with time, what is known as foam thermal conductivity aging. Thus, alternative key strategies for improving the thermal properties of foams are the use of blowing agents with low thermal conductivities that are able to stay inside the cells for along time.

This chapter includes two scientific articles whose main objective consists on **studying the effect of the fillers on the thermal conductivity and/or the mechanical properties of our RPU foams**:

-Article 4: Evaluation of the thermal conductivity and mechanical properties of water blown polyurethane rigid foams reinforced with carbon nanofibers. European Polymer Journal 108 (**2018**) 98-106.

-Article 5: Long-term thermal conductivity of cyclopentane-water blown rigid polyurethane foams reinforced with different types of fillers. Polymer International (**2019**).

Two aspects are analyzed in the articles included in this chapter: the thermal and mechanical properties of water-blown RPU foams reinforced with carbon nanofibers (CNFs), and the effect that different type of fillers (talc (T), diatomaceous earth (DE), and non-porous silica (NPS)) induces on the long-term thermal properties of the RPU foams blown with water and cyclopentane (CP) (see **Figure 5.1**). In both papers a thermal conductivity model is used to understand in depth how the fillers affect to the different heat transfer mechanisms. In the case of RPU foams blown with water, the gas inside the cells just after production is CO_2, which diffuses rapidly out of the cells. For this reason, all the gas in the structure is atmospheric air, with a higher thermal conductivity, in a short time period (a few weeks). This is the main reason of the high thermal conductivity of these foams (around 35 mW/mK). In the case of RPU foams blown with water and CP, the latter, with low thermal conductivity and a low diffusion coefficient, enhances the gas phase contribution, and thus the overall long-term

thermal conductivity, because CP is retained in the cells for long periods of time (several years) giving thermal conductivities in the range of 21 to 26 mW/mK. A brief summary of the articles are presented in **Figure 5.1**.

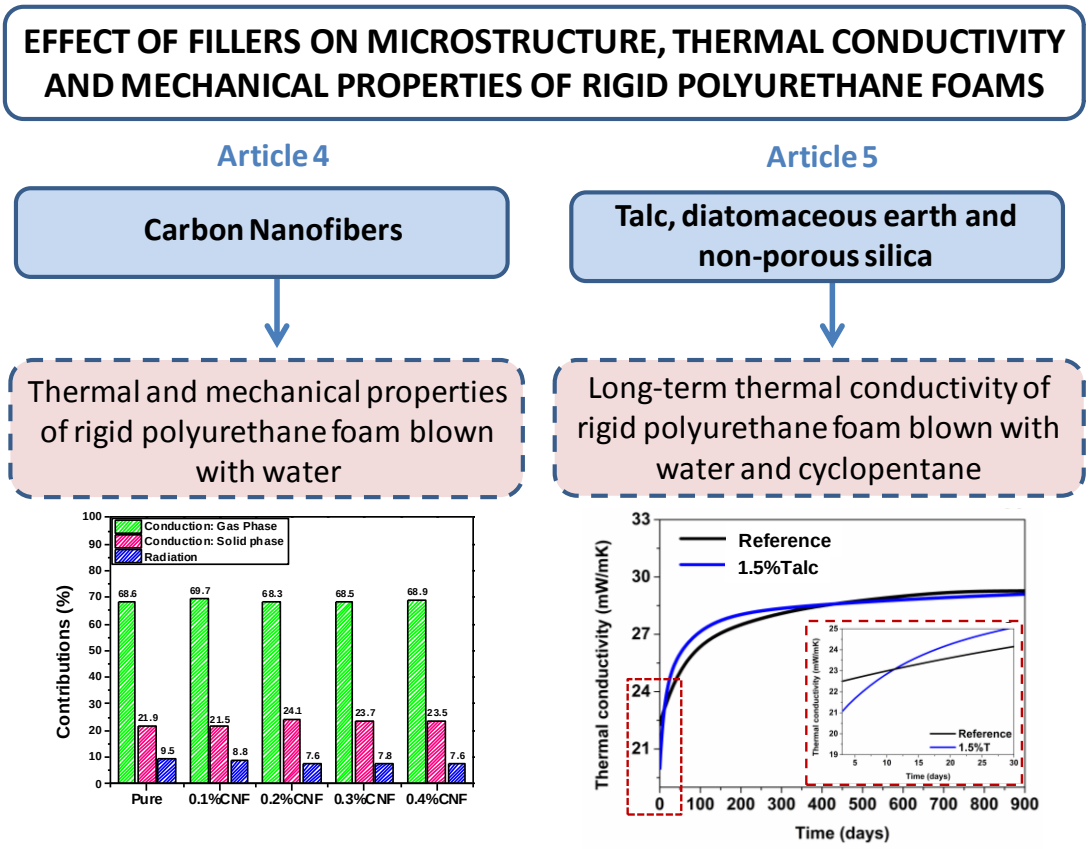

Figure 5.1. Scheme of the articles included in this chapter.

In the fourth article, a water-blown RPU foam is reinforced with small amounts of CNFs (0.1, 0.2, 0.3 or 0.4 wt%) in order to reduce the thermal conductivity, whereas the mechanical properties are maintained. The CNFs are mainly located on the struts and hardly modify the cellular structure of the foams. The contributions of the heat conduction mechanisms are quantified by measuring the extinction coefficient and by modelling the thermal conductivity. The inclusion of CNFs, which act as infrared radiation blockers, increases the experimental extinction coefficient, and thus the radiative contribution is reduced up to 20%. Therefore, an appreciable thermal enhancement is achieved at very low contents of CNFs (0.1 wt%). However, foams with CNFs contents higher than 0.1 wt% do not present higher reductions of the thermal properties, because the conduction through the solid phase increases, mainly due to the enhancement of both density and conductivity of the polymeric matrix. Moreover, the sample with 0.1 wt% of CNFs presents a slight increase in relative Young's modulus, maintaining the relative collapse stress.

In the fifth article, the long-term thermal conductivity of water-CP blown RPU composite foams has been studied along three years of aging. In the early days after production, the thermal conductivity of the samples with particles (T, DE, or NPS) is enhanced in comparison to that of the reference material. This may be explained considering that their significant decrease in cell size, which increases the extinction coefficient calculated by Glicksman equation, and thus reduces the radiative contribution to the total thermal conductivity. After some time, the first improvement is lost in many samples. A relationship has found for first time between the slope of the thermal conductivity *versus* time at the first measurements and the internal temperature reached during the foaming process. The evolution of the RPU foams in which higher internal temperatures (such as the systems with 1.5%T, 1%DE, 3%DE, or 0.2%NPS) are reached is more pronounced than in those RPU foams where lower foaming temperatures (such as the systems with 5%DE, 0.05%NPS, or 0.1%NPS) are observed. This effect is related to the kinetics of the diffusion of the gas occluded inside the cells, since the evolution of the thermal conductivity of the gas mixture calculated by the the thermal conductivity model shows similar trends to the experimental thermal conductivity. Moreover, the thermal conductivity model allows predicting the thermal conductivity values when the foams reach a stationary state (once all the gas inside the foam is air). The foams with a higher decrease of the cell size would give rise to higher extinction coefficients, and therefore to higher thermal conductivity reductions. The best systems from this point of view are talc and DE.

The conclusions obtained from these two studies have been decisive in the development of filled RPU foams with improved thermal and mechanical properties. Moreover, correlations between the foaming temperature and the evolution of the thermal conductivity with time has been established for the first time for foams modified with micro and nanoparticles, fulfilling one of the objectives of this thesis (**chapter 1**, **section 1.2**).

European polymer journal 108 (**2018**)98-106
https://doi.org/10.1016/j.eurpolymj.2018.08.051

Evaluation of the thermal conductivity and mechanical properties of water blown polyurethane rigid foams reinforced with carbon nanofibers

Mercedes Santiago-Calvo[1,*], Josías Tirado-Mediavilla[1], Jens Chr. Rauhe[2], Lars Rosgaard Jensen[2], José Luis Ruiz-Herrero[1], Fernando Villafañe[3], Miguel Ángel Rodríguez-Pérez[1]

[1] Cellular Materials Laboratory (CellMat), Condensed Matter Physics Department, Faculty of Science, University of Valladolid, Campus Miguel Delibes 7, 47011 Valladolid, Spain

[2] Department of Materials and Production, Aalborg University, Fibigerstraede 16, 9220 Aalborg East, Denmark

[3] GIR MIOMeT-IU Cinquima-Química Inorgánica, Faculty of Science, University of Valladolid, Campus Miguel Delibes 7, 47011 Valladolid, Spain

* Corresponding author: mercesc@fmc.uva.es

Abstract

This article studies the effect of carbon nanofibers (CNFs) on the morphological, thermal and mechanical properties of water-blown rigid polyurethane (PUR) foams with densities in the range of 55 to 60 kg/m^3. Different amounts of CNF have been used, 0.1, 0.2, 0.3 and 0.4 wt.% CNFs are located in the struts and produce minor modifications on open cell content, cell size, cell size distribution and anisotropy ratio of the foams. The contributions of the heat conduction mechanisms have been quantified by measuring the extinction coefficient and by modelling the thermal conductivity. The inclusion of CNFs reduces the radiative contribution by increasing the extinction coefficient and increases the conduction through the solid phase mainly due to an increase in density and an increase of the conductivity of the polymeric matrix. Due to this, a clear reduction of the heat flow by radiation and a reduction of the total thermal conductivity is achieved with only 0.1 wt.% of CNFs. Moreover, the addition of this low amount of CNF allows maintaining the mechanical properties of the foams.

Keywords: Polyurethane foam, carbon nanofibers, thermal conductivity, compression test

1. Introduction

One of the most important classes of specialty polymers is polyurethanes (PUs) [1]. They are composed by urethanes-linking moieties, obtained by the polyaddition of polyisocyanates to polyols. PUs may also contain different functional groups in the main chain, such as urea, which come from the reaction of polyisocyanates with the amines resulting from polyisocyanates hydrolysis [2, 3]. PUs are classified according to their chemical structure in thermoplastic polyurethanes (TPU) or thermosets, and according to their physical structure they may be divided into rigid solids, soft elastomers, or foams.

PUs are present in commercial coatings, adhesives, sealants, binders, elastomers and foams [1]. They are considered multipurpose polymers due to the high diversity of PUs, and they cover a surprisingly wide range of applications in areas such as automotive, medical, construction, furniture or appliances, among others [4-7]. Only large-volume commodity plastics such as polyethylene, polypropylene, polyvinyl chloride or polystyrene are ahead of PUs in overall volume used [1]. It is also noteworthy that the demand for PUs is an impressive 7.4% of the whole European polymer market [8].

Most of the PUs industrially obtained are foams, which represent almost 50% of the global foam market [9], mainly due to their interesting physical properties, such as low density, low thermal conductivity, and tailored mechanical properties as a function of the foam density. PU foams are usually classified according to their mechanical behaviour into flexible foams (used for furniture, mattresses, and automotive seats) and rigid foams (used for insulation and structural materials) [10].

One of the main applications of rigid polyurethane foams (PUR) is the thermal management for building and transportation insulation or refrigeration systems, where typically the foams are the core of sandwich panels.

The thermal conductivity of foams has been both theoretically [11-19] and experimentally [20-23] studied. The thermal conductivity of a PUR foam (considering both solid and gas phases) is well represented as the addition of conduction in gas and solid phases and radiative conductivity [24].

A method widely used to decrease the thermal conductivity and to improve the mechanical response of PUR foams is the dispersion of fillers into the PU matrix. The characteristics of both foam and additives should be considered in order to select an appropriate reinforcement. Nano-reinforcements can improve the mechanical and thermal properties. Interestingly, this improvement of the composite properties occurs for low contents of nanosize fillers. This is particularly appealing for PUR foams, because the use of a higher amount of filler could preclude the production of foams with the low densities required for thermal insulation and structural applications. The studies published so far in relation to PU nanocomposite foams include the use of different types of nanoparticles, such as nanoclays [20, 25-27], nanosilicas [28, 29], carbon nanotubes [30-34] or carbon nanofibers (CNFs) [35-38]. As expected, these works lead to conclude that the properties of the final composite depend on both the chemical composition, and on the nanoparticles size, shape, amount added and degree of dispersion and compatibilization obtained.

CNFs are cylindrical or conical nanostructures with diameters between 50 and 200 nm and lengths between microns and millimetres. They may present different morphologies, from disordered bamboo-like to highly graphitized ''cup stacked'' structures [39]. The inclusion of CNFs into polymers produces changes in their thermal and electrical conductivity, tensile and compressive strength, ablation resistance, damping properties, and flammability [40].

Although the addition of CNFs to polymers usually improves the properties of the composites formed, the number of papers dealing with adding CNFs into a rigid PU matrix is somewhat scarce [35-38]. Kabir et al. (2007) studied various process parameters for CNFs sonication dispersion into PUR components, and demonstrated that with the addition of 0.5 and 1 wt.% of CNFs in a PUR system of 240 kg/m^3, the compressive strength was improved by 10% and 20% [38]. Saha et al. (2008) investigated the effects of different nanoparticles (1 wt.% loading with either-TiO_2, platelet nanoclays, or rod-shaped CNFs) introduced by sonication dispersion on the thermal stability and mechanical performances of PUR foam with density 240 kg/m^3. The highest enhancement of both thermal stability and mechanical properties was observed in the system containing 1 wt.% CNFs [35]. Harikrishnan et al. (2010) studied the nanodispersion of CNFs in a PUR system of 35 Kg/m^3, and observed a reduction of thermal conductivity and a clear improvement of compressive modulus and of fire resistance of the nanocomposite foam with 0.5 wt.% of CNFs in the foam, without apparent changes in the foam reaction kinetics [36]. Saha et al. (2011) studied the effect of low amounts of CNF (0.01, 0.05 or 0.1 wt.%) on the reaction kinetics and concluded that the fastest polymerization reaction occurred for the PUR foam containing 0.1% CNF. Moreover, the CNF particles acted as nucleation agents, resulting in a higher number of smaller cells in the composite foam with density 65 Kg/m^3 [37].

The previous papers report that CNFs are promising nanoparticles to improve the properties of PUR foams, however only in one of them the thermal conductivity of the foams is studied. In addition, in that paper [36] the effect of the particles in the heat conduction mechanism is not discussed and the density of the foams analysed is clearly lower than the density of the foams considered in our research.

Keeping the previous ideas in mind, this paper presents a systematic study on the effect of the addition of CNFs on the heat conduction mechanisms of a water-blown PUR system used as the core material of sandwich panels. These foams must have a high compressive strength and due to this its density is in many cases relatively high (around 55 kg/m^3 in our case). Our target is reducing the thermal conductivity of these foams, which is not an easy task due to the low weight of the radiative contribution (as it is discussed below), while the mechanical properties are at less maintained. Thus, PUR foams containing different amounts of CNFs (0.1, 0.2, 0.3 or 0.4 wt.%) are obtained and their thermal and mechanical properties are measured. Thermal conductivity changes are explained in detail using both theoretical models, measurements of extinction coefficient and a detailed morphological characterization. Moreover, the effect of CNFs on mechanical properties is reported.

2. Experimental

2.1. Materials

The water-blown PUR foams used in this study were obtained from a two-component system supplied by BASF, after mixing the polyol Elastopor H1501/1 and the diphenylmethane diisocyanate ISOPMDI 9240. The polyol is a mixture of components containing polyether polyol, catalysts, stabilizers and water as blowing agent [41, 42].

The vapor grown CNFs were Pyrograf® III PR-24-XT-PS supplied by Applied Sciences Inc. The CNFs has an average diameter of 100 nm and a length of 50-200 microns. Their surface is a minimal chemically vapor deposited (CVD) layer of carbon over a graphitic tubular core [43]. The CNFs were dried in a vacuum oven and stored in a desiccator before use.

2.2. Polyurethane foam and carbon nanofiber-polyurethane foam composite production

PUR foams containing 0.1, 0.2, 0.3 and 0.4 wt.% of CNFs were obtained as follows. CNFs were firstly added to the polyol by using a Silverson L5M high shear mixer running at 4000 rpm for 30 min. while the mixture was cooled in a water bath to avoid an increase in temperature of the polyol. The isocyanate was added, and the mixture was stirred using a Pendraulik TD100 mechanical mixer running at 2500 rpm for 30s. No difference in reactions between isocyanate and polyol/CNFs mixtures and pure polyol, respectively, was observed indicating that the polyol did not experience a significant heating during the mixing procedure. The mixture was then poured into an open wooden mould with dimensions 250 x 250 x 250 mm^3 and left to foam freely in one direction. The expansion time was 232±21 seconds and the curing temperature was room temperature. After 24 hours the foam was demoulded and cut into appropriate dimensions using a bandsaw. The cured samples were also stored at room temperature before testing. PUR foams without CNFs were also obtained as a reference. In all cases the polyol and isocyanate were mixed in a ratio 100:160 by weight, so each foam formulation was fixed with the same total amount of components (isocyanate, polyol, catalyst, water and other additives).

2.3. Carbon nanofibers characterization

1 wt. % of CNFs were dispersed in tetrahydrofuran using a sonicator horn for 30s. Small drops of the solution were placed on the SEM specimen holders and the tetrahydrofuran was removed by drying in a fume hood overnight leaving CNFs dispersed on the holders. The diameters of the fibers were determined using a Zeiss EVO LS15 scanning electron microscope and ImageJ.

2.4. Foam characterization

2.4.1. Density

Foam density was measured as described by ASTM D1622/D1622M-14 [44]. Density was determined by dividing the weight of each sample by its corresponding volume of five different samples for each material. The samples were cylindrical with a diameter of 30 mm and a height of 25 mm.

2.4.2. Open cell content

The percentage of open cell content (OC) was measured with a gas pycnometer Accupyc II 1340 from Micromeritics, according to ASTM D6226-10 [45]. Nitrogen is used as the displacement medium. The OC was measured for five cylindrical samples from each material after measuring their densities. OC was calculated by using the following equation [45]:

$$OC\ (\%) = 100\left(\frac{V_{Sample} - V_{Pycnometer}}{V_{Sample}\ p}\right) \qquad \textbf{(1)}$$

Where V_{sample} is the geometrical volume of the sample (calculated from the sample dimensions), $V_{pycnometer}$ is the volume measured with the pycnometer, p is the sample porosity calculated using $\left(1 - \frac{p_{foam}}{p_{solid}}\right)$, where p_{foam} is the foam density and p_{solid} the solid matrix density. A value of 1160 kg/m^3 was used as p_{solid}.

2.4.3. Morphological characterization of foams

Optical Microscopy (OM) was used to locate the position of CNFs in the foam structure. Optical micrographs were taken using a Leica DM2500M microscope.

Scanning electron microscopy (SEM) was used to characterize the cellular structure of the foam (cells, cell walls, and struts). SEM micrographs were taken with a JEOL JSM-820 microscope. The foams were cut with blades to ensure a smooth surface, which was examined by SEM after vacuum coating with a gold monolayer. SEM micrographs were obtained in the growth plane of the foam.

The main characteristics of the cellular foam structure were determined by an image analysis technique [46] . The Image analysis was carried out with ImageJ by measuring at least 400 cells. Cell size distribution, average cell size (Φ_{3D}) and anisotropy ratio (AR) were thus determined. In addition, some statistical parameters of the cell size distribution were calculated: standard deviation (SD), normalized standard deviation (NSD), and the asymmetry coefficient (AC). NSD (ratio between SD and Φ_{3D}) is related to the width of the cell size distribution, and therefore provides information about the homogeneity of the cell size distribution (i.e. homogeneous cell distributions present small values of NSD). AC provides information about the shape of distribution, a negative coefficient indicating that the smallest cells are more separated from the average cell size value than the biggest ones, and *vice versa.*

2.4.4. Fourier transform infrared (FTIR) spectroscopy

FTIR spectra of the samples were collected using a Bruker Tensor 27 spectrometer by transmission method. Chemical reactivity between nanoparticles and PUR foam was analyzed using FTIR.

2.4.5. Thermal conductivity

The thermal conductivity measurements of the foams were performed using a Rapid K heat flowmeter from Holometrix. Measurements were made under steady heat flow conditions through the test samples, in accordance with the UNE12667 method [47], by using samples of 200 x 200 x 25 mm^3, after calibrating with a standard sample. Thermal conductivity (λ) was calculated by measuring the heat flow through the test sample, q, as a result of the temperature gradient (ΔT) across the growth plane of material. λ was calculated according to Fourier's equation [47]:

$$q = \lambda A \frac{\Delta T}{\mathrm{d}} \qquad \textbf{(2)}$$

Where *d* is sample thickness, and *A* is the cross-sectional area of the sample calculated from a standard sample. The measurements were performed at 20°C, with a temperature gradient (ΔT) of 10°C. Thermal conductivity for each sample was measured 7 times, each one during 10 minutes, in order to obtain an average value. These measurements were performed six months after the foams were produced, considering that by then all the carbon dioxide generated during foaming should have been diffused out to the atmosphere, and therefore the only gas inside the foams is air.

2.4.6. Mechanical tests

Mechanical tests were performed according to ASTM D1621-10 [48]. These experiments were performed in compression using an Instron Machine (model 5.500R6025). Stress-strain curves were obtained at room temperature at a strain rate of 10 mm/min. The maximum static strain was 75% for all the experiments and the compression direction was parallel to the cell growth direction (thickness direction) of the foam. The samples were cylindrical with a diameter of 30 mm and a height of 25 mm. Young´s modulus (E) and collapse stress (σ_C) were measured.

2.4.7. Spectral extinction coefficient ($K_{e,\lambda}$)

Sample thickness *(L)* and transmission measurements *(τ)* are needed to determine the spectral extinction coefficient ($K_{e,\lambda}$).

Sample Thickness (L)

Five to seven thin samples with a thickness (*L*) ranging between 0.8 and 2.5 mm were cut from the five different foams studied. A dynamic mechanical analyzer (DMA7) from PerkinElmer was

used to measure the thickness (*L*) of the samples with a high accuracy. A parallel-plate system with a top plate of 12 mm in diameter was used applying a force of 10 mN.

Transmission measurements (τ)

Spectra of the thin samples were collected using a Bruker Tensor 27 FTIR spectrometer in the transmission mode. The spectra were obtained after 32 scans with a resolution of 4 cm^{-1} in a wavenumbers range from 4000 and 400 cm^{-1}, after subtracting a background spectrum. The data supplied by the software were a collection of 1866 values in this range. The samples were located as close as possible to the detector in our device in order to minimize the loss of transmitted intensity due to the scattering of radiation. This is the same approach used in our previous research in which the same type of characterization was performed [24, 49].

The transmittance (τ) is the ratio of the intensity transmitted through the sample ($I_{\lambda}(x)$) with respect to the intensity without the sample ($I_{0,\lambda}$):

$$\tau_{n,\lambda} = \frac{I_{\lambda}(x)}{I_{0,\lambda}} \quad \textbf{(3)}$$

The spectral extinction coefficient ($K_{e,\lambda}$) for thin samples can be obtained from Beer's law [50]. For homogeneous samples, once $K_{e,\lambda}$ is assumed to be independent of sample thickness, the following equation is valid:

$$\tau_{n,\lambda} = e^{(-\int_0^L K_{e,\lambda} dx)} \quad \textbf{(4)}$$

Therefore, the spectral extinction coefficient ($K_{e,\lambda}$) can be expressed from the spectral transmittance $\tau_{e,\lambda}$ as:

$$K_{e,\lambda} = \frac{-\ln(\tau_{n,\lambda})}{L} \quad \textbf{(5)}$$

As a result, $K_{e,\lambda}$ can be obtained by means of a linear regression of the plot of $ln(\tau_{e,\lambda})$ *vs*. *L*.

3. Results and discussion

3.1. Foams characterization

The cellular structure and some physical properties of the foams are collected in **Table 1**. The density slightly increases up to around 5 kg/m^3 when low amounts of CNFs are added (**Table 1**). Since each system contains the same total amount of components, the small increase in density is connected with the progressive increase in the viscosity of the CNF/polyol mixture when the particles are added which reduces the volume expansion of the foams. In addition to density, the open cell content (OC) slightly increases from 8.9% up to 10.8% with CNFs addition (Table 1) which indicates that the particles are not acting as cell openers due to both their poor compatibility with the PU matrix and their lack of chemical reactions with PU formulation components, as discussed below.

Figure 1 shows SEM images of the microcellular structure of samples, whereas the average cell size (Φ_{3D}) as a function of CNF amount is presented in **Figure S1**. It is observed that the changes in cell size are very small when CNFs are incorporated in PU formulation. The cell size is reduced a 6% for the foam containing 0.2 wt.% CNFs, whereas increases a 7% for those samples with higher amounts of CNFs (0.3 and 0.4 wt.% CNFs) may be due to bubble coalescence, which is evidenced qualitatively in the SEM micrographs.

Moreover, there are hardly changes in the cell size distribution. Gaussian fitting of the distributions is displayed in **Figure S2**. All samples show relatively high homogeneity (small values of NSD) and positive AC (large cell are more separated from mean cell size than smallest cells) (**Table 1**). Additionally, anisotropy ratio (AR) values are also included in **Table 1**. All the foams have a certain degree of anisotropy in the thickness direction, but no trends as a function of the CNF content are observed.

Based on the results obtained, it is concluded that, the effect of CNFs in the cellular structure of the foams is small.

Table 1. Main cellular structure characteristics and physical properties of the manufactured PU foams: density, open cell content (OC), mean cell size (Φ_{3D}), standard deviation of the cell size distribution (SD), normalized standard deviation (NSD), asymmetry coefficient (AC) and anisotropy ratio (AR).

Samples	Density (Kg/m^3)	OC (%)	Φ_{3D} (μm)	SD	NSD	AC	AR
Pure	56.2±0.9	8.9±0.7	366	169	0.46	0.80	1.22±0.34
0.1%CNF	59.9±0.5	8.7±0.6	359	141	0.48	0.79	1.21±0.39
0.2%CNF	58.4±1.3	10.4±0.4	346	146	0.42	0.63	1.38±0.39
0.3%CNF	60.7±0.8	10.5±0.1	392	191	0.49	2.12	1.21±0.32
0.4%CNF	60.8±0.5	10.8±0.4	390	174	0.45	0.83	1.26±0.37

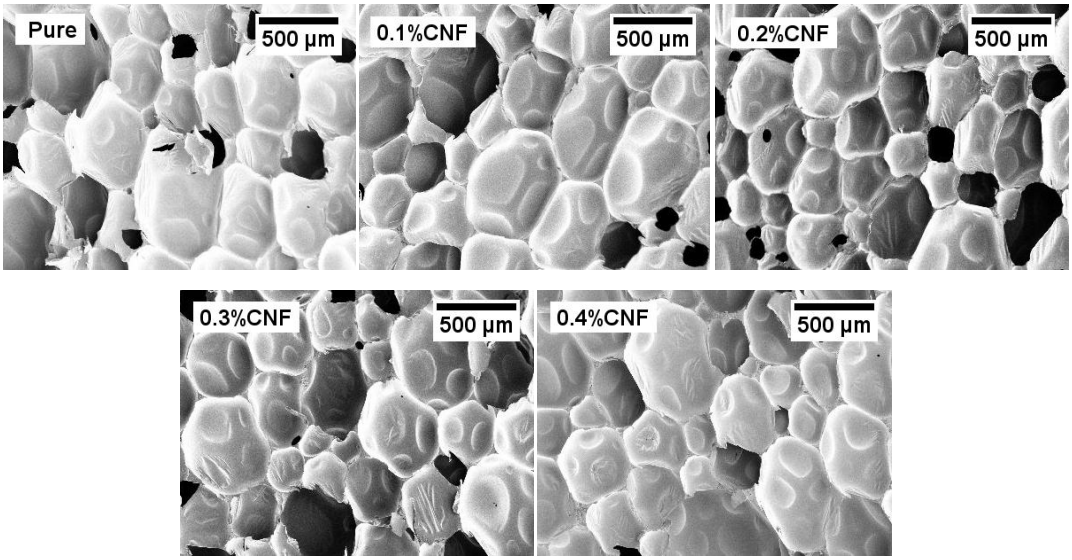

Figure 1. SEM micrographs in the growth plane of the foams: Pure material, with 0.1 wt.% CNFs, with 0.2 wt.% CNFs, with 0.3 wt.% CNF and with 0.4 wt.% CNFs.

3.2. CNFs characterization and distribution in the foam

A representative SEM image of the CNFs and a diameter distribution plot are shown in **Figure 2**. The characterization of the dimensions of CNFs gave an average diameter of 102 nm, with a standard deviation of 26 nm. Besides CNFs the material used as filler also contains small amounts of other particles such as iron catalyst particles as it can be appreciated in **Figure 2** [43].

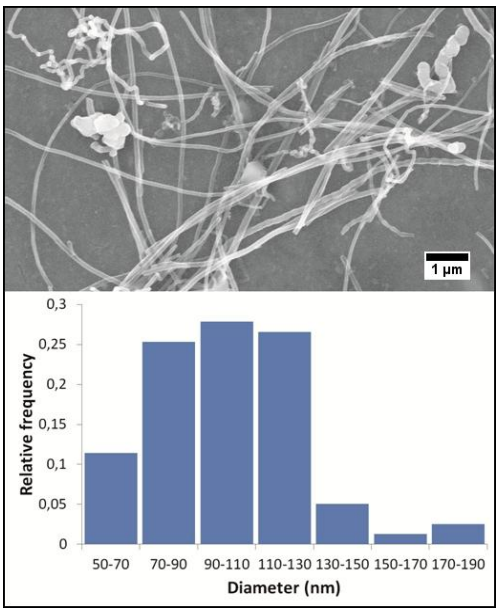

Figure 2. SEM micrograph and diameter distribution of carbon nanofibers.

CNFs could act as infrared radiation absorbent [51], and therefore their localization in the foam is important in order to understand its influence on the thermal conductivity. The solid phase in cellular materials is distributed between the two components of cells: walls and struts, and consequently the CNFs could be located in both areas. **Figure 3** shows optical micrographs for the foam containing 0.4 wt.% CNF (the results obtained for the other foams containing CNFs were similar). The cell walls are free from nanoparticles, whereas the CNFs can be only observed in the struts (**Figure 3.b**). On the other hand, the SEM micrographs in **Figure 4** confirm that the nanoparticles are mainly situated in the struts, whereas only small amounts of particles are present in the cell walls (**Figure 4.a** and **4.b**). These results were common for all the materials containing CNFs. Moreover, the poor adhesion of the CNFs in the PU matrix is also observed in the SEM images shown in **Figure 4.c** and **4.d**. This poor adhesion between the filler and the matrix could play a role on the mechanical response of the foams, as discussed below.

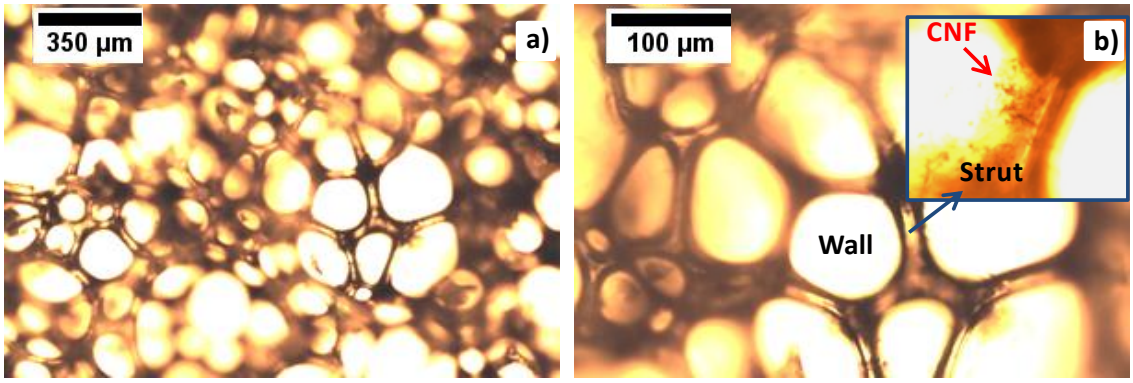

Figure 3. Optical microscopy images of the microstructure for PUR foam with 0.4 wt.% CNF. (a) General view, (b) Enlarged image showing cell walls and struts.

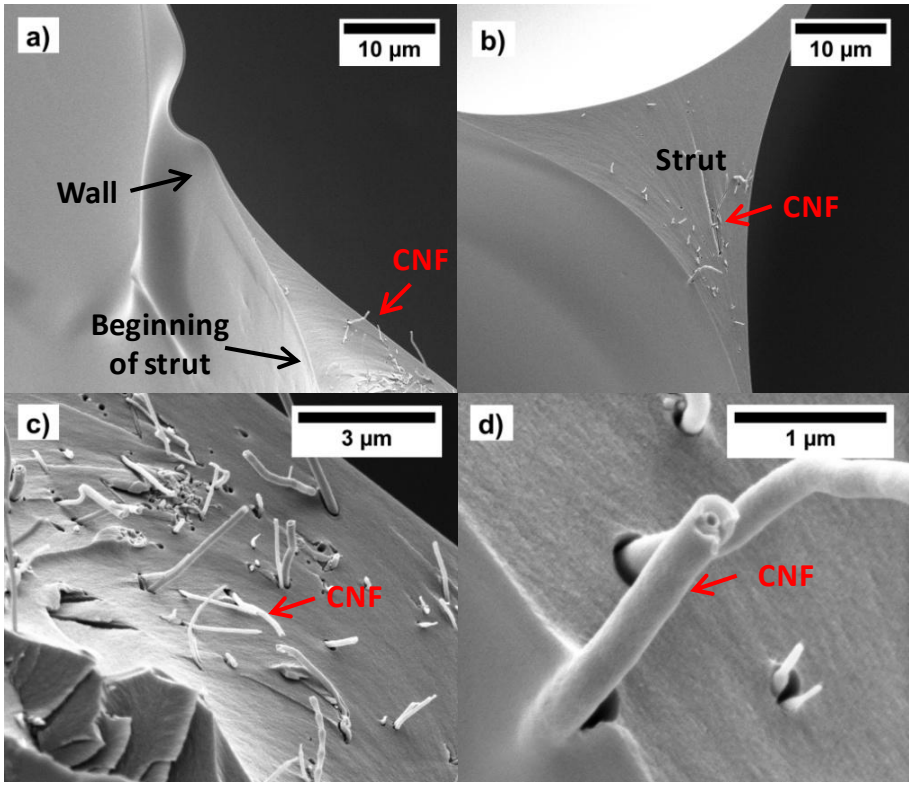

Figure 4. SEM micrographs of the microstructure for PUR foam with 0.3%CNF. (a) Wall and beginning of a strut, (b) Strut, (c) CNFs in the strut, (d) CNFs in the strut (detail).

In conclusion, both optical and SEM micrographs show that CNF nanoparticles are mainly located in the struts. A possible explanation of this result is that the cell wall thickness in these foams is in the range of 1 to 2.5 microns and the size of the struts is slightly higher, as a result the CNFs cannot be located in the walls because although they have an average diameter of 102 nm, their length is high, between 50 and 200 microns. In addition, the CNFs have a minimal chemically vapor deposited (CVD) layer of carbon on the surface, and therefore their surface hardly has functional groups which can react with other functional groups present in foam components, such as isocyanate, polyols or the blowing agent (water) [36]. This lack of chemical reaction between CNFs and foam components does not allow to redistribute the CNFs along cell walls and may also explain the poor adhesion of the CNFs present in the foam. Besides, the pure PUR foam and the PUR foams containing CNFs display the same absorptions in the FTIR spectra (**Figure 5**), supporting the no chemical reaction between the CNFs and the PU matrix.

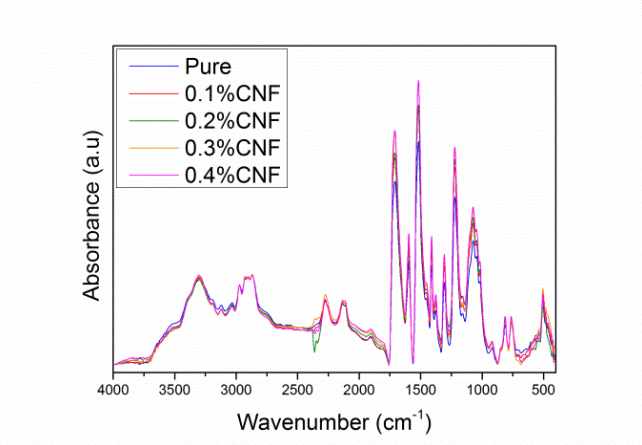

Figure 5. FTIR spectra of the PUR foams.

3.3. Study of thermal conductivity

The thermal conductivity was measured once carbon dioxide has diffused outside the cells and has been substituted by atmospheric air [24]. **Figure 6** show the thermal conductivity values obtained once this final stationary state has been reached. The thermal conductivity for the reference foam is 35.5 mW/mK. This value is in the range expected considering that the foam is water-blown, so air was in the cells when the conductivity was measured, and taking into account that the density is relatively high, 56 kg/m^3. Reducing the thermal conductivity of this foam, while keeping a high density, is not a simple task because as it will be explained later the radiative contribution (the one that it is possible to reduce by using the CNFs) has a low contribution in these systems. Despite this fact, a small number of particles (0.1 wt.%) can reduce the thermal conductivity to values of 34.8 mW/mK (**Figure 6**). Therefore, a small content of particles is needed to detect a clear reduction of the thermal conductivity. However, only this small amount can improve the results, increasing this content to values of 0.2, 0.3 or 0.4 wt.% does not further reduce the thermal conductivity.

As it is shown in **Table 1**, the inclusion of CNFs causes insignificant changes in the density, open cell content, cell size, anisotropy and cell size distribution, so that the variations in thermal conductivity cannot be explained by variations of these parameters. Thus, in order to understand the results obtained a detailed study considering measurements of the extinction coefficient and modelling of the thermal conductivity modelling has been carried out.

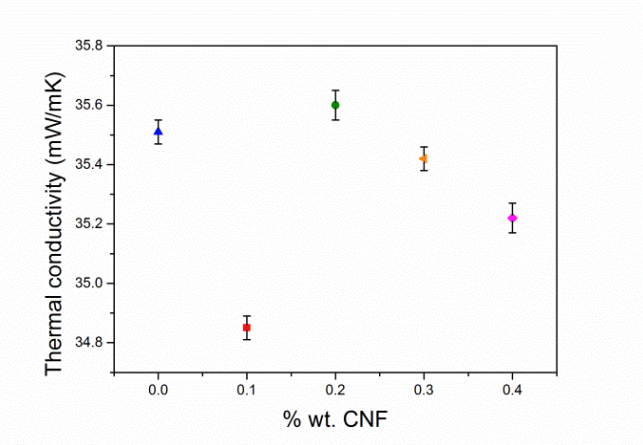

Figure 6. Thermal conductivity as a function of CNF concentration.

3.3.1. Rosseland extinction coefficient (K_R)

When thick PUR foams are used in real applications, the mean free path for radiation propagation is small enough to be considered as an optically thick medium. Radiative heat transfer through an optically thick medium can be estimated by the diffusion approximation where the radiative heat flux $q_r(x)$ is proportional to the black body emissive power (σT^4), and can be expressed as follows [11]:

$$q_r(x) = \frac{4}{3K_{e,R}}\frac{\partial e_b}{\partial x} = \frac{-16\,\sigma T^3}{3K_{e,R}}\frac{\partial T}{\partial x} = -\lambda_r\frac{\partial T}{\partial x} \qquad \textbf{(6)}$$

λr is the radiative conductivity, σ is the Stefan–Boltzmann constant, T is the mean temperature, and $K_{e,R}$ is the Rosseland mean extinction coefficient. Hence, the radiative conductivity can be approximated by the Rosseland equation [11]:

$$\lambda_r = \frac{16\,n^2\sigma T^3}{3K_{e,R}} \qquad \textbf{(7)}$$

Where *n* is the effective refraction index, and $K_{e,R}$ is the Rosseland mean extinction coefficient. In this case, *n* is close to one because the volume of gas (porosity) of the PUR foams herein studied is approximately 95%. $K_{e,R}$ is obtained from the following equation [50]:

$$\frac{1}{K_{e,R}} = \frac{\int_0^\infty \frac{1}{K_{e,\lambda}}\frac{\partial e_{b,\lambda}}{\partial T}d\lambda}{\int_0^\infty \frac{\partial e_{b,\lambda}}{\partial T}d\lambda} \qquad \textbf{(8)}$$

Where $e_{b,\lambda}$ is the spectral blackbody emissive power and λ is the wavelength. Therefore, the Rosseland mean extinction coefficient is an average value of $K_{e,\lambda}$ weighed by the local spectral

energy flux. Once, $K_{e,\lambda}$ is measured experimentally (equations 4 and 5), $K_{e,R}$ can be obtained using **equation 8**.

The Rosseland mean extinction coefficients obtained for each sample are shown in **Figure 7** and clearly increase when increasing the amounts of CNFs. There is a clear increase up to 0.3 wt.% of CNF content and then the values are stable. The trend of Rosseland extinction coefficient should be due to an increase of the extinction coefficient of the PU matrix due to the presence of CNFs because the cellular structure is similar for all the analyzed foams. All this will imply a reduction of the radiative contribution of thermal conductivity for samples with CNFs, as discussed later.

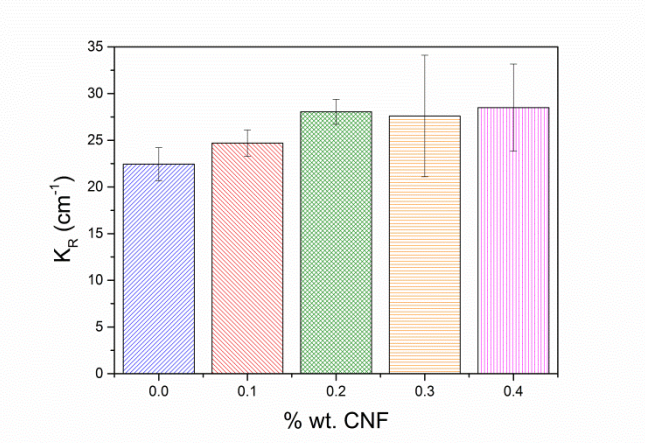

Figure 7. Experimental results for Rosseland extinction coefficient (K_R).

3.3.2. Thermal conductivity modelling

The thermal conductivity of the PUR foam (containing solid and gas phases) is well represented by the addition of four heat conduction mechanisms: conduction along the cell walls and the struts of the solid polymer (λ^s), conduction through the gas phase (λ^g), thermal radiation (λ^r), and convection within the cells (λ^c). The addition of these contributions gives the total thermal conductivity (λ^t):

$$\lambda^t = \lambda^s + \lambda^g + \lambda^r + \lambda^c \qquad \textbf{(9)}$$

The convective mechanism is considered negligible [11] due to the very small cell size of the foams under study (300-400 μm). The conductive terms of the gas and of the solid phases can be estimated by **equations 10** and **11**:

$$\lambda^g = \lambda_g V_g \qquad \textbf{(10)}$$

$$\lambda^s = \lambda_s \frac{V_s}{3}\left(\left(f_s\sqrt{AR}\right) + 2(1 - f_s)(AR)^{1/4}\right) \qquad \textbf{(11)}$$

where V_g is the volume fraction of the gas phase ($_{1-\rho_f/\rho_s}$), ρ_f and ρ_s are the density of the foams and the density of the solid respectively (ρ_s =1160 kg/m^3), V_s is the volume fraction of the solid phase ($_{\rho_f/\rho_s}$), *AR* is the anisotropy ratio, λ_g is the thermal conductivity of the gas for a given temperature, and λ_s is the thermal conductivity of the solid matrix that is unknown for the materials under study because the effect of the nanoparticles on this property cannot be measured [17]. The gas conduction (**equation 10**) depends on the nature of the gas. As indicated above, the gas inside the cells once the final stationary state has been reached is atmospheric air, whose conductivity at 20°C is 25.6 mW/mK [52].

3.3.3. Estimation of heat conduction mechanisms

An estimation of the different heat conduction mechanisms for the samples under study was conducted. The conductivity through the gas phase was calculated using **equation 10** and the radiative contribution was obtained using **equation 7** and the experimental values measured for the extinction coefficient. The conduction through the solid phase was calculated as the difference between the experimental thermal conductivity and the values of conduction in the gas phase and radiation. We used this procedure because the thermal conductivity of the solid matrix λ_s is unknown. **Figure 8** shows the contribution (in percentage) of each heat conduction mechanism.

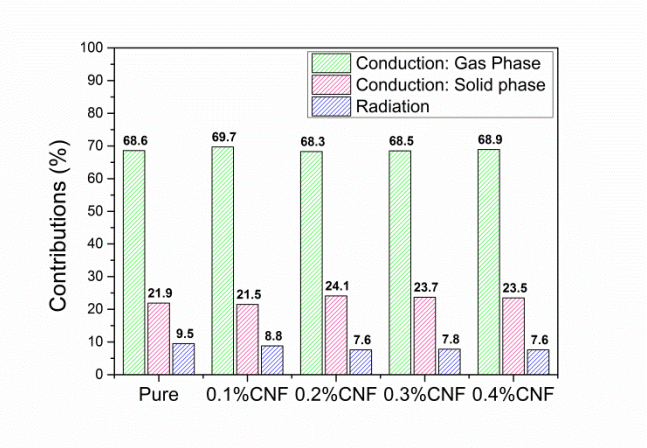

Figure 8. The contribution of the thermal conductivity mechanisms for each PU foam.

3.3.3.1. Modelling discussion: Conduction through the gas phase

As shown by **Figure 8** this contribution is the most significant in the final value of the thermal conductivity. As explained above, the thermal conductivity is measured when the composition of the gas in the cells has reached a stationary value, i.e. when all carbon dioxide (conductivity = 14.5 mWm^{-1}K^{-1}) has diffused outside the cells and has been replaced by atmospheric air (25.6 mWm^{-1}K^{-1}). Using the thermal conductivity model (**equation 9**), the conduction through the

gas phase with 100% of air concentration inside the cells is app.69% for the all the materials under study (**Figure 8**).

3.3.3.2. Modelling discussion: Radiation term

The radiative conductivity can be estimated by the Rosseland equation (**equation 9**) using the Rosseland extinction coefficient ($K_{e,R}$) obtained experimentally. The radiative contribution is app. 10% for the pure material, and the addition of CNFs results in a decrease of this contribution from 10% to around 8% (**Figure 8)**. Since the radiative conductivity is associated with changes in the extinction coefficient (cellular structure did not change when CNFs were added), the increase of extinction coefficient with CNFs addition previously discussed involves a high reduction of radiative conductivity up to 20% for the material containing CNFs. Therefore, it is concluded that a very small content of CNFs is enough to have a second phase that is acting in a very effective way as infrared blocker. It is important to remark here that the relatively high density of the foam system under study (56 kg/m^3) results in a low contribution of the radiative heat transfer, only 10%, much lower than the 20% reached for foams systems with lower densities [53-55]. Due to this reason and, as it was mentioned in the introduction, it is not an easy task to reduce the conductivity of this type of PU systems by using strategies acting on the radiative heat conduction. In this system the maximum reduction of the total thermal conductivity we could reach is 10% by completely removing the heat conduction by radiation. Therefore, the result obtained, a reduction of 20% of the radiative contribution that translates into a 2.2% reduction of the total conductivity for the material containing 0.1 wt.% of CNFs is considered a promising result.

3.3.3.3. Modelling discussion: Conduction through the solid phase

The contribution of conduction through the solid gives app. 22% for the pure PUR foam and increases as CNFs concentration grows (**Figure 8**). The relatively high density of the foams under study is the reason behind this high contribution of the solid phase [53-55]. On the one hand, the density of the foam increases when the fillers are added (see **Table 1**) and this is one of the reasons justifying the increase of this contribution when filler content increases. On the other hand, **Table 2** collects the thermal conductivity of the polymeric matrix (λs) for all samples, which is calculated by using the thermal conductivity model (**equation 9**) and the values of the heat conduction through the solid phase (**Figure 8**). As it can be seen, λs in the materials containing nanofillers increases with the CNFs contents (0.2 and 0.3 wt.%). This is probably due to an increase of the conductivity of the solid matrix due to the formation of an interconnected network of the fibers [32, 33].

Table 2. Thermal cconductivity of the polymeric matrix (λs) for the samples containing nanoparticles.

Samples	λs (mW/mK)
Pure	342
0.1%CNF	311
0.2%CNF	347
0.3%CNF	345
0.4%CNF	334

In summary, this analysis indicates that the addition of CNF particles causes an increase of the extinction coefficient, due to the activity of the particles as infrared blockers, and at the same time an increase of the conduction through the solid phase due to the increase in density of the foam and increase of the conductivity of the polymeric matrix. The optimum material is the one containing 0.1 wt.% CNF because in this system the particles are acting as IR blockers and the solid phase contribution is still low. For higher contents of particles, the increase in the solid phase contribution compensates the increase of the extinction coefficient, resulting in materials with a similar conductivity to that of the pure foam.

3.4. Mechanical properties

The compressive properties (Young's modulus and collapse stress) of PUR foams were measured at room temperature. The Gibson and Ashby relationship between mechanical properties and density [56] must be used in order to exclude the differences in densities between the foam samples. Therefore, Young's modulus and collapse stress divided by the relative density of the foam samples allow the comparison of the mechanical properties of the PU foams with different CNFs content. The relative Young's modulus and relative collapse stress of the foams are collected in **Figures 9**. It can be observed that the mechanical properties are hardly modified by the CNFs because the cellular structure of nanocomposite foams is not deteriorated by the addition of the particles. The slight reduction of relative collapse stress for foams with CNFs could be due to the poor adhesion of CNFs to the PU matrix. The most interesting result is for the foam containing 0.1 wt.% CNFs which slightly increases (8%) the relative Young's modulus and maintains the relative collapse stress, in addition to the reduction of the thermal conductivity reported in previous paragraphs. This result is remarkable because in several studies [25, 57-59] the inclusion of nanoparticles into PU foams improves some properties such as the thermal conductivity, however the mechanical properties are reduced [58, 59].

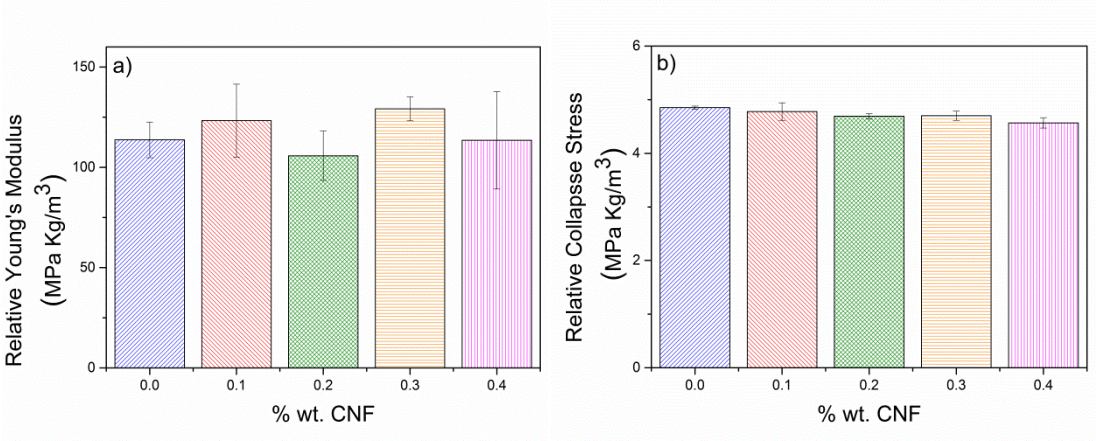

Figure 9. **a)** Relative Young's modulus and **b)** relative collapse stress for the foams corresponding to compression tests.

4. Conclusions

PUR foams with densities in the range of 55-60 kg/m^3 reinforced with small amounts of CNFs have been prepared and characterized. The cellular structure of the foams slightly changes due to the addition of CNFs. These nanoparticles are mainly situated in the struts and have a poor adhesion with the PU matrix.

The inclusion of CNFs increases the extinction coefficient of the foam, and as consequence there is a clear reduction of the radiative contribution of the thermal conductivity for the samples containing CNFs (up to 20%). The total thermal conductivity is reduced at very low contents of CNFs (0.1 wt.% of CNFs content). For this material thermal conductivity is reduced by 2% in comparison with the reference foam, which is a remarkable result taking into account that the foams under study have relatively high densities. Concentrations higher than 0.1 wt.% do not lead to higher reductions of the thermal conductivity due to an increase of the heat conduction through the solid phase, which is due to a density increase when the particles are added and to an increase of the thermal conductivity of the solid matrix. On the other hand, the sample with 0.1 wt.% of CNFs, in addition to the improved thermal insulation, presents a slight increase in relative Young's modulus and maintains the relative collapse stress.

Acknowledgement

Financial assistance from MINECO, FEDER, UE (MAT2015-69234-R) and the Junta de Castile and Leon (VA011U16) are gratefully acknowledged.

References

[1] M. Szycher, Szycher's Handbook of Polyurethanes, Second ed., CRC Press Boca Raton, Florida, USA, 2012.
[2] K. Ashida, Polyurethane and related foams: Chemistry and Technology, CRC Press2007.
[3] H.W. Engels, H.G. Pirkl, R. Albers, R.W. Albach, J. Krause, A. Hoffmann, H. Casselmann, J. Dormish, Polyurethanes: versatile materials and sustainable problem solvers for today's challenges, Angewandte Chemie, 52 (2013) 9422-9441.
[4] U. Meier-Westhues, Polyurethanes: Coatings, Adhesives and Sealants., Vincentz Network, Hannover, 2007.
[5] N.M.K. Lamba, K.A. Woodhouse, S.L. Cooper, Polyurethanes in Biomedical Applications, CRC Press, Boca Raton, Fl, US, 1997.
[6] R.M. Evans, Polyurethane sealants: technology and applications, Technomic Publishing Company, Lancaster, PA, 1993.
[7] S. Lee, Thermoplastic Polyurethane Markets in the EU: Production, Technology, Applications and Trends, Rapra Technology Limited, United Kingdom, 1998.
[8] Plastics-the Facts 2014. An analysis of European plastics production, demand and waste data for 2014., in: PlasticsEurope (Ed.), 2015.
[9] Polymer Foams Market Expected to Consume 25.3 Million Tonnes by 2019. http://www.smithersrapra.com/news/2014/may/polymer-foam-market-to-consume-25-3-million-tonnes, 2014 (accessed 16 July 2019).
[10] D. Klempner, V. Sendijarevic, Handbook of Polymeric Foams and Foam Technology, Hanser 1991.
[11] L. Glicksman, Low Density Cellular Plastics: Physical Basis of Behaviour, Springer Netherlands, London, 1994.
[12] R.J.J. Williams, C. Aldao, Thermal Conductivity of Plastic Foams, Polymer Engineering and Science, 23 (1983) 293–298.
[13] R. Boetes, C.J. Hoogendoorn, Heat Transfer in Polyurethane Foams for Cold Insulation, Proceedings of the International Centre for Heat and Mass Transfer, 1987, pp. 14-20.
[14] J. Francl, W.D. Kingery, Thermal Conductivity: IX, Experimental Investigation of Effect of Porosity on Thermal Conductivity, Journal of the American Ceramic Society, 37 (1954) 99–107.
[15] M.A. Schuetz, L.R. Glicksman, A Basic Study of Heat Transfer Through Foam Insulation, Journal of Cellular Plastics, 20 (1984) 114-121.
[16] L. Glicksman, M. Schuetz, M. Sinofsky, Radiation heat transfer in foam insulation International Journal of Heat and Mass Transfer, 30 (1987) 187–197.
[17] L.R. Glicksman, Heat transfer and ageing of cellular foam insulation, Cellular polymers, 10 (1991) 276-293.
[18] O.A. Almanza, M.A. Rodríguez-Pérez, J.A.D. Saja, Prediction of the radiation term in the thermal conductivity of crosslinked closed cell polyolefin foams, Journal of Polymer Science Part B: Polymer Physics, 38 (2000) 993–1004.
[19] J. Kuhn, H.P. Ebert, M.C. Arduini-Schuster, D. Büttner, J. Fricke, Thermal transport in polystyrene and polyurethane foam insulations, Thermal transport in polystyrene and polyurethane foam insulations, 35 (1992) 1795-1801.
[20] S.H. Kim, M.C. Lee, H.D. Kim, H.C. Park, H.M. Jeong, K.S. Yoon, B.K. Kim, Nanoclay reinforced rigid polyurethane foams, Journal of Applied Polymer Science, 117 (2010) 1992-1997.
[21] J.W. Wu, W.F. Sung, H.S. Chu, Thermal conductivity of polyurethane foams, International Journal of Heat and Mass Transfer, 31 (1999) 1100–1106.
[22] M.S. Han, S.J. Choi, J.M. Kim, Y.H. Kim, W.N. Kim, H.S. Lee, J.Y. Sung, Effects of Silicone Surfactant on the Cell Size and Thermal Conductivity of Rigid, Macromolecular Research, 17 (2009) 44–50.

[23] C.-j. Tseng, M. Vamaguch, T. Ohmori, Thermal conductivity of polyurethane foams from room temperature to 20 K, Cryogenics, 37 (1997) 305–312.
[24] S. Estravís, J. Tirado-Mediavilla, M. Santiago-Calvo, J.L. Ruiz-Herrero, F. Villafañe, M.A. Rodríguez-Pérez, Rigid polyurethane foams with infused nanoclays: Relationship between cellular structure and thermal conductivity, European Polymer Journal, 80 (2016) 1–15.
[25] X. Cao, L. James Lee, T. Widya, C. Macosko, Polyurethane/clay nanocomposites foams: processing, structure and properties, Polymer, 46 (2005) 775–783.
[26] Z. Xu, X. Tang, A. Gu, Z. Fang, Novel preparation and mechanical properties of rigid polyurethane foam/organoclay nanocomposites, Journal of Applied Polymer Science, 106 (2007) 439-447.
[27] G. Harikrishnan, T.U. Patro, D.V. Khakhar, Polyurethane Foam-Clay Nanocomposites: Nanoclays as Cell Openers, Industrial and Engineering Chemistry Research, 45 (2006) 7126–7134.
[28] M.M.A. Nikje, Z.M. Tehrani, Polyurethane Rigid Foams Reinforced by Doubly Modified Nanosilica, Journal of Cellular Plastics, 46 (2010) 159–172.
[29] M.M.A. Nikje, Z.M. Tehrani, Thermal and mechanical properties of polyurethane rigid foam/modified nanosilica composite, Polymer Engineering & Science, 50 (2010) 468–473.
[30] L. Zhang, E.D. Yilmaz, J. Schjødt-Thomsen, J.C. Rauhe, R. Pyrz, MWNT reinforced polyurethane foam: Processing, characterization and modelling of mechanical properties, Composites Science and Technology, 71 (2011) 877-884.
[31] D. Yan, L. Xu, C. Chen, J. Tang, X. Ji, Z. Li, Enhanced mechanical and thermal properties of rigid polyurethane foam composites containing graphene nanosheets and carbon nanotubes, Polymer International, 61 (2012) 1107-1114.
[32] D.-X. Yan, K. Dai, Z.-D. Xiang, Z.-M. Li, X. Ji, W.-Q. Zhang, Electrical conductivity and major mechanical and thermal properties of carbon nanotube-filled polyurethane foams, Journal of Applied Polymer Science, 120 (2011) 3014-3019.
[33] N. Athanasopoulos, A. Baltopoulos, M. Matzakou, A. Vavouliotis, V. Kostopoulos, Electrical conductivity of polyurethane/MWCNT nanocomposite foams, Polymer Composites, 33 (2012) 1302-1312.
[34] L. Madaleno, R. Pyrz, A. Crosky, L.R. Jensen, J.C.M. Rauhe, V. Dolomanova, A.M.M.V. de Barros Timmons, J.J. Cruz Pinto, J. Norman, Processing and characterization of polyurethane nanocomposite foam reinforced with montmorillonite–carbon nanotube hybrids, Composites Part A: Applied Science and Manufacturing, 44 (2013) 1–7.
[35] M.C. Saha, M.E. Kabir, S. Jeelani, Enhancement in thermal and mechanical properties of polyurethane foam infused with nanoparticles, Materials Science and Engineering: A, 479 (2008) 213-222.
[36] G. Harikrishnan, S.N. Singh, E. Kiesel, C.W. Macosko, Nanodispersions of carbon nanofiber for polyurethane foaming, Polymer, 51 (2010) 3349-3353.
[37] M.C. Saha, B. Barua, S. Mohan, Study on the Cure Kinetic Behavior of Thermosetting Polyurethane Solids and Foams: Effect of Temperature, Density, and Carbon Nanofiber, Journal of Engineering Materials and Technology, 133 (2011) 011015.
[38] M.E. Kabir, M.C. Saha, S. Jeelani, Effect of ultrasound sonication in carbon nanofibers/polyurethane foam composite, Materials Science and Engineering: A, 459 (2007) 111-116.
[39] E. Thostenson, C. Li, T. Chou, Nanocomposites in context, Composites Science and Technology, 65 (2005) 491-516.
[40] Y.S. Kim, R. Davis, A.A. Cain, J.C. Grunlan, Development of layer-by-layer assembled carbon nanofiber-filled coatings to reduce polyurethane foam flammability, Polymer, 52 (2011) 2847-2855.
[41] IsoPMDI 92140 Technical Data Sheet. BASF Poliuretanos Iberia S.A.
[42] Elastopor H 1501/2 Technical Data Sheet. BASF Poliuretanos Iberia S.A.

[43] Pyrograf® III PR-24-XT-PS Carbon Nanofibers, in: A.S. Inc. (Ed.).
[44] ASTM D1622-08: Standard Test Method for Apparent Density of Rigid Cellular Plastics.
[45] ASTM D6226-10: Standard Test Method for Open Cell Content of Rigid Cellular Plastics.
[46] J. Pinto, E. Solorzano, M.A. Rodriguez-Perez, J.A. de Saja, Characterization of the cellular structure based on user-interactive image analysis procedures, Journal of Cellular Plastics, 49 (2013) 555–575.
[47] UNE-EN 12667:2002. Thermal performance of building materials and products. Determination of thermal resistance by means of guarded hot plate and heat flow meter methods. Products of high and medium thermal resistance.
[48] ASTM D1621: Standard Test Method for Compressive Properties Of Rigid Cellular Plastics.
[49] R.A. Campo-Arnáiz, M.A. Rodríguez-Pérez, B. Calvo, J.A. de Saja, Extinction coefficient of polyolefin foams, Journal of Polymer Science Part B: Polymer Physics, 43 (2005) 1608-1617.
[50] H.R.N. Jones, Radiation Heat Transfer, Oxford Science, Oxford, 2000.
[51] J. Shen, X. Han, L.J. Lee, Nanoscaled Reinforcement of Polystyrene Foams using Carbon Nanofibers, Journal of Cellular Plastics, 42 (2016) 105-126.
[52] J.R. Howell, R. Siegel, M.P. Mengu, Thermal radiation heat transfer, 5th ed., CRC press2010.
[53] O. Almanza, M.A. Rodríguez-Pérez, J.A. de Saja, The Thermal Conductivity of Polyethylene Foams Manufactured by a Nitrogen Solution Process, Cellular Polymers, 18 (1999) 385-401.
[54] M.A. Rodríguez-Pérez, O. Alonso, J. Souto, J.A. de Saja, Thermal Conductivity of Crosslinked Closed Cell Polyolefin Foams, Polymer Testing, 16 (1997) 287-298.
[55] E. Solórzano, M.A. Rodriguez-Perez, J. Lázaro, J.A. de Saja, Influence of Solid Phase Conductivity and Cellular Structure on the Heat Transfer Mechanisms of Cellular Materials: Diverse Case Studies, Advanced Engineering Materials, 11 (2009) 818-824.
[56] L. Gibson, M. Ashby, Cellular solids: structure and properties, Pergamon Press, Oxford, 1988.
[57] T. Widya, C. Macosko, Nanoclay-Modified Rigid Polyurethane Foam, Journal of Macromolecular Science, Part B: Physics, 44 (2005) 897-908.
[58] M. Santiago-Calvo, V. Blasco, C. Ruiz, R. París, F. Villafañe, M.Á. Rodríguez-Pérez, Synthesis, characterization and physical properties of rigid polyurethane foams prepared with poly(propylene oxide) polyols containing graphene oxide, European Polymer Journal, 97 (2017) 230-240.
[59] M. Santiago-Calvo, J. Tirado-Mediavilla, J.L. Ruiz-Herrero, M.Á. Rodríguez-Pérez, F. Villafañe, The effects of functional nanofillers on the reaction kinetics, microstructure, thermal and mechanical properties of water blown rigid polyurethane foams, Polymer, 150 (2018) 138-149.

Supplementary material

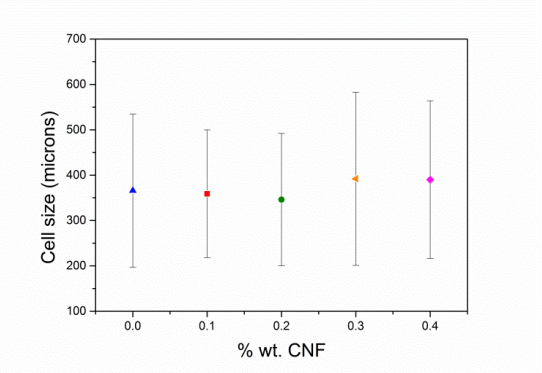

Figure S1. Average cell size vs the CNFs ratio.

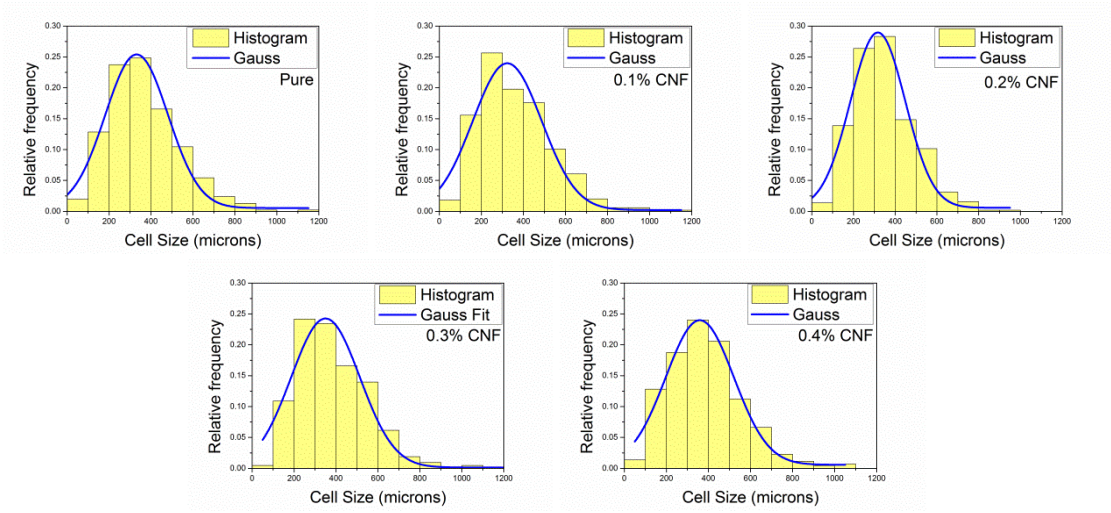

Figure S2. Cell size distribution of the foams under study.

Effect of fillers on cellular structure and physical properties of rigid polyurethane foams

Polymer international (**2019**)
https://doi.org/10.1002/pi.5893

Long-term thermal conductivity of cyclopentane-water blown rigid polyurethane foams reinforced with different types of fillers

Mercedes Santiago-Calvo[1,*], Josías Tirado-Mediavilla[1], J. L. Ruiz-Herrero[1], Fernando Villafañe[2], Miguel Ángel Rodríguez-Pérez[1]

[1] Cellular Materials Laboratory (CellMat), Condensed Matter Physics Department, Faculty of Science, University of Valladolid, Campus Miguel Delibes 7, 47011 Valladolid, Spain

[2] GIR MIOMeT-IU Cinquima-Química Inorgánica, Faculty of Science, University of Valladolid, Campus Miguel Delibes 7, 47011 Valladolid, Spain

* Corresponding author: mercesc@fmc.uva.es

Abstract

The understanding of the long-term thermal conductivity of rigid polyurethane (RPU) foams presents a great interest in the building field considering the conservation of energy efficiency. In this study, the effect of different types of particles (talc (T), diatomaceous earth (DE), and non-porous silica (NPS)) on the thermal conductivity of RPU foams blown with cyclopentane (CP) and water as blowing agents has been investigated along three years of aging. The characterization of the cellular structure shows how the addition of particles causes a cell size reduction of the foams, and consequently an enhancement of the thermal properties just after production. However, this initial reduction was not maintained, because each foam shows a different thermal conductivity evolution with time. We have found for the first time, a relationship between the slope of the thermal conductivity *versus* time at the first measurements and the internal temperature reached during the foaming process. The evolution of the RPU foams in which higher internal temperatures were reached is more pronounced than in those RPU foams where lower foaming temperatures were observed. This effect is related to the kinetics of the diffusion of the gas occluded inside the cells and imposes a new criterion for the selection of particles to reduce the thermal conductivity of RPU foams, these additives should ideally decrease the temperature reached during the foaming process. Moreover, the effect of aging on the thermal conductivity is explained by using theoretical models.

Keywords: Polyurethane; foams; thermal conductivity; foaming temperature; composites

1. Introduction

Rigid polyurethane (RPU) foams with a closed-cell structure are mainly used for thermal insulation and for structural applications especially in buildings, due to their low thermal conductivity, low density, high compression strength, and low moisture permeability [1, 2]. RPU foams are usually prepared by the polymerization reaction of a polyol with an isocyanate, which produces urethane linkages. At the same time, foam expansion occurs due to the presence of a chemical blowing agent, a physical blowing agent, or a mixture of both. Until recently, chlorofluorocarbons (CFCs) and hydrochlorofluorocarbons (HCFCs) were commonly used as physical blowing agents, but they have been recently prohibited because they play a decisive role on the destruction of the ozone layer. For this reason, more environmentally friendly blowing agents such as cyclopentane (CP) or water are currently used in many industrial applications. Water acts as a chemical blowing agent reacting with isocyanate to form CO_2 and urea linkages, giving rise to water-blown RPU foams. On the other hand, CP evaporates during as a result of the heat produced during the polymerization reaction.

Thermal conductivity is the most important property for RPU foams used as insulating materials. The thermal conductivity is determined by the following heat transfer mechanisms [3-6]: conduction along the solid phase (λ^s), conduction through the gas phase (λ^g), thermal radiation (λ^r), and convection within the cells (λ^c). The latter is negligible for the foams with small cell sizes (less than 2 mm) [7, 8]. The thermal conductivity of RPU foams depends mainly on the types and amount of blowing agents contained in the closed cells, due to the high contribution of λ^g to the total thermal conductivity (higher than 60%) [8, 9]. Thus, the use of blowing agents with low thermal conductivities is one of the key strategies to improve the thermal properties of RPU foams. Moreover, the addition of fillers to the RPU matrix may also decrease the cell size and/or block the infrared radiation, reducing the radiation contribution to the thermal conductivity [5, 10, 11].

Another important aspect to consider is the aging of the RPU foams, since the thermal conductivity values always increase with time. This aging phenomenon occurs because the blowing agents slowly diffuse out of the cells, being replaced by atmospheric air which diffuses into them. Each blowing agent presents a different diffusion rate, for example, the diffusion rate of CO_2 out the foam is high, and in fact it is replaced by air after a few weeks [11]. CP shows a very low diffusion rate out the foam, and several years are needed to be completely replaced it by atmospheric air [12]. Given its significance, different authors have thoroughly studied the aging of RPU foams. Ostrogorsky et al. [9] developed an analytical model to predict the effective diffusion coefficient of RPU foams. This model allows the rate of gas diffusion and of foam aging to be determined. The theoretical predictions of CO_2, O_2 and N_2 differed *ca.* 29% from the measured values. Wilkes et al. [13] studied the effect of storage temperature on the thermal conductivity of RPU foams containing HCFC-141b, hydrofluorocarbon (HFC)-134a, HFC-245fa, or CP. This study described the behaviour of these foams used for refrigerators and

freezers after one year of aging. Two types of samples were used: full-thickness simulated refrigerator panels in which the foam is enclosed between solid plastic sheets (acrylonitrile butadiene styrene (ABS) and high impact polystyrene (HIPS)), and slices of core foam cut from similar panels. The authors concluded that the aging rate increases with the storage temperature, and it is higher for unenclosed full-thickness core foams than for those enclosed between plastic sheets. In following works [12, 14], this group continued the study of the previous samples, measuring their thermal conductivities during four years, and comparing them with theoretical predictions of aging models. Modesti et al. [15] determined experimentally the effective diffusion coefficient of HFC-245fa, CO_2 and air in RPU foams, by means of flame ionization detector gas chromatography (FID-GC) and fourier-transform infrared spectroscopy (FT-IR). They found that the slope of the aging curves depended only on the effective diffusion coefficients, and that the comparison of the experimental and predicted thermal aging curves confirmed the accuracy and reliability of the method proposed for the determination of the effective diffusion coefficients. In a later study, the same group [16] studied the aging of foams with different blowing agents, such as HFCs, hydrocarbons (HCs), dimethoxymethane, CO_2, or air, following the method previously described for the determination of the effective diffusion coefficients. Marrucho et al. [17] measured the thermal conductivity of mixtures of N_2 and CP at different temperatures and pressures, what allowed the thermal conductivity evolution of RPU foams to be evaluated. The results obtained were correlated with the modified Wassiljewa mixing rule and predicted using the extended corresponding states theory (ECST). Murphy [18] studied the effects of moisture infusion and blowing agent diffusion by means of previous literature studies, their own experiments, and long-term aging studies. Their main conclusions were that water vapour worsens the thermal conductivity of foams, that there is no correlation between molecular weight of blowing agents and the thermal conductivity of the foam, and finally that the blowing agent (CFCs, HCFCs and ecomate®) diffusion out of the foam is much slower than atmospheric gas infusion. Kuranska et al. [19] investigated the effect of different type of blowing agents (methylal, isopentane, CP, mixture of isopentane and CP, CO_2) on the foaming process, cellular structure, mechanical properties and changes of thermal conductivity during 1 year of aging. RPU systems with isopentane and a mixture of isopentane and CP showed the lowest thermal conductivity after 360 days.

Thermal aging has been studied in previous reports [9, 12-19] for RPU foams containing different blowing agents, but so far thermal aging of RPU foams reinforced with fillers has not been studied. The use of fillers is of great interest in the field of RPU foams because their addition can improve the thermal insulation of these materials [10, 11, 20-22]. In this work we report the effect of different types of particles (talc, diatomaceous earth and non-porous silica) on the long-term thermal conductivity of RPU foams containing CP and water as blowing agents. In addition, another aim of this paper is to establish, for the first time, a correlation between the effect of the fillers during foaming and the aging performance.

2. Materials and Methods

2.1. Materials

A formulation of RPU foam with water and CP as blowing agents was used in this investigation. The polyol component, Elastopor H 1501/1 (OH index 651 mg KOH/g, density 1.07 g cm^{-3}, viscosity 650 mPa•s) from "BASF Poliuretanos Iberia S.A." (Rubí, Spain), is a mixture of components containing polyether polyol, catalysts, stabilizers and water. The isocyanate component, IsoPMDI 92140 (31.5% NCO, density 1.23 g cm^{-3}, viscosity 170-250 mPa•s) from "BASF Poliuretanos Iberia S.A." (Rubí, Spain), is a polymeric diphenylmethane diisocyanate (pMDI). The free foaming density of this formulation is 30 kg/m^3. Cyclopentane (99.9% purity) from Sigma Aldrich (Madrid, Spain) was used as blowing agent. The proportions of the three components were set at 100/160/13 by weight for the polyol, isocyanate and cyclopentane in order to have a free foaming density of 30 kg/m^3.

The particles chosen to carry out this study are: talc (T), diatomaceous earth (DE), and non-porous silica (NPS). T used is from Imerys (Graz, Austria) and has a mean particle size of 2 microns. DE used is from Cekesa (Elche de la Sierra,Spain) with a particle size from 0.58 to 28 microns. NPS used is manufactured by Glantreo (Cork, Ireland) with a particle size of 0.15 microns. The surface of the particles has been treated with C18 groups. Both T and DE were selected mainly due to their low cost, and also because as micrometric particles they are easier to disperse. In the case of DE, these particles have a porous silica structure at the nanoscale [23] which increases their superficial area and therefore it could improve their efficiency as nucleating agents. On the other hand, NPS were selected because as nanometric particles the nucleation potential is very high with low contents. Due to the low content used and the nanometric size NPS is expected to have a smaller impact on the properties of cell walls and therefore on the diffusion of the gases.

2.2. Preparation of rigid polyurethane nanocomposite foams

Different RPU foams were studied: the pure material (without particles, obtained as reference material), and those containing 1.5 wt% T, 1 wt% DE, 3 wt% DE, 5 wt% DE, 0.05 wt% NPS, 0.1 wt% NPS or 0.2 wt% NPS with respect to the final mass of the RPU foams.

An overhead stirrer (EUROSTAR Power control-visc P1, IKA) with a 50 mm diameter Lenart disc stirrer was used to premix the polyol with the particles at 250 rpm for 5 minutes. Then, CP was mixed with the polyol blend at 250 rpm for 3 minutes. Finally, polyol blend with CP and the isocyanate were mixed in a plastic cup at 1200 rpm for 10 seconds. The mixture was then poured into an open wooden mould of dimensions 35 x 35 x 5 cm^3. After 2 days the foam was demoulded and cut into samples with appropriate dimensions in order to measure the thermal conductivity and to characterize the foams.

The foaming temperature reached during foaming process by each system was measured in a plastic cup. Three thermocouples type K were introduced at different positions of a plastic cup

of 11.5 cm of diameter and 14 cm of height in order to obtain the temperature measurements. The thermocouples were placed vertically in the centre of plastic cup at the following heights: 2.0 cm, 6.5 cm and 12.5 cm from the bottom. The data collected by the thermocouples during foaming process were registered in a computer. Then, for each experiment the curves given by each thermocouple were averaged to obtain the curve average foaming temperature vs time. From these curves, the maximum values were also analysed. Three experiments were carried out for each sample The standard deviation of the average foaming temperature vs time curves (for each time) was always lower than ± 1.

2.3. Foams characterization

Foam density was measured as described by ASTM D1622/D1622M-14 [24]. Density was determined in three different samples for each material, with a diameter of 30 mm and a height of 25 mm.

After measuring the densities in the samples, open cell content (OC%) was measured by using a gas pycnometer Accupyc II 1340 from Micromeritics, according to ASTM D6226-10 [25].

The cellular morphology of the foams was observed by Scanning Electron Microscopy (SEM) with a JEOL JSM-820 microscope. The growth plane (z plane) of cured foams was examined by SEM after vacuum coating with a gold monolayer. An image analysis technique [26] of SEM micrographs was used to determine the main characteristics of the cellular structure of the foams: mean cell size (Φ_{3D}), anisotropy ratio (AR), and cell size distribution by using histograms and gaussian fitting. More than 150 cells of different areas of each material were used for this analysis. The methodology used to measure the cellular structure parameters are explained in the work by Pinto et al. [26].

The thermal conductivity measurements of the foams were performed using a Rapid K heat flowmeter from Holometrix. Measurements were performed under steady heat flow conditions through the test samples, in accordance with the UNE12667 method [27], by using samples of 30 x 30 x 2.5 cm^3. The measurements were performed at 20°C, where the temperature gradient (ΔT) goes from 5°C in the bottom surface plate to 35°C in the top surface plate. Several measurements (at least four during the first two months, see Supplementary material) were performed from the fourth day of foams production, in order to know the thermal conductivity evolution with time. These experiments were conducted along three years. The samples were stored in opened plastic bag at room temperature and atmospheric pressure. The measurements of thermal conductivity versus time were fitted to a sum of exponential functions as observed in Figures S1-S8 (Supplementary material) in order to obtain the thermal conductivity values at any time. Therefore, the thermal conductivity at time 0 of foams production (collected in Table S1 in the Supplementary material) was obtained by extrapolation using the curve fitting functions.

3. Results and Discussion

3.1. Density and cellular structure characterization

Different physical properties of the foams were determined, and the values obtained are collected in **Table 1**. The data indicate that the sample containing 1.5 wt% T has the highest density, which is ca. 4 kg/m^3 higher than that of the reference material. However, the rest of the samples with particles present similar densities respect to that of the reference material.

Table 1. Density, open cell content (OC), mean cell size (Φ_{3D}), standard deviation (SD), normalized standard deviation (NSD) and anisotropy (AR) for each foam obtained.

Material	Density (Kg/m^3)	OC (%)	Φ_{3D} (μm)	SD	NSD	AR
Reference	31.19±1.69	8.1±1.9	608	68	0.11	1.11±0.29
1.5%Talc	35.55±1.16	9.5±3.1	307	98	0.32	1.27±0.27
1%DE	31.15±0.36	8.1±0.4	409	120	0.29	1.05±0.21
3%DE	31.81±0.07	9.2±0.8	331	102	0.31	1.69±0.44
5%DE	31.46±0.60	9.0±1.0	340	105	0.31	1.18±0.25
0.05%NPS	30.70±0.39	9.0±1.0	410	110	0.27	1.39±0.31
0.1%NPS	31.55±0.43	9.4±0.8	499	110	0.22	1.05±0.19
0.2%NPS	30.27±1.24	13.0±3.8	454	117	0.26	1.14±0.21

In general, the open cell content (**Table 1**) for the foams with particles slightly increases, being the foam containing 0.2 wt% NPS that showing the highest value (*ca.* 13%).

The main characteristics of the cellular structure have been obtained with image analysis from SEM micrographs in the growth plane (**Figure 1**), and are summarized in Table 1 and Figure 2. Most notably, the addition of different types of particles into the polyol component promotes a mean cell size reduction of up to 50% for T particles, 46% for DE particles and 33% for NPS particles, respect to the value of the pure foam. Thus, the smallest mean cell size of all the samples studied is that containing 1.5 wt% T. In regard to DE systems, cell sizes are even more reduced as the amount of DE particles increases. In contrast, the cell size of foams containing NPS is minimum for the material containing 0.05 wt% NPS. The reduction of cell size with particles addition is not related to the anisotropy ratio, which does not increase for most of the samples in comparison to the reference foam. Nevertheless, the sample containing 1.5 wt% T and that containing 0.05 wt% NPS show a slight increase in their anisotropy ratio, whereas the increase of the sample with 3 wt% DE is even higher.

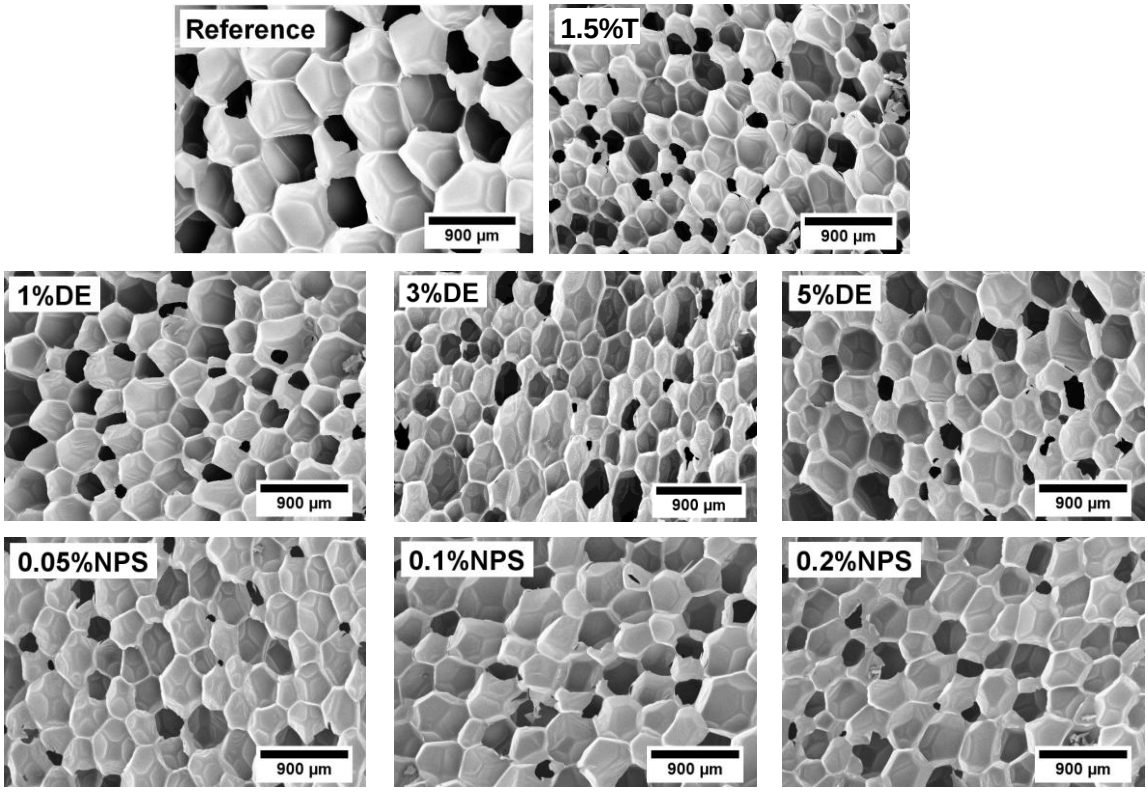

Figure 1. SEM micrographs of the foams under study showing the cell morphology.

The analysis of the SEM micrographs (**Figure 2**) provides also extra information about the cell size distribution. The study of the histograms and gaussian fitting corroborates the qualitative observations in SEM micrographs, and supports the cell size reductions, discussed above. In general, the foams with particles show a symmetric distribution and a good homogeneity.

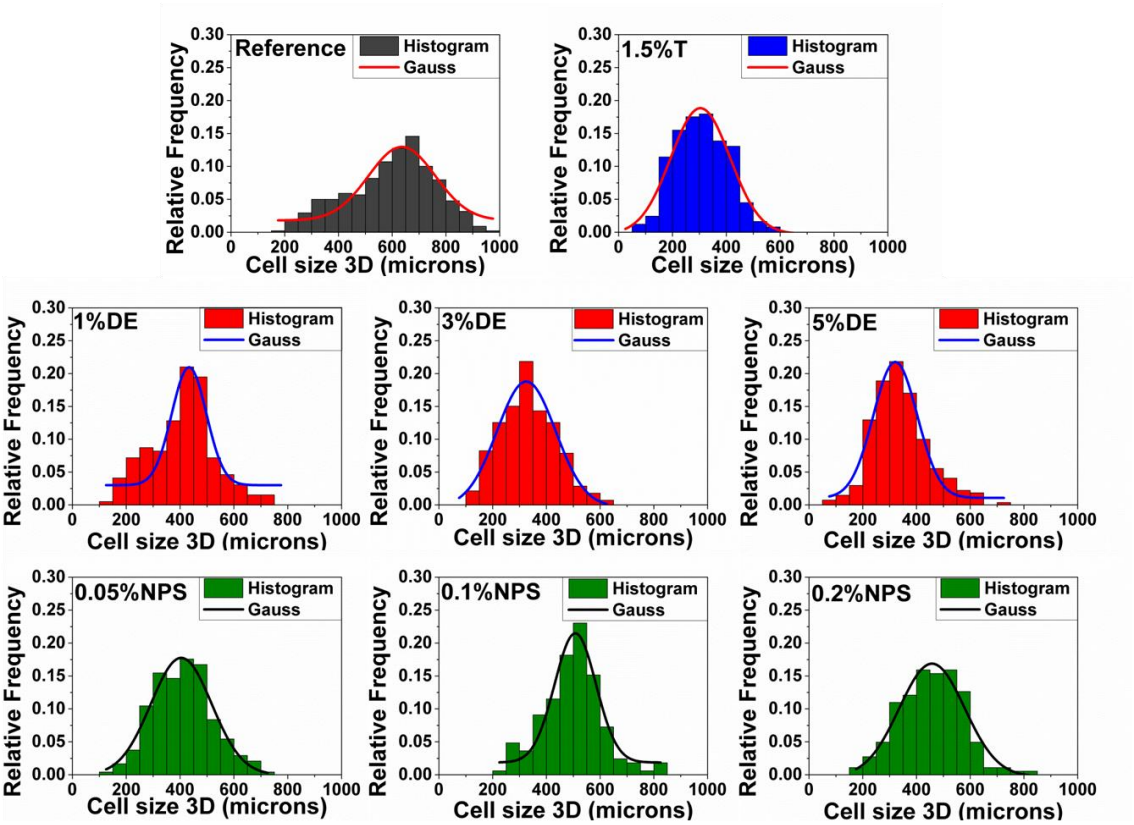

Figure 2. Cell size distribution for the foams.

3.2. Foaming temperature measurements

The foaming temperature of RPU foams can be followed because the reactions involved in PU formation are exothermic. **Figure 3** shows the average foaming temperature versus time for some representative systems. It is observed that with the addition of particles into the PU foam the temperatures reached during the foaming are higher than that of reference foam. Moreover, maximum of the average foaming temperature curves reached for each system are collected in **Table 2**.

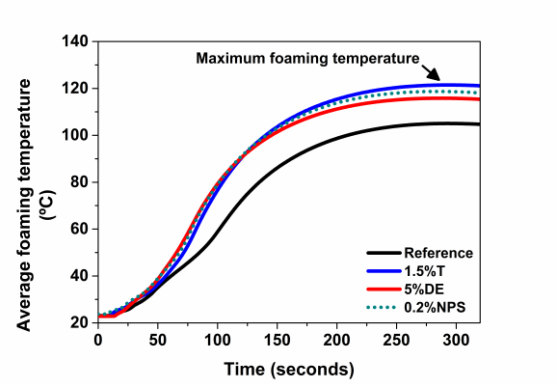

Figure 3. Average maximum foaming temperatures for several materials.

Table 2. The average foaming temperatures reached for the foams under study.

Material	Foaming temperature (°C)
Reference	105.9
1.5%Talc	121.9
1%DE	120.1
3%DE	120.6
5%DE	116.4
0.05%NPS	117.5
0.1%NPS	116.3
0.2%NPS	119.0

3.3. Study of the thermal conductivity aging

The foams under study were produced using water as a chemical blowing agent and CP as physical blowing agent. Their thermal conductivity was measured along *ca.* three years in order to study their thermal conductivity aging (**Figure 4 A**, **C** and **E**). The low thermal conductivity of all these foams (ca. 21 mW/m•K at the initial time of the foams production) is due to their low density (ca. 30 kg/m^3), and also to the use of CP (which has a low thermal conductivity and a low diffusion coefficient) as physical blowing agent. This initial value of thermal conductivity increases with time and reaches *ca.* 30 mW/m•K 3 years after foam production. The main reason for the increase of the thermal conductivity is the diffusion of the gases initially occluded inside the cells. Their thermal conductivity (14.5 mW/m•K for CO_2 and 12 mW/m•K for CP at 20 °C) is very low, but these gases slowly diffuse out of the cells, being substituted by atmospheric air, whose thermal conductivity (25.6 mW/m•K at 20 °C) is higher. The CP is retained in the cells for longer periods of time compared to those of CO_2; CO_2 leaves the foam in a time period less than 30 days [11].

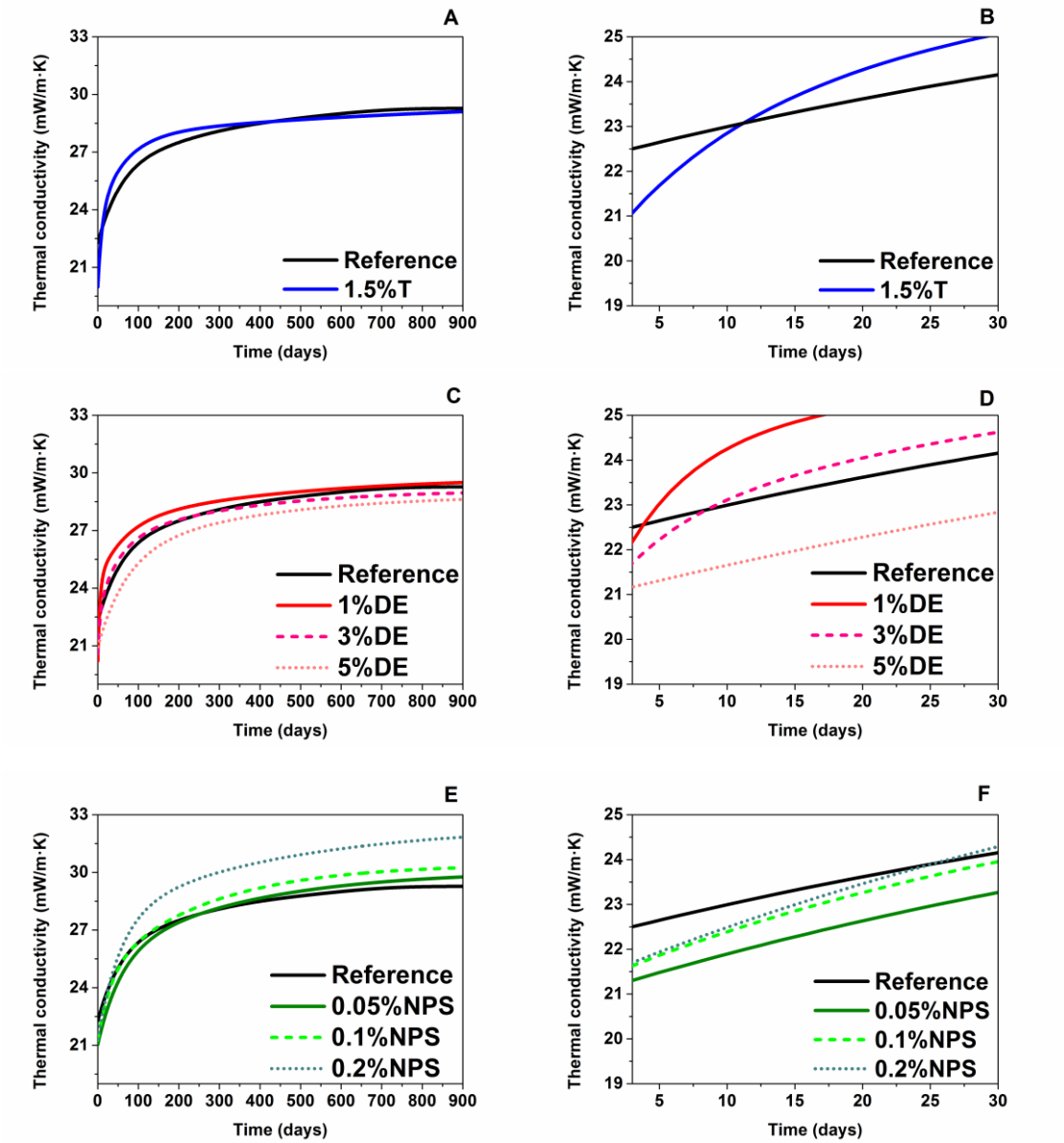

Figure 4. Thermal conductivity evolution for the pure foam and for the foams with fillers: during the first 900 days (**A**, **C** and **E**); and during 30 days (**B**, **D** and **F**).

Therefore, the analysis of the thermal conductivity evolution for the first 30 days is discussed first. The thermal conductivity values at initial times are clearly reduced for all foams with fillers in comparison with the reference material, as shown in **Figures 4** (**B, D** and **F**). This lower value of the thermal conductivity is mainly due to the smaller cell sizes of the foams containing the filler. This reduces the radiative contribution to the thermal conductivity, as discussed below. Nevertheless, **Figure 5** indicates that there is not a clear relationship between the cell sizes, the open cell contents or the density and thermal conductivities measured at initial times (less than 5 days after foam production). Therefore, other factors are playing a major role on to the thermal conductivity values. One possible explanation would be that different content of gasses inside the cells are present in each foam after the same time, i.e. the gasses

diffusion rates just after foam production are different for the different materials under study. Moreover, the initial improvement of the thermal properties is not maintained in many systems. For some of systems with the exception of 5%DE, 0.1%NPS and 0.05%NPS the conductivity of the filled material increases very quickly with time and becomes higher than the thermal conductivity of the reference material. Different reasons might explain why the concentration of gasses varies at diverse rates for each system: the properties of the foam (density, cell size, open cell content, cell window thickness, blowing agents used, initial cell gas composition, etc), the solubilities and diffusion coefficients of the gasses, and also the differences in temperature and pressure between the gasses contained in the cells and the external atmosphere, among others.

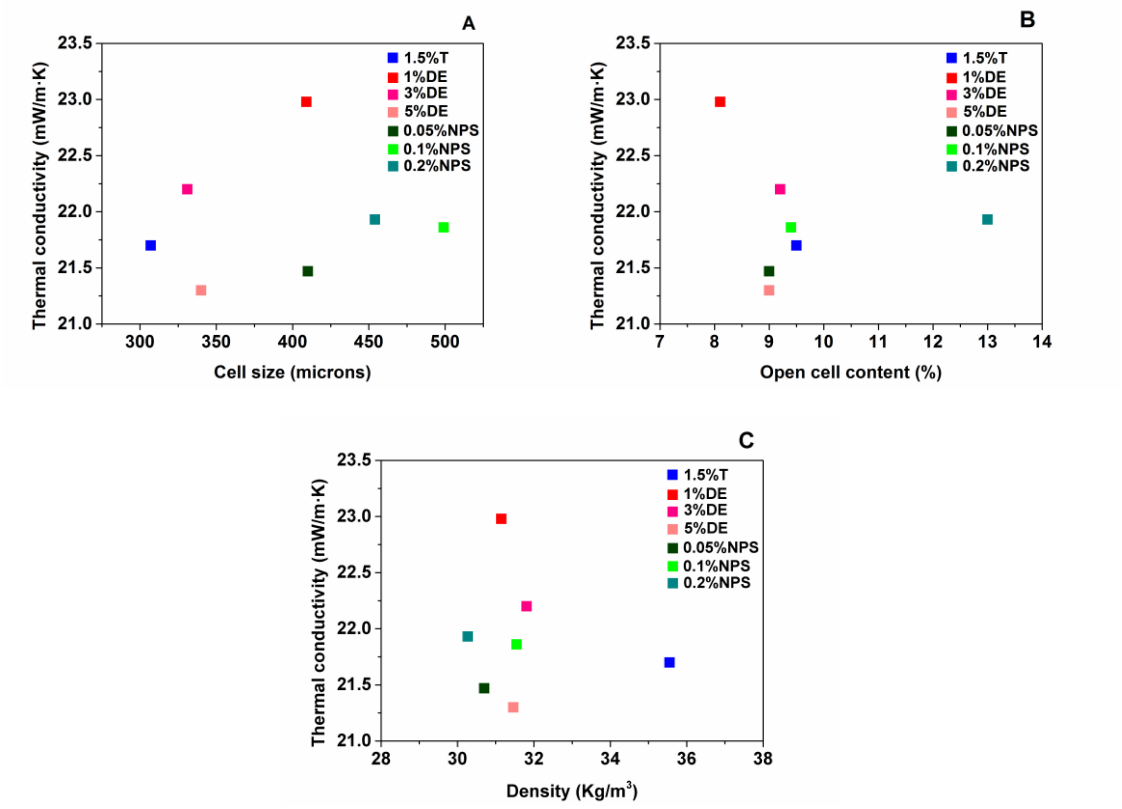

Figure 5. A) Thermal conductivity versus cell size after 5 days of the foam production; **B)** Thermal conductivity versus open cell content after 5 days of the foam production; **C)** Thermal conductivity versus density after 5 days of the foam production.

In order to analyse this change in thermal conductivity with time in the first 30 days after production, the slope of the thermal conductivity *vs.* time curve has been calculated between time 0 and 30 days. This analysis allows the variation of the rate of the concentration of gasses to be evaluated. We have found a clear relationship between the thermal conductivity slope vs time and the foaming temperature reached inside the foams during their production (**Table 2**),

as shown in **Figure 6**. Those samples reaching lower foaming temperatures (such as the systems with 5%DE, 0.05%NPS, or 0.1%NPS) display lower thermal conductivity slopes. By contrast, those samples reaching higher foaming temperatures (such as the systems with 1.5%T, 1%DE, 3%DE, or 0.2%NPS) gave higher thermal conductivity slopes. This means that the latter systems provide a very quick diffusion of the gasses out the cells. This effect can be explained taking into account the different pressure gradient of the gas inside the cells vs. the external atmospheric pressure. The developing foam is expanding against the ambient pressure until the polymerization reaction finishes, and after that the foam cools down to room temperature. Therefore, the pressure inside the cells growths depending on the amount of gas produced (which is constant in the systems herein studied) and on the temperature reached during the foaming process. When the foam finally cools down (at a cell volume approximately constant), the pressure inside the cells drops below ambient pressure, and thus the pressure in the cells would be different depending on the temperature reached during foaming. A higher temperature during foaming would cause a lower value of the pressure inside the cells and as a consequence a higher pressure gradient with the atmosphere, causing higher gas diffusion rates.

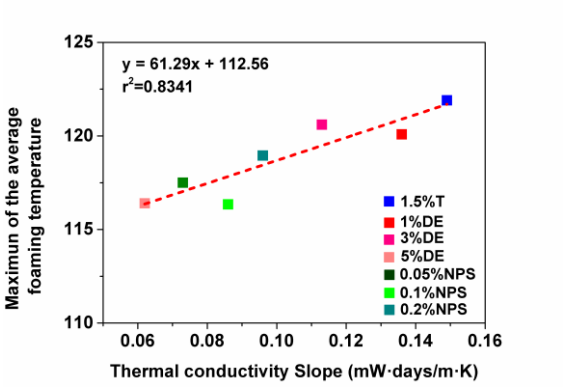

Figure 6. Maximum of the average foaming temperature curves versus thermal conductivity slope between 0 and 30 days.

Clearly, the foaming temperature in all the systems with fillers increases compared to that of the pure foam (105.9°C). A first group of foams (5%DE, 0.05%NPS and 0.1%NPS) are obtained with lower foaming temperatures displays a thermal conductivity evolution at initial time similar to that of the pure foam, as shown in **Figure 4** (**D** and **F**). In these systems there is lower pressure gradient between the cells and the atmosphere. On the other hand, the group of foams (1.5%T, 1%DE, 3%DE and 0.2%NPS) which reaches higher foaming temperatures (giving higher differences of pressure difference between the cells and the atmosphere), show a rapid growth of their thermal conductivity compared to that of the reference material. In these foams the low thermal conductivities achieved in the first days is quickly lost, due to the high diffusion of gases in them, as shown in **Figure 4** (**B**, **D** and **F**).

Figure 4 (**A**, **C** and **E**) show the thermal conductivity evolution for pure foam and for foams with fillers along 900 days. Samples with lower foaming temperatures (5%DE, 0.05%NPS and 0.1%NPS) maintain during longer times lower thermal conductivity values, because the gas diffusion is slow. Even the thermal conductivity of the system with 5%DE, which has the lowest thermal conductivity slope, is lower than that of the pure material during all the measured time (**Figure 4 D**). On the other hand, for the group of systems (1.5%T, 1%DE, 3%DE and 0.2%NPS) with higher foaming temperatures, there are some that recover the enhancement of the thermal conductivity over time. For example, the thermal conductivity value of the foam containing 1.5 wt% T is again lower than that of value of the pure material after *ca.* 400 days (**Figure 4. A**), whereas the thermal conductivity of the foam with 3 wt% DE is improved after *ca.* 300 days (**Figure 4. C**). In these cases, the recovery (1.5%T and 3%DE) or maintenance (5%DE) of the thermal conductivity reduction shown in the first measurements is remarkable (**Figure 4**). Moreover, it should be expected that the improvement of the thermal conductivity observed in the first measurements would be recovered for all the foams with fillers once they reach a stationary state where the gas concentration is the same for all of them. This is because all the foams containing fillers have lower cell sizes than the reference material.

Therefore, we have found an interesting behaviour in these systems. For those fillers increasing significantly the temperature reached during foaming there are two cross-over points of its thermal conductivity curve vs time in comparison with that of the reference foam. The first cross-over point at times lower than 30 days is due to a higher diffusion rate of the gasses inside the foam due to a low pressure inside the cells when the material cools down after foaming. The second one, occurring between 300 and 400 days after production, is due to the lower cell size of the foams containing fillers. Therefore, when the gas composition is similar to that of the reference foam the thermal conductivity is once again below that of the reference system. These considerations will be taken into account to model the thermal conductivity of the foams.

3.4. Thermal conductivity modelling

In this section, a thermal conductivity modelling is proposed in order to understand the thermal conductivity aging of the samples under study. The thermal conductivity of a RPU foam (λ^t, containing solid and gas phases) is well represented by the sum of four mechanisms: conduction along the cell walls and the struts of the solid polymer (λ^s), conduction through the gas phase (λ^g), thermal radiation (λ^r), and convection within the cells (λ^c). The addition of these contributions gives the total heat flow (λ^t) (**equations 1**)[7, 28]:

$$\lambda^t = \lambda^s + \lambda^g + \lambda^r + \lambda^c \quad \textbf{(1)}$$

The very small cell size of the foams under study (600-300 μm) makes the convective mechanism (λ^c) to be considered negligible [7, 8]. The conductive terms of the gas and of the solid phases can be estimated by **equations 2** and **3** [29]:

$$\lambda^g = \lambda_g V_g \quad \textbf{(2)}$$

$$\lambda^s = \lambda_s \frac{V_s}{3}\left(\left(f_s\sqrt{A}\right) + 2(1 - f_s)(A)^{1/4}\right) \quad \textbf{(3)}$$

where V_g is the volume fraction of the gas phase (1-ρ_r), V_s is the volume fraction of the solid phase (ρ_r), A is the anisotropy ratio, λ_g is the thermal conductivity of gas mixture, and λ_s is the thermal conductivity of solid PU (0.26 W/mK) [29]. ρ_r is the relative density (ρ_f/ρ_s), where ρ_f is the foam density and ρ_s is the solid PU density (1160 Kg/m^3).

The radiative mechanism refers to the transport of energy by electromagnetic waves, and the attenuation of radiation takes place in the forms of reflection, absorption, and scattering. The radiative conductivity can be calculated by the **Rosseland equation** [7]:

$$\lambda^r = \frac{16n^2\sigma T^3}{3K} \quad \textbf{(4)}$$

Where *n* is the effective refraction index, σ is the Stefan–Boltzmann constant, T is the mean temperature, and K is the extinction coefficient. In this case, *n* is ca. 1 because the volume of gas (porosity) of the PU foams studied here is around 97%. The radiative conductivity can be estimated by the Rosseland equation (**equation 4**) using the Glicksman extinction coefficients (K_G) that is described in the following section (**equations 5** and **6**).

3.4.1. Extinction coefficient modelling: Glicksman extinction coefficient (K_G)

The Glicksman extinction coefficient (K_G) is herein calculated for all systems studied in order to evaluate the radiative contribution of the thermal conductivity. The equation to predict the extinction coefficient of closed cell PU foams was proposed by Glicksman and coworkers [7]. They considered pentagonal dodecahedral cells as a set of randomly oriented blackbody struts that scatter radiation, and cell walls that absorb radiation. The Glicksman extinction coefficient (K_G) includes the contribution of struts (K_{edges}), and that of cell walls ($K_H K_W$)[7]:

$$K_G = K_{edges} + K_H K_W \quad \textbf{(5)}$$

$$K_G = 4.10\frac{\sqrt{f_S\frac{\rho_f}{\rho_s}}}{\phi} + (1 - f_S)\frac{\rho_f}{\rho_s}K_W \quad \textbf{(6)}$$

The extinction contribution depends on the cell size (ϕ), foam density (ρ_f), solid polyurethane density (ρ_s), mass fraction in the struts (f_S), and a constant related to the cell geometry (4.10). A value of 0.7 for the mean mass fraction in the struts is considered for this type of foams [11] [30, 31]. The cell wall contribution is valid for foams containing thin cell walls (δ < 30 μm, around 2 μm in our foams), and includes the hypothetical extinction coefficient for a uniform material which occupies the entire volume of the foam, whose

attenuation is the same to those of thin cell walls. The value of the extinction coefficient of the solid polymer (K_w =600 cm^{-1}) was obtained from the literature [7].

The values of the Glicksman extinction coefficients (K_G) calculated using **equation 6** are presented in **Figure 7**. These data show an increase of the extinction coefficient for foams with fillers, being higher for those with lower cell sizes (systems with T and DE), what implies a reduction of the radiation contribution to the thermal conductivity (**equation 4**). Therefore, the improvement of the thermal properties observed for the different materials with particles at initial times could be due to the decrease of the radiation contribution, assuming a constant gas concentration just after production.

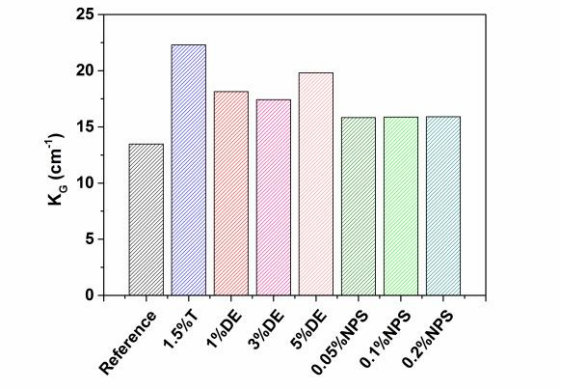

Figure 7. Calcualted Glicksman extinction coefficient for the foams under study.

3.4.2. Study of thermal conductivity of gas mixture evolution (λ_g)

The conduction through the gas phase (λ_g) is the most significant contribution to the final value of the thermal conductivity. Thus, the variations of the thermal conductivity of the gas mixture (λ_g) modify the total thermal conductivity, as can be observed in **Figure 4**. As explained previously, the gas inside the cells changes from CO_2 (14.5 mW/m•K) and CP (12 mW/m•K) to atmospheric air (25.3 mW/m•K), due to the diffusion through the PU matrix. Assuming that the conduction through the solid (λ_s) and the radiation contribution (λ_r) are time independent, the conduction through the gas contribution (λ_g) can be calculated using the thermal conductivity model (equation 1) by subtracting the solid phase and the radiation contributions from the experimental values of the thermal conductivity. The contribution of the thermal conductivity of the gas mixture (λ_g) with time can be also calculated by using the thermal conductivity model (equation 2). **Figure 8** shows the evolution of the thermal conductivity of gas mixture with time for the all the systems studied. The initial value calculated for the gas conductivity of each foam is between 13 and 16 mW/m•K, which implies that a mixture of CO_2 and CP is present in the cells (**Figure 8. A**). However, these initial values increase in different ways depending on how gas diffusion occurs for each material. Clearly, the slope of the gas mixture thermal conductivity shown in **Figure 8** follows a similar trend than those of the slopes of the thermal conductivities shown in **Figure 4**. Thus, those foams that presented a fast

thermal conductivity evolution display also a fast thermal conductivity evolution of the gas mixture (such as the systems with 1.5%T, 1%DE, 3%DE or 0.2%NPS). Nevertheless, the rest of the foams present a slightly increase of both the thermal conductivity of gas mixture and of the total thermal conductivity.

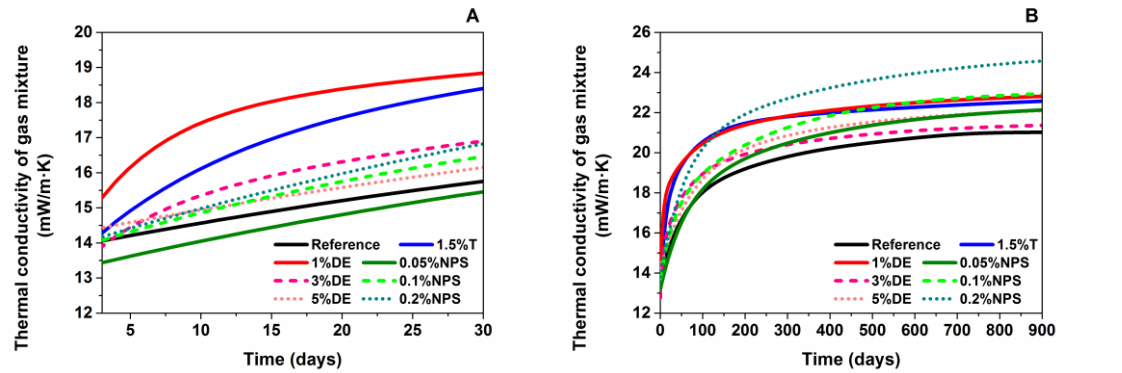

Figure 8. Thermal conductivity of the gas mixture as a function of time for all systems studied: **A)** during the first 30 days; **B)** during 900 days.

On the other hand, the value of the thermal conductivity of the gas mixture calculated after 900 days is between 20 and 25 mW/m•K, what indicates that the gas diffusion has not finished yet (**Figure 8. A**). The foam containing 0.2 wt% NPS presents the highest open cell content, and has the highest thermal conductivity of the gas mixture (around 25 mW/m•K), which means that the exchange of gases (almost all the gas inside the cells is air, whose conductivity at 20°C is 25.6 mW/m•K [32]) has practically finished.

3.4.3. Prediction of the thermal conductivity at stationary state

The thermal conductivity has been measured for 900 days, but the foams have not yet reached a stationary state at this time, as discussed in the previous section. In this section, we present a prediction of the thermal conductivity evolution supposing that the stationary state has been reached, that is, considering that all the gas inside the cells is atmospheric air. This would allow to know how the different particles added to the PU matrix affect the total thermal conductivity. **Figure 9** collects the thermal conductivity values calculated using the thermal conductivity model (**equation 1**). Clearly, the thermal properties of the foam would be enhanced by the addition of particles. This is mainly due to the decrease of the cell size, which increases the extinction coefficient (**Figure 7**), and therefore reduces the radiative contribution to the thermal conductivity. The foam containing 1.5 wt% T, which has the smallest cell size (307 µm) compared with that of reference material (608 µm), would present the highest radiative contribution reduction, and therefore the lowest thermal conductivity (around 5% lower that of the reference foam). Among the systems containing DE, the materials with 3% and with 5%DE have smaller cell sizes (331 and 340 µm respectively) than that with 1%DE (409 µm). However, a high thermal conductivity reduction (around 5%) is predicted for the foam with 5%DE in comparison to that with 3%DE because of the higher anisotropy of the later

(**Table 1**). The foams containing NPS would have a small improvement of the thermal conductivity (around 2.7 % of reduction) because their cell sizes do not decrease significantly in comparison to that of the rest of the foams with fillers (**Table 1**). Therefore, these samples present lower extinction coefficient values (**Figure 7**).

Regarding the densities of the samples, these are verysimilar to reference foam and thus this parameter does not have a signifcant influence on the thermal conductivity. Only the foam containing 1.5%T with a higher density (4 kg/m^3 more than the reference foam) could present an increase in the thermal conductivity of solid phase. However, this foam has the lowest thermal conductivity of **Figure 9**, which suggest that the reduction of the radiative contribution has a more important influence on the predicted thermal conductivity.

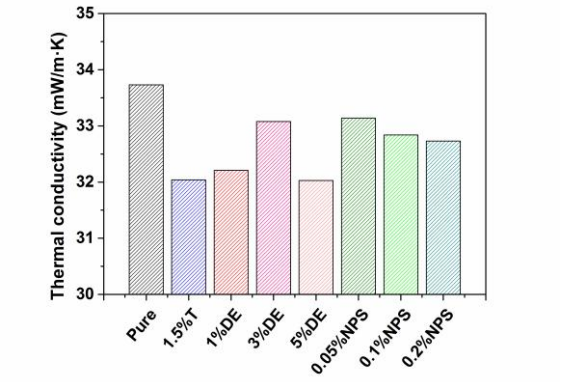

Figure 9. Thermal conductivity predicted using the thermal conductivity model assuming that air is the only gas inside the cells.

4. Conclusions

The effect of different types of particles (Talc (T), diatomaceous earth (DE) and non-porous silica (NPS)) on the thermal conductivity of the rigid polyurethane (RPU) foams with cyclopentane (CP) and water as blowing agents have been here investigated along three years of aging. The initial measurements show an improvement of the thermal conductivities due to the presence of particles into the RPU matrix, because they decrease the cell size, and thus also decrease the radiation contribution. However, the thermal conductivities evolve differently in each system, due to the variations of the gas composition inside cells with time, what in many cases leads to the loss of this first improvement of the thermal conductivity measured at initial times. We have found for the first time, a relationship between the thermal conductivity slope at initial times and the foaming temperatures reached during the foams formation. Thus, foams reaching higher foaming temperatures (systems with 1.5% T, 1%DE, 3%DE or 0.2%NPS) generate a high pressure difference between the inside and the outside of the foam cells once the material is cooled down, and consequently a very quick diffusion of the

gasses out the cells. As expected, slow diffusion of gases is observed for those foams reaching lower temperatures during their formation (systems with 5% DE, 0.05%NPS or 0.1%NPS) and as a consequence a slower rate of thermal conductivity increase vs time. Modelling the thermal conductivity of the foams allows calculating the evolution of the thermal conductivity of the gas mixture (λ_g) with time, which follows a similar trend to those of the slopes of the thermal conductivities experimentally measured. Moreover, the thermal conductivity model allows predicting the thermal conductivity values when the foams reach a stationary state (once all the gas inside the foam is air). The foams with a higher decrease of the cell size would give rise to higher extinction coefficients, and therefore to higher thermal conductivity reductions. The best systems from this point of view are T and DE.

The findings of this paper are important in the development of filled RPU foams with improved thermal conductivities. The filler has to be useful to reduce the cell size but at the same time it is needed that is does not affect the temperature of the system or that the increase of temperature associated with the addition of the filler is compensated by modifications of the formulation.

Acknowledgement

Financial assistance from MINECO, FEDER, UE (MAT2015-69234-R and RTC-2016-5285-5) and the Junta de Castile and Leon (VA275P18) are gratefully acknowledged.

References

[1] G. Oertel, Polyurethane Handbook 2nd ed., Hanser Publishers, Munich, 1993.
[2] C. Hopmann, R. Wagner, K. Fischer, A. Böttcher, One Step Production of Highperformance Sandwich Components, Cellular Polymers, 36 (2017).
[3] S.W. Choi, J.M. Jung, H.M. Yoo, S.H. Kim, W.I. Lee, Analysis of thermal properties and heat transfer mechanisms for polyurethane foams blown with water, Journal of Thermal Analysis and Calorimetry, 132 (2018) 1253-1262.
[4] H. Zhang, W.-Z. Fang, Y.-M. Li, W.-Q. Tao, Experimental study of the thermal conductivity of polyurethane foams, Applied Thermal Engineering, 115 (2017) 528-538.
[5] M. Santiago-Calvo, J. Tirado-Mediavilla, J.C. Rauhe, L.R. Jensen, J.L. Ruiz-Herrero, F. Villafañe, M.Á. Rodríguez-Pérez, Evaluation of the thermal conductivity and mechanical properties of water blown polyurethane rigid foams reinforced with carbon nanofibers, European Polymer Journal, 108 (2018) 98-106.
[6] N.V. Gama, A. Ferreira, A. Barros-Timmons, Polyurethane Foams: Past, Present, and Future, Materials, 11 (2018).
[7] L. Glicksman, Low Density Cellular Plastics: Physical Basis of Behaviour, Springer Netherlands, London, 1994.
[8] R. Hasanzadeh, T. Azdast, A. Doniavi, R.E. Lee, Multi-objective optimization of heat transfer mechanisms of microcellular polymeric foams from thermal-insulation point of view, Thermal Science and Engineering Progress, 9 (2019) 21-29.
[9] A.G.Ostrogorsky, L.R.Glicksman, D.W.Reitz, Aging of polyurethane foams, International Journal of Heat and Mass Transfer, 29 (1986) 1169-1176.

[10] M. Santiago-Calvo, J. Tirado-Mediavilla, J.L. Ruiz-Herrero, M.Á. Rodríguez-Pérez, F. Villafañe, The effects of functional nanofillers on the reaction kinetics, microstructure, thermal and mechanical properties of water blown rigid polyurethane foams, Polymer, 150 (2018) 138-149.
[11] S. Estravís, J. Tirado-Mediavilla, M. Santiago-Calvo, J.L. Ruiz-Herrero, F. Villafañe, M.A. Rodríguez-Pérez, Rigid polyurethane foams with infused nanoclays: Relationship between cellular structure and thermal conductivity, European Polymer Journal, 80 (2016) 1–15.
[12] K.E. Wilkes, D.W. Yarbrough, G.E. Nelson, J.R. Booth, Aging of Polyurethane Foam Insulation in Simulated Refrigerator Panels — Four-Year Results with Third-Generation Blowing Agents, The Earth Technologies Forum. Washington, DC, 2003.
[13] K.E. Wilkes, W.A. Gabbard, F.J. Weaver, Aging of Polyurethane Foam Insulation in Simulated Refrigerator Panels — One-Year Results with Third-Generation Blowing Agents, The Earth Technologies Forum, Washington, DC, 1999.
[14] K.E. Wilkes, W.A. Gabbard, F.J. Weaver, J.R. Booth, Aging of Polyurethane Foam Insulation in Simulated Refrigerator Panels — Two-Year Results with Third-Generation Blowing Agents, Polyurethanes Conference 2000, 2000.
[15] M. Modesti, A. Lorenzetti, C. Dall'Acqua, New experimental method for determination of effective diffusion coefficient of blowing agents in polyurethane foams, Polymer Engineering and Science, 44 (2004) 2229-2239.
[16] M. Modesti, A. Lorenzetti, C. Dall'Acqua, Long-term performance of environmentally-friendly blown polyurethane foams, Polymer Engineering & Science, 45 (2005) 260-270.
[17] I.M. Marrucho, F. Santos, N.S. Oliveira, R. Dohrn, Aging of Rigid Polyurethane Foams: Thermal Conductivity of N2 and Cyclopentane Gas Mixtures, Journal of Cellular Plastics, 41 (2005) 207-224.
[18] J. Murphy, Long-term Aging of Closed-Celled Foam Insulation, Cellular Polymers, 29 (2010) 313-326.
[19] M. Kuranska, A. Prociak, S. Michalowski, K. Zawadzinska, The influence of blowing agents type on foaming process and properties of rigid polyurethane foams, Polimery, 63 (2018) 672-678.
[20] M. Modesti, A. Lorenzetti, S. Besco, Influence of nanofillers on thermal insulating properties of polyurethane nanocomposites foams, Polymer Engineering & Science, 47 (2007) 1351-1358.
[21] G. Harikrishnan, S.N. Singh, E. Kiesel, C.W. Macosko, Nanodispersions of carbon nanofiber for polyurethane foaming, Polymer, 51 (2010) 3349-3353.
[22] A. Lorenzetti, M. Roso, A. Bruschetta, C. Boaretti, M. Modesti, Polyurethane-graphene nanocomposite foams with enhanced thermal insulating properties, Polymers for Advanced Technologies, 27 (2016) 303-307.
[23] D. Sen, A.P. Garcia, M.J. Buehler, Mechanics of Nano-Honeycomb Silica Structures: Size-Dependent Brittle-to-Ductile Transition, Journal of Nanomechanics and Micromechanics, 1 (2011) 112-118.
[24] ASTM D1622-08: Standard Test Method for Apparent Density of Rigid Cellular Plastics.
[25] ASTM D6226-10: Standard Test Method for Open Cell Content of Rigid Cellular Plastics.
[26] J. Pinto, E. Solorzano, M.A. Rodriguez-Perez, J.A. de Saja, Characterization of the cellular structure based on user-interactive image analysis procedures, Journal of Cellular Plastics, 49 (2013) 555–575.
[27] UNE-EN 12667:2002. Thermal performance of building materials and products. Determination of thermal resistance by means of guarded hot plate and heat flow meter methods. Products of high and medium thermal resistance.
[28] L. Gibson, M. Ashby, Cellular solids: structure and properties, Pergamon Press, Oxford, 1988.

[29] L.R. Glicksman, Heat transfer and ageing of cellular foam insulation, Cellular polymers, 10 (1991) 276-293.
[30] S. Pardo-Alonso, E. Solórzano, L. Brabant, P. Vanderniepen, M. Dierick, L. Van Hoorebeke, M.A. Rodríguez-Pérez, 3D Analysis of the progressive modification of the cellular architecture in polyurethane nanocomposite foams via X-ray microtomography, European Polymer Journal, 49 (2013) 999–1006.
[31] S. Pérez-Tamarit, E. Solórzano, A. Hilger, I. Manke, M.A. Rodríguez-Pérez, Multi-scale tomographic analysis of polymeric foams: A detailed study of the cellular structure, European Polymer Journal, 109 (2018) 169-178.
[32] J.R. Howell, R. Siegel, M.P. Mengu, Thermal radiation heat transfer, 5th ed., CRC press2010.

Supplementary material

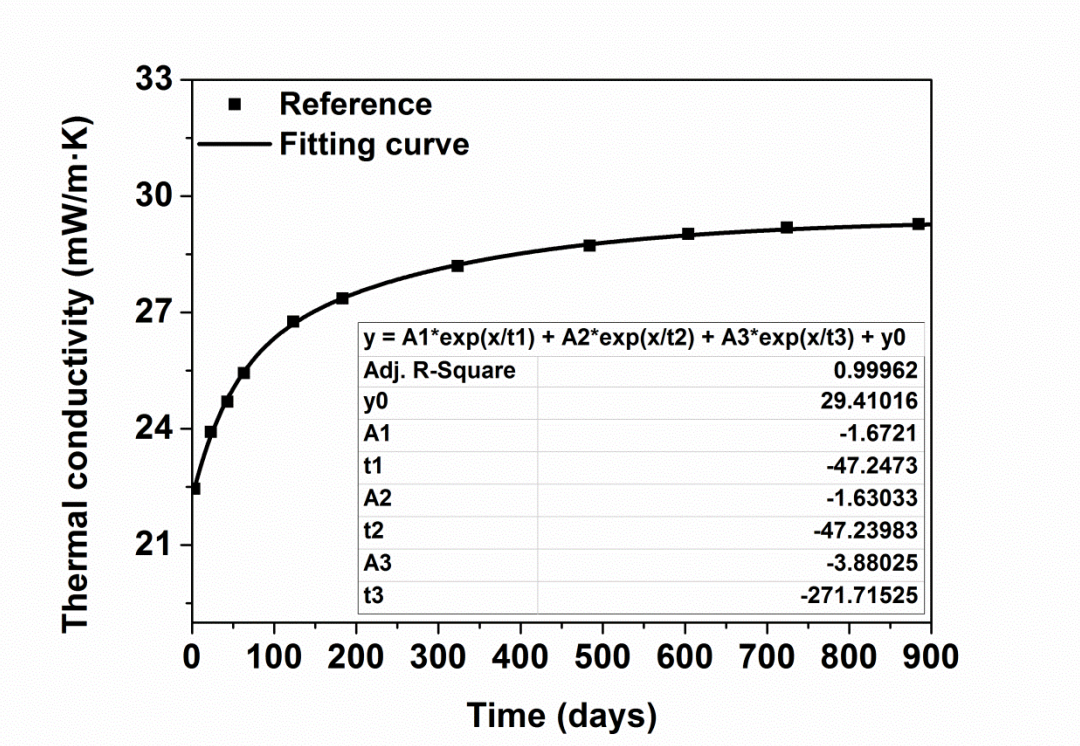

Figure S1. Measurements of thermal conductivity versus time and the corresponding fitting curve for the **reference foam.**

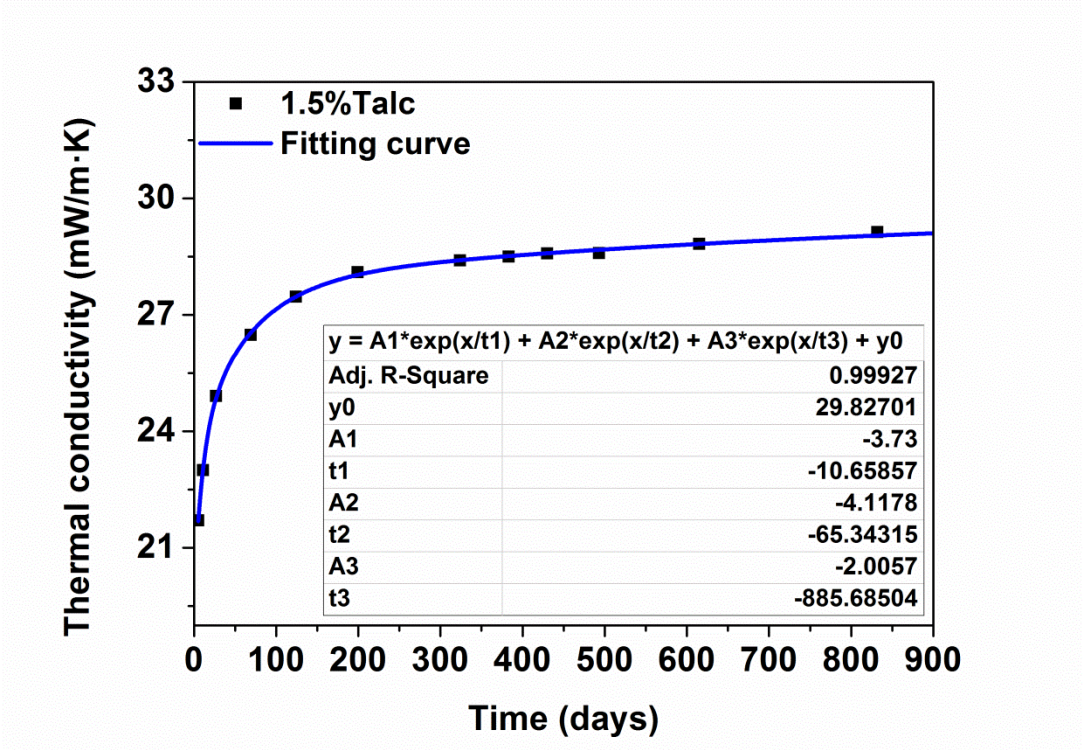

Figure S2. Measurements of thermal conductivity versus time and the corresponding fitting curve for the **foam with 1.5%Talc.**

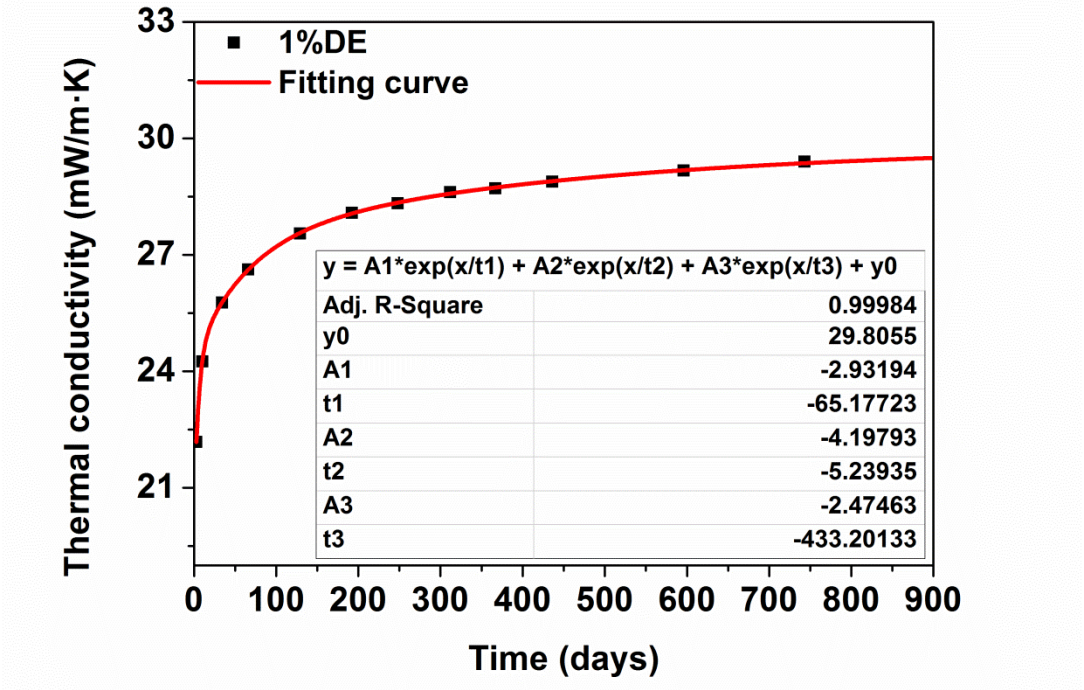

Figure S3. Measurements of thermal conductivity versus time and the corresponding fitting curve for the **foam with 1%DE.**

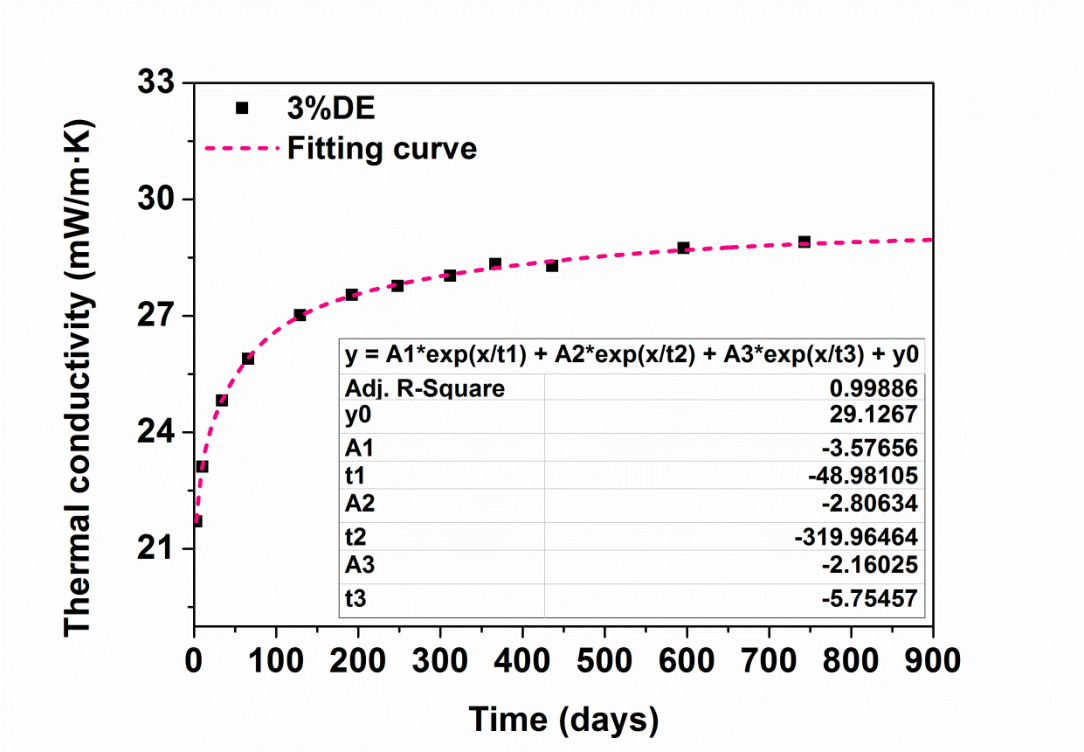

Figure S4. Measurements of thermal conductivity versus time and the corresponding fitting curve for the **foam with 3%DE.**

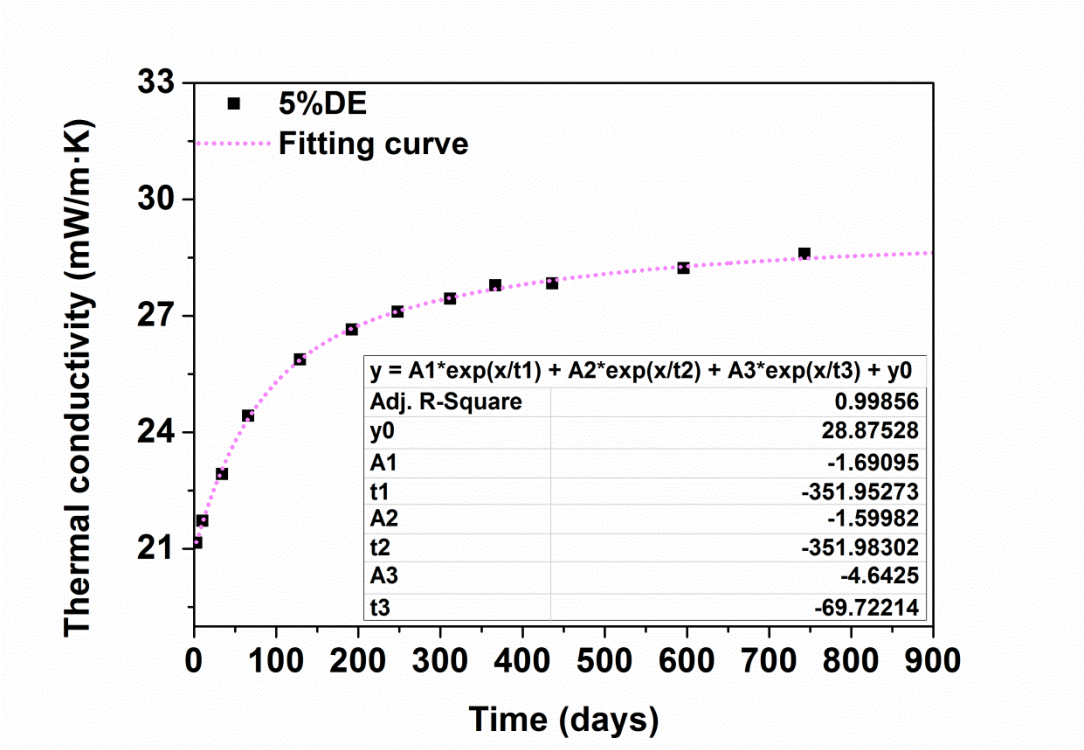

Figure S5. Measurements of thermal conductivity versus time and the corresponding fitting curve for the **foam with 5%DE.**

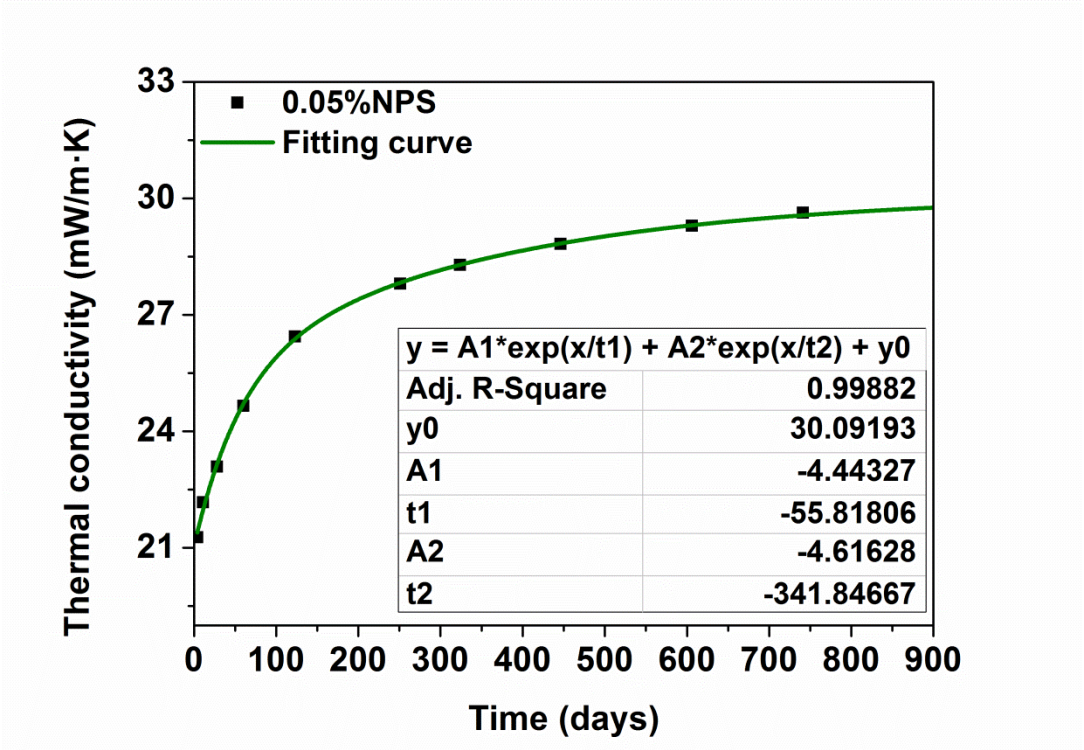

Figure S6. Measurements of thermal conductivity versus time and the corresponding fitting curve for the **foam with 0.05%NPS.**

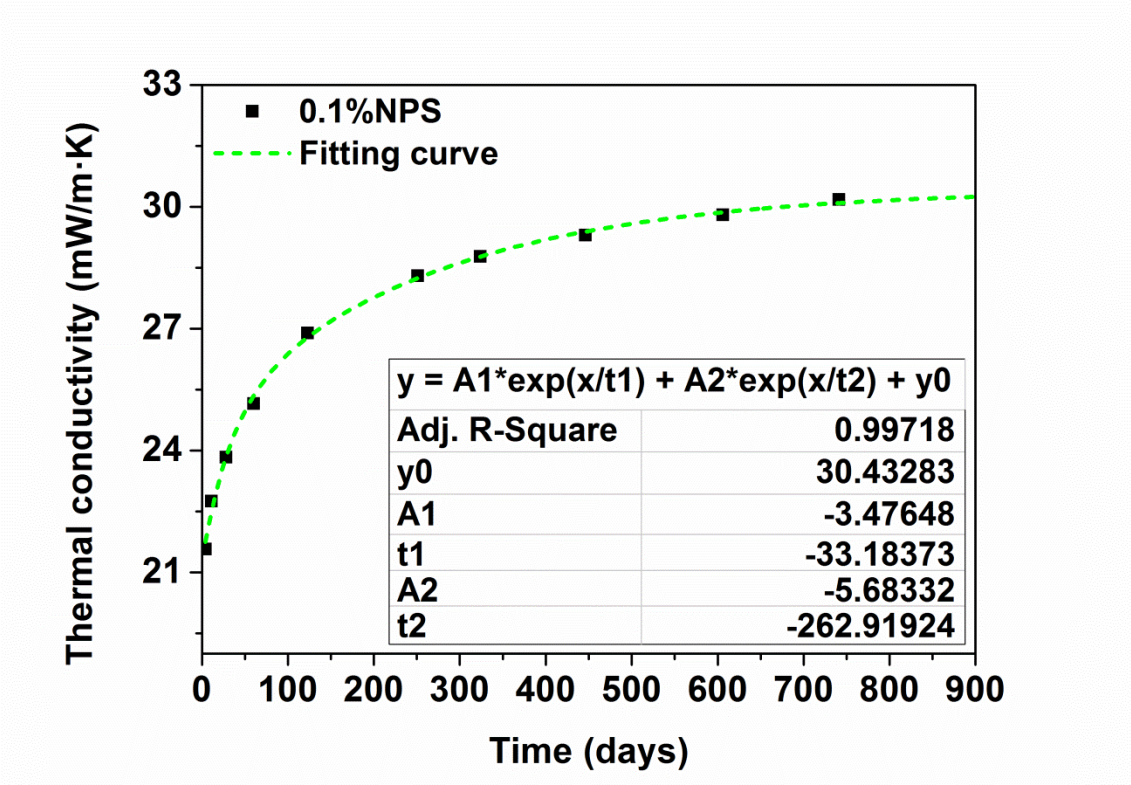

Figure S7. Measurements of thermal conductivity versus time and the corresponding fitting curve for the **foam with 0.1%NPS.**

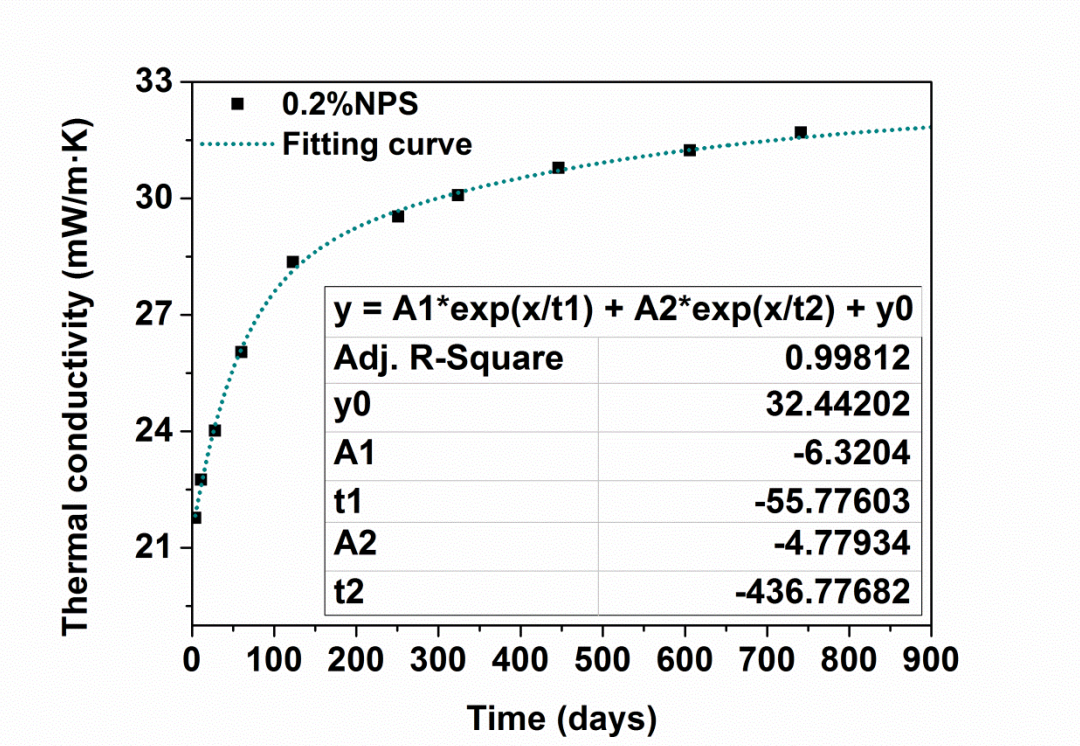

Figure S8. Measurements of thermal conductivity versus time and the corresponding fitting curve for the **foam with 0.2%NPS.**

Table S1. Thermal conductivity at time 0 obtained by extrapolation using the curve fitting functions obtained by each sample (see previous figures).

Material	Thermal conductivity (mW/m•K)
Reference	22.23
1.5%Talc	19.97
1%DE	20.20
3%DE	20.58
5%DE	20.94
0.05%NPS	21.03
0.1%NPS	21.27
0.2%NPS	21.34

CHAPTER 6:

OPTIMIZATION OF RIGID POLYURETHANE FORMULATION FROM KINETICS RESULTS TO OBTAIN RIGID POLYURETHANE FOAMS REINFORCED WITH GRAPHENE OXIDE WITH BETTER THERMAL AND MECHANICAL PROPERTIES

Mercedes Santiago Calvo

6.1- Introduction

In recent years, the addition of tiny amounts of nanofillers to the polymer matrix of polyurethane (PU) foams has allowed excellent improvements for a wide variety of physical features. This strategy is being widely studied, and several works have described the effects of nanofillers such as nanoclays, nanosilicas, carbon nanotubes (CNTs), carbon nanofibers (CNFs), graphene or graphene oxide (GO) on PU nanocomposites foams. In most of the studies, specific dispersion methods and/or special surface treatments are required in order to obtain an appropriate degree of nanofillers dispersion, which is required for superior performances. In addition, the inclusion of nanofillers into PU foams may, in many cases, modify the kinetics of the reaction, which would give rise to unexpected consequences on the final morphology of the PU matrix and on the cellular structure. Thus some properties may be improved, but others may be worsened. For this reason, understanding how the chemical reactions are modified when nanoparticles are incorporated into the PU foams should help to correct a potential reaction imbalance by changing the PU formulation. As a consequence, this strategy would allow developing PU formulations reinforced with nanofillers with positive effects on all their properties.

Two scientific articles whose main goal is **applying the methodology of monitoring the foaming process of rigid polyurethane (RPU) foams modified with nanofillers and then to optimize the PU formulation**, are included in this chapter**.** The articles are:

-Article 6: Synthesis, characterization and physical properties of rigid polyurethane foams prepared with poly(propylene oxide) polyols containing graphene oxide. European Polymer Journal 97 (**2017**) 230–240.

-Article 7: Improvement of thermal and mechanical properties by control of formulations in rigid polyurethane foams from polyols functionalized with graphene oxide. Journal of Applied Polymer Science, 136 (**2019**) 47474.

The approaches presented in this chapter in order to solve the problems mentioned for RPU nanocomposite foams have barely addressed in the previous literature. The first approach is the use of GO particles chemically linked to polyol chains, which preclude the agglomeration of nanofillers and avoid the dispersion problem previously mentioned. The second approach is to carry out an in-depth study of the effect of GO particles on the kinetics of the reactions, in order to relate the modification of reaction kinetics with the morphology of PU matrix and with the final properties of the RPU material. Finally, the kinetic information allows redefining the RPU formulation with GO, so as foam properties such as thermal and mechanical may be improved. A scheme of this chapter is shown in **Figure 6.1**.

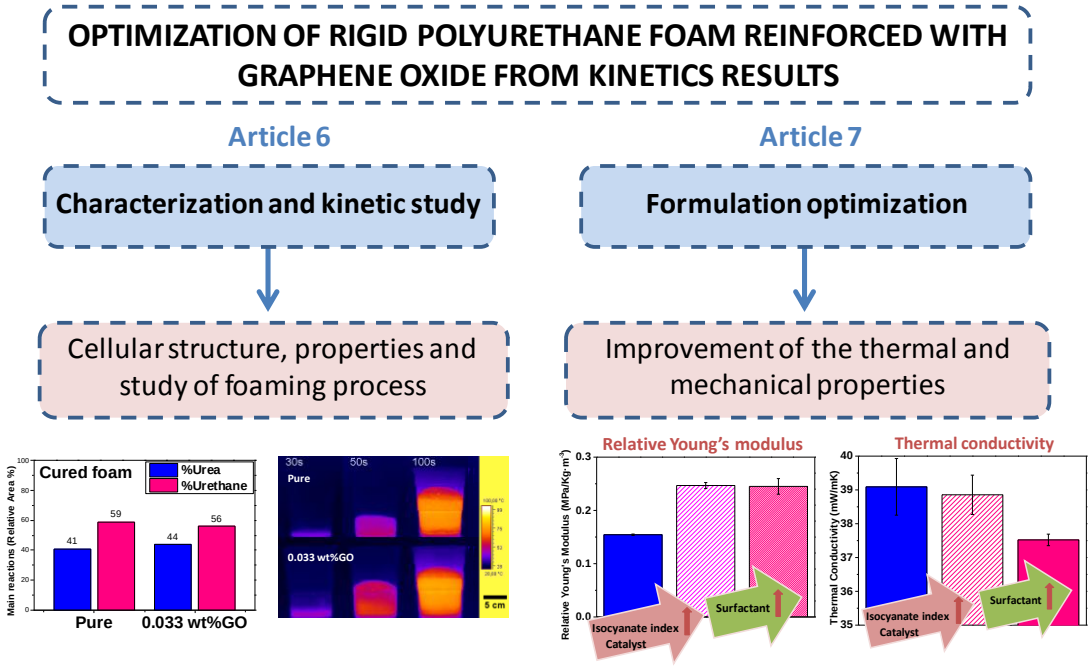

Figure 6.1. Scheme of the articles included in this chapter.

The sixth article describes the synthesis of water-blown RPU foams from polyols functionalized with very low amounts of GO (0.017, 0.033 and 0.083 wt%). In this study, the effect of GO attached to the polyols on the foaming kinetics, cellular structure, thermal conductivity and compressive mechanical properties of the RPU foams is investigated. The results of this research shows that the optimum content of GO in the final foam is 0.033 wt%. In this foam, the cell size decreases a 19%, and consequently the thermal conductivity is reduced ca. 4%, without decisive modifications of other important aspects of the cellular structure, such as density, open cell content or anisotropy. However, the Young`s modulus and collapse stress are not improved with the presence of 0.033 wt% GO, what could be due to a negative modification of the polymer morphology. For this reason, a foaming kinetic study is carried out using infrared expandometry, *in-situ* FTIR spectroscopy and temperature measurements, in order to evaluate the effects of the optimum GO content (0.033 wt%) on the foam formation process and PU morphology. The study indicates that at the beginning of the foaming process the system containing GO generates more urethane and, due to its higher viscosity, this material is able to entrap the evolving carbon dioxide, resulting in a fast expansion. On the other hand, at the late stages of the foaming process, the presence of GO enhances the blowing reaction (urea groups), due to the release of the retained water on the GO layers. Moreover, the isocyanate conversion is slightly lower for the foam containing GO, what is also consistent with the lower temperatures reached for this system.

The seventh article is based on the information collected from the previous kinetic study, so as the optimum system containing 0.033 wt% GO has been optimized in order to improve its

mechanical properties, and at the same time maintaining or improving the thermal conductivity reduction. For this purpose, a series of strategies have been followed in order to correct the effect of the GO contents on the reaction kinetics. The first strategy consists of increasing the isocyanate index or the amount of catalyst in order to promote the gelling reaction and the isocyanate conversion, which are reduced due to the presence of GO. The second strategy consists of increasing the amount of surfactant in order to stabilize the bubbles formed during nucleation. The last strategy is based on the combination of the previous strategies. The results show how, by controlling PU formulation, both the thermal and the mechanical behaviour are improved for RPU foams functionalized with 0.033 wt% GO. The highest cell size reduction (25%) and the lowest thermal conductivity (4%) are obtained for the foam, with a simultaneous increase of the isocyanate index, and catalyst and surfactant contents. Moreover, this adequate combination leads to a high improvement of a 59% of the relative Young's modulus, and of a 54% of the relative collapse stress.

In conclusion, these works have contributed to a better understanding of how the nanoparticles affect the foaming process of RPU foams. This has been managed by applying the adequate methodology in order to follow the reaction kinetics and expansion kinetics, as well as the morphology of the polymeric matrix. The information obtained from the foaming study has allowed both the optimization of a PU formulation and the correction of the undesirable changes in the mechanical properties. Thus, this chapter complies with the main objectives and motivations of this thesis (**chapter 1**, **section 1.2**).

Optimization of rigid polyurethane formulation from kinetics results to obtain rigid polyurethane foams reinforced with graphene oxide with better thermal and mechanical properties

European polymer journal 97 (**2017**) 230-240
https://doi.org/10.1016/j.eurpolymj.2017.10.013

Synthesis, characterization and physical properties of rigid polyurethane foams prepared with poly(propylene oxide) polyols containing graphene oxide

Mercedes Santiago-Calvo[1,*], Victoria Blasco[2], Carolina Ruiz[2], Rodrigo París[2], Fernando Villafañe[3], Miguel-Ángel Rodríguez-Pérez[1]

[1] Cellular Materials Laboratory (CellMat), Condensed Matter Physics Department, Faculty of Science, University of Valladolid, Campus Miguel Delibes, Paseo de Belén 7, 47011 Valladolid, Spain

[2] D.C. Technology and Corporate Venturing, Repsol S.A. C/ Agustín de Betancourt s/n, 28935 Móstoles, Spain

[3] GIR MIOMeT-IU Cinquima-Química Inorgánica, Faculty of Science, University of Valladolid, Campus Miguel Delibes, Paseo de Belén 7, 47011 Valladolid, Spain

* Corresponding author: mercesc@fmc.uva.es

Abstract

Water blown rigid polyurethane foams (RPU) are produced by using *in situ* polymerized polyols functionalized with graphene oxide (GO). The effect of the polyol functionalized with GO on the foaming kinetics, cellular structure, thermal conductivity, and compressive mechanical properties of the RPU foams is investigated. The inclusion of small amounts of GO in the system (0.017, 0.033 and 0.088 wt. %) allows reducing the cell size up to 33%. The thermal conductivity is also reduced in nanocomposites foams. The inclusion of the GO particles deteriorates the mechanical performance of the materials. On the other hand, the effect of GO on the polymerization reaction kinetics are evaluated by infrared expandometry, FTIR spectroscopy and reaction temperature measurements. These kinetic studies show that the presence of the particles induces high percentages of urea groups during foaming, and hence the resulting foams show higher expansion. Isocyanate conversion and the temperature reached for the foam containing GO slightly decrease with respect to those of the pure foam.

Keywords: Polyurethane foam, Graphene oxide, thermal conductivity, reaction kinetics

1. Introduction

Rigid polyurethane (RPU) foams present excellent features as insulating materials, and therefore they are nowadays extensively used in building, transportation insulation, refrigeration systems and pipelines, as well as in other applications [1]. The extensive use of RPU foams is mainly due to their low density, easily scalable fabrication and their low thermal conductivity, and all this favours the cost reduction and the improvement of the energy efficiency at the final product. The improvement of the thermal and mechanical responses of RPU foams may be enhanced by the incorporation of diverse fillers into the PU matrix. In particular, nanocomposites obtained after the addition of nanofillers to RPU foams, are becoming a promising option compared with conventional composites (microcomposites). Nanofillers exhibit an enormous specific surface area which allows a higher interaction with the polymer matrix, thus improving their physical properties. As a result, the addition of even low amounts of nanoparticles gives rise to important improvements of a wide variety of physical properties, such as thermal, mechanical, and barrier properties. This is particularly interesting for RPU foams, because the use of higher amounts of fillers could preclude the production of foams with the low densities required for thermal insulation. Therefore, a significant amount of studies have been published on foams based on PU nanocomposites containing different types of nanoparticles, such as nanoclays, nanosilicas, carbon nanotubes, or carbon nanofibers [2-7].

Graphene is a two-dimensional carbon allotrope with a one atom-thick planar sheet of sp^2 bonded carbon atoms densely packed in a honeycomb crystal lattice. Graphene has gathered vast attention since its discovery [8], since it is considered “the thinnest material in the universe”, showing notable thermal, mechanical and electronic properties. However, non-supported graphene cannot exist, since it will restack to give graphite, where graphene layers adhere together through π-π stacking interactions. Therefore, graphene can only be isolated on a support. Other way to stabilize individualized graphene sheets is chemical functionalization, such as the transformation into graphene oxide (GO) [9]. GO partially preserves the extraordinary graphene properties and overcome some of their deficiencies, and therefore it has been used for the fabrication of polymer-graphene nanocomposites [10]. GO is usually produced from mineral graphite flakes by thermal oxidation method [11], and is a two-dimensional material containing a high amount of epoxy and hydroxyl groups on both sides of the basal carbon plane and carboxyl groups on its edges. These oxygenated functionalities can form chemical bonds and/or non-covalent-interactions with an appropriate polymer matrix, what makes GO suitable nanofiller for polymer nanocomposites.

The number of reports dealing with RPU foams reinforced with graphene or GO is still scarce. Yan et al. [12] prepared high density (*ca*. 200 kg/m^3) RPU foams containing 0.1, 0.2 and 0.3 wt% of reduced GO (as graphene nanosheets). The foam with 0.3% of reduced GO showed a reduction of cell size by 12%, and an increase of the Young`s modulus and collapse stress by

36% and 32%, respectively. However the thermal conductivity was not improved. Bernal et al. [13] produced RPU nanocomposite foams (with density ca. 80 Kg/m^3) containing 0.17 and 0.35 wt% of functionalized graphene sheets (FGS) to obtain electromagnetic interference (EMI) shielding materials, which showed a clear reduction of the cell size by 22%. Lorenzetti et al. [14] studied the effect of 0.3 and 0.5 wt% of reduced GO (1-2 layers) on the thermal conductivity of RPU foams of density *ca.* 35 kg/m^3. The foam containing 0.3 wt% of graphene presented cell size reduction, although an increase of the graphene content up to 0.5 wt% did not decrease the cell size. The RPU-graphene nanocomposite foams showed a reduction of the thermal conductivity and a slower aging rate with respect to the pure material. In addition, the extinction coefficient was increased due to role played by the particles as IR- blockers.

In all these papers graphene or GO was added as a nanoparticle to the polyol blend and was dispersed using mechanical stirring or ultrasonication. This is a simple approach that has a main drawback: it is necessary to disperse properly the nanoparticles in the polyol. In addition, it is well known that dispersing nanoparticles in most of the cases is not a simple task, since it requires specific methods (such as high shear mixing, ultrasounds, or functionalization of the particles, for example) to reach a certain degree of dispersion. The approach followed herein is completely different and it avoids the dispersion problem previously mentioned. The polyols used have been polymerized *in situ* in the presence of GO, what allows attaching the particles to the polymer chains. This is a relatively new approach and in fact we are aware of only one previous report on polyols functionalized with graphene which are used to form RPU foams [15]. This patent describes a chemical bond method in order to prepare polyether polyol modified with reduced GO. Different RPU foams were prepared by changing the ratio between pure polyol and graphene modified polyol. The flame retardant and mechanical properties were evaluated in the materials obtained. The results of this patent show that all RPU foams reached V-0 in the UL94 test, whereas the smoke release rate of RPU foams containing graphene was significantly reduced with respect to the reference material. In addition, the tensile strength of the RPU foams was significantly improved. In spite of these promising results, this work do not report in detail how density, cellular structure and thermal conductivity and the PU reaction kinetics are affected by the presence of graphene in the polyol.

Taking the previous ideas in mind, herein we present a detailed study on RPU foams produced from a polyol functionalized with GO. Low amounts of GO (0.017, 0.033 and 0.083 wt%) are used in order to maintain a viscosity of the polyol allowing the production of RPU foams. The influence of the amount of GO in the polyol on density, cellular structure, thermal conductivity and mechanical properties are herein described. Moreover, a kinetic study is carried out by FTIR spectroscopy, infrared expandometry and temperature evolution, in order to evaluate the effects of GO on the foam formation process.

2. Experimental

2.1. Materials

IsoPMDI 92140 (31.5% NCO, density 1.23 g cm^{-3}, viscosity 170-250 mPas), a polymeric diphenylmethane diisocyanate (pMDI) from "BASF Poliuretanos Iberia S.A", was used to produce the rigid polyurethane foams. TEGOAMIN® DMCHA (N,N-dimethylcyclohexylamine) from Evonik, was used as gelling and foaming catalyst. TEGOSTAB® B 8522 (a non-hydrolysable poly-ether-polydimethyl-siloxane–stabilizer) from Evonik, was used as a surfactant. Distilled water was used as a blowing agent.

2.2. Synthesis of polyols functionalized with GO

Graphene Oxide (Graphenea S.A.) was dispersed in the triol initiator using UltraTurrax for 15 minutes at room temperature. The mixture was then added to the polymerization reactor (2 L, 600 rpm) and heated to 50 °C in presence of Propylene Oxide (Repsol) at 1 Bar of pressure and 2000 ppm of acid catalyst, according to Appel *et al*. [16]. Polymerization was stopped when a constant pressure was reached. Four poly(propylene oxide) polyols were synthesized: the pure polyol, and those containing 500, 1000 and 2500 ppm of GO.

2.3. Characterization of polyol functionalized with GO

The hydroxyl number in mg of KOH per grams of polyol and polyols functionalized with GO was calculated according to ASTM D-4274.

Brookfield viscosity was determined at 25°C using a Brookfield DV-III ULTRA Rheometer.

Glass transition temperature (T_g) was taken from the second heating in differential scanning calorimeter (DSC) experiments. Non isothermal (10°C/min from -85 to 200°C) experiments were carried out using a DSC TA Instruments Q2000 under nitrogen flow, operating with an intra-cooler under nitrogen flow. Temperature and heat flow calibrations were performed with indium as standard.

Weigh-averaged molecular weights (M_W) and polydispersity index (PDI) were determined against PEG standards by gel-permeation chromatography (GPC) using a Bruker 3800 equipped with a deflection RI detector. Tetrahydrofuran at 1 mL/min flow rate was used as eluent at 30°C.

2.4. Preparation of rigid polyurethane/graphene oxide nanocomposite foams

Four different RPU foam systems were studied: the pure material (without GO, obtained as reference material), and those containing 0.017 wt% GO (500 ppm in polyol), 0.033 wt% GO

(1000 ppm in polyol) and 0.083 wt% GO (2500 ppm in polyol) with respect to the final mass of RPU foams.

An overhead stirrer (EUROSTAR Power control-visc P1, IKA) with a 50 mm diameter Lenart disc stirrer was used to premix the polyol (100 parts by weight (ppw)) with catalyst (1 ppw), surfactant (1 ppw), and blowing agent (5 ppw) during 2 minutes at 250 rpm to obtain homogenous polyol blends (Part B). Part B and the isocyanate (Part A) at an isocyanate index of 120 were mixed in a plastic cup at 1200 rpm for 10 seconds. After the foaming, the curing process was extended for 2 days at room temperature, and then the foam samples were cut for characterization.

2.5. Foams characterization

Foam density was measured as described by ASTM D1622/D1622M-14 [17]. Density was determined in three different samples for each material, with a diameter of 30 mm and a height of 25 mm.

After measuring the densities in the samples, open cells content (OC%) was measured by using a gas pycnometer Accupyc II 1340 from Micromeritics, according to ASTM D6226-10 [18].

The cellular morphology of the foams was observed by Scanning Electron Microscopy (SEM) with a JEOL JSM-820 microscope. The growth plane (z plane) of cured foams was examined by SEM after vacuum coating with a gold monolayer. An image analysis technique [19] of SEM micrographs was used to determine the main characteristics of the cellular foam structure: mean cell size (Φ_{3D}), anisotropy ratio (AR) and cell size distribution. The calculated statistical parameters for cell size distribution were: standard deviation (SD), normalized standard deviation (NSD) (i.e. SD/ Φ_{3D}), and asymmetry coefficient (AC). NSD provides information about the homogeneity of the cell size distribution: homogeneous cell distributions present small values of this parameter. AC measures the degree of asymmetry of the distribution, so as a negative AC indicates that the smaller cells are more separated from the mean cell size than bigger ones, and vice versa. More than 150 cells of different areas of each material were used for this analysis. The detailed calculation of the cellular structure parameters are explained in the work by Pinto et al. [19].

FTIR spectra of the cured foams were collected using a Bruker ALPHA spectrometer by attenuated total reflectance (ATR) method. Polymer morphology and polymer composition of RPU foam was analyzed using deconvolution of amide I region (carbonyl region) of FTIR spectrum. The deconvolution was performed using the same method described in the following section dealing with the kinetic studies by FTIR spectroscopy.

Thermal conductivity was determined at room temperature by using a hot-disk transient plane source (TPS) thermal constant analyzer, according to ISO 22007-2:2008 method [20]. The measurements were performed using two cylindrical samples for each material with a diameter of 30 mm and a height of 25 mm. A disk shaped TPS sensor with a radius of 3.189 mm was used for all measurements, after being located in contact with the xy plane (perpendicular to growth plane) of the two samples [21]. Several measurements were performed until 40 days after the foams were produced. At that time the samples have reached the stationary state, considering that all the CO_2 generated during foaming have diffused outwards the foam by then, and it has been replaced by atmospheric air [5].

Mechanical properties in compression were measured at room temperature by using an Instron Machine (model 5.500R6025), according to ASTM D1621-10 [22]. Stress (ρ)–strain (ε) curves were obtained at a strain rate of 10 mm/min and the maximum static strain was 75% for all the experiments. The compression tests were performed in a direction parallel to the growing direction for three different samples of each material, with a diameter of 30 mm and a height of 25 mm. The samples were prepared with rigorously parallel contact surfaces. Young´s modulus (E) and collapse stress (σ_C) were calculated from the stress-strain curves.

2.6. Kinetics studies

Reaction kinetics for the reference material and for the material containing 0.033 wt% GO (1000 ppm in polyol) were studied by *in situ* FTIR, temperature evolution and IR expandometry.

In situ FTIR spectra of the samples were collected using a Bruker ALPHA spectrometer by attenuated total reflectance (ATR) method. 1 mL of the reacting foam was poured on an ATR cell to obtain the variation of FTIR spectra *versus* time. The addition of the isocyanate was taken as t = 0 for the reaction, and the maximum elapsed time between the addition of isocyanate and the acquisition of the first scan was 40 seconds. Each FTIR spectrum was obtained after 16 scans, with a resolution of 4 cm^{-1} for the range 4000-400 cm^{-1}. In order to reproduce the large scale foam temperature profile, the experiment was carried out at 70°C, as the spectrometer contains a heating device. A background spectrum was deduced from each reaction spectra, and a total of 60 spectra were taken for each experiment, which lasted 30 minutes. Baseline correction was conducted in order to correct the shifts from temperature changes in each spectrum. According to the literature,[23, 24] the asymmetric CH stretching band at 2972 cm^{-1} (which remains constant during the reaction) was used as internal reference band. The results herein reported are the average of three kinetics experiments.

The overlapped absorptions in the amide I region (carbonyl region) (1601-1760 cm^{-1}) were deconvoluted using Gaussian bands in order to follow separately the blowing and gelling reactions occurring during the foaming process. Curve fittings were adjusted by literature methods [25, 26] and the hidden bands were identified following the second derivative technique. The deconvolution range (1790-1570 cm^{-1}) allows an admissible adjustment and

avoids the absorption effects of side bands from the aromatic C=C ring stretching and from amide II bands.

The temperature profiles during foaming process were measured. Four thermocouples type K were introduced in a plastic cup of 11.5 cm of diameter and 14 cm of height in order to measure the temperature during 30 minutes at four different positions. As seen in Figure 1, thermocouples were placed vertically in the centre of plastic cup at the following heights from the base of the cylinder (**Figure 1**): 0.5 cm (thermocouple 1, T1), 2.0 cm (thermocouple 2, T2), 6.5 cm (thermocouple 3, T3) and 12.5 cm (thermocouple 4, T4). The data collected by the thermocouples were registered in a computer.

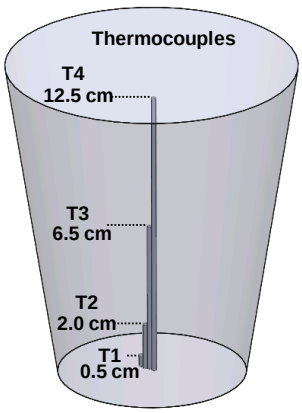

Figure 1. Schematic view of the system of thermocouples inside the plastic cup.

IR expandometry was used to measure expansion height and volume, expansion rate, expansion acceleration and maximum surface temperature reached. In this technique the foaming process is followed by using an infrared camera that records the variations of the surface temperature during foaming. The IR camera used in this paper was HotFind L from SDS Infrared. 25 images are taken every 1 second. Once all the images are taken and by using image analysis it is possible to measure the aforementioned characteristics [27].

3. Results and Discussion

3.1. Polyol characterization

Typically, poly(propylene oxide) polyols are produced by reacting a triol initiator with propylene oxide (PO) as shown in **Scheme 1** for a 3-arm polyol. The presence of GO in the reaction mixture may favour polyol linear chain grafting, since the hydroxyl groups of GO could

react with PO [16]. Therefore, polyether polyols grafting onto the GO surface are obtained. Due to the incorporation of the GO in the polyol during the synthesis it is possible to obtain an excellent dispersion of the particles solving the always difficult challenge of dispersing the particles.

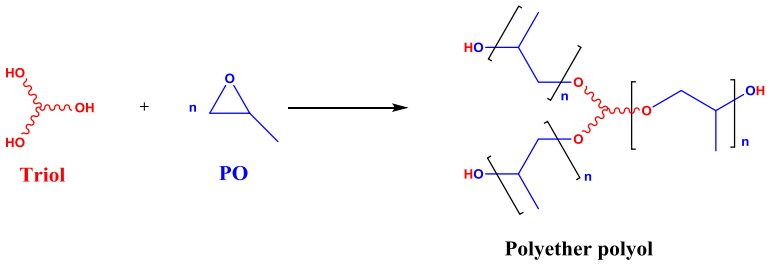

Scheme 1. Synthesis of polyether polyol.

The properties of the resulting polyether polyols are summarized in **Table 1**. The first column shows the decrease of the the hydroxyl number with the inclusion of GO, being the polyol with 1000 ppm GO that showing a lower value. The decrease of the hydroxyl number for polyols functionalized with GO could be due the reaction of some hydroxyl groups of the polyether polyol components with GO during the synthesis of the polyether polyols.

In addition, the viscosity slightly increases for the polyols containing 500 ppm and 1000 ppm GO, and it is obviously higher for the polyol containing 2500 ppm GO. In general, the viscosity is related to molecular weight. As can be appreciated on **Table 1**, the viscosity raises with the increase of the weigh-averaged molecular weight (Mw) of the polyol. The Mw value grows with the amount of GO, indicating that the GO promotes the polyol linear chain grafting, as has been mentioned previously [16]. Furthermore, the distribution of the molecular weights in the polyol is determined by the polydispersity index (PDI), which is almost constant in all the polyols prepared.

On the other hand, **Table 1** collects the glass transition temperatures (Tg), which slightly decreases when GO is added. The polyol with a higher amount of GO presents the smallest value of Tg, being this polyol that showing the higher polydispersity index.

Table 1. Properties of polyol functionalized with GO compared with the pure material.

Polyol	Hydroxyl number (mg KOH/g)	Viscosity (mPa·s at 25°C)	Tg (°C)	Mw (Dalton)	PDI
Pure	426.4	476.9	-59.6	488	1.2
500 ppm GO	399.3	553.3	-60.4	494	1.1
1000 ppm GO	358.6	547.6	-61.0	570	1.1
2500 ppm GO	377.5	4463.2	-62.8	675	1.3

3.2. Density and Cellular structure characterization

Different physical properties of the foams were determined, and the values obtained are collected in **Table 2**. The density of the foams containing 0.017 and 0.033 wt% GO increases 1 kg/m^3 compared to that of the pure material, whereas the density of the foam containing 0.083 wt% GO increases around 3-4 kg/m^3. This could be related to the significant increase of the polyol viscosity when a high GO content is incorporated (**Table 1**). The open cell content (OC) for the foam with 0.017 wt% GO is similar to that obtained for the reference foam. However, there is an evident increase of the OC with the GO addition, being the foam with the highest GO content (0.083 wt%) that showing the highest value (*ca.* 42%).

The SEM micrographs in the growth plane (**Figure 2**) allow obtaining the main characteristics of the cellular structure (**Table 2**). It is remarkable that the incorporation of small amounts of GO into polyol promotes an important cell size reduction of up to 33% for the material containing 0.083 wt% GO, demonstrating its effectiveness as cell nucleating agent. This reduction is clearly observed in the SEM micrographs shown in **Figure 2 b-d**. In addition to the clear modification of cell size, samples with low GO contents (equal or below 0.033 wt%) present similar anisotropy ratios (AR) than the reference foam. However, this anisotropy ratio is reduced for the sample with higher GO content (0.083 wt% GO). This is probably due to some cells degeneration occurring in these samples which also promotes a large open cell content, higher NSD and AC and a higher density.

The histograms and gaussian fitting depicted in **Figure 3**, as well as other quantitative information collected in **Table 2**, give extra information about the cell size distribution. Samples up to 0.033 wt% GO show a good homogeneity of the cell size distribution (small values of NSD) and a symetric distribution, with values of AC near to zero. However, the cell size distribution of the foam with 0.083 wt% GO is less homogeneous, considering its high value of NSD (0.55), and its highly asymmetric distribution, with a high and positive value of AC (1.33). As previosly mentioned, this is probably due to the degenation of the cellular structure due to cells coalescence.

Table 2. Density, open cell content (OC), mean cell size (Φ3D), standard deviation (SD), normalized standard deviation (NSD), asymmetry coefficient (AC) and anisotropy (AR) for each foam obtained.

Material	Density (Kg/m^3)	OC (%)	Φ_{3D} (μm)	SD	NSD	AC	AR
Pure (reference)	30.1±0.8	11.03±1.01	529	178	0.34	0.30	1.46±0.47
0.017 wt% GO	31.1±0.9	10.45±0.04	489	139	0.28	-0.32	1.54±0.38
0.033 wt% GO	31.7±0.7	14.05±1.93	427	140	0.33	0.15	1.57±0.36
0.083 wt% GO	34.0±2.0	41.58±10.79	355	177	0.55	1.33	1.25±1.31

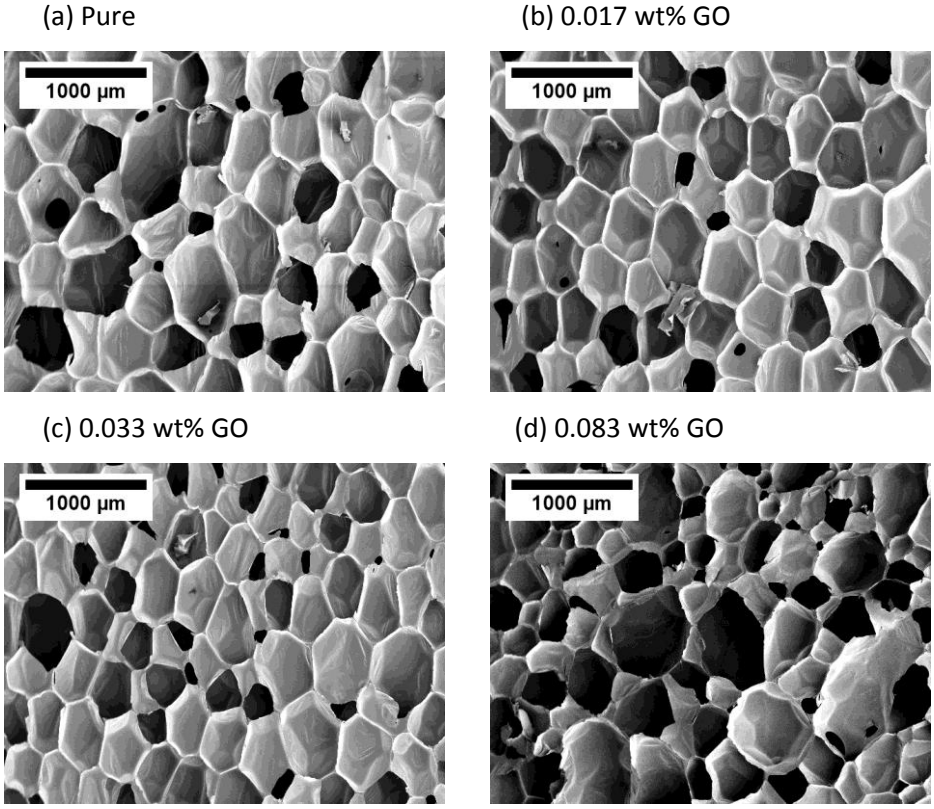

Figure 2. SEM micrographs for the growth plane of the foam: **(a)** Pure material (reference), **(b)** with 0.017 wt% GO, **(c)** with 0.033 wt% GO and **(d)** 0.083 wt% GO.

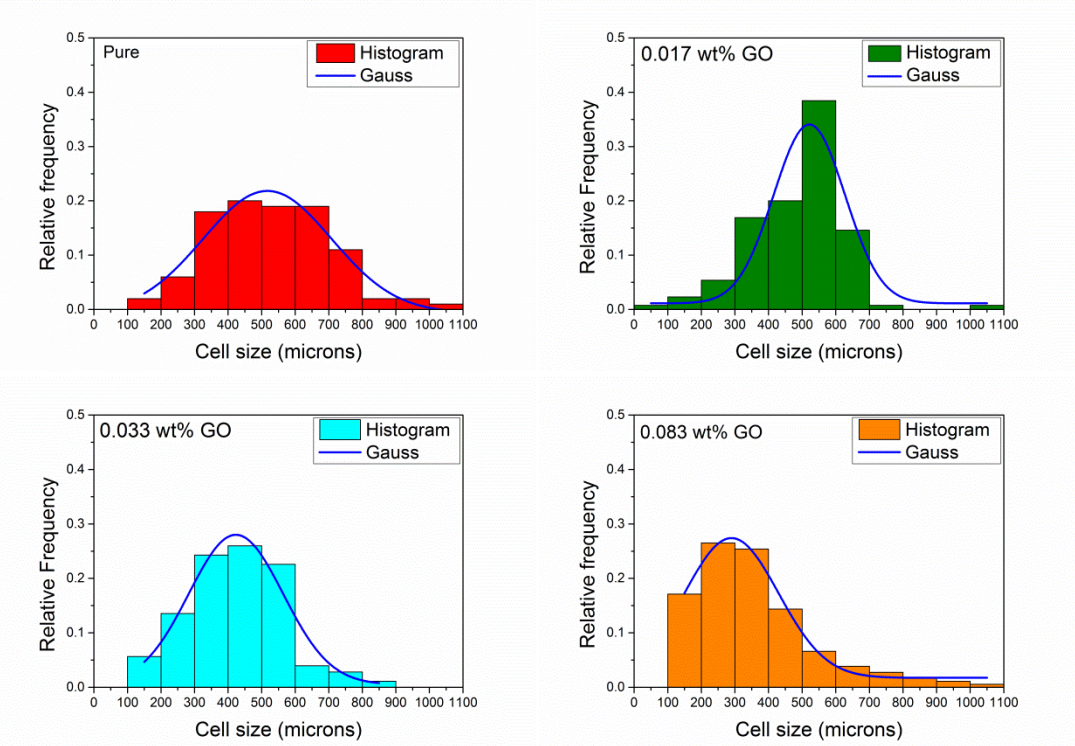

Figure 3. Cell size distributions and gaussian fits for each distribution.

3.3. Polymer morphology characterization

RPU foams present a complex polymer morphology composed of alternant soft and hard segments. Hard segments derive from the reactions of isocyanate with water and/or hydroxyl groups give rise to foam stiffness, while soft segments from polyols provide foam elasticity. The polymerization reaction creates progressively a chemical crosslinking network of RPU foams, while blowing reaction generates polyurea segments whose different polarity and chemical incompatibility with polyol segments tends to aggregate via hydrogen bonding, thus originating microphase separation domains [28]. The polyurea hard segments in foams have stronger specific hydrogen-bonding interaction and high stiffness compared to the urethane hard segments found in most elastomers. For this reason the hydrogen-bonded urea, in particular ordered urea, is frequently used for estimating the degree of microphase separation [29, 30], and has a significant influence on the mechanical properties of RPU foams. Therefore, we decided to study the composition of the PU matrix by the deconvolution of the carbonyl region of the cured RPU foams [30]. The carbonyl region comprises the different urea and urethane groups formed during the foaming process. The data collected in **Table 3** shows how the presence of GO alters the main PU reactions, and create changes in the hydrogen bonding

network of PU nanocomposites. **Table 3** shows that cured foams containing GO present a total percentage of urea slightly higher than that of the reference foam. This indicates that the blowing reaction has been favoured, being the isocyanate conversion around 90% for all the foams studied. A more detailed examination of the different types of hydrogen bonding may be inferred from these data. In general the percentage of ordered urea is slightly suppressed by the increase of GO, what indicates a lower degree of microphase separation. However, the development of the free urea in foams with GO increases and free urea is dissolved in polyol-rich soft domains, while the amount of disordered hydrogen-bonded urea enhances, and can be found both within the phase mixed and as phase-separated. Furthermore, the percentage of hydrogen-bonded urethane increases, whereas free urethane goes down with the incorporation of GO in the RPU foams.

The analysis of the polymer morphology allows concluding that the addition of GO generates a slight decrease of the polymerization reaction and, consequently, lower formation of chemical crosslinking network inside RPU foam. In addition to that, the incorporation of GO favours the blowing reaction, but there are more urea hard segments dissolved in polyol-rich soft domains than urea microphase separation domains. It is well known that these two modifications should have a negative influence on the mechanical properties of RPU foams with GO [28, 31, 32], as discussed below.

Table 3. Relative area percentage of the absorbances of urea and urethane carbonyls detected in the amide I region after one month when foams are cured [33].

Material	Urea relative area %			Urethane relative area %		Main reaction relative area %	
	% Ordered H-Bonded urea carbonyl	% Disordered H-Bonded urea carbonyl	% Free Urea carbonyl	% H-Bonded urethane carbonyl	% Free urethane carbonyl	% Total Urea	% Total Urethane
Pure (reference)	23.1	17.6	18.1	29.4	29.4	41.2	58.8
0.017 wt% GO	23.0	17.7	20.6	29.6	26.8	43.6	56.4
0.033 wt% GO	23.4	17.9	20.3	29.7	26.7	43.6	56.4
0.083 wt% GO	22.3	17.3	19.9	29.5	28.2	42.3	57.7

3.4. Thermal conductivity

Thermal conductivity is a crucial parameter for RPU foams, given their applications as insulation materials. The values of the thermal conductivity of PUR foams (pure and containing GO) is shown in **Figure 4**. These thermal measurements were performed 40 days after the foams production, when the foam has reached a stationary state, what means that the

foaming agent inside the cells (CO_2 generated during the foaming reaction) has been totally substituted by atmospheric air [5].

It is well known that thermal conductivity generally decreases with cell size reduction and/or with an increase of the extinction coefficient, as both modifications reduce the radiative contribution to thermal conductivity [5, 34-36]. These effects are clearly seen in the samples under study. **Table 2** shows a significant cell size reduction with the addition of GO from 529 µm for pure material to 355 µm for the foam containing 0.083 wt% GO. Moreover, it is expected that the GO attached to polyol chains will be properly distributed in the walls and struts of the foams. Since GO is an infrared radiation blocker, it would increase the extinction coefficient of the cell walls and struts, decreasing the radiative contribution of the thermal conductivity of these foams.

Therefore, these results indicate the addition of very small amounts of GO (from 0.017 wt% to 0.083 wt%) enhances the thermal properties, which reach a minimum for 0.033 wt% GO. The thermal conductivity is reduced around 5% in comparison with the reference material. When the amount of GO is increased to 0.083 wt%, the maximum cell size reduction is achieved. Despite this, the thermal conductivity of the foam containing 0.083 wt% GO is higher than expected, and this seems to be due to the significant modifications observed in the cellular structure in this material, which has a higher density, a more heterogeneous cellular structure, and a high open cell content (**Table 2**). Moreover, an increase in the GO content could induce an definite increment of the contribution to conduction through the solid phase [37].

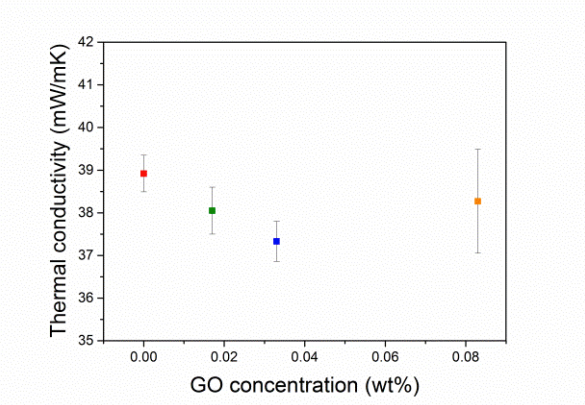

Figure 4. Thermal conductivity values for PU nanocomposite foams.

3.5. Mechanical properties

The compression behaviour of the foams containing GO has been also measured. As the foams studied have slightly different densities, and density plays a significant role on the mechanical properties, we have used the scaling relationship between mechanical properties and density [38] in order to exclude the effect of density on the properties. For this reason **Figure 5** collects the relative collapse stress and relative Young's modulus (collapse stress and Young's modulus divided by the density of the foam sample).

As shown in the figure, the mechanical properties decrease with the increase of GO content, and they are always lower than those of the pure material. This reduction of these properties is small for the two materials containing lower amounts of GO particles, and it is more significant for the materials containing the highest amount of GO. For the samples with low GO contents this slight decrease should be related with a different polymer morphology in the matrix of the foams, because the cellular structure of two materials is not worse than that of the reference foam. This has been already explained in the section dealing with polymer morphology characterization. For the material with a high amount of GO (0.083 wt%) the decrease should be a combination of the mentioned modification of the polymer morphology with the deterioration of the cellular structure already described.

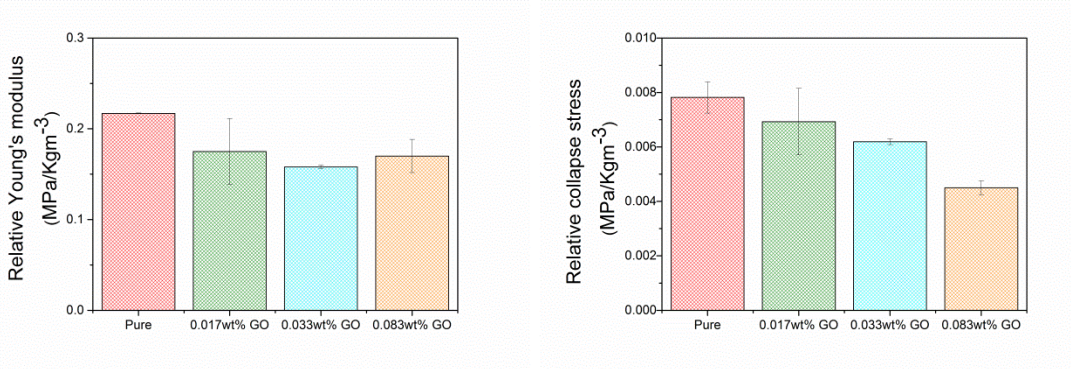

Figure 5. Relative Young's modulus and relative collapse stress for PU nanocomposite foams.

3.6. Kinetic study

RPU foam formation involves two main competing reactions of polymerization and foaming: the reaction of isocyanate with polyol (gelling or polymerization reaction) produces urethane groups, whereas the reaction of isocyanate with water (blowing or foaming reaction) gives rise to the foam expansion by formation of CO_2 and final formation of urea groups [1]. In order to obtain a PU foam with the desired cellular structure and physical properties, an adequate control of these two simultaneous reactions is required. Therefore, a kinetic study would help to understand the changes in the reaction kinetics and the overall kinetic balance of the system under study. The analysis of cellular structure and of thermal properties described

above indicates that the optimum properties are obtained for the PU foam containing 0.033 wt% of GO. Therefore, this system has been chosen to identify the effect of the presence of GO on the reaction kinetics.

Infrared expandometry

The exothermic nature of the foaming process allows following the expansion kinetics of RPU foams by infrared expandometry [27]. **Figure 6** shows six selected images of the growing foams taken with the infrared camera. The comparison of the two first images (at 30 and 50 seconds) leads to conclude that the foam containing GO grows faster than pure foam in a first stage (until *ca.* 50s). However, from this moment the evolution of both foams is similar.

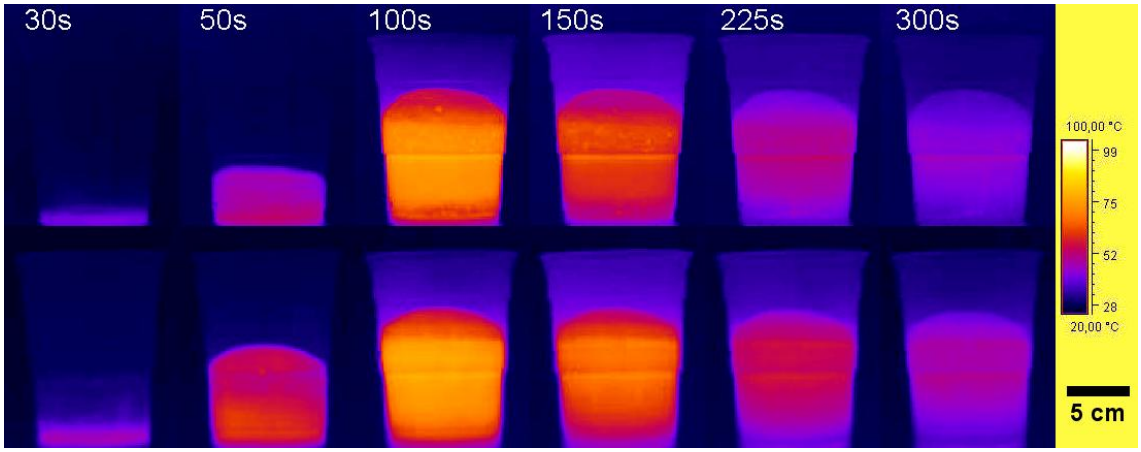

Figure 6. Comparative images of infrared camera for the pure foam (above) and the foam containing 0.033 wt% GO (below) at different reaction times.

Height and volume evolution *versus* time are presented in **Figure 7**. Both sample height and volume are slightly higher for the foam containing 0.033 wt% GO than for the pure foam (*ca*. 0.5 cm and *ca*. 80 cm^3, respectively). Both foams reach the final expansion approximately at the same time.

Moreover, expansion rate and expansion acceleration were also studied, and the results are shown in **Figure 8**. The foam containing 0.033 wt% GO reaches faster and with higher acceleration the maximum expansion rate and acceleration (*ca*. 10 seconds), both being slightly higher (ca. 2 cm^3/s and 0.1 cm^3/s^2 respectively) than those of the pure foam. After that, the expansion rates are similar for both samples.

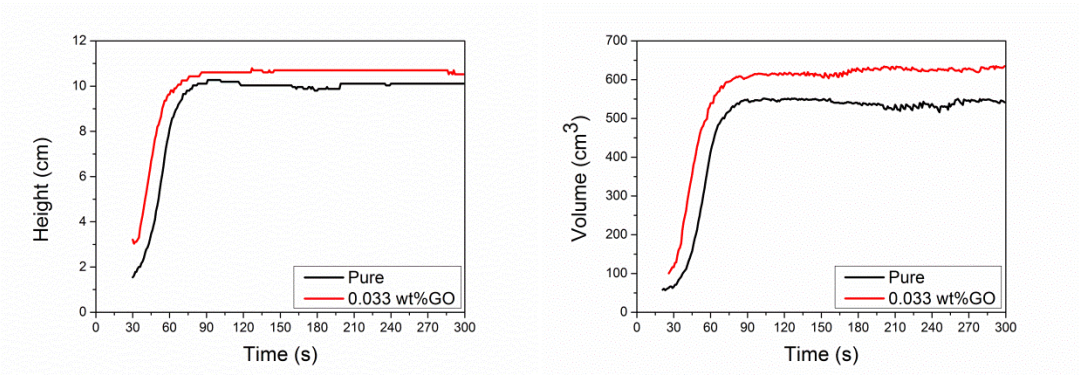

Figure 7. Sample height (left) and sample volume (right) from the expandometry monitorization results for the pure foam (in black) and for the foam containing 0.033 wt% GO (in red).

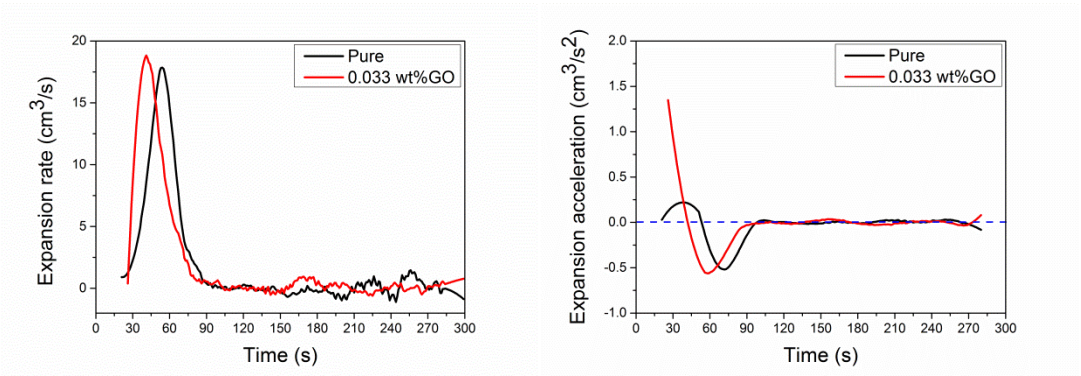

Figure 8. Expansion rate (left) and expansion acceleration (right) curves for the pure material (in black) and for the foam containing 0.033 wt% GO (in red).

The maximum of the surface temperatures *versus* time considering the whole sample are shown in **Figure 9**. Both the maxima temperatures and the trends are similar for both systems. However, after the maxima, the temperature drops slightly slower for the foam with GO, what might be a consequence of the lower thermal conductivity of this material. Moreover, this behavior is confirmed by **Figure 6**, as the surface temperature of the foam containing GO after 300 seconds is slightly higher than that of the pure material, what points to a smaller heat dissipation for the foam containing GO.

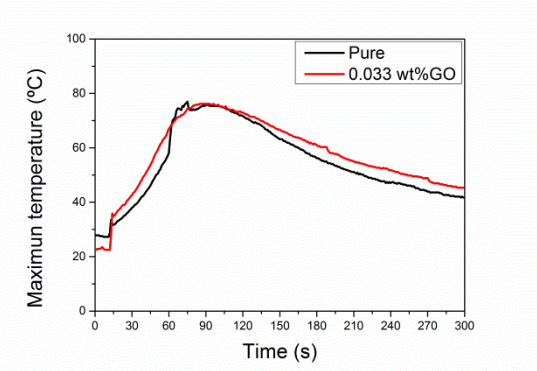

Figure 9. Maxima surface temperatures detected by the infrared camera for both samples.

FTIR measurements

The reaction kinetics of RPU foams has been followed by *in situ* FTIR spectroscopy. The isocyanate consumption is evaluated by the decrease of the isocyanate asymmetric stretching vibration at 2270 cm^{-1}, whereas the generation of urethane and urea products are followed considering the increase of the carbonyl stretching vibrations of the Amide I Region in the range 1610-1760 cm^{-1}. An example of the reaction monitoring of the pure foam by *in situ* FTIR spectra is depicted in **Figure 10**, where the isocyanate consumption and products generation are highlighted.

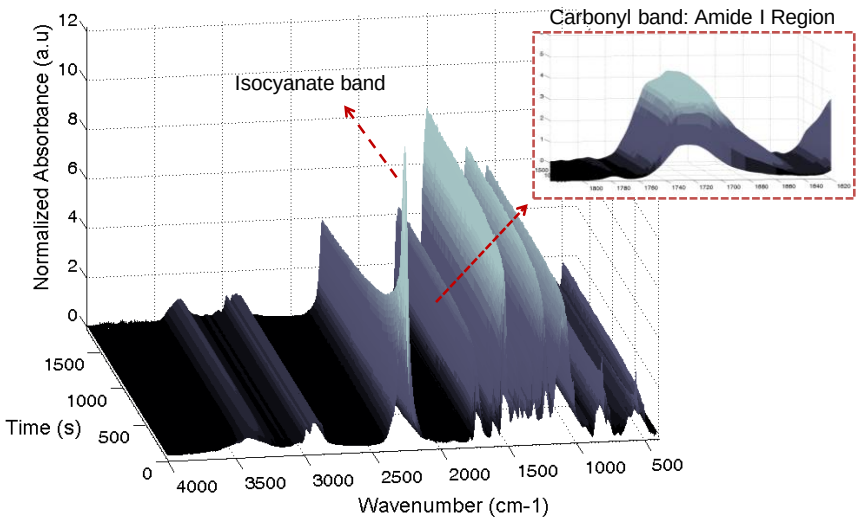

Figure 10. FTIR spectra for pure foam during 30 minutes.

Firstly, the isocyanate group conversion (*p*NCO) during the foaming process is quantified by the decay (equation 1) [24] of the isocyanate absorption band, located between 2500 and 2000 cm^{-1}:

$$pNCO = \frac{A_0 - A_{max}}{A_0} \quad (1)$$

where A_0 is the absorbance extrapolated of the isocyanate band for t = 0, and A_{max} is the integrated absorbance of the isocyanate band at time = t. **Figure 11** shows the isocyanate conversion obtained from this equation for the pure material and for the foam with 0.033 wt% GO. A higher isocyanate conversion is observed for the pure foam respect to the foam containing 0.033 wt% GO during foaming process, but both foams show very similar final isocyanate consumption (of *ca*. 70% after 30 minutes of reaction and *ca.* 90% after one month, once the foams are cured). In the case of the pure foam, the isocyanate rate conversion increases rapidly during the early stages of the foaming reaction (first 600 seconds), and more slowly after this point. The slower isocyanate reaction for the foam with GO might be related to the higher viscosity of polyol with GO respect to the polyol without GO.

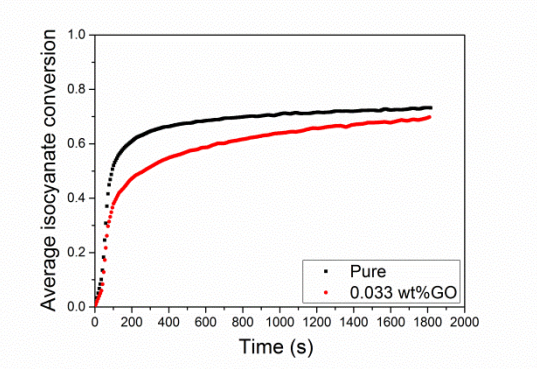

Figure 11. Average isocyanate conversion *versus* time for pure foam (in black) and for the foam containing 0.033 wt% GO (in red).

Moreover, the amide I absorptions were monitored and deconvoluted [25]. This procedure allows obtaining quantitative measurements of the relative ratio between the carbonyl groups present in the reaction mixture corresponding to urethane and urea compounds. The relative area percentages of ureas or urethanes respect the whole area of all the carbonyl absorptions permit to follow the course of the main reactions, i.e. foaming and polymerization reactions, which can be characterized separately. **Figure 12** collects the relative area obtained at initial time (in fact *ca*. 40 seconds after mixing the reactants) and 30 minutes later. **Figure 12** shows how the presence of GO clearly affects the overall reaction kinetics. At initial time the

urethane percentage of the foam containing GO is higher than that of the pure foam. However, after 30 minutes the final urea percentage is increased when GO is incorporated to the foam compared to the pure material. Finally, one month after the foam production the cured foam containing GO presents a urea percentage slightly higher (44%) than the cured reference material (41%). Therefore, the foam containing GO slightly favours the blowing reaction (responsible of both urea linkages formation and gas formation) in comparison to the pure foam. This result may be explained considering that the GO layers are able to retain water on its layer structure, what has been experimentally evidenced previously [39].

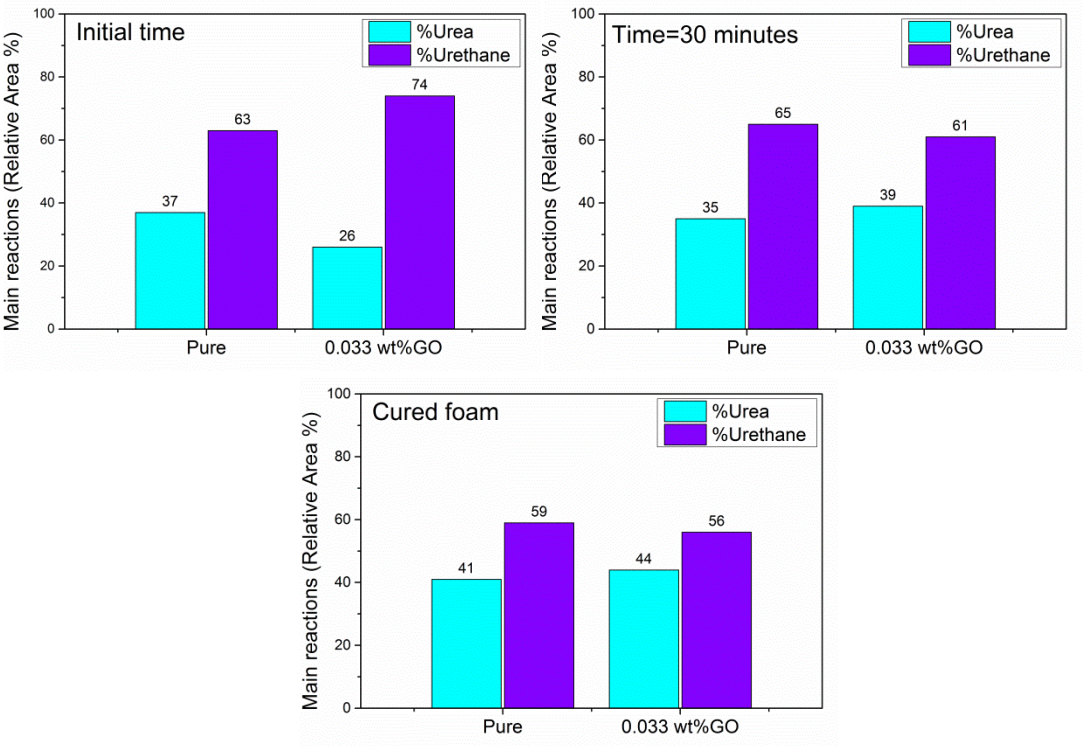

Figure 12. Relative area percentage of the absorbances of urea or urethane detected in the amide I region at initial time, after 30 minutes and one month after the foams production.

Reaction temperature measurements

Gelling and blowing reactions generated during foaming are exothermic reactions. As the cellular structure of the RPU foam is being formed, the center of foam is isolated from its surroundings, so it may be considered as an adiabatic system. Thus, the adiabatic temperature monitoring of the RPU foam may be related to the reactions kinetics, and hence to the

consumption of isocyanate in both gelling and blowing reactions [40]. **Figure 12** shows the adiabatic temperature evolution *versus* time at the different heights where the four thermocouples are placed in the plastic cup during RPU formation (**Figure 1**). Both foams show similar temperatures rising profiles, independently on the zone studied. As expected, higher temperatures are reached at thermocouples placed at higher heights in comparison with those placed below. Moreover, the maxima temperatures reached at the different heights are greater for the pure material compared to those for the foam with GO. This may be related to the higher isocyanate consumption occurring during the formation of the pure foam (as shown by FTIR measurements) which generates more amount of products.

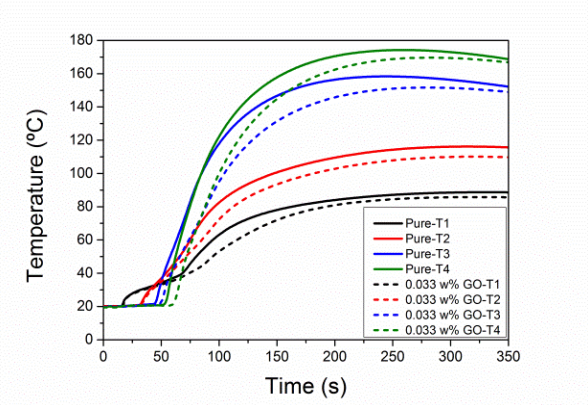

Figure 12. Temperature evolution during foaming process detected by thermocouples for all the analysed samples.

Kinetic studies: a summary

Considering the amount of information provided by the techniques used, we can make a proposal about how the reaction kinetics is modified when polyol functionalized with GO is used to obtain RPU foams.

At the first stages of the foaming process, the infrared expandometry shows a faster growing of the foam containing GO respect to the pure foam, reaching earlier the maxima expansion rate. On the other hand, the FTIR spectroscopy shows more urethane formation for the foam with GO, and the polyol functionalized with GO has also higher viscosity. All this could make the viscosity in the polymer appropriate to prevent the escape of carbon dioxide generated in the blowing reaction, what could explain the rapid grow of the foam containing GO at the beginning of the reaction. In addition to the main reactions involved in PU foams, additional processes may occur. The isocyanate might also react with carboxyl and/or hydroxyl groups of the GO surface, giving rise to the formation of amides and CO_2 and/or urethanes, respectively [41]. Therefore, the higher urethane percentage obtained when GO is present may be due not only to the gelling reaction between isocyanate and polyol, but also to the reaction between isocyanate and the hydroxyl groups on the GO surface [41].

At the final stages of the foaming process, the FTIR results show that the presence of GO slightly enhances the blowing reaction, thus giving higher percentages of urea groups, and hence a higher expansion for the foam containing 0.033 wt% of GO. This result may be explained considering that the GO layers are able to retain water on its layer structure [39], and that the retained water is more easily released at high reaction temperatures, increasing the blowing reaction at the late stages of the foaming process.

Considering isocyanate consumption, it is slightly higher for the pure material, indicating that the reactions to obtain the pure foam generate more products. This is also consistent with the higher temperatures reached in this system.

4. Conclusions

Polyols functionalized with GO and their use for obtaining water-blown RPU foams are herein described. The use of polyol functionalized with GO precludes the agglomeration of fillers, making unnecessary its dispersion in the PU matrix. This solves one of the main challenges of making polymer nanocomposites.

The optimum content of GO in the final foam is 0.033 wt%, since it leads to reduce the cell size, and consequently the thermal conductivity, without decisive modifications of other important aspects of the cellular structure, such as density, open cell content or anisotropy. The mechanical properties are not improved when GO is present, mainly because there is a negative modification of the polymer morphology in all foams, and also a deterioration of the cellular structure occurs in the case of the foam with higher GO content (0.083 wt%).

The kinetic studies show how the reaction kinetics are modified by the presence of GO. In summary, at the beginning of the foaming process the system with GO presents more urethane generation and, due to its higher viscosity, this material is able to entrap the evolving carbon dioxide, resulting in a fast expansion. On the other hand, at the late stages of the foaming process, the presence of GO enhances the blowing reaction, due to the release of the retained water on GO layers. Moreover, the foam containing GO presents a slightly decrease of isocyanate conversion, and this is also consistent with the lower temperatures reached for this system.

Acknowledgements

Financial assistance from MINECO, FEDER, UE (MAT2015-69234-R) and the Junta de Castile and Leon (VA011U16) are gratefully acknowledged. Authors thank Graphenea S.A. for supplying us with Graphene Oxide and for the technical discussion.

References

[1] M. Szycher, Szycher's Handbook of Polyurethanes, Second ed., CRC Press Boca Raton, Florida, USA, 2012.
[2] G. Harikrishnan, S.N. Singh, E. Kiesel, C.W. Macosko, Nanodispersions of carbon nanofiber for polyurethane foaming, Polymer, 51 (2010) 3349-3353.
[3] M.C. Saha, M.E. Kabir, S. Jeelani, Enhancement in thermal and mechanical properties of polyurethane foam infused with nanoparticles, Materials Science and Engineering: A, 479 (2008) 213-222.
[4] S.H. Kim, M.C. Lee, H.D. Kim, H.C. Park, H.M. Jeong, K.S. Yoon, B.K. Kim, Nanoclay reinforced rigid polyurethane foams, Journal of Applied Polymer Science, 117 (2010) 1992-1997.
[5] S. Estravís, J. Tirado-Mediavilla, M. Santiago-Calvo, J.L. Ruiz-Herrero, F. Villafañe, M.A. Rodríguez-Pérez, Rigid polyurethane foams with infused nanoclays: Relationship between cellular structure and thermal conductivity, European Polymer Journal, 80 (2016) 1–15.
[6] M.M.A. Nikje, Z.M. Tehrani, Thermal and mechanical properties of polyurethane rigid foam/modified nanosilica composite, Polymer Engineering & Science, 50 (2010) 468–473.
[7] L. Zhang, E.D. Yilmaz, J. Schjødt-Thomsen, J.C. Rauhe, R. Pyrz, MWNT reinforced polyurethane foam: Processing, characterization and modelling of mechanical properties, Composites Science and Technology, 71 (2011) 877-884.
[8] K.S. Novoselov, A.K. Geim, S.V. Morozov, D. Jiang, Y. Zhang, S.V. Dubonos, I.V. Grigorieva, A.A. Firsov, Electric Field Effect in Atomically Thin Carbon Films, Science, 190 (2004) 666.
[9] S. Eigler, A. Hirsch, Chemistry with graphene and graphene oxide-challenges for synthetic chemists, Angewandte Chemie, 53 (2014) 7720-7738.
[10] K. Hu, D.D. Kulkarni, I. Choi, V.V. Tsukruk, Graphene-polymer nanocomposites for structural and functional applications, Progress in Polymer Science, 39 (2014) 1934-1972.
[11] W. Hummers, R. Offeman, Preparation of Graphitic Oxide, Journal of American Chemistry Society, 80 (1958) 1339.
[12] D. Yan, L. Xu, C. Chen, J. Tang, X. Ji, Z. Li, Enhanced mechanical and thermal properties of rigid polyurethane foam composites containing graphene nanosheets and carbon nanotubes, Polymer International, 61 (2012) 1107-1114.
[13] M.M. Bernal, M. Martin-Gallego, I. Molenberg, I. Huynen, M.A. López Manchado, R. Verdejo, Influence of carbon nanoparticles on the polymerization and EMI shielding properties of PU nanocomposite foams, RSC Advances, 4 (2014) 7911.
[14] A. Lorenzetti, M. Roso, A. Bruschetta, C. Boaretti, M. Modesti, Polyurethane-graphene nanocomposite foams with enhanced thermal insulating properties, Polymers for Advanced Technologies, 27 (2016) 303-307.
[15] A Graphene chemically-modified hard polyurethane foam. China Patent CN 104844781 A. 2015.
[16] A.-K. Appel, R. Thomann, R. Mülhaupt, Hydroxyalkylation and Polyether Polyol Grafting of Graphene Tailored for Graphene/Polyurethane Nanocomposites, Macromolecular Rapid Communications, 34 (2013) 1249-1255.
[17] ASTM D1622-08: Standard Test Method for Apparent Density of Rigid Cellular Plastics.

[18] ASTM D6226-10: Standard Test Method for Open Cell Content of Rigid Cellular Plastics.
[19] J. Pinto, E. Solorzano, M.A. Rodriguez-Perez, J.A. de Saja, Characterization of the cellular structure based on user-interactive image analysis procedures, Journal of Cellular Plastics, 49 (2013) 555–575.
[20] ISO 22007-2:2008. Plastics-Determination of Thermal Conductivity and Thermal Diffusivity—Part 2: Transient Plane Heat Source (Hot Disc) Method.
[21] O. Almanza, M.A. Rodríguez-Pérez, J.A. de Saja, Applicability of the Transient Plane Source Method To Measure the Thermal Conductivity of Low-Density Polyethylene Foams, Journal of Polymer Science: Part B: Polymer Physics, 42 (2004) 1226–1234.
[22] ASTM D1621: Standard Test Method for Compressive Properties Of Rigid Cellular Plastics.
[23] M.J. Elwell, A.J. Ryan, H.J.M. Grünbauer, H.C.V. Lieshout, In-Situ Studies of Structure Development during the Reactive Processing of Model Flexible Polyurethane Foam Systems Using FT-IR Spectroscopy, Synchrotron SAXS, and Rheology, Macromolecules, 29 (1996).
[24] M.J. Elwell, A.J. Ryan, An FT i.r. study of reaction kinetics and structure development in model flexible polyurethane foam systems, Polymer, 37 (1996) 1353–1361.
[25] D.P. Queiroz, M.N. de Pinho, C. Dias, ATR-FTIR Studies of Poly(propylene oxide)/Polybutadiene Bi-Soft Segment Urethane/Urea Membranes, Macromolecules, 36 (2003) 4195–4200.
[26] A. Marcos-Fernández, A.E. Lozano, L. González, A. Rodríguez, Hydrogen Bonding in Copoly(ether-urea)s and Its Relationship with the Physical Properties, Macromolecules, 30 (1997) 3584–3592.
[27] M. Santiago-Calvo, S. Pérez-Tamarit, J. Tirado-Mediavilla, F. Villafañe, M.A. Rodríguez-Pérez, Infrared expandometry: a novel methodology for monitoring blowing kinetics of cellular materials with exothermic foaming mechanisms, Polymer Testing, 66 (2018) 383–393.
[28] J. Zou, Y. Chen, M. Liang, H. Zou, Effect of hard segments on the thermal and mechanical properties of water blown semi-rigid polyurethane foams, Journal of Polymer Research, 22 (2015).
[29] W. Li, A.J. Ryan, Effect of Chain Extenders on the Morphology Development in Flexible Polyurethane Foam, Macromolecules, 35 (2002) 6306–6312.
[30] A.M. Heintz, D.J. Duffy, C.M. Nelson, Y. Hua, S.L. Hsu, W. Suen, C.W. Paul, A Spectroscopic Analysis of the Phase Evolution in Polyurethane Foams, Macromolecules, 38 (2005) 9192-9199.
[31] D.V. Dounis, G.L. Wilkes, Structure-property relationships of flexible polyurethane foams, Polymer 38 (1997) 2819-2828.
[32] M.F. Sonnenschein, B.L. Wendt, Design and formulation of soybean oil derived flexible polyurethane foams and their underlying polymer structure/property relationships, Polymer, 54 (2013) 2511-2520.
[33] L. Ning, W. De-Ning, Y. Sheng-Kang, Hydrogen-Bonding Properties of Segmented Polyether Poly(urethane urea) Copolymer, Macromolecules, 30 (1997) 4405–4409.
[34] M.A. Rodríguez-Pérez, O. Alonso, J. Souto, J.A. de Saja, Thermal Conductivity of Crosslinked Closed Cell Polyolefin Foams, Polymer Testing, 16 (1997) 287-298.
[35] O. Almanza, M.A. Rodríguez-Pérez, J.A. de Saja, The Thermal Conductivity of Polyethylene Foams Manufactured by a Nitrogen Solution Process, Cellular Polymers, 18 (1999) 385-401.
[36] E. Solórzano, M.A. Rodriguez-Perez, J. Lázaro, J.A. de Saja, Influence of Solid Phase Conductivity and Cellular Structure on the Heat Transfer Mechanisms of Cellular Materials: Diverse Case Studies, Advanced Engineering Materials, 11 (2009) 818-824.

[37] T. Kuilla, S. Bhadra, D. Yao, N.H. Kim, S. Bose, J.H. Lee, Recent advances in graphene based polymer composites, Progress in Polymer Science, 35 (2010) 1350-1375.
[38] L. Gibson, M. Ashby, Cellular solids: structure and properties, Pergamon Press, Oxford, 1988.
[39] D.R. Dreyer, A.D. Todd, C.W. Bielawski, Harnessing the chemistry of graphene oxide, Chemical Society reviews, 43 (2014) 5288-5301.
[40] L.D. Artavia, C.W. Macosko, Foams kinetics, Journal of Cellular Plastics, 26 (1990) 490-511.
[41] S. Stankovich, R.D. Piner, S.T. Nguyen, R.S. Ruoff, Synthesis and exfoliation of isocyanate-treated graphene oxide nanoplatelets, Carbon, 44 (2006) 3342-3347.

Optimization of rigid polyurethane formulation from kinetics results to obtain rigid polyurethane foams reinforced with graphene oxide with better thermal and mechanical properties

Applied polymer science 136 (**2019**) 47474
https://doi.org/10.1002/app.47474

Improvement of thermal and mechanical properties by control of formulations in rigid polyurethane foams from polyols functionalized with graphene oxide

Mercedes Santiago-Calvo[1,*], Victoria Blasco[2], Carolina Ruiz[2], Rodrigo París[2], Fernando Villafañe[3], Miguel-Ángel Rodríguez-Pérez[1]

[1] Cellular Materials Laboratory (CellMat), Condensed Matter Physics Department, Faculty of Science, University of Valladolid, Campus Miguel Delibes, Paseo de Belén 7, 47011 Valladolid, Spain

[2] D.C. Technology and Corporate Venturing, Repsol S.A. C/ Agustín de Betancourt s/n, 28935 Móstoles, Spain

[3] GIR MIOMeT-IU Cinquima-Química Inorgánica, Faculty of Science, University of Valladolid, Campus Miguel Delibes, Paseo de Belén 7, 47011 Valladolid, Spain

* Corresponding author: mercesc@fmc.uva.es

Abstract

This paper addresses the optimization of water-blown rigid polyurethane foams (RPU) obtained from a polyol functionalized with graphene oxide (GO). For this purpose, a series of RPU foams are herein synthesized by varying either the isocyanate index, the contents of catalyst or the contents of surfactant, or a combination of these three components. The modifications introduced in the formulation are based on the effect of GO on the reaction kinetics. These strategies are mainly focused on the increase of both isocyanate conversion and polymerization reaction, which decrease for the foams containing GO. Density, cellular structure, thermal conductivity, and mechanical properties of the resulting foams are herein investigated. The results show how controlling PU formulation allows to improve both the thermal and the mechanical behaviour in these RPU foams containing GO. The highest cell size reduction of 25% and the lowest thermal conductivity are obtained for the sample with a simultaneous increase of isocyanate index, catalyst content, and surfactant content.

Moreover, the adequate combination of these components leads to a high improvement of 59% of the relative Young's modulus, and of 54% of the relative collapse stress.

Keywords: Polyurethane foam; graphene oxide; formulation; thermal conductivity; mechanical properties

1. Introduction

Rigid polyurethane (RPU) foams are one of the most important thermal insulating materials, since they can also be used simultaneously as structural materials, due to their combination of low weight, low thermal conductivity and good mechanical strength. Therefore, RPU foams play an essential role in many industries, such as construction, refrigeration, and piping [1].

In recent years, the promising characteristics displayed by polymer nanocomposite foams [2] have led them to gain significance in the group of lightweight materials. The addition of tiny amounts of nanoparticles to the polymer matrix may give rise to excellent improvements of a wide variety of physical features, such as thermal, mechanical, and barrier properties. This topic is being widely studied, in particular by several works reporting the effects of nanoparticles such as nanoclays, nanosilicas, carbon nanotubes, carbon nanofibers, graphene or graphene oxide (GO) on PU nanocomposites [3-11]. A proper dispersion of the nanoparticles in the PU matrix is essential to optimize their behaviour, what requiring special surface treatments and/or specific dispersion methods. The inclusion of nanoparticles into PU foams may also modify the kinetics of the reactions, which would give rise to unexpected consequences on the final properties of the final PU matrix, since some properties may be improved, but others may be worsened.

The chemistry of PU foams is based on two simultaneous reactions: the polymerization or gelling reaction, where an isocyanate and a polyol generate the three-dimensional polyurethane network, and the foaming or blowing reaction, where a gas is generated by the addition of physical or chemical blowing agents [12]. Water is commonly used as chemical blowing agent in RPU foams, since it reacts with isocyanate giving urea groups and CO_2, which contributes to the foam expansion. Physical blowing agents, such as cyclopentane or isopentane, can also be added since their vaporization contributes to the foam expansion. The PU formulation determines the final density, morphology and rigidity of the foam, thus defining which PU foams are appropriate for a desired application.

In a previous study we described the formation of water-blown RPU foams from polyols functionalized with low amounts of graphene oxide (GO) (0.017, 0.033 and 0.083 wt%) [13]. One of the main advantages of this approach is that GO particles are chemically incorporated into polyol chains, which precludes the agglomeration of fillers. Among the RPU foams therein obtained, that containing 0.033 wt% GO (optimum system) gave the better insulating properties. This foam displayed a cell size decrease of 19%, and consequently a thermal

conductivity reduction of *ca*. 4% compared with that of the pure material without GO particles. However, the Young`s modulus and collapse stress did not improve with the presence of GO. This reduction of the mechanical properties for the optimum system was explained considering a different polymer morphology in the matrix of the foams, since the cellular structure did not worsen. Therefore, a detailed kinetic study was carried out by infrared expandometry [14], FTIR spectroscopy, and temperature measurements in order to identify the effect of the polyol functionalized with GO on the reaction kinetics, and consequently on the final polymer morphology. This study showed how the presence of GO increased the amount of urethane groups when the foaming process started, and how the higher viscosity of this firstly formed foam favoured the entrapment of the evolving CO_2, resulting in a fast expansion. However, at the late stages of the foaming process, the presence of GO enhanced the urea generation, due to the release of the retained water on the GO layers. Furthermore, the foams containing GO showed a slight decrease of isocyanate conversion, and consequently lower temperatures were achieved with respect to pure material. In summary, it was concluded that the presence of GO in the polyol modified the reaction kinetics and therefore the properties. Consequently, this formulation could be more finely tuned in order to improve certain properties.

The present work is based on the information collected from the aforementioned research [13], the main target being to improve the mechanical properties of RPU foams functionalized with GO, whereas the thermal conductivity is maintained or improved. For this purpose, we have chosen as starting material the better foam previously obtained, i.e. that containing 0.033 wt%. Using the previous data referring to the modifications of the reaction kinetics induced by the presence of GO in the polyol, a series of RPU foams are herein synthesized by varying the isocyanate index, the amounts of catalyst, the amounts of surfactant, or a combination of these components. Density, cellular structure, thermal conductivity and mechanical properties of the resulting foams are herein evaluated. The results show that, by a proper control of the PU formulation, the use of polyol functionalized with GO allows improving both the thermal and the mechanical properties simultaneously.

2. Experimental

2.1. Materials

IsoPMDI 92140 (31.5% NCO, density 1.23 g cm^{-3}, viscosity 170-250 mPa·s), a polymeric diphenylmethane diisocyanate (pMDI) from BASF Poliuretanos Iberia S.A (Rubí, Spain), was used to produce the RPU foams. TEGOAMIN® DMCHA (N,N-dimethylcyclohexylamine) from Evonik Nutrition & Care GmbH (Essen, Germany), was used as gelling and foaming catalyst. TEGOSTAB® B 8522 (a non-hydrolysable poly-ether-polydimethyl-siloxane–stabilizer) from

Evonik Nutrition & Care GmbH (Essen, Germany), was used as surfactant. Distilled water was used as a blowing agent. Polyol functionalized with 1000 ppm of GO (OH index 358 mg KOH/g, viscosity 547.6 mPa·s, 570 Da) was synthesized by Repsol S.A (Móstoles, Spain) [13].

2.2. Preparation of rigid polyurethane/graphene oxide nanocomposite foams

RPU foam containing 0.033 wt% GO (1000 ppm in polyol) is the reference material whose components were modified in order to study their effect on the RPU properties [13]. Isocyanate index was varied from 115 to 130 (**Table 1**), gelling and foaming catalyst from 0.5 parts per weight (ppw) to 2 ppw (**Table 2**), and surfactant from 1 ppw to 2 ppw (**Table 3**). Moreover, a combination of the above strategies was also considered (**Table 4**).

An overhead stirrer (EUROSTAR Power control-visc P1, IKA) with a 50 mm diameter Lenart disc stirrer was used to premix the polyol with the catalyst, surfactant, and blowing agent during 2 minutes at 250 rpm, to obtain a homogenous polyol blend (labelled as Part B = Polyol component). Part B and the isocyanate (Part A) were mixed in a plastic cup at 1200 rpm for 10 seconds. Free-rise foams were cured for 2 days at room temperature, and then the foam samples were cut for characterization.

Table 1. PUR formulations with different isocyanate index from 115 to 130.

	Isocyanate component	**Polyol component**			
Samples	**Isocyanate index**	**Polyol [ppw]**	**Surfactant [ppw]**	**Catalyst [ppw]**	**Blowing agent (H_2O) [ppw]**
PU-115ISO	115	100	1	1	5
PU-120ISO (Reference)	120	100	1	1	5
PU-125ISO	125	100	1	1	5
PU-130ISO	130	100	1	1	5

Table 2. PUR formulations with different amount of catalyst from 0.5 ppw to 2 ppw.

	Isocyanate component	**Polyol component**			
Samples	**Isocyanate index**	**Polyol [ppw]**	**Surfactant [ppw]**	**Catalyst [ppw]**	**Blowing agent (H_2O) [ppw]**
PU-0.5CAT	120	100	1	0.5	5
PU-1CAT (Reference)	120	100	1	1	5
PU-1.5CAT	120	100	1	1.5	5
PU-2CAT	120	100	1	2	5

Table 3. PUR formulations with different amount of surfactant from 1 ppw to 2 ppw.

	Isocyanate component	**Polyol component**			
Samples	**Isocyanate index**	**Polyol [ppw]**	**Surfactant [ppw]**	**Catalyst [ppw]**	**Blowing agent (H_2O) [ppw]**
PU-1SURF (Reference)	120	100	1	1	5
PU-2SURF	120	100	2	1	5

Table 4. PUR formulations with different amount of isocyanate index, catalyst and surfactant.

	Isocyanate component	**Polyol component**			
Samples	**Isocyanate index**	**Polyol [ppw]**	**Surfactant [ppw]**	**Catalyst [ppw]**	**Blowing agent (H_2O) [ppw]**
PU-120ISO-1CAT-1SURF (Reference)	120	100	1	1	5
PU-130ISO-2CAT-1SURF	130	100	1	2	5
PU-130ISO-2CAT-2SURF	130	100	2	2	5

2.3. Foams characterization

Foam density was measured as described by ASTM D1622/D1622M-14 [15], in three different samples for each material. The samples had a diameter of 30 mm and a height of 25 mm.

After measuring the densities in the samples, open cells content (OC%) was measured by using a gas pycnometer Accupyc II 1340 from Micromeritics, according to ASTM D6226-10 [16].

The cellular morphology of the foams was determined by Scanning Electron Microscopy (SEM) with a JEOL JSM-820 microscope. The growth plane (z plane) of cured foams was examined by SEM after vacuum coating with a gold monolayer. An image analysis technique [17] of SEM micrographs was used to determine the main characteristics of the cellular foam structure: mean cell size (Φ_{3D}), anisotropy ratio (AR), and cell size distribution. The calculated statistical parameters for cell size distribution were: standard deviation (SD), normalized standard deviation (NSD) (i.e. SD/ Φ_{3D}), and asymmetry coefficient (AC). NSD provides information about the homogeneity of the cell size distribution: homogeneous cell distributions present small values of this parameter. AC measures the degree of asymmetry of the distribution, so as a negative AC indicates that the smaller cells are more separated from the mean cell size than bigger ones, and vice versa. More than 150 cells of different areas of each material were used for this analysis. The detailed calculation of the cellular structure parameters were explained by Pinto et al. [17].

Thermal conductivity was determined at room temperature by using a hot-disk transient plane source (TPS) thermal constant analyzer, according to ISO 22007-2:2008 method [18]. The measurements were performed using two cylindrical samples for each material with a diameter of 30 mm and a height of 25 mm. A disk shaped TPS sensor with a radius of 3.189 mm was used for all measurements, after being located in contact with the xy plane (perpendicular to growth plane) of the two samples [19]. Several measurements were performed after 1 month of the foams production. At that time the samples have reached the stationary state, because all the CO_2 generated during foaming have diffused outwards the foam, and it has been replaced by atmospheric air [6].

Mechanical properties in compression were measured at room temperature by using an Instron Machine (model 5.500R6025), according to ASTM D1621-10 [20]. Stress–strain curves were obtained at a strain rate of 10 mm/min and the maximum static strain was 75% for all the experiments. As one of main potential applications of the RPU foams under study is as thermal insulator in the core of sandwich panels for the construction sector or in refrigerators, therefore the direction of interest to perform the compression tests was the growing direction. Three different samples with a diameter of 30 mm and a height of 25 mm were measured for each material. The samples were prepared with rigorously parallel contact surfaces. Young´s modulus and collapse stress were calculated from the stress-strain curves.

3. Results and Discussion

In a previous work describing the properties of PUR containing GO, we reported that the optimum content of GO in the final foam was 0.033 wt% [13]. This produced a significant cell size reduction of 19% in comparison to pure foam without GO, and consequently the thermal conductivity was also reduced around 4%. At the same time, other important features such as density, open cell content or anisotropy were not modified. Despite these positive performances, the mechanical properties were reduced around 20% when GO was present due to the negative modification of the polymer morphology. Our previous report [13] included a detailed study of the reaction kinetics carried out by infrared expandometry, FTIR spectroscopy, and reaction temperature measurements. This allowed evaluating the modifications produced by the incorporation of GO on the polymer morphology and on the foaming expansion (**Table 5** and **Figure 1)**. Those kinetic studies showed that the internal temperature reached for the foam containing GO during the foaming process was lower than that of pure foam, and this effect was related to a slightly decrease of isocyanate conversion (**Table 5**). At the initial steps of the foaming process, more urethane groups were formed in the foam containing GO (**Table 5**). These groups favored an increase of the viscosity, and therefore the entrapment of the evolving CO_2 was also favoured, resulting in a fast expansion (**Figure 1**). On the other hand, at the final stages of the foaming process (30 minutes later) the presence of GO favoured a slight decrease of the polymerization reaction, therefore less percentages of urethane groups were obtained, giving rise to a lower crosslinking network inside the RPU foam (**Table 5**). However, the enhancement of the blowing reaction due to the presence of GO generated higher percentages of urea groups and CO_2 (**Table 5**), and also a higher expansion for the foam containing 0.033 wt% of GO with respect to the pure material (**Figure 1**).

Table 5. Results of the evaluation of reaction kinetics by FTIR spectroscopy, and reaction temperature measurements for the material without GO and for the material containing 0.033 wt% [13].

Reaction time	Pure (without GO)				0.033 wt% GO			
	Average isocyanate conversion (%)	Total Urea (%)	Total Urethane (%)	Average internal temperature (ºC)	Average isocyanate conversion (%)	Total Urea (%)	Total Urethane (%)	Average internal temperature (ºC)
Initial time (around 40 s)	13±0.05	37	63	134±0.9	8±0.04	26	74	129±0.5
30 minutes	73±0.03	35	65		70±0.03	39	61	

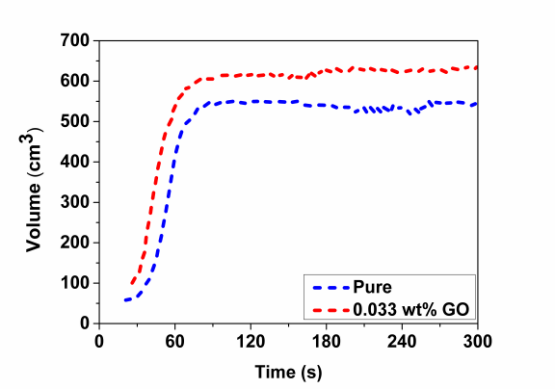

Figure 1. Sample volume *vs.* time from the infrared expandometry monitoring for the pure foam without GO and for the foam containing 0.033 wt% GO.

Considering all the above results, we decided to focus the present study on the RPU formulation based on the polyol containing 0.033 wt% of GO, which displayed the better performance. Our objective was obtaining enhanced mechanical properties, and at the same time maintaining or improving the thermal conductivity properties. For this purpose, a sequence of RPU foams are herein described by varying the isocyanate index, the amounts of catalyst and surfactant, and/or a combination of these components. The two first strategies, that is, the variation of isocyanate index and of catalyst content, are based on the kinetic results previously mentioned, and hence are aimed to promote a higher isocyanate consumption in the polymerization reaction. The third strategy is based on the increase of surfactant, which should stabilize the formation of gas bubbles formed during nucleation, hindering degeneration phenomena such as coalescence. The last strategy combines these different options (isocyanate index, catalyst and surfactant) in order to find synergies looking for significant improvements of the thermal and mechanical properties.

3.1. Influence of isocyanate index

Firstly, a series of foams with higher isocyanate index have been obtained, in an attempt to enhance the isocyanate consumption. This should lead to an increase of both the polymerization and the cross-linking network in the polymer matrix, making the foam stiffer and consequently improving its mechanical properties.

The effect of isocyanate index in density and cellular structure has been evaluated, and the results are collected in **Table 6**. An increase of the density when the isocyanate index rises is observed, so that the density of the sample with higher isocyanate index (PUR-130ISO) increases *ca*. 1.5 kg/m^3 compared to that of the reference foam. The high isocyanate index results in a higher foam density because increasing the amount of isocyanate in the polymerization reaction leads to an increase of the total amount of polymer network [21]. However, the OC is scarcely altered.

SEM analysis (**Table 6** and **Figure 2**) shows a slight decrease of cell size. Moreover, cell size distribution is relatively homogeneous for all samples, since NSD values are low. The AC values reveal that asymmetry slightly increases with isocyanate index, therefore large cells are more separated from the average value than those smaller. Considering the anisotropy, the foams with higher isocyanate indexes (125 and 130) present a slightly decrease of AR.

Table 6. Density, open cell content (OC), mean cell size (Φ3D), normalized standard deviation (NSD), asymmetry coefficient (AC) and anisotropy ratio (AR) for the foams with different isocyanate index.

Samples	Density (Kg/m^3)	OC (%)	Φ3D (µm)	NSD	AC	AR
PU-115ISO	34.2±0.0	8.61±1.38	373±77	0.21	-0.10	1.38±0.29
PU-120ISO (Reference)	33.1±0.1	7.09±0.45	406±103	0.25	0.56	1.38±0.31
PU-125ISO	34.9±0.7	7.65±0.10	375±97	0.26	0.45	1.27±0.30
PU-130ISO	34.5±1.4	6.90±1.20	381±62	0.16	0.13	1.33±0.37

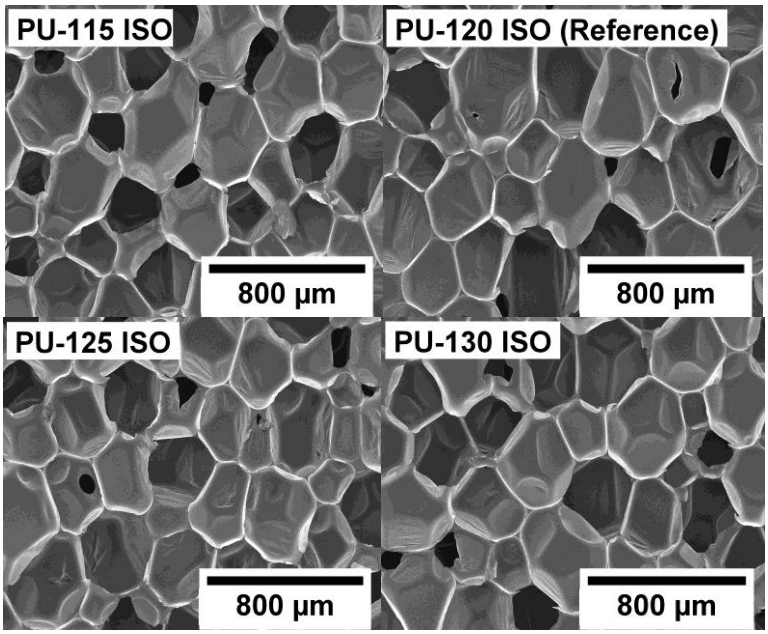

Figure 2. SEM micrographs of foams with different isocyanate index.

On the other hand, we have calculated the relative collapse stress and relative Young's modulus (collapse stress and Young's modulus divided by the density of the foam sample) [22] because it allows comparing the mechanical properties of foams regardless of their density. The relative mechanical properties for foams with different isocyanate index are collected in **Figure 3.a** and show a slight increase with the isocyanate index. Consequently, the sample with 130 isocyanate index reaches the highest improvement, since it reaches an increase of 14% of the relative Young's modulus, and of 10% of the relative collapse stress, compared to the reference foam. As expected, this improvement could be due to the higher cross-linking density expected for a higher isocyanate index. In addition, the cellular structure of these foams is not deteriorated, as observed in **Table 6**, and thus the improvement on the polymer matrix morphology is translated into improvements in the mechanical behaviour.

We have also investigated the effect of isocyanate index on the thermal properties of the foams. The values of the thermal conductivity of foams are presented in **Figure 3.b**, and show a slight increase with the isocyanate index content. This feature should be mainly due to the small increase of the density when the isocyanate index is increased, which should also increase the conduction through the solid phase, considering that the cellular structure is scarcely modified [23, 24].

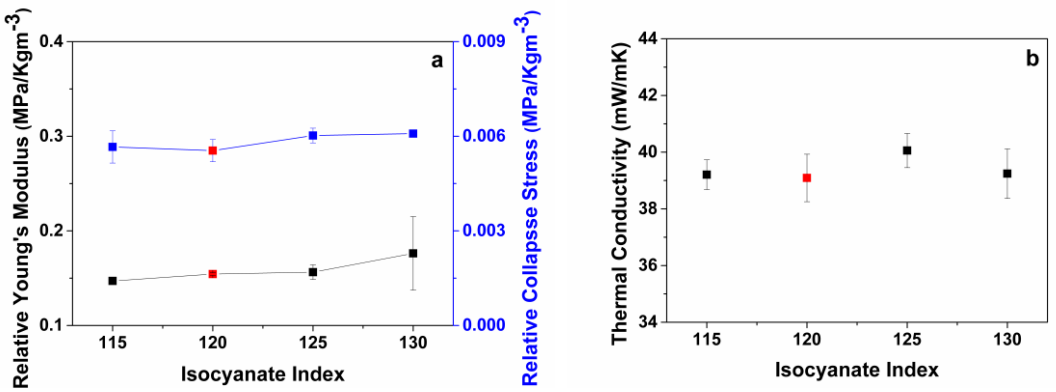

Figure 3. (a) Mechanical and **(b)** thermal properties for the foams with different isocyanate index.

3.2. Influence of catalyst

Another way to achieve a higher isocyanate conversion is increasing the catalyst content. Thus, samples with different content of catalyst from 0.5 to 2 ppw were prepared, and their density and cellular structure values measured (**Table 7)**. The density slightly decreases with the catalyst content. The samples with larger density decreases (*ca*. 1 kg/m^3) are those with higher catalyst contents (1.5 and 2 ppw) respect to the reference foam. This may be explained considering that the blowing reaction is favored in these conditions. Moreover, the OC slightly increases with the addition of catalyst.

On the other hand, the sample with the highest amount of catalyst (PUR_2CAT) affords the larger cell size reduction (15%), what might be attributed to the formation of important amount of gas bubbles [25]. This reduction is clearly observed in the SEM micrographs, shown in **Figure 4**. Furthermore, the sample with the highest amount of catalyst content (PUR_2CAT) is the most homogeneous and displays a highly symmetric cell size distribution, as indicated by the very small value of NSD and by a AC value near to zero. Additionally, AR increases with the catalyst content, being the sample with the highest content (PUR_2CAT) being the one with the higher AR value.

Table 7. Density, open cell content (OC), mean cell size (Φ3D), normalized standard deviation (NSD), asymmetry coefficient (AC) and anisotropy ratio (AR) for foams with different catalyst content.

Samples	Density (Kg/m^3)	OC (%)	Φ3D (µm)	NSD	AC	AR
PU-0.5CAT	33.7±0.3	8.12±0.62	427±98	0.23	0.39	1.30±0.28
PU-1CAT (Reference)	33.1±0.1	7.09±0.45	406±103	0.25	0.56	1.38±0.31
PU-1.5CAT	31.8±0.4	8.12±0.62	361±87	0.24	1.11	1.40±0.30
PU-2CAT	31.9±0.7	8.43±0.31	346±63	0.18	-0.22	1.49±0.45

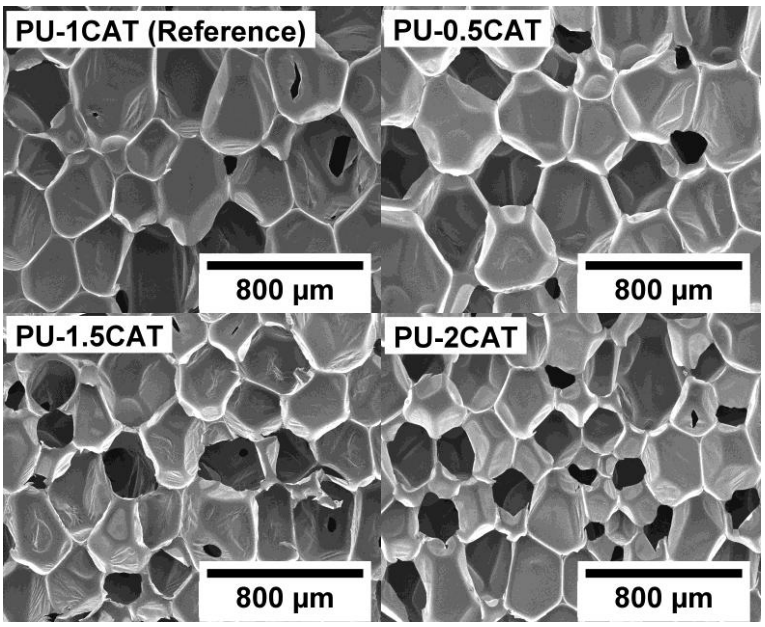

Figure 4. SEM micrographs of foams with different catalyst content.

The relative collapse stress and relative Young's modulus of foams with different content of catalyst (**Figure 5.a**) evidence a slight increase of the mechanical properties with the increasing content of catalyst in the PU formulation. Therefore, the sample with the highest content (PUR_2CAT) achieves the highest enhancement. Compared to the reference foam, that obtained with 2 ppw of catalyst exhibits an increase of a 19% of the relative Young's modulus, and a 15% of the relative collapse stress. As in the case of the foams with different isocyanate index, the cellular structure for the foams is not deteriorated when the catalyst content increases. Therefore, the improvement of the mechanical behaviour could be due to the higher isocyanate conversion promoted by the catalyst increase, and also to the decrease of the cell size.

As a general trend, the value of thermal conductivity decreases with the catalyst content (**Figure 5.b**). As mentioned above, the increase of the catalyst content produces a significant cell size reduction in the foams, which would imply a decrease of the radiation contribution to the thermal conductivity [6, 23, 24]. Furthermore, the density decrease of the foams with higher catalyst content involves a decrease of the solid phase conduction contribution to the thermal conductivity. Therefore, the result obtained in figure 4b can be clearly explained taking into account the density and cellular structure results.

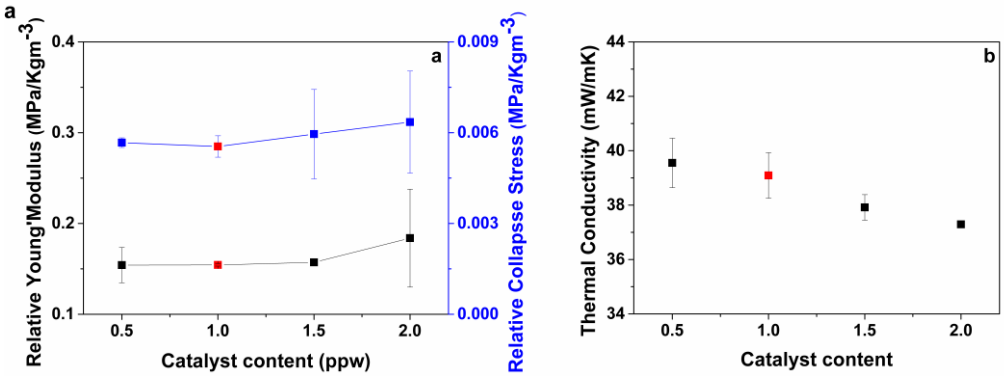

Figure 5. (a) Mechanical and **(b)** thermal properties for the foams with different catalyst content.

3.3. Influence of surfactant

The presence of surfactants has an important role in the PU formulation because they stabilize the gas bubbles formed during nucleation, thus inhibiting coalescence. For these reasons, the surfactant content has been increased from 1 ppw to 2 ppw, and the effect of this increase on the RPU foam properties has been evaluated. As shown in **Table 8**, no changes of density and of cellular structure parameters are detected when the surfactant content is increased. **Figure 6** shows how the cells of the RPU foam remain small and uniform when the surfactant content is increased to 2 ppw.

Table 8. Density, open cell content (OC), mean cell size (Φ3D), normalized standard deviation (NSD), asymmetry coefficient (AC) and anisotropy ratio (AR) for foams with different surfactant content.

Samples	Density (Kg/m^3)	OC (%)	Φ3D (µm)	NSD	AC	AR
PUR-1SURF (Reference)	33.1±0.1	7.09±0.45	406±103	0.25	0.56	1.38±0.31
PUR-2SURF	32.0±1.4	6.86±1.28	393±96	0.24	-0.26	1.48±0.28

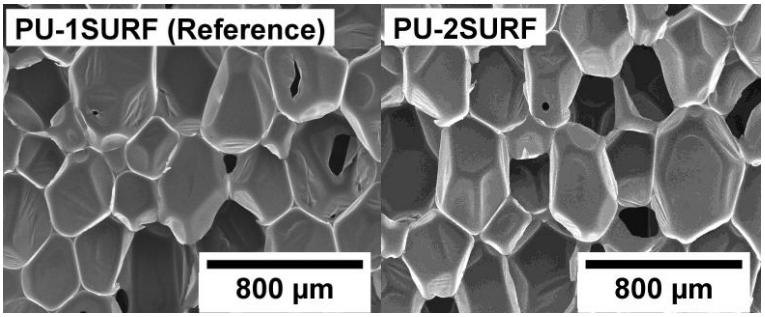

Figure 6. SEM micrographs of foams with different surfactant content.

The effect of the surfactant on the mechanical properties of RPU foam is observed in **Figure 7.a**. The compressive properties slightly increase when the surfactant content rises from 1 to 2 ppw, increasing the relative Young's modulus by 10% and the relative collapse stress by 17%. Since the cellular structure is maintained when the surfactant content increases, this slight improvement of the mechanical properties could be due to either the modification of the polymer matrix morphology either to a different distribution of the material in cell walls and struts.

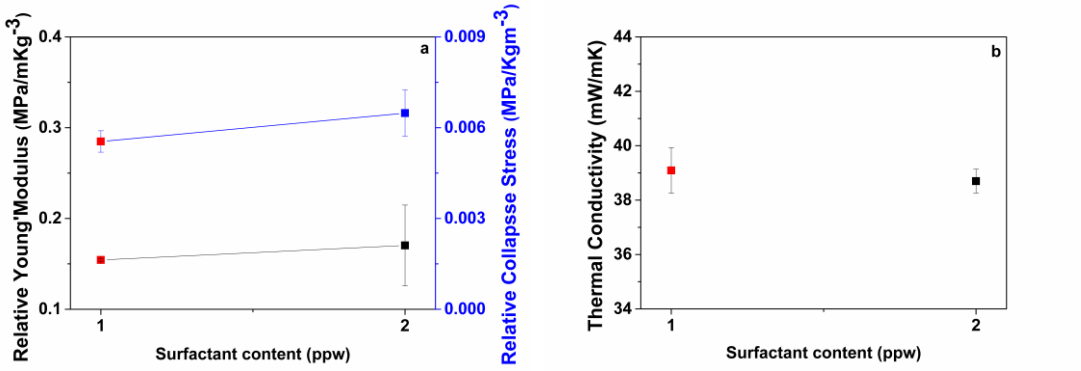

Figure 7. (a) Mechanical and **(b)** thermal properties for the foams with different surfactant content.

On the other hand, the thermal conductivity of the RPU foam containing 2 ppw of surfactant is similar to that of the reference foam, as shown in **Figure 7.b**. Thus, the thermal properties hardly change when the surfactant content is increased mainly because the cellular structure and density are not modified.

3.4. Combination of modifications

Based on the results described above, where the effect of isocyanate index, catalyst or surfactant on the cellular structure and properties of the foam were separately studied, we have made a combination of the contents of each component with the aim of generating a substantial improvement in the thermal and mechanical foam properties. Therefore, two new materials (PUR-130ISO-2CAT-1SURF and PUR-130ISO-2CAT-2SURF) with changes in the PU formulation, have been designed and their properties have been compared with those of the reference material (PUR-120ISO-1CAT-1SURF). The isocyanate index (130) and the catalyst content (2ppw) have been increased and the surfactant content is maintained (1 ppw) in the PUR-130ISO-2CAT-1SURF sample. On the other hand, the isocyanate index (130), the catalyst content (2ppw), and also the surfactant content (2 ppw) have been increased in the PUR-130ISO-2CAT-2SURF sample.

Table 9 collects densities and cellular structure characteristics for these new RPU foams. The density of the sample with higher isocyanate index and catalyst content increases by 3 kg/m^3 compared to that of the reference foam, whereas the density of the foam with higher isocyanate index, catalyst and surfactant contents decreases by around 1 kg/m^3. The open cell content (OC) value is slightly lower for the PUR-130ISO-2CAT-1SURF sample than that of the reference foam. However, an evident decrease of the OC value is observed when the surfactant content is also increased, since the PUR-130ISO-2CAT-2SURF sample gives a lower OC value. Furthermore, a decisive cell size reduction is obtained for these new foams, being 22% for PUR-130ISO-2CAT-1SURF, and 25% for the PUR-130ISO-2CAT-2SURF sample. This

reduction is clearly observed in the SEM micrographs shown in **Figure 8**. The PUR-130ISO-2CAT-2SURF sample presents similar AR value than that of the reference material, although this AR value is reduced for the PUR-130ISO-2CAT-1SURF sample. All foams studied have a high homogeneity (with small NSD) and a high symmetry (AC near to zero).

Table 9. Density, open cell content (OC), mean cell size (Φ3D), normalized standard deviation (NSD), asymmetry coefficient (AC) and anisotropy ratio (AR) for foams with different combination of components.

Samples	Density (Kg/m^3)	OC (%)	Φ3D (µm)	NSD	AC	AR
PUR-120ISO-1CAT-1SURF (Reference)	33.1±0.1	7.09±0.45	406±103	0.25	0.56	1.38±0.31
PUR-130ISO-2CAT-1SURF	36.2±0.1	6.37±0.56	318±53	0.17	0.07	1.11±0.20
PUR-130ISO-2CAT-2SURF	31.9±0.2	4.32±0.03	306±65	0.21	0.39	1.39±0.28

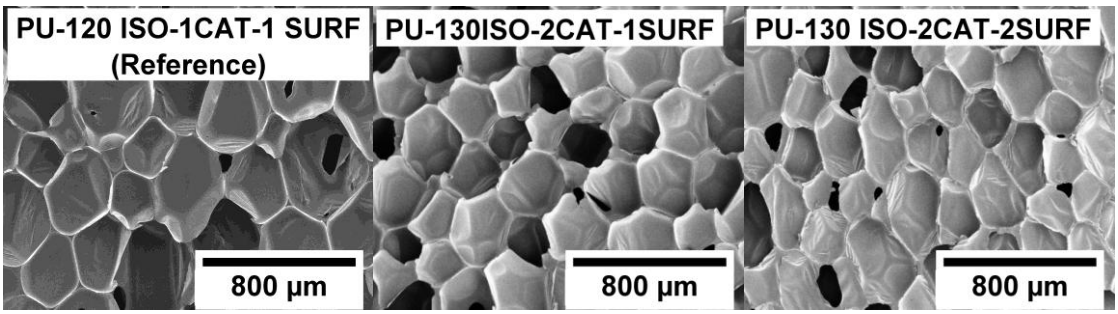

Figure 8. SEM micrographs of foams with different combination of components.

The values of relative Young's modulus and relative collapse stress of these foams are collected in **Figure 9.a**, and show a noticeable improvement of the mechanical properties. Compared to the reference foam, the sample with higher isocyanate index and catalyst (PUR-130ISO-2CAT-1SURF) presents an increase of 60% in the compressive modulus, and of 40% in the collapse stress. On the other hand, the sample with higher isocyanate index, catalyst and surfactant (PUR-130ISO-2CAT-2SURF) reaches an increase of 59% in the compressive modulus,

whereas the increase of the collapse stress is 54%. This enhancement of the mechanical properties could be mainly due to the higher isocyanate conversion promoted by the catalyst and isocyanate increase, and also to the improvement of the cellular structure by these components combination.

The values of the thermal conductivity of these two RPU foams are shown in **Figure 9.b**. As expected, thermal conductivity decreases with cell size reduction, because the radiative contribution to thermal conductivity is also reduced [6, 23, 24]. The significant cell size reduction achieved with these combined formulations can be appreciated from **Table 9**. The sample with higher isocyanate index and catalyst (PUR-130ISO-2CAT-2SURF) displays smaller cell size, but its thermal conductivity is not significantly reduced because it presents a higher density, which instead contributes to the solid phase conductivity increase [23, 24]. However, the thermal conductivity of the sample with higher isocyanate index, catalyst and surfactant (PUR-130ISO-2CAT-2SURF) is reduced by *ca*. 4%, compared to that of the reference material. In this case, this may be explained not only by the cell size reduction, but also by the decrease of the density and of the OC value, as well as a by its homogenous cellular structure.

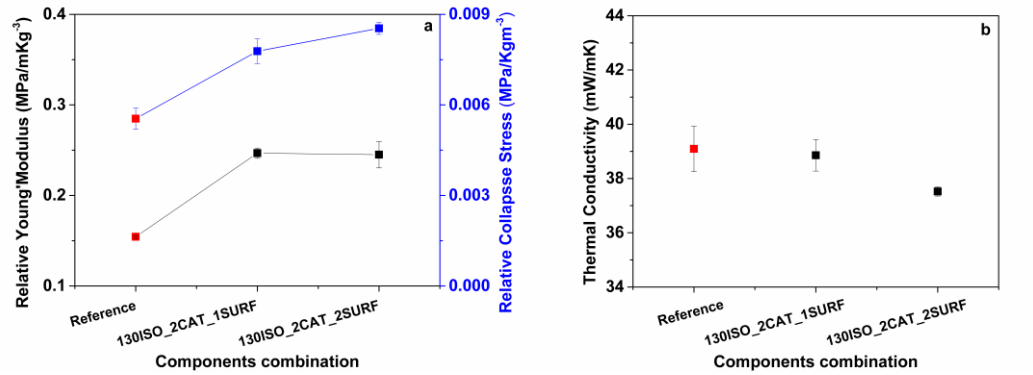

Figure 9. Mechanical and thermal properties for the foams with different combination of components.

The main purpose of this study was improving the mechanical properties of the RPU foam containing GO, and at the same time maintaining or reducing the thermal conductivity. In conclusion, the synergy between the adequate combination of these three components in the PU formulation (isocyanate index, catalyst and surfactant) made possible to achieve a maximum enhancement of the mechanical and thermal properties.

4. Conclusions

The formulation of a water-blown RPU foam from a polyol functionalized with GO have been modified in order to improve their mechanical properties. Starting from the experimental data on the reaction kinetics of the system containing GO in comparison with the system without GO, a series of modifications has been defined and tested. In particular, the effects of either the isocyanate index, catalyst, or surfactant contents, as well as a combination of these modifications of these three components, on the density, cellular structure, and mechanical and thermal properties of the final foams have been evaluated.

The best performing formulation is that containing 130 of isocyanate index, 2 ppw of catalyst and 2 ppw of surfactant, which gives rise to a final foam where the cell size is reduced by 25%, as well as to significant reductions of density, and of open cell content. Correspondingly, the thermal conductivity is reduced by 4%. Moreover, the mechanical properties are highly improved, so as the Young's modulus and the collapse stress are increased by 59% and 54% respectively.

In conclusion, the strategies used in this paper has resulted in significant improvements of both mechanical and thermal properties for a RPU foam obtained from a polyol functionalized with GO.

Acknowledgments

Financial assistance from Spanish Ministry of Economy and Competitiveness, European Regional Development Fund, RETOS COLABORACION Project: NUMASTA. RTC-2016-5285-5 is gratefully acknowledged. Authors thank Graphenea S.A. for supplying us with Graphene Oxide and for the technical discussion.

References

[1] M. Szycher, Szycher's Handbook of Polyurethanes, Second ed., CRC Press Boca Raton, Florida, USA, 2012.
[2] L. Chen, D. Rende, L.S. Schadler, R. Ozisik, Polymer nanocomposite foams, Journal of Materials Chemistry A, 1 (2013) 3837.
[3] G. Harikrishnan, S.N. Singh, E. Kiesel, C.W. Macosko, Nanodispersions of carbon nanofiber for polyurethane foaming, Polymer, 51 (2010) 3349-3353.
[4] M.C. Saha, M.E. Kabir, S. Jeelani, Enhancement in thermal and mechanical properties of polyurethane foam infused with nanoparticles, Materials Science and Engineering: A, 479 (2008) 213-222.

[5] S.H. Kim, M.C. Lee, H.D. Kim, H.C. Park, H.M. Jeong, K.S. Yoon, B.K. Kim, Nanoclay reinforced rigid polyurethane foams, Journal of Applied Polymer Science, 117 (2010) 1992-1997.
[6] S. Estravís, J. Tirado-Mediavilla, M. Santiago-Calvo, J.L. Ruiz-Herrero, F. Villafañe, M.A. Rodríguez-Pérez, Rigid polyurethane foams with infused nanoclays: Relationship between cellular structure and thermal conductivity, European Polymer Journal, 80 (2016) 1–15.
[7] M.M.A. Nikje, Z.M. Tehrani, Thermal and mechanical properties of polyurethane rigid foam/modified nanosilica composite, Polymer Engineering & Science, 50 (2010) 468–473.
[8] L. Zhang, E.D. Yilmaz, J. Schjødt-Thomsen, J.C. Rauhe, R. Pyrz, MWNT reinforced polyurethane foam: Processing, characterization and modelling of mechanical properties, Composites Science and Technology, 71 (2011) 877-884.
[9] D. Yan, L. Xu, C. Chen, J. Tang, X. Ji, Z. Li, Enhanced mechanical and thermal properties of rigid polyurethane foam composites containing graphene nanosheets and carbon nanotubes, Polymer International, 61 (2012) 1107-1114.
[10] M.M. Bernal, M. Martin-Gallego, I. Molenberg, I. Huynen, M.A. López Manchado, R. Verdejo, Influence of carbon nanoparticles on the polymerization and EMI shielding properties of PU nanocomposite foams, RSC Advances, 4 (2014) 7911.
[11] A. Lorenzetti, M. Roso, A. Bruschetta, C. Boaretti, M. Modesti, Polyurethane-graphene nanocomposite foams with enhanced thermal insulating properties, Polymers for Advanced Technologies, 27 (2016) 303-307.
[12] G. Oertel, Polyurethane Handbook 2nd ed., Hanser Publishers, Munich, 1993.
[13] M. Santiago-Calvo, V. Blasco, C. Ruiz, R. París, F. Villafañe, M.Á. Rodríguez-Pérez, Synthesis, characterization and physical properties of rigid polyurethane foams prepared with poly(propylene oxide) polyols containing graphene oxide, European Polymer Journal, 97 (2017) 230-240.
[14] M. Santiago-Calvo, S. Pérez-Tamarit, J. Tirado-Mediavilla, F. Villafañe, M.A. Rodríguez-Pérez, Infrared expandometry: a novel methodology for monitoring blowing kinetics of cellular materials with exothermic foaming mechanisms, Polymer Testing, 66 (2018) 383–393.
[15] ASTM D1622-08: Standard Test Method for Apparent Density of Rigid Cellular Plastics.
[16] ASTM D6226-10: Standard Test Method for Open Cell Content of Rigid Cellular Plastics.
[17] J. Pinto, E. Solorzano, M.A. Rodriguez-Perez, J.A. de Saja, Characterization of the cellular structure based on user-interactive image analysis procedures, Journal of Cellular Plastics, 49 (2013) 555–575.
[18] ISO 22007-2:2008. Plastics-Determination of Thermal Conductivity and Thermal Diffusivity—Part 2: Transient Plane Heat Source (Hot Disc) Method.
[19] O. Almanza, M.A. Rodríguez-Pérez, J.A. de Saja, Applicability of the Transient Plane Source Method To Measure the Thermal Conductivity of Low-Density Polyethylene Foams, Journal of Polymer Science: Part B: Polymer Physics, 42 (2004) 1226–1234.
[20] ASTM D1621: Standard Test Method for Compressive Properties Of Rigid Cellular Plastics.
[21] H. Fan, A. Tekeei, G.J. Suppes, F.-H. Hsieh, Physical Properties of Soy-Phosphate Polyol-Based Rigid Polyurethane Foams, International Journal of Polymer Science, 2012 (2012) 1-8.
[22] L. Gibson, M. Ashby, Cellular solids: structure and properties, Pergamon Press, Oxford, 1988.
[23] O. Almanza, M.A. Rodríguez-Pérez, J.A. de Saja, The Thermal Conductivity of Polyethylene Foams Manufactured by a Nitrogen Solution Process, Cellular Polymers, 18 (1999) 385-401.
[24] E. Solórzano, M.A. Rodriguez-Perez, J. Lázaro, J.A. de Saja, Influence of Solid Phase Conductivity and Cellular Structure on the Heat Transfer Mechanisms of Cellular Materials: Diverse Case Studies, Advanced Engineering Materials, 11 (2009) 818-824.
[25] K.H. Choe, D.S. Lee, W.J. Seo, W.N. Kim, Properties of Rigid Polyurethane Foams with Blowing Agents and Catalysts, Polymer Journal, 36 (2004) 368-373.

CHAPTER 7:
INTERNATIONAL RESEARCH STAY: THERMOPLASTIC POLYURETHANE FOAMS

Mercedes Santiago Calvo

7.1- Introduction

The study of foams based on thermoplastic polyurethanes (TPU) is growing in importance in recent years, even though most of polyurethane (PU) foams are thermoset. On the one side, TPU foams present attractive properties, such as light-weight, high flexiblility, great cushioning effect, and fast energy restoration in compression. On the other side, the use of TPU foams shows significant advantages compared to the mostly used thermoset PU foams, since TPU foams are elastic thermoplastically processable materials, and they can also be reprocessed or recycled, due to their non-chemical crosslinked structure. TPU can be foamed by different foaming processes, such as extrusion foaming, injection foaming, reaction foaming, and gas dissolution foaming in an autoclave. Although extrusion and injection foaming are the two most popular processes, gas dissolution foaming in an autoclave is recently being used because it gives rise to high quality foams.

The main objective of the a scientific article included in the present chapter is **studying the foaming behavior of a series of TPU materials with different hard segments (HS) contents by using gas dissolution foaming process.**

-Article 8: Synthesis, characterization, and foaming of thermoplastic polyurethane with different hard segment contents. Submitted to Polymer.

The first part of this work consists of the synthesis and characterization of TPUs with different HS contents. It was carried out during a three-months stay at the Polymers & Peptides Research Group of the School of Materials of the University of Manchester (UK), under the supervision of Professor Alberto Saiani. In addition to this, this research stay allowed fulfilling one of the requirements in order to obtain the International Mention Thesis. The second part of this work was completed at CellMat, and it was focused on the foaming of the previously synthesized TPUs by gas dissolution foaming.

In the eighth article, the influence of HS contents from 40 to 60 wt. % in TPU materials foamed by one-step gas dissolution foaming process has been studied by analyzing the density and cellular structure(see **Figure 7.1**). Firstly, the effect of the foaming temperature is evaluated from 140°C to 180°C, fixing a saturation pressure of 20 MPa and a saturation time of 1 h. Among the TPUs studied, only that containing 50 wt. % HS gives a stable foam, and its better features are reached by foaming at 170 °C. Higher or lower HS ratios does not allow to obtain TPU foams, since that with 60 wt. % HS has a high crystallinity and rigidity, and that with 40 wt. % HS presents a low viscosity, which does not allow stabilizing the developed cellular structure. Finally, the foaming of TPU with 50 wt. % HS has been optimized by varying the saturation pressure from 10 MPa to 25 MPa, at 170°C for 1h. The optimum saturation and foaming conditions are 25 MPa and 170 °C for 1h, what provides foams with the lowest relative density (0.739), the smallest average cell size of 4 μm, and the higher cell nucleation density of $8.0x10^9$ nuclei/cm^3.

Most of the previous works reported in the literature have studied the foaming of commercial TPUs in which the composition is not usually known, but this research is pioneer as it allows to relate the TPU composition with the foaming behaviour.

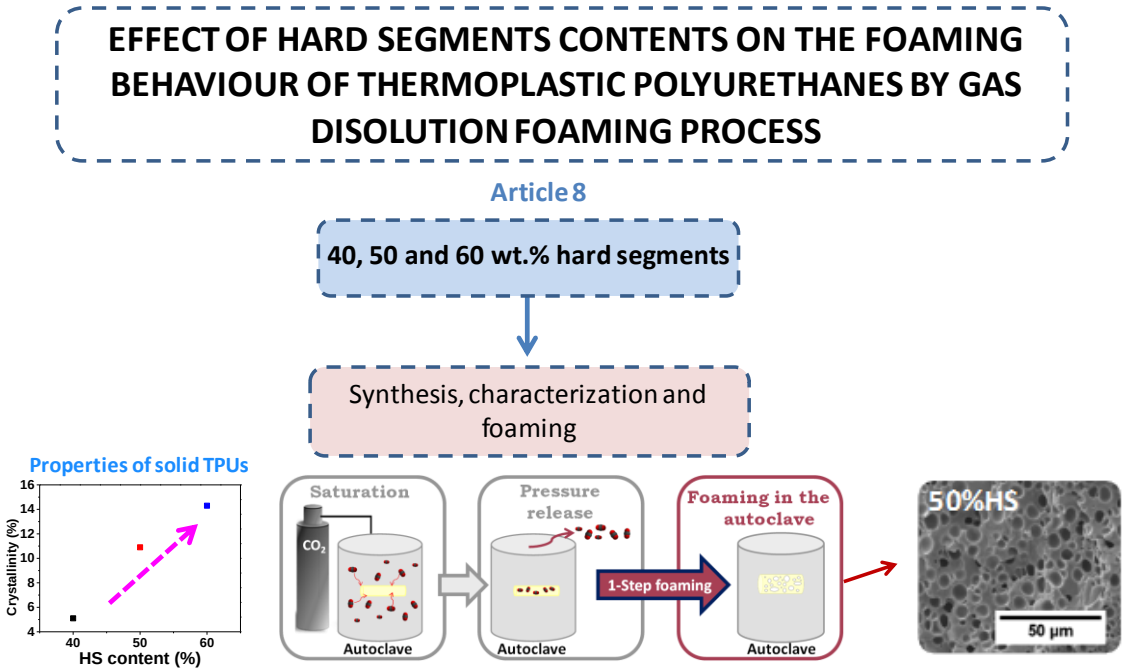

Figure 7.1. Scheme of the main objective of the scientific article include in this chapter.

Submitted to Polymer

Synthesis, characterization, and foaming of thermoplastic polyurethane with different hard segment contents

Mercedes Santiago-Calvo[1,*], Haneen Naji[2], Victoria Bernardo[1], Judith Martín-de León[1], Alberto Saiani[2], Fernando Villafañe[3], Miguel Ángel Rodríguez-Pérez[1]

[1] Cellular Materials Laboratory (CellMat), Condensed Matter Physics Department, Faculty of Science, University of Valladolid, Campus Miguel Delibes 7, 47011 Valladolid, Spain

[2] School of Materials, The University of Manchester, Oxford Road, Manchester M13 9PL, UK

[3] GIR MIOMeT-IU Cinquima-Química Inorgánica, Faculty of Science, University of Valladolid, Campus Miguel Delibes 7, 47011 Valladolid, Spain

* Corresponding author: mercesc@fmc.uva.es

Abstract

A series of thermoplastic polyurethanes (TPUs) with different amounts of hard segments (HS) (40, 50 and 60 wt. %) are synthesized by a pre-polymer method. Shore hardness, gel permeation chromatography (GPC), differential scanning calorimetry (DSC), wide angle X-ray diffraction (WAXD), dynamic mechanical thermal analysis (DMTA), and rheology of the synthesized TPUs are determined. These materials are then foamed by one-step gas dissolution foaming process. The effect of foaming temperature from 140°C to 180°C on the cellular structure and on density is evaluated, fixing a saturation pressure of 20 MPa and a saturation time of 1 h. Among the TPUs studied, only that with 50 wt. % HS allows to obtain a stable foam, whose better features are reached after foaming at 170 °C. Finally, the foaming of TPU with 50 wt. % HS is optimized by varying the saturation pressure from 10 MPa to 25 MPa, at 170°C. The optimum saturation and foaming conditions are 25 MPa and 170 °C for 1h, which give foams with the lowest relative density of 0.739, the smallest average cell size of 4 μm, and the higher cell nucleation density of $8.0x10^9$ nuclei/cm^3.

Keywords: Thermoplastic polyurethane; foams; gas dissolution foaming

International research stay: Thermoplastic polyurethane foams

1. Introduction

Foaming polymers are widely used in almost all industrial sectors, due to their interesting value-added properties, such as low density, low thermal conductivity, and adaptable mechanical properties depending on their relative density. Polyurethane (PU) is the polymer par excellence, considering foams obtained industrially, which represent almost the 50% of the global foam market [1]. Although most of PU foams are thermoset, the study of foams based on thermoplastic polyurethanes (TPU) are gaining importance in recent years, because they are elastic thermoplastically processable materials, and also because they can be reprocessed or recycled. Thus, TPU foams are nowadays very interesting materials for several industries, such as furniture, automotive, sportswear, and packaging.

TPUs are block copolymers composed of alternating soft segments (SS) and hard segments (HS), produced by the polyaddition reaction of a diisocyanate with a medium molecular weight macrodiol and with a low molecular weight diol, which acts as chain extender. The presence of SS and HS gives rise to a two-phase microstructure, in which the HS from the isocyanate and the chain extender segregate into semicrystalline domains, whereas the SS from the polyol chains form amorphous domains in which the HS are dispersed [2]. Therefore, HS offers rigidity, and SS provides flexibility to the TPU material, and their ratio and distribution are determined by a large number of chemical and structural factors, including the polymerization procedure used for their synthesis and processing conditions, and at the same time determine the properties and performance of TPUs.

Gas dissolution foaming process is one of the most reliable methods developed in order to produce thermoplastics foams, where carbon dioxide (CO_2) is normally used as blowing agent. This technology allows to manufacture large samples by using a green solvent (CO_2), which can be removed leaving no residues nor pollutant compounds. Many studies have been published on the use of this method, and different cellular polymers have been obtained, such as poly(methylmethacrylate) (PMMA), polystyrene (PS), poly(lactic acid) (PLA), polycarbonate (PC), polyethylene (PE), or polypropylene (PP) among others [3-5]. Nevertheless, the number of reports dealing with TPU foams obtained by gas dissolution foaming process using CO_2 as the blowing agent is still rather limited [6-13].

Dai et al. [6] foamed TPU films synthesized from 4,4-diphenylmethanediisocyanate (MDI), poly-tetramethyleneglycol (PTMG) and 1,3-propylenediamine components by a one-step foaming method. Processing conditions, such as pressure, temperature, and foaming time, and their effect on the foam morphology were investigated. The resulting TPU foams showed an improvement in their damping performance. TPU foamed at 35 °C, 18 MPa and 160 min reached the lowest cell size of *ca*. 4μm, a cell density of *ca*. 10^{11} cells/cm^3 and a foam density of *ca*. 0.4 g/cm^3. Ito et al. [7] studied the effect of the chain length of the SS and the HS contents on the cellular structure of TPU foams obtained by a two-step foaming. They concluded that the solubility of CO_2 in the SS is considerably higher than that in the HS. Rizvi et al. [8] obtained TPU nanocomposites foams produced by one-step foaming from a commercial

TPU reinforced with different concentration (from 0 to 10 wt. %) of multiwall carbon nanotubes (MWNTs). TPU foam with 4 wt. % of MWNT has the smallest cell size of 2.7 µm, the greatest cell density of 6.7 x 10^{10} cells/cm^3 and a relative density of *ca.* 0.46. The thermal, electrical and piezoresistive properties of these nanocomposites foams were investigated and correlated with the MWNT concentration, and with the microstructure of the materials. Prasad et al. [9] used commercial TPUs with different hardness to obtain porous chemical mechanical polishing (CMP) pads, changing the processing conditions. They concluded that the cellular structure of the TPU foams synthesized by a two-step foaming is related to the hardness of the polymer matrix. Yeh et al. [10] foamed a commercial TPU with Cloisite® 30B nanoclay (1,3 and 5 wt%) in order to promote cell nucleation and to increase the cell density. The cell size of the final nanocomposite foams decreased to 1 µm, and the cell density increased to 3 x 10^{11} cells/cm^3 even after using a short foaming time of 5 s either at 150°C in a two-step foaming, either at a lower foaming temperature (70°C) in a one-step foaming. In a later study, this group [11] obtained a nanocellular TPU foam by adding Cloisite® 30B nanoclay, at 60°C in a one-step foaming. The lowest cell size reached was *ca*. 0.45 µm when the saturation and foaming conditions were 13.79 MPa and 50°C. This foaming process gave a cell density of 10^{11} cells/cm^3, and a relative density of 0.9–0.95. The same group [12] later reported the synthesis of a TPU based on MDI, 1,4-butanediol (BD) and polypropylene glycol (PPG). One-step foaming afforded a cell size reduction up to 2 µm when the foaming temperature decreased up to 20°C. The decrease of cell size was stabilized at 20°C, but the foam presented a non-uniform cell structure below 20°C. Moreover, the authors also reported that pre-mixing TPU before foaming produced a higher cell size reduction, and a more homogeneous cellular structure. In a posterior study, these researchers [13] used three different approaches in order to obtain TPU nanocellular foams by a one-step foaming from previously synthesized TPU: increasing the HS content, replacing the SS type, and adding a graphene nucleation agent. All three approaches were able to produce cell sizes of less than 1 µm. Although increasing the HS content generated a minimum average cell size of 0.5 µm, the cell size distribution was heterogeneous and the relative density was as high as 0.91, for saturation and foaming conditions of 50°C and 13.6 MPa. The best results were obtained for TPU foams with 0.1 wt. % of graphene, because their cell structure was homogeneous with an average cell size of 0.7 µm, the cell density improved to 4.94 × 10^{11} cells/cm^3, and a low relative density of 0.77 was reached, for saturation and foaming conditions of 20°C and 13.6 MPa.

Considering the scarcity of reports on synthesized TPU foams, we have focused our research on synthesizing a new series of TPUs with different characteristics in order to obtain TPU foams. In particular, we herein report the synthesis of TPUs based on MDI, poly(ethyleneglycol)-block-poly(propyleneglycol-block-poly(ethylen-glycol) (PEG-PPG-PEG) and 1,5-pentanediol (1,5-PDO) components, with different HS contents (40, 50 and 60 wt. %) by using the pre-polymer method. These TPUs are herein characterized by shore hardness, GPC, DSC, WAXD, DMTA and rheology. The foaming behaviour of these materials is also extensively analysed at different saturation and foaming conditions by one-step gas dissolution foaming process, as well as the density and cellular structure of the resulting foams.

2. Materials and Methods

2.1. Materials

The reactants used to obtain TPU are: MDI with a molecular weight of 250.25 g/mol and a functionality of 2, PEG-PPG-PEG as macrodiol with an average M_n of ~2000 g/mol and OH index of 56-59 mg KOH/g, 1,5-PDO as chain extender with a molecular weight of 104.15 g/mol and a functionality of 2, 1,4-Diazabicyclo[2.2.2]octane (DABCO) as catalyst and N,N-Dimethylacetamide (DMAc) as solvent. All of them were supplied by Sigma Aldrich and used as received, except PEG-PPG-PEG and 1,5-PDO, which were dried in a vacuum oven overnight at 80°C and then were stored in sealed glass jars with molecular sieves, and DABCO, which was deoxygenated by bubbling nitrogen before use. Medical grade CO_2 (99.9% purity) was used as blowing agent for the gas dissolution foaming experiments.

2.2. TPU synthesis

Three samples of TPU were synthesized with different weight fraction of HS: 40%HS, 50%HS and 60%HS (% indicated is by weight). The synthesis of TPUs was carried out in a reaction flask by a two-step, pre-polymer method under dry nitrogen atmosphere. Firstly, PEG-PPG-PEG was added drop wise from a funnel to an excess of MDI and this mixture was heated to in an oil bath at 80°C for 2 h with stirring at 400 rpm. In the second step, the mixture of an additional amount of MDI and the prepolymer previously obtained in DMAc (240 mL), was added drop wise from the funnel to a preheated mixture of 1,5-PDO and DABCO (0.3 g, 0.003 mmol, 0.3%) in DMAc (60 mL). This reaction mixture was stirred at 400 rpm for 2h in an oil bath at 80°C. Finally, the solution containing the TPU was poured into silicone moulds and maintained in an oven at 80°C for 3 days to obtain TPU casts.

The amount of each component used for the different TPUs is collected in **Table 1**. The molar ratio of NCO/OH was adjusted as 1.02. The pre-polymer formulation (first step of synthesis) used is calculated having a molar ratio of the number of moles of MDI and PEG-PPG-PEG polyol as 6:1 for TPU 50%HS and TPU 60%HS, and as 4:1 for TPU 40%HS. 100 g of TPU material were produced in each synthesis.

Table 1. The amount of each component used for first and second step of TPU synthesis.

	FIRST STEP		SECOND STEP		
TPU SAMPLES	MDI Isocyanate	PEG-PPG-PEG Polyol	PREPOLYMER	MDI Isocyanate	1,5-PDO Chain extender
40%HS	43.8 g, 0.175 mol	85.8 g, 0.043 mol	90.6 g	0 g, 0 mol	9.4 g, 0.090 mol
50%HS	64.2 g, 0.257 mol	85.8 g, 0.043 mol	87.4 g	0 g, 0 mol	12.6 g, 0.121 mol
60%HS	64.2 g, 0.257 mol	85.8 g, 0.043 mol	69.9 g	13.4 g, 0.054 mol	16.7 g, 0.160 mol

2.3. Samples production of solid TPU

Compression molded samples were prepared by using a hot plate press. The material was first heated at a temperature above melting temperature (between 165-180 °C) for 3 min, raising the pressure to 100 bar at 0.5 bar/s. Then the samples were pressed under a constant pressure of 10 MPa for 7 min, lowering the temperature to 60°C at 25°C/min. These compression molded samples were prepared to characterize their shore hardness, WAXD, DMTA and rheology.

Extruded samples with 1.5±0.5 mm of diameter were also prepared by TWELVindex extrusion plastometer from ATS Faar using a temperature above melting temperature (between 165-180 °C). These extruded samples were prepared to carry out the foaming tests.

All the samples were dried in a vacuum oven overnight at 80°C before characterization and foaming process.

2.4. Solid TPU characterization

2.4.1. Density

Density of the solid TPUs (ρ_s) (extruded samples) was measured with a gas pycnometer Accupyc II 1340 from Micromeritics.

2.4.2. Shore hardness

Shore A and B hardness tenting was measured with a Bareiss U72 durometer following the "ISO 868:2003: Plastics and ebonite. Determination of indentation hardness by means of a duromer (Shore hardness)" procedure. The measurements were taken for 1 s at the temperature of 23°C. Three samples of each material from the compressed sheet with dimensions 10 x 10 x 2 mm^3 were used.

2.4.3. Gel permeation chromatography (GPC)

Number-averaged molecular weights (M_n), weigh-averaged molecular weights (Mw) and polydispersity index (PDI) were determined by GPC. A dilute solution of 1 mg/ml of synthesized TPU was prepared in tetrahydrofuran (THF) and stirred for 2 hours. The solutions were filtered through a 0.2 µm polyamide filter. Three measurements of each synthesized TPU were carried out in order to obtain an average.

2.4.4. Differential scanning calorimetry (DSC)

DSC was performed using a DSC30 Mettler Toledo Instrument. Tests were carried out under nitrogen atmosphere at a heating rate of 10 °C min^{-1} from -90 to 220 °C. All DSC measurements were done in aluminium pans with 8 mg of extruded TPU.

2.4.5. Wide angle X-ray diffraction (WAXD)

WAXD patterns were obtained using a PANalytical X'Pert Pro (XRD 5) instrument employing Cu Kα radiation (λ = 1.54 Å) as the X-ray source, and a voltage of 40 KV and 40 mA of current. The diffraction angle was scanned from 5° to 90°. The samples were cut from the compressed sheet, with dimensions 10 x 10 x 2 mm^3.

2.4.6. Dynamic mechanical thermal analysis (DTMA)

DTMA tests were carried out using a Q800 DMA instrument (TA) in single cantilever mode at a heating rate of 3 °C/min, an amplitude of 15 µm and a frequency of 1 Hz. The samples were cut from the compressed sheet, with dimensions 17 x 6 x 2 mm^3. Three samples of each sample were measured to obtain an average. The storage modulus (E'), loss modulus (E'') and tan δ were recorded and glass transition temperature (Tg) of hard segments (HS) and soft segments (SS) were calculated from the peak tan δ.

2.4.7. Shear rheology

Cylindrical samples obtained by compression molding with a thickness of 1 mm and a diameter of 25 mm were used for the rheological tests. Rheological measurements were carried out on a strain-controlled rheometer (ARES-G2, TA Instruments) with parallel plate geometry (diameter 25 mm, gap 1 mm) under a nitrogen atmosphere. The rheological characterization was performed in frequency sweep tests at 200 °C, a constant strain of 10% and an angular

frequency range from 0.1 to 100 rad s^{-1}. Strain was chosen in order to measure all the samples in the linear viscoelastic region (LVR), and was estimated by an initial study through amplitude sweep test at strains ranging from 0.01% to 10000%, an angular frequency of 1 rad/s and 200 °C.

2.5. Gas dissolution foaming experiments

A high pressure vessel (model PARR 4681) provided by Parr Instrument Company with a capacity of 1 L was used for the foaming tests. The maximum temperature and pressure reached by this device are 350 °C and 41 MPa, respectively. The pressure was automatically controlled by an accurate pressure pump controller (model SFT-10) provided by Supercritical Fluid Technologies Inc. The vessel is equipped with a clamp heater of 1200 W, and its temperature is controlled by a CAL 3300 temperature controller. This set up has been used to get a set of experiments by using a one-step foaming process. Firstly, samples were introduced in the pressure vessel under certain pressure and temperature conditions for the saturation stage. After saturation, pressure was rapidly released and the samples expanded in the pressure vessel after depressurization. Two sets of experiments were performed for the extruded samples. Firstly, the effect of the foaming temperature was analysed by fixing the saturation pressure to 20 MPa and the saturation time to 1 h, and varying the foaming temperature between 140, 150, 160, 170 and 180 °C. Secondly, the influence of the saturation pressure was evaluated by choosing four different saturation pressures: 10, 15, 20 and 25 MPa at 170 °C for 1 h. Extruded TPU samples were foamed and then were left to desorb the remaining CO_2 before characterizing their density and cellular structure.

2.6. Characterization of TPU foams

2.6.1. Density

Density of the TPU foams was determined with the water-displacement method based on Archimedes' principle using a density determination kit with an AT261 Mettler-Toledo balance. The density of TPU foams was measured when all CO_2 was desorbed. Relative density (ρ_r) has been calculated by the ratio between the density of TPU foam (ρ_f) and the density of the solid TPU (extruded samples) with the same chemical composition (ρ_s).

2.6.2. Cellular structure

With the aim of maintaining the cellular structure for the microscopic visualization, samples were cooled in liquid nitrogen and fractured. The cellular morphology of the extruded samples was observed by Scanning Electron Microscopy (SEM) with a JEOL JSM-820 microscope. The perpendicular plane of the extrusion direction was examined by SEM after vacuum coating

with a gold monolayer. An image analysis technique [14] of SEM micrographs was used to determine the average cell size (Φ) of the cellular structure of the TPU foamed. More than 100 cells of different areas of each cellular material have been used for this analysis.

Cell nucleation density (N_0) [14] has been determined according to Equation 1 where N_v is the cell density, Φ is the average cell size and ρ_r is the relative density.

$$_0 = \frac{N_v}{\rho_r} = \frac{6\,(1n\rho_r)}{\rho_r \pi \Phi^3} \qquad \textbf{Equation 1}$$

3. Results and Discussion

3.1. Characterization of Solid TPU

A complete characterization of the TPU samples allows to relate the TPU properties with the gas dissolution foamability. Relevant properties of the samples studied are collected in **Table 2**. The density slightly increases when the HS content increases in the TPU material. The measurement of Shore hardness allows to test the TPU resistance into two categories: Shore A is used for more flexible types of TPU whereas Shore D is referred to more rigid varieties. **Table 2** shows that the shore hardness increases with HS content. TPU 60%HS is not classified in Shore A scale, thus being the most rigid material of all those studied.

In **Table 2**, GPC measurements of the samples with different contents of HS show that the molecular weights are higher for TPUs with low contents of HS (40%HS and 50%HS) than for TPU 60%HS. The polydispersity index, it is close to 2 in all TPU studied.

Table 2. Properties of TPU samples: the density of the solid TPU (ρ_s), shore hardness, number-averaged molecular weights (M_n), weigh-averaged molecular weights (M_w) and polydispersity index (PDI).

TPU SAMPLES	ρ_s (Kg/m^3)	Hardness (Shore A)	Hardness (Shore D)	M_n (g/mol)	M_w (g/mol)	PDI
40%HS	1.068±0.002	78.8±0.4	22.6±0.5	18583±1046	36556±1576	1.97±0.06
50%HS	1.125±0.003	88.6±0.5	37.6±0.9	26403±1469	51468±1274	1.95±0.06
60%HS	1.101±0.003	-	45.6±0.5	8552±1602	18325±535	2.18±0.32

The DSC thermograms of the TPU under study are shown in **Figure 1** and the results obtained are collected in **Table 3**. DSC thermograms of all TPU samples display a first transition at ca. -45°C associated with the glass transition of the SS (TgSS), which is similar for all the materials studied. The second transition is observed at *ca.* 90°C, and is associated with the annealing

temperatures, since the samples had been dried in a vacuum oven overnight at 80°C before the characterization and the foaming experiments. Several endothermic peaks associated with the melting temperatures (Tm 1-3) of the HS crystalline are observed at higher temperatures, between 150°C and 180°C (**Table 3**). The observation of several Tm peaks is related to the different order of crystalline structures. Tm of TPU systems is shifted to higher temperatures when the HS content increases, and the TPU with high HS content (60%HS) presents a sharp endothermic peak at 180°C, which may be related to the formation of highly ordered crystalline structures. Moreover, the HS crystallinity of the samples grows from 5.1% to 14.3% when the HS content increases from 40 wt. % to 60 wt. % (**Table 3**).

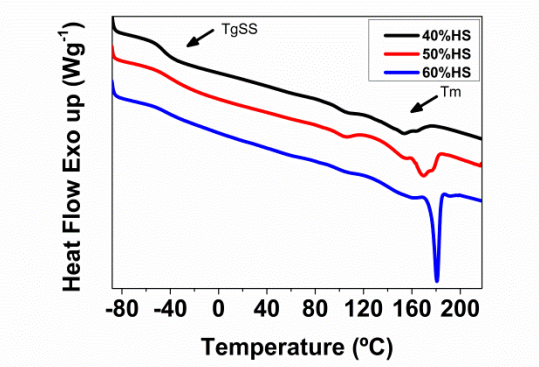

Figure 1. DSC thermograms of solid TPUs with different HS%.

Table 3. DSC data of solid TPUs with different HS%.

TPU SAMPLES	Tg SS (°C)	Tm 1 (°C)	Tm 2 (°C)	Tm 3 (°C)	HS crystallinity (%)
40%HS	-47	-	154	165	5.1
50%HS	-41	154	169	177	10.9
60%HS	-49	-	162	180	14.3

WAXD patterns for TPU systems are shown in **Figure 2**. The diffraction peaks near 2θ = 19°, 20°, 21°, 22°, 24° and 26° are obviously attributed to the presence of TPU crystals. The intensity of these peaks increases when TPU samples include more HS contents (50%HS and 60%HS), because these samples present higher crystallinities. In the case of TPU 40%HS, the material is more amorphous what explains the absence crystalline peaks. The decrease of crystallinity shown in the WAXD pattern for the TPUs under study is also observed in the DSC results.

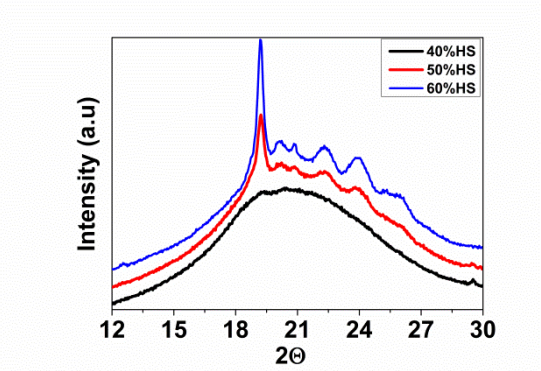

Figure 2. WAXD pattern of solid TPUs with different HS%.

The viscoelastic properties of the TPU samples were measured by DMTA. **Figure 3** shows the storage modulus, the loss modulus, and damping factor (tan δ), as a function of the temperature for the TPU samples prepared. The increase of HS% leads to an increase of the storage modulus, and to a decrease of the peak intensity maximum of both the loss modulus and the tan δ [15]. The increase of HS implies an increase in cristallinity which provide rigidity to the material, and consequently the storage modulus increases [16]. Moreover, the onset of the peak of Tg measured by DMTA shows similar temperatures to those measured by DSC.

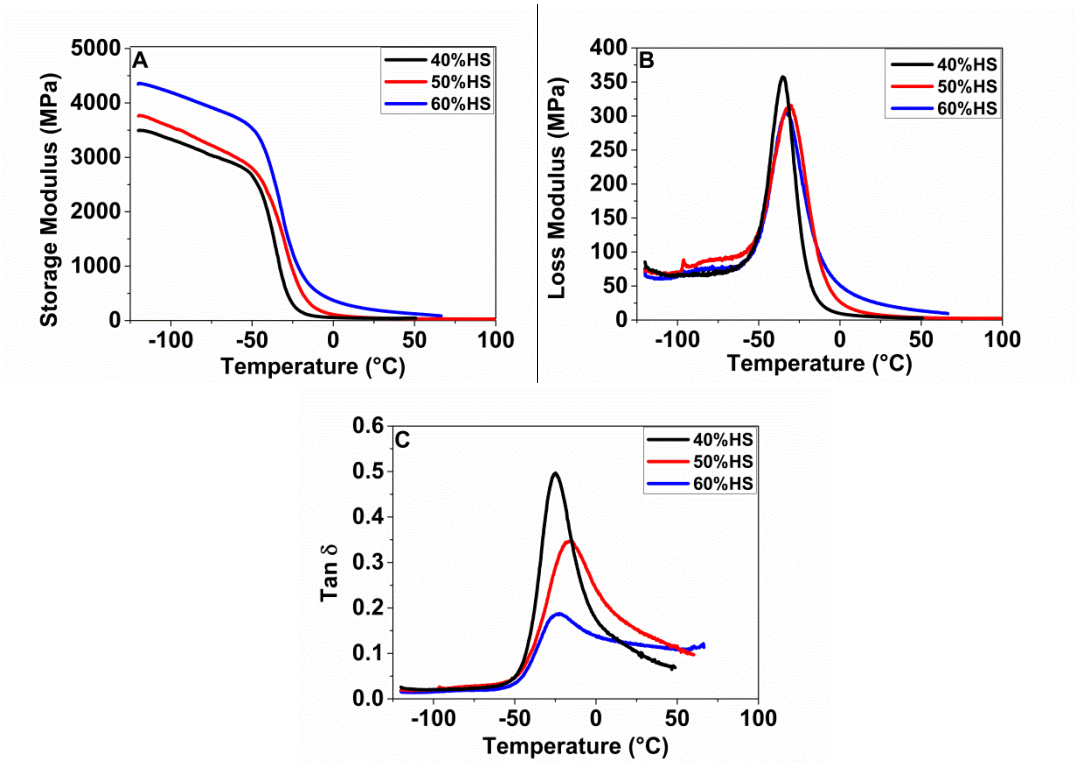

Figure 3. Dynamic mechanical analysis of solid TPUs with different HS%.

A rheological characterization was performed for the TPU samples with different HS% to determine the complex viscosity curves shown in **Figure 4**. TPU 40%HS and TPU 60%HS show small complex viscosities at low frequencies, whereas TPU 50%HS displays a considerably increase of complex viscosity. The difference in melt viscosity becomes smaller at relatively high shear frequency. Clearly, the TPU with 50 wt. % HS greatly increases the melt viscosity in all the angular frequencies respect to the rest of TPU systems, what could favor its foamability capability. These complex viscosities are in concordance with the molecular weights of each material (**Table 2**), being the TPU with 50 wt. % HS that has higher molecular weight and complex viscosity than the rest of materials. Moreover, TPU with 50 wt. % HS exhibits plastic behavior, since the slope of the regression line is -0.96 [17]. However, TPU 40%HS and TPU 60%HS have a Newtonian behavior, because the slopes of their regression lines are -0.06 and -0.03, respectively [17].

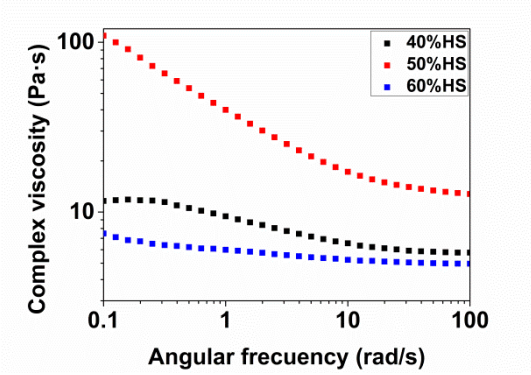

Figure 4. Complex viscosity as function of the angular frequency for TPUs with different HS%.

3.2. Study of TPU foaming

The TPUs previously prepared were foamed by gas dissolution foaming process in one-step, in order to study the effect of HS content (40 wt%, 50 wt% and 60 wt. %) in the foaming behaviour. We selected low contents in HS since previous studies showed that most of the CO_2 used for foaming process is dissolved in SS [7].

In the first part of the study, we evaluated the influence of the foaming temperature by using five different foaming temperatures: 140 °C, 150°C, 160 °C, 170 °C and 180 °C. The saturation pressure and foaming time were kept constant at 20 MPa and 1h respectively. **Figure 5** shows the SEM micrographs of the TPU samples after the foaming process. Only the TPU with 50 wt. % HS shows a stable cellular structure for the different foaming conditions used. However, the TPU with 60 wt. % HS does not foam, probably due to its high HS content, that results in a high crystallinity (DSC results in **Table 3** and WAXD pattern in **Figure 2**) and a high rigidity (Shore harness in **Table 2**), and also its low viscosity (**Figure 4**). Conversely, the TPU with 40 wt. % HS with low crystallinity (DSC results in **Table 3**) gives rise to a highly deteriorated cellular

structure, clearly seen in **Figure 5**, especially for high foaming temperatures. The low quality of this cellular structure can be attributed mainly to the low viscosity of the TPU matrix (**Figure 4**), which could reduce the stability of the cellular structure, thus producing cell coalescence and/or collapsing.

Hence, the characteristics of the TPU with 50 wt. % HS are optimum in order to get a better foamability. The relative density, average cell size, and cell nucleation density of the samples foamed with 50 wt. % HS were measured, and the values obtained are presented in **Figure 6**. **Figure 6.A** shows that the relative density decreases as the foaming temperature increases, reaching maximum values of expansion at 170°C, when the saturation pressure and foaming time are maintained. On the one hand, the average cell size decreases when the foaming temperature increases (**Figure 5** and **Figure 6.B**), the cellular structure being less homogeneous at lower foaming temperatures (140°C and 150°C) possibly due to the crystalline part of TPU is not melted at these temperatures. The TPU foamed at 170 °C displays a small cell size of 5 microns, and a homogeneous cellular structure. The cell nucleation density increases as the foaming temperature increases (**Figure 6.C**), what points to a higher number of cells in the foams produced. A maximum cell nucleation density of $3.5x10^9$ nuclei/cm^3 is reached at 170 °C for all the foaming experiments, which coincides with the lowest cell size of 5 microns and with the lowest relative density of 0.814. These results indicate that the most efficient foaming is reached at 170°C. At 180°C, the cell nucleation density is slightly reduced, and consequently both cell sizes and relative densities slightly increase. These results are a consequence of the softening of the TPU polymer, which foams above the melting temperature.

Since the TPU 50%HS is the optimum content of HS, it was selected in order to optimize the foaming of our TPU system in the second part of this study. For this purpose, the influence of the saturation pressure for TPU 50%HS was evaluated using four different saturation pressures: 10, 15, 20 and 25 MPa, whereas the foaming temperature and foaming time were kept constant at 170 °C and 1 h respectively. These conditions were chosen since the TPU foams with the best characteristics had been previously obtained with this foaming temperature. SEM micrographs and parameters of the TPU foams with 50 wt. % HS are collected in **Figure 7** and **Figure 8**. **Figure 8.A** shows the relative density values, which decrease with the saturation pressure, achieving the lowest relative density when using 25 MPa. Moreover, **Figure 8.B** indicates that a saturation pressure increase leads to important cell size reduction, what is clearly observed in the SEM micrographs shown in **Figure 7**. Thus, the lowest cell size reduction is obtained for TPU foamed at 25 MPa. All these results are in concordance with the trend of the cell nucleation densities shown in **Figure 8.C**, which increase when increasing the saturation pressure. In general, the increase of the saturation pressure causes a higher amount of gas dissolved in TPU matrix, what leads to smaller relative densities and cell sizes, and also a to a higher cell nucleation density. Nevertheless, the TPU material is scarcely foamed at low saturation pressure (10 MPa), as observed in **Figure 7**.

In conclusion, the optimum foaming and saturation conditions for the TPU with 50 wt. % HS are 170 °C of saturation pressure, 25 MPa of foaming pressure and 1h of saturation time. The resulting TPU foam has the lowest relative density (0.739), the smallest cell size (4 microns), and the maximum cell nucleation density ($8.0x10^9$). In the literature [13], a TPU synthesized with similar components to that used in our study (MDI as isocyanate, macrodiol as polyol and diol as chain extender) and with a similar HS% (48 wt. % HS) was foamed in one-step, and it presented a heterogeneous cellular structure with the smallest cell size of *ca.* 0.5 µm, its relative density was 0.91 and the cell density was 4 x 10^9 cells/cm^3. Therefore, the relative density (0.739) of TPU foam under our study is lower than that of the TPU foam found in the literature (0.91) [13] and also our material has an homogeneous cellular structure.

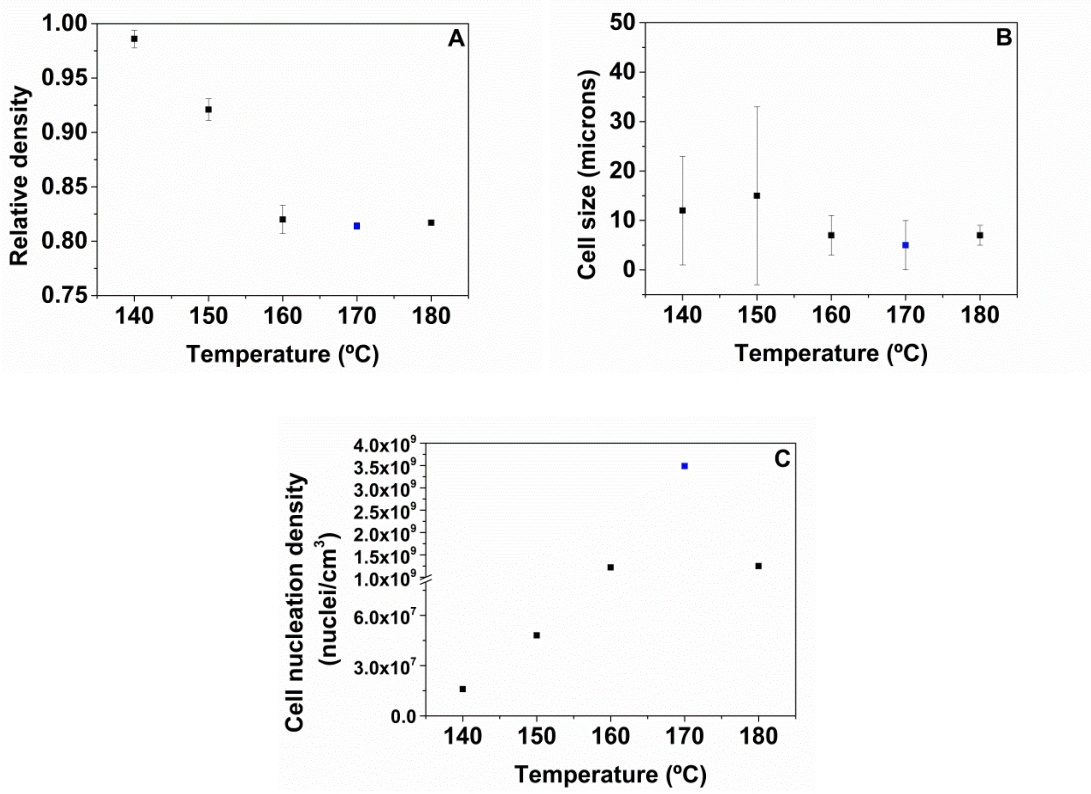

Figure 6. Relative density **(A)**, cell size **(B)** and cell nucleation density **(C)** of TPU 50%HS foamed by 1-step between 140-180°C, 20 MPa and 1h.

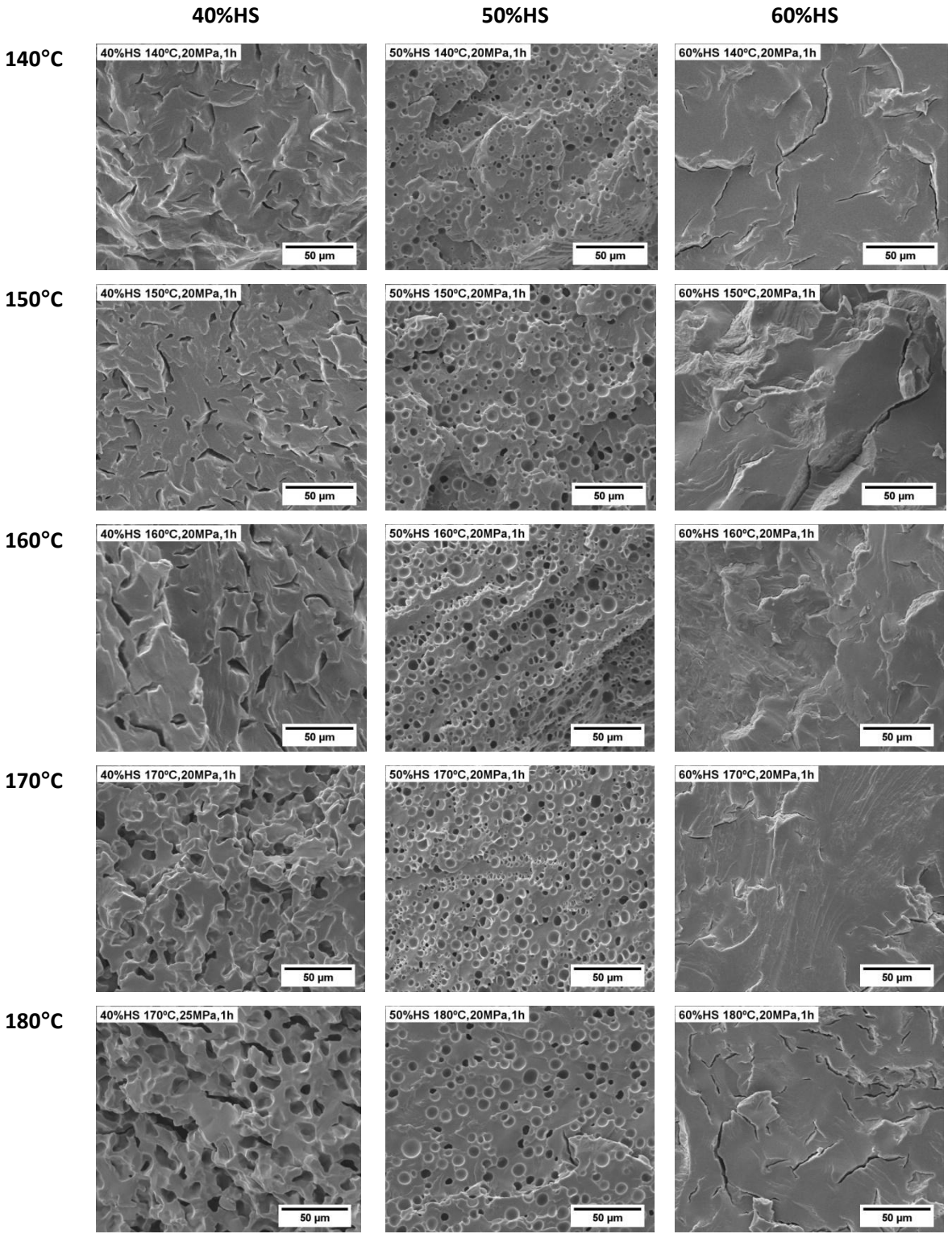

Figure 5. SEM micrographs of TPU with different HS% foamed by one-step between 140-180°C, 20 MPa and 1h.

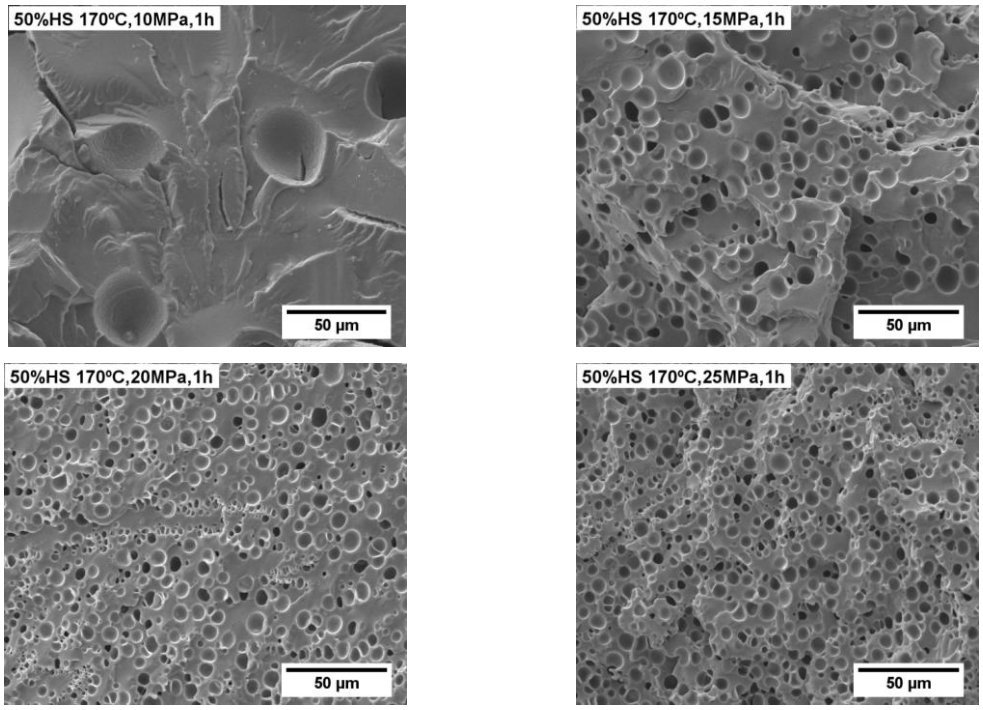

Figure 7. SEM micrographs of TPU 50%HS foamed by one-step between 10-25MPa, 170°C and 1h.

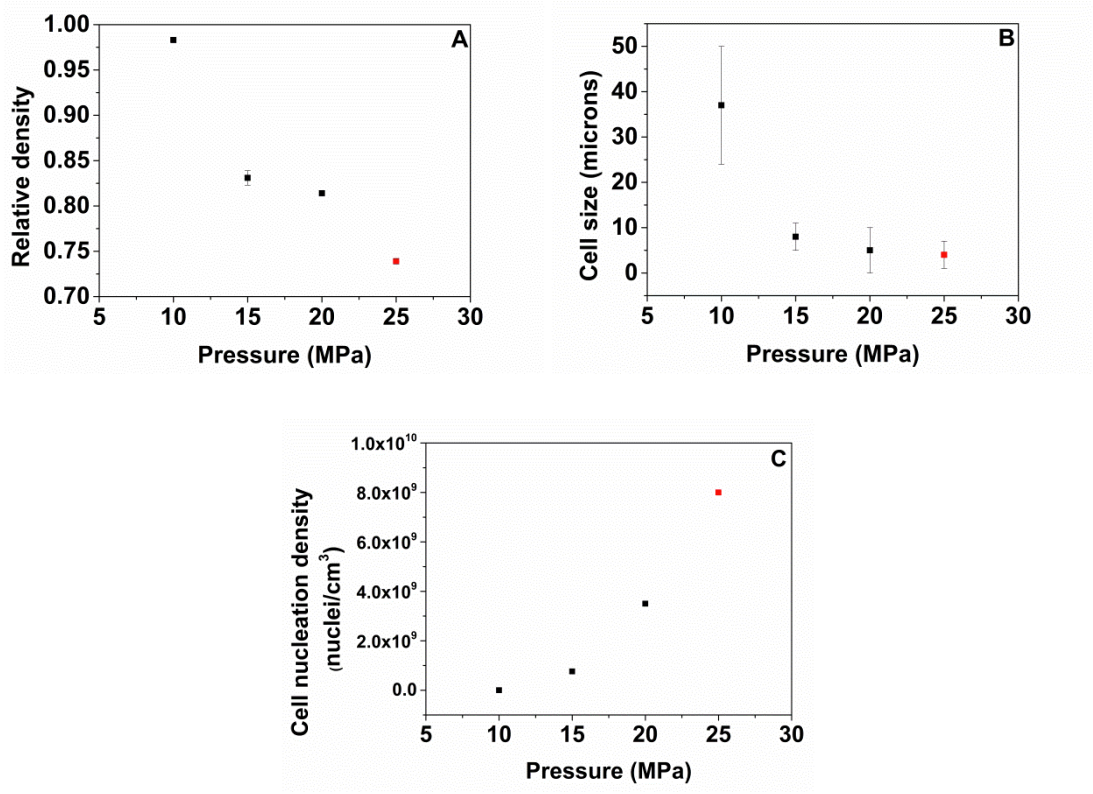

Figure 8. Relative density **(A)**, cell size **(B)** and cell nucleation density **(C)** of TPU 50%HS foamed by one step between 10-25MPa, 170°C and 1h.

4. Conclusions

A series of TPU based on MDI, PEG-PPG-PEG and 1,5-PDO components with low contents of HS (40, 50 and 60 wt. %) are synthesized using the pre-polymer method. These TPUs are well characterized by measuring their densities, shore hardness, GPC, DSC, WAXD, DMTA and rheology.

These TPUs are foamed by using CO_2 gas dissolution one-step foaming process. The study of the influence of the foaming temperatures from 140°C to 180°C, maintaining a saturation pressure of 20 MPa and a foaming time of 1h allows to conclude that (a) the optimum HS content to obtain TPU foams is 50 wt. %; and (b) the best foaming temperature is 170°C, because at this temperature the lower relative density is reached. Higher or lower HS ratios do not lead to TPU foams, since that with 60 wt. % HS has a high crystallinity and rigidity, and that with 40 wt. % HS has a low viscosity which no allow to stabilize the developed cellular structure.

Finally, the conditions to obtain the TPU foam with 50 wt. % HS were optimized by varying the saturation pressure from 10 to 25 MPa, whereas the foaming temperature (170 °C), and the foaming time (1 h) were maintained. The best foaming and saturation conditions are 170°C, 25 MPa and 1 h, since these conditions led to TPU foams with the lowest relative density (0.739), the smallest average cell size (4 microns), and a improved cell nucleation density ($8.0x10^9$).

In the field of TPU foams, there are very few reports that deal with synthesized TPU foamed by using CO_2 gas dissolution foaming process. As a main conclusion of our study, new series of synthesized TPUs have been researched in order to produce TPU foams with optimal characteristics.

Acknowledgments

Financial support from FPU grant FPU14/02050 (Victoria Bernardo) from the Spanish Ministry of Education and Junta of Castile and Leon grant (Judith Martín-de León) is gratefully acknowledged. Financial assistance from MINECO, FEDER, UE (MAT2015-69234-R) and the Junta de Castile and Leon (VA011U16) are gratefully acknowledged. Alberto Saiani is grateful to the Engineering and Physical Sciences Research Council (EPSRC Fellowship Grant No. EP/K016210/1) for financial support. Haneen Naji is grateful to the Iraqi Ministery of Higher Education and Scientific Research (MOHESR) for sponsoring her PhD. All research data supporting this publication are directly available within this publication.

References

[1] Polymer Foams Market Expected to Consume 25.3 Million Tonnes by 2019. http://www.smithersrapra.com/news/2014/may/polymer-foam-market-to-consume-25-3-million-tonnes, 2014 (accessed 16 July 2019).
[2] C. Prisacariu, Polyurethane elastomers, Wien New York: Springer, 2011.
[3] S.G. Kazarian, Polymer Processing with Supercritical Fluids, Polymer Science, Series C, 42 (2000) 78-101.
[4] I. Tsivintzelis, A.G. Angelopoulou, C. Panayiotou, Foaming of polymers with supercritical CO2: An experimental and theoretical study, Polymer, 48 (2007) 5928-5939.
[5] E. Reverchon, S. Cardea, Production of controlled polymeric foams by supercritical CO2, The Journal of Supercritical Fluids, 40 (2007) 144-152.
[6] X. Dai, Z. Liu, Y. Wang, G. Yang, J. Xu, B. Han, High damping property of microcellular polymer prepared by friendly environmental approach, The Journal of Supercritical Fluids, 33 (2005) 259-267.
[7] S. Ito, K. Matsunaga, M. Tajima, Y. Yoshida, Generation of microcellular polyurethane with supercritical carbon dioxide, Journal of Applied Polymer Science, 106 (2007) 3581-3586.
[8] R. Rizvi, H. Naguib, Porosity and composition dependence on electrical and piezoresistive properties of thermoplastic polyurethane nanocomposites, Journal of Materials Research, 28 (2013) 2415-2425.
[9] A. Prasad, G. Fotou, S. Li, The effect of polymer hardness, pore size, and porosity on the performance of thermoplastic polyurethane-based chemical mechanical polishing pads, Journal of Materials Research, 28 (2013) 2380-2393.
[10] S.-K. Yeh, Y.-C. Liu, W.-Z. Wu, K.-C. Chang, W.-J. Guo, S.-F. Wang, Thermoplastic polyurethane/clay nanocomposite foam made by batch foaming, Journal of Cellular Plastics, 49 (2013) 119-130.
[11] S.-K. Yeh, Y.-C. Liu, C.-C. Chu, K.-C. Chang, S.-F. Wang, Mechanical Properties of Microcellular and Nanocellular Thermoplastic Polyurethane Nanocomposite Foams Created Using Supercritical Carbon Dioxide, Industrial & Engineering Chemistry Research, 56 (2017) 8499-8507.
[12] C.-C. Chu, S.-K. Yeh, S.-P. Peng, T.-W. Kang, W.-J. Guo, J. Yang, Preparation of microporous thermoplastic polyurethane by low-temperature supercritical CO2 foaming, Journal of Cellular Plastics, 53 (2017) 135-150.
[13] S.-K. Yeh, Y.-R. Chen, T.-W. Kang, T.-J. Tseng, S.-P. Peng, C.-C. Chu, S.-P. Rwei, W.-J. Guo, Different approaches for creating nanocellular TPU foams by supercritical CO2 foaming, Journal of Polymer Research, 25 (2017) 30.
[14] J. Pinto, E. Solorzano, M.A. Rodriguez-Perez, J.A. de Saja, Characterization of the cellular structure based on user-interactive image analysis procedures, Journal of Cellular Plastics, 49 (2013) 555–575.
[15] Kim_et_al, Preparation and Properties of Segmented Thermoplastic Polyurethane Elastomers with Two Different Soft Segments, Journal_of_Applied_Polymer_Science, (1999).
[16] V. Costa, A. Nohales, P. Felix, C. Guillem, D. Gutierrez, C.M. Gomez, Structure–property relationships of polycarbonate diol-based polyurethanes as a function of soft segment content and molar mass, Journal of Applied Polymer Science, (2015).
[17] S. Scognamillo, E. Gioffredi, M. Piccinini, M. Lazzari, V. Alzari, D. Nuvoli, R. Sanna, D. Piga, G. Malucelli, A. Mariani, Synthesis and characterization of nanocomposites of thermoplastic polyurethane with both graphene and graphene nanoribbon fillers, Polymer, 53 (2012) 4019-4024.

CHAPTER 8:

CONCLUSIONS AND FURURE WORK

Mercedes Santiago Calvo

8.1- Conclusions

This section summarizes the main conclusions and achievements of the research performed in this thesis, which are in accordance with the objectives initially presented (**chapter 1, section 1.3**).

As a general achievement of this thesis, new knowledge has been acquired in the two methods that can be used to manufacture foamed materials based on polyurethane (PU): by reactive foaming (thermoset PU foams) and by gas dissolution foaming (thermoplastic PU (TPU) foams) (see **Figure 8.1**). The study of thermoset PU foams constitutes the main part of the thesis (**chapters 4, 5 and 6**), whereas the study of TPU foams is complementary to this and was begun during the international stay in the University of Manchester (**chapter 7**). The conclusions of each part are presented separately in the next sections.

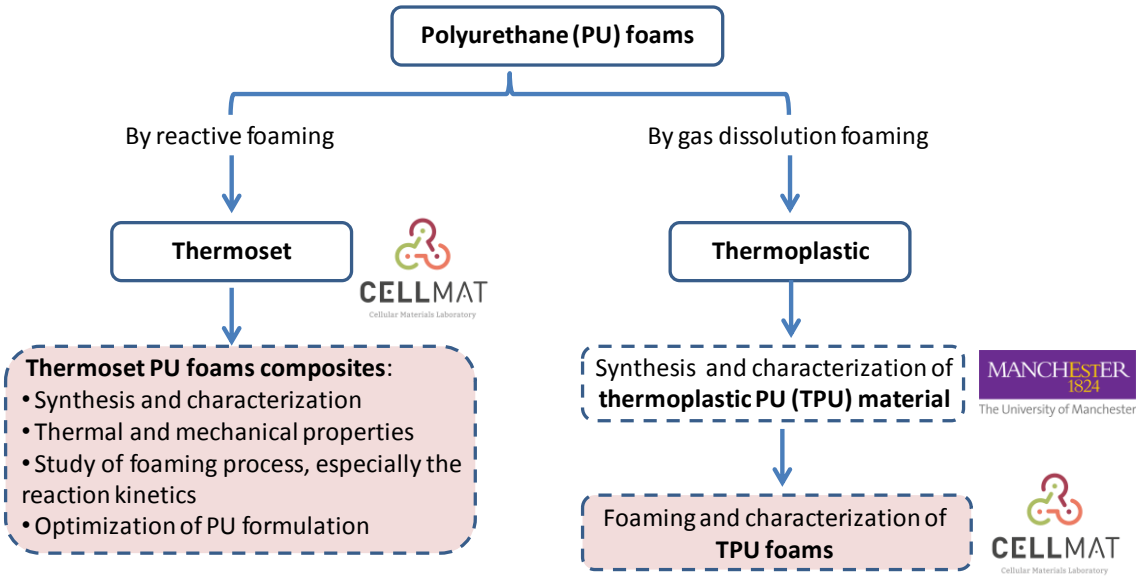

Figure 8.1. Simplified scheme of the investigations developed in this thesis.

8.1. Thermoset polyurethane foams

The work developed in the present thesis continues the research line based on PU foams of CellMat laboratory, but for the first time mainly focusing the research on the chemical aspects. In thermoset PU foams are crucial the balance between the reactions implicated in the PU foam formation (blowing and gelling reactions) in order to obtain a foam with desired properties. However, the inclusion of particles in the PU matrix with the aim of improving the foam properties may modify the kinetics of the reactions, giving rise to unexpected consequences on the properties of the final foam. Therefore, understanding these effects is

necessary to make better use of particles, and finally to get better cellular structure and foam properties. Therefore, the **first objective** of this thesis was:

Acquiring new knowledge about the **thermoset PU foams** (particularly RPU foams), focusing on the study of the foaming process, especially the reaction kinetics of the gas generation (blowing reaction) and polymerization (gelling reaction) when micro- and/or nanoparticles are incorporated into the PU matrix to improve the thermal and mechanical properties.

To fulfill this objective a methodology that allows evaluating the changes produced in the foaming process when fillers are incorporated in the PU matrix in order to get better foam properties has been established. This methodology is based on the use of the following complementary techniques: *in-situ* FTIR spectroscopy, infrared (IR) expandometry, foaming temperature measurements, and *in-situ* X-ray radioscopy. Three articles that deal with these techniques are presented in **chapter 4** and their main conclusions are summarized below (**see Figure 8.2**).

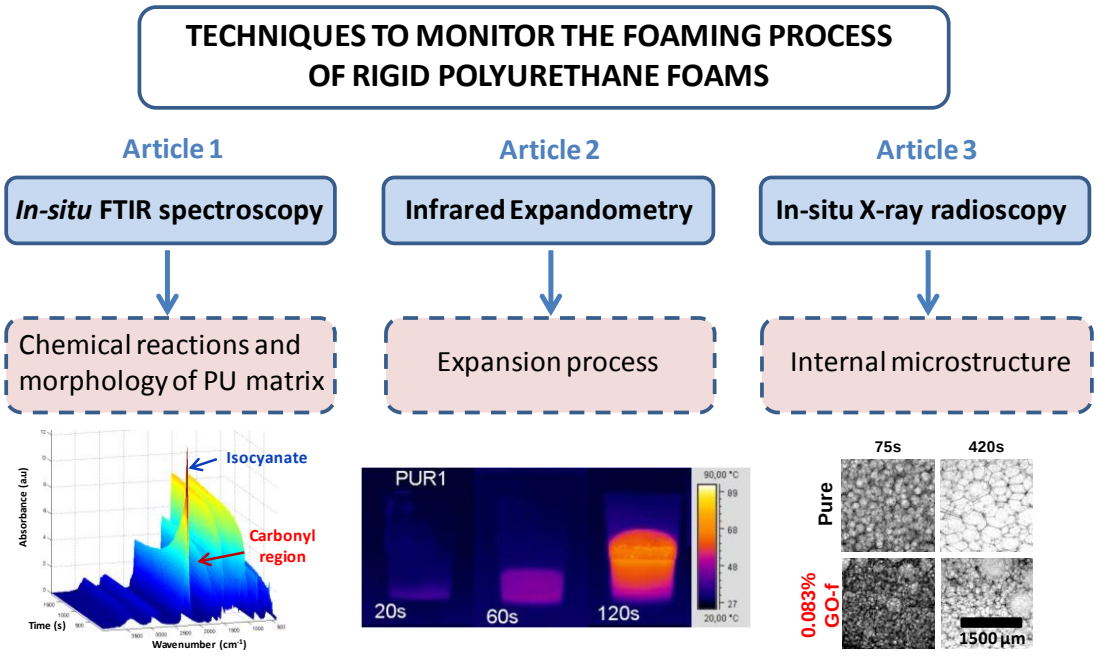

Figure 8.2. Scheme of the techniques used to follow the foaming process of RPU foams.

In the first article, a methodology based on *in-situ* FTIR spectroscopy has been established in order to study the kinetics of the main chemical reactions (blowing and gelling) and the morphology of the polymeric matrix during the foaming process of RPU foams (**see Figure 8.2**)**.** This work allows obtaining the following conclusions:

- **Reaction kinetics.**
  - This methodology is tested for water-blown RPU foams reinforced with 5 wt% of different nanoclays and nanosilicas: nanosilica A200 (hydrophilic), nanosilica R812 (hydrophobic), nanosilica R974 (partially hydrophilic/partially hydrophobic), CNa+ (hydrophilic) and C30B (partially hydrophilic/partially hydrophobic).
  - The kinetic data allows correlating the isocyanate consumption with the type of nanoparticles and their superficial groups. Thus, the foams containing nanosilicas show higher isocyanate conversions than those containing nanoclays, whereas those nanoparticles containing hydrophobic groups afford higher isocyanate conversions.
  - The quantification of urethane and urea, obtained by deconvolution of the carbonyl region absorptions, enables to follow the blowing and gelling reactions during the foaming process. This information allows concluding that nanoparticles containing hydrophilic groups on their surface (A200 and CNa+) enhance the blowing reaction, giving higher percentages of urea products (38.4% and 34.25 for A200 and CNa+ respectively) in comparison with pure foam (33.3%). Moreover, R974 also exhibits a blowing reaction increase (37.6% of urea products), due to its dual behavior with hydrophilic and hydrophobic groups on its surface. One of the possible reasons for the increase of blowing reaction could be the water present on these hydrophilic particles, which could be released during the foaming process. Instead, nanosilica R812, that only contains hydrophobic groups on the surface (90% methyl groups), and nanoclay C30B, which contains both hydrophilic and hydrophobic groups on their surface, enhance the gelling reaction (70.5% and 73.1 of urethane products for R812 and C30B, respectively) in comparison with pure foam (66.7% of urethane products).
- **Properties of the foams.**
  - The effect of the modification of the reaction kinetics induced by the nanoparticles on the density, cellular structure, viscoelastic properties, thermal conductivity and mechanical properties is discussed.
  - Density is reduced for systems in which the blowing reaction is enhanced (foams with R974 and CNa+). However, when the blowing reaction is accelerated in a significant extent the strong decoupling between blowing and gelling promotes a deterioration of the cellular structure, as observed for the A200 system (with the highest urea percentage, 38.4%).
  - The conversion degree clearly affects the viscoelastic properties of the foams, since a higher isocyanate conversion promotes both a higher glass transition temperature and a lower degree of mobility of the polymer chains. The foam containing nanosilica R812 (with the highest isocyanate conversion) displays the highest Tg, whereas the foam containing nanoclay CNa+ (with the smallest isocyanate conversion) affords the lowest Tg value.
  - In addition to these effects, all the analyzed nanoparticles act as nucleating agents during the process, reducing the average cell size and decreasing the homogeneity of the cell size distribution. Cell size is highly reduced up to 34% by nanoclays, and up to 22% by nanosilicas, compared to the value of the pure foam. Thus, nanoclays

are more effective than nanosilicas, possibly because the specific surface area of nanoclays is higher than those of nanosilicas.

- Moreover, the high content of particles used induces an increase of the open cell content. Clearly, nanosilicas give rise to higher open cell content (15% and 23% for R812 and R974) compared to those of nanoclays (11% and 8% for CNa+ and C30B, respectively) and pure foam (5%).
- These modifications of the cellular structure lead to a reduction of the thermal conductivity for the systems containing clays since these present a cell size reduction which promotes the reduction of the heat transfer by radiation and the open cell content does not increase significantly in comparison with that of the pure foam. However, the system containing nanosilicas present similar (R812) or higher (R974) thermal conductivity than of the reference material. This is probably due to the high open cell content of these two materials, which induces a significant increase of the heat transfer by radiation in spite of their reduced cell size.
- A decrease of the compressive properties is obtained for all the studied foams, which is mainly due to the increase of the open cell content by the particle addition.

In the second work, a novel experimental technique, infrared expandometry, is introduced in order to monitor the expansion process of RPU foams, by taking advantage of their exothermic foaming process (**see Figure 8.2**)**.** This work allows obtaining the following conclusions:

- **The main characteristic of this technique.**
  - This technique is based on the infrared radiation emitted by a body at a given temperature. Considering the exothermic foaming process of RPU foam, the expansion process can be recorded using an infrared camera and the analysis of the images acquired allows determining the evolution versus time of important parameters of the foaming process, such as height, volume, expansion rate, acceleration rate, and surface temperature. Moreover, the homogeneity of the surface temperature is evaluated by several parameters, such as the normalized standard deviation, the normalized temperature variation, and the evolution of the vertical profile of the surface temperature.
  - Some of the advantages of this technique are the following: the in-situ monitoring of foaming kinetics from the initial time, the study of samples without size restrictions and the measurement of surface temperature at certain points of the surface or for the whole sample surface. In addition to this, the surface temperatures are measured without interfering with the expansion process, as opposed to traditional thermocouple measurement**s.** Finally, this technique allows a quick and simple processing of the images by image analysis due to the important temperature differences between the sample and the background that gives a high image contrast**.**

- **Tested polyurethane systems.**
  - Infrared expandometry is herein tested for four different water-blown RPU foams, which differ in the amount of water (2 or 5 ppw) and in the blowing catalyst used (0 or 2 ppw).
  - PUR1 and PUR2 have been obtained by using the same amount of water in the PU formulation (2 ppw), which is lower than that used in foams PUR3 and PUR4 (5 ppw). Since water acts a blowing agent, the final expansion of the two latter foams is higher. On the one hand, PUR1 and PUR2 reach approximately 9 cm in height, and consequently *ca.* 600 cm^3 in volume. On the other hand, PUR3 and PUR4 show a higher final expansion, reaching 15 cm in height, and reaching a total volume close to 1000 cm^3.
  - The studied samples also can be divided into two separated groups depending on the presence of the blowing catalyst in the PU formulation. PUR1 and PUR3, which do not contain blowing reaction catalyst, expand relatively slowly, with a maximum peak in the expansion rate curves located at *ca*. 70s. Since the formulation of PUR2 and PUR4 contain 2 parts of the blowing reaction catalyst, the expansion of these two samples is very fast. On the other hand, when foams with the same amount of catalyst are compared (PUR1 vs. PUR3, and PUR2 vs. PUR4) foams containing higher amounts of water in the PU formulation (PUR3 and PUR4) reach higher maximum expansion rates.
  - PUR2 and PUR4, which contain the blowing catalyst, reach higher temperatures (both average and maximum temperatures), and these temperatures are reached in a shorter time compared with PUR1 and PUR3, which do not contain blowing catalyst. When formulations containing the same amount of catalyst are compared, the presence of water in the reaction also accelerates the sample heating. Moreover, the surface temperature measured during foaming with the infrared camera was supported by the temperature measurement with a thermocouple placed near to the surface, since both methods showed the same trend.
  - The evolution of the vertical profiles of surface temperature allows evaluating the inhomogeneities of temperature in the surface of the samples. Figure 15 shows that all the foams reach the maximum temperature approximately in the center of the sample. The vertical profiles of surface temperature allow evaluating the inhomogeneities of temperature in the surface of the samples. These are less homogeneous for the foams containing blowing catalyst (PUR2 and PUR4) than those for foams without blowing catalyst (PUR1 and PUR3).
  - Therefore, this work demonstrates the potential of this technique in order to follow the expansion kinetics of PU foams.

In the third article, in-situ X-ray radioscopy is applied to study the internal microcellular structure and relative density during the foaming process of RPU foams (**see Figure 8.2**)**.** This work allows obtaining the following conclusions:

- **Foaming behavior.**
  - This technique is used to compare the foaming behavior of two series of foams: those prepared from polyols functionalized with GO (GO chemically linked to polyol chains labeled as GO-f) and those containing GO dispersed into the polyol (labeled as GO-d) by high shear mixing (loading of 0.017 and 0.033 wt%). From X-ray radioscopy experiments, the relative density, cell size and cell nucleation density at intermediate stages of the foaming process are evaluated.
  - At the end of the foaming process (*ca.* 560 s), the foams with GO-f reach relative densities slightly higher than that of the reference material, as the amount of GO-f increases. However, the opposite result is found for the foam with higher GO-d content (0.083 wt. %), since a slightly decrease in relative density with respect to pure material is observed.
  - The radioscopy results show that the cell size decreases as the GO-f content increases in comparison to the reference system, the reduction reached for 0.017 wt. % and 0.083 wt. % of GO-f being 16 % and 30%, respectively. Conversely, the cell size is reduced by *ca.* 20% for the foam with 0.017 wt. % GO-d, whereas the cell size is not reduced for the foam with 0.083 wt. % GO-d in comparison to the values of the reference material. This result could be explained considering that a low content of GO may be easily dispersed, whereas a high content could form aggregates.
  - At the early stages, the results show that the number of nucleation sites increases for the samples with GO-f compared to the reference material, the cell nucleation density being superior for the highest GO-f content. The evolution of the cell nucleation density shows that there is coalescence in all the systems under study, because the cell nucleation density decreases with time, this coalescence being more pronounced in systems with GO-f. Despite this, the enhanced nucleation experienced by foams with GO-f prevails at the final stages over the cell degeneration processes, what is in accordance with the cell size reduction described above. In the case of foam with 0.017 wt% GO-d, this does not present an increase in cell nucleation density respect to reference foam, but less degeneration mechanism occurs. For this reason, this foam presents cell nucleation density similar to that of foam with 0.017 wt% GO-f.
  - The systems with GO-d present less reproducibility than those of the foams with GO-f. Thus, the results obtained demonstrate that the use of polyol functionalized with GO-f offers a great improvement of the cellular structure and also makes the results more reproducible**.**
- **Comparison of results from the radioscopy experiment and from the final foam.**
  - The foams produced during the X-ray radioscopy experiment present higher values of relative density (0.155±0.031 more) and smaller values of cell size (118±22 less) than those of the final foams. This is because these parameters are measured for smaller samples after 560 s, when the foaming process has not been yet completed, and the reduced size of the samples scanned by radioscopy limits the temperature generation reducing the foam expansion. However, the trends

observed in the radioscopy samples correspond to those of the larger samples, which allows validating the X-ray radioscopy results.

Once, the methodology of monitoring the foaming process has been established, it can be used to carry out an in-depth study of the effect of nanoparticles on the foaming behavior of an RPU foam system. This allowed getting **the second important objective** of this thesis:

Studying the effect that modifying the reactions could have on the structure and properties of the final materials.

Once, the modification of the PU reactions by nanoparticles addition is identified, this can be explained the morphology of the PU matrix and the final properties of the foam. Thus, this information allows fulfilling the third **important objective** of this thesis:

Optimizing the formulations of RPU systems containing particles using the kinetic information obtained.

Thus, to fulfill the above objectives, the water-blown RPU foams produced with polyols functionalized with GO are selected, since the previously X-ray radioscopy study showed that the use of GO-f provided many improvements in the cellular structure of the foams. These studies are included in **chapter 6** (article 6 and 7 of this thesis) and the conclusions obtained are summarized below (**see Figure 8.3**).

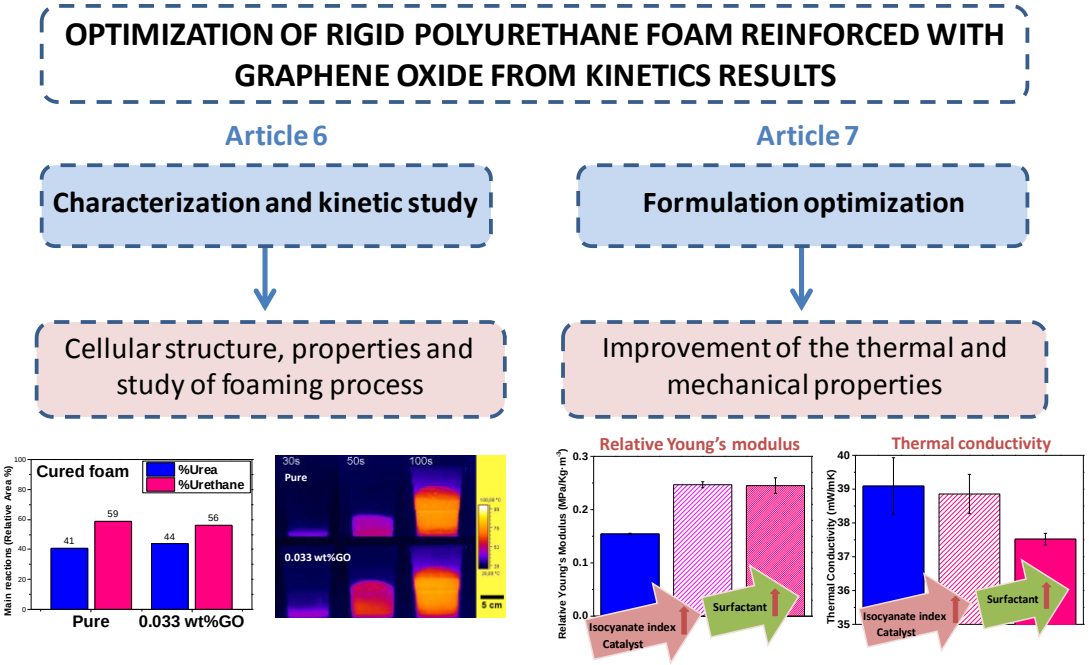

Figure 8.1. Scheme of the research focused on studying the effect of GO on the cellular structure, the properties and the foaming process, and the subsequent optimization of the PU formulation basing on the results of the previous foaming study.

In the sixth article, the methodologies of monitoring the foaming process are applied in water-blown RPU foams prepared with polyols functionalized with GO, and then correlations between the reaction kinetics, the final morphology of the polymer matrix, the cellular structure and the foam properties are established (**see Figure 8.2**)**.** This work allows obtaining the following conclusions:

- **Properties of the polyols functionalized with GO.**
  - Four different polyols are used to produce the water-blown RPU foams: the pure polyol, and those containing 500, 1000 and 2500 ppm of GO. GO is chemically linked to the polyol chains during the synthesis of the polyols.
  - The inclusion of GO decreases the hydroxyl number, being the polyol with 1000 ppm GO that showing a lower value.
  - The viscosity slightly increases for the polyols containing 500 ppm and 1000 ppm GO (553 mPa•s and 547 mPa•s, respectively), and it is obviously higher for the polyol containing 2500 ppm GO (4463 mPa•s) in comparison with that of the pure polyol (477 mPa•s).
  - The Mw value grows with the amount of GO, indicating that the GO promotes the polyol linear chain grafting.
  - The use of polyol functionalized with GO precludes the agglomeration of fillers, solving the usual problems of particles dispersion in polymer nanocomposites. In addition, small amounts of GO are necessary for improving foam properties.
- **Properties of the polyurethane foams from polyols functionalized with GO.**
  - Four different RPU foams are studied: the pure material (without GO, obtained as reference material), and those containing 0.017 wt% GO (500 ppm in polyol), 0.033 wt% GO (1000 ppm in polyol) and 0.083 wt% GO (2500 ppm in polyol) with respect to the final mass of RPU foams.
  - The density of the foams containing 0.017 and 0.033 wt% GO increases 1 kg/m^3 compared to that of the pure material, whereas the density of the foam containing 0.083 wt% GO increases around 3-4 kg/m^3. This could be related to the significant increase of the polyol viscosity when a high GO content is incorporated.
  - Open cell content increases with the GO addition, being the foam with the highest GO content (0.083 wt%) that showing the highest value (*ca.* 42%).
  - It is remarkable that the incorporation of small amounts of GO into polyol promotes an important cell size reduction of up to 33% for the material containing 0.083 wt% GO, demonstrating its effectiveness as cell nucleating agent.
  - Foams with low GO contents (equal or below 0.033 wt%) present similar anisotropy ratios than the reference foam.
  - Samples up to 0.033 wt% GO show a good homogeneity of the cell size distribution and a symmetric distribution, whereas the cell size distribution of the foam with 0.083 wt% GO is less homogeneous and highly asymmetric.
  - The addition of very small amounts of GO enhances the thermal properties because the cell size is reduced (from 529 μm for pure material to 355 μm for the foam containing 0.083 wt% GO) and the GO particles act as an infrared blocker, which reduces the radiation contribution to the thermal conductivity. The highest

reduction of around 5% is obtained with 0.033 wt% GO, thus this is the optimum GO content. Although the foam containing 0.083 wt% GO has the maximum cell size reduction, the thermal conductivity of this foam is higher than expected, and this seems to be due to the significant modifications observed in its cellular structure, which has a higher density, a more heterogeneous cellular structure, and a high open cell content. Moreover, an increase in the GO content could induce an increment of the contribution to conduction through the solid phase.

- The inclusion of the GO particles deteriorates the compressive mechanical properties of the foams. For the samples with low GO contents this slight decrease should be related with a different polymer morphology in the matrix of the foams, because the cellular structure of two materials is not worse than that of the reference foam. For the material with a high amount of GO (0.083 wt%) the decrease should be a combination of the mentioned modification of the polymer morphology with the deterioration of the cellular structure.

- **Kinetic study.**
  - The effect of GO on the foaming process is evaluated by infrared expandometry, FTIR spectroscopy and reaction temperature measurements. The kinetic studies are carried out for the pure foam and the optimum foam that is that with 0.033 wt% GO.
  - At the beginning of the foaming process, the FTIR spectroscopy shows more urethane formation for the foam with GO, and the polyol functionalized with GO has also higher viscosity. All this could make the viscosity in the polymer appropriate to prevent the escape of carbon dioxide generated in the blowing reaction, resulting in a fast expansion observe by infrared expandometry. On the other hand, the isocyanate might also react with carboxyl and/or hydroxyl groups of the GO surface, giving rise to the formation of amides and CO_2 and/or urethanes, respectively. Thus, the higher urethane percentage obtained when GO is present may be due not only to the gelling reaction between isocyanate and polyol, but also to the reaction between isocyanate and the hydroxyl groups on the GO surface.
  - At the late stages of the foaming process, the FTIR results show that the presence of GO enhances the blowing reaction (39% of urea products for foam with GO versus 35% of urea products for pure foam), what could be due to the release of the retained water on GO layers. Moreover, the foam containing GO presents a slightly decrease of isocyanate conversion (73%) respect to the pure foam (70%), what is also consistent with the lower temperatures reached for this system (the average maximum temperature reached was 129°C for foam with GO and 134 °C for the pure foam).

In the seventh article, the formulation of RPU foam with optimum content of GO (0.033 wt. %) is optimized in order to compensate the reduction in mechanical properties using the kinetic information (**see Figure 8.2**)**.** This work allows obtaining the following conclusions:

- **Optimized foams.**
  - A series of modifications in the formulation are defined and tested, such as the increases of the isocyanate index (from 115 to 130), of the contents of catalyst (from 1.5 to 2 ppw), or of the contents of surfactant (from 1 to 2 ppw), as well as the combination of these three components. These strategies are based on the effect of GO on the reaction kinetics and are mainly focused on the increase of both isocyanate conversion and polymerization reaction, which decreased for the foams containing GO.
  - The best performing formulation is that with a simultaneous increase of isocyanate index (130), catalyst content (2ppw), and surfactant content (2 ppw), which gives rise to a final foam where the cell size is reduced by a 25%, as well as to significant reductions of density (1 Kg/m^3 less), and of open cell content (from 7% for reference foam to 4% for the optimized foam). Correspondingly, the thermal conductivity is reduced by 4% and the mechanical properties are highly improved, so as Young's modulus and collapse stress are increased by 59% and 54% respectively.

Moreover, another objective of this thesis was to study the thermal conductivity and/or the mechanical properties of RPU foams reinforced with other interesting fillers. This objective was fulfilled in the works presented in **chapter 5** (articles 4 and 5 of this thesis). The main conclusions obtained from these works are summarized below (see **Figure 8.4**).

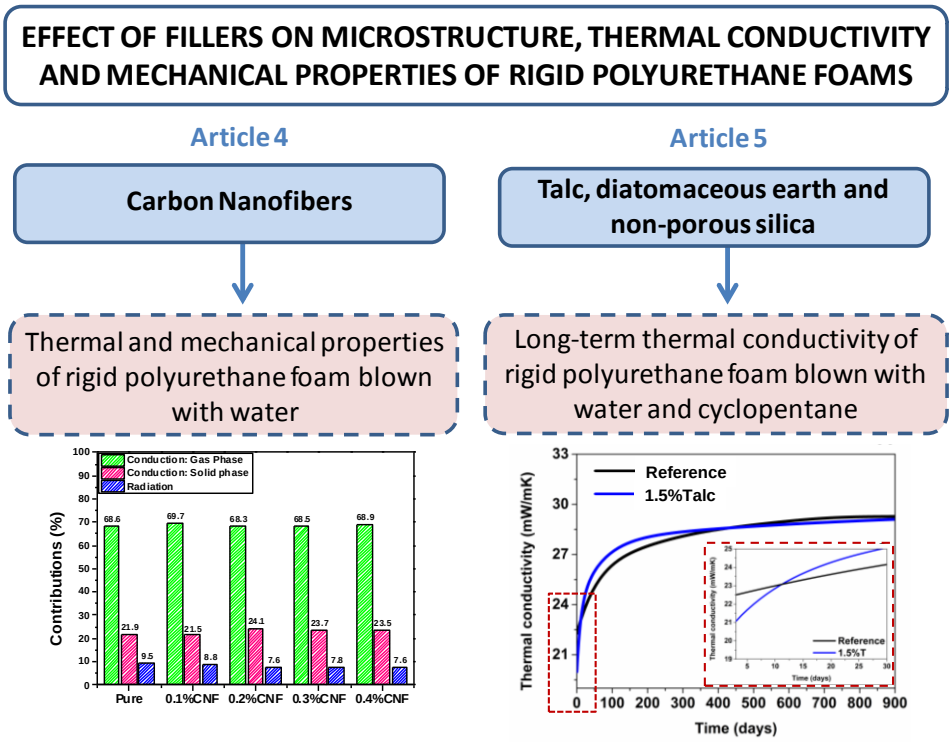

Figure 8.4. Scheme of the works focused on studying the effect of filler on microstructure, thermal conductivity and mechanical properties of RPU foams.

The thermal and mechanical properties of water-blown RPU foams are improved by reinforcement with carbon nanofibers (CNFs). This work allows obtaining the following conclusions:

- **Characteristics of the polyurethane foams.**
  - PUR foams with densities in the range of 55-60 kg/m^3 reinforced with small amounts of CNFs (0.1, 0.2, 0.3 and 0.4 wt%) are prepared and characterized.
  - The density slightly increases up to around 5 kg/m^3 when low amounts of CNFs are added. This increase in density is connected with the progressive increase in the viscosity of the CNF/polyol mixture when the particles are added.
  - Both open cell content and cellular structure of the foams slightly change with the addition of CNFs. The open cell content slightly increases from a value of 8.9% up to a value of 10.8% with CNFs addition. The cell size is reduced a 6% for the foam containing 0.2 wt.% CNFs, whereas increases a 7% for those samples with higher amounts of CNFs (0.3 and 0.4 wt% CNFs). Moreover, there are hardly changes in the cell size distribution and in the anisotropy..
  - Optical and SEM micrographs show that CNF nanoparticles are mainly situated in the struts and present a poor adhesion to the PU matrix due to their surface hardly has functional groups which can react with other functional groups present in foam components.
- **Thermal conductivity and mechanical properties.**
  - Moreover, the contributions of the heat conduction mechanisms are quantified by measuring the extinction coefficient and by modeling the thermal conductivity.
  - The inclusion of CNFs increases the extinction coefficient of the foam up to 27%, and as a consequence the radiative contribution of the thermal conductivity is reduced up to 20%.
  - The total thermal conductivity is reduced by 2% for the foam with only 0.1 wt% of CNFs. This is a remarkable result taking into account the relatively high densities of the foams studied and the small amount of CNF used. Concentrations higher than 0.1 wt% do not lead to higher reductions of the thermal conductivity due to an increase of the heat conduction through the solid phase (due to the density increase when the particles are added and to an increase of the thermal conductivity of the solid matrix).
  - On the other hand, the sample with 0.1 wt.% of CNFs added to the improved thermal insulation (2%), presents a slight increase in relative Young's modulus (8%) and maintains the relative collapse stress.

The long-term thermal conductivity of cyclopentane-water RPU foams reinforced with a different type of fillers (talc (T), diatomaceous earth (DE), and non-porous silica (NPS)) is measured along three years of aging.

- **Characteristics of the polyurethane foams.**
  - Different RPU foams blown with cyclopentane(CP) and water were studied: the pure material (without particles), and those containing 1.5 wt% T, 1 wt% DE, 3

wt% DE, 5 wt% DE, 0.05 wt% NPS, 0.1 wt% NPS or 0.2 wt% NPS with respect to the final mass of the RPU foams.

- The sample containing 1.5 wt% T has the highest density, which is *ca.* 4 kg/m^3 higher than that of the reference material. However, the rest of the samples with particles present similar densities respect to that of the reference material.
- The open cell content for the foams with particles slightly increases, being the foam containing 0.2 wt% NPS that showing the highest value (*ca.* 13%).
- Most notably, the addition of different types of particles into the polyol component promotes a mean cell size reduction of up to 50% for T particles, 46% for DE particles and 33% for NPS particles, respect to the value of the pure foam.
- Anisotropy does not increase for most of the samples in comparison to the reference foam (with 1.11 of anisotropy). Nevertheless, the sample containing 1.5 wt% T and that containing 0.05 wt% NPS show a slight increase in their anisotropy ratio (1.27 and 1.39, respectively) whereas the increase of the sample with 3 wt% DE is even higher (1.69).
- In general, the foams with particles show a symmetric distribution and a good homogeneity.

- **Thermal conductivity evolution of the polyurethane foams.**
  - In the early days after foam production, the thermal conductivity is enhanced in the samples with particles, in comparison to the reference material, principally due to the significant decrease in cell size, what is promoted by the reduction of the radiative contribution. However, the thermal conductivities evolve differently in each system, due to the variations of the gas composition inside cells with time, what in many systems (with the exception of 5%DE, 0.1%NPS and 0.05%NPS) lead to the loss of this first improvement of the thermal conductivity measured at initial times.
  - We have found for the first time, a relationship between the thermal conductivity slope at initial times and the foaming temperatures reached during the foam formation. The foams reaching higher foaming temperatures (systems with 1.5% T, 1%DE, 3%DE or 0.2%NPS) generate a high-pressure difference between the inside and the outside of the foam cells once the material is cooled down, and consequently a very quick diffusion of the gasses out the cells occurs. Meanwhile, the opposite behavior is observed for those foams reaching lower temperatures during their formation (systems with 5% DE, 0.05%NPS or 0.1%NPS).
  - The samples with lower foaming temperatures (5%DE, 0.05%NPS and 0.1%NPS) maintain during longer times lower thermal conductivity values, because the gas diffusion is slow. Even the thermal conductivity of the system with 5%DE, which has the lowest thermal conductivity slope, is lower than that of the pure material during 900 days. On the other hand, for the group of systems (1.5%T, 1%DE, 3%DE and 0.2%NPS) with higher foaming temperatures, there are some that recover the enhancement of the thermal conductivity over time. For example, the thermal conductivity value of the foam containing 1.5 wt% T is again lower than that of the value of the pure material after *ca.* 400 days, whereas the thermal conductivity of the foam with 3 wt% DE is improved after *ca.* 300 days. Moreover, it should be

expected that the improvement of the thermal conductivity observed in the first measurements would be recovered for all the foams with fillers once they reach a stationary state where the gas concentration is the same for all of them. This is because all the foams containing fillers have lower cell sizes than the reference material.

- Modeling the thermal conductivity of the foams allows calculating the evolution of the thermal conductivity of the gas mixture (λ_g) with time, which follows a similar trend to those of the slopes of the thermal conductivities experimentally measured.
- Moreover, the thermal conductivity model allows predicting the thermal conductivity values when the foams reach a stationary state (once all the gas inside the foam is air). The foams with a higher decrease of the cell size (T and D) would give rise to higher extinction coefficients, and therefore to higher thermal conductivity reductions. The best systems from this point of view are T and DE.
- This effect is related to the kinetics of the diffusion of the gas occluded inside the cells and imposes a new criterion for the selection of particles to reduce the thermal conductivity of RPU foams, these additives should ideally decrease the temperature reached during the foaming process. Moreover, the effect of aging on thermal conductivity is explained by using theoretical models.
- The findings of this study are important in the development of filled RPU foams with improved thermal conductivities. The filler has to be useful to reduce the cell size but at the same time it is needed that does not affect the temperature of the system or that the increase of temperature associated with the addition of the filler is compensated by modifications of the formulation.

8.2. Thermoplastic polyurethane foams

On the other hand, a small part of this thesis has been focused on the study of the foaming behavior of TPU materials using gas dissolution foaming (**Chapter 7**). The **objective of this part** was:

> Studying the foaming behavior of **TPU materials** using gas dissolution foaming in order to generate knowledge about TPU foams.

To fulfill this objective **a new series of TPUs with low contents of hard segments (HS) (40, 50 and 60 wt. %) has been synthesized by a pre-polymer method and from this series the effect that the different TPU composition has on the foaming behavior has been analyzed** (see **Figure 8.5**). This work allows obtaining the following conclusions:

- **Synthesis of TPUs.**
  - TPUs based on 4,4-diphenylmethanediisocyanate (MDI), poly(ethyleneglycol)-block-poly(propyleneglycol-block-poly(ethylen-glycol) (PEG-PPG-PEG) and 1,5-

pentanediol (1,5-PDO) components, with different HS contents (40, 50 and 60 wt. %), are synthesized by using the pre-polymer method.

- Extruded samples are prepared in order to examine their foaming behavior.

- **Characterization of solid TPUs.**
  - TPUs are well characterized by measuring their densities, shore hardness, GPC, DSC, WAXD, DMTA and rheology.
  - The density slightly increases when the HS content increases in the TPU material (from 1.068 Kg/m^3 for 40%HS to 1.101 Kg/m^3 for 50%HS).
  - The same happens with the shore D hardness, this increases from 22.3 for TPU 40%HS to 45.6 for 60%HS, which indicates that the material with 60 wt% HS is the most rigid of all those studied.
  - GPC measurements show that the molecular weights are higher for TPUs with low contents of HS (40%HS and 50%HS) than for TPU 60%HS.
  - DSC thermograms of all TPU samples display a first transition at *ca.* -45°C associated with the glass transition of the SS (TgSS), which is similar for all the materials studied. The second transition is observed at *ca.* 90°C, and is associated with the annealing temperatures, since the samples had been dried in a vacuum oven overnight at 80°C before the characterization and the foaming experiments. Finally, several endothermic peaks associated with the melting temperatures (Tm 1-3) of the HS crystalline are observed at higher temperatures, between 150°C and 180°C. Tm of TPU systems is shifted to higher temperatures when the HS content increases, and the HS crystallinity of the samples grows from 5.1% to 14.3% when the HS content increases from 40 wt. % to 60 wt. %.
  - The increase of crystallinity shown in the DSC results for the TPUs under study is also observed in the WAXD pattern.
  - The viscoelastic properties of the TPU samples were measured by DMTA. The increase of HS% leads to an increase of the storage modulus because this implies an increase in cristallinity which provide rigidity to the material. Also, the increase of HS% leads to a decrease in the peak intensity maximum of both the loss modulus and the damping factor (tan δ).
  - Rheological characterization shows that the TPU with 50 wt. % HS greatly increases the melt viscosity in all the angular frequencies respect to the rest of TPU systems, what could favor its foamability capability. These complex viscosities are in concordance with the molecular weights of each material, being the TPU with 50 wt. % HS that has higher molecular weight and complex viscosity than the rest of the materials.

- **TPU foams**.
  - TPUs are foamed by using CO_2 gas dissolution one-step foaming process and the density and cellular structure (cell size and cell nucleation density) of the resulting foams are also determined.
  - Firstly, the effect of foaming temperature from 140°C to 180°C is evaluated, fixing a saturation pressure of 20 MPa and a saturation time of 1 h. Among the TPUs studied, only with TPU with 50 wt% HS has obtained a stable foam. TPU with 60 wt. % HS does not foam due to its high HS content which results in a high

crystallinity and rigidity, and also its low viscosity. Conversely, TPU with 40 wt. % HS with low crystallinity gives rise to a highly deteriorated cellular structure. The low quality of this cellular structure can be attributed mainly to the low viscosity of the TPU matrix, which does not allow stabilizing the developed cellular structure.

Hence, the characteristics of the TPU with 50 wt% HS are optimum in order to get a better foamability. The relative density decreases as the foaming temperature increases, reaching maximum values of expansion at 170°C (0.814). On the one hand, the average cell size decreases when the foaming temperature increases, the cellular structure being less homogeneous at lower foaming temperatures (140°C and 150°C) possibly due to the crystalline part of TPU 50%HS is not melted at these temperatures. The TPU foamed at 170 °C displays a small cell size of 5 microns, and a homogeneous cellular structure. The cell nucleation density increases as the foaming temperature increases. A maximum cell nucleation density of $3.5x10^9$ nuclei/cm^3 is reached at 170 °C, which coincides with the smallest cell size of 5 microns and with the lowest relative density of 0.814. At 180°C, the cell nucleation density is slightly reduced, and consequently both cell sizes and relative densities slightly increase. These results are a consequence of the softening of the TPU polymer, which foams above the melting temperature.

- Finally, the foaming of TPU with 50 wt. % HS is optimized by varying the saturation pressure from 10 to 25 MPa, whereas the foaming temperature (170 °C), and the foaming time (1 h) are maintained. The relative density and cell size decrease with the saturation pressure, achieving the lowest relative density (0.739) and the lowest cell size reduction (4 microns) when using 25 MPa. Thus, the cell nucleation density increases with the pressure, reached the highest value ($8.0x10^9$ nuclei/cm^3) at 25 MPa. In general, the increase of the saturation pressure causes a higher amount of gas dissolved in TPU matrix, what leads to smaller relative densities and cell sizes, and also a to a higher cell nucleation density.

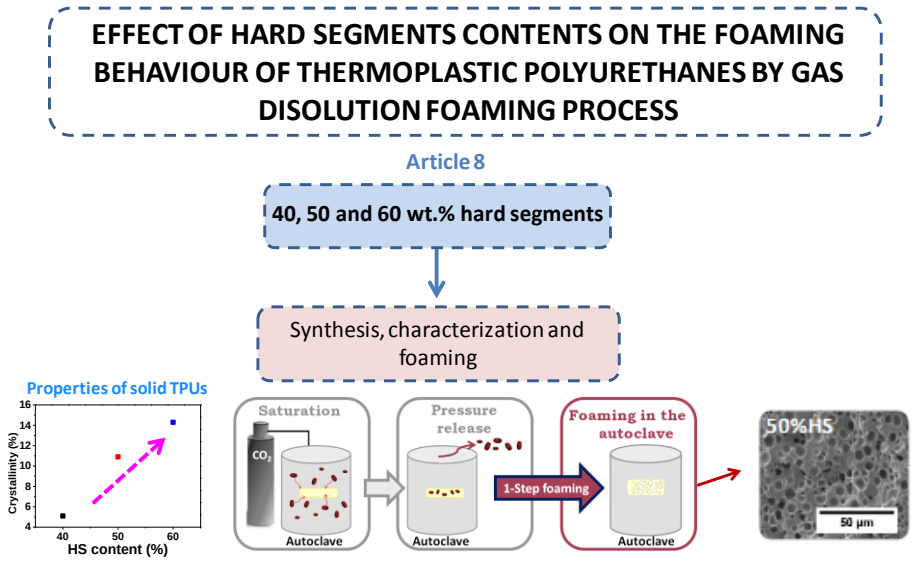

Figure 8.5. Scheme of the main objective of the scientific article about TPU foams.

8.2- Future work

The work performed in this thesis has opened several interesting research topics in the line of PU foams, which will be the focus of CellMat research in the following years. In the first place, the following ideas are proposed in order to continue generating knowledge in the area of **the thermoset PU foams** that have a large market:

- Evaluating the effect of air bubbles introduced when the isocyanate and polyol components are mixed by using different high shear mixing. In the case of RPU foams modified with microparticles and/or nanoparticles, this study would be interesting in order to separate the effect of both particles and air bubbles. To this end, different experiments could be carried out without air bubbles, for example by foaming under vacuum or by foaming with and injection machine. This approach would allow knowing the true effect of the particles on the cellular structure and on the properties of final foams.

- Looking for new strategies destined to improve the thermal insulation performance of RPU foams (with 4–35 mW/mK at low density, 25–50 kg/m^3). For example, the incorporation of aerogel particles in PU matrixes has scarcely studied and seems to be a promising strategy. Since one of the most important properties of aerogels is their low thermal conductivity (<20 mW/mK), the RPU foams reinforced with aerogels could reduce the thermal conductivity of the solid phase contribution, what is usually increased by conventional fillers. Therefore, it would be interesting to study in-depth RPU systems reinforced with commercial or synthesized aerogel particles, especially those based on PU that have not yet been manufactured. Another example could be the incorporation of liquid compounds such as ionic liquids, which would solve the dispersion problems presented by solid particles.

- Expanding the methodology used to analyze the reaction kinetics of the PU foams, starting to use other techniques such as DMTA or rheology. These techniques could give additional information to that obtained with the techniques presented in this thesis. The proposed techniques allow evaluating the modulus development during the foaming process, which could relate to the viscosity of the reactive mixture. Moreover, there are very few studies that follow the foaming process with these techniques, which suppose an opportunity to generate new knowledge in the field of PU foams. In addition to this, more information about products generation could be obtained by real-time FTIR spectroscopy. In general, the foaming process of PU foams is very fast and thus the use of real-time FTIR spectroscopy allows evaluating the reactions from the first seconds, which are lost using the FTIR-spectroscopy without less time resolution.

- Applying the monitoring methodology of the foaming process, which has been developed in this thesis, in other PU foams such as polyisocyanurate foams, flexible PU foams or semi-rigid PU foams.

- Establishing a methodology to measure the gas composition inside the cells of RPU foams blown with a physical blowing agent by gas chromatography. This would allow understanding the long-term thermal conductivity of RPU foams.

- Using alternative blowing agents such as Hydrofluoroolefins (HFO) and hydrochlorofluoroolefins (HCFO) that belong to the 4th generation of foaming agents used in RPU foams. These are interesting since these results in a very low global warming potential and thus could be considered an 'eco-friendly' gas.

- Obtaining thermoset PU foams by high-pressure CO_2 foaming. This foaming method showed very effective with thermoplastics (for example TPU) because microcellular and nanocellular foams have been obtained which have enhanced thermal insulating and mechanical properties as compared to the conventional foams. However, the preparation of thermoset PU foams by high-pressure CO_2 foaming is more complicated than for TPU foams, due to the reactions involved in the foaming process. This study is interesting because microcellular thermoset PU foams could be obtained and even nanocellular thermoset PU foams.

In the second place, a new branch in the research line of PU foams based on the **green thermoset PU foams** from environmental-friendly raw materials may be also proposed. Some ideas are the following:

- Studying PU foams based on bio-based polyols. The use of polyols from natural resources such as vegetable oils and natural fats has a great interest because of their important availability, sustainability, biodegradability, and added values.
- Studying non-isocyanate PU (NIPU) foams without requiring either phosgene or isocyanates in order to avoid special safety, health, and handling precautions and to meet the demands of green chemistry.

The last proposal would be to continue the study of **TPU foams** because they present huge advantages compared to thermoset PU foams. For example, TPU foams are elastic thermoplastically processable materials, and they can be reprocessed or recycled due to their non-chemical crosslinked structure. Different foaming process could be studied, such as bead foaming, extrusion foaming or injection foaming.